Electro-Magnetic Transients Program (EMTP)

Theory Book

CONTENTS

(Click topic to jump to its location)

Branch of System Engineering
Bonneville Power Administration
Portland, Oregon 97208-3621
United States of America

PREFACE

To operate an electric power system reliably, and to plan its expansion properly, utility engineers perform a variety of network studies. The most common types of network studies are

- short circuit (or fault) analysis,
- power (or load) flow analysis,
- stability analysis, and
- analysis of electromagnetic transients.

Among these, studies concerned with electromagnetic transients are probably the most complicated ones. For the beginner, there is the difficulty of developing an understanding of the nature of electromagnetic transients in power systems, in addition to the difficulty of learning how to simulate them with the Electromagnetic Transients Program (EMTP). The problem is much easier for the expert, who needs only minimal advice on how to use the EMTP properly. Both the beginner and the expert must have some understanding of the limitations and inherent errors of EMTP simulations, however.

Thus began the writing of the original prime contractor who was paid by BPA to assemble this work, Prof. Hermann W. Dommel of the University of British Columbia in Vancouver (Canada). More modern history can be found in Can/Am EMTP News, the newsletter of the North American user group. Pasting from the July, 1994, and July, 1995, issues is the following story about the conversion to computer storage:

July, 1994 : BPA EMTP Theory Book in WP 5.1

The 700-page EMTP Theory Book of BPA is being converted to WordPerfect 5.1 storage from the crummy, old, paper copy that was submitted by Prof. Hermann W. Dommel of the University of British Columbia (located in Vancouver, B.C., Canada) in 1987. More information

should be provided in the next (October) newsletter. Work has been started by Kwang-yi Ger, Dr. Tsu-huei Liu's daughter, who recently finished her second year as a student of journalism at the University of Washington in Seattle (USA). Ms. Ger is a good writer, and she knows WordPerfect. Initially, the content of all figures will be ignored. If any reader has ideas about how best to handle graphics of BPA's Theory Book, he is encouraged to share his understanding with the Can/Am user group. Current thinking is that, initially, all figures might be scanned to produce bitmaps. To avoid making this added burden mandatory, the files should be kept external. Later, one at a time, some of these then might be replaced by vector storage.

For those readers who may have forgotten, or may never have known, Prof. Dommel signed a contract with BPA around the end of August, 1981. Among other things (cable research by Luis Marti), this contract provided payment of about $100K to Prof. Dommel for delivery of the book within 4 years. Well, the 4 years passed, but the Theory Book (named *Reference Manual* only for purposes of the contract) was not ready. This was around the end of August, 1985. So, without penalty, BPA allowed Prof. Dommel another entire year. This time, the manuscript was submitted. However, it was not yet usable because it included many pieces of intellectual property that belonged to others, and for which the professor had not obtained permission to use. This explains paragraph 3 of the official BPA form letter by Drs. Liu and Meyer dated June 10, 1987: *"Since the early fall of 1986 when BPA received the manuscript from the contractor, there has been an effort to obtain permission for BPA to publish all portions of the book that were copyrighted by others. This has been completed to the satisfaction of the BPA contracting officer, who just recently gave his approval for BPA to print this work, and to distribute copies to others."*

Back to the first paragraph. The perceptive reader might already have asked himself: convert from *paper* to WordPerfect? Did Prof. Dommel never supply BPA with a computer-stored (e.g., magnetically-stored) copy of the text? That is correct: only a paper copy was supplied by Prof. Dommel, who claimed that his disk files somehow had been lost. So, the keying by Kwang-yi Ger continues in West Linn.

July, 1995 :   BPA EMTP Theory Book in WP 5.1

The 700-page EMTP Theory Book of BPA has been converted to WordPerfect 5.1 storage from the crummy, old, paper copy that was submitted to BPA in 1987 by its contractor, Hermann Dommel.   The present mention is a continuation of the story in the January issue.

Kwang-yi Ger, the daughter of Drs. Tsu-huei Liu and Kai-hwa Ger, did all the non-table text (including all equations) with some help from her mother, recall. Now, Kwang-chien Ger, the younger son, has completed the operation by adding all figures as .TIF bitmaps. Both high- (300 dpi) and low- (75 dpi) resolution copies were produced, and then included by WP5.1 to convert to equivalent, compressed .WPG files. The .WPG files are stored externally, and there are two sets. Compressed sizes of these are 2763 and 531 Kbytes, respectively. After unzipping, these become 7091 and 1091 Kbytes.

Improved resolution of some figures is a result that may surprise the average reader. Normally, creating a bitmap from an original results in distortion that includes loss of resolution. But what if the original already involves substantial distortion,   typically due to substantial photoreduction? Using a photocopy machine, there is no way to recover the lost resolution. But with computer scanning, human intelligence can be applied in the form of graphical editing of the bitmap. The H-P software that allows this is *HP Paintbrush*, which Kwang-chien has been using effectively on some figures such as 6.33 and 12.1. If some figures look significantly better than the original printed copy that was submitted by contractor Dommel, it is because they have been improved!

Co-Chairmen of Canadian/American EMTP User Group

Dr. W. Scott Meyer
The Fontaine, Unit 6B
1220 N.E. 17-th Avenue
Portland, Oregon 97232
U.S.A.
E-mail: atp@agora.rain.com

Dr. Tsu-huei Liu
3179 Oak Tree Court
West Linn, Oregon 97068
U.S.A
E-mail: thliu@bpa.gov

1. INTRODUCTION TO THE SOLUTION METHOD USED IN THE EMTP

This manual discusses by and large only those solution methods which are used in the EMTP. It is therefore not a book on the complete theory of solution methods for the digital simulation of electromagnetic transient phenomena. The developers of the EMTP chose methods which they felt are best suited for a general-purpose program, such as the EMTP, and it is these methods which are discussed here. For analyzing specific problems, other methods may well be competitive, or even better. For example, Fourier transformation methods may be preferable for studying wave distortion and attenuation along a line in cases where the time span of the study is so short that reflected waves have not yet come back from the remote end.

The EMTP has been specifically developed for power system problems, but some of the methods have applications in electronic circuit analysis as well. While the developers of the EMTP have to some extent been aware of the methods used in electronic circuit analysis programs, such as TRAC or ECAP, the reverse may not be true. A survey of electronic analysis programs published as recently as 1976 [22] does not mention the EMTP even once.

Computer technology is changing very fast, and new advances may well make this manual obsolete by the time it is finished. Also, better numerical solution methods may appear as well, and replace those presently used in the EMTP. Both prospects have been discouraging for the writer of this manual; what has kept him going is the hope that those who will be developing better programs and who will use improved computer hardware will find some useful information in the description of what exists today.

Digital computers cannot simulate transient phenomena continuously, but only at discrete intervals of time (step size Δt). This leads to truncation errors which may accumulate from step to step and cause divergence from the true solution. Most methods used in the EMTP are numerically stable and avoid this type of error build-up.

The EMTP can solve any network which consists of interconnections of resistances, inductances, capacitances, single and multiphase π-circuits, distributed-parameter lines, and certain other elements. To keep the explanations in this introduction sample, only single-phase network elements will be considered and the more complex multiphase network elements as well as other complications will be discussed later. Fig. 1.1 shows the details of a larger network just for the region around node 1. Suppose that voltages and currents have already been computed at time instants 0, Δt, $2\Delta t$, etc., up to t-Δt, and that the solution must now be found at instant t. At any instant of time, the sum of the currents flowing away from node 1 through the branches must be equal to the injected current i_1:

$$i_{12}(t) \; + \; i_{13}(t) \; + \; i_{14}(t) \; + \; i_{15}(t) \; = \; i_1(t) \tag{1.1}$$
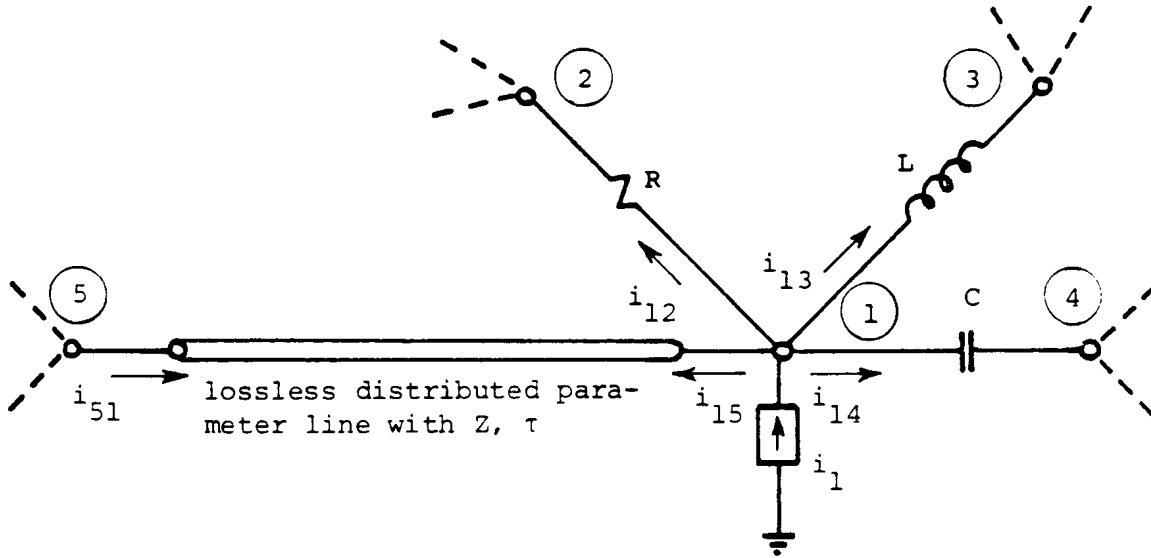
Fig. 1.1 - Details of a larger network around node no. 1

Node voltages are used as state variables in the EMTP. It is therefore necessary to express the branch currents, i_{12}, etc., as functions of the node voltages. For the resistance,

$$i_{12}(t) = \frac{1}{R} \{v_1(t) - v_2(t)\}$$

(1.2)

For the inductance, a simple relationship is obtained by replacing the differential equation

$$v = L\frac{di}{dt}$$

with the central difference equation

$$\frac{v(t) + v(t-\Delta t)}{2} = L\frac{i(t) - i(t-\Delta t)}{\Delta t}$$

This can be rewritten, for the case of Fig. 1.1, as

$$i_{13}(t) = \frac{\Delta t}{2L} \{v_1(t) - v_3(t)\} + hist_{13}(t-\Delta t)$$

(1.3a)

with $hist_{13}$ known from the values of the preceding time step,

$$hist_{13}(t-\Delta t) = i_{13}(t-\Delta t) + \frac{\Delta t}{2L} \{v_1(t-\Delta t) - v_3(t-\Delta t)\}$$

(1.3b)

The derivation for the branch equation of the capacitance is analogous, and leads to

1-2

$$i_{14}(t) = \frac{2C}{\Delta t}\{v_1(t) - v_4(t)\} + hist_{14}(t-\Delta t) \qquad (1.4a)$$

with $hist_{14}$ again known from the values of the preceding time step,

$$hist_{14}(t-\Delta t) = -i_{14}(t-\Delta t) - \frac{2C}{\Delta t}\{v_1(t-\Delta t) - v_4(t-\Delta t)\} \qquad (1.4b)$$

Readers fresh out of University, or engineers who have read one or one too many textbooks on electric circuits and networks, may have been misled to believe that Laplace transform techniques are only useful for "hand solutions" or rather small networks, and more or less useless for computer solutions of problems of the size typically analyzed with the EMTP. Since even new textbooks perpetuate the myth of the usefulness of Laplace transforms, Appendix I has been added for the mathematically-minded reader to summarize numerical solution methods for linear, ordinary differential equations.

For the transmission line between nodes 1 and 5, losses shall be ignored in this introduction. Then the wave equations

$$-\frac{\partial v}{\partial x} = L'\frac{\partial i}{\partial t}$$

$$-\frac{\partial i}{\partial x} = C'\frac{\partial v}{\partial t}$$

where

        L', C' = inductance and capacitance per unit length[1],

        x = distance from sending end,

have the well-known solution due to d'Alembert:

$$i = F(x - ct) - f(x + ct)$$
$$v = ZF(x - ct) + Zf(x + ct) \qquad (1.5a)$$

with

        $\left.\begin{array}{l}F(x - ct) \\ f(x = ct)\end{array}\right]$ = functions of the composite expressions $x - ct$ and $x + ct$,

        Z = surge impedance $Z = \sqrt{L'/C'}$ (constant),

        c = velocity of wave propagation (constant).

        If the current in Eq. (1.5a) is multiplied by Z and added to the voltage, then

---

[1]The prime is used on L', C' to distinguish these distributed parameters from lumped parameters L, C.

$$v + Zi = 2ZF(x - ct) \qquad (1.5b)$$

Note that the composite expression v + Zi does not change if x - ct does not change. Imagine a fictitious observer travelling on the line with wave velocity c. The distance travelled by this observer is x = x_0 + ct (x_0 = location of starting point), or x - ct is constant. If x - ct is indeed constant, then the value of v + Zi seen by the observer must also remain constant. With travel time

$$\tau = \text{line length} / c \ ,$$

an observer leaving node 5 at time t - τ will see the value of v_5(t - τ) + Zi_{51}(t - τ), and upon arrival at node 1 (after the elapse of travel time τ), will see the value of v_1(t) - Zi_{15}(t) (negative sign because i_{15} has opposite direction of i_{51}). But since this value seen by the observer must remain constant, both of these values must be equal, giving, after rewriting,

$$i_{15}(t) = \frac{1}{Z} v_1(t) + hist_{15}(t - \tau) \qquad (1.6a)$$

where the term $hist_{15}$ is again known from previously computed values,

$$hist_{15}(t-\tau) = -\frac{1}{Z} v_5(t-\tau) - i_{51}(t-\tau) \qquad (1.6b)$$

Example: Let Δt = 100 μs and τ = 1 ms. From equations (1.6) it can be seen that the known "history" of the line must be stored over a time span equal to τ, since the values needed in Eq. (1.6b) are those computed 10 time steps earlier. Eq. (1.6) is an exact solution for the lossless line if Δt is an integer multiple of τ; if not, linear interpolation is used and interpolation errors are incurred. Losses can often be represented with sufficient accuracy by inserting lumped resistances in a few places along the line, as described later in Section 4.2.2.5. A more sophisticated treatment of losses, especially with frequency dependent parameters, is discussed in Section 4.2.2.6.

If Eq. (1.2), (1.3a), (1.4a) and (1.6a) are inserted into Eq. (1.1), then the node equation for node 1 becomes

$$\left(\frac{1}{R} + \frac{\Delta t}{2L} + \frac{2C}{\Delta t} + \frac{1}{Z} \right) v_1(t) - \frac{1}{R} v_2(t) - \frac{\Delta t}{2L} v_3(t) - \frac{2C}{\Delta t} v_4(t) =$$

$$i_1(t) - hist_{13}(t-\Delta t) - hist_{14}(t-\Delta t) - hist_{15}(t-\tau) \qquad (1.7)$$

which is simply a linear, algebraic equation in unknown voltages, with the right-hand side known from values of preceding time steps.

For any type of network with n nodes, a system of n such equations can be formed[2],

$$[G] [v(t)] = [i(t)] - [hist] \qquad (1.8a)$$

---

[2]Brackets are used to indicate matrix and vector quantities.

with $[G]$ = n x n symmetric nodal conductance matrix,

          $[v(t)]$ = vector of n node voltages,

          $[i(t)]$ = vector of n current sources, and

          $[hist]$ = vector of n known "history" terms.

Normally, some nodes have known voltages either because voltage sources are connected to them, or because the node is grounded. In this case Eq. (1.8a) is partitioned into a set A of nodes with unknown voltages, and a set B of nodes with known voltages. The unknown voltages are then found by solving

$$[G_{AA}][v_A(t)] = [i_A(t)] - [hist_A] - [G_{AB}][v_B(t)] \tag{1.8b}$$

for $[v_A(t)]$.

      The actual computation in the EMTP proceeds as follows: Matrices $[G_{AA}]$ and $[G_{AB}]$ are built, and $[G_{AA}]$ is triangularized with ordered elimination and exploitation of sparsity. In each time step, the vector on the right-hand side of Eq. (1.8b) is "assembled" from known history terms, and known current and voltage sources. Then the system of linear equations is solved for $[v_A(t)]$, using the information contained in the triangularized conductance matrix. In this "repeat solution" process, the symmetry of the matrix is exploited in the sense that the same triangularized matrix used for downward operations is also used in the backsubstitution. Before proceeding to the next time step, the history terms hist of Eq. (1.3b), (1.4b) and (1.6b) are then updated for use in future time steps.

      Originally, the EMTP was written for cases starting from zero initial conditions. In such cases, the history terms $hist_{13}$, $hist_{14}$ and $hist_{15}$ in Eq. (1.7) are simply preset to zero. But soon cases arose where the transient simulation had to be started from power frequency (50 or 60 Hz) ac steady-state initial conditions. Originally, such ac steady-state initial conditions were read in[3], but this put a heavy burden on the program user, who had to use another steady-state solution program to obtain them. Not only was the data transfer bothersome, but the separate steady-state solution program might also contain network models which could differ more or less from those used in the EMTP. It was therefore decided to incorporate an ac steady-state solution routine directly into the EMTP, which was written by J.W. Walker.

      The ac steady-state solution shall again be explained for the case of Fig. 1.1. Using node equations again, Eq. (1.1) now becomes

$$I_{12} + I_{13} + I_{14} + I_{15} = I_1 \tag{1.9}$$

where the currents I are complex phasor quantities $|I| \cdot e^{j\alpha}$ now. For the lumped elements, the branch equations are obvious. For the resistance,

$$I_{12} = \frac{1}{R}(V_1 - V_2) \tag{1.10}$$

---

[3]This option is still available in the EMTP, but it has become somewhat of a historic relic and has seldom been used after the addition of a steady-state solution routine. For some types of branches, it may not even work ([1], p. 37c).

for the inductance,
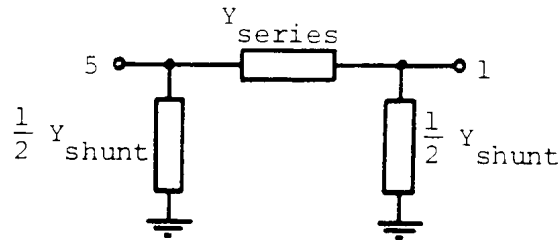
$$I_{13} = \frac{1}{j\omega L}(V_1 - V_3) \tag{1.11}$$

and for the capacitance,

$$I_{14} = j\omega C(V_1 - V_4) \tag{1.12}$$

For a line with distributed parameters R', L', G', C', the exact steady-state solution is

$$\begin{bmatrix} I_{15} \\ I_{51} \end{bmatrix} = \begin{bmatrix} Y_{series} + \frac{1}{2} Y_{shunt} & -Y_{series} \\ -Y_{series} & Y_{series} + \frac{1}{2} Y_{shunt} \end{bmatrix} \begin{bmatrix} V_1 \\ V_5 \end{bmatrix} \tag{1.13}$$

if the equivalent π-circuit representation of Fig. 1.2 is used, with

Fig. 1.2 - Equivalent π-circuit for ac steady-state
solution of transmission line

$$Y_{series} = \frac{1}{Z_{series}}, \quad with \ Z_{series} = \mathcal{L}(R' + j\omega L')\frac{\sinh(\gamma \mathcal{L})}{\gamma \mathcal{L}}$$

$$\frac{1}{2} Y_{shunt} = \frac{\mathcal{L}}{2}(G' + j\omega C')\frac{\tanh\left(\frac{\gamma \mathcal{L}}{2}\right)}{\frac{\gamma \mathcal{L}}{2}} \tag{1.14}$$

and sometimes equally useful,

$$Y_{series} + \frac{1}{2} Y_{shunt} = \cosh(\gamma \mathcal{L}) \cdot Y_{series}$$

where γ is the propagation constant,

$$\gamma = \sqrt{(R' + j\omega L')(G' + j\omega C')} \tag{1.15}$$

For the lossless case with R' = 0, and G' = 0, Eq. (1.14) simplifies to

$$Z_{series} = \mathcal{L} \cdot j\omega L' \cdot \frac{\sin(\omega\mathcal{L}\sqrt{L'C'})}{\omega\mathcal{L}\sqrt{L'C'}}$$

$$\frac{1}{2}Y_{shunt} = \frac{\mathcal{L}}{2} \cdot j\omega C' \cdot \frac{\tan\left(\frac{\omega\mathcal{L}}{2}\sqrt{L'C'}\right)}{\frac{\omega\mathcal{L}}{2}\sqrt{L'C'}} \tag{1.16}$$

$$Y_{series} + \frac{1}{2}Y_{shunt} = \cos(\omega\mathcal{L}\sqrt{L'C'}) \cdot Y_{series}$$

If the value of $\omega\mathcal{L}$ is small, typically $\mathcal{L} \leq 100$ km at 60 Hz for overhead lines, then the ratios sinh(x) / x and tanh(x/2) / x/2 in Eq. (1.14), as well as sin(x) / x and tan(x/2) / x/2 in Eq. (1.16) all become 1.0. This simplified π-circuit is usually called the "nominal" π-circuit,

$$Z_{series} = \mathcal{L} \cdot (R' + j\omega L')$$

$$\frac{1}{2}Y_{shunt} = \frac{\mathcal{L}}{2}(G' + j\omega C') \qquad \text{if } \omega\mathcal{L} \text{ is small.} \tag{1.17}$$

With the equivalent π-circuit of Fig. 1.2, the branch equation for the lossless line finally becomes

$$I_{15} = (Y_{series} + \frac{1}{2}Y_{shunt})V_1 - Y_{series}V_5 \tag{1.18}$$

Now, we can again write the node equation for node 1, by inserting Eq. (1.10), (1.11), (1.12) and (1.18) into Eq. (1.9),

$$\left(\frac{1}{R} + \frac{1}{j\omega L} + j\omega C + Y_{series} + \frac{1}{2}Y_{shunt}\right)V_1 - \frac{1}{R}V_2 - \frac{1}{j\omega L}V_3 - j\omega C V_4 - Y_{series}V_5 = I_1$$

$$\tag{1.19}$$

For any type of network with n nodes, a system of n such equations can be formed,

$$[Y][V] = [I] \tag{1.20}$$

with   [Y] = symmetric nodal admittance matrix, with complex elements,

        [V] = vector of n node voltages (complex phasor values),

        [I] = vector of n current sources (complex phasor values).

Again, Eq. (1.20) is partitioned into a set A of nodes with unknown voltages, and a set B of nodes with known

voltages. The unknown voltages are then found by solving the system of linear, algebraic equations

$$[Y_{AA}][V_A] = [I_A] - [Y_{AB}][V_B] \qquad\qquad (1.21)$$

Bringing the term $[Y_{AB}][V_B]$ from the left-hand side in Eq. (1.20) to the right-hand side in Eq. (1.21) is the generalization of converting Thevenin equivalent circuits (voltage vector $[V_B]$ behind admittance matrix $[Y_{AB}]$) into Norton equivalent circuits (current vector $[Y_{AB}][V_B]$ in parallel with admittance matrix $[Y_{AB}]$).
Norton equivalent circuits (current vector $[Y_{AB}][V_B]$ in parallel with admittance matrix $[Y_{AB}]$).

2. LINEAR, UNCOUPLED LUMPED ELEMENTS

Linear, uncoupled lumped elements are resistances R, self inductances L, and capacitances C. They usually appear as parts of equivalent circuits, which may represent generators, transformers, short sections of transmission lines, or other components of an electric power system, or they may represent a component by itself.

2.1 Resistance R

Resistance elements are used to represent, among other things,

(a)   closing and opening resistors in circuit breakers,

(b)   tower footing resistance (as a crude approximation [8] of a complicated, frequency-dependent grounding impedance),

(c)   resistance grounding of transformer and generator neutrals,

(d)   "metering" - resistance in places where currents of branch voltages cannot be obtained in other ways by the EMTP,

(e)   as parts of equivalent networks, e.g., in parallel with inductances to produce proper frequency-dependent damping (see Section 2.2.2).

(f)   for the representation of long lines in lightning surge studies if no reflection comes back from the remote end during the duration t_{max} of the study.

Example (f) is easily derived from Eq. (1.6b) if it is assumed that the initial conditions on the line are zero. In that case, $hist_{15}(t - \tau) = 0$ for $t < \tau$ since it takes time τ for any nonzero condition occurring in node 5 after $t \geq 0$ to show up in node 1. If nothing is connected to node 5 ("open-ended line"), then I_{15} would remain zero for $t < 2\tau$. The EMTP recognizes this simplification if

(1) $\tau > t_{max}$, and

(2)   zero initial conditions[1].

If both conditions (1) and (2) are met, then the EMTP represents the line simply as two shunt resistances (Fig. 2.1). This simplification saves not only computer time but storage space as well, because no history terms have to be stored for the line. This long-line model is mostly used in lightning surge studies and
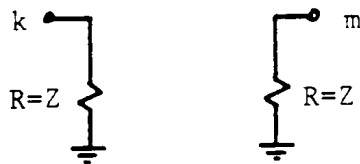
Fig. 2.1 - Equivalent circuit of long line if no reflections come back from other end

---

[1]It is possible to modify this simplification for cases starting from linear ac steady-state conditions as well; in that case, nodes 5 and 1 in Fig. 2.1 would have ac steady-state current sources connected to them. Unfortunately, the EMTP does not yet contain this modification.

in transient recovery voltage studies, where the unfaulted lines leaving the substation under study are preferably modelled this way.

The equation of a lumped resistance R between nodes k and m,

$$i_{km}(t) = \frac{1}{R}\left(v_k(t) - v_m(t)\right) \tag{2.1}$$

is solved accurately by the EMTP, as long as the value of R is not "unreasonably" small.

2.1.1 Error Analysis

Very large values of R are acceptable and do not degrade the solution of the complete network. In the limiting case, $R = \infty$, its reciprocal value 1/R simply gets lost in [G] of Eq. (1.8), that is, it will not have any influence on the network solution, as it should be. A practical limit for very large resistances is the approximate square root of the largest real number which the computer can handle (e.g., $R < 10^{38}$ if the computer accepts numbers up to 10^{76}). This is because intermediate expressions of the form $R^2 + X^2$ are computed in the steady-state solution in the conversion from impedances to admittances. Extremely large values of R have been used in the past to obtain voltage differences between nodes with such "metering"-resistance branches; in newer EMTP versions, voltage differences can be obtained directly.

Very large resistances can be used to replace the series R-L elements in symmetric multiphase π-circuits, if one is only interested in the capacitive coupling among the phases, as explained in Fig. 2.2. This trick reduces the number of nodes, but more importantly, it avoids accuracy problems which may occasionally show up if the π-circuit represents a very short line section[2]. In the steady-state solution of Eq. (1.20) the value of the series

---

[2]It may be worth adding a diagnostic printout in the EMTP if the admittances of the series and shunt elements are too far apart in orders of magnitude. This would require a comparison of $1/\omega L$ and ωC in the steady-state solution, and of $\Delta t/2L$ and $2C/\Delta t$ in the transient solution.
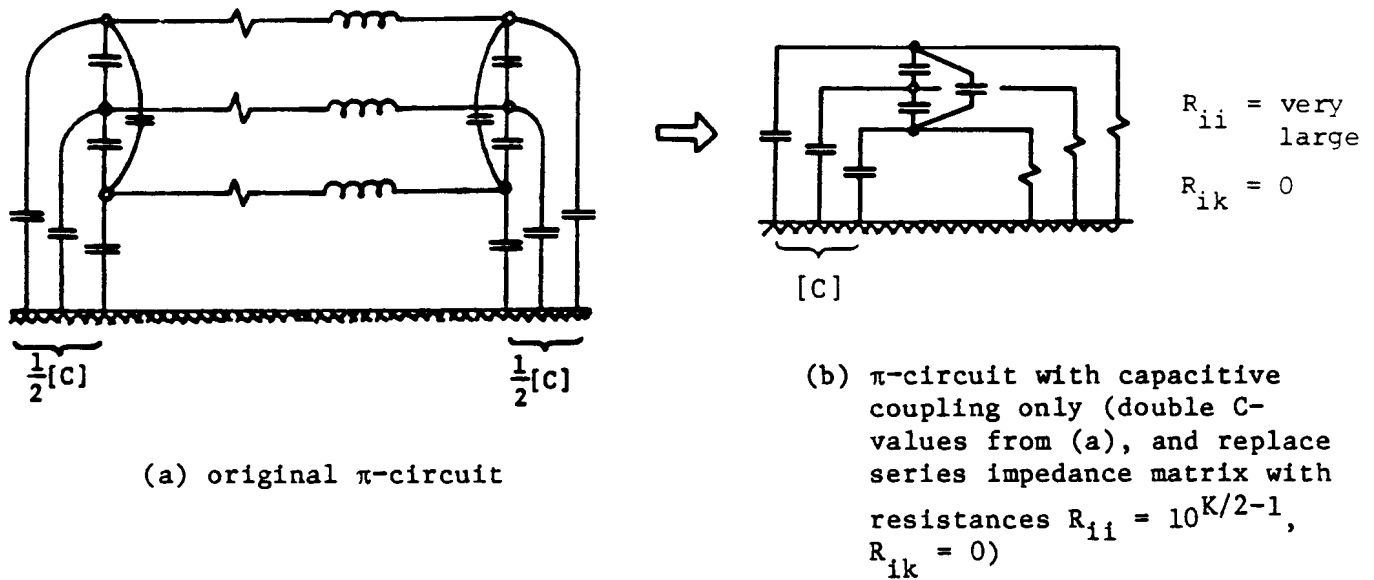
(a) original π-circuit

(b) π-circuit with capacitive coupling only (double C-values from (a), and replace series impedance matrix with resistances $R_{ii} = 10^{K/2-1}$, $R_{ik} = 0$)

R_{ii} = very large

$R_{ik} = 0$

[C]

Fig. 2.2 - Conversion of nominal π-circuit for short line into π-circuit with capacitive coupling only

element is entered as $1/\mathscr{L}[Z']^{-1}$ into [Y], where [Z'] is the impedance per unit length and $\mathscr{L}$ the length of the short section. For a short length, $\mathscr{L}$ is small and $1/\mathscr{L}[Z']^{-1}$ accordingly relatively large. At the same time, the shunt susceptances $1/2\mathscr{L} \cdot j\omega[C']$ entered into [Y] become relatively small. As $\mathscr{L}$ is decreased, the capacitive coupling effect will eventually get lost in the solution. In a practical case of capacitive coupling between 500 kV circuits at 60 Hz, this accuracy problem showed up with the shortest line section being 1.6 km; it was discovered accidentally because the single-precision solution (accuracy approx. 7 decimal digits) on an IBM 370 differed unexpectedly by 10% from the double-precision solution (accuracy approx. 14 decimal digits). For reasonable step sizes of Δt, the problem is less severe in the transient calculation, as can easily be seen if $j\omega$ in Eq. (1.19) is replaced by $2/\Delta t$ in Eq. (1.7). In this example, with $\Delta t = 100~\mu s$, the value of the series element would be smaller by a factor of 53, while the value of the shunt element would be larger by a factor of 53. Or in other words, a similar accuracy problem would appear during the transient simulation if the line were shortened by a factor of 53 ($\mathscr{L} = 30$ m instead of 1.6 km).

Very small values of R do create accuracy problems, for the same reason as discussed in the preceding paragraph: Very small values of R create very large conductance values 1/R in the matrix [Y] of steady-state solutions and in the matrix [G] of transient solutions, which can "swamp out" the effects of other elements connected to that resistance. Very small values of R have been used in the past primarily to separate switches, since earlier EMTP versions allowed only one switch to be connected to a node with unknown voltage. In newer versions, this limitation on the location of switches no longer exists, and the need for using very small values of R should therefore no longer exist in these later versions.

Hints about the use of small resistances are given in [1], pp. 6b-6c.

2-3

2.1.2 Example for Network with Resistances

Practical examples for purely resistive networks are rather limited. A simple case is shown in Fig. 2.3. Assume a dc voltage source with negligible source impedance is connected to a line through a circuit breaker with a closing resistor of value R_{close}. If we are interested in what happens after closing of contact I in the first short time period during which reflections have not yet come back from the remote end, then this case can be studied with the circuit of Fig. 2.3(b). If we choose $R_{close} = Z$, we see that the voltage at the sending end will be 0.5 p.u., which will double to 1.0 p.u. at the open receiving end. Therefore, no overvoltage will appear as long as contact II is still open. A real case is obviously more complicated because

| (a) network | (b) equivalent circuit |
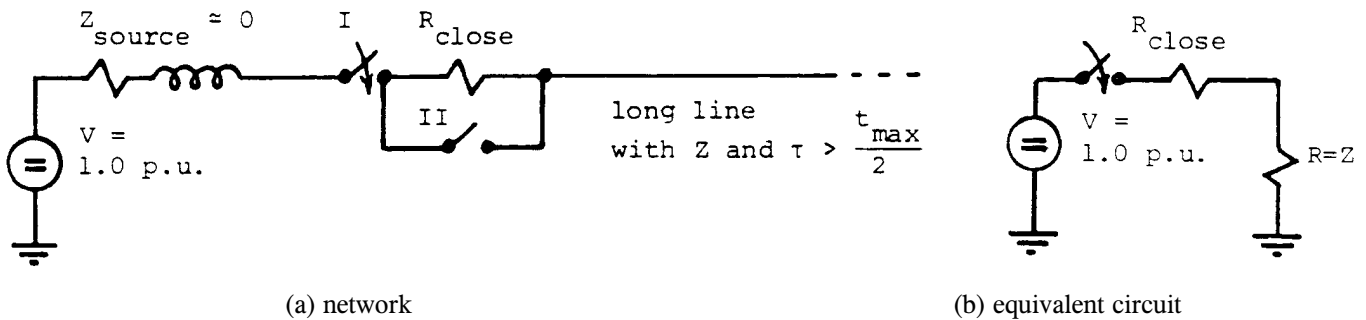
**Fig. 2.3** - Energization of a very long line (Z = surge impedance, τ = travel time)

- contact II will close (typically 8 to 10 ms later) as well,
- the system is three-phase,
- the line is not lossless,
- multiple reflections will occur as we study a longer time period,
- closing of contact I does not necessarily occur at maximum voltage (approximated as a dc source in Fig. 2.3), but may occur anywhere on the sine-wave,
- the source impedance is not zero,
- the three poles in a three-phase system do not close simultaneously, and because of many other factors.

In a typical system, maximum switching surge overvoltages may be 2.4 to 2.8 p.u. without closing resistors (versus 2.0 p.u. in Fig. 2.3), which would typically be reduced to 1.5 to 2.2 p.u. with closing resistors (versus 1.0 p.u. in Fig. 2.3) [69].

2.2 Self Inductance L

Magnetically coupled circuits are so prevalent in power systems, starting from the generator, through the transformer, to the magnetically coupled phase conductors of a three-phase line, that inductances usually appear as coupled inductances. There are cases, however, of uncoupled self inductances. Among other things, self

inductances are used to represent

(a) normal three-phase connection

(b) four-reactor compensation scheme
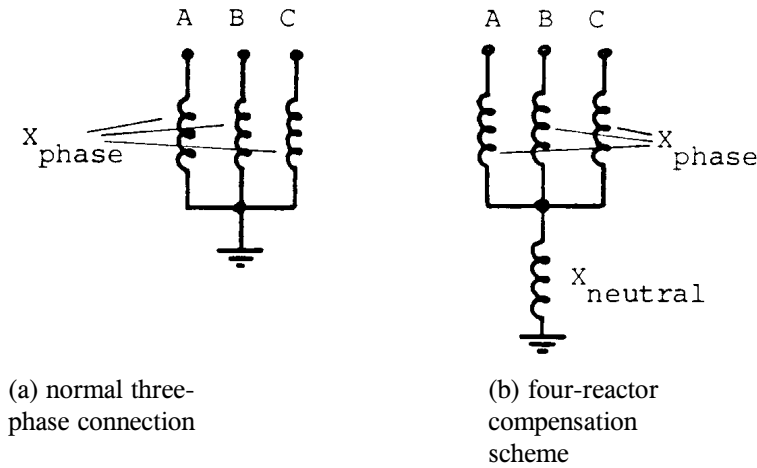
Fig. 2.4 - Shunt reactor connections

(a)   single-phase shunt reactors and neutral reactors in shunt compensation schemes (Fig. 2.4),

(b)   part of discharge circuits in series-capacitor stations,

(c)   equipment in HVDC converter stations, such as smoothing reactors, anode reactors, parts of filters on the ac and dc side,

(d)   inductive part of source impedances in Thevenin equivalent circuits for the "rest of the system" when positive and zero sequence parameters are identical (Fig. 2.5),

(e)   inductive part of single-phase nominal π-circuits in the single-phase representation of balanced (positive or negative sequence) operation or of zero sequence operation (Fig. 2.6),

(f)   part of equivalent circuit for loads (Fig. 2.7), even though load modelling at higher frequencies is a very complicated topic [9], and loads are therefore, or for other reasons, often ignored,
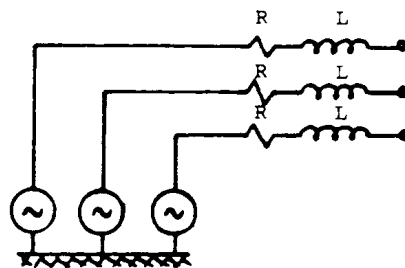
Fig. 2.5 - Thevenin equivalent circuit with $Z_{pos} = Z_{neg} = Z_{zero}$
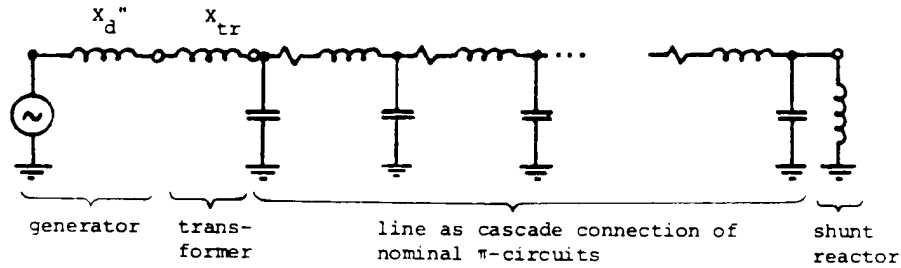
2-5

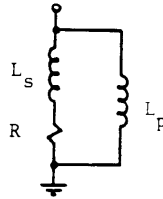**Fig. 2.6** - Typical positive sequence network representation

Fig. 2.7 - Load model for harmonics studies [9]

(g)   part of surge arrester models to simulate the dynamic characteristics of the arrester [10],

(h)   parts of electronic circuits.

Choke coils used for power-line carrier communications are normally ignored in switching surge studies, but may have to be modelled in studies involving higher frequencies. Current transformers are usually ignored, unless the current transformer itself is part of the investigation (e.g., in studying the distortion of the secondary current through saturation effects).

The equation of a self inductance L between nodes k and m is solved accurately in the ac steady-state solution with Eq. (1.11). The only precaution to observe is that ωL_{km} should not be extremely small, for the same reasons as explained in Section 2.1.1 for the case of small resistance values.

For the transient simulation, the exact differential equation

$$v_k - v_m = L\frac{di_{km}}{dt} \tag{2.2}$$

is replaced by the approximate central difference equation

$$\frac{v_k(t) - v_m(t) + v_k(t-\Delta t) - v_m(t-\Delta t)}{2} = L\frac{i_{km}(t) - i_{km}(t-\Delta t)}{\Delta t} \tag{2.3}$$

The same difference equation is obtained if the trapezoidal rule of integration is applied to the integral in

$$i_{km}(t) = i_{km}(t-\Delta t) + \frac{1}{L}\int_{t-\Delta t}^{t}\left[v_k(u) - v_m(u)\right]du \tag{2.4}$$

giving

$$i_{km}(t) = i_{km}(t-\Delta t) + \frac{\Delta t}{2L}\{v_k(t) - v_m(t) + v_k(t-\Delta t) - v_m(t-\Delta t)\} \tag{2.5}$$

Eq. (2.3) and (2.5) can be rewritten into the desired branch equation

$$i_{km}(t) = \frac{\Delta t}{2L}\{v_k(t) - v_m(t)\} + hist_{km}(t-\Delta t) \tag{2.6}$$

with the "history term" $hist_{km}(t - \Delta t)$ known from the solution at the preceding time step,

$$hist_{km}(t-\Delta t) = i_{km}(t-\Delta t) + \frac{\Delta t}{2L}\{v_k(t-\Delta t) - v_m(t-\Delta t)\} \tag{2.7}$$

Eq. (2.6) can conveniently be represented as an equivalent resistance $R_{equiv} = 2L/\Delta t$, in parallel with a known current source $hist_{km}(t - \Delta t)$, as shown in Fig. 2.8. Once all the node voltages have been found at a particular time step at instant t, the history term of Eq. (2.7) must be updated for
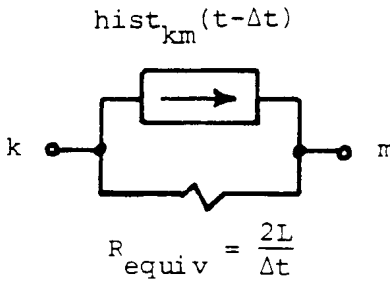
Fig. 2.8 - Equivalent resistive circuit for transient solution of lumped inductance

each inductive branch for use in the next time step at $t + \Delta t$. To do this, the branch current must first be found from Eq. (2.6), or alternatively, if both equations are combined, the recursive updating formula

$$hist_{km}(t) = \frac{\Delta t}{L}\{v_{km}(t) - v_m(t)\} + hist_{km}(t-\Delta t) \tag{2.8}$$

can be used. If branch current output is requested, then Eq. (2.6) is used.

2.2.1 Error Analysis

Since the differential equation (2.2) is solved approximately, it is important to have some understanding about the errors caused by the application of the trapezoidal rule of integration. As explained in Section I.4 of Appendix I, the trapezoidal rule is numerically stable, and the solution does therefore not "run away" (see Fig. I.4 in Appendix I). Fortunately, there is also a physical interpretation of the error, because Eq. (2.5) resulting from the

trapezoidal rule is identical with the exact solution of the short-circuited lossless line in the arrangement of Fig. 2.9 This was first pointed out to the writer by H. Maier, Technical University Stuttgart, Germany, in a personal communication in 1968, for the case of a shunt inductance. From a paper by P.B. Johns [12], it became obvious that this identity is valid for any connection of the inductance. To derive the parameters of such a "stub-line" representation, it is reasonable to start with the requirement that the distributed inductance L', multiplied by the stub-line length $\mathcal{L}$, should be equal to the value of the lumped inductance

$$L'\mathcal{L} = L \tag{2.9}$$
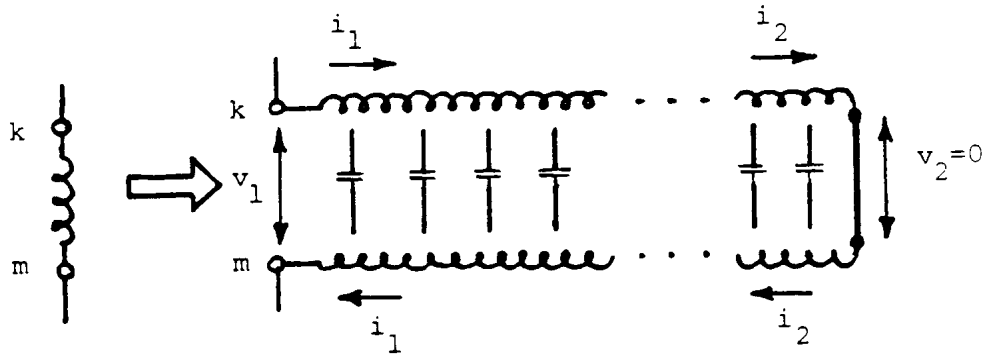
Fig. 2.9 - Lumped inductance replaced by short-circuited stub-line with Z = 2L/Δt and τ = Δt/2

With L'$\mathcal{L}$ known, the next parameter to be determined is the travel time τ of the stub-line. Since

$$\tau = \sqrt{(L'\mathcal{L})(C'\mathcal{L})} \tag{2.10}$$

the shorter the travel time, the smaller will be the value of the "parasitic" but unavoidable capacitance C'$\mathcal{L}$. The shortest possible travel time for a transient simulation with step size Δt is

$$\tau = \frac{\Delta t}{2} \tag{2.11}$$

With this value, conditions at terminal 1 at t - Δt arrive at the shorted end at t - Δt/2 and get reflected back to terminal 1 at t. Therefore, the best possible stub-line representation has

$$Z = \frac{2L}{\Delta t}, \qquad \tau = \frac{\Delta t}{2} \tag{2.12}$$

Assume that the smoothing reactor on a dc line has L = 0.5H, and that the step size is 100 μs. Then Z = 10,000 Ω, and the unavoidable total capacitance C'$\mathcal{L}$ becomes 5 nF, which appears to be negligible, at least if the reactor has a shunt capacitor of 1.2 μF connected to it anyhow, as in the case of the HVDC Pacific Intertie [11]. Now it remains to be shown that the exact solution for the lossless stub-line with parameters from Eq. (2.12) is identical with Eq. (2.5). As explained in Section 1, the expression (v + Zi) along a lossless line for a fictitious observer riding

on the line with wave speed remains constant, or going from 1 to 2 in Fig. 2.9,

$$v_1(t - \Delta t) + Zi_1(t - \Delta t) = Zi_2\left(t - \frac{\Delta t}{2}\right)$$

and travelling back again from 2 to 1,

$$-Zi_2\left(t - \frac{\Delta t}{2}\right) = v_1(t) - Zi_1(t)$$

which, combined, yields

$$i_1(t) = \frac{1}{Z}v_1(t) + \left\{\frac{1}{Z}v_1(t-\Delta t) + i_1(t-\Delta t)\right\} \tag{2.13}$$

which is indeed identical with Eq. (2.5). This identity explains the numerical stability of the solution process: The chosen step size may be too large, and thereby create a fairly inaccurate stub-line with too much parasitic capacitance

$$C'\mathcal{L} = \frac{(\Delta t)^2}{4L} \tag{2.14}$$

from Eq. (2.10), but since the wave equation is still solved accurately[3], the solution will not run away. The "mathematical oscillations" sometimes seen on voltages across inductances, and further explained in Section 2.2.2, are undamped wave oscillations travelling back and forth between terminals 1 and 2 (Fig. 2.9).

The identity of the trapezoidal rule solution with the exact stub-line solution makes it easy to assess the error as a function of frequency [13]. Assume that an inductance L is connected to a voltage source of angular frequency ω, through some resistance R for damping purposes. The transient simulation of this case will eventually lead to the correct steady-state solution of the stub-line (or not drift away from the steady-state answer if the simulation starts from correct steady-state initial conditions). This steady-state solution at any angular frequency ω is known from the exact equivalent π-circuit of Fig. 1.2. By short-circuiting terminal 5, the input impedance becomes

$$Z_{input} = \frac{1}{Y_{series} + \frac{1}{2}Y_{shunt}} \tag{2.15}$$

or with Eq. (1.16),

---

[3]Except for round-off errors caused by the finiteness of the word length in digital computers, which are normally negligible. There is no interpolation error, which occurs in the simulation of real transmission lines whenever τ is not an integer multiple of Δt (see Section 4.2.2.2).

$$Z_{input} = j\omega L \cdot \frac{\tan\left(\omega\dfrac{\Delta t}{2}\right)}{\omega\dfrac{\Delta t}{2}} \qquad (2.16)$$

Therefore, the ratio between the apparent inductance resulting from the stub-line representation or from the trapezoidal rule solution, and the exact inductance becomes

$$\frac{L_{trapezoidal}}{L} = \frac{\tan\left(\omega\dfrac{\Delta t}{2}\right)}{\omega\dfrac{\Delta t}{2}} \qquad (2.17)$$

The phase error is zero over the entire frequency range. Since power systems are basically operated as constant voltage networks, it makes sense in many cases to assume that the voltage $V_L(j\omega)$ across the inductance is more or less fixed, and that the current $I_L(j\omega)$ follows from it. If we compare this current of the stub-line representation or trapezoidal rule solution with the current of the exact solution for the lumped inductance, then we obtain the frequency response of Fig. 2.10, where the ratio (the reciprocal of Eq. (2.17)) is shown as a function of the Nyquist frequency

$$f_{Nyquist} = \frac{1}{2\Delta t} \qquad (2.18)$$
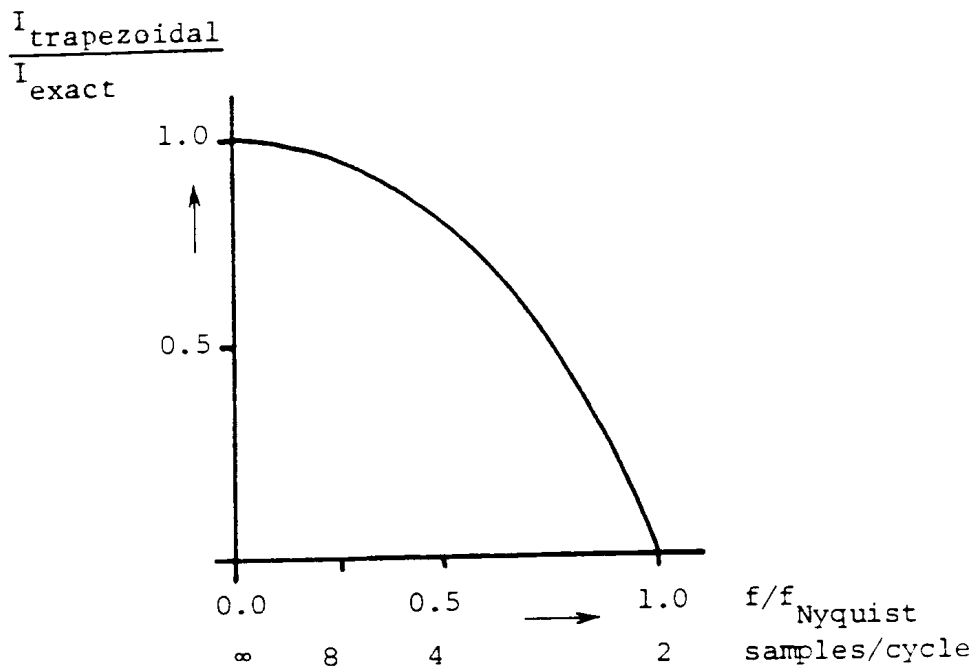
Fig. 2.10 - Amplitude ratio $I_{trapezoidal}/I_{exact}$ through an inductance as a function of frequency

This frequency is the theoretically highest frequency of interest for a step size Δt, amounting to 2 samples/cycle. From a practical standpoint, at least 4 to 8 samples/cycle are needed to reproduce a particular frequency even crudely. From Fig. 2.10 or from Eq. (2.17) it can be seen that the error in the current will be -5.2% at a crude sampling rate of 8 samples/cycle, or -0.8% at a more reasonable sampling rate of 20 samples/cycle. Furthermore, Fig. 2.10 also shows that the trapezoidal rule filters out the higher frequency currents, since the curve goes down as the frequency increases, as pointed out by R.W. Hamming [14].

Because of the error in Eq. (2.17), there is a small discrepancy between the initial conditions found with Eq. (1.11), and the response to power frequency in the time step loop. For 60 Hz, this error would be 0.012% with $\Delta t = 100$ μs, or 1.2% with $\Delta t = 1$ ms. It is debatable whether Eq. (2.17) should be used for the steady-state solution, instead of Eq. (1.11), to match both solutions perfectly. This issue appears with other network elements as well. If a perfect match is desired, then it may be best to have two options for steady-state solutions, one intended for initialization (using Eq. (2.17) in this example), and the other one intended for steady-state answers at one or more frequencies (using Eq. (1.11) in this example).

Very large values of L are acceptable as long as $(\omega L)^2$ or $2L/\Delta t$ is not larger than the largest floating point number which the computer can handle. To obtain flux $= \int v dt$ across a branch, a large inductance can be added in parallel and current output be requested. The need for this may arise if a flux-current plot is required for a nonlinear inductance. With $L = 10^{10}$ H, 10^{10} - times the current would be the flux.

Very small values of ωL or of $2L/\Delta t$ do create accuracy problems the same way as small resistances (see Section 2.1.1).

2.2.2 Damping of "Numerical Oscillations" with Parallel Resistance

While the trapezoidal rule filters out high-frequency currents in inductances connected to voltage sources, it unfortunately also amplifies high-frequency voltages across inductances in situations where currents are forced into them. In the first case, the trapezoidal rule works as an integrator, for which is performs well, whereas in the second case it works as a differentiator for which is performs badly. The problem shows up as "numerical oscillations" in cases where the derivative of the current changes abruptly, e.g., when a current is interrupted in a circuit breaker (Fig. 2.11). The exact solution for v_L is shown as a solid line, with a sudden jump to zero at the
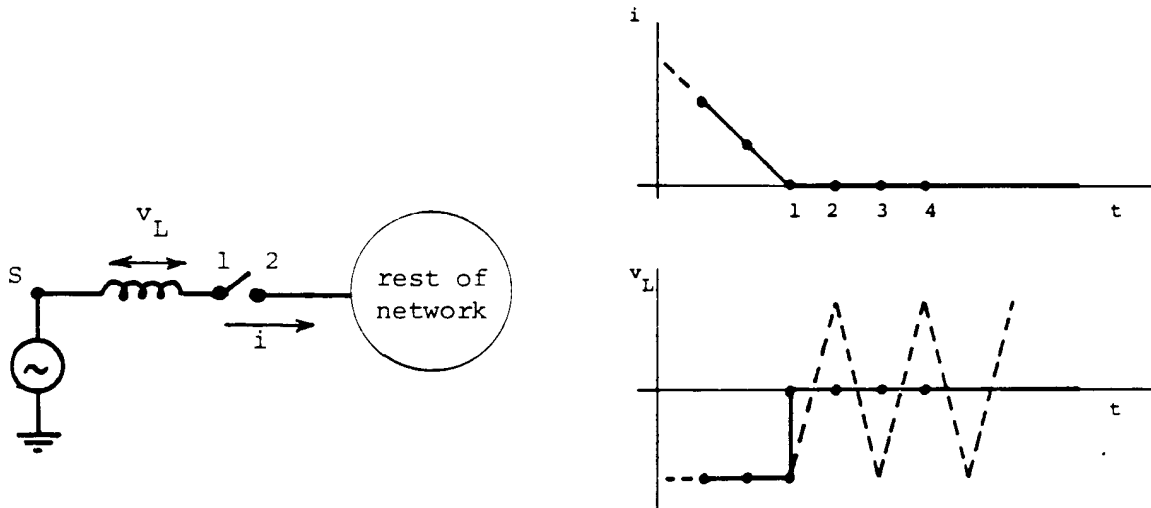
Fig. 2.11 - Voltage after current interruption

instant of current interruption, whereas the EMTP solution is shown as a dotted line. Since

$$v_L(t) = \frac{2L}{\Delta t}\{i(t) - i(t-\Delta t)\} - v_L(t-\Delta t) \qquad (2.19)$$

and assuming that the voltage solution was correct prior to current interruption, it follows that $v_L(t) = -v_L(t - \Delta t)$ in points 2, 3, 4,... as soon as the currents at $t - \Delta t$ and t both become zero; therefore, the solution for v_L will oscillate around zero with the amplitude of the pre-interruption value.

There are cases where the sudden jump would be an unacceptable answer anyhow, and would indicate improper modelling of the real system. An example would be the calculation of transient recovery voltages, since any circuit breaker would reignite if the voltage were to rise with an infinite rate of rise immediately after current interruption. For a transient recovery voltage calculation, the cure would be to include the proper stray capacitance from node 1 to ground (and possibly also from 1 to 2 and from 2 to ground).

On the other hand, there are cases where the user is not interested in the details of the rapid voltage change, and would be happy to accept answers with a sudden jump. A typical example would be sudden voltage changes caused by transformer saturation with two-slope inductance models for the nonlinearity, as indicated in
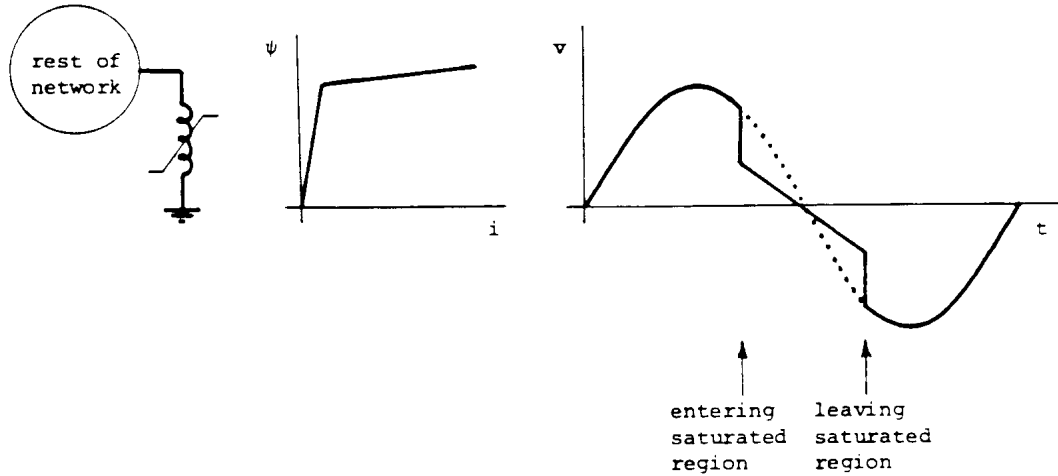
Fig. 2.12 - Voltage jumps caused by transformer saturation

Fig. 2.12. It should be pointed out that these "numerical oscillations" always oscillate around the correct answer (around zero in Fig. 2.11) and plots produced with a smoothing option would produce the correct curves. Nonetheless, it would be nice to get rid of them, especially since they can cause numerical problems in other parts of the network, as has happened occasionally in turbine-generator models [26, p.45].

The "textbook answer" would be re-initialization of variables at the instant of the jump. This would be fairly easy if the equations were written in state-variable form [dx/dt] = [A][x]. With nodal equations as used in the EMTP, re-initialization was thought to be very tricky, until B. Kulicke showed how to do it [15]. His method is summarized in Appendix II. Whether re-initialization should be implemented is debatable, since the damping method described next seems to cure this problem, and also seems to have a physical basis as shown in Section 2.2.3.

V. Brandwajn [16] and F. Alvarado [17] both describe a method for damping these "numerical oscillations" with parallel damping resistances (Fig. 2.13). For a given current injection, the trapezoidal rule solution of the parallel circuit of Fig. 2.13 becomes

$$v(t) \;=\; \frac{1}{\dfrac{\Delta t}{2L}+\dfrac{1}{R_p}}\{i(t)-i(t-\Delta t)\} \;-\; \frac{R_p-\dfrac{2L}{\Delta t}}{R_p+\dfrac{2L}{\Delta t}}\,v(t-\Delta t) \tag{2.20}$$

If a current impulse is injected into this circuit (in a form which the EMTP can handle, e.g., as
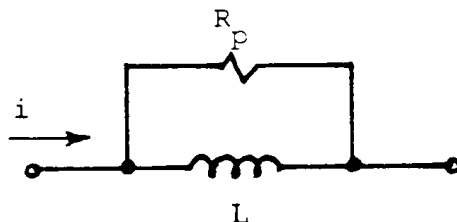

Fig. 2.13 - Parallel damping

2-13

a "hat," with i rising linearly to I_{max} between 0 and Δt, dropping linearly back to zero between Δt and $2\Delta t$, and staying at zero thereafter), then, after the impulse has dropped back to zero, the first term in Eq. (2.20) will disappear, and we are left with the second term which causes the numerical oscillations,

$$v(t) \ = \ -\alpha \cdot v(t-\Delta t)$$

with

$$\alpha \ = \ \frac{R_p \ - \ \dfrac{2L}{\Delta t}}{R_p \ + \ \dfrac{2L}{\Delta t}} \tag{2.21}$$

being the reciprocal of the damping factor. This oscillating term will be damped if $\alpha < 1$; it is shown in Fig. 2.14 for $R_p = 10 \cdot 2L/\Delta t$ or $\alpha = 9/11$, and for $R_p = 2 \ 2L/\Delta t$ or $\alpha = 1/3$. The oscillation would disappear in one time step for $R_p = 2L/\Delta t$ or $\alpha = 0$ (critically damped case)[4]. If R_p is too large, then the damping effect is too small. On the other hand, if R_p is reduced until it approaches the value $2L/\Delta t$ (ideal value for damping), then too much of an error is introduced into the inductance representation. Fig. 2.15 shows the magnitude and phase error of the impedance for $R_p = 4 \ 2L/\Delta t$ and $R_p = 8 \ 2L/\Delta t$, as well as the magnitude error from Eq. (2.17) which already exists for the inductance alone with the trapezoidal rule. It is interesting that the magnitude error with a parallel resistance is actually slightly smaller than the error which already exists for the inductance alone because of the trapezoidal rule. Therefore, the parallel resistance has no detrimental effect on the magnitude frequency response. It does introduce losses, however, as expressed by the phase error. As shown in the next section, these losses are often not far off from those which actually occur in equipment modelled with inductances. From a purely numerical standpoint, a good compromise between reasonable damping
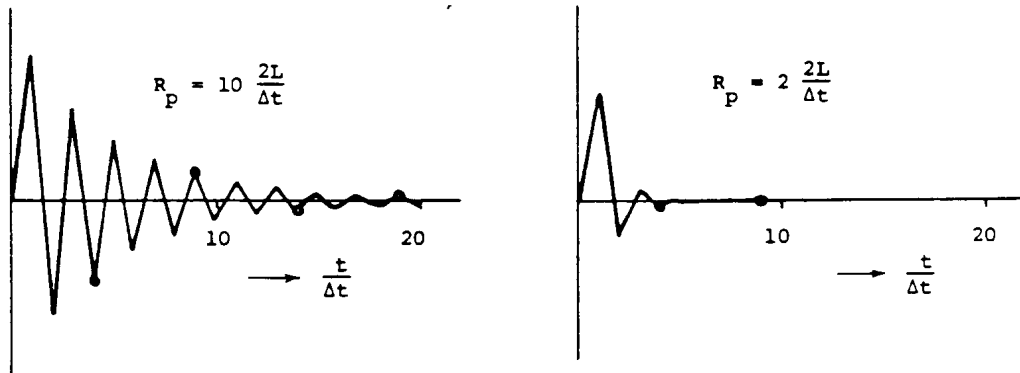
Fig. 2.14 - Oscillating term [17]. Reprinted by permission of F. Alvarado

---

[4]The critically damped trapezoidal rule with $R_p = 2L/\Delta t$ is identical with the backward Euler method, as explained in Appendix I.9.
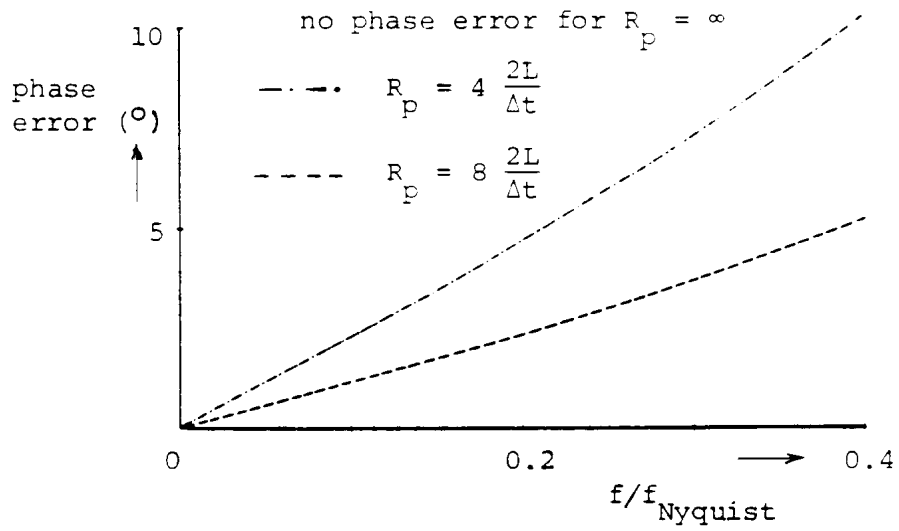
Fig. 2.15 - Phase and magnitude error with parallel resistance [16]

(R_p as low as possible) and acceptable phase error (R_p as high as possible) leads to values of

$$5.4\frac{2L}{\Delta t} \le R_p \le 9.4\frac{2L}{\Delta t} \quad \textit{according to Brandwagn} \text{ [16]} \tag{2.22}$$

or

$$R_p = \frac{20}{3} \cdot \frac{2L}{\Delta t} \quad \textit{according to Alvarado [17]} \tag{2.23}$$
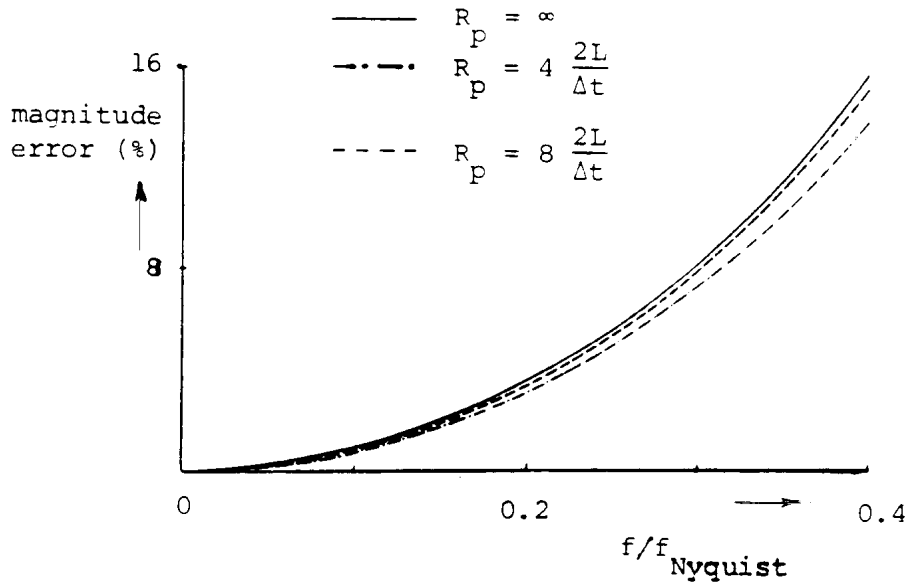
with Brandwajn's lower limit determined by specified acceptable phase error at power frequency.

The errors introduced into the parallel connection of Fig. 2.13 through the trapezoidal rule are seen in Fig. 2.16, in which $R_{series} + jX_{series} = R_p(jX)/(R_p + jX)$ is shown for the exact solution with $X = \omega L$, and for the trapezoidal rule solution with $\omega L_{trapezoidal}$ from Eq. (2.17).
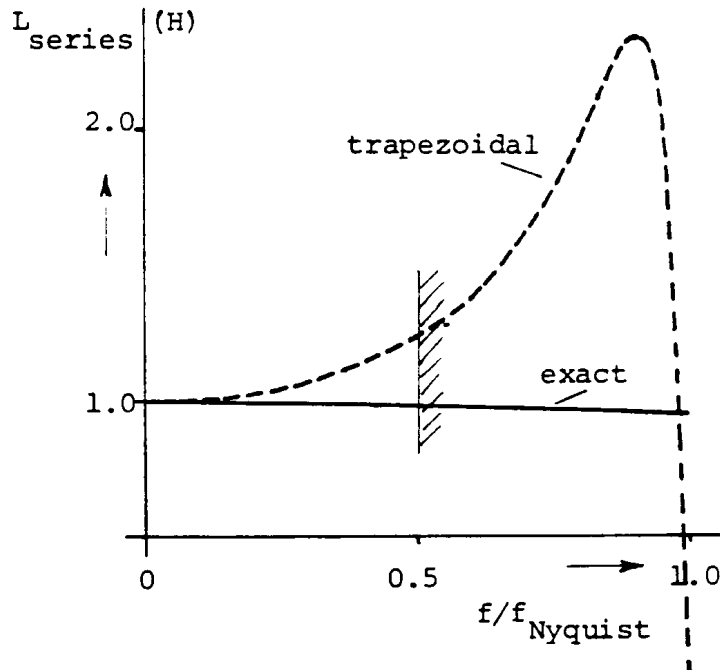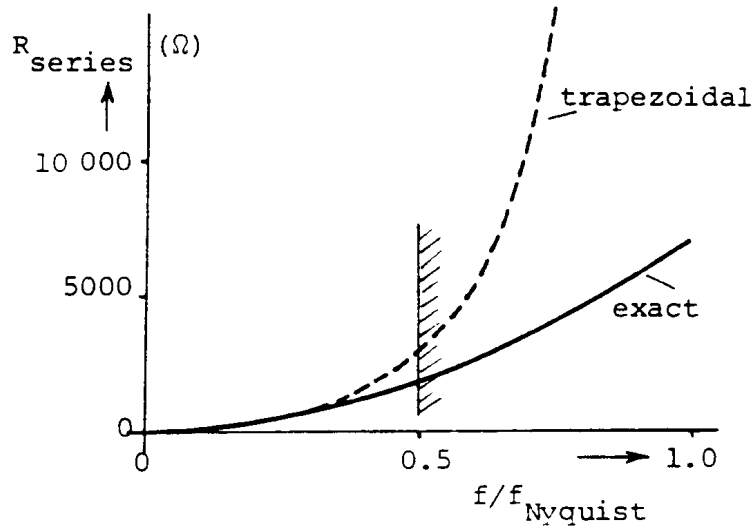
Fig. 2.16 - Apparent series resistance and series inductance for the parallel connection of Fig. 2.13, with $R_p = (20/3) \bullet (2L/\Delta t)$. The region to the right of $f/f_{Nyquist} = 0.5$ is of little practical interest because the sampling rate would be too low to show these frequencies adequately

Whether the EMTP will be changed to include parallel resistances automatically remains to be seen. It is interesting to note that the electronic analysis program SYSCAP of Rockwell International Corp., which seems to use techniques very similar to the EMTP, has R_p and R_s of Fig. 2.18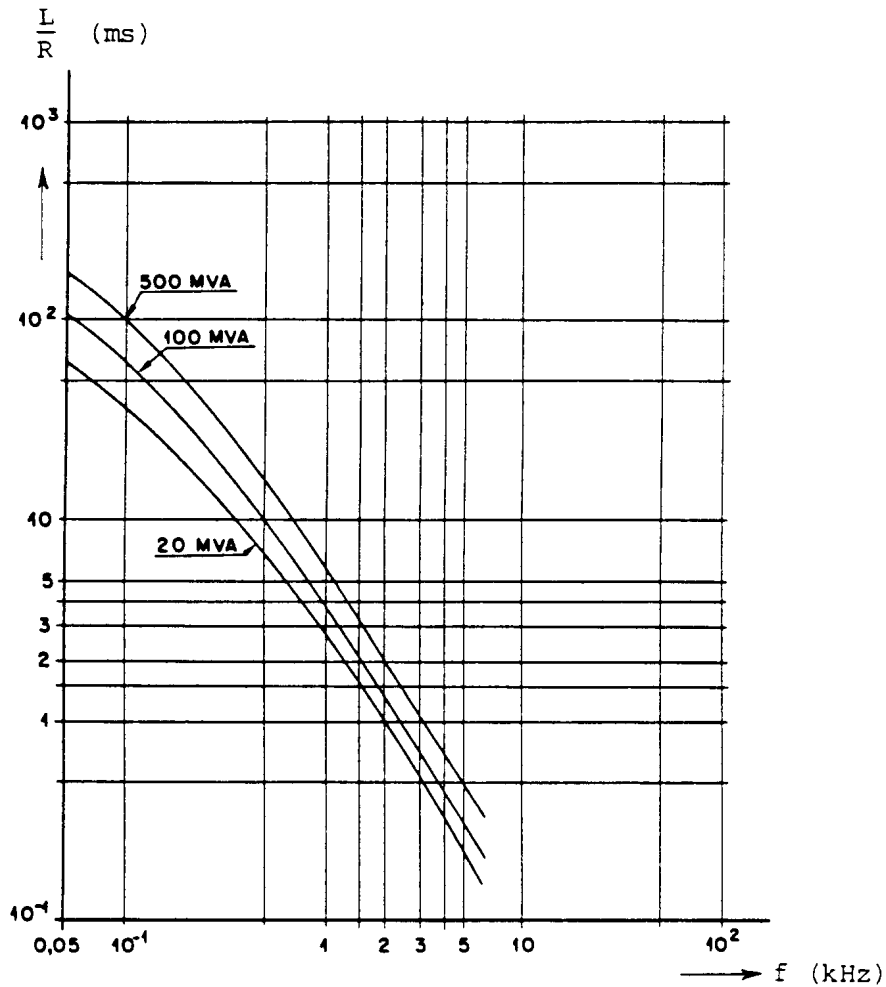 built into the inductor model, with default values of $R_s = 0.1\ \Omega$ and $R_p = 10^{12}\ \Omega$ [22, p. 715]. The possibility of numerical oscillations is mentioned as well, in cases where the time constants of the inductor model of Fig. 2.18 are small compared with Δt [22, p. 773].

Fig. 2.17 - L/R-ratio of the short-circuit impedance of typical transformers [18]. Reprinted by permission of CIGRE

2-17
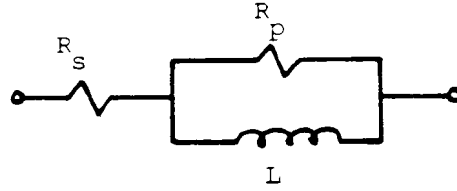
Fig. 2.18 - Equivalent circuit for the short-circuit impedance of a transformer

2.2.3 Physical Reasons for Parallel Resistance

There are many situations in which inductances should have parallel resistances for physical reasons. In some cases, the values of these resistances will be lower than those of Eq. (2.22) or (2.23), which will make the damping of the numerical noise even better. Typical applications of damping resistances are described next. These examples may not cover all applications, but should at least be representative.

(a)   Short-circuit impedance of transformers

The short-circuit impedance of transformers does not have a constant L/R-ratio; instead, the L/R-ratio decreases with an increase in frequency, as shown in Fig. 2.17 taken from [18]. If we use the curve for the 100 MVA transformer, and assume L = 1H (or mH, or p.u.) as well as $\Delta t = 100\ \mu s$, then a value of R_p = 163,000 Ω (or mΩ, or p.u.) will produce the proper L/R-ratio at 1 kHz. This value lies nicely in between the limits of 108,000 Ω and 188,000 Ω recommended in Eq. (2.22). A series resistance of R_s = 9.4 Ω (or mΩ, or. p.u.) can then be added to obtain the correct L/R-ratio at 50 Hz, which leads to the equivalent circuit of Fig. 2.18 for the short-circuit impedance of the transformer. With Z_{input} from Eq. (2.16), the $L_{trapezoidal}$/R-ratio of this equivalent circuit is shown as a dotted line in Fig. 2.19, which is a reasonably good match for the experimental curve (solid line), and much better than a constant L/R-ratio without R_p[5]. It is interesting that a CIGRE Working Group on Interference Problems recommends the same equivalent circuit of Fig. 2.18 for the analysis of harmonics [9], with

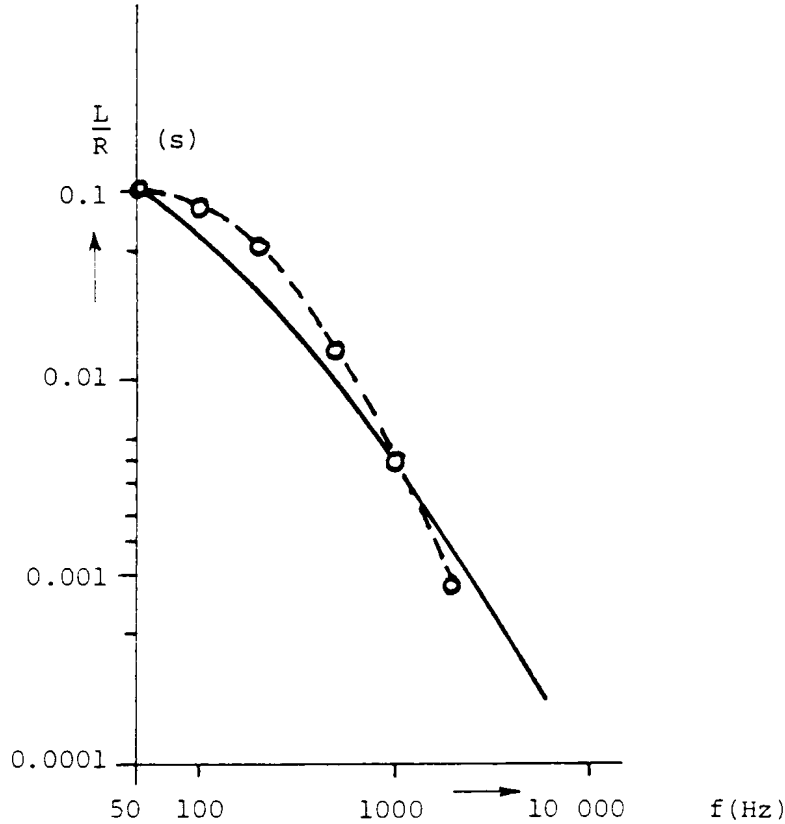$$13 < \frac{S_N R_p}{V_N^{\ 2}} < 30$$
(2.24)

and

$$90 < \frac{V_N^{\ 2}}{S_N R_s} < 110$$
(2.25)

---

[5]In the EMTP, the L/R-ratio without R_p would actually increase with frequency, since $L_{trapezoidal}$ of Eq. (2.17) increases with frequency.

Fig. 2.19 - L/R-ratio of the short-circuit impedance of a 100 MVA transformer (dotted line from equivalent circuit of Fig. 2.18 with L being solved by trapezoidal rule, solid line from [18]). Reprinted by permission of CIGRE

where S_N is the rated power and V_N the rated voltage of the transformer. If we assume $X_{short-circuit} = 0.05$ to 0.10 p.u. at 50 Hz ([9] talks about 50 Hz), then Eq. (2.24) becomes with $\omega L = (0.05$ to $0.10) \cdot V_N^2/S_N$,

$$(40,841 \text{ to } 81,681) \cdot L < R_p < (94,248 \text{ to } 188,496) \cdot L \qquad (2.26)$$

or with a typical step size of $\Delta t = 100 \ \mu s$,

$$(2.04 \text{ to } 4.08) \ 2L/\Delta t < R_p < (4.07 \text{ to } 9.4) \ 2L/\Delta t,$$

with the higher numbers for the lower short-circuit reactance of 0.05 p.u. Again, the value of R_p lies in the same range as Eq. (2.22). Eq. (2.25) implies an L/R-ratio at 50 Hz of 0.014 to 0.018 for a 0.05 p.u. short-circuit reactance, or of 0.028 to 0.035 for a 0.10 p.u. short-circuit reactance, which is lower than the values at 50 Hz in Fig. 2.17.

(b)   Magnetizing impedance of transformers and iron-core reactors

As discussed in more detail in Section 6.6, parallel resistances are added to the magnetizing inductance of transformers for a crude approximation of the hysteresis and eddy current losses. Similarly, the equivalent circuit of Fig. 2.18 is recommended for iron-core reactors [20], with R_s representing I^2R-losses in the winding, and R_p representing iron-core losses.

(c)   Synchronous generators

2-19

A CIGRE Working Group on Interference Problems recommends a resistance in parallel with the negative sequence inductance (which is practically identical to $(L''_d + L''_q)/2$), but feels that is it premature to propose a probable order of magnitude [9]. A typical curve for L''_d/R-ratios of generators, similar to Fig. 2.19 has been published in [18], and could be used to find reasonable values of R_p.

(d)   Nominal π-circuits

Cascade connections of nominal π-circuits are used to represent transmission lines on transient network analyzers. To suppress the spurious oscillations which are caused by the lumpy approximation of distributed parameters, it is customary to add parallel resistances (Fig. 2.20). Typical values appear to be $R_p = 5$ Z_{surge}, which would lead to a value of $R_p = 5 \; 2L/\Delta t$ in the stub-line representation of the inductance in Fig. 2.9. Reasonable values of R_p for cascade connections are discussed in [18].
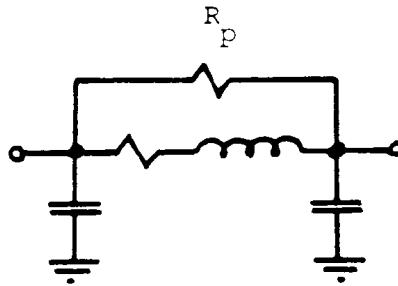
Fig. 2.20 - Damping resistance in nominal π-circuit

(e)   Source impedances

The Thevenin equivalent circuit of Fig. 2.5 is obviously a crude approximation for the rest of the system at frequencies different from the power frequency. To make the frequency-response of this circuit more realistic, damping resistances are often connected in parallel with the R-L branch.

2.2.4 Example for Network with Inductances[6]

A simple yet realistic example of an R-L circuit arises from short-circuit calculations. Assume that a three-phase system has been reduced to a steady-state Thevenin equivalent circuit seen from the fault location, similar to that of Fig. 2.5, with the sequence impedances $Z_{pos} = Z_{neg} = R_{pos} + jX_{pos}$ and $Z_{zero} = R_{zero} + jX_{zero}$ then known. As shown by Eq. (3.4), these sequence parameters can be converted to self and mutual impedances. A single-phase-to-ground fault can then be simulated with a switch closure in the circuit of Fig. 2.21(a), where it is assumed that the self impedance Z_s consists of a resistance R_s in series with an inductance L_s[7]. Fig. 2.21(b) shows the fault current

---

[6]This is one of the few examples with per-unit quantities, simply to show that they can be used. The writer prefers actual values, for reasons explained in Appendix IV.

[7]This assumption is obviously only correct at power frequency, but seems to be reasonable over a wider frequency range in many cases. It would give wrong answers if the system were to consist of a power plant/transmission line/series capacitor connection, since this requires an R-L-C representation, possibly with a capacitor protection circuit similar to Fig. 2.28 (see Section 2.3.4 as well). A detailed fault calculation with the

obtained with the EMTP for $R_s = 0.18$ p.u. and $L_s = 0.712$ p.u. If $R_s << X_s$ at power frequency, which is not quite true here, then there is a minimum offset ("symmetrical fault current") if the fault occurs when the voltage is at its peak value, and a maximum offset ("asymmetrical fault current") if the fault occurs at zero crossing of the voltage. The influence of Δt on the results, as well as the exact solution

$$i(t) = \frac{V_{\max}}{\sqrt{R_s^2 + (\omega L_s)^2}} \{\sin(\omega t + \ominus - \varphi) - \sin(\ominus - \varphi) e^{-tR_s/L_s}\}$$

with

$$\varphi = \tan^{-1}(\omega L_s / R_s)$$

are shown in Fig. 2.21(c). The EMTP results with $\Delta t \leq 500$ μs are indistinguishable from the exact solution.

EMTP, which shows travelling wave effects and compares results with field tests in the Hydro-Quebec System, is described in [19].

(a)

$V_{max}\sin(\omega t + \Theta)$ R_s L_s closes at t=0

(b)

I (p.u.)

2.0

$\Theta = 90°$ $\Theta = 0°$

0

20   40   t (ms)

-2.0

(c)

I (p.u.)

2.0

$\Delta t = 2$ ms

exact and
$\Delta t \leq 500$ μs

0

20   40   t (ms)

-2.0
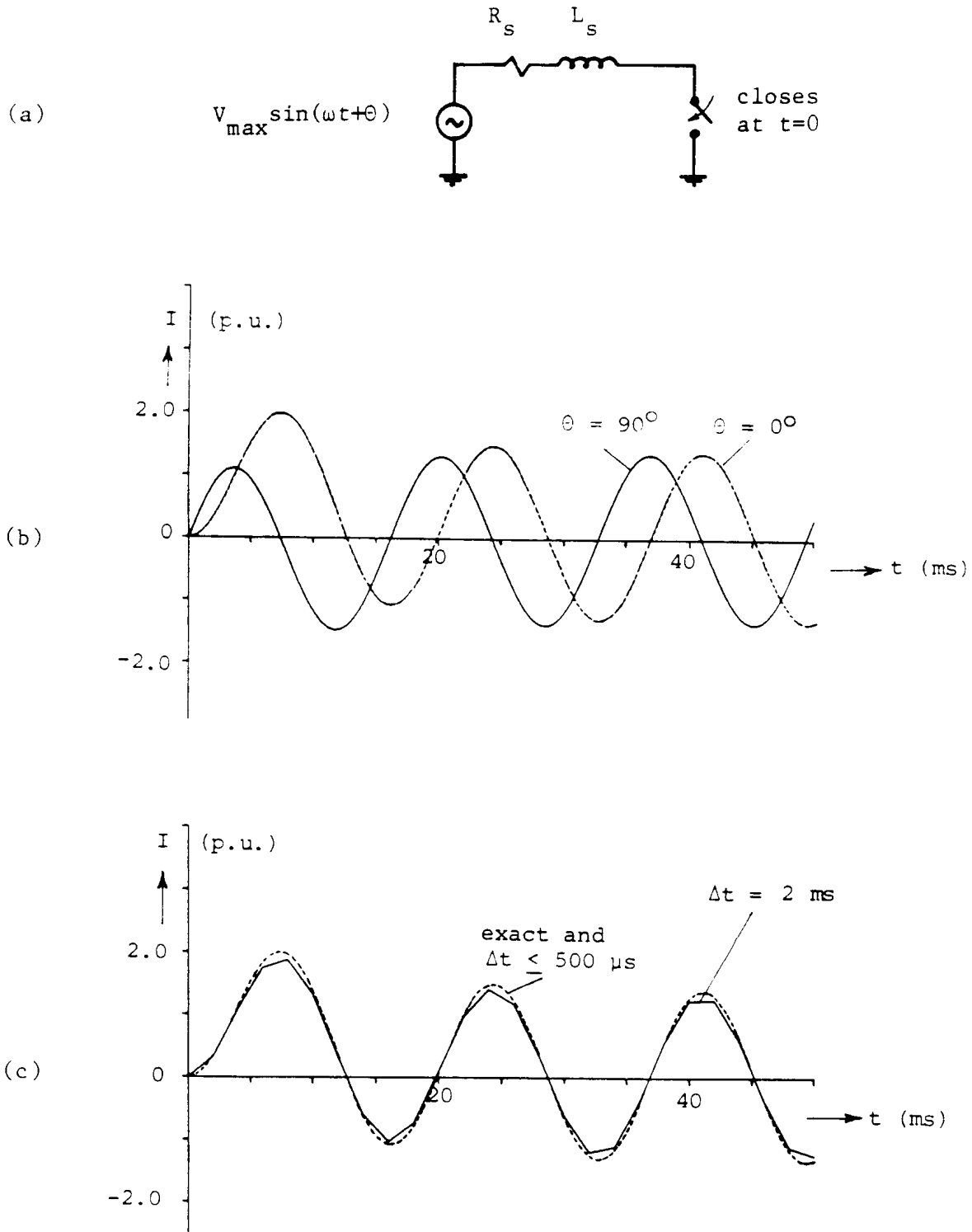
Fig. 2.21 - Single-phase-to-ground fault
(a) Equivalent circuit,
(b) Fault currents for $R_s/X_s = 0.2528$, f = 60 Hz, $\Delta t \leq 500$ μs, for different closing times,
(c) Influence of Δt

2-22

2.3 Capacitance C

Capacitance elements are used to represent, among other things,

(a)   series and shunt capacitors,

(b)   shunt capacitances in nominal π-circuit representations of transmission lines,

(c)   equipment in HVDC converter stations, such as parts of snubber circuits and filters, and surge capacitors,

(d)   stray capacitances of transformers, generators, etc., especially in transient recovery voltage and lightning surge studies, where impedances ωL become so high at higher frequencies that the parallel impedances of stray capacitances 1/ωC become dominant,

(e)   capacitive potential transformers and capacitive voltage dividers,

(f)   parts of surge generators.

The equation of a lumped capacitance C between nodes k and m is solved accurately in the ac steady-state solution with Eq. (1.12). The only precaution to observe is that ωC should not be extremely large, which is unlikely to occur in practice anyhow, for the same reasons as explained for small resistances in Section 2.1.1.

For the transient simulation, the exact differential equation

$$i_{km} = C \frac{d(v_k - v_m)}{dt} \tag{2.27}$$

is replaced by the approximate central difference equation

$$\frac{i_{km}(t) + i_{km}(t-\Delta t)}{2} = C \frac{\{v_k(t) - v_m(t)\} - \{v_k(t-\Delta t) - v_m(t-\Delta t)\}}{\Delta t} \tag{2.28}$$

which gives the desired branch equation

$$i_{km}(t) = \frac{2C}{\Delta t}\{v_k(t) - v_m(t)\} + hist_{km}(t-\Delta t) \tag{2.29}$$

with the "history term" $hist_{km}(t - \Delta t)$ known from the solution at preceding time step,

$$hist_{km}(t-\Delta t) = -i_{km}(t-\Delta t) - \frac{2C}{\Delta t}\{v_k(t-\Delta t) - v_m(t-\Delta t)\} \tag{2.30}$$

Again, analogous to inductance, identical results would be obtained from an integration of Eq. (2.27) with the trapezoidal rule. Eq. (2.29) can be represented as an equivalent resistance $R_{equiv} = \Delta t/2C$, in parallel with a known current source $hist_{km}(t - \Delta t)$, as shown in Fig. 2.22. Once all

$$R_{equiv} = \frac{\Delta t}{2C}$$
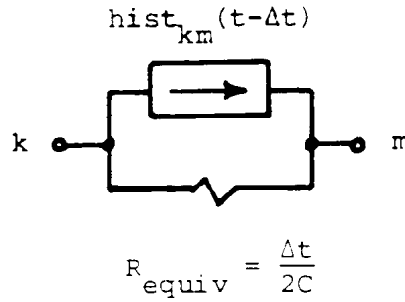
Fig. 2.22 - Equivalent resistive circuit
for transient solution of lumped
capacitance

the node voltages have been found at a particular time step at instant t, the history term of Eq. (2.30) must be updated for each capacitive branch for use in the next time step at t + Δt. To do this, one must first find the current from Eq. (2.29). Alternatively, the recursive updating formula

$$hist_{km}(t) = -\frac{C}{\Delta t}\{v_k(t) - v_m(t)\} - hist_{km}(t - \Delta t)$$ (2.31)

can be used, which is the same as Eq. (2.8) for the inductance if followed by a sign reversal.
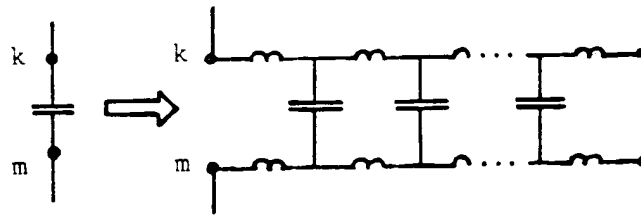
Fig. 2.23 - Lumped capacitance replaced by stub-line with Z
= Δt/2C and τ = Δt/2

2.3.1 Error Analysis

Not surprisingly, the error analysis is analogous to that of the inductance. For a physical interpretation of the errors, the stub-line representation of Fig. 2.23 is used, in which the lumped capacitance is replaced by an open-ended lossless line. To obtain the parameters, it is reasonable to make the total distributed capacitance equal to the lumped capacitance,

$$C'\mathscr{L} = C$$ (2.32)

With C'$\mathscr{L}$ known, the next parameter to be determined is travel time τ. Eq. (2.10) shows that the shorter the travel time, the smaller will be the value of the "parasitic" but unavoidable inductance L'$\mathscr{L}$. For a step size Δt, the shortest possible travel time is

$$\tau = \frac{\Delta t}{2} \qquad (2.33)$$

With Eq. (2.32) and (2.33) the surge impedance becomes $Z = \Delta t/2C$.

Without going through the details, let it simply let it be said that the exact solution for the stub-line of Fig. 2.23 is identical with the trapezoidal rule solution of Eq. (2.29) and (2.30). This identity will again be used to assess the error as a function of frequency. Assume that a capacitance C is connected to a source with angular frequency ω, through some network with damping. The transient simulation will then settle down to the correct steady-state solution of the stub-line of Fig. 2.23, or not drift away from it if the simulation was started from correct steady-state initial conditions. This steady-state solution is known from the exact equivalent π-circuit of Fig. 1.2, with terminal 5 being open-ended,

$$Y_{input} = (Y_{series} + \frac{1}{2}Y_{shunt}) - \frac{Y_{series}^2}{Y_{series} + \frac{1}{2}Y_{shunt}} \qquad (2.34)$$

or after some manipulations with Eq. (1.16),

$$Y_{input} = j\omega C \cdot \frac{\tan\left(\omega\frac{\Delta t}{2}\right)}{\omega\frac{\Delta t}{2}} \qquad (2.35)$$

This is analogous with Eq. (2.16) for the inductance, except that the analogous error now applies to the capacitance C rather than to the inductance L, or

$$\frac{C_{trapezoidal}}{C} = \frac{\tan\left(\omega\frac{\Delta t}{2}\right)}{\omega\frac{\Delta t}{2}} \qquad (2.36)$$

Again, the phase error is zero over the entire frequency range. If we force a current $I_c(j\omega)$ into the capacitance, then the voltage across the stub-line, compared with the exact solution, will have the frequency response of Fig. 2.24, which is identical with Fig. 2.10 if the current ratio is replaced by the voltage ratio. The trapezoidal rule filters out the higher frequency voltages.
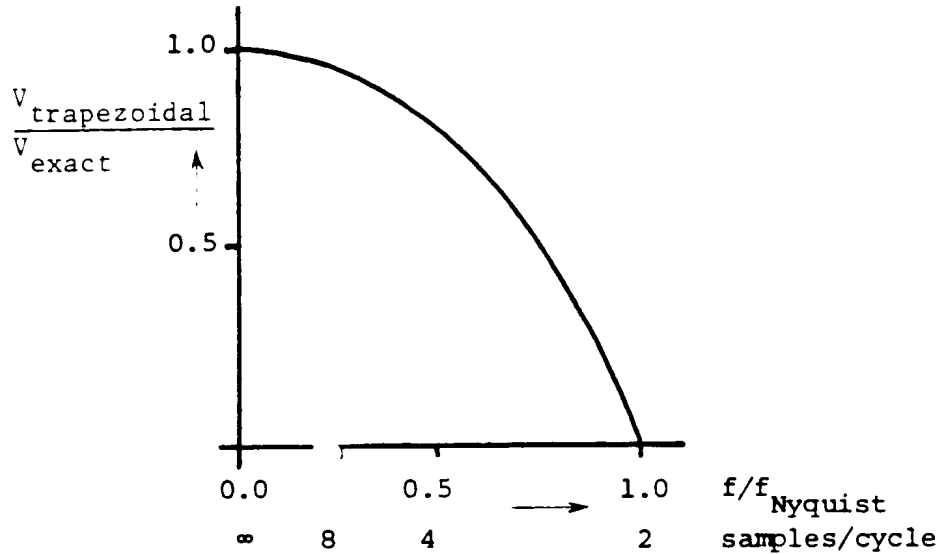
Fig. 2.24 - Amplitude ratio $V_{trapezoidal}/V_{exact}$ of a capacitance as a function of frequency

Again, there is a small discrepancy between the initial conditions found with Eq. (1.12), and the response to power frequency from Eq. (2.35) in the time step loop (at 60 Hz, 0.012% error with $\Delta t = 100$ μs, or 1.2% with $\Delta t = 1$ ms). Whether it should be eliminated has already been discussed in the second-last paragraph of Section 2.2.1.

Very small values of C are acceptable as long as $(1/\omega C)^2$ or $\Delta t/2C$ is not larger than the largest floating point number which the computer can handle. Very large values of C do create accuracy problems the same way as small resistances (see Section 2.1.1), but they are unlikely to occur in practice.

2.3.2 Damping of "Numerical Oscillations" with Series Resistance

While the trapezoidal rule filters out high-frequency voltages across capacitances for given current injections, it also amplifies high-frequency currents for given voltages across C. The numerical oscillations discussed for the inductance in Section 2.2.2 would appear in capacitance currents if there is an abrupt change in dv_c/dt. For some reason, numerical oscillations have seldom been a problem in capacitances, either because there are very few situations where they would appear, or simply because currents through capacitances are seldom included in the output. Analogous to the inductance, these numerical oscillations could be damped with series resistances R_s (Fig. 2.25). Using Alvarado's arguments [17], the trapezoidal rule solution for a voltage impulse applied to the circuit of Fig. 2.25 would be

$$i(t) = \frac{1}{\dfrac{\Delta t}{2C}+R_s}\{v(t)-v(t-\Delta t)\} - \frac{\dfrac{\Delta t}{2C}-R_s}{\dfrac{\Delta t}{2C}+R_s}i(t-\Delta t) \tag{2.37}$$

2-26
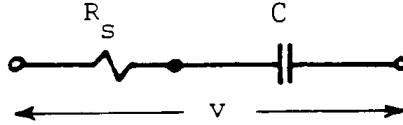
Fig. 2.25 - Series damping resistance

After the voltage impulse v has dropped back to zero, we are left with the second term, which causes the numerical oscillations,

$$i(t) = -\alpha \cdot i(t - \Delta t)$$

$$with \qquad \alpha = \frac{\dfrac{\Delta t}{2C} - R_s}{\dfrac{\Delta t}{2C} + R_s} \tag{2.38}$$

In analogy to Eq. (2.23), a reasonable value for the damping resistance would be

$$R_s = 0.15 \frac{\Delta t}{2C} \tag{2.39}$$

2.3.3 Physical Reasons for Series Resistance

None are known to the writer at this time which would justify a series resistance as high as that of Eq. (2.39). G.W.A. Dummer [23] suggests the equivalent circuit of Fig. 2.26, and says that R_s is dominant at very high frequencies, while R_p is dominant at very low frequencies, but
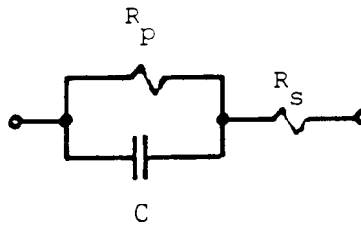
Fig. 2.26 - Equivalent circuit for capacitor with losses

his comments refer to capacitors used in electronics. The typical textbook circuit has no series resistance, which would imply that the loss factor decreases inversely proportional with frequency. This contradicts the curve in Fig. 2.27 given by A. Roth for high-voltage capacitors [24]. Assuming C = 1 μF and Δt = 100 μs and using $C_{trapezoidal}$ instead of C to duplicate the EMTP behavior, a value of R_s = 0.344 Ω (ignoring R_p) would more or less match tanδ at 2 kHz, as shown in Fig. 2.27. Note that this value of R_s is one order of magnitude lower than the recommended damping resistance of Eq. (2.39). SYSCAP, an electronic analysis program with solution techniques similar to the EMTP, has R_p and R_s of Fig. 2.26 built into the capacitor model, with default values of R_s = 0.1 Ω and R_p = 10^{12} Ω [22, p. 715].

2-27
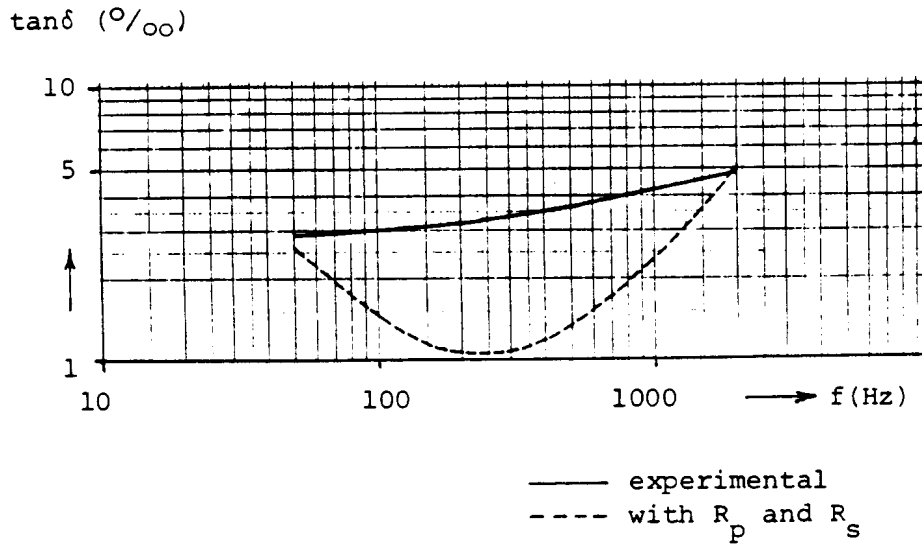
Fig. 2.27 - Loss factor [24]. Reprinted by permission of Springer-Verlag and A.W. Roth

Note that capacitors which may be subjected to short-circuits often have series resistors built in. Similarly, the overvoltage protection of series capacitors with spark gaps (Fig. 2.28) includes current-limiting R-L elements in the discharge circuit, with a typical "ringing" frequency of 400 Hz during discharge.
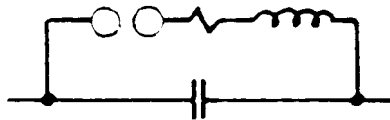
Fig. 2.28 - Spark gap protection of series capacitor

2.3.4 Example for Network with Capacitances

Let us modify the fault current study of Section 2.2.4 for a case in which the transmission line is series-compensated with capacitors (Fig. 2.29). Let us further assume that L_s in Section 2.2.4 represented the net reactance $X_{net} = \omega L - 1/\omega C$ at 60 Hz, to make both results directly comparable. With $R_s = 0.18$ p.u., $X_s = 1.0833$ p.u., $\omega C = 2.695$ p.u. and $\Delta t = 100$ μs, the fault current of Fig. 2.30 is obtained (data taken from [74], with connection from fault location to infinite bus left off). For comparison purposes, the fault current with the net reactance represented by L_s, as done in Section 2.2.4, is shown as well; it differs appreciably from the more accurate solution with the circuit model of Fig. 2.29. This difference has consequences for the accuracy of stability simulations, since net reactances are practically always used in stability studies. Fig. 2.31 compares the swing curves obtained with a net reactance and an L-C representation for a case similar to the IEEE benchmark model for subsynchronous resonance studies [21].
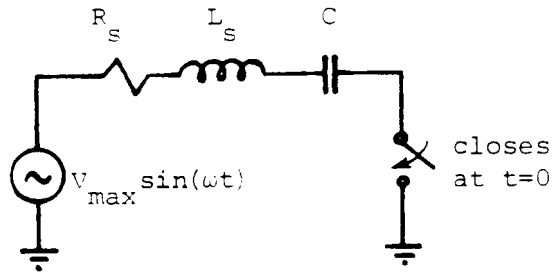
Fig. 2.29 - Single-phase-to-ground fault in a system with a series capacitor
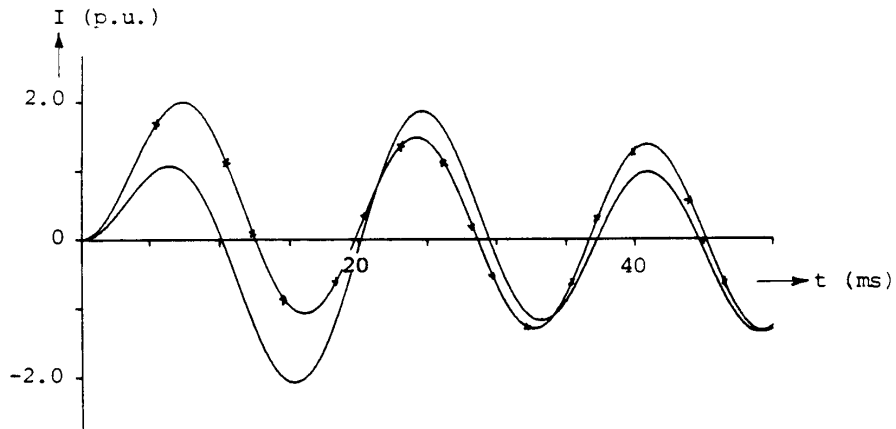
Fig. 2.30 - Fault current in series-compensated network of Fig. 2.29 (line without symbols). For comparison, results from Fig. 2.21 with net reactance are shown as well (line with symbols)
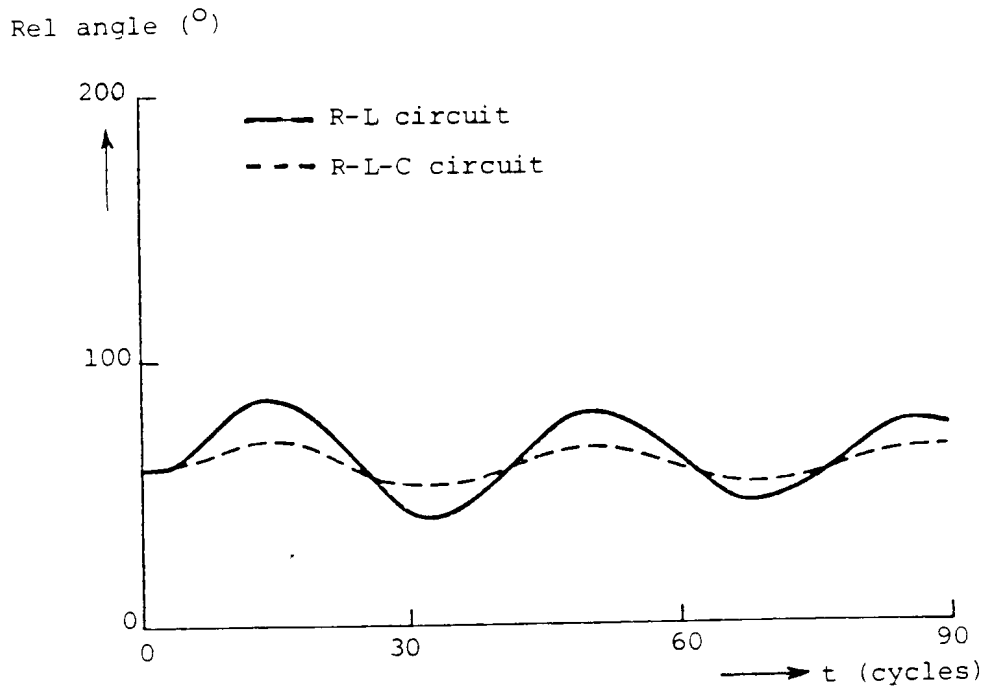
Fig. 2.31 - Swing curves with R-L and R-L-C representations

2-29

2.4 Series Connection of R, L, C

If lumped elements R, L, C frequently occur in pairs as series connections of R-L, R-C, or L-C, or as a series connection of all three elements R-L-C, then it becomes more efficient to treat the series connection as a single branch, thereby reducing the number of nodes and nodal equations. This has been implemented in the EMTP for the series connection of R-L-C (Fig. 2.32). For the steady-state solution, the branch equation is simply

$$I_{km} = \frac{1}{R+j(\omega L-1/\omega C)} (V_k-V_m)$$
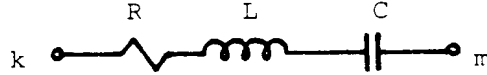
Fig. 2.32 - Series connection of R, L, C

To derive the branch equation for the transient simulation, add the three voltage drops across R, L, and C

$$v_k - v_m = v_R + v_L + v_c$$

with the voltage drops expressed as a function of the current with Eq. (2.1), (2.6) and (2.29),

$$v_k(t) - v_m(t) = \left(R + \frac{2L}{\Delta t} + \frac{\Delta t}{2C}\right) i_{km}(t) - \frac{2L}{\Delta t} hist_L(t-\Delta t) - \frac{\Delta t}{2C} hist_C(t-\Delta t) \tag{2.40}$$

After replacing the history terms $hist_L$ and $hist_C$ with the expressions of Eq. (2.7) and (2.30), this leads to the branch equation

$$i_{km}(t) = G_{series}\{v_k(t) - v_m(t)\} + hist_{series}(t-\Delta t) \tag{2.41a}$$

with

$$G_{series} = \frac{1}{R + \frac{2L}{\Delta t} + \frac{\Delta t}{2C}} \tag{2.41b}$$

and the combined history term

$$hist_{series}(t-\Delta t)=G_{series}\left\{\left(\frac{2L}{\Delta t}-R-\frac{\Delta t}{2C}\right)i(t-\Delta t)+v_k(t-\Delta t)-v_m(t-\Delta t)-2v_C(t-\Delta t)\right\}. \tag{2.42}$$

For updating this history term, the new current is first calculated from Eq. (2.41a), and the new capacitor voltage v_C from

$$v_C(t) = v_C(t-\Delta t) + \frac{\Delta t}{2C}\{i(t) + i(t-\Delta t)\}$$

2-30

Eq. (2.42) is not the only way of expressing the combined history term, but it is the one being used in the EMTP.

2.5 Single-Phase Nominal π-Circuit

This is a special case of the M-phase nominal π-circuit discussed in Section 3.4. Earlier EMTP versions recognize the special case of M = 1, and use scalar equations in place of matrix equations, whereas newer EMTP versions go through the matrix manipulations with M = 1. Since single-phase π-circuits are seldom used, it is reasonable to eliminate the special code for the scalar case.

3. LINEAR, COUPLED LUMPED ELEMENTS

Coupled lumped elements appear primarily in the M-phase π-circuit representation of transmission lines, in the representation of transformers as coupled impedances, and as source impedances in cases where positive and zero sequence parameters are not equal.

3.1 Coupled Resistances [R]

Coupled resistances, in the form of branch resistance matrices [R], appear primarily

(a)   as part of the series impedance matrix in M-phase nominal π-circuits,

(b)   as long line representations in lightning surge studies if no reflections come back from the remote end during the duration t_{max} of the study.

The diagonal elements of [R] are the self resistances, and the off-diagonal elements are the mutual resistances. The off-diagonal terms in the series resistance matrix of an M-phase line are caused by the presence of the earth as a potential current return path. The earth is not modelled as a conductor as such; instead, it is used as a reference point for measuring voltages. If it were explicitly modelled as a conductor, its equation for a three-phase line could have the form

$$-\frac{dV_E}{dx} = Z'_{EA}I_A + Z'_{EB}I_B + Z'_{EC}I_C + Z'_{EE}I_E$$

Since the voltages are measured with respect to earth, $V_E = 0$, and therefore,

$$I_E = -\frac{Z'_{EA}}{Z'_{EE}}I_A - \frac{Z'_{EB}}{Z'_{EE}}I_B - \frac{Z'_{EC}}{Z'_{EE}}I_C$$

which, when inserted into the voltage drop equations for the phases A, B, C, produces

$$-\frac{dV_A}{dx} = \left(Z'_{AA} - \frac{Z'_{AE}Z'_{EA}}{Z'_{EE}}\right)I_A + \left(Z'_{AB} - \frac{Z'_{AE}Z'_{EB}}{Z'_{EE}}\right)I_B + \left(Z'_{AC} - \frac{Z'_{AE}Z'_{EC}}{Z'_{EE}}\right)I_C$$

and similar for B, C. This is the form used in M-phase π-circuits, with earth being an implicit, rather than explicit, current conductor. Assuming purely inductive coupling $Z'_{ik} = jX'_{ik}$, the terms $Z'_{AE}Z'_{EB}/Z'_{EE}$ etc. will obviously contain real parts since the self impedance of the earth Z'_{EE} contains a real part. Whether the real part thus produced can strictly be treated as a resistance for all frequencies is open to debate, as explained in Section 4.1.2.4.

The EMTP automatically converts a long line with distributed parameters into a shunt resistance matrix [R] if

(1) $\tau > t_{max}$ for all M modes[1] of the M-phase line,

---

[1]Modes are explained in Section 4.1.5.

(2)   zero initial conditions.

This representation is simply an M-phase generalization of the single-phase case discussed in Section 2.1. For the high-frequency lossless line model, which is often used in lightning surge studies and described in more detail in Section 4.1.5.2, this shunt resistance matrix has the elements

$$R_{ii} = 60 \ell n \frac{2h_i}{r_i}, \quad R_{ik} = 60 \ell n \frac{D_{ik}}{d_{ik}} \tag{3.1}$$

with h_i = average height above ground, r_i = conductor radius, D_{ik} = distance from conductor i to image of conductor k, d_{ik} = direct distance between conductors i and k. These are the well-known self and mutual surge impedances of an M-phase line [8].

The equations for coupled resistances

$$[i_{km}(t)] = [R]^{-1} \left\{ [v_k(t)] - [v_m(t)] \right\} \tag{3.2}$$

are solved accurately by the EMTP, as long as [R] is non-singular and not extremely ill-conditioned. In all cases known so far, [R] is symmetric, and the EMTP has therefore been written in such a way that it only accepts symmetric matrices [R].

The EMTP does not have an input option for coupled resistances by themselves; instead, they must be specified as part of the M-phase nominal π-circuit of Section 3.4, with L and C left zero. For long lines with $\tau >$ t_{max} and zero initial conditions, the EMTP converts the distributed-parameter model internally to the form of Eq. (3.2). Since [R] is symmetric, the EMTP stores and processes the elements of these and all other coupled-branch matrices as one-dimensional arrays in and above the diagonal (e.g. R_{11} stored in X(1), R_{12} in X(2), R_{22} in X(3), R_{13} in X(4), etc.).

3.1.1 Error Analysis

As already mentioned, [R] must be non-singular if a resistance matrix is read in. If its inverse [R]$^{-1}$ is read in, then this requirement can be dropped, since [R]$^{-1}$ is allowed to be singular without causing any problems. Also, the resistances shouldn't be so small that [R]$^{-1}$ becomes so large that it "swamps out" the effect of other connected elements, as mentioned in Section 2.1.1. On the other hand, very small values of [R]$^{-1}$ are acceptable (see "very large resistances" in Section 2.1.1).

3.1.2 Insertion of Coupled Branches into Nodal Equations

Since coupled branches have not been discussed in the introduction to the solution methods, their inclusion into the system of nodal equations shall briefly be explained. Assume that three branches ka-ma, kb-mb, kc-mc are coupled (Fig. 3.1). In forming the nodal equation for node ka, the current $i_{ka,ma}$ is needed,
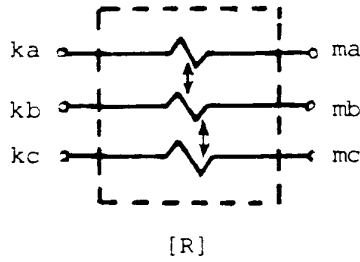
Fig. 3.1 - Three coupled
resistances

$$i_{ka,ma} = G_{aa}^{branch}\left(v_{ka} - v_{ma}\right) + G_{ab}^{branch}\left(v_{kb} - v_{mb}\right) + G_{ac}^{branch}\left(v_{kc} - v_{mc}\right)$$

with G_{ik}^{branch} being elements of the branch conductance matrix $[R]^{-1}$. This means that in the formation of the nodal equation for node ka, G_{aa}^{branch} enters into element $G_{ka,ka}$ of the nodal conductance matrix in Eq. (1.8a), $-G_{aa}^{branch}$ into $G_{ka,ma}$, G_{ab}^{branch} into $G_{ka,kb}$, $-G_{ab}^{branch}$ into $G_{ka,mb}$, etc. If this is done systematically, the matrix $[R]^{-1}$ will be added to two diagonal blocks, and subtracted from two off-diagonal blocks of the nodal conductance matrix $[G]$, as indicated in Fig. 3.2. Unfortunately, rows and columns ka, kb, kc and ma, mb, mc do not follow each other that neatly, and the entries in $[G]$ will therefore be all over the place, but this is simply a programming task. It is worth pointing out that the entry of coupled branches into the nodal conductance matrix can always be explained with an equivalent network of uncoupled elements. For three coupled resistances, the equivalent network with uncoupled elements would contain 15 uncoupled resistances (see Fig. 7 in Chapter II of [26]). Such equivalent networks with
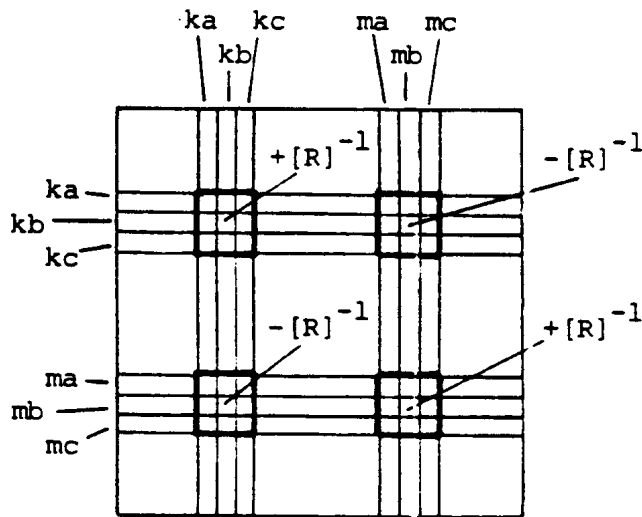
Fig. 3.2 - Contributions of three coupled branches to the
nodal conductance matrix

uncoupled elements are useful for assessing the sparsity of a matrix, but they can be misleading by seemingly indicating galvanic connections where none exist. For example, the steady-state branch equations for two-winding transformers, which are well known from power flow and short-circuit analysis,

$$\begin{bmatrix} I_{ka,ma} \\ I_{kb,mb} \end{bmatrix} = \begin{bmatrix} Y & -tY \\ -tY & t^2Y \end{bmatrix} \begin{bmatrix} V_{ka} & -V_{ma} \\ V_{kb} & -V_{mb} \end{bmatrix} \qquad (3.3)$$

simply imply the connection of Fig. 3.3(a), and nothing more. The equivalent network with uncoupled elements is

shown in Fig. 3.3(b), which produces the well-known transformer model of Fig. 3.3(c) if

nodes ma and mb are grounded.

| (a) | Coupled elements | (b) | Uncoupled elements | (c) | Uncoupled elements with nodes ma and mb grounded |
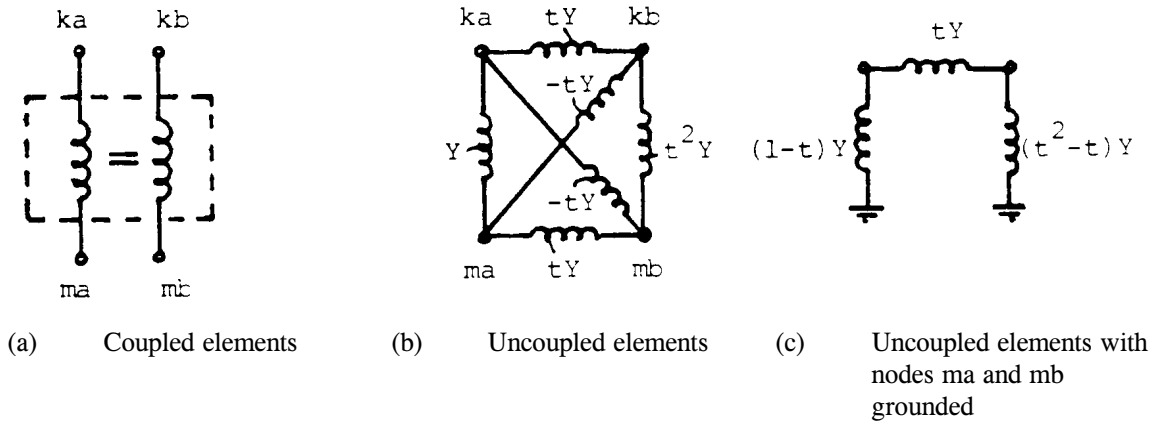
Fig. 3.3 - Two-winding transformer as two coupled branches

3.1.3 Example for Coupled Resistance

Assume that a lightning stroke, represented by a current source i(t), hits phase A of a three-phase line (Fig.

3.4). Let us then find the voltage build-up in all 3 phases over a time span
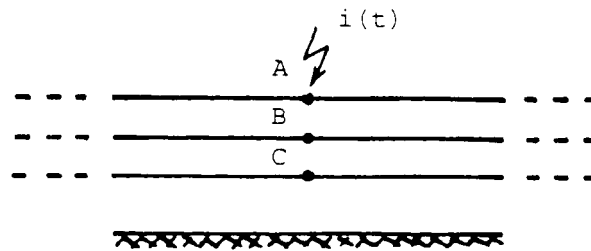
Fig. 3.4 - Lightning stroke to phase A of a three-phase
line

during which reflections have not yet come back from the remote ends of the line, using the high-frequency lossless

line model of Eq. (3.1). Assume a flat tower configuration typical of 220 kV lines, with an average height above

ground = 12.5 m, spacing between conductors = 7.58 m, and conductor radius 14.29 mm. Then from Eq. (3.1),

$$[R] = \begin{bmatrix} 448.02 & 74.24 & 39.41 \\ 74.24 & 448.02 & 74.24 \\ 39.41 & 74.24 & 448.02 \end{bmatrix} \Omega$$

The left as well as the right part of the line is then represented by [R] connected from A, B, C to ground, and the

voltages become

$$v_A(t) = 224.01 \, i(t)$$
$$v_B(t) = 37.12 \, i(t)$$
$$v_C(t) = 19.71 \, i(t)$$

or 16.6% of v_A appears in phase B, and 8.8% in phase C. An interesting variation of this case is the calculation of the effect which this lightning stroke has on the equipment in a substation. Assume that the travel time τ between the stroke location and the substation is such that no reflection comes back from the stroke location during the time t_{max} of the study, with the time count starting when the waves hit the substation (Fig. 3.5). In such cases, the waves coming into the substation can be represented as a three-phase voltage source with amplitudes equal to twice the value of the voltages at the stroke location, behind the resistance matrix [R]. This, in turn, can be converted to a current source in parallel with a shunt resistance matrix [R]. Since

$$[v_{source}] = 2 \cdot \frac{1}{2}[R] \begin{bmatrix} i(t) \\ 0 \\ 0 \end{bmatrix}$$

it follows that the equivalent current source injected into the substation simply becomes equal to the lightning current at the stroke location [i(t), 0, 0] which together with the shunt resistance matrix [R], represents the waves coming into the substation as long as no reflections have come back yet from the stroke location.

3-5
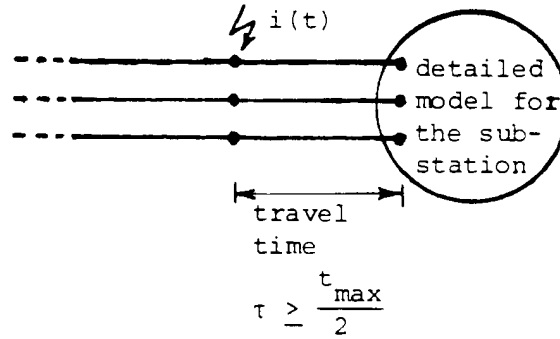
(a) Network configuration
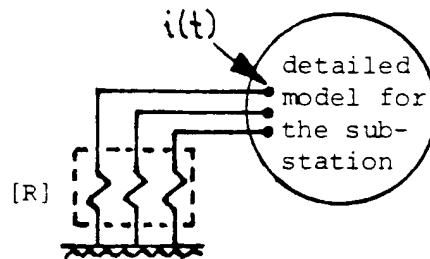
(b) Equivalent network for line and lightning stroke

Fig. 3.5 - Waves coming into substation

3.2 Coupled Inductances [L]

Coupled inductances, in the form of branch inductance matrices, are used to represent magnetically coupled circuits, such as

(a)   inductive part of transformers,

(b)   inductive part of source impedances in three-phase Thevenin equivalent circuits for the "rest of the system" when positive and zero sequence parameters differ,

(c)   inductive part of M-phase nominal π-circuits.

The diagonal elements of [L] are the self inductances, and the off-diagonal elements are the mutual inductances. In all cases known so far, [L] is symmetric, and the EMTP only accepts symmetric matrices, with the storage scheme described in the last paragraph before Section 3.1.1.

The source impedances mentioned earlier under (b) above are often specified as positive and zero sequence parameters Z_{pos}, Z_{zero} which can be converted to self and mutual impedances

$$Z_s = \frac{1}{3}\left(2Z_{pos} + Z_{zero}\right), \qquad Z_m = \frac{1}{3}\left(Z_{zero} - Z_{pos}\right) \tag{3.4}$$

of the coupled impedance matrix

$$[Z] = \begin{bmatrix} Z_s & Z_m & Z_m \\ Z_m & Z_s & Z_m \\ Z_m & Z_m & Z_s \end{bmatrix} \tag{3.5}$$

Of course, these self and mutual impedances can in turn be converted back to sequence parameters,

$$Z_{pos} = Z_s - Z_m , \qquad Z_{zero} = Z_s + 2Z_m \tag{3.6}$$

For a generalization of this data conversion to any number of phases M, see Eq. (4.60) in Section 4.1.3.2.

The equations for coupled inductances between a set of nodes ka, kb,... and a set of nodes ma, mb,... (Fig. 3.6) are solved accurately in the ac steady-state solution with

$$[I_{km}] = \frac{1}{j\omega}[L]^{-1}\{[V_k] - [V_m]\} \tag{3.7}$$

The only precaution to observe is that $[L]^{-1}$ should not be extremely large, for reasons explained in Section 2.1.1.
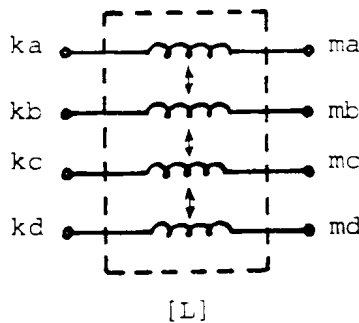
Fig. 3.6 - Four coupled inductances

For the transient simulation, Eq. (2.6) and (2.7) for the scalar case are simply generalized for the matrix case, which produces the desired branch equations

$$[i_{km}(t)] = \frac{\Delta t}{2}[L]^{-1}\{[v_k(t)] - [v_m(t)]\} + [hist_{km}(t-\Delta t)] \tag{3.8}$$

with the history term $[hist_{km}(t - \Delta t)]$ known from the solution at the preceding time step,

$$[hist_{km}(t-\Delta t)] = [i_{km}(t-\Delta t)] + \frac{\Delta t}{2}[L]^{-1}\{[v_k(t-\Delta t)] - [v_m(t-\Delta t)]\} \tag{3.9}$$

Just as in the uncoupled case, Eq. (3.8) can be represented as an equivalent resistance matrix $[R_{equiv}] = (2/\Delta t)[L]$, in parallel with a vector $[hist_{km}(t - \Delta t)]$ of known current sources. The matrix $[R_{equiv}]^{-1}$ enters into the nodal

conductance matrix of the transient solution in the same way as described in Section 3.1.2 (for the steady-state solution, simply replace $[R_{equiv}]^{-1}$ by $(1/j\omega)[L]^{-1}$). While the current source hist_{km} of an uncoupled inductance enters only into two components k and m of the right-hand side in Eq. (1.8b), the vector $[\text{hist}_{km}]$ must now be subtracted from components ka, kb, kc,…, and added to components ma, mb, mc,….

Once all the node voltages have been found at a particular time step at instant t, the history term of Eq. (3.9) must be updated for each group of coupled inductances. This could be done recursively with the matrix equivalent of the scalar equation (2.8). The EMTP does not have an input option for coupled inductances alone; instead, they must be specified as part of the M-phase nominal π-circuit of Section 3.4, where the updating formulas used by the EMTP are discussed in more detail.

There are situations where [L] may not exist, but where $[L]^{-1}$ can be specified as a singular matrix. Such an example is the transformer model of Eq. (3.3). If resistances are ignored, Eq. (3.3) can be used for transient studies with

$$[L]^{-1} = j\omega \begin{bmatrix} Y & -tY \\ -tY & t^2Y \end{bmatrix} \tag{3.10}$$

where Y = 1/(jX), with X being the short-circuit input reactance of the transformer measured from winding ka-ma. It is therefore advisable to have input options for $[L]^{-1}$ as well as for [L], as further discussed in Section 3.4.2.

3.2.1 Error Analysis

The errors are the same as for the uncoupled inductance, that is, the ratio $\tan(\omega\,\Delta t/2)/(\omega\,\Delta t/2)$ of Eq. (2.17) applies to every element in the matrix [L], or its reciprocal to every element in $[L]^{-1}$. The stub-line representation of Fig. 2.9 becomes an M-phase stub-line, if M is the size of the matrix [L]. There is no need to use modal analysis for this stub-line because all travel times are equal, as mentioned in Section 4.1.5.2. In that case, the single-phase line equations can be generalized to M-phase line equations by simply replacing scalars with matrix quantities. Eq. (2.9), (2.12) and (2.14) therefore become

$$\mathcal{L}[L'] = [L], \qquad [Z] = \frac{2}{\Delta t}[L], \qquad and \quad \mathcal{L}[C'] = (\frac{\Delta t}{2})^2 [L]^{-1}$$

3.2.2 Damping of "Numerical Oscillations" with Coupled Parallel Resistances

Again, the explanations of Section 2.2.2 for the uncoupled inductance are easily generalized to the matrix case if all elements of [L] are to have the same ratio R_p/L. Since $[L]^{-1}$ is used in Eq. (3.8), it is preferable to express the parallel resistances in the form of a conductance matrix, e.g., with Alvarado's recipe of Eq. (2.23),

$$[G_p] = 0.15\frac{\Delta t}{2}[L]^{-1} \tag{3.11}$$

If $[L]^{-1}$ is singular, $[G_p]$ would be singular as well, but the singularity would not cause any problems. If the coupled

inductances go from nodes ka, kb,…to nodes ma, mb,… (Fig. 3.6), then $[G_p]$ would be connected in the same way from nodes ka, kb,… to nodes ma, mb,…

3.2.3 Physical Reasons for Coupled Parallel Resistances

The reasons are the same as those listed in Section 2.2.3 in those situations in which the single-phase case can be generalized to the M-phase case.

3.2.4 Example for Network with Coupled Inductances

Let us go back to the example of the single-phase-to-ground fault described in Section 2.2.4, but treat it as a three-phase Thevenin equivalent circuit now, with coupled resistances and inductances (Fig. 3.7). Assume that $Z_{pos} = 0.02 + j0.404$ p.u. and $Z_{zero} = 0.5 + j1.329$ p.u., or with Eq. (3.4) $Z_s = 0.18 + j0.712$ p.u., $Z_m = 0.16 + j0.308$ p.u. There are three voltage sources now,

$$v_{A\text{-}SOURCE} = V_{max}\sin(\omega t)$$

$$v_{B\text{-}SOURCE} = V_{max}\sin(\omega t - 120°)$$

$$v_{C\text{-}SOURCE} = V_{max}\sin(\omega t + 120°)$$
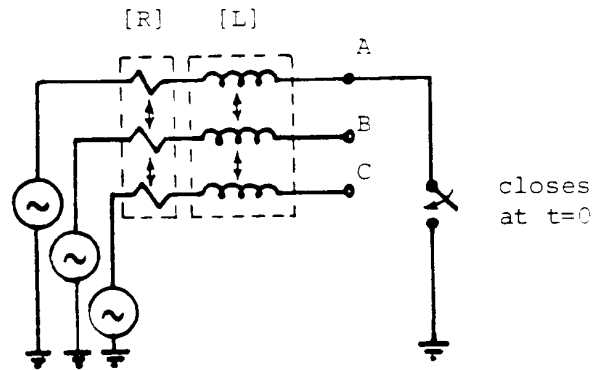
Fig. 3.7 - Single-phase-to-ground fault with three-phase
Thevenin equivalent circuit

With the same values of R_s and L_s as in Section 2.2.4, the fault current will be identical with the curves of Fig. 2.21(b) and (c). In addition, we can now obtain the overvoltages in the unfaulted phases B and C, which are shown in Fig. 3.8.

3-9
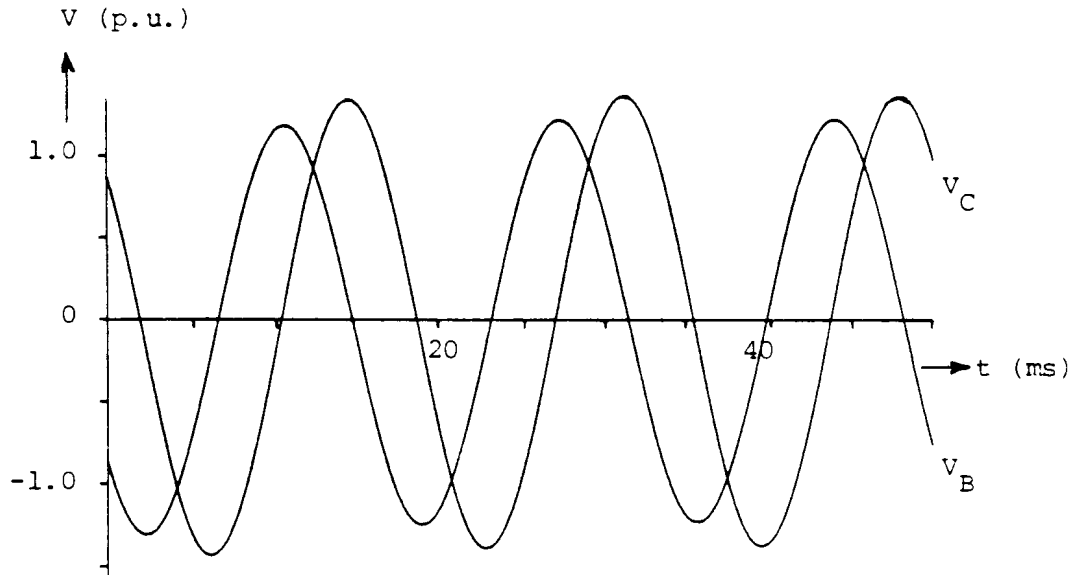
Fig. 3.8 - Overvoltages in unfaulted phases B and C

The steady-state solution can of course be easily obtained from the phasor equations

$$
\begin{bmatrix} V_A \\ V_B \\ V_C \end{bmatrix} = \begin{bmatrix} V_{A\text{-}SOURCE} \\ V_{B\text{-}SOURCE} \\ V_{C\text{-}SOURCE} \end{bmatrix} - \begin{bmatrix} Z_s & Z_m & Z_m \\ Z_m & Z_s & Z_m \\ Z_m & Z_m & Z_s \end{bmatrix} \begin{bmatrix} I_A \\ 0 \\ 0 \end{bmatrix}
\tag{3.12a}
$$

The first row produces, with $V_A = 0$,

$$
I_A = \frac{V_{A\text{-}SOURCE}}{Z_s}
\tag{3.12b}
$$

and the second the third rows produce the voltage changes in the unfaulted phases

$$
\Delta V_B = \Delta V_C = -\frac{Z_m}{Z_s} V_{A\text{-}SOURCE}
\tag{3.12c}
$$

If these voltage changes are shown in a phasor diagram (Fig. 3.9), then it becomes obvious why the overvoltages in phases B and C are unequal, unless the ratio Z_m/Z_s is a real (rather than complex) number. In the latter case the dotted changes become vertical in B and C in Fig. 3.9, and the overvoltages become equal.

3-10
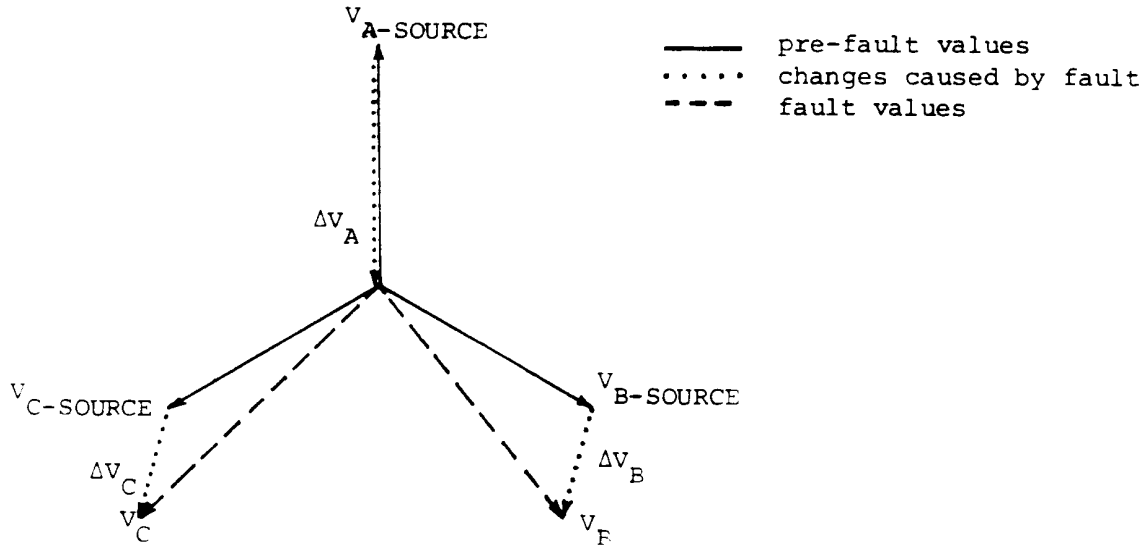
Fig. 3.9 - Phasor diagram of voltage changes caused by single-phase-to-ground fault

3.3 Coupled Capacitances [C]

Coupled capacitances, in the form of branch capacitance matrices, appear as the shunt elements of M-phase nominal π-circuits (Fig. 3.10). One could argue that the capacitances are not really coupled, since they appear as 6 uncoupled capacitances in Fig. 3.10. However, the same argument can be made for coupled resistances and inductances, as explained in Fig. 3.3 of Section 3.1.2, and the fact remains that the shunt capacitances of M-phase lines appear as matrix quantities in the derivation of the equations.
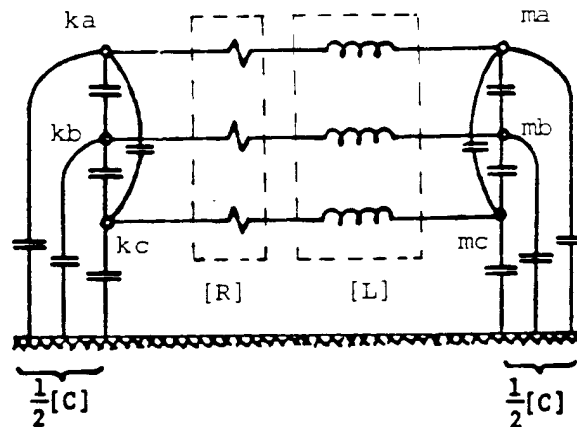
Fig. 3.10 - Three-phase nominal π-circuit

Since the only known application of coupled capacitances is as shunt elements of M-phase nominal π-circuits, the EMTP accepts them only in that form, that is, as equal branch capacitance matrices 1/2 [C] at each end of the π-circuit, from nodes ka, kb,... to ground, and from nodes ma, mb,... to ground. In all cases, [C] is symmetric, and this symmetry is exploited with the storage scheme described in the last paragraph before Section

3.1.1. The diagonal element C_{kaka} of [C] is the sum of all capacitances between phase a and the other phases b, c,... as well as between phase a and ground, whereas the off-diagonal element C_{kakb} is the <u>negative</u> value[2] of the capacitance between phases a and b.

Sometimes, shunt capacitances of three-phase lines are specified as positive and zero sequence parameters C_{pos}, C_{zero}, which can be converted to the diagonal and off-diagonal elements

$$C_s = \frac{1}{3}(2C_{pos} + C_{zero}) , \quad C_m = \frac{1}{3}(C_{zero} - C_{pos}) \tag{3.13}$$

of the coupled capacitance matrix

$$[C] = \begin{bmatrix} C_s & C_m & C_m \\ C_m & C_s & C_m \\ C_m & C_m & C_s \end{bmatrix} \tag{3.14}$$

C_m must be negative because the off-diagonal element is the negative value of the coupling capacitance between two phases, therefore, $C_{zero} < C_{pos}$. For a generalization of this data conversion to any number of phases M, see Eq. (4.61) in Section 4.1.3.2.

The steady-state equations for coupled capacitances in the shunt connection of Fig. 3.10, and <u>with the factor 1/2</u>, are

$$[I_{k0}] = \frac{1}{2}j\omega[C][V_k], \quad [I_{m0}] = \frac{1}{2}j\omega[C][V_m] \tag{3.15}$$

with subscripts "k0" and "m0" indicating that the currents flow from nodes ka, kb,... to ground ("0"), and from nodes ma, mb,... to ground. Eq. (3.15) is solved accurately in the steady-state solution. The only precaution to observe is that $\omega[C]$ should not be extremely large, for reasons explained in Section 2.1.1, but this is very unlikely to occur in practice anyhow.

For the transient simulation, Eq. (2.29) and (2.30) are again generalized for the matrix case, which produces the desired branch equations (taking care of the factor 1/2!),

$$[i_{k0}(t)] = \frac{1}{\Delta t}[C][v_k(t)] + [hist_{k0}(t-\Delta t)] \tag{3.16}$$

with the history term $[hist_{k0}(t - \Delta t)]$ known from the solution at the preceding time step,

---

[2]It might be worthwhile to have the EMTP check for the negative sign, and automatically make it negative, with an appropriate warning message, in cases where the negative sign was forgotten. The writer is not aware of any situation in which the off-diagonal element would not be negative.

$$[hist_{k0}(t-\Delta t)] = -\frac{1}{\Delta t}[C][v_k(t-\Delta t)] - [i_{k0}(t-\Delta t)] \qquad (3.17)$$

The equations for the shunt capacitance 1/2 [C] at the other end (nodes ma, mb,…) are the same if subscript k is replaced by m. As in the uncoupled case, Eq. (3.16) can be represented as an equivalent resistance matrix $\Delta t[C]^{-1}$, in parallel with a vector $[hist_{km}(t - \Delta t)]$ of known current sources. The matrix $1/\Delta t$ [C] enters into the nodal conductance matrix of the transient solution only in the diagonal block of rows and columns ka, kb,… and in the diagonal block of rows and columns ma, mb,… (Fig. 3.2), because of the shunt connection, while the vector $[hist_{k0}]$ must be subtracted from components ka, kb,… (analogous for $[hist_{m0}]$).

Once all the node voltages have been found at a particular time step at instant t, the history term of Eq. (3.17) is updated recursively,

$$[hist_{k0}(t)] = -\frac{2}{\Delta t}[C][v_k(t)] - [hist_{k0}(t-\Delta t)] \qquad (3.18)$$

and analogous for $[hist_{m0}]$. Recursive updating is efficient here, in contrast to coupled inductances, because the branches consist only of capacitances here, unless currents are to be computed as well. In the latter case, $[i_{k0}(t)]$ is first found from Eq. (3.16), and then inserted into Eq. (3.17) to obtain the updated history term, with both formulas using the same matrix $1/\Delta t$ [C].

3.3.1 Error Analysis

The errors are the same as for the uncoupled capacitance, that is, the ratio tan(ω Δt/2) / (ω Δt/2) of Eq. (2.35) applies to every element in the matrix 1/2 [C]. The stub-line representation of Fig. 2.23 becomes an M-phase stub-line, with the second set of nodes being ground in this case. There is no need to use modal analysis, as explained in Section 3.2.1.

3.3.2 Damping of "Numerical Oscillations" with Series Resistances

Again, the explanations of Section 2.3.2 for the uncoupled capacitance are easily generalized to the matrix case if all elements of 1/2 [C] are to have the same time constant R_sC. Eq. (2.39) would then become

$$[R_s] = 0.15 \ \Delta t[C]^{-1} \qquad (3.19)$$

(factor 1/2 of Eq. (2.39) disappeared because the equations have been written for 1/2 [C] here). As mentioned in Section 2.3.2, numerical oscillations in capacitive currents have seldom been a problem.

3.3.3 Physical Reasons for Coupled Series Resistances

None are known to the writer at this time. The discussions of Section 2.3.3 do not apply to shunt capacitances of overhead lines, but they may be relevant to the capacitances of underground or submarine cables.

3.3.4 Example for Network with Coupled Capacitances

Assume that a power plant with a number of generator-transformer units in parallel is connected into the 230 kV switchyard through a number of parallel underground cables. The circuit breakers at the end of the cables are open, when a single-phase-to-ground fault occurs on the power plant side of the breakers (Fig. 3.11).
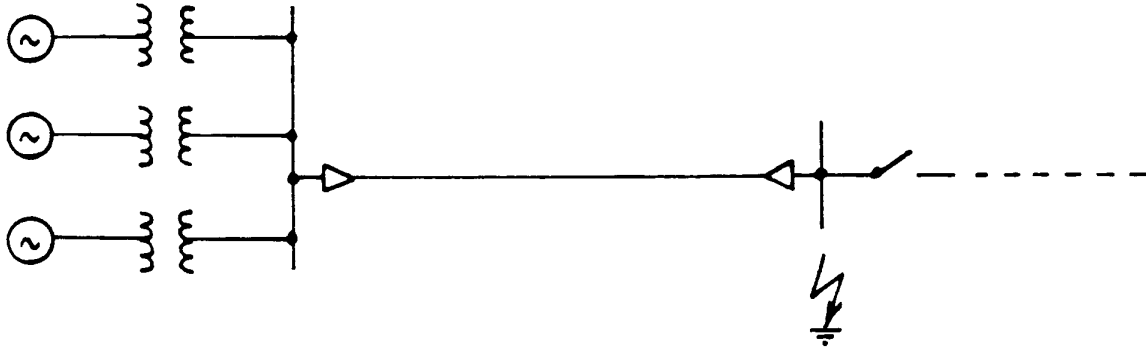
Fig. 3.11 - Cable circuit with single-phase-to-ground fault. Fault occurs in phase A when source voltage in A is at its peak. Generator-transformers represented as three-phase voltage sources of 230 kV (RMS, line-to-line) behind coupled reactances with $X_{pos} = 8\ \Omega$, $X_{zero} = 2.8\ \Omega$ (referred to 230 kV side). Cables represented as three-phase nominal π-circuit with $Z_{pos} = Z_{zero} = 0.015834\ \Omega$, $\omega C_{pos} = \omega C_{zero} = 897.6\ \mu S$, $R_{FAULT} = 1\ \Omega$

The data resembles the situation at Ground Coulee before the Third Powerhouse was built, except that $Z_{zero} = Z_{pos}$ for the cables is an unrealistic assumption. Also note that the shunt capacitances of the nominal π-circuit are actually uncoupled in this case because $C_m = 0$, which is always true in high voltage cables where each phase is electrostatically shielded. Nonetheless, this cable circuit was chosen because it illustrates the effects of shunt capacitances better than a case with overhead lines where $C_m \neq 0$.

Fig. 3.12(a) shows the voltages in the two unfaulted phases at the fault location, with oscillations superimposed on the 60 Hz so typical of cable circuits. Fig. 3.12(b) shows the fault current; the high-frequency oscillations at the beginning are caused by discharging the shunt capacitance through the fault resistance of 1 Ω. With zero fault resistance, this discharge would theoretically consist of an infinite current spike at t = 0, which leads to the undamped numerical oscillations across the correct 60 Hz - values discussed in Section 2.3.2 (Fig. 3.12(c)). These numerical oscillations would not appear if the cables were modelled as lines with distributed parameters; instead, physically based travelling wave oscillations would appear which would still look similar to those of Fig. 3.12(b).
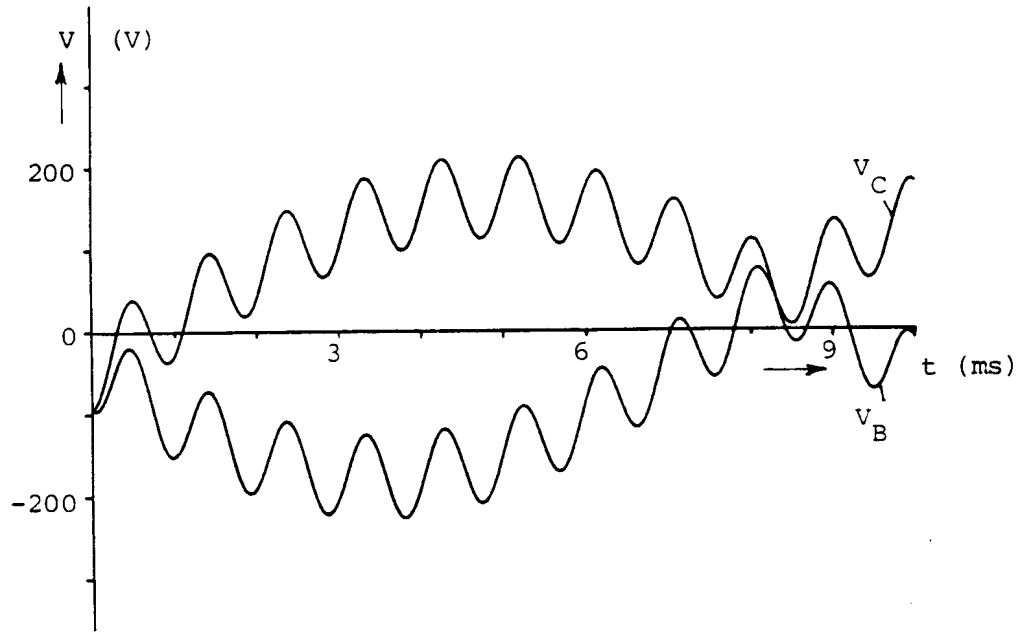
(a)   Overvoltages
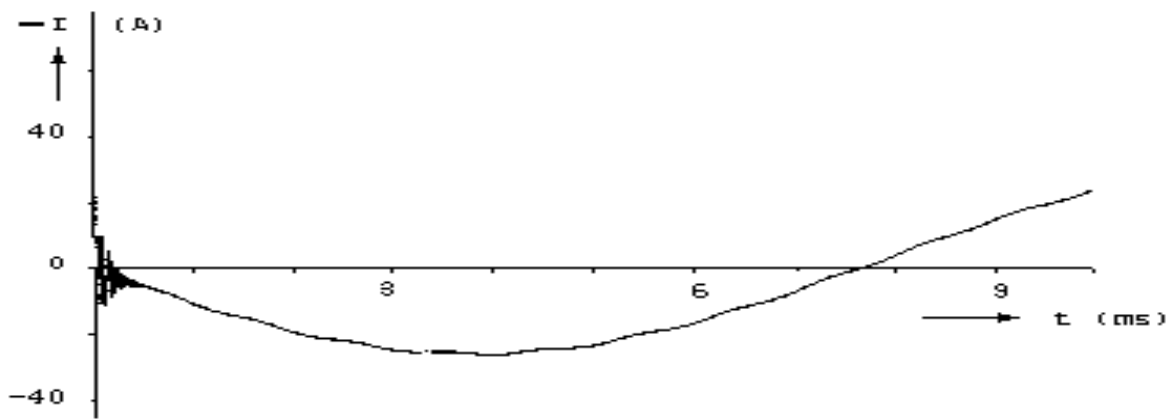
(b)   Fault current for $R_{FAULT} = 1\ \Omega$ (negative value shown)
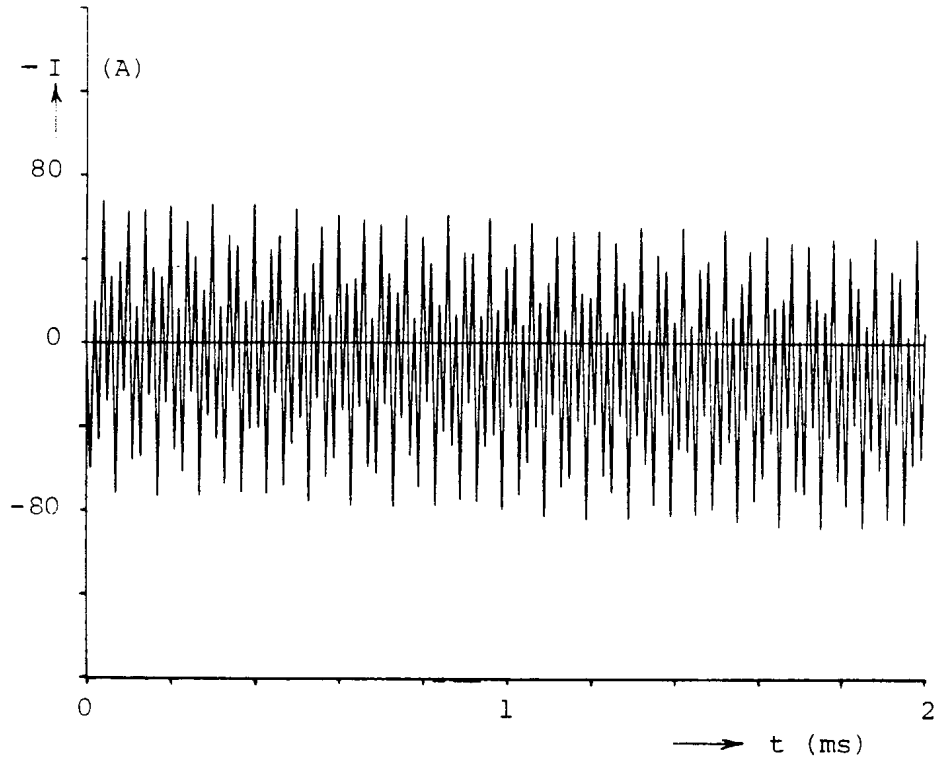
(c)   Fault current for $R_{FAULT} = 0$ (different scale than in (b), but value again
        negative)

Fig. 3.12
- Overvoltages and fault current for a single-phase-to-ground fault in the cable circuit of Fig. 3.11 ($\Delta t = 10\mu s$; small step size chosen to allow comparisons with distributed parameter model of cable with $Z_{surge} = 4.2\Omega$, $\tau = 10\mu s$)

3.4 M-Phase Nominal π-Circuit

Series connections of coupled resistances and coupled inductances first appeared as part of M-phase nominal π-circuits (Fig. 3.10) when the EMTP was developed. It was therefore decided to handle such series connections as part of an M-phase nominal π-circuit input option. By allowing the shunt capacitance 1/2 [C] to be zero, this π-circuit input option can then be used for series connections of [R] and [L] as well.

The equations for the shunt capacitance matrices 1/2 [C] at both ends are solved as discussed in Section 3.3. [C] = 0 is not recognized by the EMTP as a special case; instead, the calculations are done as if [C[were nonzero.

What remains to be shown is the series connection of [R] and [L] as one single set of M coupled branches. The derivation of the coupled branch equations is similar to that of the scalar case discussed in Section 2.4, if scalar quantities are replaced by matrices. When the series [R] - [L] connection was first implemented in the EMTP, it was not recognized that [L] may not always exist. With the appearance of singular [L]$^{-1}$ matrices, e.g., in the transformer model of Eq. (3.3), an alternative formulation was developed. Both formulations have been implemented, as discussed in the next two sections.

3-16

3.4.1 Series Connection of [R] and [L]

For the steady-state solution, the branch equations are

$$I_{km} = \{[R] + j\omega[L]\}^{-1}\{[V_k] - [V_m]\} \tag{3.20}$$

They are solved accurately. For the transient simulation, the branch equations are derived by adding the voltage drops across [R] and [L]. From Eq. (3.2) and (3.8),

$$[i_{km}(t)] = [G_{series}]\{[v_k(t)] - [v_m(t)]\} + [hist_{series}(t-\Delta t)] \tag{3.21a}$$

with

$$[R_{series}] = [R] + \frac{2}{\Delta t}[L] \ , \quad and \quad [G_{series}] = [R_{series}]^{-1} \tag{3.21b}$$

and the history term

$$[hist_{series}(t-\Delta t)] = [G_{series}]\{[v_k(t-\Delta t)] - [v_m(t-\Delta t)] +$$

$$\left(\frac{2}{\Delta t}[L] - [R]\right)[i_{km}(t-\Delta t)]\} \tag{3.22}$$

Direct updating of the history term with Eq. (3.22) involves three matrix multiplications because $[i_{km}]$ must first be found from Eq. (3.21a). Unless currents must be computed anyhow, as part of the output quantities, updating with the following recursive formula is more efficient,

$$[hist_{series}(t) = [H]\{[v_k(t)] - [v_m(t)] + [R_{series}][hist_{series}(t-\Delta t)]\} -$$

$$[hist_{series}(t-\Delta t)] \tag{3.23a}$$

since it involves only two matrix multiplications. Matrix [H] is

$$[H] = 2\{[G_{series}] - [G_{series}][R][G_{series}]\} \tag{3.23b}$$

All matrices $[R_{series}]$, $[G_{series}]$ and [H] are still symmetric, which is exploited by the EMTP with the storage scheme discussed in the last paragraph before Section 3.1.1. Symmetry is not automatically assured. For instance, the alternative updating formula

$$[hist_{series}(t)] = [F][i_{km}(t)] - [hist_{series}(t-\Delta t)]$$

which, in combination with Eq. (3.21a), would be preferable in situations where current output is requested, has an unsymmetric matrix [F],

$$[F] = [H][R_{series}]$$

All equations in this section can handle the special case of either [R] = 0 or [L] = 0 as long as [R$_{series}$] of Eq. (3.21b) can be inverted.

3.4.2 Series Connections of [R] and [L]$^{-1}$

Singular matrices [L]$^{-1}$ appear in transformer representations if exciting currents are ignored. By itself, [L]$^{-1}$ is easily handled with Eq. (3.8) and (3.9). In series connections with [R], however, the equations of the preceding section cannot be used directly because [L] does not exist.

For the steady-state solution, the matrix [R] + jω [L] is rewritten as

$$[R] + j\omega[L] = [j\omega L]\{[j\omega L]^{-1}[R] + [U]\}$$

with [U] being the identity matrix, which upon inversion, produces the inverse required in Eq. (3.20),

$$\{[R] + j\omega[L]\}^{-1} = \{[U] + [j\omega L]^{-1}[R]\}^{-1}[j\omega L]^{-1} \tag{3.24}$$

Eq. (3.24) produces a symmetric matrix, even though the matrix [U] + [jωL]$^{-1}$[R] needed as an intermediate step is unsymmetric. The symmetry of the result from Eq. (3.24) can be shown by rewriting the matrix [R] + jω[L] as

$$[R] + j\omega[L] = [j\omega L]\{[j\omega L]^{-1}[R][j\omega L]^{-1} + [j\omega L]^{-1}\}[j\omega L]$$

from which the inverse is obtained as

$$\{[R]+j\omega[L]\}^{-1} = [j\omega L]^{-1}\{[j\omega L]^{-1}[R][j\omega L]^{-1} + [j\omega L]^{-1}\}^{-1}[j\omega L]^{-1} \tag{3.25}$$

Each of the three factors of the product is a symmetric matrix, which is obvious for the two outer factors and which can easily be proved for the inner factor by showing that its transpose is equal to the original. With all three factors being symmetric, the triple product [A][B][A] is symmetric, too. The EMTP uses Eq. (3.24) rather than (3.25), because the latter would fail if [R] = 0 and [L]$^{-1}$ singular. The EMTP does not use complex matrix inversion, followed by matrix multiplication with an imaginary matrix, however. Instead, Eq. (3.24) is reformulated as the solution of a system of N linear equations with N right-hand sides,

$$\{j[U] + [\omega L]^{-1}[R]\}[Y] = [\omega L]^{-1} \tag{3.26}$$

where the inverse [Y] is now directly obtained as the N solution vectors. To avoid complex matrix coefficients, Eq. (3.26) is further rewritten as 2N real equations,

$$[\omega L]^{-1}[R][Y_r] - [Y_i] = [\omega L]^{-1} \tag{3.27}$$

$$[Y_r] + [\omega L]^{-1}[R][Y_i] = 0 \tag{3.28}$$

By replacing [Y$_r$] in Eq. (3.27) with the expression from Eq. (3.28), the imaginary part of [Y] is found by solving the N real equations

$$\left\{ \left([\omega L]^{-1}[R]\right)^2 + [U] \right\} [Y_i] = -[\omega L]^{-1} \tag{3.29}$$

and the real part is then calculated from Eq. (3.28).

For the transient simulation, $[R_{series}]$ of Eq. (3.21b) is rewritten as

$$[R] + \frac{2}{\Delta t}[L] = \frac{2}{\Delta t}[L]\left\{ \frac{\Delta t}{2}[L]^{-1}[R] + [U] \right\}$$

which, upon inversion, produces the matrix $[G_{series}]$ required in Eq. (3.21a),

$$[G_{series}] = \left\{ [U] + \frac{\Delta t}{2}[L]^{-1}[R] \right\}^{-1} \frac{\Delta t}{2}[L]^{-1} \tag{3.30}$$

Again, the matrix $[U] + \Delta t/2 \ [L]^{-1}[R]$ needed as an intermediate step is unsymmetric, while the final result $[G_{series}]$ becomes symmetric. Symmetry is proved with Eq. (3.25) by simply replacing $j\omega$ by $2/\Delta t$. As in the steady-state case, the inverse of Eq. (3.30) is found by solving N linear equations

$$\left\{ [U] + \frac{\Delta t}{2}[L]^{-1}[R] \right\}[G_{series}] = \frac{\Delta t}{2}[L]^{-1} \tag{3.31}$$

To initialize the history term $[hist_{series}]$, Eq. (3.21a) can be used directly. To update it, neither Eq. (3.22) nor Eq. (3.23a) can be used because $[L]$ and $[R_{series}]$ do not exist. Instead, Eq. (3.23a) is rewritten as

$$[hist_{series}(t)] = [H]\{[v_k(t)] - [v_m(t)]\} + [hist_{series}(t-\Delta t)] +$$

$$[G_{series}][-2R][hist_{series}(t-\Delta t)] \tag{3.32}$$

By storing the symmetric matrices $[H]$, $[G_{series}]$ and $-2[R]$, the updating with Eq. (3.32) can be done with three matrix multiplications, starting with the product $-2[R][hist_{series}(t - \Delta t)]$. An alternative updating formula, which requires the storage of only two symmetric matrices $[G_{series}]$ and $-2[R]$, and produces the currents $[i_{km}]$ as a by-product, is

$$[hist_{series}(t)] = [G_{series}]\{[v_k(t)] - [v_m(t)] + [-2R][i_{km}(t)]\} + [i_{km}(t)] \tag{3.33}$$

if the current is first found from Eq. (3.21a), followed by the multiplication $-2[R][i_{km}(t)]$, etc. Eq. (3.33) is derived from Eq. (3.22) by rewriting $2/\Delta t \ [L] - [R]$ as $[R_{series}] \ -2[R]$.

All equations in this section have symmetric matrices, and can handle the special case of either $[R] = 0$ or $[L]^{-1} = 0$ as long as $[U] + \Delta t/2 \ [L]^{-1}[R]$ in Eq. (3.30) can be inverted. Note, however, that $[L]^{-1} = 0$ implies infinite inductances, that is, the M coupled branches are really M open switches.

4. OVERHEAD TRANSMISSION LINES

4.1 Line Parameters

The parameters R', L', and C' of overhead transmission lines are evenly distributed along the line[1], and can, in general, not be treated as lumped elements. Some of them are also functions of frequency; therefore, the term "line constants" is avoided in favor of "line parameters." For short-circuit and power flow studies, only positive and zero sequence parameters at power frequency are needed, which are readily available from tables in handbooks, or can easily be calculated from simple formulas. For the line models typically needed in EMTP studies, however, these simple formulas are not adequate enough. Usually, the line parameters must therefore be computed, with either one of the two supporting routines LINE CONSTANTS or CABLE CONSTANTS.

These supporting routines produce detailed line parameters for the following types of applications:

(a)   Steady-state problems at power frequency with complicated coupling effects. An example is the calculation of induced voltages and currents in a de-energized three-phase line which runs parallel with an energized three-phase line. Both lines would be represented as six coupled phases in this case.

(b)   Steady-state problems at higher frequencies. Examples are the analysis of harmonics, or the analysis of power line carrier communication, on untransposed lines.

(c)   Transients problems. Typical examples are switching and lightning surge studies.

Line parameters could be measured after the line has been built; this is not easy, however, and has been done only occasionally. Also, lines must often be analyzed in the design stage, and calculations are the only means available for obtaining line parameters in that case.

The following explanations describe primarily the theory used in the supporting routines LINE CONSTANTS and CABLE CONSTANTS, though other methods are occasionally mentioned, especially if it appears that they might be used in EMTP studies some day. The supporting routine LINE CONSTANTS is heavily based on the work done by M.H. Hesse [27], though some extensions to it were added.

4.1.1 Line Parameters For Individual Conductors

The solution method is easier to understand for a specific example. Therefore, a double-circuit three-phase line with twin bundle conductors and one ground wire will be used for the explanations (Fig. 4.1). There are 13 conductors in this configuration. They will be called

---

[1]The "prime" in R', L' and C' is used to indicate distributed parameters in Ω/km, H/km and F/km.
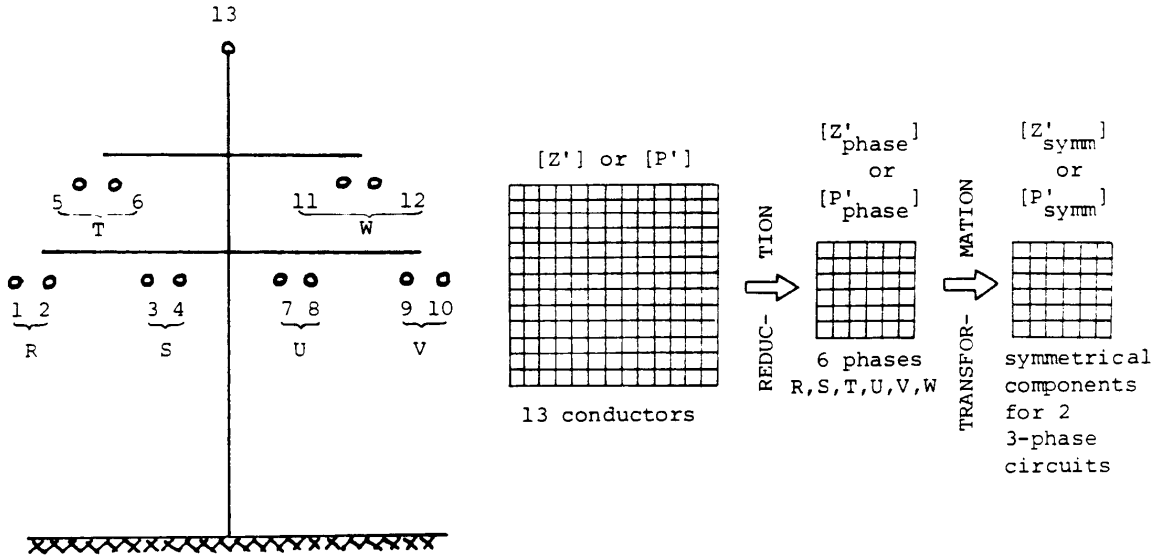
Fig. 4.1 - Line parameters

individual conductors[2], to distinguish them from the 6 equivalent phase conductors which are obtained after pairs have been bundled into phase conductors and after the ground wire has been eliminated.

4.1.1.1 Series Impedance Matrix

It is customary to describe the voltage drop along a transmission line in the form of partial differential equations, e.g., for a single-phase line as

$$-\frac{\partial v}{\partial x} = R'i + L'\frac{\partial i}{\partial t} \tag{4.1}$$

The parameters R' and L' of overhead lines are not constant, however, but functions of frequency. In that case it is improper to use Eq. (4.1); instead, the voltage drops must be expressed in the form of phasor equations for ac steady state conditions at a specific frequency. For the case of Fig. 4.1,

$$-\begin{bmatrix} \dfrac{dV_1}{dx} \\ \dfrac{dV_2}{dx} \\ . \\ . \\ . \\ \dfrac{dV_{13}}{dx} \end{bmatrix} = \begin{bmatrix} Z'_{11} & Z'_{12} & \cdots & Z'_{1,13} \\ Z'_{21} & Z'_{22} & \cdots & Z'_{2,13} \\ & & \cdots\cdots\cdots & \\ Z'_{13,1} & Z'_{13,2} & \cdots & Z'_{13,13} \end{bmatrix} \begin{bmatrix} I_1 \\ I_2 \\ . \\ . \\ . \\ I_{13} \end{bmatrix} \tag{4.2a}$$

---

[2]In the output of the supporting routine LINE CONSTANTS, they are called "physical conductors."

with V_i = voltage phasor, measured from conductor i to ground,

           I_i = current phasor in conductor i,

or in general

$$-\left[\frac{dV}{dx}\right] = [Z'][I] \tag{4.2b}$$

with [V] = vector of phasor voltages (measured from conductor to ground), and

       [I] = vector of phasor currents in the conductors.

Implied in Eq. (4.2) is the existence of ground as a return path, to which all voltages are referenced. The matrix $[Z'] = [R'(\omega)] + j\omega [L'(\omega)]$ is called the series impedance matrix; it is complex and symmetric. The diagonal element $Z'_{ii} = R'_{ii} + j\omega L'_{ii}$ is the series self impedance per unit length of the loop formed by conductor i and ground return. The off-diagonal element $Z'_{ik} = Z'_{ki} = R'_{ki} + j\omega L'_{ki}$ is the series mutual impedance per unit length between conductors i and k, and determines the longitudinally induced voltage in conductor k if a current flows in conductor i, or vice versa. The resistive terms in the mutual coupling are introduced by the presence of ground, as briefly explained in Section 3.1.

Formulas for calculating Z'_{ii} and Z'_{ik} were developed by Carson and Pollaczek in the 1920's for telephone circuits [28, 29]. These formulas can also be used for power lines. Both seem to give identical results for overhead lines, but Pollaczek's formula is more general inasmuch as it can also be used for buried (underground) conductors or pipes. Carson's formula is easier to program than Pollaczek's and is therefore used in both supporting routines LINE CONSTANTS and CABLE CONSTANTS, except that the latter includes an extension of Carson's formula for the case of multilayer stratified earth [30] as well. Carson's, Pollaczek's and other earth return formulas are compared in [31].

Two recent new approaches to the calculation of earth-return impedances are those of Hartenstein, Koglin and Rees [32], and of Gary, Deri, Tevan, Semlyen and Castanheira [33, 34]. Hartenstein, Koglin and Rees treat the ground as a system of conducting layers 1, 2, 3…n, with uniform current distribution in each layer (Fig. 4.2(a)). Their results come close to those obtained with Carson's formula. One advantage of their method is the fact that it is very easy to assume difference earth resistivities for each of the layers. Gary, Deri, et al. calculate self and mutual impedances with the simple formulas originally proposed by Dubanton,

$$Z'_{ii} = R'_{i-internal} + j\left\{\omega\frac{\mu_0}{2\pi}\ell n\frac{2(h_i+\bar{p})}{r_i} + X'_{i-internal}\right\} \tag{4.3}$$

and

$$Z'_{ik} = j\omega\frac{\mu_0}{2\pi}\ell n\frac{\sqrt{(h_i+h_k+2\bar{p})^2 + x^2_{ik}}}{d_{ik}} \tag{4.4}$$

in which p represents a complex depth,

$$\overline{p} = \sqrt{\frac{\rho}{j\omega\mu_0}} \tag{4.5}$$

All other parameters are explained after Eq. (4.8), except for x_{ik} = horizontal distance between conductors i and k (Fig. 4.4), and ρ = earth resistivity. The results agree very closely with those obtained from Carson's formula, with the differences peaking at 9% in the frequency range between 100 Hz and 10 kHz and being lower elsewhere. This is a very good agreement, indeed, and Eq. (4.3) and (4.4) may therefore supplant Carson's formula some day. Fig. 4.2(b) shows a comparison of positive and zero sequence parameters for a typical 500 kV line.
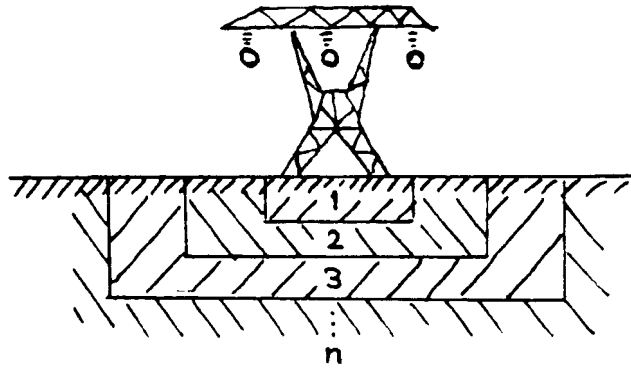
Fig. 4.2(a) - Alternative to Carson's formula: Ground represented as layers 1, 2,…n

Carson's formula

Carson's formula for homogeneous earth is normally accurate enough for power system studies, especially since the data for a more detailed multilayer earth return is seldom available. The supporting routine CABLE CONSTANTS does have an option for multilayer or stratified earth, however. Carson's formula is based on the following assumptions:

(a)   The conductors are perfectly horizontal above ground, and are long enough so that three-dimensional end effects can be neglected (this makes the field problem two-dimensional). The sag is taken into account indirectly by using an average height above ground (Fig. 4.3).
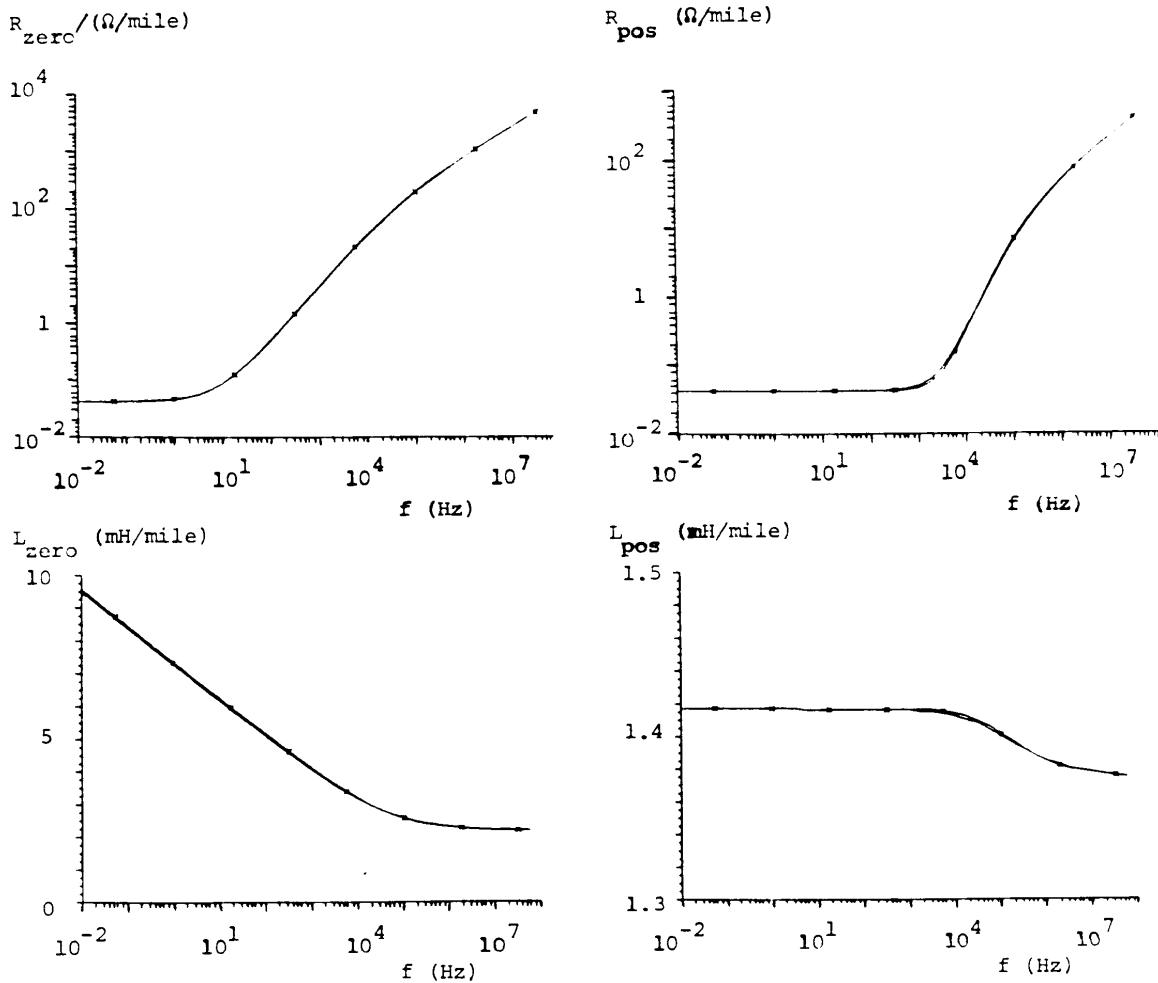
Fig. 4.2(b) - Alternative to Carson's formula: formula by Gary, Deri et al. (comparison with Carson's formula for a typical 500 kV line with bundle conductors; skin effect in conductors ignored)

(b) The aerial space is homogeneous without loss, with permeability μ_0 and permittivity ε_0.

(c) The earth is homogeneous with uniform resistivity ρ, permeability μ_0 and permittivity ε_0, and is bounded by a flat plane with infinite extent, to which the conductors are parallel. The earth behaves as a conductor, i.e., $1/\rho \gg \omega\varepsilon_0$, and hence the displacement currents may be neglected. Above the critical frequency $f_{critical} = 1/(2\pi\varepsilon_0\rho)$, other formulas [35, 36] must be used (for $\rho = 10,000$ Ωm in rocky ground, $f_{critical} = 1.8$ MHz, which is still on the high side for most EMTP line models).

(d) The spacing between conductors is at least one order of magnitude larger than the radius of the conductors, so that proximity effects (current distribution within one conductor influenced by current in an adjacent conductor) can be ignored.

The conductor profile between towers (Fig. 4.3) can be described

(a) as a parabola for spans ≤ 500 m,

(b) as a catenary for $500 \leq$ spans ≤ 2000 m, and

(c) as an elastic line for spans > 2000 m.

4-5
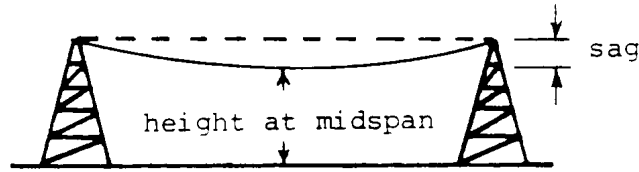
Fig. 4.3 - Conductor profile between towers

If the parabola is accurate enough, then the average height above ground is

$$h = height \ at \ midspan + \frac{1}{3} sag,$$ (4.6)

(4.6)

which is the formula used by both supporting routines LINE CONSTANTS and CABLE CONSTANTS. The elements of the series impedance matrix can then be calculated from the geometry of the tower configuration (Fig. 4.4) and from characteristics of the conductors. For the self impedance,

$$Z'_{ii} = (R'_{i-internal} + \Delta R'_{ii}) + j(\omega \frac{\mu_0}{2\pi} \ln \frac{2h_i}{r_i} + X'_{i-internal} + \Delta X'_{ii})$$ (4.7)
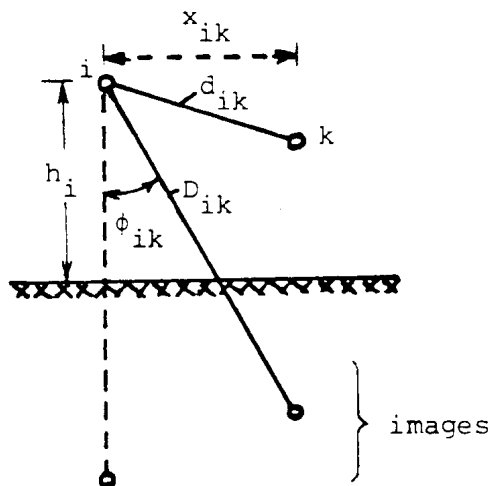
Fig. 4.4 - Tower geometry

and for the mutual impedance

$$Z'_{ik} = Z'_{ki} = \Delta R'_{ik} + j(\omega \frac{\mu_0}{2\pi} \ln \frac{D_{ik}}{d_{ik}} + \Delta X'_{ik})$$ (4.8)

with μ_0 = permeability of free space. Using

$$\mu_0/2\pi = 2 \cdot 10^{-4} \ H/km$$ (4.9)

produces impedances in Ω/km. The parameters in Eq. (4.7) and (4.8) are

$R'_{i\text{-internal}}$ = ac resistance of conductor i in Ω/unit length,

h_i = average height above ground of conductor i,

D_{ik} = distance between conductor i and image of conductor k,

d_{ik} = distance between conductors i and k,

r_i = radius of conductor i,

$X_{i\text{-internal}}$ = internal reactance of conductor i,

ω = $2\pi f$ with f = frequency in Hz,

$\Delta R'$, $\Delta X'$ = Carson's correction terms for earth return effects.

Carson's correction terms $\Delta R'$ and $\Delta X'$ in Eq. (4.7) and (4.8) account for the earth return effect, and are functions of the angle ϕ (ϕ = 0 for self impedance, $\phi = \phi_{ik}$ in Fig. 4.4 for mutual impedance), and of the parameter a:

$$a = 4\pi\sqrt{5} \cdot 10^{-4} \cdot D \cdot \sqrt{\frac{f}{\rho}}$$ (4.10)

with D = $2h_i$ in m for self impedance,

$\quad$ D_{ik} in m for mutual impedance,

$\quad$ ρ = earth resistivity in Ωm.

$\Delta R'$ and $\Delta X'$ become zero for a → ∞ (case of very low earth resistivity). Carson gives an infinite integral for $\Delta R'$ and $\Delta X'$, which he developed into the sum of four infinite series for a ≤ 5. Rearranged for easier programming, it can be written as one series, and for impedances in Ω/km, becomes

$\Delta R' =$	$4\omega \bullet 10^{-4}\{\pi/8$	$\Delta X' =$	$4\omega \bullet \{1/2(0.6159315 - 1na)$
	$-b_1 a \bullet \cos\phi$		$+b_a a \bullet \cos\phi$
	$+b_2[(c_2 - 1na)a^2\cos2\phi + a^2\sin2\phi]$		$-d_2 a^2\cos2\phi$
	$+b_3 a^3\cos3\phi$		$+b_3 a^3\cos3\phi$
	$-d_4 a^4\cos4\phi$		$-b_4[(c_4 - 1na)a^4\cos4\phi + \phi a^4\sin g4\phi]$
	$-b_5 a^5\cos5\phi$		$+b_5 a^5\cos5\phi$

$$+b_6[(c_6-1na)a^6\cos6\phi + \phi a^6\sin6\phi \qquad\qquad -d_6a^6\cos6\phi$$

$$+b_7a^7\cos7\phi \qquad\qquad\qquad\qquad\qquad +b_7a^7\cos7\phi$$

$$-d_8a^8\cos8\phi \qquad\qquad\qquad\qquad\qquad -b_8[(c_8-1na)a^8\cos8\phi + \phi a^8\sin8\phi]$$

$$- ...\} \qquad\qquad\qquad\qquad\qquad\qquad\qquad + ...\}$$

$$\text{in } \Omega/\text{km} \quad (4.11)$$

Each 4 successive terms for a repetitive pattern. The coefficients b_i, c_i and d_i are constants, which can be precalculated and stored in lists. They are obtained from the recursive formulas:

$$b_1 = \frac{\sqrt{2}}{6} \text{ for odd subscripts,}$$

$$b_i = b_{1-2}\frac{sign}{i(i+2)} \text{ with the starting value}$$

$$b_2 = \frac{1}{16} \text{ for even subscripts,} \qquad\qquad (4.12)$$

$$c_i = c_{1-2} + \frac{1}{i} + \frac{1}{i+2} \text{ with the starting value } c_2 = 1.3659315,$$

$$d_i = \frac{\pi}{4}\cdot b_i,$$

with sign $= \pm 1$ changing after each 4 successive terms (sign $= \pm 1$ for i = 1, 2, 3, 4; sign = -1 for i = 5, 6, 7, 8 etc.).

The trigonometric functions are calculated directly from the geometry,

$$\cos\phi_{ik} = \frac{h_i + h_k}{D_{ik}} \qquad and \qquad \sin\phi_{ik} = \frac{x_{ik}}{D_{ik}}$$

and for higher-order terms in the series from the recursive formulas

$$a^i cosi\phi = [a^{i-1}\cos(i-1)\phi\cdot\cos\phi - a^{i-1}\sin(i-1)\phi\cdot\sin\phi]\cdot a$$

$$a^i sini\phi = [a^{i-1}\cos(i-1)\phi\cdot\sin\phi + a^{i-1}\sin(i-1)\phi\cdot\cos\phi]\cdot a \qquad\qquad (4.13)$$

For power circuits at power frequency only few terms are needed in the infinite series of Eq. 4.11. However, at frequencies and for wider spacings (e.g., in interference calculations) more and more terms must be taken into account as the parameter a becomes larger and larger [37, discussion by Dommel]. Once Carson's series starts to converge, it does so fairly rapidly. How misleading the results can be with too few terms in the series of Eq. 4.11 is illustrated for the case of a = 4 and ϕ = 0: If the series were truncated after the 1st, 2nd,..., 15th term, the percent error in $Re\{Z'_{ii}\}$ would be

+312, -748, -16, +798, -416, +365, -121, -93, +28, -15, +5.2,

+1.7, -0.35, +0.14, -0.04

For a > 5 the following finite series [38] is best used:

$$\Delta R' = \left(\frac{\cos\phi}{a} - \frac{\sqrt{2}\cos2\phi}{a^2} + \frac{\cos3\phi}{a^3} + \frac{3\cos5\phi}{a^5} - \frac{45\cos7\phi}{a^7} \right) \cdot \frac{4\omega \cdot 10^{-4}}{\sqrt{2}}$$

$$\Delta X' = \left(\frac{\cos\phi}{a} - \frac{\cos3\phi}{a^3} + \frac{3\cos5\phi}{a^5} + \frac{45\cos7\phi}{a^7} \right) \cdot \frac{4\omega \cdot 10^{-4}}{\sqrt{2}} \quad in \ \Omega/km \tag{4.14}$$

Internal impedance and skin effect

In the old days of slide-rule calculations, the internal reactance $X'_{reactance}$ and external reactance $\omega \mu_0/2\pi \, \ell n$ 2h/r for lossless earth were often combined into one expression, by replacing radius r with the smaller "geometric mean radius" GMR to account for the internal magnetic field,

$$\omega\frac{\mu_0}{2\pi}\ell n\frac{2h}{r} + X'_{internal} = \omega\frac{\mu_0}{2\pi}\ell n\frac{2h}{GMR} \tag{4.15}$$

GMR was often included in conductor tables. Instead of or in addition to GMR, North American handbooks have also frequently given the "reactance at 1 foot spacing"[3] X'_A, which is related to GMR,

$$X'_A = \omega\frac{\mu_0}{2\pi}\ell n\frac{1(foot)}{GMR(feet)} \tag{4.16}$$

with GMR in feet (or in m if X'_A is to be the reactance at 1 m spacing).

The concept of geometric mean radius was originally developed for nonmagnetic conductors at power frequency where uneven current distribution (skin effect) can be ignored. In that case, its meaning is indeed purely geometric, with GMR being equal to the geometric mean distance among all elements on the conductor cross section area if this area were divided into an infinite number of equal, infinitesimally small elements. For a solid, round, nonmagnetic conductor at low frequency,

$$GMR/r = e^{-1/4}$$

This formula changes to

$$GMR/r = e^{-\mu_r/4}$$

if the conductor is made of magnetic material with relative permeability μ_r; its geometric meaning is then lost. If skin effect is taken into account, its geometric meaning is lost as well. The name geometric mean radius is therefore

---

[3]The name comes form the positive sequence reactance formula $X'_{pos} = \omega \mu_0/2\pi \, \ell n$ GMD/GMR discussed in Eq. (4.56), for the case where the spacing among the three phases (expressed as geometric mean distance GMD) is 1 foot, with GMR given in feet as well.

misleading, and it is questionable whether it should be retained.

Eq. (4.15) gives the conversion formula between GMR and internal reactance,
The internal reactance can be calculated for certain types of conducts [39, 40] as part of the internal impedance $R'_{internal} + jX'_{internal}$. Since $GMR/r = e^{-X'_{internal}/(\omega\frac{\mu_0}{2\pi})}$ is only a very small part of the total reactance for nonmagnetic conductors, its accurate determination is somewhat academic. More important is the calculation of $R'_{internal}$, because the increase of resistance with frequency due to skin effect can be considerable.

$$(4.17)$$

The internal impedance of solid, round wires can be calculated with well-known skin effect formulas, with $R'_{internal}$ being of more practical interest than $X'_{internal}$. Stranded conductors can usually be approximated as solid conductors of the same cross-sectional area[4] [41]. It has been claimed that steel-reinforced aluminum cables (ACSR) can usually be approximated as tubular conductors when the influence of the steel core is negligible, which is more likely to be the case with an even number of layers of aluminum strands, since the magnetization of the steel core caused by one layer spiralled in one direction is more or less cancelled by the next layer spiralled in the opposite direction. The supporting routine LINE CONSTANTS uses this approximation of an ACSR as a tubular conductor. If the magnetic material of the steel core is of influence, then calculations probably become unreliable, and current-dependent, measured values should be used instead. Since the solid conductor is a special case of the tubular conductor, the supporting routine LINE CONSTANTS uses only the formula for the latter, which is described as Eq. (5.7b) in Section 5.1.

Table 4.1 shows the increase in resistance and the decrease in internal inductance due to skin effect for a tubular conductor with $R'_{dc} = 0.0398$ Ω/mile, ratio inside radius/outside radius $q/r = 0.2258$ (Fig. 4.5), and $\mu_r = 1.0$. The internal inductance of a tube at dc is [48, p. 64]

$$L'_{dc} = 2 \cdot 10^{-4} \left\{ \frac{q^4}{(r^2-q^2)^2} \ell n \frac{r}{q} - \frac{3q^2-r^2}{4(r^2-q^2)} \right\} H/km$$

or $0.454866 \cdot 10^{-4}$ H/km in this case. At high frequencies, $R'_{internal} = X'_{internal}$, with both components being proportional to $\sqrt{\omega}$. This is the region of pronounced skin effect. From Table 4.1 it can be seen that $R'_{internal}$ and $X'_{internal}$ are almost equal at 10 kHz (difference 2.2%), with the difference decreasing to 0.7% at 100 kHz, or 0.2% at 1 MHz.

---

[4]There are cases, however, where this approximation is not good enough. More accurate formulas are needed, for instance, for calculating the attenuation in power line carrier problems [39], as explained in Appendix VII.

Table 4.1 - Skin effect in a tubular conductor

f(Hz)	R'_{ac}/R'_{dc}	$L'_{internal-ac}/L'_{internal-dc}$
2	1.0002	0.99992
4	1.0007	0.99970
6	1.0015	0.99932
8	1.0026	0.99879
10	1.0041	0.99812
20	1.0164	0.99254
40	1.0632	0.97125
60	1.1347	0.93898
80	1.2233	0.89946
100	1.3213	0.85639
200	1.7983	0.66232
400	2.4554	0.47004
600	2.9421	0.38503
800	3.3559	0.33418
1000	3.7213	0.29924
2000	5.1561	0.21204
4000	7.1876	0.15008
6000	8.7471	0.12258
8000	10.0622	0.10617
10000	11.2209	0.09497
20000	15.7678	0.06717
40000	22.1988	0.04750
60000	27.1337	0.03879
80000	31.2942	0.03359
100000	34.9597	0.03004
200000	49.3413	0.02124
400000	69.6802	0.01502
600000	85.2870	0.01227
800000	98.4441	0.01062
1000000	110.0357	0.00950
2000000	155.5154	0.00672
4000000	219.8336	0.00475
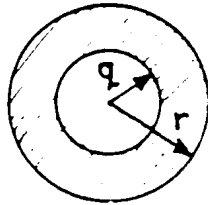
Fig. 4.5 - Tubular conductor
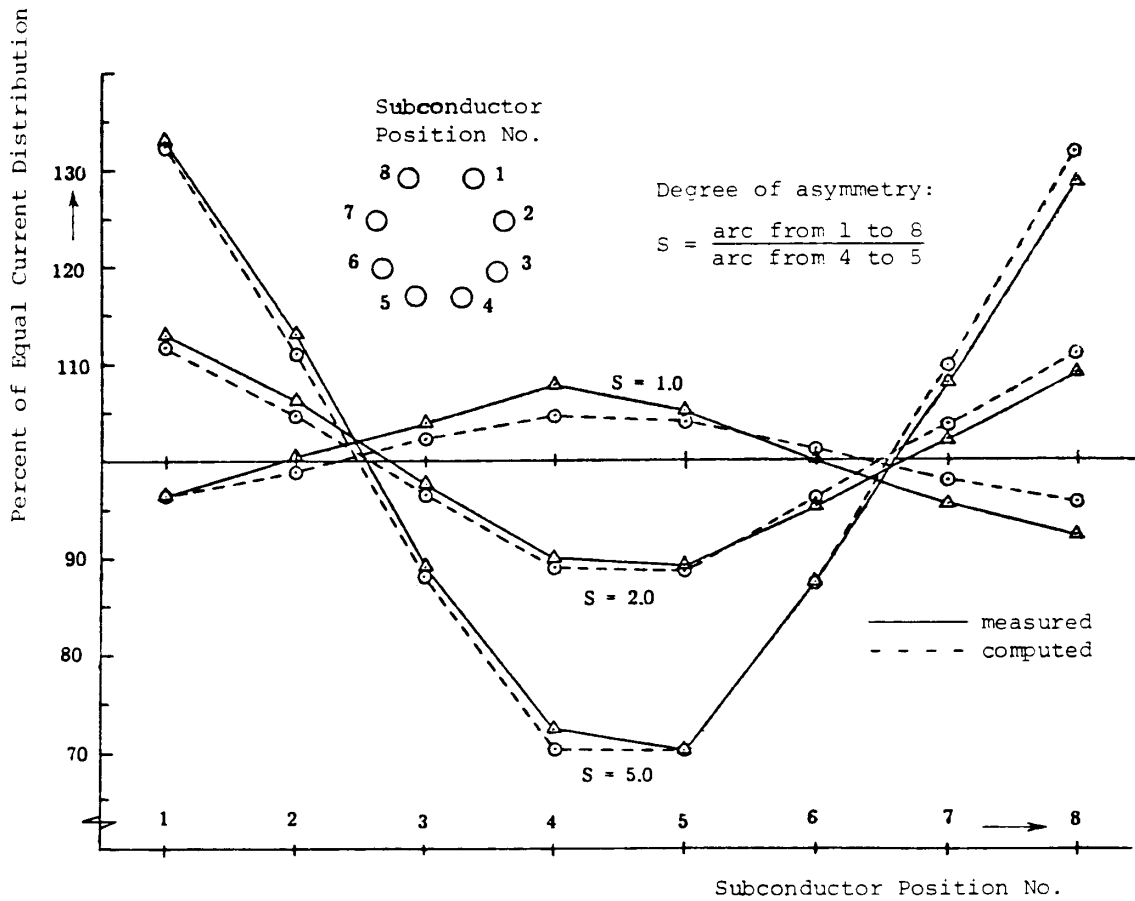
Fig. 4.6 - Current distribution within an 8-conductor bundle [42].

Example for using series impedance matrix of individual conductors

The matrix of Eq. (4.2) can be used to study the uneven current distribution within a bundle conductor. Fig. 4.6 shows measured and calculated values for the unequal current distribution in the 8 subconductors of an asymmetrical bundle for various degrees of asymmetry [42]. Asymmetrical bundling was proposed to reduce audible noise, but this advantage is offset by the unequal current distribution. The currents in this case were found from Eq. (4.2) with an 8 x 8 matrix, assuming equal voltage drops in the 8 conductors,

$$[I] = -[Z']^{-1}[dV/dx] \tag{4.18}$$

4.1.1.2 Shunt Capacitance Matrix

The voltages from the 13 conductors in Fig. 4.1 to ground are a function of the line charges:

$$
\begin{bmatrix} v_1 \\ v_2 \\ . \\ . \\ . \\ v_{13} \end{bmatrix} = \begin{bmatrix} P'_{11} & P'_{12} & \cdots & P'_{1,13} \\ P'_{21} & P'_{22} & \cdots & P'_{2,13} \\ \cdots & & & \\ \cdots & & & \\ \cdots & & & \\ P'_{13,1} & P'_{13,2} & \cdots & P'_{13,13} \end{bmatrix} \begin{bmatrix} q_1 \\ q_2 \\ . \\ . \\ . \\ q_{13} \end{bmatrix}
\qquad (4.19a)
$$

with q_i = charge per unit length on conductor i, or in the general case

$$
[v] = [P'][q]
\qquad (4.19b)
$$

Maxwell's potential coefficient matrix [P'] is real and symmetric. Its elements are easy to compute from the geometry of the tower configuration and from the conductor radii if the following two assumptions are made: (a) the air is lossless and the earth is uniformly at zero potential, (b) the radii are at least an order of magnitude smaller than the distances among the conductors. Both assumptions are reasonable for overhead lines. Then the diagonal element becomes

$$
P'_{ii} = \frac{1}{2\pi\epsilon_0} \ln \frac{2h_i}{r_i}
\qquad (4.20)
$$

and the off-diagonal element

$$
P'_{ik} = P'_{ki} = \frac{1}{2\pi\epsilon_0} \ln \frac{D_{ik}}{d_{ik}}
\qquad (4.21)
$$

with ϵ_0 = permittivity of free space. The factor $1/(2\pi\epsilon_0)$ in these equations is $c^2 \cdot \mu_0/2\pi$, where c is the speed of light. With c = 299,792.5 km/s and $\mu_0/(2\pi) = 2 \cdot 10^{-4}$ H/km, it follows that

$$
1/(2\pi\epsilon_0) = 17.975109 \cdot 10^6 \quad km/F
\qquad (4.22)
$$

The inverse relationship of Eq. (4.19) yields the shunt capacitance matrix [C'],

$$
[q] = [C'][v], \quad with \ [C'] = [P']^{-1}
\qquad (4.23)
$$

The supporting routine LINE CONSTANTS uses a version of the Gauss-Jordan process for this matrix inversion which takes advantage of symmetry [43]. This process was chosen because it can easily be modified to handle matrix reductions as well, which are needed for eliminating ground wires and for bundling conductors. Appendix III explains this Gauss-Jordan process in more detail.

The capacitance matrix [C'] is in nodal form. This means that the diagonal element C'_{ii} is the sum of the shunt capacitances per unit length between conductor i and all other conductors as well as ground, and the off-diagonal element $C'_{ik} = C'_{ki}$ is the <u>negative</u> shunt capacitance per unit length between conductors i and k. An example for a three-phase circuit from [44, p. 457] is shown in Fig. 4.7, with

$$[C'] = \begin{bmatrix} 12.161 & -2.625 & -2.625 \\ -2.625 & 11.729 & -1.349 \\ -2.625 & -1.349 & 11.729 \end{bmatrix} \ nF/mile$$

or $C'_{12\text{-mutual}} = 2.625$, $C'_{13\text{-mutual}} = 2.625$, $C'_{23\text{-mutual}} = 1.349$, $C_{2\text{-ground}} = 7.755$ nF/mile, etc.
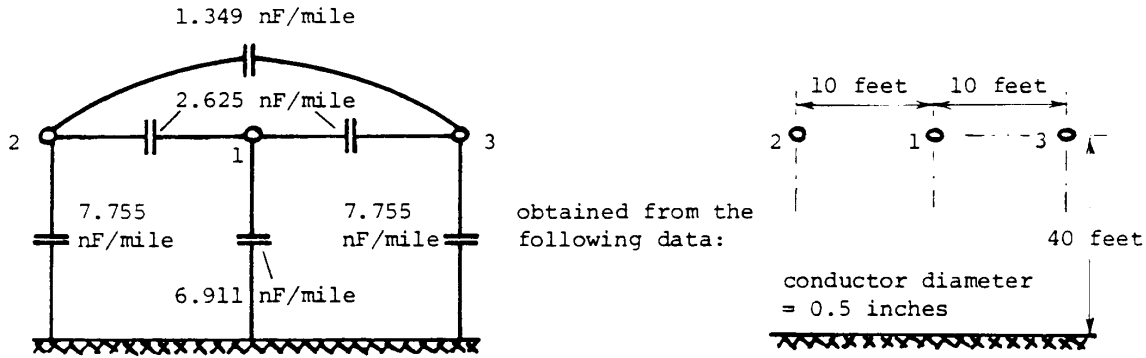
Fig. 4.7 - Mutual and shunt capacitances

For ac steady-state conditions, the vector of charges (as phasor values) is related to the vector of leakage currents [-dI/dx] by

$$[Q] = -\frac{1}{j\omega}\left[\frac{dI}{dx}\right] \tag{4.24}$$

Therefore, the second system of differential equations is

$$-\left[\frac{dI}{dx}\right] = j\omega\,[C'][V] \tag{4.25}$$

which, together with Eq. (4.2), completely describes the ac steady-state behavior of the multi-conductor line. Shunt conductances G' have been ignored in Eq. (4.25), because their influence is negligible on overhead lines, except at very low frequencies approaching dc, where the line behavior is determined by R' and G', with $\omega L'$ and $\omega C'$ becoming negligibly small. With G', the complete equation is

$$-\left[\frac{dI}{dx}\right] = [Y'][V] \tag{4.26a}$$

where

$$[Y'] = [G'] + j\omega\,[C'] \tag{4.26b}$$

At very high frequencies, the shunt capacitances are also influenced by earth conduction effects, and correction terms must then be added to Eq. (4.20) and (4.21). However, the earth conduction effect is normally

negligible below 100 kHz to 1 MHz [45]. In that case, the capacitances are constant, in contrast to series resistances and series inductances which are functions of frequency.

4.1.2 Line Parameters for Equivalent Phase Conductors

Equations (4.2) and (4.19) for all individual conductors contain more information than is usually needed. Generally, only the phase quantities are of interest. For the case of Fig. 4.1, the reduction from 13 equations to 6 equations for the phases R, S, T, I, V, W is accomplished by introducing the following conditions,

for grounding conductor 13: $dV_{13}/dx = 0$ in (4.2), $v_{13} = 0$ in (4.19),

for bundling conductors 1 and 2 into phase R:

$$I_1 + I_2 = I_R, \quad dV_1/dx = dV_2/dx = dV_R/dx \text{ in (4.2),}$$

and

$$q_1 + q_2 = q_R, \quad v_1 = v_2 = v_R \text{ in (4.19)}$$

and analogous for bundling the other phases. With these conditions, the matrices can be reduced to 6 x 6, as explained next. These reduced matrices will be called matrices for the equivalent phase conductors.

4.1.2.1 Elimination of Ground Wires

Normally, ground wires are continuous and grounded at every tower[5], which are typically 250 to 350 m apart. In that case it is permissible for frequencies up to approximately 250 kHz to assume that the ground wire potential is continuously zero [46]. This allows a reduction in the order of the [Z']- and [P']-matrices, with the reduction procedure being the same for both. Let the matrices and vectors in Eq. (4.2) be partitioned for the set "u" of ungrounded conductors, and for the set "g" of ground wires,

$$-\begin{bmatrix} [dV_u/dx] \\ [dV_g/dx] \end{bmatrix} = \begin{bmatrix} [Z'_{uu}] & [Z'_{ug}] \\ [Z'_{gu}] & [Z'_{gg}] \end{bmatrix} \begin{bmatrix} [I_u] \\ [I_g] \end{bmatrix} \tag{4.27}$$

Since $[V_g]$ and $[dV_g/dx]$ are zero, Eq. (4.27) can be reduced by eliminating $[I_g]$,

$$-\begin{bmatrix} \dfrac{dV_u}{dx} \end{bmatrix} = [Z'_{reduced}] \ [I_u] \tag{4.28a}$$

where

$$[Z'_{reduced}] = [Z'_{uu}] - [Z'_{ug}] [Z'_{gg}]^{-1} [Z'_{gu}] \tag{4.28b}$$

Rather than using straightforward matrix inversion and matrix multiplications in Eq. (4.28b), the more efficient Gauss-Jordan reduction process of Appendix III is used in the supporting routine LINE CONSTANTS. [P'] is reduced in the same way, and [C'$_{reduced}$] is found by inverting [P'$_{reduced}$]. At first sight it may appear as if less work

---

[5]Non-continuous "segmented" ground wires are discussed in Section 4.1.2.5.

were involved in reducing [C'], where the reduction simply consists of "scratching out" the rows and columns for ground wires "g." However, [C'] must first be found from the inversion of [P'], and it is faster to reduce a matrix than to invert it.

4.1.2.2 Bundling of Conductors

On high voltage power lines, bundle conductors are frequently used, where each "phase" or bundle conductor consists of two or more subconductors held together by spacers (typically 100 m apart). The bundle is usually symmetrical (S = 1.0 in Fig. 4.6), but unsymmetrical bundles have been proposed as well. Two methods can be used for calculating the line parameters of bundle conductors. With the first method, the parameters are originally calculated with each subconductor being represented as an individual conductor. Since the voltages are equal for the subconductors within a bundle, this voltage equality is then used to reduce the order of the matrices to the number of "equivalent phase conductors." With the second method, the concept of geometric mean distances is used to replace the bundle of subconductors by a single equivalent conductor. Both methods can be used with the supporting routine LINE CONSTANTS. The supporting routine CABLE CONSTANTS is limited to the second method.

Method 1 - Bundling of subconductors by matrix reduction

As in the elimination of ground wires, the matrix reduction process is the same for [Z'] and [P'], and will therefore only be explained for [Z']. Let us assume that the individual conductors i, k, l, m are to be bundled to make up phase R. Then the conditions

$$I_i \ + \ I_k \ + \ I_\mathcal{L} \ + \ I_m \ = \ I_R$$

and

$$\frac{dV_i}{dx} \ = \ \frac{dV_k}{dx} \ = \ \frac{dV_\mathcal{L}}{dx} \ = \ \frac{dV_m}{dx} \ = \ \frac{dV_R}{dx}$$

must be introduced into Eq. (4.2). The first step is to get I_R into the equations. This is done by writing I_R in place of I_i. By doing this, an error is of course made, which amounts to the addition of terms

$$Z'_{\mu i}(I_k \ + \ I_\mathcal{L} \ + \ I_m)$$

in all rows μ; they must obviously be subtracted again to keep the equations correct. In effect, this means subtraction of column i from columns k, $\mathcal{L}$, m. These changes are shaded in Fig. 4.8.

4-16
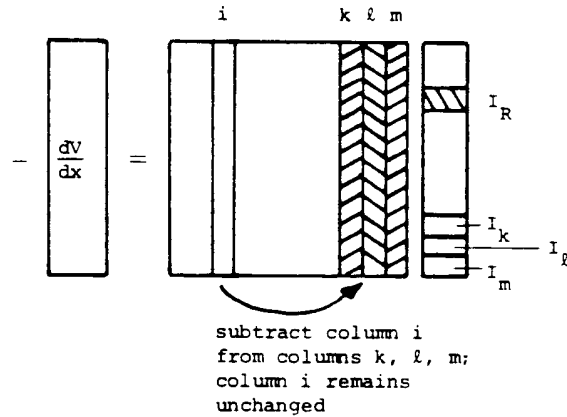
Fig. 4.8 - First step in bundling procedure

Columns k, ℓ, m are assumed to be the last ones in the matrix to make the explanation easier. The currents I_k, I_ℓ, I_m are still in the equations after execution of the first step of Fig. 4.8. To be able to eliminate them, there should be zeros in the left-hand side of the respective rows. This is easily accomplished by subtracting row i from rows k, ℓ, m, which produces zeros because $dV_i/dx = dV_k/dx$ etc. These changes are shaded in Fig. 4.9. The equations are now in a form which permits elimination of I_k, I_ℓ, I_m, in the same way as elimination of ground wires in Eq. (4.28). The four rows and columns for subconductors i, k, ℓ, m are thereby reduced to a single row and column for bundle conductor R.

Method 1 is more general than method 2 discussed next. For instance, it can easily handle the unequal current distribution in asymmetrical bundles described in Fig. 4.6.
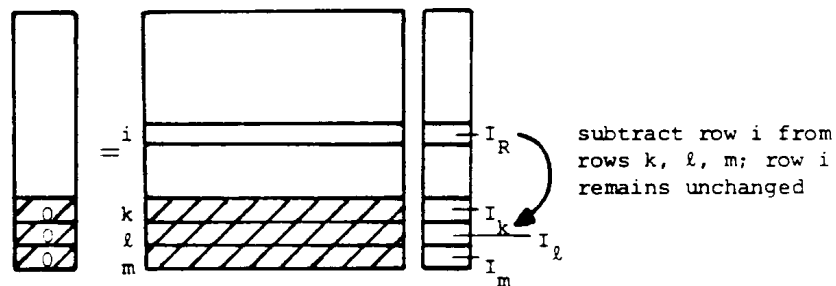
Fig. 4.9 - Second step in bundling procedure

Method 2 - Replacing bundled subconductors with equivalent single conductor

This method was developed for hand calculations [47], and while theoretically not limited to symmetrical bundles, formulas have usually only been derived for the more important case of symmetrical bundles. The following formulas are based on the assumption that

(a)   the bundle is symmetrical (S = 1.0 in Fig. 4.6), and

(b)   the current distribution among the individual subconductors within a bundle is uniform.
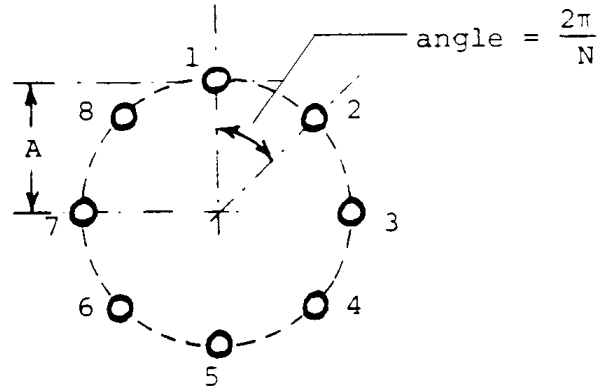
Fig. 4.10 - Symmetrical bundle with N individual subconductors

With these assumptions, the bundle can be treated as a single equivalent conductor in Eq. (4.15) by replacing GMR with the equivalent geometric mean radius of the bundle,

$$GMR_{equiv} = \sqrt[N]{N \cdot GMR \cdot A^{N-1}} \qquad (4.29)$$

where

GMR = geometric mean radius of individual subconductor in bundle,

A = radius of bundle (Fig. 4.10).

Similarly, the radius r in Eq. (4.20) must be replaced with the equivalent radius

$$r_{equiv} = \sqrt[N]{N \cdot r \cdot A^{N-1}} \qquad (4.30)$$

Comparison between methods 1 and 2

Both methods for bundling conductors give practically identical answers, at least in the example chosen for this comparison. The example was a 500 kV three-phase line with horizontal tower configuration, with phases 40 feet apart at an average height above ground of 50 feet. The symmetrical bundle consisted of 4 subconductors spaced 18 inches apart. Conductor diameter = 0.9 inches, dc resistance = 0.1686 Ω/mile, GMR = 0.3672 inches, r_{equiv} = 7.80524 inches from Eq. (4.30), and GMR_{equiv} = 7.41838 inches from Eq. (4.29). Table 4.2 compares the results in the form of positive and zero sequence parameters at 60 Hz. Obviously, the results are practically identical.

Table 4.2 - Comparison between methods 1 and 2 for bundling

Positive and zero sequence parameters at 60 Hz	Method 1 (Bundling by matrix reduction)	Method 2 (Equivalent conductors)

R'$_{pos}$ (Ω/mile)	0.042223	0.042205
X'$_{pos}$ (Ω/mile)	0.53394	0.53399
C'$_{pos}$ (μF/mile)	0.021399	0.021397
R'$_{zero}$ (Ω/mile)	0.31740	0.31738
X'$_{zero}$ (Ω/mile)	2.0065	2.0065
C'$_{zero}$ (μF/mile)	0.013456	0.013455

4.1.2.3 Reduced Matrices for Equivalent Phase Conductors

For the case of Fig. 4.1, elimination of ground wires and bundling of subconductors reduces the 13 x 13 matrices for the individual conductors to 6 x 6 matrices for the phases, e.g., for the series impedances,

$$-\frac{d}{dx}\begin{bmatrix}V_R\\V_S\\V_T\\V_U\\V_V\\V_W\end{bmatrix}=\begin{bmatrix}Z'_{RR}&Z'_{RS}&Z'_{RT}&Z'_{RU}&Z'_{RV}&Z'_{RW}\\Z'_{SR}&Z'_{SS}&Z'_{ST}&Z'_{SU}&Z'_{SV}&Z'_{SW}\\Z'_{TR}&Z'_{TS}&Z'_{TT}&Z'_{TU}&Z'_{TV}&Z'_{TW}\\Z'_{UR}&Z'_{US}&Z'_{UT}&Z'_{UU}&Z'_{UV}&Z'_{UW}\\Z'_{VR}&Z'_{VS}&Z'_{VT}&Z'_{VU}&Z'_{VV}&Z'_{VW}\\Z'_{WR}&Z'_{WS}&Z'_{WT}&Z'_{WU}&Z'_{WV}&Z'_{WW}\end{bmatrix}\begin{bmatrix}I_R\\I_S\\I_T\\I_U\\I_V\\I_W\end{bmatrix}$$

or in general,

$$-\left[\frac{dV_{phase}}{dx}\right]=[Z'_{phase}][I_{phase}] \tag{4.31}$$

and

$$-\left[\frac{dI_{phase}}{dx}\right]=j\omega[C'_{phase}][V_{phase}] \tag{4.32}$$

For a three-phase single circuit with phases A, B, C, Eq. (4.31) would have the form

$$-\begin{bmatrix}\dfrac{dV_A}{dx}\\[2mm]\dfrac{dV_B}{dx}\\[2mm]\dfrac{dV_C}{dx}\end{bmatrix}=\begin{bmatrix}Z'_{AA}&Z'_{AB}&Z'_{AC}\\Z'_{BA}&Z'_{BB}&Z'_{BC}\\Z'_{CA}&Z'_{CB}&Z'_{CC}\end{bmatrix}\begin{bmatrix}I_A\\I_B\\I_C\end{bmatrix} \tag{4.33}$$

The diagonal element Z'$_{kk}$ in Eq. (4.33) is the series self impedance of phase k for the loop formed by phase k with return through ground and ground wires, and the off-diagonal element Z'$_{ik}$ is the series mutual impedance between phases i and k. The self impedance of phase k <u>is not</u> the positive sequence impedance. To obtain impedances which

come close to the positive sequence values, we would have to assume symmetrical currents in Eq. (4.33),

$$I_B = a^2 I_A \quad and \quad I_C = a I_A , \quad with \quad a = e^{j\,120°}$$

and then express the voltage drop in phase A as a function of I_A only,

$$-\frac{dV_A}{dx} = Z'_{A\text{-}symm} I_A, \quad with \ Z'_{A\text{-}symm} = (Z'_{AA} + a^2 Z'_{AB} + a Z'_{AC}) \tag{4.34a}$$

and similarly for phases B and C,

$$-\frac{dV_B}{dx} = Z'_{B\text{-}symm} I_B, \quad with \ Z'_{B\text{-}symm} = (Z'_{BB} + a Z'_{AB} + a^2 Z'_{BC}) \tag{4.34b}$$

$$-\frac{dV_C}{dx} = Z'_{C\text{-}symm} I_C, \quad with \ Z'_{C\text{-}symm} = (Z'_{CC} + a^2 Z'_{AC} + a Z'_{BC}) \tag{4.34c}$$

The values of the three impedances $Z'_{A\text{-}symm}$, $Z'_{B\text{-}symm}$, $Z'_{C\text{-}symm}$ in Eq. (4.34) are not exactly equal, but their average value is the positive sequence impedance. Because of slight differences in the three values, the voltage drops are slightly unsymmetrical (or the currents become slightly unsymmetrical for given symmetrical voltage drops). As discussed in Section 4.1.3, transposing a line eliminates or reduces these unsymmetries at power frequency, though not necessarily at higher frequencies.

In the capacitance matrix of a three-phase line, C'_{AA} would be the sum of the coupling capacitances to phases B and C and of the capacitance to ground, and C_{AB} would be the negative value of the coupling capacitance between phases A and B. Assuming symmetrical voltages, Eq. (4.32) would show slight unsymmetry in $[dI_{phase}/dx]$, analogous to that of Eq. (4.34).

4.1.2.4 Nominal π-Circuit for Equivalent Phase Conductors

The matrices in Eq. (4.31) and (4.32) are the basis for practically all EMTP line models. Even in studies where ground wires must be retained, it is still these matrices which are used, with phase numbers assigned to the ground wires as well. A three-phase line with one ground wire is conceptually a four-phase line, with phase no. 1, 2, 3 for phase conductors A, B, C and phase no. 4 for the ground wire.

One type of line representation uses cascade connections of nominal π-circuits, as discussed in Sections 4.2.1.1 and 4.2.2.1. This polyphase nominal π-circuit with a series impedance matrix and equal shunt capacitance matrices at both ends, as shown in Fig. 3.10, is directly obtained from the matrices in Eq. (4.31) and (4.32),

$$[R] + j\omega[L] = \mathcal{L} \cdot [Z'_{phase}] \tag{4.35}$$

and

$$\frac{1}{2}j\omega[C] \;=\; \frac{1}{2}j\omega\mathscr{L}\,[C^{/}_{phase}] \tag{4.36}$$

where $\mathscr{L}$ is the length of the line.

The cascade connection of nominal π-circuits approximates the even distribution of the line parameters reasonably well up to a certain frequency. It does ignore the frequency dependence of the resistances and inductances per unit length, however, and is therefore reasonably accurate only within a certain frequency range.

Strictly speaking, it may not be quite correct to treat the real part of $[Z'_{phase}]$ as a resistance, and the imaginary part as a reactance, as done in Eq. (4.35), especially for lines with ground wires. For a three-phase line with phases A, B, C and ground wire g, the original 4 x 4-matrix is reduced to a 3 x 3-matrix with elements

$$Z^{/}_{ik-reduced} \;=\; Z^{/}_{ik-original} \;-\; \frac{Z^{/}_{ig-original}\,Z^{/}_{kg-original}}{Z^{/}_{g\,g-original}} \tag{4.37}$$

Even if $Z'_{ik\text{-original}}$ could be separated into resistance and reactance without any doubt, the real part of the second term in Eq. (4.37) depends on the imaginary parts of the three impedances as well, unless the R/X-ratios of all three impedances were equal. There is also some doubt about separating $Z'_{ik\text{-original}}$ into resistance and reactance because of the earth as an implied return conductor, as mentioned in Section 3.1. Nonetheless, experience has shown that nominal π-circuits do give reasonable answers in many cases, and they are at least correct at the frequency at which the matrices were calculated (and probably reasonably accurate in a frequency range around that specific frequency).

Example for using nominal π-circuits

Electrostatic and magnetic coupling effects from energized power lines to parallel objects, such as fences or de-energized power lines, are important safety issues, and have been well described in two IEEE Committee Reports [37, 49]. A case of a fence running parallel to a power line (Fig. 4.11) is discussed here, as an application example for nominal π-circuits.[6] By simply treating the fence as a fourth phase conductor, the following series impedance and shunt capacitance matrices are obtained:

$$[Z^{/}_{phase}] = \begin{bmatrix} 0.4054 + j0.9859 & symmetric! \\ 0.0574 + j0.4265 & 0.4054 + j0.9859 \\ 0.0574 + j0.4265 & 0.0574 + j0.3742 & 0.4054 + j0.9859 \\ 0.0581 + j0.3168 & 0.0581 + j0.3291 & 0.0581 + j0.3044 & 1.8607 + j0.9953 \end{bmatrix} \Omega/km$$

and

---

[6]For electrically short lines, as in this example, electrostatic coupling effects can be solved by themselves with $[C'_{phase}]$, and magnetic coupling effects by themselves with $[Z'_{phase}]$. For solving such cases with the EMTP, it is usually easier to use nominal π-circuits which combine both effects. With that approach, electrically long lines can be studied as well, provided an appropriate number of π-circuits are connected in cascade.

$$[C'_{phase}] = \begin{bmatrix} 7.5709 & symmetric \\ -1.6266 & 7.3088 \\ -1.6304 & -0.8349 & 7.2999 \\ -0.1688 & -0.2758 & -0.1189 & 6.9727 \end{bmatrix} nF/km$$

From these matrices, the nominal π-circuit matrices are calculated with Eq. (4.35) and (4.36).

Power line conductors:
  $R'_{internal}$ = 0.348 Ω/km
  X'_A = 0.4755 Ω/km (60 Hz)
  (reactance at 1 m spacing)
  diameter = 12.7 mm
  frequency = 60 Hz
Fence:
  $R'_{internal}$ = 1.802 Ω/km
  solid conductor (nonmagnetic)
  diameter = 4.064 mm
  length = 2 km
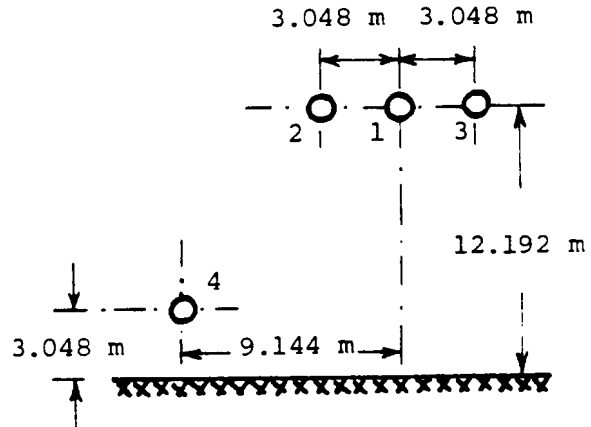
Fig. 4.11 - Fence 4 running parallel with power line phase conductors 1, 2, 3

Assume that the fence is insulated from the posts and nowhere grounded. To find the voltage on the fence due to capacitive coupling, simply connect voltage sources to phases 1, 2, 3 at the sending end, and leave 1, 2, 3 at the receiving end as well as 4 at both ends open-ended. Assuming V = 345 kV RMS, line-to-line, the fence voltage becomes V_4 = 3.97 kV. If phase 1 were at zero potential because of a phase-to-ground fault, with phases 2 and 3 still at rated voltage 345/√3 kV, then the fence voltage would increase to V_4 = 6.84 kV. These answers are practically independent of fence length.

Now assume that the 2 km long fence is grounded at the sending end and open-ended at the receiving end. To find the voltage in the fence for a load current of 1 kA RMS, simply add current sources to phases 1, 2, 3 at the receiving end, with symmetrical voltage sources at the sending end. Phase 4 is connected to ground at the sending end and open-ended at the receiving end. The answer will be $V_{4\text{-receiving end}}$ = 0.043 kV, which increases dramatically to 6.442 kV if the currents are changed to I_1 = 10 kA, I_2 = I_3 = 0 to simulate a phase-to-ground fault. For this last case, the fence current would be 1.526 kA if the fence were grounded at both ends. These answers are practically independent of the voltage on phases 1, 2, 3, which can easily be verified by setting them zero.

4.1.2.5 Continuous and Segmented Ground Wires

(a)   Circulating Currents in Continuous Ground Wires

Assume that ground wire no. 13 of Fig. 4.1 is grounded at each tower. If the ground wire is not eliminated,

then the series impedance matrix for equivalent phase conductors will be a 7 x 7 matrix. Its elements can then be used to calculate the longitudinally induced voltage in the ground wire,

$$-\frac{dV_g}{dx} = Z'_{gR} I_R + Z'_{gS} I_S + \ldots Z'_{gW} I_W + Z'_{gg} I_g \tag{4.38}$$

If tower and tower footing resistances are ignored, then $V_g = 1$ at all towers as long as span $<<$ wavelength, or

$$I_g = -\frac{Z'_{gR} I_R + Z'_{gS} I_S + \ldots Z'_{gW} I_W}{Z'_{gg}} \tag{4.39}$$

Since the mutual impedances from the phase conductors to the ground wire are never exactly equal, the numerator in Eq. (4.39) does not add up to zero even if the phase currents are symmetrical. Therefore, there is a nonzero ground wire current I_g, produced by positive sequence currents, which circulates through ground wire, towers and ground (Fig. 4.12). This circulating current produces additional losses, which show up as an increase in the value of the positive sequence resistance, compared with the resistance of the phase conductors. Handbook formulas would not contain this increase, but the elimination of the ground wires discussed in Section 4.1.2.1 will produce it automatically. In one particular case of a single-circuit 500 kV line, this increase was 6.5%.
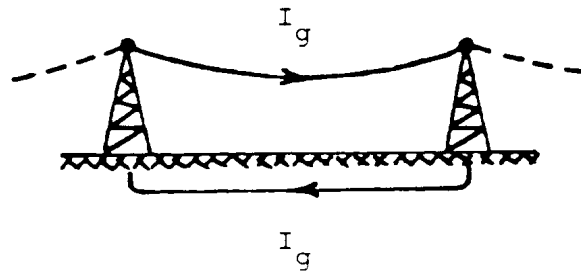
Fig. 4.12 - Circulating current in ground wire

The inclusion of tower and tower footing resistances may change the results of Eq. (4.39) somewhat. If we assume equal resistance at all towers, then it appears that the voltage drop produced by the current in the left loop (Fig. 4.13) is canceled by the voltage drop produced by the current in the middle loop, and Eq. (4.39) should therefore still be correct, except in the very first and very last span of the line. This assumes that the phase currents do not change from one span to the next, which is reasonable up to a certain frequency.
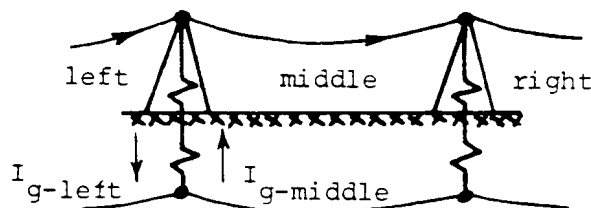
Fig. 4.13 - Cascade connection of loops

(b)   Segmented Ground Wires

    To avoid the losses associated with these circulating currents, some utility companies use segmented ground wires which are grounded at one tower, and insulated at adjacent towers to both ends of the segmentation interval, where they are interrupted as well (Fig. 4.14).

"T-configuration"
in segmentation interval
Δ = insulator
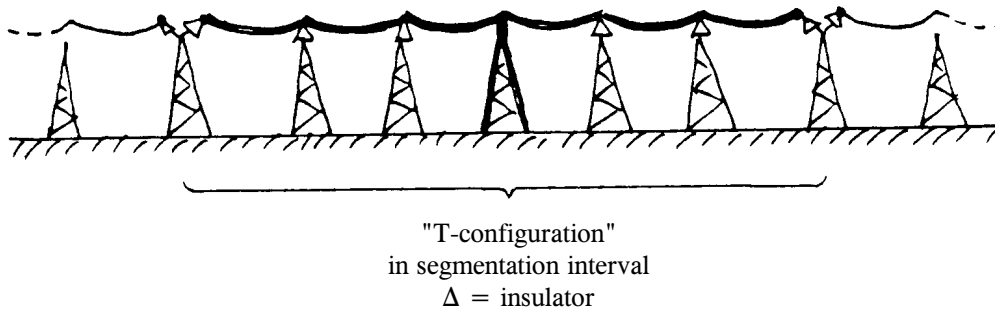
Fig. 4.14 - Segmented ground wires

They still act as electrostatic shields for lightning protection, but when struck by lightning, the segmentation gaps and the small insulators will flash over, thereby making the ground wire continuous again. The supporting routine LINE CONSTANTS has an option for segmented ground wires, which ignores[7] them in the calculation of the series impedance matrix since they have no influence on the voltage drops in the phase conductors, but takes them into account in the calculation of the capacitance matrix because the electrostatic field is not influenced by segmentation.

(c)   Reduction Effect of Continuous Ground Wires on Interference

    Interference from power lines in parallel telephone lines becomes a problem if there are high zero-sequence currents in the power line, e.g., in case of a single-phase-to-ground fault. Assume a three-phase line with one ground wire g and a parallel telephone line P as shown in Fig. 4.15. For zero sequence currents, which implies equal currents in phases A, B, C, the voltages in P induced by currents in A, B, C will add up in the same direction (Fig. 4.16). The voltage induced by the ground wire current I_g will have opposite polarity, however, since this

---

[7]An exception are studies where it can be assumed that the gaps and insulators have flashed over. For such studies, ground wires must be treated as continuous, as suggested by W.A. Lewis. Switching and lightning surge studies may fall into this category.
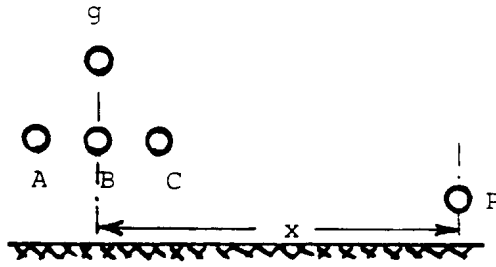
Fig. 4.15 - Parallel telephone line P close to a power line with phases A, B, C and ground wire g

current flows in opposite direction, thereby reducing the total induced voltage - dV_p/dx. Part of this beneficial reduction may be offset by an increase in the zero sequence currents because ground wires also reduce the zero sequence impedance of lines (typically by 5 to 15% with one
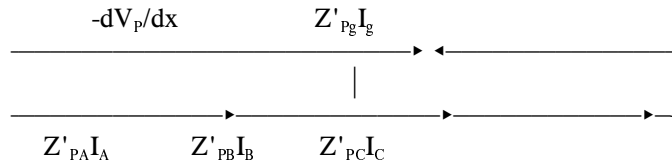
Fig. 4.16 - Induced voltage caused by currents $I_A = I_B = I_C$ and by I_g

steel ground wire, or 15 to 30% with one ACSR ground wire). The reduction effect of the ground wire on interference can be included in the calculations in two different ways:

(a)   Obtain the mutual impedances from matrices in which ground wires have been eliminated and in which the parallel telephone lines has been retained as an additional conductor. Then the reduction effect of the ground wires is automatically contained in calculating the magnetically induced voltage from

$$-\frac{dV_P}{dx} = Z'_{PA-reduced}I_A + Z'_{PB-reduced}I_B + Z'_{PC-reduced}I_C \tag{4.40a}$$

and, if needed, the electrostatically induced voltage for an insulated parallel telephone line from

$$0 = C'_{PA-reduced}V_A + C'_{PB-reduced}V_B + C'_{PC-reduced}V_C + C'_{PP-reduced}V_P \tag{4.40b}$$

(b)   Calculate the mutual impedances from P to the phases as well as to the ground wires (or obtain them from matrices in which the ground wires were retained), and recover the value of the ground wire currents with a "screening matrix" from the phase currents. By setting $V_g = 0$ in Eq. (4.27), the ground wire currents are obtained as

$$[I_g] = \underbrace{-[Z'_{gg}]^{-1}[Z_{gu}]}_{[F_{screen}]}[I_u] \tag{4.41}$$

with "u" indicating ungrounded phase currents here. The screening matrix $[F_{screen}]$ is the transpose of the distribution factor matrix $[D_{12}]$ of Eq. (III.14) in Appendix III, and as indicated there, can easily be obtained as a by-product of the matrix reduction process. As an example, Fig. 4.17 shows the standing waves of the phase currents of the sixth harmonic of 60 Hz in the two poles A, B of the Pacific Intertie HVDC line, as well as the currents in the two ground wires recovered with Eq. (4.41) [11].
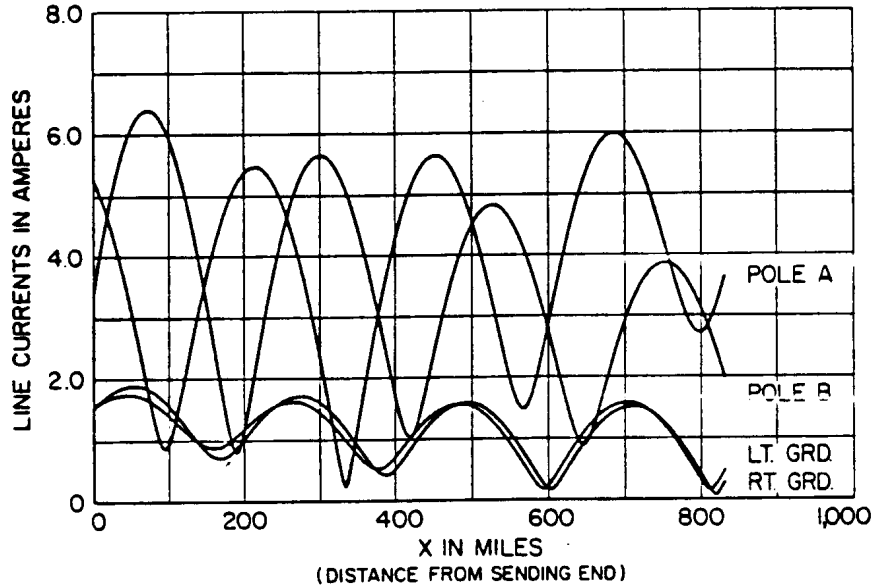
Fig. 4.17 - Currents of sixth harmonic in HVDC line [11]. [©] 1969 IEEE

4.1.3 Positive and Zero Sequence Parameters of Balanced[8] Lines

A "balanced" transmission line shall be defined as a line where all diagonal elements of $[Z'_{phase}]$ and $[C'_{phase}]$ are equal among themselves, and all off-diagonal elements are equal among themselves,

$$
\begin{bmatrix}
Z'_s & Z'_m & ..... & Z'_m \\
Z'_m & Z'_s & ..... & Z'_m \\
. & . & . & . \\
. & . & . & . \\
. & . & . & . \\
Z'_m & Z'_m & ..... & Z'_s
\end{bmatrix}
\begin{bmatrix}
C'_s & C'_m & ..... & C'_m \\
C'_m & C'_s & ..... & C'_m \\
. & . & . & . \\
. & . & . & . \\
. & . & . & . \\
C'_m & C'_m & ..... & C'_s
\end{bmatrix}
\qquad (4.42)
$$

---

[8]Also called "continuously transposed" in the EMTP Rule Book.
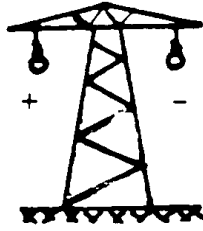
Fig. 4.18 - Bipolar dc line

The only line which is truly balanced is the symmetric bipolar dc line (Fig. 4.18), where $Z'_{11} = Z'_{22} = Z'_s$ and $Z'_{12} = Z'_m$. Single-circuit three-phase lines become more or less balanced if the line is transposed, as shown in Fig. 4.19, provided the length of the "barrel" (= 3 sections, or one cycle of the transposition scheme) is much less than the wavelength of the frequencies involved in the particular study. While the Westinghouse Reference Book [51, p. 777] mentions that a barrel may be 80 to 160 km in length on long lines, a German handbook [52, p. 555] recommends that one barrel be no longer than 80 km (at 50 Hz, or 67 km at 60 Hz) for lines with triangular conductor configuration, or 40 km (at 50 Hz, or 33 km at 60 Hz) for other conductor configurations. Whatever the length of the barrel, it is important to realize that while
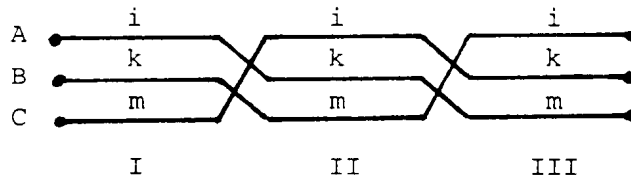
Fig. 4.19 - Transposition scheme for single three-phase circuit

a line may be reasonably balanced at power frequency, there may be enough unbalance at higher frequencies[9]. If the barrel length is much shorter than the wavelength, then series impedances can be averaged by themselves through the three sections, and shunt capacitances can be averaged by themselves, e.g., for the impedances of the line in Fig. 4.19,

$$\frac{1}{3}\left[\begin{bmatrix} Z'_{ii} & Z'_{ik} & Z'_{im} \\ Z'_{ki} & Z'_{kk} & Z'_{km} \\ Z'_{mi} & Z'_{mk} & Z'_{mm} \end{bmatrix} + \begin{bmatrix} Z'_{kk} & Z'_{km} & Z'_{ki} \\ Z'_{mk} & Z'_{mm} & Z'_{mi} \\ Z'_{ik} & Z'_{im} & Z'_{ii} \end{bmatrix} + \begin{bmatrix} Z'_{mm} & Z'_{mi} & Z'_{mk} \\ Z'_{im} & Z'_{ii} & Z'_{ik} \\ Z'_{km} & Z'_{ki} & Z'_{kk} \end{bmatrix}\right] = \begin{bmatrix} Z'_s & Z'_m & Z'_m \\ Z'_m & Z'_s & Z'_m \\ Z'_m & Z'_m & Z'_s \end{bmatrix}$$

with

---

[9]At the time of writing, studies at B.C. Hydro seem to indicate that transposed single-circuit lines with horizontal conductor configuration cannot be treated as balanced lines in switching surge studies.

$$Z'_s = \frac{1}{3}(Z'_{ii} + Z'_{kk} + Z'_{mm})$$

$$Z'_m = \frac{1}{3}(Z'_{ik} + Z'_{km} + Z'_{mi}) \qquad (4.43)$$

The averaging process for the shunt capacitances is analogous.

4.1.3.1 Positive and Zero Sequence Parameters of Single-Circuit Three-Phase Lines

Balanced single-circuit three-phase lines can be studied much easier with symmetrical or α, β, 0-components because the three coupled equations in the phase domain,

$$-\left[\frac{dV_{phase}}{dx}\right] = \begin{bmatrix} Z'_s & Z'_m & Z'_m \\ Z'_m & Z'_s & Z'_m \\ Z'_m & Z'_m & Z'_s \end{bmatrix}[I_{phase}] \qquad (4.44)$$

become three decoupled equations with symmetrical components,

$$-dV_{zero}/dx = Z'_{zero}I_{zero}$$
$$-dV_{neg}/dx = Z'_{pos}I_{neg}$$
$$-dV_{pos}/dx = Z'_{pos}I_{pos} \qquad (4.45)$$

or with α, β, 0-components,

$$-dV_{zero}/dx = Z'_{zero}I_{zero}$$

$$-dV_{\alpha}/dx = Z'_{pos}I_{\alpha} \qquad (4.46)$$

$$-dV_{\beta}/dx = Z'_{pos}I_{\beta}$$

Since transformation to symmetrical components involves complex coefficients, symmetrical components are not well suited for transient analysis where all variables are real, and are therefore only briefly discussed in Section 4.1.4. The impedances needed in both systems (4.45) and (4.46) are the same, however, namely Z'_{zero} and Z'_{pos}. The balanced distributed-parameter line models in the EMTP use transformations to α, β, 0-components, due to Edith Clarke [44],

$$[v_{phase}] = [T][v_{0\alpha\beta}] \qquad [v_{0\alpha\beta}] = [T]^{-1}[v_{phase}]$$

and

$$[i_{phase}] = [T][i_{0\alpha\beta}] \qquad [i_{0\alpha\beta}] = [T]^{-1}[i_{phase}] \tag{4.47}$$

where

$$[v_{0\alpha\beta}] = \begin{bmatrix} v_0 \\ v_\alpha \\ v_\beta \end{bmatrix}$$

with

$$[T] = \frac{1}{\sqrt{3}} \begin{bmatrix} 1 & \sqrt{2} & 0 \\ 1 & -\frac{1}{\sqrt{2}} & \frac{\sqrt{3}}{\sqrt{2}} \\ 1 & -\frac{1}{\sqrt{2}} & -\frac{\sqrt{3}}{\sqrt{2}} \end{bmatrix}$$

and

$$[T]^{-1} = \frac{1}{\sqrt{3}} \begin{bmatrix} 1 & 1 & 1 \\ \sqrt{2} & -\frac{1}{\sqrt{2}} & -\frac{1}{\sqrt{2}} \\ 0 & \frac{\sqrt{3}}{\sqrt{2}} & -\frac{\sqrt{3}}{\sqrt{2}} \end{bmatrix} \tag{4.48}$$

The columns in [T] and [T]$^{-1}$ are normalized; in that case [T] is orthogonal,

$$[T]^{-1} = [T]^t \tag{4.49}$$

Applying this transformation to Eq. (4.44) produces

$$-\begin{bmatrix} dV_0/dx \\ dV_\alpha/dx \\ dV_\beta/dx \end{bmatrix} = \begin{bmatrix} Z'_s + 2Z'_m & 0 & 0 \\ 0 & Z'_s - Z'_m & 0 \\ 0 & 0 & Z'_s - Z'_m \end{bmatrix} \begin{bmatrix} I_0 \\ I_\alpha \\ I_\beta \end{bmatrix}$$

which is identical with Eq. (4.46), with

$$Z'_{zero} = Z'_s + 2Z'_m \tag{4.50a}$$

Eq. (4.50) and its inverse relationship is the same as discussed previously in Eq. (3.6) and (3.4). Going from the

$$Z'_{pos} = Z'_s - Z'_m \tag{4.50b}$$

three coupled equations in (4.44) to the three decoupled equations in (4.46) allows us to solve the line as if it consisted of three single-phase lines, which is much simpler than trying to solve the equations of a three-phase line.

The positive sequence inductance of overhead lines is practically constant, while the positive sequence resistance remains more or less constant until skin effect in the conductors becomes noticeable, as shown in Fig. 4.20. Zero sequence inductance and resistance are very much frequency-dependent, due to skin effects in the earth return.
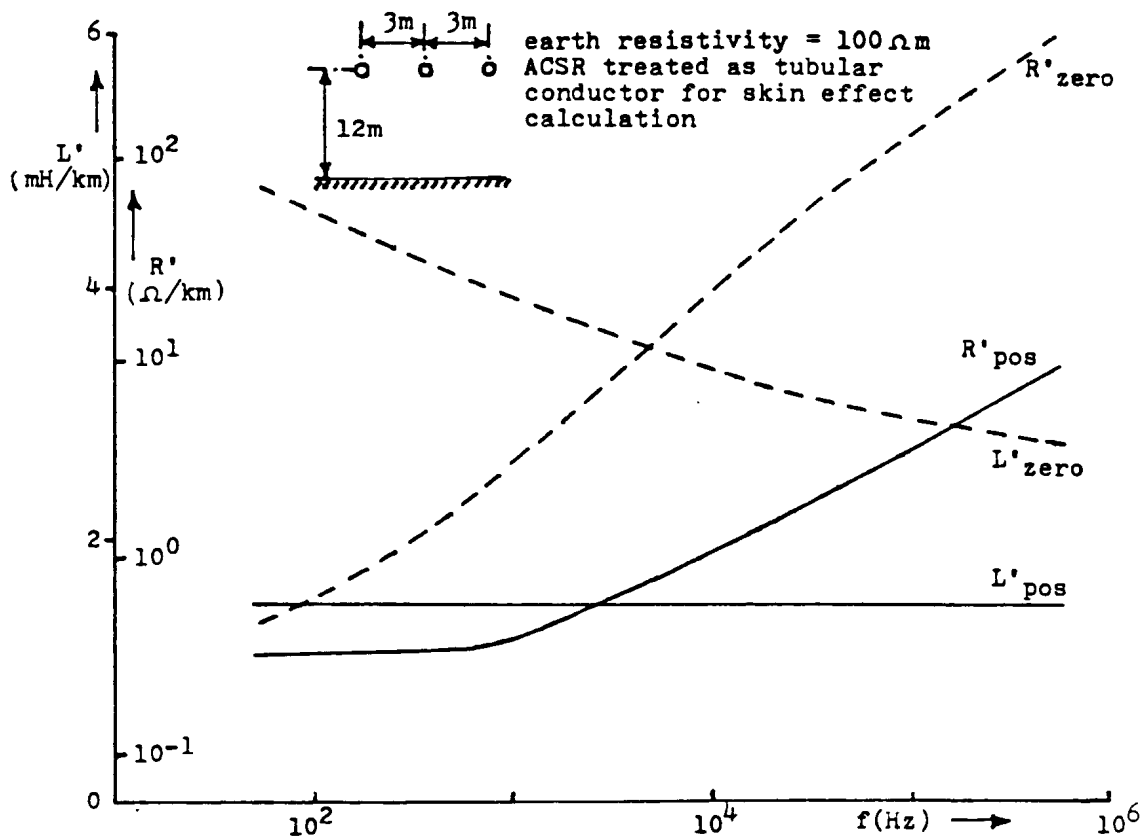
Fig. 4.20 - Positive and zero sequence resistance and inductance of a three-phase line

The shunt capacitance matrix of a balanced three-phase line becomes diagonal in α, β, 0-components as well, with

$$C'_{zero} = C'_s + 2C'_m \tag{4.51a}$$

$$C'_{pos} = C'_s - C'_m \tag{4.51b}$$

4-30

which is the inverse relationship of Eq. (3.13). The capacitances are constant over the frequency range of interest to power engineers.

Comparison with results from handbook formulas

The positive and zero sequence parameters obtained from the supporting routines LINE CONSTANTS and CABLE CONSTANTS may differ from those obtained with handbook formulas. Since some EMTP users may make comparisons, it may be worthwhile to explain the major differences for a specific example. Assume a typical 500 kV line with horizontal phase configuration, with phases 40 feet apart at an average height above ground of 50 feet. Each phase consists of a symmetrical bundle with 4 subconductors spaced 18 inches apart. Subconductor diameter = 0.9 inches, dc resistance = 0.1686 Ω/mile, GMR = 0.3672 inches. Throughout this comparison, the bundle conductors are represented as equivalent conductors with r_{equiv} = 7.80524 inches from Eq. (4.30) and GMR_{equiv} = 7.41838 inches from Eq. (4.29).

For positive sequence capacitance, most handbooks give the formula

$$C'_{pos} = \frac{2\pi\varepsilon_0}{\ln\dfrac{d_m}{r_{\equiv}}} \tag{4.52}$$

with $d_m = \sqrt[3]{d_{AB}d_{AC}d_{BC}}$ (geometric mean distance among the three phases).

This produces a value approx. 4% lower than the more accurate value from Eq. (4.51) for the 500 kV line described above. The formula for zero sequence capacitance in [52] and [53],

$$C'_{zero} = \frac{2\pi\varepsilon_0}{\ln\dfrac{2h_m D_m{}^2}{r_{equiv}d_m{}^2}} \qquad (Siemens) \tag{4.53}$$

with

$\quad h_m = \sqrt[3]{h_A h_B h_C}$ (geometric mean height),

$\quad D_m = \sqrt[3]{D_{AB}D_{AC}D_{BC}}$ (geometric mean distance between one phase and image of another phase),

can be derived by averaging the diagonal and off-diagonal elements in the [P'$_{phase}$]-matrix among themselves to account for transposition. Eq. (4.51) has this averaging process implied in the [C'$_{phase}$]-matrix. Both give practically the same answer, with results from Eq. (4.53) 0.23% lower than those from Eq. (4.51). In [51], Eq. (4.53) is further simplified by assuming $D_m \approx 2h_m$,

$$C'_{zero} = \frac{2\pi\varepsilon_0}{\ln\dfrac{(2h_m)^3}{r_{equiv}d_m{}^2}} \qquad (Westinghouse) \tag{4.54}$$

which produces a value 4% higher than the value from Eq. (4.51). While Eq. (4.54) is theoretically less accurate, the value may actually be closer to measured values because the influence of towers, which is neglected in all

4-31

formulas, typically increases the calculated zero sequence capacitance by about 8 to 9% on 110 kV lines, about 6% on 220 and 380 kV lines, and about 4% on 700 kV lines [54, p. 218].

The formulas for zero and positive sequence impedances in most handbooks are based on the assumption that parameter a in Eq. (4.10) is so small that only the first term in the series of Eq. (4.11) must be retained. For normal phase spacings this is probably a reasonable assumption at power frequency 50 or 60 Hz. Then, after all diagonal and off-diagonal elements have been averaged out among themselves through transposition,

$$\Delta R'_s = \Delta R'_m \approx \frac{\omega \pi \cdot 10^{-4}}{2} \quad in \ \Omega/km$$

and

$$\Delta X'_s \approx 2\omega \cdot 10^{-4}[0.6159315 - \ln(2h_m k \frac{\sqrt{f}}{\sqrt{\rho}})] \quad in \ \Omega/km \tag{4.55}$$

$$\Delta X'_m \approx 2\omega \cdot 10^{-4}[0.6159315 - \ln(D_m k \frac{\sqrt{f}}{\sqrt{\rho}})] \quad in \ \Omega/km$$

with

$$k = 4\pi \cdot \sqrt{5} \cdot 10^{-4}$$

This leads to the expression

$$Z'_{pos} = R'_{ac} + j2\omega \cdot 10^{-4} \ln\frac{d_m}{GMR_{equiv}} \quad in \ \Omega/km \tag{4.56}$$

with R'_{ac} = ac resistance of equivalent phase conductor. It is interesting that the influence of ground resistivity and of conductor height, which is present in Z'_s and Z'_m, completely disappears here in taking the difference, $Z'_{pos} = Z'_s - Z'_m$. Eq. (4.56) is the formula found in most handbooks. Table 4.3 compares results from Eq. (4.50) with results from Eq. (4.56) for the 500 kV line described above with the following additional assumptions: Earth resistivity = 100 Ωm; skin effect within conductors ignored to limit differences to influence of earth return (that is, $R'_{ac} = R'_{dc}$ and GMR_{equiv} = constant).

Table 4.3 - Accurate and approximate positive sequence resistance and inductance

	ACCURATE R'$_{pos}$ and L'$_{pos}$ from Eq. (4.50)		APPROXIMATE R'$_{pos}$ and L'$_{pos}$ from Eq. (4.56)	
f (Hz)	R' (Ω/mile)	L' (mH/mile)	R' (Ω/mile)	L' (mH/mile)

10^{-6}	0.04215	1.417	0.04215	1.417
10	0.04215	1.416	0.04215	1.417
100	0.04229	1.416	0.04215	1.417
1 000	0.05003	1.416	0.04215	1.417
10 000	0.3528	1.413	0.04215	1.417
100 000	6.229	1.401	0.04215	1.417

Table 4.3 shows that L'$_{pos}$ from Eq. (4.56) is quite accurate over a wide frequency range, whereas R'$_{pos}$ becomes less accurate as the frequency increases (0.33% error at 100 Hz, but wrong by orders of magnitude at 100 kHz). The increase in R'$_{pos}$ in the higher frequency range is caused by eddy currents in the earth, as indicated in Fig. 4.21 for a bipolar dc line. Ground wires also influence the positive sequence impedance, as mentioned in Section 4.1.2.5 (a). Both influences are ignored in Eq. (4.56), but automatically included in the method described here.
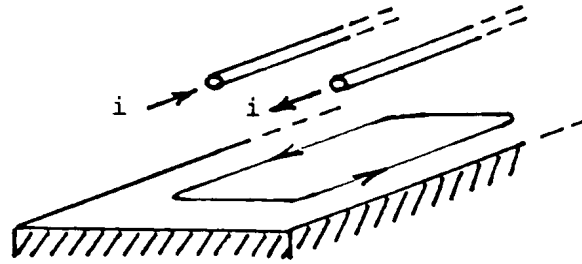
Fig. 4.21 - Eddy currents in earth

The zero sequence impedance obtained from Eq. (4.55) is

$$Z'_{zero} = (R'_{ac} + \frac{3\omega\pi \cdot 10^{-4}}{2}) + j6\omega \cdot 10^{-4} \ln\left(\frac{658.87\frac{\sqrt{\rho}}{\sqrt{f}}}{3\sqrt{GMR_{equiv} \cdot d_m^2}} \right) \quad in \ \Omega/km \qquad (4.57)$$

with f in Hz, ρ in Ωm, and GMR$_{equiv}$ and d$_m$ in m. Eq. (4.57) is the same equation as in [51, 52, 53]. Table 4.4 compares the approximate results from Eq. (4.57) with the accurate results from Eq. (4.50). The inductance L'$_{zero}$ is reasonably accurate over a wide frequency range (-0.75% error at 100 Hz, -33% error at 100 kHz), but the resistance R'$_{zero}$ is less accurate (4.6% error at 100 Hz, 159% error at 100 kHz).

Table 4.4 - Accurate and approximate zero sequence resistance and inductance

	ACCURATE		APPROXIMATE	
	R'$_{zero}$ and L'$_{zero}$ from Eq. (4.50)		R'$_{zero}$ and L'$_{zero}$ from Eq. (4.57)	
f (Hz)	R' (Ω/mile)	L' (mH/mile)	R' (Ω/mile)	L' (mH/mile)

4-33

10^{-6}	0.04215	13.94	0.04215	13.94
10	0.08905	6.170	0.08980	6.158
100	0.4960	5.084	0.05187	5.046
1 000	4.169	4.052	4.807	3.934
10 000	32.12	3.164	47.69	2.823
100 000	184.0	2.568	476.6	1.711

4.1.3.2 Positive and Zero Sequence Parameters of Balanced M-Phase Lines

The EMTP can handle balanced distributed-parameter lines not only for the case of a three-phase line, but for any number of phases M. For this general case, the α, β, 0-transformation of Eq. (4.47) has been generalized to M phases, with the transformation matrix [55]

$$[T] = \begin{bmatrix} \dfrac{1}{\sqrt{M}} & \dfrac{1}{\sqrt{2}} & \dfrac{1}{\sqrt{6}} & \cdots & \dfrac{1}{\sqrt{J(J-1)}} & \cdots & \dfrac{1}{\sqrt{M(M-1)}} \\[2ex] \dfrac{1}{\sqrt{M}} & -\dfrac{1}{\sqrt{2}} & \dfrac{1}{\sqrt{6}} & \cdots & \dfrac{1}{\sqrt{J(J-1)}} & \cdots & \dfrac{1}{\sqrt{M(M-1)}} \\[2ex] \dfrac{1}{\sqrt{M}} & 0 & -\dfrac{2}{\sqrt{6}} & . & . & . & . \\[2ex] . & . & . & . & -\dfrac{(J-1)}{\sqrt{J(J-1)}} & . & . \\[2ex] . & . & . & . & 0 & . & . \\[2ex] . & . & . & . & . & . & . \\[2ex] \dfrac{1}{\sqrt{M}} & 0 & 0 & . & 0 & . & -\dfrac{(M-1)}{\sqrt{M(M-1)}} \end{bmatrix} \qquad (4.58)$$

where again

$$[T]^{-1} = [T]^{t} \qquad (4.59)$$

[T] of Eq. (4.48) is a special case of Eq. (4.58) for M = 3 if we assume that the phases are numbered 2, 3, 1 in Eq. (4.47) and if the α, β, 0-quantities are ordered 0, β, -α (sign reversal on α).

Applying this M-phase α, β, 0-transformation[10] to the matrices of M-phase balanced lines produces diagonal matrices of the form

---

[10]In the UBC EMTP, and in older versions of the BPA EMTP, Karrenbauer's transformation [57] is used instead, which produces the same diagonal matrices, but does not have the property of Eq. (4.59). This property is important because it makes the balanced line just a special case of the untransposed line discussed in Section 4.1.5.

$$
\begin{bmatrix}
Z'_{zero} & & & & & \\
& Z'_{pos} & & & & \\
& & Z'_{pos} & & & \\
& & & \cdot & & \\
& & & & \cdot & \\
& & & & & \cdot & \\
& & & & & & Z'_{pos}
\end{bmatrix}
$$

with the first diagonal element being the zero sequence (ground mode) impedance, and the next M-1 diagonal elements being the positive sequence (aerial mode) impedance,

$$Z'_{zero} = Z'_s + (M - 1)Z'_m \tag{4.60a}$$

$$Z'_{pos} = Z'_s - Z'_m \tag{4.60b}$$

and similarly for the capacitances,

$$C'_{zero} = C'_s + (M - 1)C'_m \tag{4.61a}$$

$$C'_{pos} = C'_s - C'_m \tag{4.61b}$$

To refer to the two distinct diagonal elements as zero and positive sequence may be confusing, because the concept of sequence values has primarily been used for three-phase lines. "Ground mode" and "aerial mode" may be more appropriate. Confusion is most likely to arise for double-circuit three-phase lines, where each three-phase line has its own zero and positive sequence values defined by Eq. (4.50) and (4.51) with symmetrical components used for each three-phase circuit, while in the context of this section the double-circuit line is treated as a six-phase line with different zero and positive sequence values defined by Eq. (4.60) and (4.61). The fact that the terms zero and positive sequence are used for $M \neq 3$ as well comes from the generalization of symmetrical components of Section 4.1.4 to M phases with the transformation matrix [56, p. 155]

$$
[S_{M-phase}] =
\begin{bmatrix}
s_{11} & s_{12} & \cdots & s_{1M} \\
s_{21} & s_{22} & \cdots & s_{2M} \\
\cdot & \cdot & \cdot & \cdot \\
s_{M1} & s_{M2} & \cdots & s_{MM}
\end{bmatrix}
\tag{4.62a}
$$

with

$$s_{ik} = \frac{1}{\sqrt{M}} \exp\{-j\frac{2\pi}{M}(i-1)(k-1)\} \tag{4.62b}$$

A special case of interest for symmetric bipolar dc lines[11] is M = 2. In this case [T] of Eq. (4.58) and [S] of Eq. (4.62a) are identical,

$$[T_{2-phase}] = \frac{1}{\sqrt{2}}\begin{bmatrix} 1 & 1 \\ 1 & -1 \end{bmatrix} \tag{4.63}$$

4.1.3.3 Two Identical Three-Phase Lines with Zero Sequence Coupling Only

Just as a transposed single-circuit three-phase line can usually be approximated as a balanced line, so two identical and parallel three-phase lines can often be approximated as "almost balanced" lines with an impedance matrix of the form

$$\begin{bmatrix} Z'_s & Z'_m & Z'_m & Z'_p & Z'_p & Z'_p \\ Z'_m & Z'_s & Z'_m & Z'_p & Z'_p & Z'_p \\ Z'_m & Z'_m & Z'_s & Z'_p & Z'_p & Z'_p \\ Z'_p & Z'_p & Z'_p & Z'_s & Z'_m & Z'_m \\ Z'_p & Z'_p & Z'_p & Z'_m & Z'_s & Z'_m \\ Z'_p & Z'_p & Z'_p & Z'_m & Z'_m & Z'_s \end{bmatrix} \tag{4.64}$$

The transposition scheme of Fig. 4.22 would produce such a matrix form, which implies that the two circuits are only coupled in zero sequence, but not in positive or negative sequence. Such a complicated transposition scheme is seldom, if ever, used, but the writer suspects that positive and negative sequence couplings in the more common double-circuit transposition scheme of Fig. 4.23 is often so weak that the model discussed here may be a useful approximation for the case of Fig. 4.23 as well.

---

[11]To be consistent, lines with M = 1 and M = 2 are called "single-phase" and "two-phase" lines, respectively, in this manual. This differs from the IEEE Standards [76, p. 647], in which circuits with one phase conductor and one neutral conductor (which could be replaced by ground return), as well as circuits with two phase conductors and one neutral conductor (or ground return) are both called single-phase circuits for historical reasons. For M ≥ 3, the definition in the IEEE Standards is the same as in this manual.
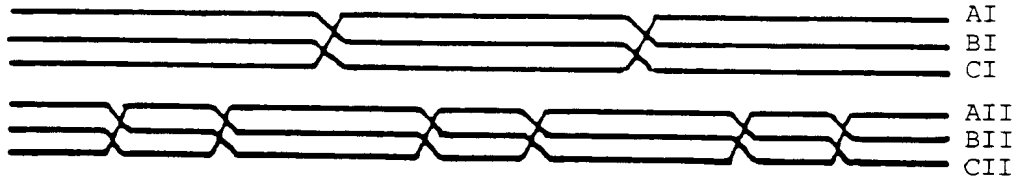
Fig. 4.22 - Double-circuit transposition scheme with zero sequence coupling only

T h e

matrix of Eq. (4.64) is diagonalized by modifying the transformation matrix of Eq. (4.58) to

$$[T] = \frac{1}{\sqrt{6}} \begin{bmatrix} 1 & 1 & \sqrt{3} & 1 & 0 & 0 \\ 1 & 1 & -\sqrt{3} & 1 & 0 & 0 \\ 1 & 1 & 0 & -2 & 0 & 0 \\ 1 & -1 & 0 & 0 & \sqrt{3} & 1 \\ 1 & -1 & 0 & 0 & -\sqrt{3} & 1 \\ 1 & -1 & 0 & 0 & 0 & -2 \end{bmatrix} \tag{4.65}$$

with $[T]^{-1} = [T]^t$ again, which produces the diagonal matrix

$$\begin{bmatrix} Z'_G & & & & & \\ & Z'_{IL} & & & & \\ & & Z'_L & & & \\ & & & Z'_L & & \\ & & & & Z'_L & \\ & & & & & Z'_L \end{bmatrix} \tag{4.66}$$

If each circuit has three-phase sequence parameters Z'_{zero}, Z'_{pos}, and if the three-phase zero sequence coupling between the two circuits is $Z'_{zero\text{-}coupling}$, then the ground mode G, inter-line mode IL and line mode L values required by the EMTP are found from

$$Z'_G = Z'_{zero} + Z'_{zero\text{-}coupling}$$
$$Z'_{IL} = Z'_{zero} - Z'_{zero\text{-}coupling} \tag{4.67}$$
$$Z'_L = Z'_{pos}$$

with identical equations for the capacitances.

If the two three-phase circuits are not identical, then the transformation matrix of Eq. (4.65) can no longer be used; instead, [T] depends on the particular tower configuration.

4-37

4.1.4 Symmetrical Components

Symmetrical components are not used as such in the EMTP, except that the parameters of balanced lines after transformation to M-phase α, β, 0-components are the same as the parameters of symmetrical components, namely zero and positive sequence values. The supporting routine LINE CONSTANTS does have output options for more detailed symmetrical component information, however, which may warrant some explanations.

In addition to zero and positive sequence values, LINE CONSTANTS also prints full symmetrical component matrices. Its diagonal elements are the familiar zero and positive sequence values of the line; they are correct for the untransposed line as well as for a line which has been balanced through proper transpositions. The off-diagonal elements are only meaningful for the untransposed case, because they would become zero for the balanced line. For the untransposed case, these off-diagonal elements are used to define unbalance factors [47, p. 93]. The full symmetrical component matrices are no longer symmetric, unless the columns for positive and negative sequence are exchanged [27]. This exchange is made in the output of the supporting routine LINE CONSTANTS with rows listed in order "zero, pos, neg,..." and columns in order "zero, neg, pos,...". With this trick, matrices can be printed in triangular form (elements in and below the diagonal), as is done with the matrices for individual and equivalent phase conductors.

Symmetrical components for two-phase lines are calculated with the transformation matrix of Eq. (4.63), while those of three-phase lines are calculated with

$$[v_{phase}] = [S][v_{symm}] \quad and \quad [v_{symm}] = [S]^{-1}[v_{phase}] \tag{4.68a}$$

identical for currents,

$$where \quad [v_{symm}] = \begin{bmatrix} v_{zero} \\ v_{pos} \\ v_{neg} \end{bmatrix}$$

$$[S] = \frac{1}{\sqrt{3}} \begin{bmatrix} 1 & 1 & 1 \\ 1 & a^2 & a \\ 1 & a & a^2 \end{bmatrix}$$

$$[S]^{-1} = \frac{1}{\sqrt{3}} \begin{bmatrix} 1 & 1 & 1 \\ 1 & a & a^2 \\ 1 & a^2 & a \end{bmatrix} \tag{4.68b}$$

and $a = e^{j120°}$.

The columns in these matrices are normalized[12]; in that form, [S] is unitary,

$$[S]^{-1} = [S^{\star}]^t \tag{4.69}$$

---

[12]The electric utility industry usually uses unnormalized transformation, in which the factor for the [S]-matrix is 1 instead of $1 / \sqrt{3}$, and for the [S]$^{-1}$-matrix 1/3 instead of $1 / \sqrt{3}$. The symmetrical component impedances are identical in both cases, but the sequence currents and voltages differ by a factor of $\sqrt{3}$.

where "*" indicates conjugate complex and "t" transposition.

For M ≥ 3, the supporting routine LINE CONSTANTS assumes three-phase lines in parallel. Examples:

M = 6: Two three-phase lines in parallel

M = 9: Three-phase lines in parallel

M = 8: Two three-phase lines in parallel, with equivalent phase conductors no. 7 and 8 ignored in the transformation to symmetrical components.

The matrices are then transformed to three-phase symmetrical components and <u>not to M-phase symmetrical components</u> of Eq. (4.62). For example for M = 6 (double-circuit three-phase line),

$$[Z'_{symm}] = \begin{bmatrix} [S]^{-1} & 0 \\ 0 & [S]^{-1} \end{bmatrix} [Z'_{phase}] \begin{bmatrix} [S] & 0 \\ 0 & [S] \end{bmatrix} \tag{4.70}$$

with [S] defined by Eq. (4.68), Eq. (4.70) produces the three-phase symmetrical component values required in Eq. (4.67).

Balancing of double-circuit three-phase lines through transpositions never completely diagonalizes the respective symmetrical component matrices. The best that can be achieved is with the seldom-used transposition scheme of Fig. 4.22, which leads to

$$[Z'_{symm}] = \begin{bmatrix} Z'_{zero-I} & 0 & 0 & Z_{zero-coupling} & 0 & 0 \\ 0 & Z'_{pos-I} & 0 & 0 & 0 & 0 \\ 0 & 0 & Z'_{pos-I} & 0 & 0 & 0 \\ Z_{zero-coupling} & 0 & 0 & Z'_{zero-II} & 0 & 0 \\ 0 & 0 & 0 & 0 & Z'_{pos-II} & 0 \\ 0 & 0 & 0 & 0 & 0 & Z'_{pos-II} \end{bmatrix}$$

$$\tag{4.71}$$

If both circuits are identical, then Z'$_{zero-I}$ = Z'$_{zero-II}$ = Z'$_{zero}$, and Z'$_{pos-I}$ = Z'$_{pos-II}$ = Z'$_{pos}$; in that case, the transformation matrix of Eq. (4.65) can be used for diagonalization. The more common transposition scheme of Fig. 4.23 produces positive and zero sequence coupling between the two
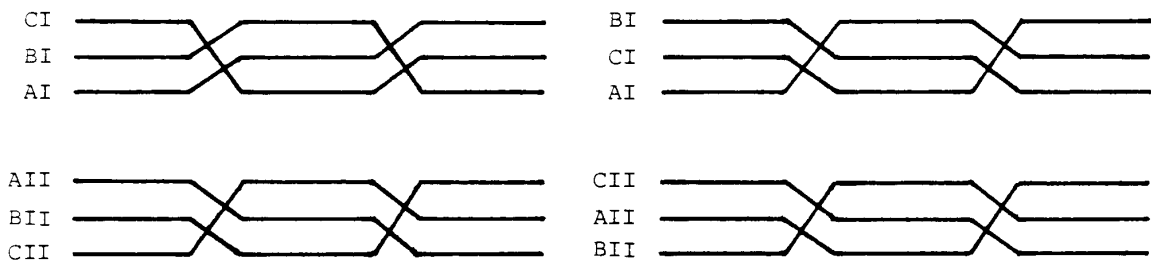
(a)   barrels rolled in   (b)   barrels rolled in
       opposite direction   same direction

Fig. 4.23 - Double-circuit transposition scheme

circuits as well, with the nonzero pattern of the matrix in Eq. (4.71) changing to

$$
\begin{bmatrix}
X & 0 & 0 & | & X & 0 & 0 \\
0 & X & 0 & | & 0 & X & 0 \\
0 & 0 & X & | & 0 & 0 & X \\
\overline{X} & \overline{0} & \overline{0} & | & \overline{X} & \overline{0} & \overline{0} \\
0 & X & 0 & | & 0 & X & 0 \\
0 & 0 & X & | & 0 & 0 & X
\end{bmatrix}
$$

where "X" indicates nonzero terms. Re-assigning the phases in Fig. 4.23(b) to CI, BI, AI, AII, BII, CII from top to bottom would change the matrix further to cross-couplings between positive sequence of one circuit and negative sequence of the other circuit, and vice versa,

$$
\begin{bmatrix}
X & 0 & 0 & | & X & 0 & 0 \\
0 & X & 0 & | & 0 & 0 & X \\
0 & 0 & X & | & 0 & X & 0 \\
\overline{X} & \overline{0} & \overline{0} & | & \overline{X} & \overline{0} & \overline{0} \\
0 & 0 & X & | & 0 & X & 0 \\
0 & X & 0 & | & 0 & 0 & X
\end{bmatrix}.
$$

4.1.5 Modal Parameters

From the discussions of Section 4.1.3 it should have become obvious that the solution of M-phase transmission line equations becomes simpler if the M coupled equations can be transformed to M decoupled equations. These decoupled equations can then be solved as if they were single-phase equations. For balanced lines, this transformation is achieved with Eq. (4.58).

Many lines are untransposed, however, or each section of a transposition barrel may no longer be short compared with the wave length of the highest frequencies occurring in a particular study, in which case each section must be represented as an untransposed line. Fortunately, the matrices of untransposed lines can be diagonalized as well, with transformations to "modal" parameters derived from eigenvalue/eigenvector theory. The transformation matrices for untransposed lines are no longer known a priori, however, and must be calculated for each particular pair of parameter matrices $[Z'_{phase}]$ and $[Y'_{phase}]$.

To explain the theory, let us start again from the two systems of equations (4.31) and (4.32),

$$-\left[\frac{dV_{phase}}{dx}\right] = [Z'_{phase}]\,[I_{phase}] \tag{4.72a}$$

and

$$-\left[\frac{dI_{phase}}{dx}\right] = [Y'_{phase}][V_{phase}] \tag{4.72b}$$

with $[Y'_{phase}] = j\omega[C'_{phase}]$ if shunt conductances are ignored, as is customarily done. By differentiating the first equation with respect to x, and replacing the current derivative with the second equation, a second-order differential equation for voltages only is obtained,

$$\left[\frac{d^2V_{phase}}{dx^2}\right] = [Z'_{phase}]\,[Y'_{phase}]\,[V_{phase}] \tag{4.73a}$$

Similarly, a second-order differential equation for currents only can be obtained,

$$\left[\frac{d^2I_{phase}}{dx^2}\right] = [Y'_{phase}]\,[Z'_{phase}]\,[I_{phase}] \tag{4.73b}$$

where the matrix products are now in reverse order from that in Eq. (4.73a), and therefore different. Only for balanced matrices, and for the lossless high-frequency approximations discussed in Section 4.1.5.2, would the matrix products in Eq. (4.73a) and (4.73b) be identical.

With eigenvalue theory, it becomes possible to transform the two coupled equations (4.73) from phase quantities to "modal" quantities in such a way that the equations become decoupled, or in terms of matrix algebra, that the associated matrices become diagonal, e.g., for the voltages,

$$\left[\frac{d^2V_{mode}}{dx^2}\right] = [\Lambda]\,[V_{mode}] \tag{4.74}$$

with $[\Lambda]$ being a diagonal matrix. To get from Eq. (4.73a) to (4.74), the phase voltages must be transformed to mode voltages, with

$$[V_{phase}] = [T_v]\,[V_{mode}] \tag{4.75a}$$

and

$$[V_{mode}] = [T_v]^{-1}\,[V_{phase}] \tag{4.75b}$$

Then Eq. (4.73a) becomes

$$\left[\frac{d^2V_{mode}}{dx^2}\right] = [T_v]^{-1}\,[Z'_{phase}]\,[Y'_{phase}]\,[T_v]\,[V_{mode}] \tag{4.76a}$$

4-41

which, when compared with Eq. (4.74), shows us that

$$[\Lambda] = [T_v]^{-1} [Z'_{phase}] [Y'_{phase}] [T_v] \qquad (4.76b)$$

To find the matrix $[T_v]$ which diagonalizes $[Z'_{phase}][Y'_{phase}]$ is the eigenvalue/eigenvector problem. The diagonal elements of $[\Lambda]$ are the eigenvalues of the matrix product $[Z'_{phase}][Y'_{phase}]$, and $[T_v]$ is the matrix of eigenvectors or modal matrix of that matrix product. There are many methods for finding eigenvalues and eigenvectors. The most reliable method for finding the eigenvalues seems to be the QR-transformation due to Francis [3], while the most efficient method for the eigenvector calculation seems to be the inverse iteration scheme due to Wilkinson [4, 5]. In the supporting routines LINE CONSTANTS and CABLE CONSTANTS, the "EISPACK"-subroutines [67] are used, in which the eigenvalues and eigenvectors of a complex upper Hessenberg matrix are found by the modified LR-method due to Rutishauser. This method is a predecessor of the QR-method, and where applicable, as in the case of positive definite matrices, is more efficient than the QR-method [68]. To transform the original complex matrix to upper Hessenberg form, stabilized elementary similarity transformations are used. For a given eigenvalue λ_k, the corresponding eigenvector $[t_{vk}]$ (= k-th column of $[T_v]$) is found by solving the system of linear equations

$$\{[Z'_{phase}] [Y'_{phase}] - \lambda_k[U]\} [t_{vk}] = 0 \qquad (4.77)$$

with [U] = unit or identity matrix. Eq. (4.77) shows that the eigenvectors are not uniquely defined in the sense that they can be multiplied with any nonzero (complex) constant and still remain proper eigenvectors[13], in contrast to the eigenvalues which are always uniquely defined.

Floating-point overflow may occur in eigenvalue/eigenvector subroutines if the matrix is not properly scaled. Unless the subroutine does the scaling automatically, $[Z'_{phase}][Y'_{phase}]$ should be scaled before the subroutine call, by dividing each element by $-(\omega^2\varepsilon_0\mu_0)$, as suggested by Galloway, Shorrows and Wedepohl [39]. This division brings the matrix product close to unit matrix, because $[Z'_{phase}][Y'_{phase}]$ is a diagonal matrix with elements $-\omega^2\varepsilon_0\mu_0$ if resistances, internal reactances and Carson's correction terms are ignored in Eq. (4.7) and (4.8), as explained in Section 4.1.5.2. The eigenvalues from this scaled matrix must of course be multiplied with $-\omega^2\varepsilon_0\mu_0$ to obtain the eigenvalues of the original matrix. In [39] it is also suggested to subtract 1.0 from the diagonal elements after the division; the eigenvalues of this modified matrix would then be the p.u. deviations from the eigenvalues of the lossless high-frequency approximation of Section 4.1.5.2, and would be much more separated from each other than the unmodified eigenvalues which lie close together. Using subroutines based on [67] gave identical results with and without this subtraction of 1.0, however.

In general, a different transformation must be used for the currents,

$$[I_{phase}] = [T_i] [I_{mode}] \qquad (4.78a)$$

---

[13]This is important if matrices $[T_v]$ obtained from different programs are compared. The ambiguity can be removed in a number of ways, e.g., by agreeing that the elements in the first row should always be 1.0, or by normalizing the columns to a Euclidean vector length of 1.0, that is, by requiring $t_{v1}t_{v1}^* + t_{v2}t_{v2}^* + \ldots = 1.0$, with t^* = conjugate complex of t. In the latter case, there is still ambiguity in the sense that each column could be multiplied with a rotation constant $e^{j\alpha}$ and still have vector length = 1.0.

and

$$[I_{mode}] = [T_i]^{-1} [I_{phase}] \tag{4.78b}$$

because the matrix products in Eq. (4.73a) and (4.73b) have different eigenvectors, though their eigenvalues are identical. Therefore, Eq. (4.73b) is transformed to

$$\left[\frac{d^2 I_{mode}}{dx^2}\right] = [\Lambda] [I_{mode}] \tag{4.79}$$

with the same diagonal matrix as in Eq. (4.74). While $[T_i]$ is different from $[T_v]$, both are fortunately related to each other [58],

$$[T_i] = [T_v^t]^{-1} \tag{4.80}$$

where "t" indicates transposition. It is therefore sufficient to calculate only one of them.

Modal analysis is a powerful tool for studying power line carrier problems [59-61] and radio noise interference [62, 63]. Its use in the EMTP is discussed in Section 4.1.5.3. It is interesting to note that the modes in single-circuit three-phase lines are almost identical with the α, β, 0-components of Section 4.1.3.1 [58]. Whether the matrix products in Eq. (4.73) can always be diagonalized was first questioned by Pelissier in 1969 [64]. Brandao Faria and Borges da Silva have shown in 1985 [65] that cases can indeed be constructed where the matrix product cannot be diagonalized. It is unlikely that such situations will often occur in practice, because extremely small changes in the parameters (e.g., in the 8th significant digit) seem to be enough to make it diagonalizable again. Paul [66] has shown that diagonalization can be guaranteed under simplifying assumptions, e.g., by neglecting conductor resistances.

The physical meaning of modes can be deduced from the transformation matrices $[T_v]$ and $[T_i]$. Assume, for example, that column 2 of $[T_i]$ has entries of (-0.6, 1.0, -0.4). From Eq. (4.78a) we would then know that mode-2 current flows into phase B in one way, with 60% returning in phase A and 40% returning in phase C.

4.1.5.1 Line Equations in Modal Domain

With the decoupled equations of (4.74) and (4.79) in modal quantities, each mode can be analyzed as if it were a single-phase line. Comparing the modal equation

$$\frac{d^2 V_{mode-k}}{dx^2} = \lambda_k V_{mode-k}$$

with the well-known equation of a single-phase line,

$$\frac{d^2 V}{dx^2} = \gamma^2 V$$

with the propagation constant γ defined in Eq. (1.15), shows that the modal propagation constant γ_{mode-k} is the square

root of the eigenvalue,

$$\gamma_{mode-k} \;=\; \alpha_k \;+\; j\beta_k \;=\; \sqrt{\gamma_k} \tag{4.81}$$

with

α_k = attenuation constant of mode k (e.g., in Np/km),

β_k = phase constant of mode k (e.g., in rad/km).

The phase velocity of mode k is

$$phase\ velocity \;=\; \frac{\omega}{\beta_k} \tag{4.82a}$$

and the wavelength is

$$wave\ length \;=\; \frac{2\pi}{\beta_k} \tag{4.82b}$$

While the modal propagation constant is always uniquely defined, the modal series impedance and shunt admittance as well as the modal characteristic impedance are not, because of the ambiguity in the eigenvectors. Therefore, modal impedances and admittances only make sense if they are specified together with the eigenvectors used in their calculation. To find them, transform Eq. (4.72a) to modal quantities

$$-\left[\frac{dV_{mode}}{dx}\right] \;=\; [T_v]^{-1}\,[Z'_{phase}]\,[T_i]\,[I_{mode}] \tag{4.83}$$

The triple matrix product in Eq. (4.83) is diagonal, and the modal series impedances are the diagonal elements of this matrix

$$[Z'_{mode}] \;=\; [T_v]^{-1}\,[Z'_{phase}]\,[T_i] \tag{4.84a}$$

or with Eq. (4.80),

$$[Z'_{mode}] \;=\; [T_i{}^t]\,[Z'_{phase}]\,[T_i] \tag{4.84b}$$

Similarly, Eq. (4.72b) can be transformed to modal quantities, and the modal shunt admittances are then the diagonal elements of the matrix

$$[Y'_{mode}] \;=\; [T_i]^{-1}\,[Y'_{phase}]\,[T_v] \tag{4.85a}$$

or with Eq. (4.80),

$$[Y'_{mode}] \;=\; [T_v{}^t]\,[Y'_{phase}]\,[T_v] \tag{4.85b}$$

4-44

The proof that both $[Z'_{mode}]$ and $[Y'_{mode}]$ are diagonal is given by Wedepohl [58]. Finally, the modal characteristic impedance can be found from the scalar equation

$$Z_{char-mode-k} = \frac{\sqrt{Z'_{mode-k}}}{\sqrt{Y'_{mode-k}}}$$

(4.86a)

or from the simpler equation

$$Z_{char-mode-k} = \frac{\gamma_{mode-k}}{Y'_{mode-k}}$$

(4.86b)

A good way to obtain the modal parameters may be as follows: First, obtain the eigenvalues λ_k and the eigenvector matrix $[T_v]$ of the matrix product $[Z'_{phase}][Y'_{phase}]$. Then find $[Y'_{mode}]$ from Eq. (4.85b), and the modal series impedance from the scalar equation

$$Z'_{mode-k} = \frac{\lambda_k}{Y'_{mode-k}}$$

(4.86c)

The modal characteristic impedance can then be calculated from Eq. (4.86a), or from Eq. (4.86b) if the propagation constant from Eq. (4.81) is needed as well. If $[T_i]$ is needed, too, it can be found efficiently from Eq. (4.85a)

$$[T_i] = [Y'_{phase}] [T_v] [Y'_{mode}]^{-1}$$

(4.85c)

because the product of the first two matrices is available anyhow when $[Y'_{mode}]$ is found, and the post-multiplication with $[Y'_{mode}]^{-1}$ is simply a multiplication of each column with a constant (suggested by Luis Marti). Eq. (4.85c) also establishes the link to an alternative formula for $[T_i]$ mentioned in [57],

$$[T_i] = [Y'_{phase}] [T_v] [D]$$

with $[D]$ being an arbitrary diagonal matrix. Setting $[D] = [Y'_{mode}]^{-1}$ leads us to the desirable condition $[T_i] = [T_v^t]^{-1}$ of Eq. (4.80). If the unit matrix were used for $[D]$, all modal matrices in Eq. (4.84) and (4.85) would still be diagonal, but with the strange-looking result that all modal shunt admittances become 1.0 and that the modal series impedances become λ_k. Eq. (4.80) would, of course, no longer be fulfilled. For a lossless line, the modal series impedance would then become a negative resistance, and the modal shunt admittance would become a shunt conductance with a value of 1.0 S. As long as the case is solved in the frequency domain, the answers would still be correct, but it would obviously be wrong to associate such modal parameters with

$$-\frac{\partial v}{\partial x} = R'i \qquad and \qquad -\frac{\partial i}{\partial x} = G'v$$

(with R' negative and G' = 1.0) in the time domain.

4.1.5.2 Lossless High-Frequency Approximation

In lightning surge studies, many simplifying assumptions are made. For example, the waveshape and amplitude of the current source representing the lightning stroke is obviously not well known. Similarly, flashover criteria in the form of volt-time characteristics or integral formulas [8] are only approximate. In view of all these uncertainties, the use of highly sophisticated line models is not always justified. Experts in the field of lightning surge studies normally use a simple line model in which all wave speeds are equal to the speed of light, with a surge impedance matrix $[Z_{surge}]$ in phase quantities, where

$$Z_{ii-surge} = 60 \ln(2h_i/r_i) \qquad (4.87a)$$

$$Z_{ik-surge} = 60 \ln(D_{ik}/d_{ik}) \qquad (4.87b)$$

$$all \ \ wave \ \ speeds \ = \ speed \ \ of \ \ light \qquad (4.87c)$$

with r_i being the radius of the conductor, or the radius of the equivalent conductor from Eq. (4.30) in case of a bundle conductor.[14]

Typically, each span between towers is represented separately as a line, and only a few spans are normally modelled (3 for shielded lines, or 18 for unshielded lines in [8]). For such short distances, losses in series resistances and differences in modal travel times are negligible. The effect of corona is sometimes included, however, by modifying the simple model of Eq. (4.87) [8].

It is possible to develop a special line model based on Eq. (4.87) for the EMTP, in which all calculations are done in phase quantities. But as shown here, the simple model of Eq. (4.87) can also be solved with modal parameters as a special case of the untransposed line. The simple model follows from Eq. (4.72) by making two assumptions for a "lossless high-frequency approximation":

1. Conductor resistances and ground return resistances are ignored.
2. The frequencies contained in the lightning surges are so high that all currents flow on the surface of the conductors, and on the surface of the earth.

Then the elements of $[Z'_{phase}]$ become

$$Z'_{ii} = j\omega\frac{\mu_0}{2\pi}\ln(2h_i/r_i) \ , \quad Z'_{ik} = j\omega\frac{\mu_0}{2\pi}\ln(D_{ik}/d_{ik}) \qquad (4.88)$$

while $[Y']$ is obtained by inverting the potential coefficient matrix,

$$[Y'] = j\omega[P']^{-1} \qquad (4.89)$$

with the elements of $[P']$ being the same as in Eq. (4.88) if the factor $j\omega\mu_0/(2\pi)$ is replaced by $1/(2\pi\epsilon_0)$. Then both matrix

---

[14]Ground wires are usually retained as phase conductors in such studies. If they are eliminated, the method of Section 4.1.2.1 must be used on $[Z_{surge}]$.

products in Eq. (4.73) become diagonal matrices with all elements being

$$\lambda_k = -\omega^2 \varepsilon_0 \mu_0, \quad k=1,...M \tag{4.90}$$

These values are automatically obtained from the supporting routines LINE CONSTANTS and CABLE CONSTANTS as the eigenvalues of the matrix products in Eq. (4.73), by simply using the above two assumptions in the input data (all conductor resistances = 0, GMR/r = 1.0, no Carson correction terms). The calculation of the eigenvector matrix $[T_v]$ or $[T_i]$ needed for the untransposed line model of Section 4.2 breaks down, however, because the matrix products in Eq. (4.73) are already diagonal. To obtain $[T_v]$, let us first assume equal, but nonzero conductor resistances R'. Then the eigenvectors $[t_{vk}]$ are defined by

$$(-\omega^2 \varepsilon_0 \mu_0 [U] + j\omega R'[P']^{-1}) [t_{vk}] = \lambda_k [t_{vk}] \tag{4.91}$$

with the expression in parentheses being the matrix product $[Z'_{phase}][Y'_{phase}]$, and $[U]$ = unit matrix. Eq. (4.91) can be rewritten as

$$[P']^{-1} [t_{vk}] = \lambda_{k-modified} [t_{vk}] \tag{4.92}$$

with modified eigenvalues

$$j\omega R' \lambda_{k-modified} = \lambda_k + \omega^2 \varepsilon_0 \mu_0 \tag{4.93}$$

Eq. (4.92) is valid for any value of R', including zero. It therefore follows that $[T_v]$ is obtained as the eigenvectors of $[P']^{-1}$, or alternatively as the eigenvectors of $[P']$ since the eigenvectors of a matrix are equal to the eigenvectors of its inverse. The eigenvalues of $[P]^{-1}$ are not needed because they are already known from Eq. (4.90), but they could also be obtained from Eq. (4.93) by setting R' = 0.

For this simple mode, $[T_v]$ is a real, orthogonal matrix,

$$[T_v] [T_v]^t = [U] \tag{4.94}$$

and therefore,

$$[T_i] = [T_v] \tag{4.95}$$

D.E. Hedman has solved this case of the lossless high-frequency approximation more than 15 years ago [45]. He recommended that the eigenvectors be calculated from the surge impedance matrix of Eq. (4.87), which is the same as calculating them from $[P']$ since both matrices differ only by a constant factor.

One can either modify the line constants supporting routines to find the eigenvectors from $[P']$ for the lossless high-frequency approximation, as was done in UBC's version, or use the same trick employed in Eq. (4.91) in an unmodified program: Set all conductor resistances equal to some nonzero value R', set GMR/r = 1, and ask for zero Carson correction terms. If the eigenvectors are found from $[P']$, then it is advisable to scale this matrix first by multiplying all elements with $2\pi\varepsilon_0$.

The lossless high-frequency approximation produces eigenvectors which differ from those of the lossy case

at very high frequencies [61]. This is unimportant for lightning surge studies, but important for power line carrier problems.

Example: For a distribution line with one ground wire (Fig. 4.24) the lossless high-frequency approximation produces the following modal surge impedances and transformation matrix,

mode	$Z_{surge\text{-}mode}$ (Ω)
1	993.44
2	209.67
3	360.70
4	310.62
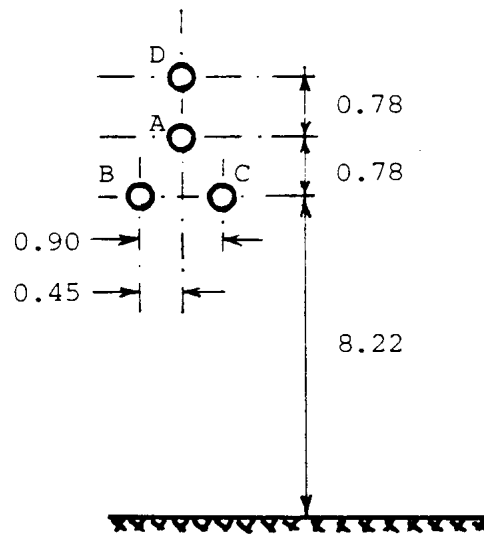
Fig. 4.24 - Position of phase conductors A, B, C and ground wire D (average height, all dimensions in m). Conductor diameter = 10.1092 mm

$$
\begin{matrix}
0.52996 & 0.82860 & -0.18 \\
0.49080 & -0.21322 & 0.462 \\
0.49080 & -0.21322 & 0.462 \\
0.48721 & -0.47170 & -0.73
\end{matrix}
$$

Converted to phase quantities, the surge impedance matrix becomes $[T_v][Z_{surge\text{-}mode}][T_v]^t$, or

$$
[Z_{surge\text{-}phase}] = \begin{bmatrix}
490.33 & & & \\
176.95 & 484.89 & symmetric & \\
176.95 & 174.27 & 484.89 & \\
190.74 & 144.26 & 144.26 & 495.31
\end{bmatrix} \ \Omega
$$

4-48

The elements from Eq. (4.87) are slightly larger, by a factor of 300,000/299,792, because the supporting routine LINE CONSTANTS uses 299,792 km/s for the speed of light, versus 300,000 km/s implied in Eq. (4.87).

Representation in EMTP then would be by means of a 4-phase, constant-parameter, lossless line. The following branch cards are for the first of 4 such cascaded sections:

```
-11A  2A        993.44 .3E-6    2  4
-11B  2B        993.44 .3E-6    2  4
-11C  2C        993.44 .3E-6    2  4
-11D  2D        993.44 .3E-6    2  4
```

The modelling of long lines as coupled shunt resistances $[R] = [Z_{surge-phase}]$ has already been discussed in Section 3.1.3. In the example above, such a shunt resistance matrix could be used to represent the rest of the line after the 4 spans from the substation. Simply using the 4 x 4 matrix would be unrealistic with respect to the ground wire, however, because it would imply that the ground wire is ungrounded on the rest of the line. More realistic, though not totally accurate, would be a 3 x 3 matrix obtained from $[Z'_{phase}]$ and $[Y'_{phase}]$ in which the ground wire has been eliminated. This model implies zero potential everywhere on the ground wire, in contrast to the four spans where the potential will more or less oscillate around zero because of reflections up and down the towers.

Comparison with More Accurate Models: For EMTP users who are reluctant to use the simple model described in this section, a few comments are in order. First, let us compare exact values with the approximate values. If we use constant parameters and choose 400 kHz as a reasonable frequency for lightning surge studies, then we obtain the results of table 4.5 for the test example above, assuming T/D = 0.333 for skin effect correction and internal inductance calculation with the tubular conductor formula, $R'_{dc} = 0.53609$ Ω/km, and $\rho = 100$ Ωm.

Table 4.5 - Exact line parameters at 400 kHz

mode	$Z_{surge-mode}$ (Ω)	wave velocity (m/s)	R' (Ω/km)
1	1027.6-j33.9	285.35	597.4
2	292.0-j0.5	299.32	7.9
3	361.9-j0.5	299.37	8.2
4	311.1-j0.5	299.32	8.0

The differences are less than 0.5% in surge impedance and wave speed for the aerial modes 2 to 4, and not more than 5% for the ground return mode 1. These are small differences, considering all the other approximations which are made in lightning surge studies. If series resistances are included by lumping them in 3 places, totally erroneous results may be obtained if the user forgets to check whether $R/4 \leq Z_{surge}$ in the ground return mode. For the very short line length of 90 m in this example, this condition would still be fulfilled here.

Using constant parameters at a particular frequency is of course an approximation as well, and some users may therefore prefer frequency-dependent models. For very short line lengths, such as 90 m in the example, most frequency-dependent models are probably unreliable, however. It may therefore be more sensible to use the simple model

described here, for which answers are reliable, rather than sophisticated models with possibly unreliable answers.

A somewhat better lossless line model for lightning surge studies than the preceding one has been suggested by V. Larsen [92]. To obtain this better model, the line parameters are first calculated in the usual way, at a certain frequency which is typical for lightning surges (e.g., at 400 kHz). The resistances are then set to zero when the matrix product $[Z'_{phase}][Y'_{phase}]$ is formed, before the modal parameters are computed. With this approach, $[T_i]$ will always be real. Table 4.6 shows the modal parameters of this better lossless model. They differ very little from those in Table 4.5.

Table 4.6 - Approximate modal parameters at 400 kHz with R=0

mode	$Z_{surge\text{-}mode}$ (Ω)	wave velocity (m/s)
1	1026.3	285.50
2	292.0	299.32
3	362.0	299.37
4	311.1	299.32

In particular, the wave velocity of the ground return mode 1 is now much closer to the exact value of Table 4.5. The transformation matrix which goes with the modal parameters of Table 4.6 is

$$[T_i] = \begin{bmatrix} 0.40795 & 0.84115 & -0.22316 & 0 \\ 0.55628 & -0.18448 & 0.44910 & -0.70711 \\ 0.55628 & -0.18448 & 0.44910 & 0.70711 \\ 0.46335 & -0.47371 & -0.73947 & 0 \end{bmatrix}$$

In this case $[T_v]$ is no longer to $[T_i]$; Eq. (4.80) must be used instead.

4.1.5.3 Approximate Transformation Matrices for Transient Solutions

The transformation matrices $[T_v]$ and $[T_i]$ are theoretically complex, and frequency-dependent as well. With a frequency-dependent transformation matrix, modes are only defined at the frequency at which the transformation matrix was calculated. Then the concept of converting a polyphase line into decoupled single-phase lines (in the modal domain) cannot be used over the entire frequency range. Since the solution methods for transients are much simpler if the modal composition is the same for all frequencies, or in other words, if the transformation matrices are constant with real coefficients, it is worthwhile to check whether such approximate transformation matrices can be used without producing too much error. Fortunately, this is indeed possible for overhead lines [66, 78].

Guidelines for choosing approximate (real and constant) transformation matrices have not yet been worked out at the time when these notes are being written. The frequency-dependent line model of J. Marti discussed in Section 4.2.2.6 needs such a real and constant transformation matrix, and wrong answers would be obtained if a complex transformation matrix were used instead. Since a real and constant transformation matrix is always an approximation,

its use will always produce errors, even if they are small and acceptable. The errors may be small in one particular frequency region, and larger in other regions, depending on how the approximation is chosen.

One choice for an approximate transformation matrix would be the one used in the lossless approximations discussed in Section 4.1.5.2. This may be the best choice for lightning surge studies.

For switching surge studies and similar types of studies, the preferred approach at this time seems to be to calculate $[T_v]$ at a particular frequency (e.g., at 1 kHz), and then to ignore the imaginary part of it. In this approach, $[T_v]$ should be predominantly real before the imaginary part is discarded. One cannot rely on this when the subroutine returns the eigenvectors, since an eigenvector multiplied with $e^{j50°}$ or any other constant would still be a proper eigenvector. Therefore, the columns of $[T_v]$ should be normalized in such a way that its components lie close to the real axis. One such normalization procedure was discussed by V. Brandwajn [79]. The writer prefers a different approach, which works as follows:

1. Ignore shunt conductances, as is customarily done. Then $[Y'_{phase}]$ is purely imaginary. Use Eq. (4.85) to find the diagonal elements of the modal shunt admittance matrix $Y'_{mode-k-preliminary}$.

2. In general, these "preliminary" modal shunt admittances will not be purely imaginary, but $j\omega C'_{mode-k}e^{-j\alpha k}$ instead. Then normalize $[T_v]$ by multiplying each column with $e^{j\,\alpha k/2}$. With this normalized transformation matrix, the modal shunt admittances will become $j\omega C'_{mode-k}$, or purely imaginary as in the phase domain.

3. To obtain the approximate (real and constant) transformation matrix, discard the imaginary part of the normalized matrix from step 2.

4. Use the approximate matrix $[T_{v-approx.}]$ from step 3 to find modal series impedances and modal shunt admittances from Eq. (4.84) and (4.85) over the frequency range of interest. If $[T_i]$ is needed, use

$$[T_{i-approx.}] \;=\; [T^t_{v-approx.}]^{-1} \tag{4.96}$$

5. If the line model requires nonzero shunt conductances, add them as modal parameters. Usually, only conductances from phase to ground are used (with phase-to-phase values being zero); in that case, the modal conductances are the same as the phase-to-ground conductances if the latter are equal for all phases.

An interesting method for finding approximate (real and constant) transformation matrices has been suggested by Paul [66]. By ignoring conductor resistances, and by assuming that the Carson correction terms $\Delta R'_{ii} + j\Delta X'_{ii}$ in Eq. (4.7) and $\Delta R'_{ik} + j\Delta X'_{ik}$ in Eq. (4.8) are all equal (all elements in the matrix of correction terms have one and the same value), the approximate transformation matrix $[T_{i-approx.}]$ is obtained as the eigenvectors of the matrix product

$$[C'_{phase}]\begin{bmatrix}111...1\\.......\\111...1\end{bmatrix}$$

with all elements of the second matrix being 1. To find $[T_{v-approx.}]$, Eq. (4.96) would have to be used. Wasley and

Selvavinayagamoorthy [93] find the approximate transformation matrices by simply taking the magnitudes of the complex elements, with an appropriate sign reflecting the values of their arguments. They compared results using these approximate matrices with the exact results (using complex, frequency-dependent matrices), and report that fairly high accuracy can be obtained if the approximate matrix is computed at a low frequency, even for the case of double-circuit lines.

If the M-phase line is assumed to be balanced (Section 4.1.3.2), then the transformation matrix is always real and constant, and known a priori with Eq. (4.58) and Eq. (4.59). Two identical and balanced three-phase lines with zero sequence coupling only have the real and constant transformation matrix of Eq. (4.65).

4.2 Line Models in the EMTP

The preceding Section 4.1 concentrated on the line parameters per unit length. These are now used to develop line models for liens of a specific length.

For steady-state solutions, lines can be modelled with reasonable accuracy as nominal π-circuits, or rigorously as equivalent π-circuits. For transient solutions, the methods become more complicated, as one proceeds from the simple case of a single-phase lossless line with constant parameters to the more realistic case of a lossy polyphase line with frequency-dependent parameters.

4.2.1 AC Steady-State Solutions

Lines can be represented rigorously in the steady-state solution with exact equivalent π-circuits. Less accurate representations are sometimes used, however, to match the model to the one used in the transient simulation (e.g., lumping R in three places, rather than distributing it evenly along the line, or using approximate real transformation matrices instead of exact complex matrices). For lines of moderate "electrical" length (typically ≤ 100 km at 60 Hz), nominal π-circuits are often accurate enough, and are probably the best models to use for steady-state solutions at power frequency. If the steady-state solution is followed by a transient simulation, or if steady-state solutions are requested over a wide frequency range, then the nominal π-circuit must either be replaced by a cascade connection of shorter nominal π-circuits, or by an exact equivalent π-circuit derived from the distributed parameters.

4.2.1.1 Nominal M-Phase π-Circuit

For the nominal M-phase π-circuit of Fig. 3.10, the series impedance matrix and the two equal shunt susceptance matrices are obtained from the per unit length matrices by simply multiplying them with the line length, as shown in Eq. (4.35) and (4.36). The equations for the coupled lumped elements of this M-phase π-circuit have already been discussed at length in Section 3, and shall not be repeated here.

Nominal π-circuits are fairly accurate if the line is electrically short. This is practically always the case if complicated transposition schemes are studied at power frequency (60 Hz or 50 Hz). Fig. 4.25 shows a typical example, with three circuits on the same right-of-way. In this case, each of the five transposition sections (1-2, 2-3, 3-4, 4-5, 5-6) would be represented as a nominal 9-phase π-circuit. While a nominal π-circuit would already be reasonably accurate

for the total line length of 95 km, nominal π-circuits are certainly accurate for each transposition section, since the longest section is only 35 km long. A comparison between measurements on the de-energized line L3 and computer results is shown in table 4.7 [80]. The coupling in this case is predominantly capacitive.
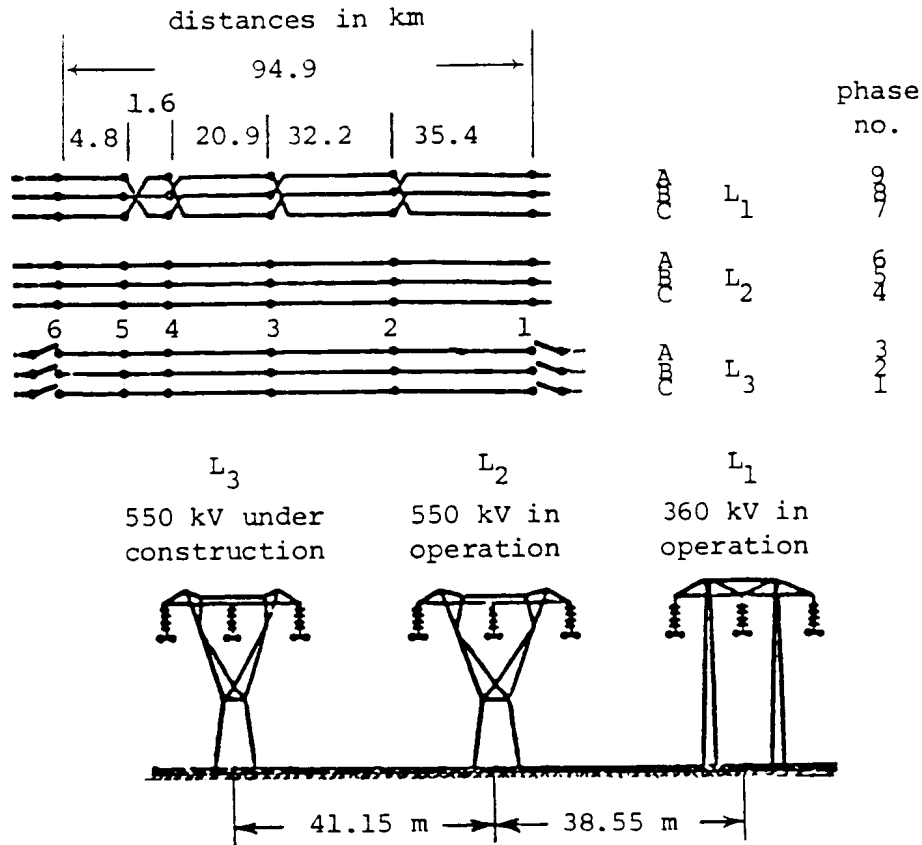
Fig. 4.25 - Transposition scheme for three adjacent circuits

Table 4.7 - Comparison between measurements and EMTP results (voltages on energized line L1 = 372 kV and on L2 = 535 kV)

	phase	measurement	EMTP results
Induced voltages on de-energized line L3 if open at both ends	A	30 kV	27.5 kV
	B	15 kV	13.8 kV
	C	10 kV	7.8 kV
Grounding currents if de-energized line L3 is grounded at right end	A	11 A	10.5 A
	B	5 A	3.2 A
	C	1 A	1.5 A

Because nominal π-circuits are so useful for studying complicated transposition schemes, a "CASCADED PI" option was added to the BPA EMTP. With this option, the entire cascade connection is converted to one single π-circuit, which is an exact equivalent for the cascade connection. This is done by adding one "component" at a time, as shown in Fig. 4.26. The "component" may either be an M-phase π-circuit, or other types of network elements such as

shunt reactors or series capacitors. Whenever component k is added, the nodal admittance matrix
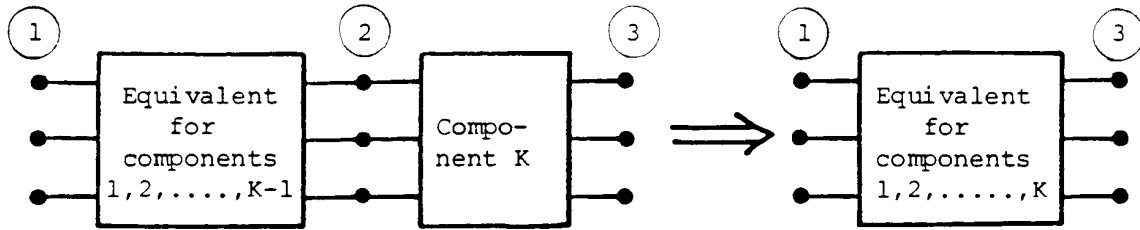
Fig. 4.26 - Schematic illustration of cascading operation for K-th component

for nodes 1, 2, 3 is reduced by eliminating the inner nodes 2, to form the new admittance matrix of the equivalent for the cascaded components 1, 2, ... K. This option keeps the computational effort in the steady-state solution as low as possible by not having to use nodal equations for the inner nodes of the cascade connection, at the expense of extra computational effort for the cascading procedure.

4.2.1.2 Equivalent π-Circuit for Single-Phase Lines

Lines defined with distributed parameters at input time are always converted to equivalent π-circuits for the steady-state solution.

For lines with frequency-dependent parameters, the exact equivalent π-circuit discussed in Section 1 is used, with Eq. (1.14) and (1.15). The same exact equivalent π-circuit is used for distortionless and lossless line models with constant parameters.

In many applications, line models with constant parameters are accurate enough. For example, positive sequence resistances and inductances are fairly constant up to approximately 1 kHz, as shown in Fig. 4.20. But even with constant parameters, the solution for transients becomes very complicated (except for the unrealistic assumption of distortionless propagation). Fortunately, experience showed that reasonable accuracy can be obtained if L' and C' are distributed and if

$$R = R' \mathcal{L}$$ (4.97)

is lumped in a few places as long as $R \ll Z_{surge}$. In the EMTP, R/2 is lumped in the middle and R/4 at both ends of an otherwise lossless line, as shown in Fig. 4.27, and as further discussed in Section 4.2.2.5. For this transient representation, the EMTP uses the same assumption[15] in the

---

[15]The EMTP should probably be changed to by-pass this option if only steady-state solutions are requested, either at one frequency or over a range of frequencies.
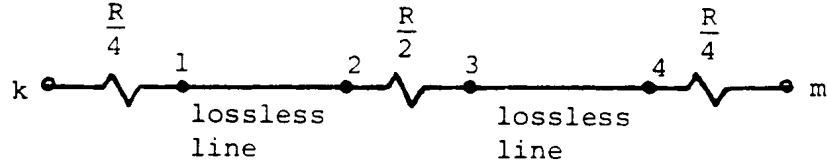
Fig. 4.27 - Line representation with lumped resistances

steady-state solution, to avoid any discrepancies between ac steady-state initialization and subsequent transient simulation, even though experiments have shown that the differences are extremely small at power frequency. By using equivalent π-circuits for each lossless, half-length section in Fig. 4.27, and by eliminating the "inner" nodes 1, 2, 3, 4, an equivalent π-circuit (Fig. 1.2) was obtained by R.M. Hasibar with

$$Z_{series} = R\cos^2\omega\tau - \left(0.5 + 0.03125\frac{R^2}{Z^2}\right)R \sin^2\omega\tau + j \sin\omega\tau \cos\omega\tau \cdot$$
$$(0.375\frac{R^2}{Z} + 2Z)$$

$$\frac{1}{2}Y_{shunt} = \frac{(-2 - 0.125\frac{R^2}{Z^2})\sin^2\omega\tau + j\frac{R}{Z}\sin\omega\tau\cos\omega\tau}{Z_{series}} \tag{4.98}$$

where

$$\tau = length \sqrt{L'C'}$$

$$Z = \sqrt{\frac{L'}{C'}}$$

$$R = length \cdot R' \tag{4.99}$$

4.2.1.3 Equivalent M-Phase π-Circuit

To obtain an equivalent M-phase π-circuit, the phase quantities are first transformed to modal quantities with Eq. (4.84) and (4.85) for untransposed lines, or with Eq. (4.58) and (4.59) for balanced lines. For identical balanced three-phase lines with zero sequence coupling only, Eq. (4.65) is used. For each mode, an equivalent single-phase π-circuit is then found in the same way as for single-phase lines; that is, either as an exact equivalent π-circuit with Eq. (1.14) and (1.15), or with Eq. (4.98) and (4.99) for the case of lumping R in three places. These single-phase modal π-circuits each has a series admittance $Y_{series-mode}$ and two equal shunt admittances 1/2 $Y_{shunt-mode}$. By assembling these admittances as diagonal matrices, the admittance matrices of the M-phase π-circuit in phase quantities are obtained from

$$[Y_{series}] = [T_i] [Y_{series-mode}] [T_i]^t \tag{4.100}$$

and

$$\frac{1}{2}[Y_{shunt}] = \frac{1}{2}[T_i][Y_{shunt-mode}][T_i]^t \tag{4.101}$$

While it is always possible to obtain the exact equivalent M-phase π-circuit at any frequency in this way, approximations are sometimes used to match the representation for the steady-state solution to the one used in the transient solution. One such approximation is the lumping of resistances as shown in Fig. 4.27. Another approximation is the use of real and constant transformation matrices in Eq. (4.100) and (4.101), as discussed in Section 4.1.5.3.

4.2.2 Transient Solutions

Historically, the first line models in the EMTP were cascade connections of π-circuits, partly to prove that computers could match switching surge study results obtained on transient network analyzers (TNA's) at that time. On TNA's, balanced three-phase lines are usually represented with decoupled 4-conductor π-circuits, as shown in Fig. 4.28. This representation can easily be derived from Eq. (4.44) by rewriting it as

$$-\frac{dV_A}{dx} = (Z'_s - Z'_m)I_A + Z'_m(I_A + I_B + I_C) \tag{4.102}$$
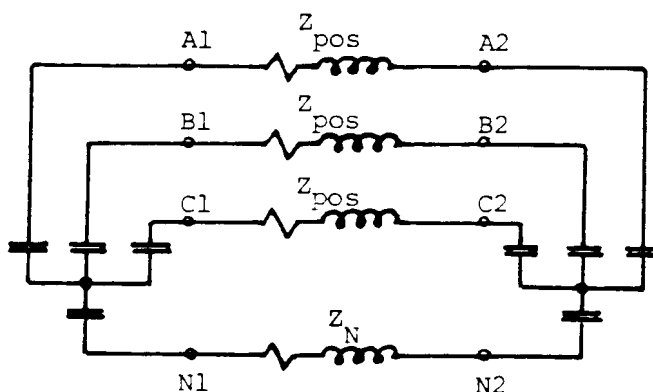
Fig. 4.28 - Four-conductor π-circuit used on TNA's

for phase A, and similar for phases B and C. The first term in Eq. (4.102) is $Z'_{pos}I_A$ (or branch A1-A2 in Fig. 4.28), while the second term is the common voltage drop caused by the earth and ground wire return current $I_A + I_B + I_C$ (branch N1-N2 in Fig. 4.28). Note, however, that Fig. 4.28 is only valid if the sum of the currents flowing out through a line returns through the earth and ground wires of that same line. For that reason, the neutral nodes N2, N3, ... must be kept floating, and only N1 at the sending end is grounded. Voltages with respect to ground at location i are obtained by measuring between the phase and node N_i. In meshed networks with different R/X-ratios, this assumption is probably not true. For this reason, and to be able to handle balanced as well as untransposed lines with any number of phases, M-phase π-circuits were modelled directly with M x M matrices, as discussed in Section 4.1.2.4. Voltages to ground are then simply the node voltages. Comparisons between these M-phase π-circuits, and with the four-conductor π-circuits of Fig. 4.28 confirmed that the results are identical.

The need for travelling wave solutions first arose in connection with rather simple lightning arrester studies, where lossless single-phase line models seemed to be adequate. Section 1 briefly discusses the solution method used in the EMTP for such lines. This method was already known in the 1920's and 1930's and strongly advocated by Bergeron [81]; it is therefore often called Bergeron's method. In the mathematical literature, it is known as the method of characteristics, supposedly first described by Riemann.

It soon became apparent that travelling wave solutions were much faster and better suited for computers than cascaded π-circuits. To make the travelling wave solutions useful for switching surge studies, two changes were needed from the simple single-phase lossless line: First, losses had to be included, which could be done with reasonable accuracy by simply lumping R in three places. Secondly, the method had to be extended to M-phase lines, which was achieved by transforming phase quantities to modal quantities. Originally, this was limited to balanced lines with built-in transformation matrices, then extended to double-circuit lines, and finally generalized to untransposed lines. Fig. 4.29 compared EMTP results with results obtained on TNA's, using the built-in transformation matrix for balanced three-phase lines and simply lumping R in three places.
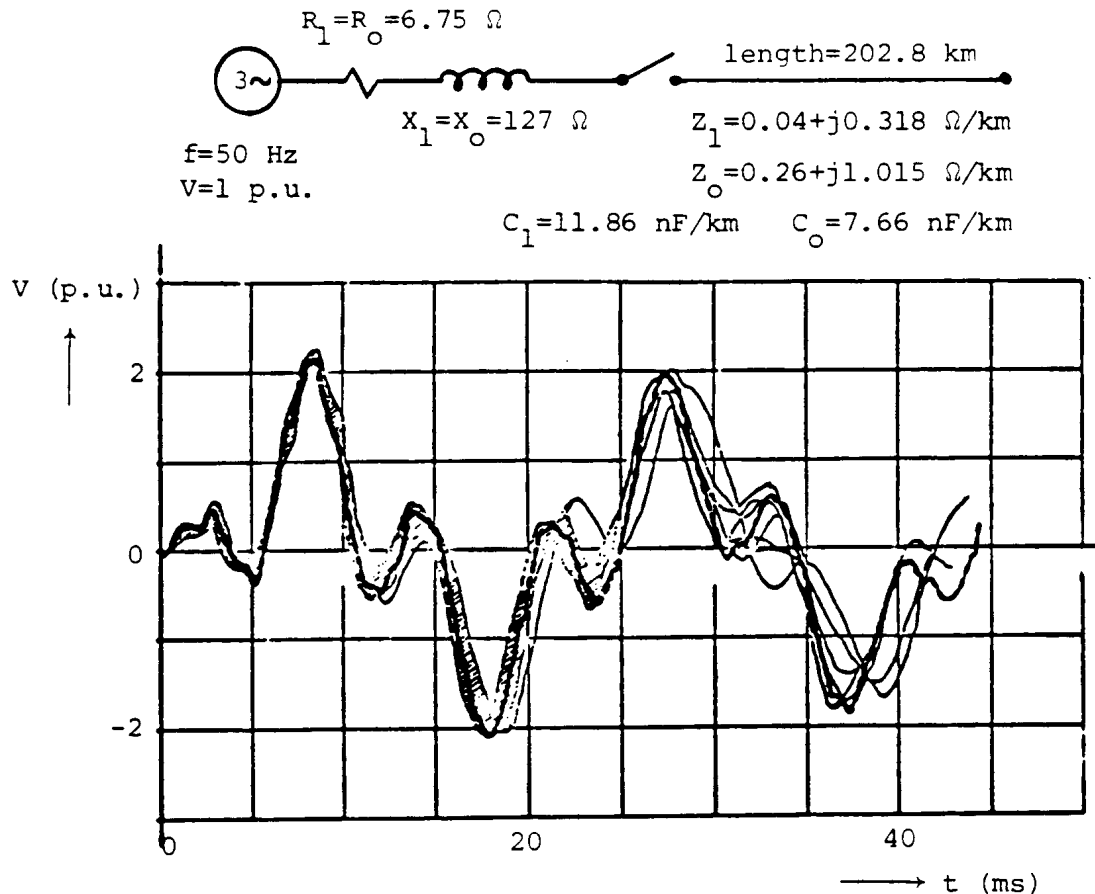
Fig. 4.29 - Energization of a three phase line. Computer simulation results (dotted line) superimposed on 8 transient

network analyzer results for receiving end voltage in phase B. Breaker contacts close at 3.05 ms in phase A, 8,05 ms in phase B, and 5.55 ms in phase C (t=0 when source voltage of phase A goes through zero from negative to positive) [82]. Reprinted by permission of CIGRE

While travelling wave solutions with constant distributed L', C' and constant lumped R produced reasonable accurate answers in many cases, as shown in Fig. 4.29, there were also cases where the frequency dependence, especially of the zero sequence impedance, could not be ignored. Choosing constant line parameters at the dominant resonance frequency sometimes improved the results. Eventually, frequency-dependent line models were developed by Budner [83], by Meyer and Dommel [84] based on work of Snelson [85], by Semlyen [86], and by Ametani [87]. A careful re-evaluation of frequency-dependence by J. Marti [88] led to a fairly reliable solution method, which seems to become the preferred option as these notes are being written. J. Marti's method will therefore be discussed in more detail.

4.2.2.1 Nominal π-Circuits

Nominal π-circuits are generally not the best choice for transient solutions, because travelling wave solutions are faster and usually more accurate. Cascade connections of nominal π-circuits may be useful for untransposed lines, however, because one does not have to make the approximations for the transformation matrix discussed in Section 4.1.5.3. On the other hand, one cannot represent frequency-dependent line parameters and one has to accept the spurious oscillations caused by the lumpiness. Fig. 4.30 shows these oscillations for the simple case of a single-phase line being represented with 8 and 32 cascaded nominal π-circuits. The exact solution with distributed parameters is shown for comparison purposes as well. The proper choice of the number of π-circuits for one line is discussed in [89], as well as techniques for damping the spurious oscillations with damping resistances in parallel with the series R-L branches of the π-circuit of Fig. 4.28.
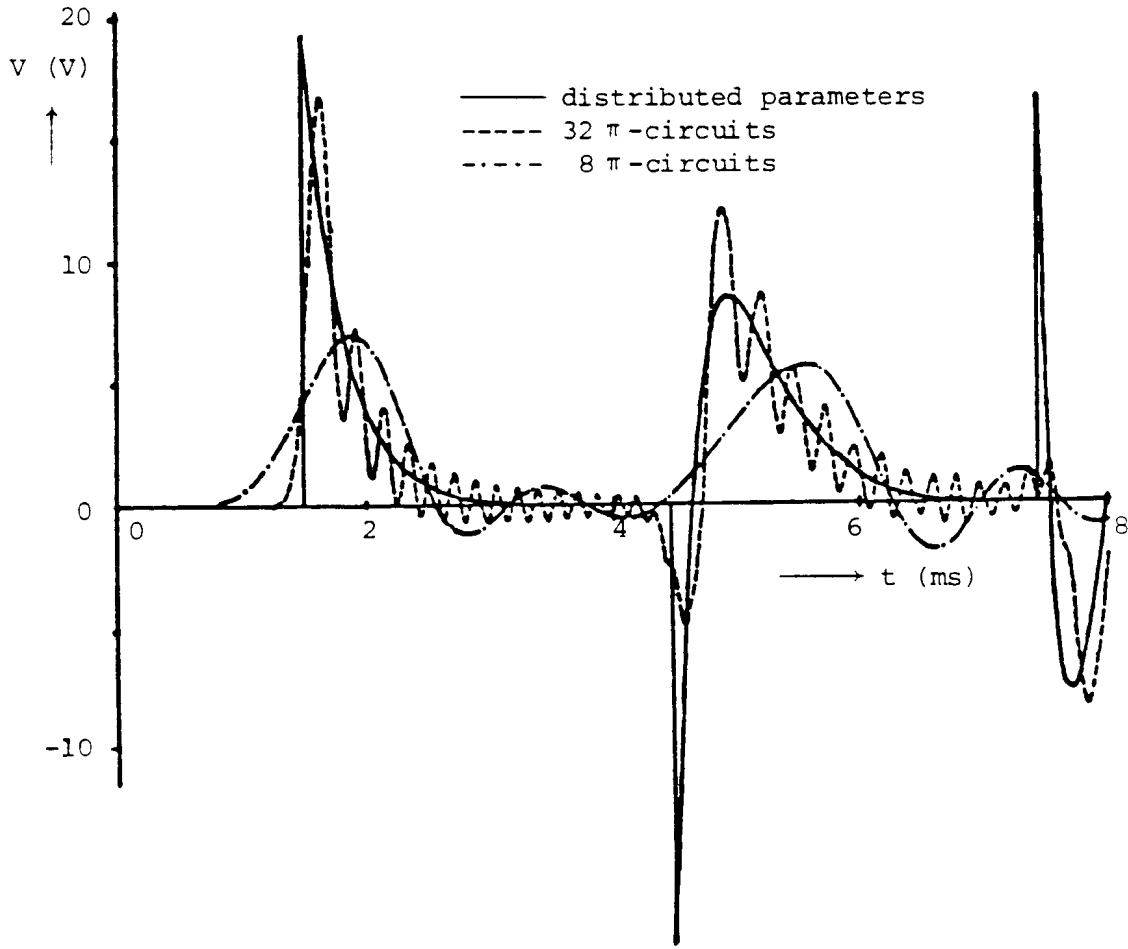
Fig. 4.30 - Voltage at receiving end of a single phase line if a dc voltage of 10 V is connected to the sending end at t=0 (line data: R=0.0376 Ω/mile, L=1.52 mH/mile, C=14.3 nF/mile, length-320 miles; receiving end terminated with shunt inductance of 100 mH)

The solution methods for nominal π-circuits have already been discussed in Section 3.4. With M-phase nominal π-circuits, untransposed lines (or sections of a line) are as simple to represent as balanced lines. In the former case, one simply uses the matrices of the untransposed line, whereas in the latter case one would use matrices with averaged equal diagonal and averaged equal off-diagonal elements.

4.2.2.2 Single-Phase Lossless Line with Constant L' and C'

The solution method for the single-phase case has already been explained in Section 1. The storage scheme for the history terms is the same as the one discussed in the next Section 4.2.2.3 for M-phase lossless lines, except that each single-phase line occupies only one section in the table, rather than M section for M modes. Similarly, the initialization of the history terms for cases starting from linear ac steady-state initial conditions is the same as in Eq. (4.108).
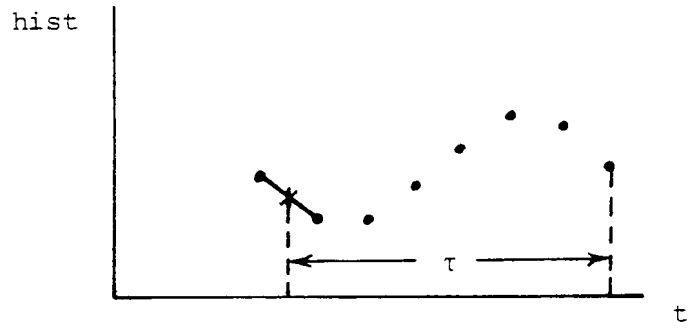
Fig. 4.31 - Linear interpolation
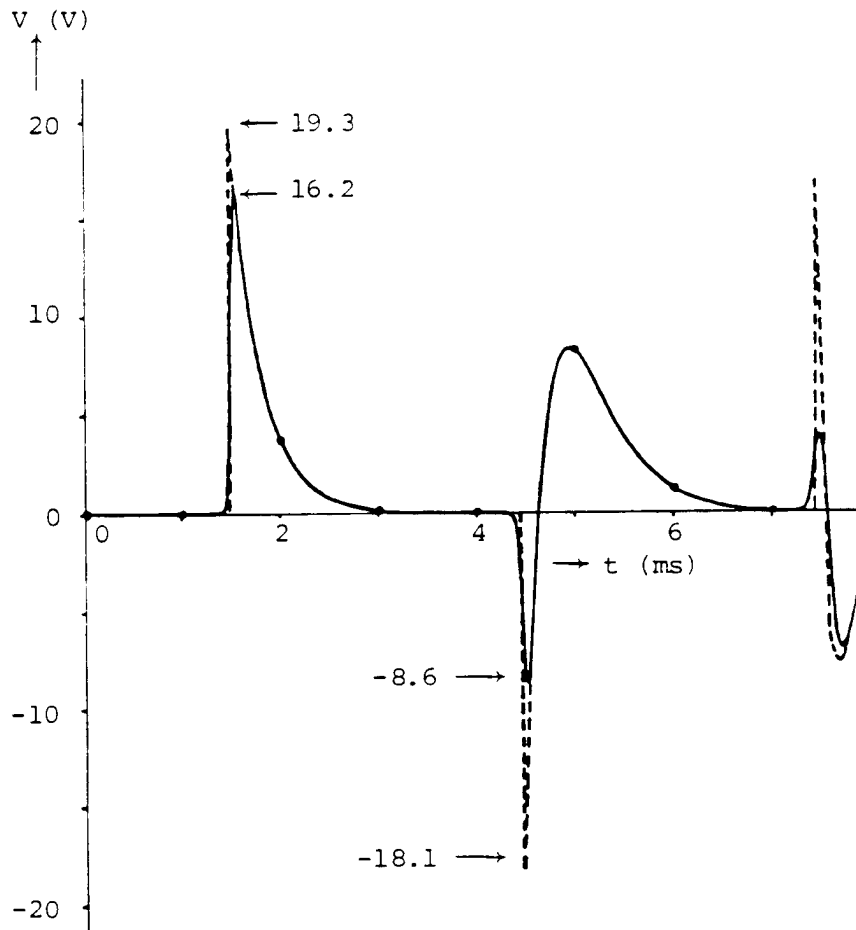
Fig. 4.32 - Effect of linear interpolation on sharp peaks. Dotted line: $\Delta t =$ 9.324...μs to make τ integer multiple of Δt. Solid line: $\Delta t = 10$ μs (τ not integer multiple of Δt)

The solution is exact as long as the travel time τ is an integer multiple of the step size Δt. If this is not the case, then linear interpolation is used in the EMTP, as indicated in Fig. 4.31. Linear interpolation is believed to be a reasonable approximation for most cases, since the curves are usually smooth rather than discontinuous. If discontinuities or very sharp peaks do exist, then rounding τ to the nearest integer multiple of Δt may be more sensible than interpolation, however. There is no option for this rounding procedure in the EMTP, but the user can easily accomplish this through changes in the input data. Fig. 4.32 compares results for the case of Fig. 4.30 with sharp peaks with and without linear interpolation. The line was actually not lossless in this case, but the losses were represented in a simple way by subdividing the line into 64 lossless sections and lumping resistances in between and at both ends. The interpolation errors are more severe if lines are split up into many sections, as was done here. If the line were only split up into two lossless sections, with R lumped in between and at both ends, then the errors in the peaks would be less (the first peak would be 18.8, and the second peak would be -15.4).

The accumulation of interpolation errors on a line broken up into many sections, with τ of each section not being an integer multiple of Δt, can easily be explained. Assume that a triangular pulse is switched onto a long, lossless line, which is long enough so that no reflections come back from the remote end during the time span of the study (Fig. 4.33). Let us look at how this pulse becomes distorted through interpolation as it travels down the line if

(a)   the line is broken up into short sections of travel time 1.5 Δt each, and

(b)   the line from the sending end to the measuring point is represented as one section ($\tau = k \cdot 1.5 \Delta t$, with k = 1, 2, 3,...).
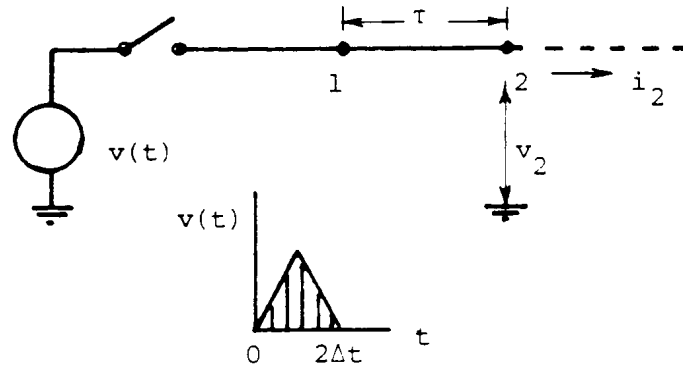
Fig. 4.33 - Single-phase lossless line energized with triangular pulse

At any point on the line, the current will be

$$i = \frac{1}{Z} v$$

and between points 1 and 2 separated by τ (Fig. 4.33),

$$v2(t + \tau) = v1(t)$$

This last equation was used in Fig. 4.34, together with linear interpolation, to find the shape of the pulse as it travels

down the line. The pulse loses its amplitude and becomes wider and wider if it is broken up into sections of travel time 1.5 Δt each. On the other hand, the pulse shape never becomes as badly distorted if the line is represented as one single section.

What are the practical consequences of this interpolation error? Table 4.8 compares peak overvoltages from a BPA switching surge study on a 1200 kV three-phase line[16], 133 miles long. Each section was split up into two lossless half-sections, with R lumped in the middle and

Table 4.8 - Interpolation errors in switching surge study with $\Delta t = 50$ µs

Run	Line model	Peak overvoltages (MV)		
		phase A	phase B	phase C
1	single section	1.311	1.191	1.496
2	7 sections	1.276	1.136	1.457
3	single section with τ rounded	1.342	1.167	1.489

at both ends, as explained in Section 4.2.2.4. Run no. 1 shows the results of the normal line representation as one section. Run no. 2 with subdivision into 7 sections produces differences of 2.6 to 4.7%. In run no. 3 the zero and positive sequence travel times $\tau_0 = 664.93$ µs and $\tau_1 = 445.74$ µs were rounded to 650 and 450 µs, respectively, to make them integer multiples of $\Delta t = 50$ µs. These changes could be interpreted as a decrease in both L'_0 and C'_0 of 2.25%, and as an increase in both L'_1 and C'_1 of 0.96%, with the surge impedances remaining unchanged. Since line parameters are probably no more accurate than ±5% at best anyhow, these implied changes are quite acceptable. With rounding, a slightly modified case is then solved without interpolation errors. Whether an option for rounding τ to the nearest integer multiple of Δt should be added to the EMTP is debatable. In general, rounding may imply much larger changes in L', C' than in this case, and if implemented, warning messages with the magnitude of these implied changes should be added as well. In Table 4.8, runs no. 3 to 1 differ by no more than 2.3%, and the interpolation error is therefore acceptable if the line is represented as one section. Breaking the line up into very many sections may produce unacceptable interpolation errors, however.

If the user is interested in a "voltage profile" along the line, then a better alternative to subdivisions into sections would be a post-processor "profile program" which would calculate

---

[16]The problem of interpolation errors is basically the same for single-phase and M-phase lines; therefore, a three-phase case is presented here for which data was already available. Choosing a step size Δt which makes the travel time τ an integer multiple of Δt is more difficult for three-phase lines, however, because there are two travel times for the positive and zero sequence mode on balanced lines (or three travel times for the 3 modes on untransposed lines).

(a)

LINE FROM SENDING END TO X
BROKEN UP INTO SECTIONS OF
$\tau = 1.5\ \Delta t$

at sending end

1.5 Δt down the line

3 Δt down the line

4.5 Δt down the line

6 Δt down the line

7.5 Δt down the line

9 Δt down the line

(b)

LINE FROM SENDING END TO X
REPRESENTED AS ONE SINGLE
SECTION
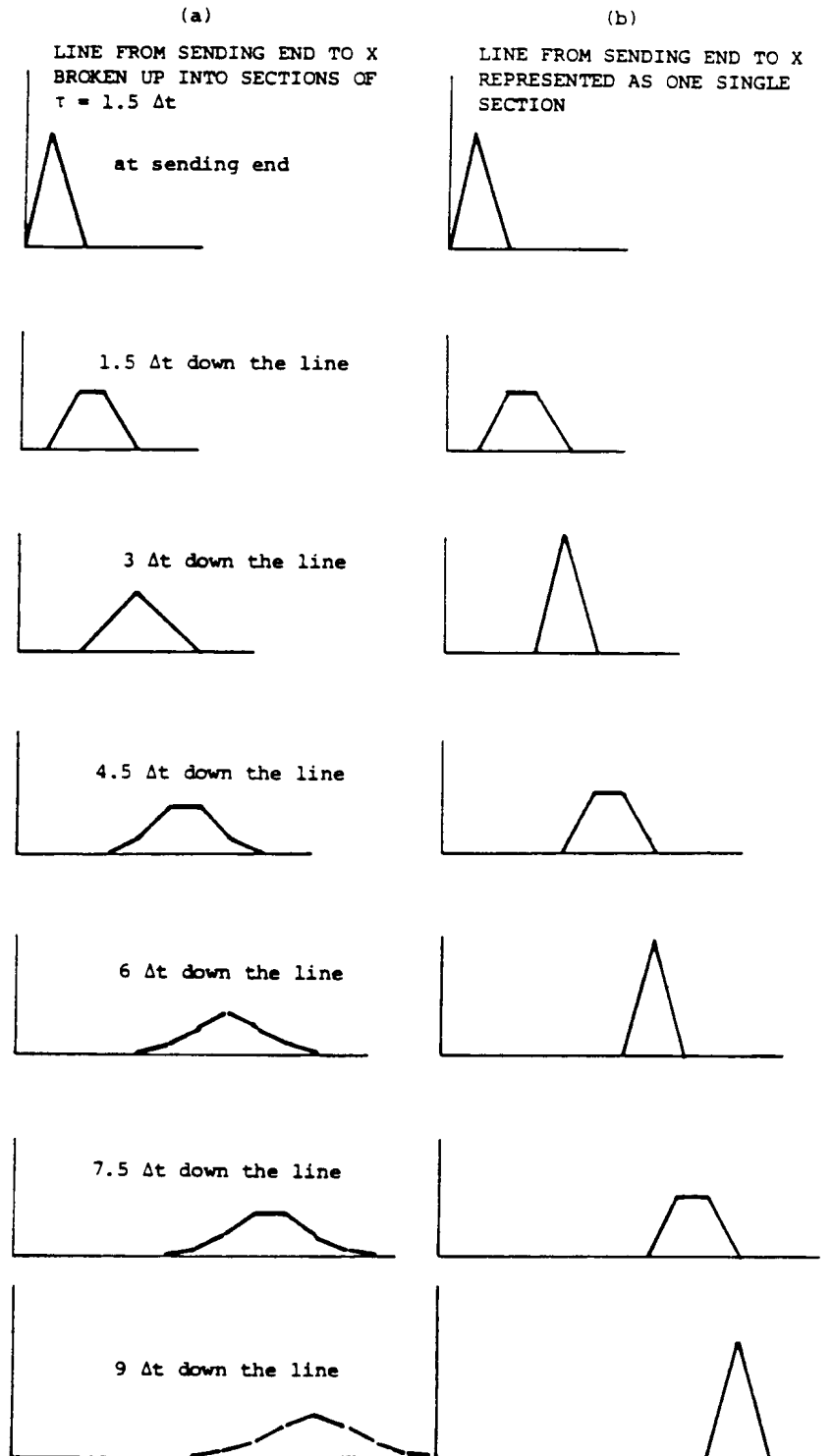
Fig. 4.34 - Pulse at incremental distances down the line

voltages and currents at intermediate points along the line from the results at both ends of the line. Such a program is easy to write for lossless and distortionless lines. Luis Marti developed such a profile algorithm for the more complicated frequency-dependent line models, which he merged into the time step loop of the EMTP [90]. This was used to produce moves of travelling waves by displaying the voltage profile at numerous points along the line at time intervals of Δt.

Fig. 4.34(a) suggests a digital filtering effect from the interpolation which is similar to that of the trapezoidal rule described in Section 2.2.1. To explain this effect, Eq. (1.6) must first be transformed from the time domain

$$\frac{1}{Z} v_k(t) - i_{km}(t) = \frac{1}{Z} v_m(t-\tau) + i_{mk}(t-\tau)$$

into the frequency domain,

$$I = \frac{1}{Z} V_k - I_{km} = \left(\frac{1}{Z} V_m + I_{mk} \right) \cdot e^{-j\omega\tau} \tag{4.103}$$

For simplicity, let us assume that voltage and current phasors V_m and I_{mk} at node m are known, and that we want to find $I = V_k/Z - I_{km}$ at node k. Without interpolation errors, Eq. (4.103) provides the answer. If interpolation is used, and if for the sake of simplicity we assume that the interpolated value lies in the middle of an interval Δt, then Eq. (4.103) becomes

$$I_{interpolated} = \left(\frac{1}{Z} V_m + I_{mk} \right) \cdot \frac{1}{2} \cdot \left(e^{-j\omega(\tau+\frac{\Delta t}{2})} + e^{-j\omega(\tau-\frac{\Delta t}{2})} \right) \tag{4.104}$$

Therefore, the ratio of the interpolated to the exact value becomes

$$\frac{I_{interpolated}}{I_{exact}} = \cos\left(\omega \frac{\Delta t}{2} \right) \tag{4.105}$$

which is indeed somewhat similar to Fig. 2.10 for the error produced by the trapezoidal rule.

Single-phase lossless line models can obviously only approximate the complicated phenomena on real lines. Nonetheless, they are useful in a number of applications, for example

(a)   in simple studies where one wants to gain insight into the basic phenomena,

(b)   in lightning surge studies, and

(c)   as a basis for more sophisticated models discussed later.

For lightning surge studies, single-phase lossless line models have been used for a long time. They are probably accurate enough in many cases because of the following reasons:

(1)   Only the phase being struck by lightning must be analyzed, because the voltages induced in the other phases will be much lower.

(2)   Assumptions about the lightning stroke are by necessity very crude, and very refined line models are therefore not warranted.

4-64

(3)   The risk of insulation failure in substations is highest for backflashovers at a distance of approx. 2 km or less. Insulation co-ordination studies are therefore usually made for nearby strokes. In that case, the modal waves of an M-phase line "stay together," because differences in wave velocity and distortion among the M waves are still small over such short distances. They can then easily be combined into one resultant wave on the struck phase. There seems to be some uncertainty, however, about the value of the surge impedance which should be used in such simplified single-phase representations. It appears that the "self surge impedance" $Z_{ii\text{-surge}}$ of Eq. (4.87a) should be used. For nearby strokes it is also permissible to ignore the series resistance. Attenuation caused by corona may be more important than that caused by conductor losses. At the time of writing these notes, corona is still difficult to model, and it may therefore be best to ignore losses altogether to be on the safe side.

4.2.2.3 M-Phase Lossless Line with Constant L' and C'

Additional explanations are needed for extending the method of Section 1 from single-phase lines to M-phase lines. In principle, the equations are first written down in the modal domain, where the coupled M-phase line appears as if it consisted of M single-phase lines. Since the solution for single-phase lines is already known, this is straightforward. For solving the line equations together with the rest of the network, which is always defined in phase quantities, these modal equations must then be transformed to phase quantities, as schematically indicated in Fig. 4.35.
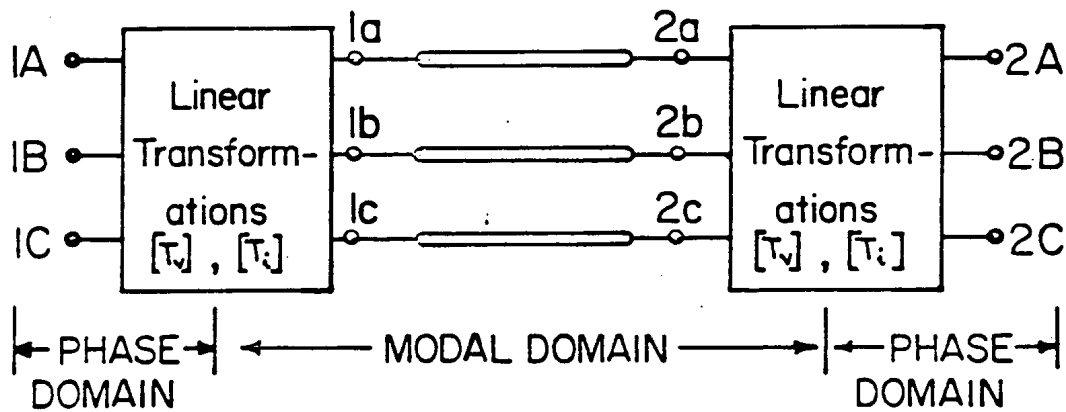
Fig. 4.35 - Transformation between phase and modal domain on a three-phase line

For simplicity, let us assume that the line has 3 phases. Then, with the notations from Fig. 4.35, each mode is described by an equation of the form of Eq. (1.6), or

$$i_{1a-2a}(t) = \frac{1}{Z_a}v_{1a}(t) + hist_{1a-2a}(t-\tau_a)$$
$$i_{1b-2b}(t) = \frac{1}{Z_b}v_{1b}(t) + hist_{1b-2b}(t-\tau_b)$$

$$(4.106)$$

$$i_{1c-2c}(t) = \frac{1}{Z_c} v_{1c}(t) + hist_{1c-2c}(t-\tau_c)$$

where each history term hist was computed and stored earlier. For mode a, this history term would be

$$hist_{1a-2a}(t-\tau_a) = -\frac{1}{Z_a} v_{2a}(t-\tau_a) - i_{2a-1a}(t-\tau_a) \qquad (4.107)$$

and analogous for modes b and c. These history terms are calculated for both ends of the line as soon as the solution has been obtained at instant t, and entered into a table for use at a later time step. As indicated in Fig. 4.36, the history terms of a three-phase line would occupy 3 sections of the history tables for modes a, b, c, and the length of each section would be $\tau_{increased}/\Delta t$, with $\tau_{increased}$ being the travel time of the particular mode increased to the nearest integer multiple of Δt[17]. Since the modal travel times τ_a, τ_b, τ_c differ from each other, the 3 sections in this table are generally of different length. This is also the reason for storing history terms as modal values, because one has to go back different travel times for each mode in picking up history terms. For the solution at time t, the history terms of Eq. (4.106) are obtained by using linear interpolation on the top two entries of each mode section.

---

[17]A single-phase line would simply occupy one section, whereas a six-phase line would occupy six sections in this table.

starting address
for mode a of a
line

mode a

mode b

oldest 2 values $\begin{cases} t{-}\tau_{increased} \\ \quad . \\ \quad . \end{cases}$
used for inter-
polation

mode c

$t{-}2\Delta t$

enter $t{-}\Delta t$
newest values $\longrightarrow$ t
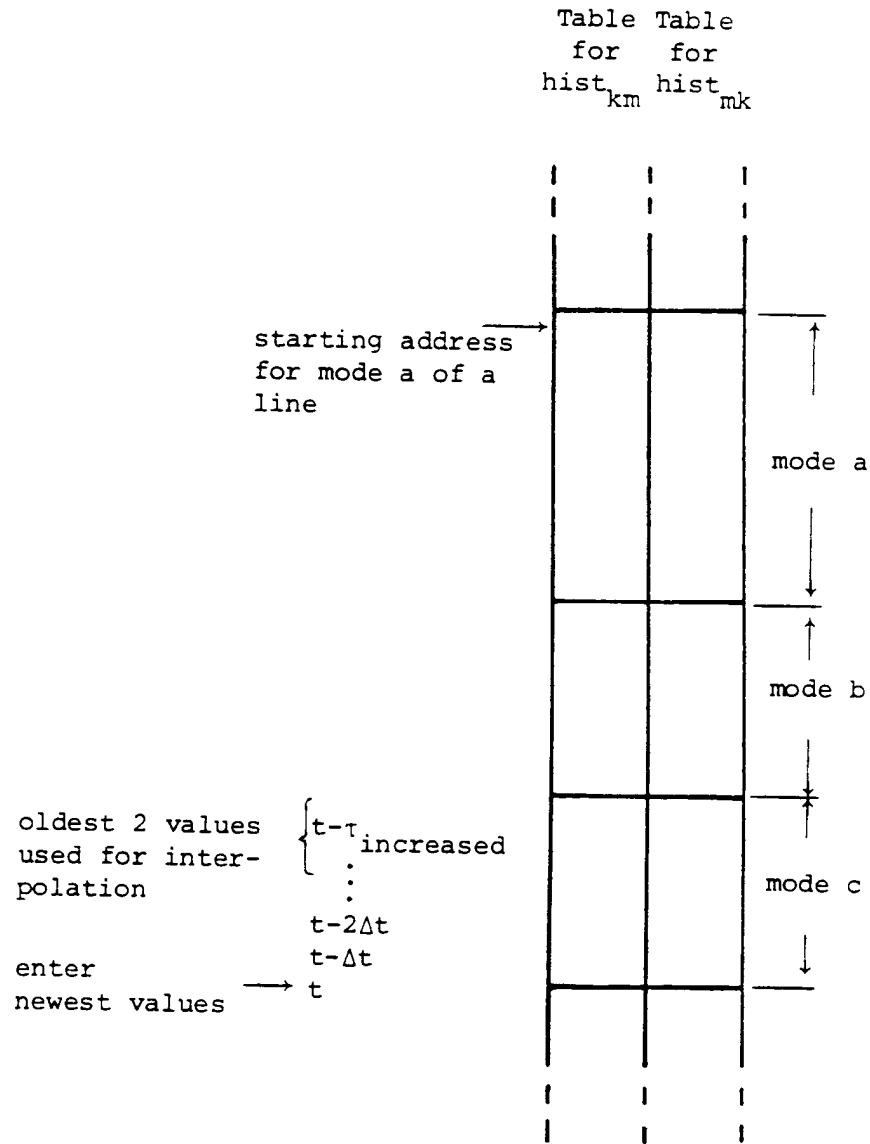
Fig. 4.36 - Table for history terms of transmission lines

After   the

solution in each time step, the entries in the tables of Fig. 4.36 must be shifted upwards by one location, thereby throwing away the values at the oldest point at t-$\tau_{increased}$. This is then followed by entering the newly calculated history terms hist(t) at the newest point t. Instead of physically shifting values, the EMTP moves the pointer for the starting address of each section down by 1 location. When this pointer reaches the end of the table, it then goes back again to the beginning of the table ("wrap-around table") [91].

The initial values for the history terms must be known for t = 0, -Δt, -2Δt, ... -$\tau_{increased}$. The necessity for knowing them beyond t = 0 comes from the fact that only terminal conditions are recorded. If the conditions were also given along the line at travel time increments of Δt, then the initial values at t = 0 would suffice. For zero initial conditions, the history table is simply preset to zero. For linear ac steady-state conditions (at one frequency ω), the history terms are first computed as phasors (peak, not rms),

$$HIST_{km} = -\frac{1}{Z}V_m - I_{mk} \tag{4.108a}$$

where V_m and I_{mk} are the voltage and current phasors at line end m (analogous for $HIST_{mk}$). With $HIST = |HIST| \cdot e^{j\alpha}$, the instantaneous history terms are then

$$hist_{km}(t) = |HIST_{km}| \cdot \cos(\omega t + \alpha) \ , \quad with \ t=0, \ -\Delta t, \ -2\Delta t, \ \dots$$

$$\tag{4.108b}$$

Eq. (4.108) is used for single-phase lines as well as for M-phase lines, except that mode rather than phase quantities must be used in the latter case.

Eq. (4.106) are interfaced with the rest of the network by transforming them from modal to phase quantities with Eq. (4.78a),

$$\left[i_{1-2}^{phase}\right] = \left[Y_{surge}\right]\left[v_1^{phase}\right] + \left[hist_{1-2}^{phase}\right] \tag{4.109a}$$

with the surge admittance matrix in phase quantities,

$$\left[Y_{surge}\right] = \left[T_i\right]\begin{bmatrix} Z_a^{-1} & 0 & 0 \\ 0 & Z_b^{-1} & 0 \\ 0 & 0 & Z_c^{-1} \end{bmatrix}\left[T_i\right]^t \tag{4.109b}$$

and the history terms in phase quantities,

$$\left[hist_{1-2}^{phase}\right] = \left[T_i\right]\begin{bmatrix} hist_{1a-2a} \\ hist_{1b-2b} \\ hist_{1c-2c} \end{bmatrix} \tag{4.109c}$$

For a lossless line with constant L' and C', the transformation matrix $[T_i]$ will always be real, as explained in the last paragraph of Section 4.1.5.2. It is found as the eigenvector matrix of the product [C'][L'] for each particular tower configuration, where [L'] and [C'] are the per unit length series inductance and shunt capacitance matrices of the line. For balanced lines, $[T_i]$ is known a priori from Eq. (4.58), and for identical balanced three-phase lines with zero sequence coupling only it is known a priori from Eq. (4.65).

The inclusion of Eq. (4.109) into the system of nodal equations (1.8a) for the entire network is quite straightforward. Assume that for the example of Fig. 4.35, rows and columns for nodes 1A, 1B, 1C follow each other, as do those for nodes 2A, 2B, 2C (Fig. 4.37). Then the 3 x 3 matrix $[Y_{surge}]$ enters into two 3 x 3 blocks on the diagonal, as indicated in Fig. 4.37, while the history terms $[hist_{1-2}^{phase}] = [hist_{1A-2A}, hist_{1B-2B}, hist_{1C-2C}]$ of Eq. (4.109c) enter into rows 1A, 1B, 1C, on the right-hand side with negative signs. Analogous history terms for terminal 2 enter into rows 2A, 2B,

2C on the right-hand side. While $[Y_{surge}]$ is entered into [G] only once outside the time-step loop, the history terms must be added to the right-hand side in each time step.
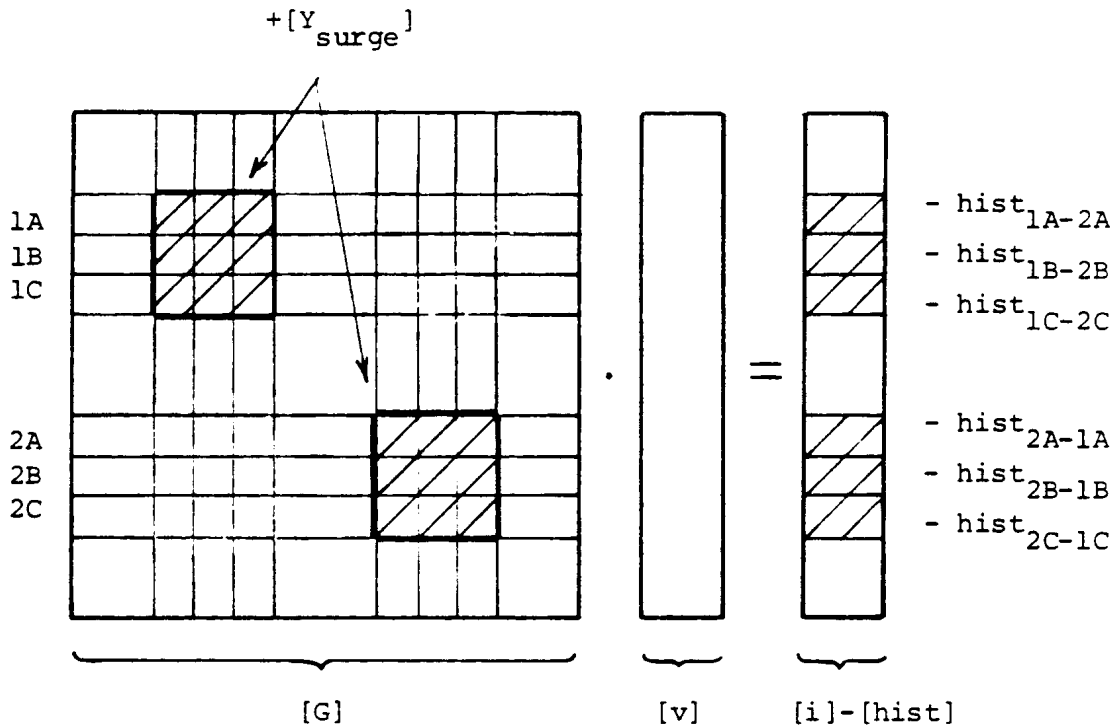
$$+[Y_{surge}]$$

Fig. 4.37 - Entries for a three-phase line into system of equations

M-phase lossless line models are useful, among other things, for

(a)   simple studies where one wants to investigate basic phenomena,

(b)   in lightning surge studies, where single-phase models are no longer adequate, and

(c)   as a basis for more sophisticated models discussed later.

Lightning surge studies cannot always be done with single-phase models. For simulating backflashovers on lines with ground wires, for example, the ground wire and at least the struck phase must be modelled ("2-phase line"). Since it is not always known which phase will be struck by the backflashover, it is probably best to model all three phases in such a situation ("4-phase line"). An example for such a study is discussed in Section 4.1.5.2, with 4-phase lossless line models representing the distribution line, and single-phase lossless line models representing the towers. Not included in the data listing are switches (or some other elements) for the simulation of potential flashovers from the tower top (nodes D) to phases A, B, C.

4.2.2.4 Single and M-Phase Distortionless Lines with Constant Parameters

Distortionless line models are seldom used, because wave propagation on power transmission lines is far from distortionless. They have been implemented in the EMTP, nonetheless, simply because it takes only a minor modification to change the lossless line equation into the distortionless line equation.

A single-phase transmission line, or a mode of an M-phase line, is distortionless if

$$\frac{R'}{L'} = \frac{G'}{C'} \qquad (4.110)$$

Losses are incurred in the series resistance R' as well as in the shunt conductance G'. The real shunt conductance of an overhead line is very small (close to zero), however. If its value must be artificially increased to make the line distortionless, with a resulting increase in shunt losses, then it is best to compensate for that by reducing the series resistance losses. The EMTP does this automatically by regarding the input value R'_{INPUT} as an indicator for the total losses, and uses only half of it for R',

$$\frac{R'}{L'} = \frac{G'}{C'} = \frac{1}{2}\frac{R'_{INPUT}}{L'} \qquad (4.111)$$

With this formula, the ac steady-state results are practically identical for the line being modelled as distortionless or with R lumped in 3 places; the transient response differs mainly in the initial rate of rise. From Eq. (4.111), the attenuation constant α becomes

$$\alpha = \frac{R'_{INPUT}}{2}\sqrt{\frac{C'}{L'}} \qquad (4.112)$$

The factor 1/2 can also be justified by using an approximate expression for the attenuation constant for lines with low attenuation and low distortion [48, p. 257],

$$\alpha = \frac{R'_{INPUT}}{2}\sqrt{\frac{C'}{L'}} + \frac{G'_{INPUT}}{2}\sqrt{\frac{L'}{C'}} \qquad (4.113)$$

which is reasonably accurate if R' << ωL' and G' << ωC'. This condition is fulfilled on overhead lines, except at very low frequencies. Eq. (4.112) is then obtained by dropping the term with G'_{INPUT} and by ignoring the fact that the waves are not only attenuated but distorted as well.

If a user wants to represent a truly distortionless line where G' is indeed nonzero, then the factor 1/2 should of course not be used. The factor 1/2 is built into the EMTP, however, and the user must therefore specify R'_{INPUT} twice as large as the true series resistance in this case.

With α known, an attenuation factor $e^{-\alpha\mathfrak{L}}$ is calculated ($\mathfrak{L}$ = length of line). The lossless line of Eq. (1.6) is then changed into a distortionless line by simply multiplying the history term of Eq. (1.6b) with this attenuation factor,

$$hist_{km}(t-\tau) = \left[-\frac{1}{Z}v_m(t-\tau) - i_{mk}(t-\tau)\right]\cdot e^{-\alpha\mathfrak{L}} \qquad (4.114)$$

The surge impedance remains the same, namely √L'/C'.

For M-phase lines, any of the M modes can be specified as distortionless. Mixing is allowed (e.g., mode 1 could be modelled with lumped resistances, and modes 2 and 3 as distortionless).

4-70

Better results are usually obtained with the lumped resistance model described next, even though lumping of resistances in a few places is obviously an approximation, whereas the distortionless line is solved exactly if the travel time is an integer multiple of Δt.

4.2.2.5 Single and M-Phase Lines with Lumped Resistances

Experience has shown that a lossy line with series resistance R' and negligible shunt conductance can be modelled with reasonable accuracy as one or more sections of lossless lines with lumped resistances in between. The simplest such approach is one lossless line with two lumped resistances R/2 at both ends. The equation for this model is easily derived from the cascade connection of R/2 - lossless line - R/2, and leads to a form which is identical with that of Eq. (1.6),

$$i_{km}(t) = \frac{1}{Z_{modified}} v_k(t) + hist_{km}(t-\tau)$$

(4.115)

except that the values for the surge impedance and history terms are slightly modified. With Z, R and τ calculated from Eq. (4.99),

$$Z_{modified} = Z + \frac{R}{2}$$

and

$$hist_{km}(t-\tau) = -\frac{1}{Z_{modified}}\left[v_m(t-\tau) + (Z-\frac{R}{2})i_{mk}(t-\tau)\right]$$

This model with R/2 at both ends is not used in the EMTP. Instead, the EMTP goes one step further and lumps resistances in 3 places, namely R/4 at both ends and R/2 in the middle, as shown in Fig. 4.27. This approach was taken because the form of the equation still remains the same as in Eq. (4.115), except that

$$Z_{modified} = Z + \frac{R}{4}$$

(4.116)

now. The history term becomes more complicated[18], and contains conditions from both ends of the line at t - τ,

$$hist_{km}(t-\tau) = -\frac{Z}{Z_{modified}^2}\left[v_m(t-\tau) + (Z-\frac{R}{4})i_{mk}(t-\tau)\right]$$

---

[18]The equation at the bottom of p. 391, left column, in [50] contains an error. I_k and I_m should not be computed from Eq. (7b); instead, use $I_k = -(1/Z) e_k(t - \tau) - hi_{k,m}(t - \tau)$ with the notation of [50], where Z is $Z_{modified}$ of Eq. (4.116). For I_m, exchange subscripts k and m.

$$-\frac{R/4}{Z^2_{modified}}\left[v_k(t-\tau) \;+\; (Z-\frac{R}{4})\,i_{km}(t-\tau)\right] \tag{4.117}$$

Users who want to lump resistances in more than 3 places can do so with the built-in three-resistance model, by simply subdividing the line into shorter segments in the input data. For example, 32 segments would produce lumped resistances in 65 places. Interestingly enough, the results do not change much if the number of lumped resistances is increased as long as R << Z. For example, results in Fig. 4.30 for the distributed-parameter case were practically identical for lumped resistances in 3, 65, or 301 places. Fig. 4.29 shows as well that TNA results are closely matched with R lumped in 3 places only.

One word of caution is in order, however. The lumped resistance model gives reasonable answers only if R/4 << Z, and should therefore not be used if the resistance is high. High resistances do appear in lightning surge studies if the parameters are calculated at a high frequency, e.g., at 400 kHz in Table 4.5, where R' = 597.4 Ω/km in the zero sequence mode. Lumping R in 3 places would still be reasonable in the case discussed there where each tower span of 90 m is modelled as one line, since 13.4 Ω is still reasonably small compared with Z = 1028 Ω. If it were used to model a longer line, say 90 km, then R/4 = 13,400 Ω, which would produce totally erroneous results[19]. In such a situation it might be best to ignore R altogether, or to use the frequency-dependent option if higher accuracy is required.

For M-phase lines, any of the M modes can be specified with lumped resistances. Mixing is allowed (e.g., mode 1 could be modelled with lumped resistances, and modes 2, ... M as distortionless). The lumped resistances do not appear explicitly as branches, but are built into Eq. (4.115) (4.116) and (4.117) for each mode. Should a user want to add them explicitly as branches, e.g., for testing purposes, then they would have to be specified as M x M - matrices [R] in phase quantities, which could easily be done with the M-phase nominal π-circuit input option by setting   L = 0 and C = 0. All modes would have to use the lumped resistance model in this set-up, that is, mixing of models would not be allowed in it.

4.2.2.6 Single and M-Phase Lines with Frequency-Dependent Parameters

The two important parameters for wave propagation are the characteristic impedance

$$Z_c \;=\; \sqrt{\frac{R' + j\omega L'}{G' + j\omega C'}} \tag{4.118}$$

and the propagation constant

$$\gamma \;=\; \sqrt{(R' + j\omega L')(G' + j\omega C')} \tag{4.119}$$

Both parameters are functions of frequency, even for constant distributed parameters R', L', G', C' (except for lossless and distortionless lines). The line model with frequency-dependent parameters can handle this case of constant

---

[19]The UBC version of the EMTP stops with an error message if R/4 > Z. It would be advisable to add a warning message as well as soon as R/4 gets fairly large (e.g. > 0.05 * Z).

distributed parameters[20], even though it has primarily been developed for frequency-dependent series impedance parameters R'(ω) and L'(ω). This frequency-dependence of the resistance and inductance is most pronounced in the zero sequence mode, as seen in Fig. 4.20. Frequency-dependent line models are therefore important for types of transients which contain appreciable zero sequence voltages and currents. One such type is the single line-to-ground fault.

To develop a line model with frequency-dependent parameters which fits nicely into the EMTP, it is best to use an approach which retains the basic idea behind Bergeron's method. Let us therefore look at what the expression v + Zi used by Bergeron looks like now, as one travels down the line. Since the parameters are given as functions of frequency, this expression must first be derived in the frequency domain. At any frequency, the exact ac steady-state solution is described by the equivalent π-circuit of Eq. (1.13), or in an input-output relationship form more convenient here,

$$\begin{bmatrix} V_k \\ I_{km} \end{bmatrix} = \begin{bmatrix} \cosh(\gamma\mathcal{L}) & Z_c\sinh(\gamma\mathcal{L}) \\ \dfrac{1}{Z}\sinh(\gamma\mathcal{L}) & \cosh(\gamma\mathcal{L}) \end{bmatrix} \begin{bmatrix} V_m \\ -I_{mk} \end{bmatrix} \tag{4.120}$$

which can be found in any textbook on transmission lines. Assume that we want to travel with the wave from node m to node k. Then the expression $V + Z_cI$ is obtained by subtracting Z_c times the second row from the first row in Eq. (4.120),

$$V_k - Z_cI_{km} = (V_m + Z_cI_{mk}) \cdot e^{-\gamma\mathcal{L}} \tag{4.121a}$$

or rewritten as

$$I_{km} = V_k/Z_c - (V_m/Z_c + I_{mk}) \cdot e^{-\gamma\mathcal{L}} \tag{4.121b}$$

with a negative sign on I_{km} since its direction is opposite to the travel direction. Eq. (4.121) is very similar to Bergeron's method; the expression $V + Z_cI$ encountered when leaving node m, after having been multiplied with a propagation factor $e^{-\gamma\mathcal{L}}$, the same when arriving at node k. This is very similar to Bergeron's equation for the distortionless line, except that the factor is $e^{-\alpha\mathcal{L}}$ there, and that Eq. (4.121) is in the frequency domain here rather than in the time domain.

Before proceeding further, it may be worthwhile to look at the relationship between the equations in the frequency and time domain for the simple case of a lossless line. In that case,

$$Z_c = \sqrt{\dfrac{L'}{C'}}, \quad \gamma = j\omega\sqrt{L'C'}, \quad and \quad e^{-\gamma\mathcal{L}} \approx e^{-j\omega\tau}$$

Anybody familiar with Fourier transformation methods for transforming an equation from the frequency into the time domain will recall that a phase sift of $e^{-j\omega\tau}$ in the frequency domain will become a time delay τ in the time domain. Furthermore, Z_c is now just a constant (independent of frequency), and Eq. (4.121) therefore transforms to

---

[20]This case differs from the line with lumped resistances inasmuch as the resistance becomes truly distributed now.

$$v_k(t) - Z_c i_{km}(t) = v_m(t-\tau) + Z_c i_{mk}(t-\tau)$$

which is indeed Bergeron's equation (1.6).

For the general lossy case, the propagation factor

$$A(\omega) = e^{-\gamma \mathcal{L}} = e^{-\alpha \mathcal{L}} \cdot e^{-j\beta \mathcal{L}}$$

with $\gamma = \alpha + j\beta$, contains an attenuation factor $e^{-\alpha \mathcal{L}}$ as well as a phase shift $e^{-j\beta \mathcal{L}}$, which are both functions of frequency. To explain its physical meaning, let us connect a voltage source V_{source} to the sending end m through a source impedance which is equal to $Z_c(\omega)$, to avoid reflections in m (Fig. 4.38). In that case, $V_m + Z_c I_{mk} = V_{source}$. Furthermore, let us assume that the receiving end k is open. Then from Eq. (4.121),

$$V_k = V_{source} \cdot A(\omega) \tag{4.122}$$
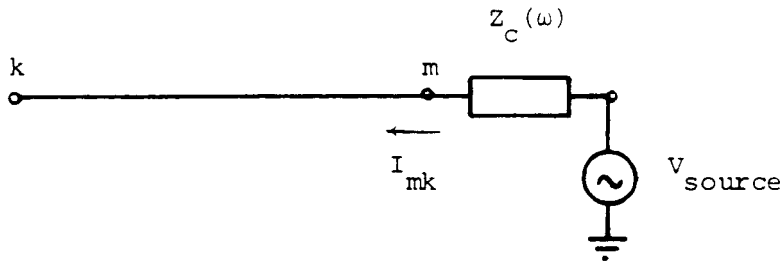
Fig. 4.38 - Voltage source connected to end m through matching impedance

that is, the propagation factor is the ratio (receiving end voltage) / (source voltage) of an open-ended line if the line is fed through a matching impedance $Z_c(\omega)$ to avoid reflections at the sending end[21]. If $V_{source} = 1.0$ at all frequencies from dc to infinity, then its time domain transform $v_{source}(t)$ would be a unit impulse (infinitely high spike which is infinitely narrow with an area of 1.0), and the integral of $v_{source}(t)$ would be a unit step. Setting $V_{source} = 1.0$ in Eq. (4.122) shows that $A(\omega)$ transformed to the time domain must be the impulse which arrives at the other end k, if the source is a unit impulse. This response to the unit impulse,

$$a(t) = \textit{inverse Fourier transform of } \{A(\omega)\} \tag{4.123}$$

will be attenuated (no longer infinitely high), and distorted (no longer infinitely narrow). Fig. 4.39 shows these responses for a typical 500 kV line of 100 miles length. They were obtained

---

[21]One could also connect a matching impedance $Z_c(\omega)$ from node k to ground to avoid reflections at the receiving end as well. In that case, the left-hand side of Eq. (4.122) becomes $2V_k$ rather than V_k. Note that the ratio $e^{-\gamma \mathcal{L}}$ starts from 1.0 and becomes less than 1.0 as the line length (or frequency) is increased. This is in contrast to the open-circuit response $V_k/V_m = 1.0/\cosh(\gamma \mathcal{L})$ more familiar to power engineers, which increases with length or frequency (Ferranti rise).
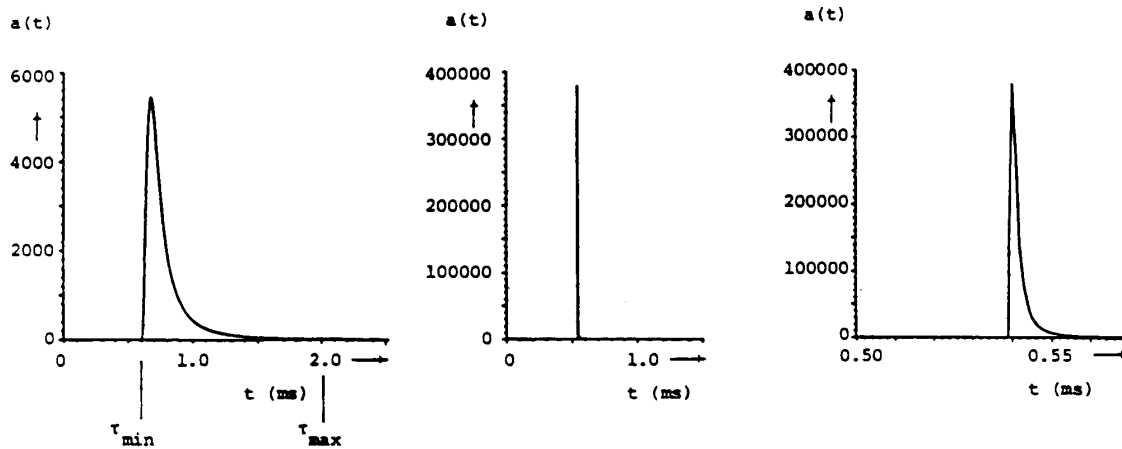
(a)   zero sequence mode

(b)   positive sequence
       mode with same
       scale as (a)

(c)   positive sequence
       mode with
       expanded scale

Fig. 4.39 - Receiving end response $v_k(t) = a(t)$ for the network of Fig. 4.38 if $v_{source}(t)$ = unit impulse [94]. Reprinted by permission of J. Marti

from the inverse Fourier transformation of $A(\omega) = \exp(-\gamma\mathcal{L})$ calculated by the LINE CONSTANTS supporting routine at a sufficient number of points in the frequency domain. The amplitude of the propagation factors $A(\omega)$ for the case of Fig. 4.39 is shown in Fig. 4.40.

The unit impulse response of a lossless line would be a unit impulse at $t = \tau$ with an area of 1.0. In Bergeron's method, this implies picking up the history term $v_m/Z + i_{mk}$ at $t - \tau$ with a weight of 1.0. In the more general case here, history terms must now be picked up at more than one point, and weighted with the "weighting function" $a(t)$. For the example of Fig. 4.39(a),
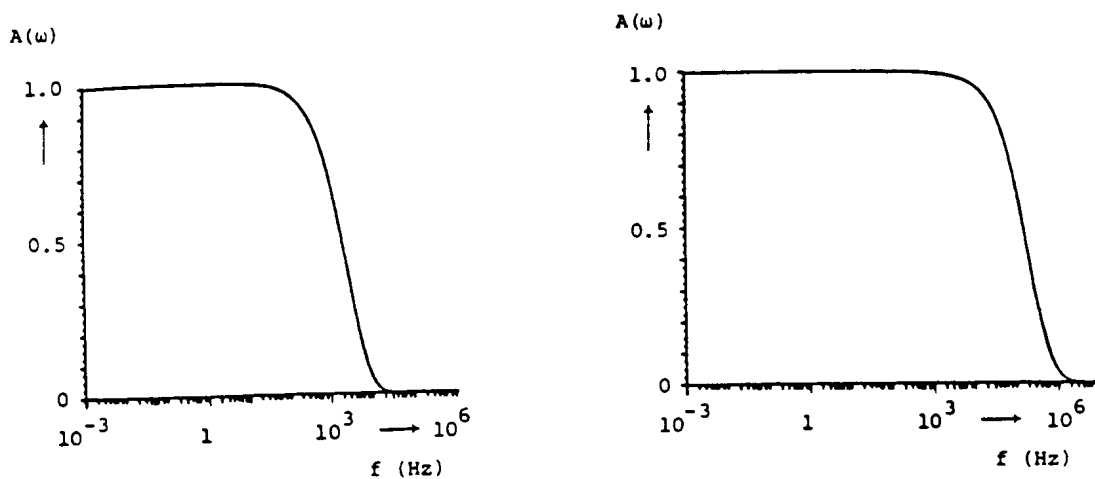
(a) zero sequence mode

(b) positive sequence mode

Fig. 4.40 - Propagation factor $A(\omega)$ for the line of Fig. 4.39 [94]. Reprinted by permission of J. Marti

history terms must be picked up starting at $\tau_{min} = 0.6$ ms back in time, to approx. $\tau_{max} = 2.0$ ms back in time. The value τ_{min} is the travel time of the fastest waves, while τ_{max} is the travel time of the slowest waves. Each terms has its own weight, with the highest weight of approx. 5400 around $\tau = 0.7$ ms back in time. Mathematically, this weighting of history at the other end of the line is done with the convolution integral

$$hist_{propagation} \ = \ - \int_{\tau_{min}}^{\tau_{max}} i_{m-total}(t-u)a(u)du \tag{4.124}$$

which can either be evaluated point by point, or more efficiently with recursive convolution as discussed later. The expression $i_{m-total}$ in Eq. (4.124) is the sum of the line current i_{mk} and of a current which would flow through the characteristic impedance if the voltage v_m were applied to it (expression $I_{mk} + V_m/Z_c$ in the frequency domain).

With propagation of the conditions from m to k being taken care of through Eq. (4.124), the only unresolved issue is the representation of the term V_k/Z_c in Eq. (4.121b). For the same 500 kV line used in Fig. 4.39, the magnitude and angle of the characteristic impedance Z_c are shown in Fig. 4.41. If the shunt conductance per unit length G' were ignored, as is usually done, Z_c would become infinite at $\omega = 0$. This complicates the mathematics somewhat, and since G' is not completely zero anyhow, it was therefore decided to use a nonzero value, with a default option of 0.03 μs/km. As originally suggested by E. Groschupf [96] and further developed by J. Marti [94], such a frequency-dependent impedance can be approximated with a Foster-I R-C
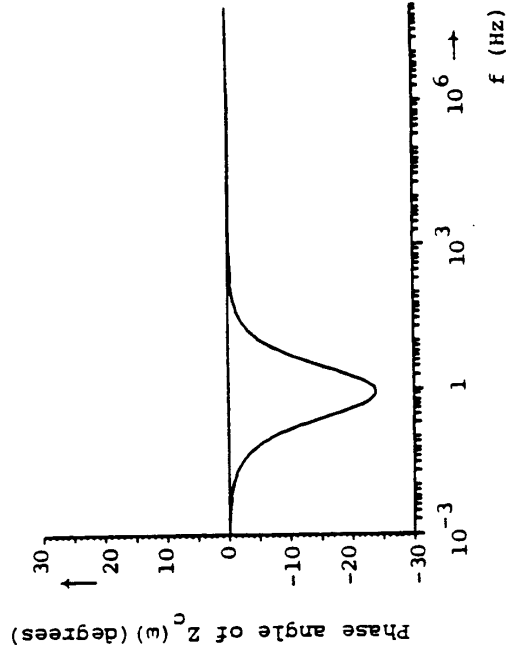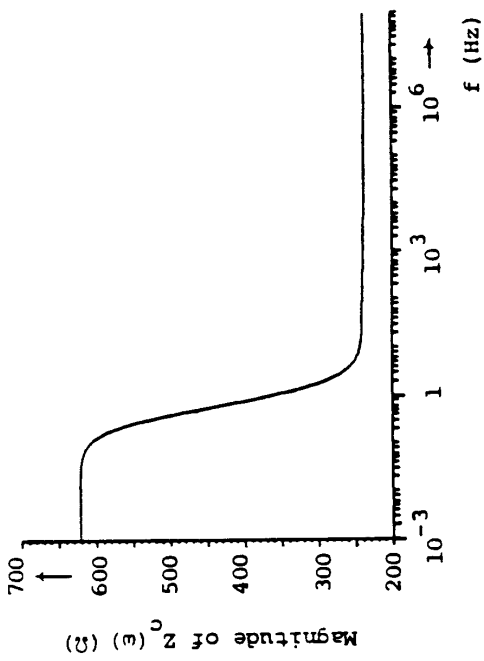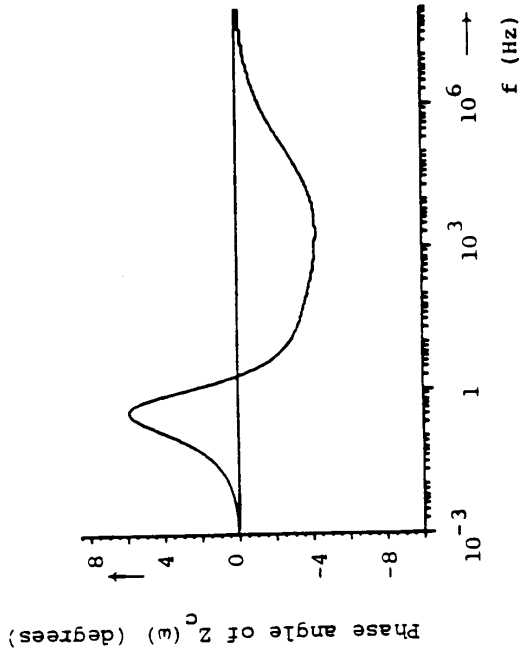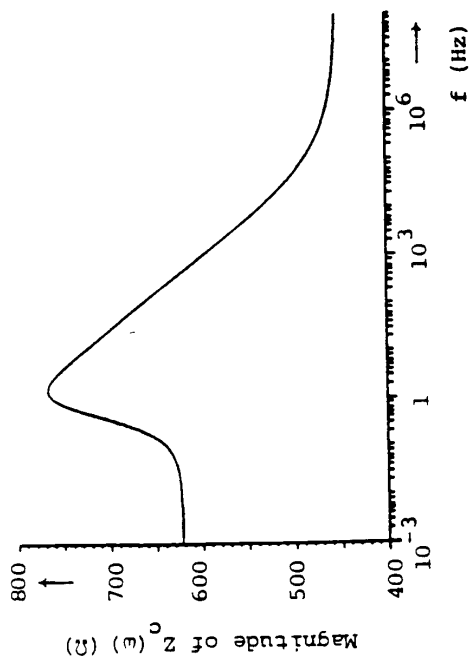
Fig. 4.41 – Characteristic impedance $Z_c(\omega)$ for the line of Fig. 4.39 [94]. Reprinted by permission of J. Marti

(a) zero sequence mode

(b) positive sequence mode

network. Then the line seen from node k becomes a simple R-C network in parallel with a current source $hist_{propagation}$ (Fig. 4.42(a)). One can then apply the trapezoidal rule of integration to the capacitances, or use any other method of implicit integration. This transforms each R-C block into a current source in parallel with an equivalent resistance. Summing these for all R-C blocks produces one voltage source in series with one equivalent resistance, or one current source in parallel with one equivalent resistance (Fig. 4.42(b)). In the solution of the entire network with Eq. (1.8), the frequency-dependent line is then simply represented again as a constant resistance R_{equiv} to ground, in parallel with a current source $hist_{RC} + hist_{propagation}$, which has exactly the same form as the equivalent circuit for the lossless line.

To represent the line in the form of Fig. 4.42 in the EMTP, it is necessary to convert the line parameters into a weighting function a(t) and into an R-C network which approximates the characteristic impedance. To do this, Z_c and γ are first calculated with the support routine LINE CONSTANTS, from dc to such a high frequency where both $A(\omega) = \exp(-\gamma \mathcal{L})$ becomes negligibly small and $Z_c(\omega)$ becomes practically constant. J. Marti [94] has shown that it is best to approximate $A(\omega)$ and $Z_c(\omega)$ by rational functions directly in the frequency domain. The weighting function a(t) can then be written down explicitly as a sum of exponentials, without any need for numerical inverse Fourier transformation. Similarly, the rational function approximation of $Z_c(\omega)$ produces directly the values of R and C in the R-C network in Fig. 4.42.

(a)   with R-C network

(b)   with equivalent resistance after
        applying implicit integration
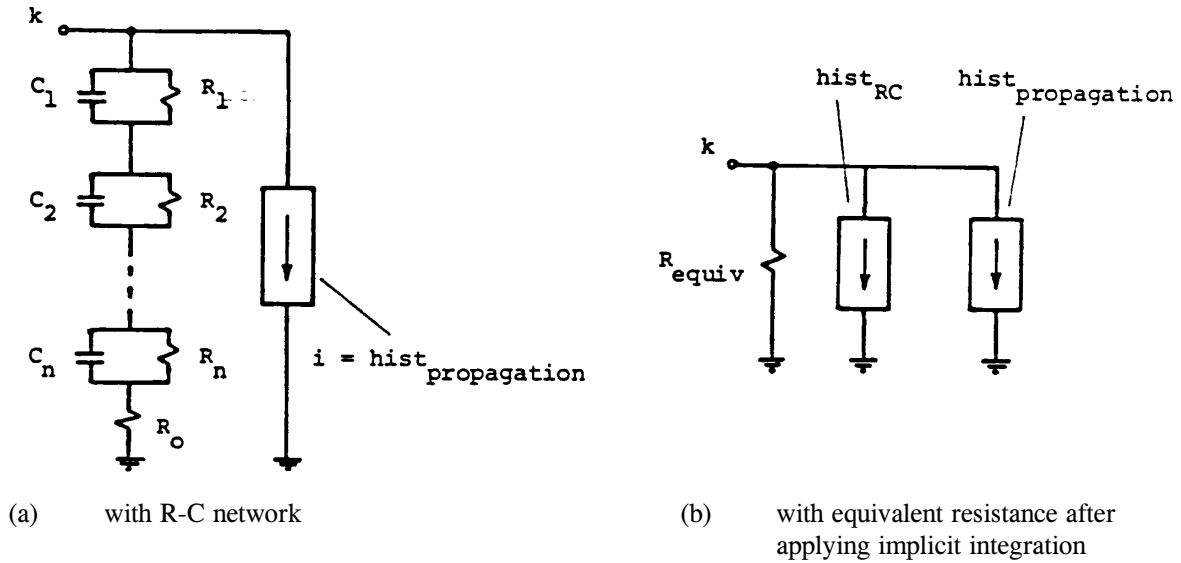
Fig. 4.42 - Frequency-dependent line representation seen from line end k

The rational function which approximates $A(\omega)$ has the form

$$A_{approx}(s) \; = \; e^{-s\tau_{min}} \, k \, \frac{(s+z_1)(s+z_2)\ldots(s+z_n)}{(s+p_1)(s+p_2)\ldots(s+p_m)} \tag{4.125}$$

with $s = j\omega$ and $n < m$. The subscript "approx" indicates that Eq. (4.125) is strictly speaking only an approximation to the given function $A(\omega)$, even though the approximation is very good. The factor $e^{-j\omega\tau min}$ is included to take care of the fact that $a(t)$ in Fig. 4.39 is zero up to $t = \tau_{min}$; this avoids fitting exponentials through the portion $0 \le t \le \tau_{min}$ where the values are zero anyhow (remember that a time shift $-\tau$ in the time domain is a phase shift $e^{-j\omega\tau}$ in the frequency domain). All poles p_i and zeros z_i in Eq. (4.125) are negative, real and simple (multiplicity one). With $n < m$, the rational function part of Eq. (4.125) can be expanded into partial fractions,

$$k \, \frac{(s+z_1)(s+z_2)\ldots(s+z_n)}{(s+p_1)(s+p_2)\ldots(s+p_m)} \; = \; \frac{k_1}{s+p_1} + \frac{k_2}{s+p_2} \ldots + \frac{k_m}{s+p_m} \tag{4.126}$$

The corresponding time-domain form of Eq. (4.15) then becomes

$$a_{approx}(t) \; = \; \left[k_1 e^{-p_1(t-\tau_{min})} + k_2 e^{-p_2(t-\tau_{min})} \ldots + k_m e^{-p_m(t-\tau_{min})} \right] for \; t \ge \tau_{min}$$

$$= \; 0 \qquad \qquad for \; t < \tau_{min} \tag{4.127}$$

This weighting function $a_{approx}(t)$ is used to calculate the history term $hist_{propagation}$ of Eq. (4.124) in each time step. Because of its form as a sum of exponentials, the integral can be found with recursive convolution much more efficiently

than with a point-by-point integration. If we look at the contribution of one exponential term $k_i e^{-p_i(t-\tau_{min})}$,

$$s_i(t) = \int_{\tau_{min}}^{\infty} i(t-u)k_i e^{-p_i(t-\tau_{min})} du \qquad (4.128)$$

then $s_i(t)$ can be directly obtained from the value $s_i(t - \Delta t)$ known from the preceding time step, with only 3 multiplications and 3 additions,

$$s_i(t) = c_1 \cdot s_i(t-\Delta t) + c_2 \cdot i(t-\tau_{min}) + c_3 \cdot i(t-\tau_{min}-\Delta t) \qquad (4.129)$$

as explained in Appendix V, with c_1, c_2, c_3 being constants which depend on the particular type of interpolation used for i.

The characteristic impedance $Z_c(\omega)$ is approximated by a rational function of the form [94]

$$Z_{c-approx}(s) = k \frac{(s+z_1)(s+z_2)...(s+z_n)}{(s+p_1)(s+p_2)...(s+p_n)} \qquad (4.130)$$

with $s = j\omega$. All poles and zeros are again real, negative and simple, but the number of poles is equal to the number of zeros now. This can be expressed as

$$Z_{c-approx}(s) = k_0 + \frac{k_1}{s+p_1} + \frac{k_2}{s+p_2}...\frac{k_n}{s+p_n} \qquad (4.131)$$

which corresponds to the R-C network of Fig. 4.42, with

$$R_0 = k_0$$

$$R_i = \frac{k_i}{p_i}, \quad C_i = \frac{1}{k_i}, \quad i=1,...n \qquad (4.132)$$

Rather than applying the trapezoidal rule to the capacitances in Fig. 4.42, J. Marti chose to use implicit integration with Eq. (I.3) of Appendix I[22], with linear interpolation on i. For each R-c block

$$i = \frac{v_i}{R_i} + C_i \frac{dv_i}{dt}$$

which has the exact solution

$$v_i(t) = e^{-\alpha_i \Delta t} \cdot v_i(t-\Delta t) + \frac{1}{C_i} \int_{t-\Delta t}^{t} e^{-\alpha_i(t-u)} i(u)du \qquad (4.133)$$

---

[22]This method is identical to the recursive convolution of Appendix V applied to Eq. (4.131). Whether recursive convolution is better than the trapezoidal rule is still unclear.

with $\alpha_i = 1/(R_iC_i)$. By using linear interpolation on i, the solution takes the form of

$$v_i(t) = R_{equiv-i} \cdot i(t) + e_i(t-\Delta t)$$
(4.134)

with $e_i(t - \Delta t)$ being known values of the preceding time step (formula omitted for simplicity), or after summing up over all R-C blocks and R_0,

$$v(t) = R_{equiv} \cdot i(t) + e(t-\Delta t)$$
(4.135a)

with

$$R_{equiv} = R_0 + \sum_{i=1}^{n} R_{equiv-i} \quad and \quad e = \sum_{i=1}^{n} e_i$$
(4.135b)

which can be rewritten as

$$i(t) = \frac{1}{R_{equiv}} v(t) + hist_{RC}$$
(4.136)

The equivalent resistance R_{equiv} enters into matrix [G] of Eq. (1.8), whereas the sum of the history terms $hist_{RC} + hist_{propagation}$ enters into the right hand side.

The key to the success of this approach is the quality of the rational function approximations for $A(\omega)$ and $Z_c(\omega)$. J. Marti uses Bode's procedure for approximating the magnitudes of the functions. Since the rational functions have no zeros in the right-hand side of the complex plane, the corresponding phase functions are uniquely determined from the magnitude functions (the rational functions are minimum phase-shift approximations in this case) [94]. To illustrate Bode's procedure, assume that the magnitude of the characteristic impedance in decibels is plotted as a function of the logarithm of the frequency, as shown in Fig. 4.43 [94]. The basic principle is to approximate the given curve by straight-line segments which are either horizontal or have a slope which is a multiple of 20 decibels/decade. The points where the slopes change define the poles and zeros of the rational function. By taking the logarithm on both sides of Eq. (4.130), and multiplying by 20 to follow the convention of working with decibels, we obtain

$$20\log|Z_{c-approx}(s)| = 20\log k + 20\log|s+z_1|\ldots + 20\log|s+z_n|$$
$$- 20\log|s+p_1|\cdots - 20\log|s+p_n|$$
(4.137)

For $s = j\omega$, each one of the terms in this expression has a straight-line asymptotic behavior with respect to ω. For instance, $20\log|j\omega + z_1|$ becomes $20\log z_1$ for $\omega \ll z_1$, which is constant, and $20\log\omega$ for $\omega \gg z_1$, which is a straight line with a slope of 20 db/decade. The approximation to Eq. (4.137) is constructed step by step: Each time a zero corner (at $\omega = z_i$) is added, the slope of the asymptotic curve is increased by 20 db, or decreased by 20 db each time a pole corner (at $\omega = p_i$) is added. The straight-line segments in Fig. 4.43 are only asymptotic traces; the actual function becomes a smooth curve without sharp corners. Since the entire curve is traced from dc to the

Fig. 4.43 - Asymptotic approximation of the magnitude of $Z_c(\omega)$ [94].
Reprinted by permission of J. Marti.
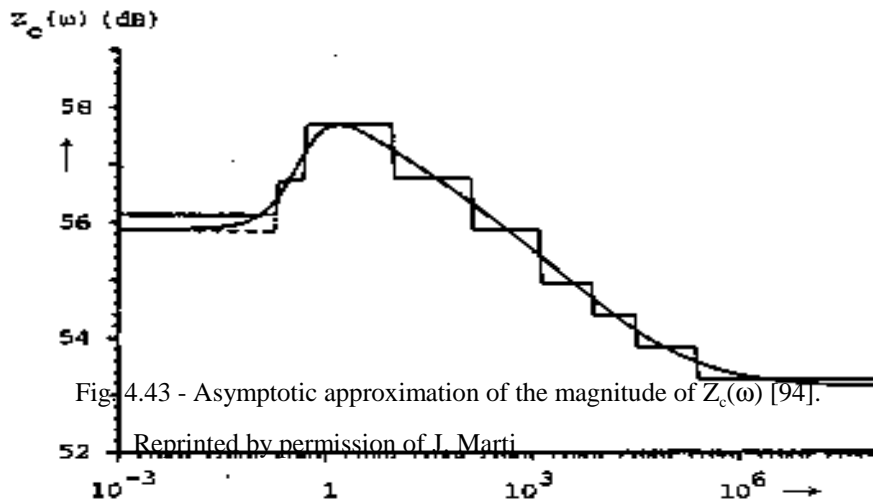
highest frequency at which the approximated function becomes practically constant, the entire frequency range is approximated quite closely, with the number of poles and zeros not determined a priori. J. Marti improves the accuracy further by shifting the location of the poles and zeros about their first positions. Fig. 4.44 shows the magnitude and phase errors of the approximation of $A(\omega)$, and Fig. 4.45 shows the errors for the approximation of $Z_c(\omega)$ for the line used in Fig. 4.39.

L. Marti has recently shown [95] that very good results can be obtained by using lower-order approximations with typically 5 poles and zeros rather than the 15 poles and zeros used in Fig. 4.44 and 4.45. Furthermore, he shows that positive and zero sequence parameters at power frequency (50 or 60 Hz) can be used to infer what the tower geometry of the line was, and use this geometry in turn to generate frequency-dependent parameters. With this approach, simple input data (60 Hz parameters) can be used to generate a frequency-dependent line model internally which is fairly accurate.
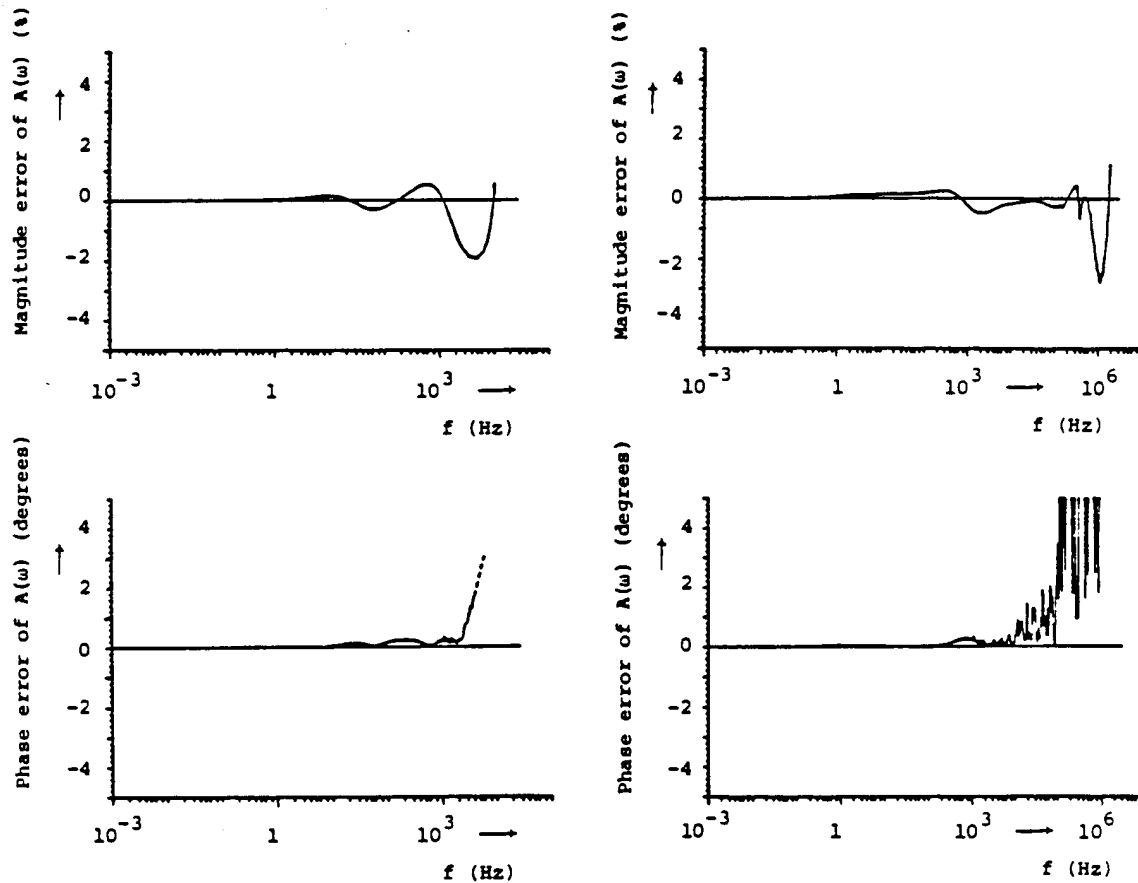
(a)   zero sequence mode   (b)   positive sequence mode
         (15 zeros and 20 poles)   (13 zeros and 17 poles)

Fig. 4.44 - Errors in approximation of $A(\omega)$ for line of Fig. 4.39 [94]. Reprinted by permission of J. Marti

For M-phase lines, any of the M modes can be specified as frequency-dependent, or with lumped resistances, or as distortionless. Mixing is allowed. A word of caution is in order here, however: At the time of writing these notes, the frequency-dependent line model works only reliably for balanced lines. For untransposed lines, approximate real and constant transformation matrices must be used, as explained in Section 4.1.5.3, which seems to produce reasonably
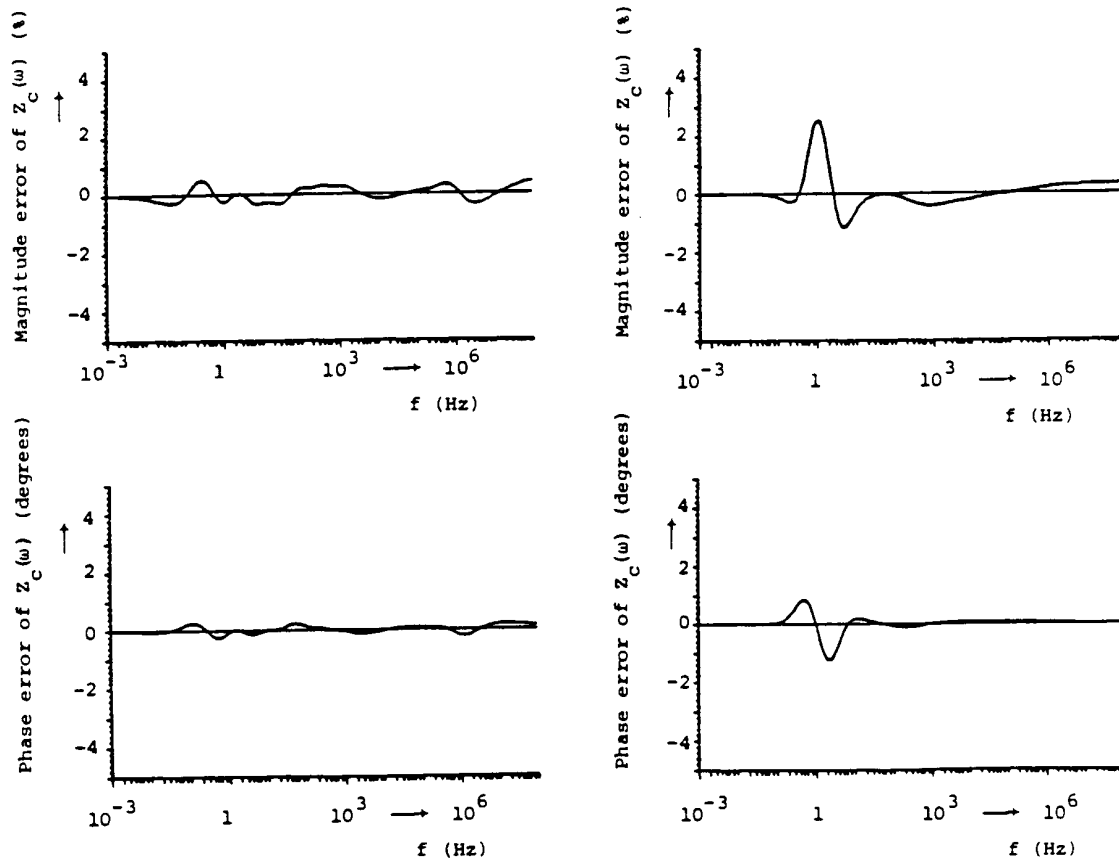
(a)   zero sequence mode   (b)   positive sequence mode
       (15 zeros and poles)   (16 zeros and poles)

Fig. 4.45 - Errors in approximation of $Z_c(\omega)$ for line for Fig. 4.39 [94]. Reprinted by permission of J. Marti

accurate results for single-circuit lines, but not for double-circuit lines. Research by L. Marti into frequency-dependent transformation matrices in connection with models for underground cables will hopefully improve this unsatisfactory state of affairs.
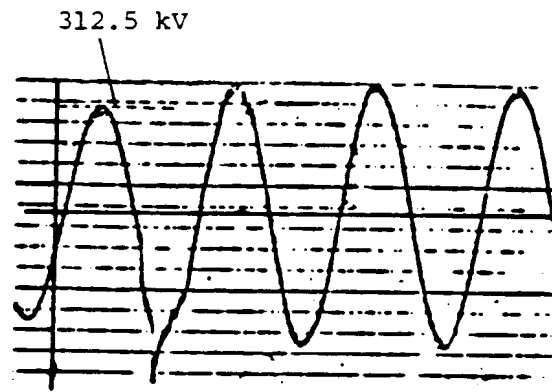
(a)
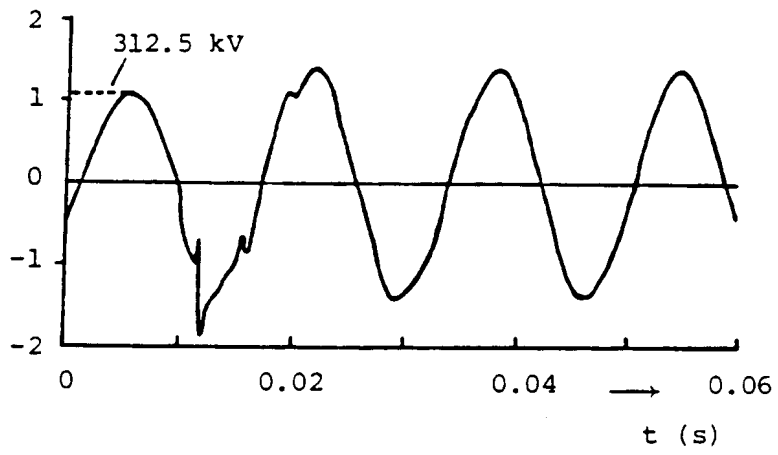
(b)
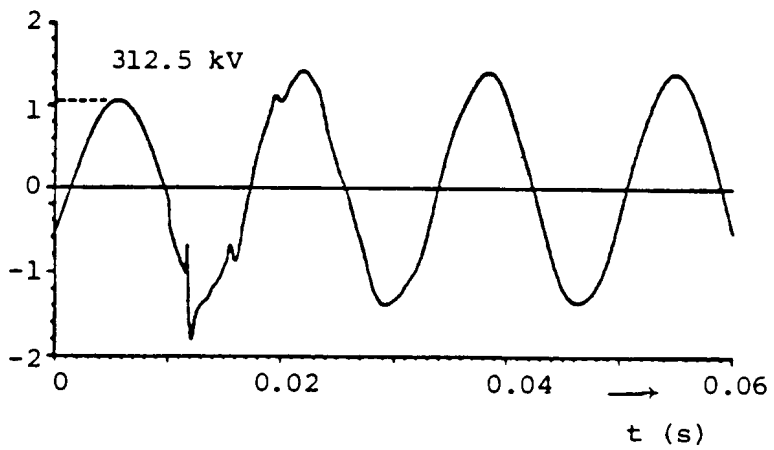
(c)

Fig. 4.46 - Comparison between voltages at phase b for [94]:
      (a) Field test oscillograph
      (b) BPA's frequency-dependence simulation
      (c) New model simulation
      Reprinted by permission of J. Marti

Field test results for a single-line-to-ground fault from Bonneville Power Administration have been sued by various authors to demonstrate the accuracy of frequency-dependent line models [84]. Fig. 4.46 compares the field test results with simulation results from an older method which used two weighting functions a_1 and a_2 [84], and from the newer method described here. The peak overvoltage in the field test was 1.60 p.u., compared with 1.77 p.u. in the older method and 1.71 p.u. in the newer method. Constant 60 Hz parameters would have produced an answer of 2.11 p.u.

5. UNDERGROUND CABLES

There is such a large variety of cable designs on the market, that it is difficult, if not impossible, to develop one computer program which can calculate the parameters R', L', C' for any type of cable.

For lower voltage ratings, the cables are usually unscreened and insulated with polyvinyl chloride. An example of a three-phase 1 kV cable with neutral conductor and armor is shown in Fig. 5.1.
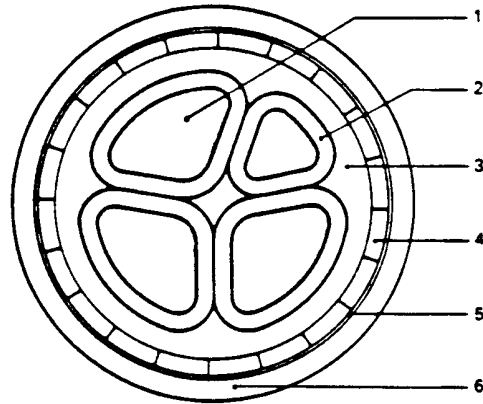
Fig. 5.1 - Armored 1 kV cable (1 = stranded conductor, 2 = insulation, 3 = bedding, 4 = flat steel wire armor, 5 = helical steel tape, 6 = plastic outer sheath). Reprinted by permission from Siemens Catalog 1980
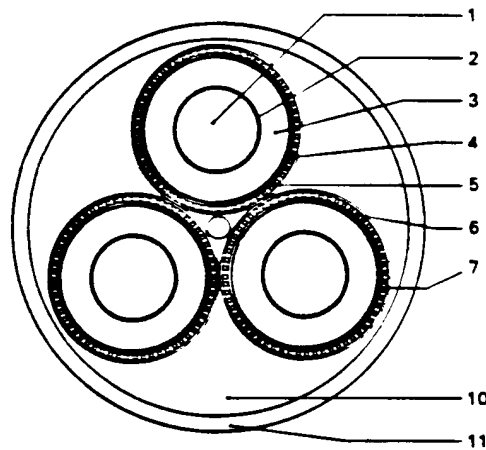
Fig. 5.2 - 12 to 35 kV distribution cable with concentric neutral conductors (1 = stranded conductor, 2, 4 = conductive layers, 3 = plastic insulation , 5 = conductive tape, 6 = concentric neutral conductors, 7 = helical copper tape, 10 = inner sheath, 11 = plastic outer sheath). Reprinted by permission from Siemens Catalog 1980

At the distribution voltage level, the cables are usually screened with concentric neutral conductors, as shown in Fig. 5.2.

At the transmission voltage level, two types of cables are in widespread use today, namely the pipe-type cable (Fig. 5.3) and the self-contained cable (Fig. 5.4). In the pipe-type cable, three paper-insulated oil-impregnated cables are drawn into a steel pipe at the construction site. The helical skid wires make it easier to pull the cables. After evacuation, the pipe is filled with oil and pressurized to a high pressure of approx. 1.5 kPa. Pipe-type cables are used for voltages from 69 to 345 kV, with 550 kV cables under development. The typical

Steel pipe
(filled with insulating oil)

Skid wires

Metallic tapes

Paper/oil insulation

Screen

Conductor
(stranded copper)
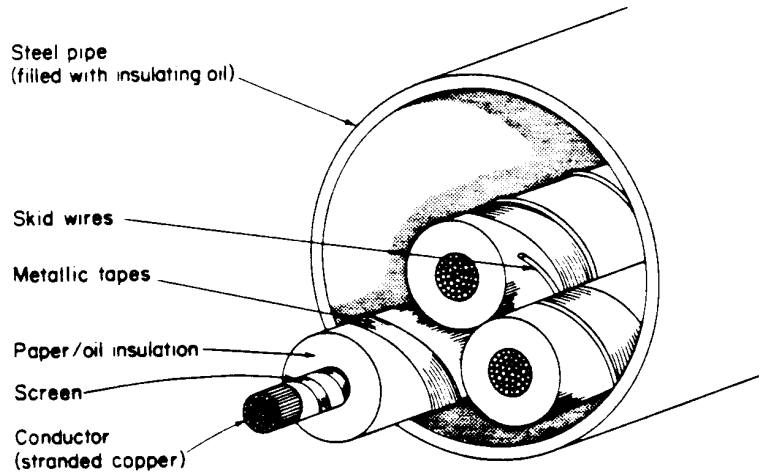
Fig. 5.3 - Pipe-type oil-filled cable [148]. © 1979 John Wiley & Sons,
Ltd. Reprinted by permission of John Wiley & Sons, Ltd

self-contained oil-filled cable is a single-core cable (Fig. 5.4). Its stranded core conductor has a hollow duct which is filled with oil and kept pressurized with low-pressure bellow-type expansion tanks. Underground and submarine self-contained cables are essentially identical, except that underground cables do not always have an armor.
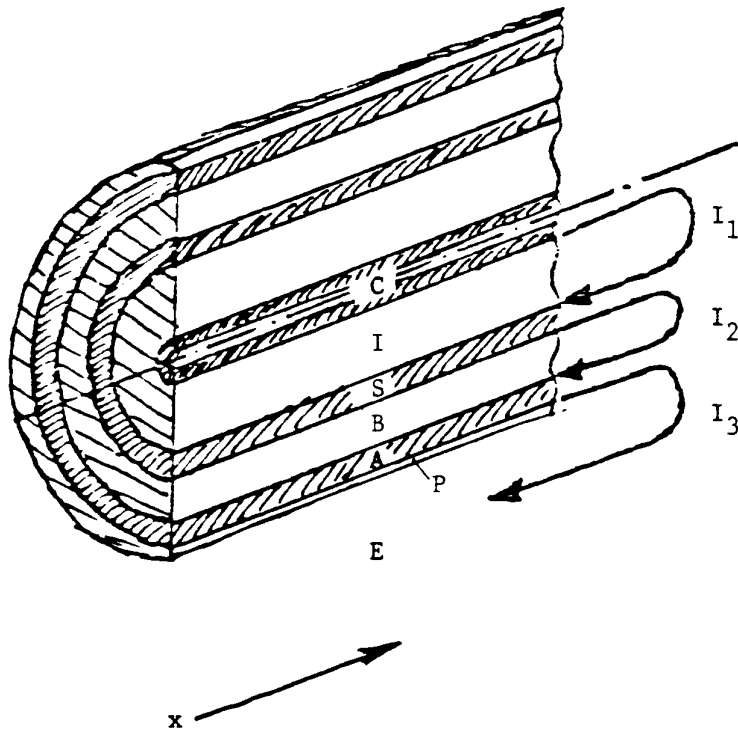
Fig. 5.4 - Single-core self-contained cable (C = stranded core conductor with oil-filled duct, I = paper insulation, S = metallic sheath, B = bedding, A = armor, P = plastic sheath). Details of conductive layers left out

Gas-insulated systems with compressed SF_6 gas are used for compact substation designs. The busses in such substations consist of tubular conductors inside a metallic sheath, with the conductors held in place by plastic spacers at certain intervals (Fig. 5.5). SF_6-busses are in use in lengths of up to 300 m. A similar design can be used for cables, but SF_6-cables are still experimental, with the sheath usually being corrugated. In EMTP studies, such relatively short

(a) Single-phase   (b) Three-phase
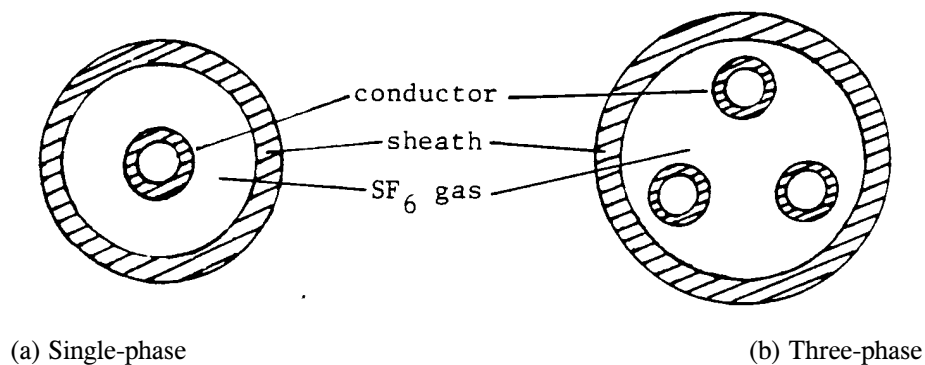
Fig. 5.5 - SF_6 bus

busses can often be ignored, or represented as a lumped capacitance. Only in studies of fast transients with high frequencies must SF_6-busses be represented as transmission lines. Since the single-phase geometry is essentially

similar to that of a self-contained cable, and since the three-phase geometry is similar to that of a pipe-type cable, no special programs are needed to handle SF_6-busses or cables, except that the three-phase arrangement of Fig. 5.5(b) has no electrostatic screens as in the case of a pipe-type cable of Fig. 5.3.

Fig. 5.1 to 5.5 are only a few examples for the large variety of cable designs. The support routine CABLE CONSTANTS was developed by A. Ametani essentially for the coaxial single-core cable design of Fig. 5.4 and 5.5(a), and later expanded for the pipe-type cable of Fig. 5.3 and for the three-phase SF_6-busses of Fig. 5.5(b). At this time, there is no support routine for the types of lower voltage cables shown in Fig. 5.1 and 5.2, but calculation methods applicable to such non-coaxial arrangements are briefly discussed in Section 5.7.

5.1 Single-Core Cables

The cable parameters of coaxial arrangements, as in Fig. 5.4, are derived in the form of equations for coaxial loops [150, 152]. In Fig. 5.4, loop 1 is formed by the core conductor C and the metallic sheath S as return, loop 2 by the metallic sheath S and metallic armor A as return, and finally loop 3 by the armor A and either earth or sea water as return.

5.1.1 Series Impedances

The series impedances of the three loops are described by three coupled equations

$$-\begin{bmatrix} \dfrac{dV_1}{dx} \\ \dfrac{dV_2}{dx} \\ \dfrac{dV_3}{dx} \end{bmatrix} = \begin{bmatrix} Z'_{11} & Z'_{12} & 0 \\ Z'_{21} & Z'_{22} & Z'_{23} \\ 0 & Z'_{32} & Z'_{33} \end{bmatrix} \begin{bmatrix} I_1 \\ I_2 \\ I_3 \end{bmatrix} \tag{5.1}$$

The self impedance Z'_{11} of loop 1 consists of 3 parts,

$$Z'_{11} = Z'_{core\text{-}out} + Z'_{core/sheath\text{-}insulation} + Z'_{sheath\text{-}in} \tag{5.2}$$

with

$Z'_{core\text{-}out}$ = internal impedance (per unit length) of tubular core conductor with return path outside the tube (through sheath here)

$Z'_{core/sheath\text{-}insulation}$ = impedance (per unit length) of insulation between core and sheath, and

$Z'_{sheath\text{-}in}$ = internal impedance (per unit length) or tubular sheath with return path inside the tube (through core conductor here).

Similarly,

$$Z'_{22} = Z'_{sheath\text{-}out} + Z'_{sheath/armor\ insulation} + Z'_{armor\text{-}in} \tag{5.3}$$

and

$$Z'_{33} = Z'_{armor-out} + Z'_{armor/earth-insulation} + Z'_{earth} \qquad (5.4)$$

with analogous definitions as for Eq. (5.2). The coupling impedances $Z'_{12} = Z'_{21}$ and $Z'_{23} = Z'_{32}$ are negative because of opposing current directions (I_2 in negative direction in loop 1, I_3 in negative direction in loop 2),

$$Z'_{12} = Z'_{21} = -Z'_{sheath-mutual} \qquad (5.5a)$$

$$Z'_{23} = Z'_{32} = -Z'_{armor-mutual} \qquad (5.5b)$$

with $Z'_{sheath-mutual} =$ mutual impedance (per unit length) of tubular sheath between the inside loop 1 and the outside loop 2, and

           $Z'_{armor-mutual} =$ mutual impedance (per unit length) of tubular armor between the inside loop 2 and the outside loop 3.

Finally, $Z'_{13} = Z'_{31} = 0$ because loop 1 and loop 3 have no common branch.

The simplest terms to calculate are the impedances of the insulation, which are simply

$$Z'_{insulation} = j\omega \frac{\mu_0}{2\pi} \ln\frac{r}{q} \qquad (5.6)$$

with μ_0 = permeability of insulation ($\mu_0 = 2 \cdot 10^{-4}$ H/km),

      r = outside radius of insulation,

      q = inside radius of insulation,   in identical units (e.g. in mm)

If the insulation is missing, e.g., between armor and earth, then $Z'_{insulation} = 0$.

The internal impedance and the mutual impedance of a tubular conductor with inside radius q and outside radius r (Fig. 4.5) are a function of frequency, and are found with modified Bessel functions [149].

$$Z'_{tube-in} = \rho m/2\pi q D \{I_0(mq) K_1(mr) + K_0(mq) I_1(mr)\} \qquad (5.7a)$$

$$Z'_{tube-out} = \rho m/2\pi r D \{I_0(mr) K_1(mq) + K_0(mr) I_1(mq)\} \qquad (5.7b)$$

$$Z'_{tube-mutual} = \rho/2\pi q r D \qquad (5.7c)$$

with $D = I_1(mr) K_1(mq) - I_1(mq) K_1(mr) \qquad (5.7d)$

The parameter

$$m = \sqrt{j\omega\mu/\rho} \qquad (5.7e)$$

is the reciprocal of the complex depth of penetration (OVERLINE) p defined earlier in Eq. (4.5).

A subroutine SKIN for calculating the impedance $Z'_{tube-out}$ of Eq. (5.7b) was developed at BPA for the support routine LINE CONSTANTS, and later modified at UBC to "TUBE" for the calculation of $Z'_{tube-in}$ and $Z'_{tube-mutual}$ as well. All arguments of the modified Bessel functions I_0, I_1, K_0, K_1 are complex numbers with a phase angle of 45° because of Eq. (5.7e). In such a case, the following real functions of a real variable can be used instead:

$$ber(x) + jbei(x) = I_0(x\sqrt{j})$$

$$ber'(x) + jbei'(x) = \sqrt{j}I_1(x\sqrt{j}) \qquad (5.8)$$

$$ker(x) + jkei(x) = K_0(x\sqrt{j})$$

$$ker'(x) + jkei'(x) = -\sqrt{j}K_1(x\sqrt{j})$$

These functions are evaluated numerically with the polynomial approximations of Eq. (9.11.1) to (9.11.14) of [149]. For arguments $x \le 8$, the absolute error is $< 10^{-7}$, whereas for arguments $x > 8$, the relative error is $< 3 \bullet 10^{-7}$. To avoid too large numbers in the numerator and denominator for large arguments of x, the expressions f(x) and g(x) in Eq. (9.22.9) and (9.11.10) of [149] are multiplied with exp (- 1 + j/√2 x). If both arguments mq and mr have absolute values greater than 8, then in addition to the above multiplication, the K_0- and K_1- functions are further multiplied by exp (2mq) to avoid indefinite terms 0/0 for very large arguments.

When the support routine CABLE CONSTANTS was developed, subroutine TUBE did not yet exist, and A. Ametani chose slightly different polynomial approximations for the functions I_0, I_1, K_0, K_1 in Eq. (5.7). He uses Eq. (9.8.1) to (9.8.8) of [149] instead, with the accuracy being more or less the same as in the polynomials used in subroutine TUBE.

Simpler formulas with hyperbolic cotangent functions in place of Eq. (5.7) were developed by M. Wedepohl [150], which also give fairly accurate answers as long as the condition $(r-q)/(r+q) < 1/8$ is fulfilled. This was verified by the author for the data of a 500 kV submarine cable.

The only term which still remains to be defined is Z'_{earth} in Eq. (5.4). This is the earth or sea return impedance of a single buried cable, which is discussed in more detail in Section 5.3.

Submarine cables always have an armor, while underground cables may only have a sheath. The armor often consists of spiralled steel wires, which can be treated as a tube of equal cross section with $\mu_r = 1$, without too much error (153). A more accurate representation is discussed in [151].

Eq. (5.1) is not yet in a form suitable for EMTP models, in which the voltages and currents of the core, sheath, and armor must appear, in place of loop voltages and currents. The transformation is achieved by introducing the terminal conditions

$$V_1 = V_{core} - V_{sheath} \qquad\qquad I_1 = I_{core}$$
$$V_2 = V_{sheath} - V_{armor} \qquad and \qquad I_2 = I_{sheath} + I_{core}$$
$$V_3 = V_{armor} \qquad\qquad I_3 = I_{armor} + I_{sheath} + I_{core} \qquad (5.9)$$

where V_{core} = voltage from core to ground,

V_{sheath} = voltage from sheath to ground,

V_{armor} = voltage from armor to ground.

By adding row 2 and 3 or Eq. (5.1) to the first row, and by adding row 3 to the second row, we obtain

$$-\begin{bmatrix} dV_{core}/dx \\ dV_{sheath}/dx \\ dV_{armor}/dx \end{bmatrix} = \begin{bmatrix} Z'_{cc} & Z'_{cs} & Z'_{ca} \\ Z'_{sc} & Z'_{ss} & Z'_{sa} \\ Z'_{ac} & Z'_{as} & Z'_{aa} \end{bmatrix} \begin{bmatrix} I_{core} \\ I_{sheath} \\ I_{armor} \end{bmatrix} \tag{5.10}$$

with
$$Z'_{cc} = Z'_{11} + 2Z'_{12} + Z'_{22} + 2Z'_{23} + Z'_{33},$$

$$Z'_{cs} = Z'_{sc} = Z'_{12} + Z'_{22} + 2Z'_{23} + Z'_{33},$$

$$Z'_{ca} = Z'_{ac} = Z'_{sa} = Z'_{as} = Z'_{23} + Z'_{33},$$

$$Z'_{ss} = Z'_{22} + 2Z'_{23} + Z'_{33},$$

$$Z'_{aa} = Z' \tag{5.10b}$$

Some authors use equivalent circuits without mutual couplings, in place of the matrix representation of Eq. (5.10) with self impedances (diagonal elements) and mutual impedances (off-diagonal elements). For example, [150] shows the equivalent circuit of Fig. 5.6 for a single-core cable without armor, which is essentially the same as the TNA four-conductor representation of overhead lines in Fig. 4.28.
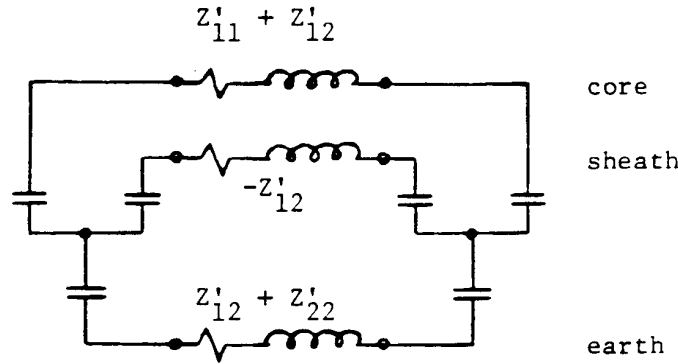
Fig. 5.6 - Three conductor π-circuit suitable for TNA's

5.1.2 Shunt Admittances

For the current changes along the cable of Fig. 5.4, the loop equations are not coupled,

$$-dI_1/dx = (G'_1 + j\omega C'_1)V_1$$

$$-dI_2/dx = (G'_2 + j\omega C'_2)V_2 \tag{5.11}$$

$$-dI_3/dx = (G'_3 + j\omega C'_3)V_3$$

G'_i and C'_i are the shunt conductance and shunt capacitance per unit length for each insulation layer. If there is no insulation (e.g., armor in direct contact with the earth), then replace Eq. (5.11) by

$$V_i = 0 \tag{5.12}$$

The shunt capacitance of tubular insulation with inside radius q and outside radius r is

$$C^{/} = \frac{2\pi\varepsilon_0\varepsilon_r}{\ln\dfrac{r}{q}}$$

(5.13)

with ε_0 = absolute permittivity or dielectric constant of free space (ε_0 defined in Eq. (4.22)) and ε_r = relative permittivity or relative dielectric constant of the insulation material. Typical values for ε_r are shown in Table 5.1 [54].

Table 5.1 - Relative permittivity and loss factor of insulation material [54]. Reprinted by permission of Springer-Verlag and the authors

Insulation Material	Relative Permittivity at 20°C	Loss Factor tanδ at 50 Hz and 20°C
butyl rubber	3.0 to 4.0	0.05
insulating oil	2.2 to 2.8	0.001 to 0.002
oil-impregnated paper	3.3 to 4.2	0.003 to 0.008
polyvinyl chloride	3.0 to 4.0	0.02 to 0.10
polyethylene	2.3	0.0002
crosslinked polyethylene	2.4	0.0004

The shunt conductance G' is ignored in the support routine CABLE CONSTANTS, which is probably reasonable in most cases. It cannot be ignored, however, if buried pipelines are to be modelled as cables, as explained in Section 5.6. If values for G' are available for cables, it is normally in the form of a dielectric loss angle δ or loss factor tanδ. Then

$$G' = \omega C' \bullet \tan\delta$$

(5.14)

Typical values for tanδ are shown in Table 5.1. In the literature on electromagnetics, the shunt conductance is usually included by assuming that ε_r in Eq. (5.13) is a complex number $\varepsilon_r = \varepsilon' - j\varepsilon''$, with Eq. (5.13) rewritten as

$$G^{/} + j\omega C^{/} = \frac{j\omega2\pi\varepsilon_0}{\ln\dfrac{r}{q}}(\varepsilon^{/} - j\varepsilon^{//})$$

(5.15)

For cross-linked polyethylene, both ε' and ε'' are more or less constant up to 100 mHz [168], with the typical values of Table 5.1. For oil-impregnated paper insulation, both ε' and ε'' vary with frequency. Measured values between 10 kHz and 100 mHz [154] showed variations in ε' of approximately 20%, whereas ε'' varied much more. Fig. 5.7 shows the variations which can be expressed as a function of frequency with the empirical formula

$$\epsilon_r = 2.5 + \frac{0.94}{(1+j\omega6\cdot10^{-9})^{0.315}} \tag{5.16}$$
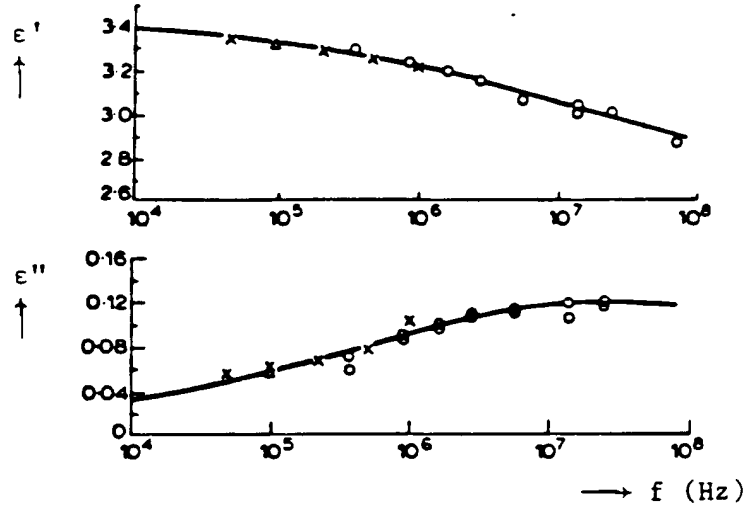
Fig. 5.7 - Measured values of ϵ' and ϵ'' for a cable with oil-impregnated paper insulation at 20°C [154]. Reprinted by permission of IEE and the authors

The support routine CABLE CONSTANTS now assumes $\epsilon'' = 0$ and ϵ' being constant, but it could easily be changed to include empirical formulas based on measurements, such as Eq. (5.16). At this time, formulas based on theory are not available because the frequency-dependent behavior of dielectrics is too complicated. Except for very short pulses ($< 5~\mu$s), the dielectric losses are of little importance for the attenuation [154], and using a constant ϵ' with $\epsilon'' = 0$ should therefore give reasonable answers in most cases.

Again, Eq. (5.11) is not yet in a form suitable for EMTP models. With the conditions of Eq. (5.9), they are transformed to

$$-\begin{bmatrix} dI_{core}/dx \\ dI_{sheath}/dx \\ dI_{armor}/dx \end{bmatrix} = \begin{bmatrix} Y'_1 & -Y'_1 & 0 \\ -Y'_1 & Y'_1+Y'_2 & -Y'_2 \\ 0 & -Y'_2 & Y'_2+Y'_3 \end{bmatrix} \begin{bmatrix} V_{core} \\ V_{sheath} \\ V_{armor} \end{bmatrix} \tag{5.17}$$

where $Y'_i = G'_i + j\omega C'_i$.

5.2 Parallel Single-Core Cables

There are not many cases where single-core cables can be represented with single-phase models. A notable exception is the submarine cable system, where the individual cables are laid so far apart (to reduce the risk of anchors damaging more than one phase) that coupling between the phases can be ignored. In general, the three

single-core cables of a three-phase underground installation are laid close together so that coupling between the phases must be taken into account.

If we start out with loop analysis, then it is apparent that it is only the most outer loops (armor with earth return, or sheath with earth return in the absence of armor) through which the phases become coupled. The magnetic field outside the cable produced by loop 1 and 2 in Fig. 5.4 is obviously zero, because the field created by I_1 in the core is exactly cancelled by the
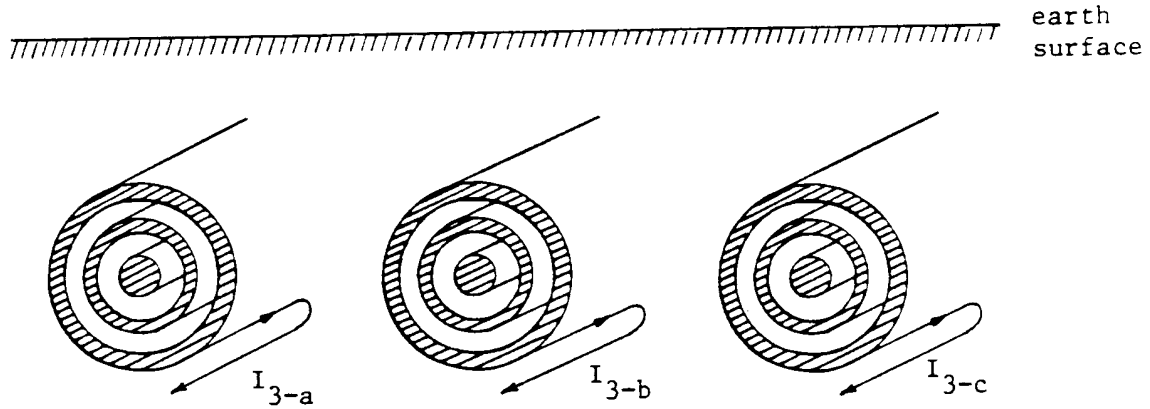
Fig. 5.8 - Three single-core cables

returning current I_1 in the sheath, etc. The first two equations in (5.1) are therefore still valid, whereas the third equation now has coupling terms among the three phases a, b, c, or

$$
[Z'_{loop}] =
\begin{bmatrix}
\begin{bmatrix} Z'_{11}a & Z'_{12}a & 0 \\ Z'_{21}a & Z'_{22}a & Z'_{23}a \\ 0 & Z'_{32}a & Z'_{33}a \end{bmatrix} & \begin{bmatrix} 0 & 0 & 0 \\ 0 & 0 & 0 \\ 0 & 0 & Z'_{ab} \end{bmatrix} & \begin{bmatrix} 0 & 0 & 0 \\ 0 & 0 & 0 \\ 0 & 0 & Z'_{ac} \end{bmatrix} \\
& \begin{bmatrix} Z'_{11}b & Z'_{12}b & 0 \\ Z'_{21}b & Z'_{22}b & Z'_{23}b \\ 0 & Z'_{32}b & Z'_{33}b \end{bmatrix} & \begin{bmatrix} 0 & 0 & 0 \\ 0 & 0 & 0 \\ 0 & 0 & Z'_{bc} \end{bmatrix} \\
\text{symmetric} & & \begin{bmatrix} Z'_{11}c & Z'_{12}c & 0 \\ Z'_{21}c & Z'_{22}c & Z'_{23}c \\ 0 & Z'_{32}c & Z'_{33}c \end{bmatrix}
\end{bmatrix}
\tag{5.18}
$$

with Z'_{ab}, Z'_{ac}, Z'_{bc} being the mutual impedances between the three outer loops of Fig. 5.8. By using Eq. (5.9) for the transformation from loop to phase (core, sheath, armor) quantities, the matrix in Eq. (5.18) becomes

$$[Z'_{phase}] = \begin{bmatrix} [Z'_{self\text{-}a}] & [Z'_{mutuala\text{-}b}] & [Z'_{mutuala\text{-}c}] \\ & [Z'_{self\text{-}b}] & [Z'_{mutualb\text{-}c}] \\ symmetric & & [Z'_{self\text{-}c}] \end{bmatrix} \qquad (5.19)$$

The 3 x 3 submatrices $[Z_{self\text{-}a}]$ etc. on the diagonal are identical to the matrix in Eq. (5.10a) for each cable by itself, whereas the 3 x 3 off-diagonal matrices have identical elements, e.g.,

$$[Z'_{mutuala\text{-}b}] = \begin{bmatrix} Z'_{ab} & Z'_{ab} & Z'_{ab} \\ Z'_{ab} & Z'_{ab} & Z'_{ab} \\ Z'_{ab} & Z'_{ab} & Z'_{ab} \end{bmatrix} \qquad (5.20)$$

The only elements not yet defined are the mutual impedances Z'_{ab}, Z'_{ab}, Z'_{bc} of the outer earth return loops, which are discussed in more detail in Section 5.3. If one of the cables does not have an armor, its self submatrix is obviously a 2 x 2 matrix and its mutual submatrix is a 2 x 3 matrix. For cables without sheath and armor, the submatrices become 1 x 1 and 1 x 3, respectively.

There is no coupling among the three phases in the shunt admittances. Therefore, the shunt admittance matrix for the three-phase system is simply

$$[Y'_{phase}] = \begin{bmatrix} [Y'_a] & 0 & 0 \\ 0 & [Y'_b] & 0 \\ 0 & 0 & [Y'_c] \end{bmatrix} \qquad (5.21)$$

where $[Y'_a]$ is the 3 x 3 matrix of Eq. (5.17) for phase a, etc.

The screening effect of the sheath and armor depends very much on the method of grounding. For example, if cable a is operated at 100 A between core and ground, with sheath and armor ungrounded and open-circuited, then the full 100 A will flow in the outer loop (loop currents $I_1 = 100$, $I_2 = 100$, $I_3 = 100$ in Fig. 5.4). This will produce maximum induced voltages in the conductors of a neighboring cable b. How much nuisance this induction effect creates depends again on the method of grounding within cable b itself. If cable b is operated between core and ground (loads connected from core to ground), and if its sheath and armor are ungrounded and open-circuited, then the induced voltage will drive a circulating current through the core, ground and load impedances. If cable b is operated between core and sheath (loads connected from core to sheath), then there will be no circulating current in that loop, because according to Eq. (5.20), the induced voltages are identical in core and sheath. There would be a circulating current through the sheath and armor in parallel with earth return if the sheath (and armor) is grounded at both ends.

If both the sheath and armor in the current-carrying cable a are grounded at both ends, then the voltage induced in the conductors of the neighboring cable b would be small. For the practical example of a 500 kV ac

submarine cable at 60 Hz, 14% of the core current would return through the sheath, 87.8% through the armor, and only 5.6% through the outermost loop with ground or sea water return. The induction effect in neighboring cables would then be only 5.6% compared to the case with ungrounded sheath and armor. The algebraic sum is larger than 100% because there are phase shifts among the three currents ($I_{sheath} = 14e^{-j148°}$, $I_{armor} = 87.8e^{+j179°}$, $I_{earth} = 5.6e^{-j86°}$).

5.3 Earth-Return Impedances[1]

In Eq. (5.4), the impedance of the loop formed by the outermost tubular conductor and the earth (or sea water) as return path is needed. This shall be called the "self earth-return impedance." For the matrix of Eq. (5.18), the "mutual earth-return impedance" Z'_{ik} between the loop formed by the outermost tubular conductor and the earth return path of cable i, and the analogous loop of cable k, is needed as well.

The four main methods of installing cables are as follows [148]:

(a)   The cable is laid directly in the soil, in a trench which is filled with a backfill consisting of either the original soil or of other material with lower or more stable thermal resistivity.

(b)   The cable is laid in ducts or troughs, usually of earthenware or concrete.

(c)   The cable is drawn into circular ducts or pipes, which allows additional cables to be installed without excavation.

(d)   The cable is installed, in air, e.g. in tunnels built for other purposes.

In cases (a), (b) and (c) the cable is clearly buried underground, and formulas for buried conductors must therefore be used. In case (a), the radius R of the outermost insulation is simply the outside radius of the cable. In cases (b) and (c) it should be the inside radius of the duct if the duct has a similar resistivity as the soil, or the outside radius if it is a very bad conductor, or possibly some average radius if it is neither a good nor a bad conductor. What to do in case (d) is somewhat unclear. Reasonable answers might be obtained by representing the tunnel with an equivalent circular cross section of radius R. Another alternative is to assume that the tunnel floor is the surface of the earth, and then use the earth-return impedance formula for overhead conductors. This would ignore current flows in the earth above the tunnel floor.

5.3.1 Buried Conductors in Semi-Infinite Earth

Exact formulas for the self and mutual earth-return impedances of buried conductors were first derived by Pallaczek [29]. In these formulas, the earth is treated as semi-infinite, extending from the surface downwards and sideways to infinity. If the horizontal distance between cable i and cable k is x, and if cable i and k are buried at depth h and y, respectively (Fig. 5.9), then the mutual earth-return impedance is [150]

$$Z'_{mutual} = \frac{\rho m^2}{2\pi}\left\{K_0(md) - K_0(mD) + \int_{-\infty}^{\infty} \frac{\exp\{-(h+y)\sqrt{\alpha^2 + m^2}}{|\alpha| + \sqrt{\alpha^2 + m^2}} \exp(j\alpha x)\, d\alpha\right\}$$

(5.22)

where

$d = \sqrt{x^2 + (h-y)^2}$ = direct distance between cables i and k,

$D = \sqrt{x^2 + (h+y)^2}$ = distance between cable i and image of cable k in air,

m = reciprocal of depth of penetration for earth from Eq. (5.7e),

α = integration constant.
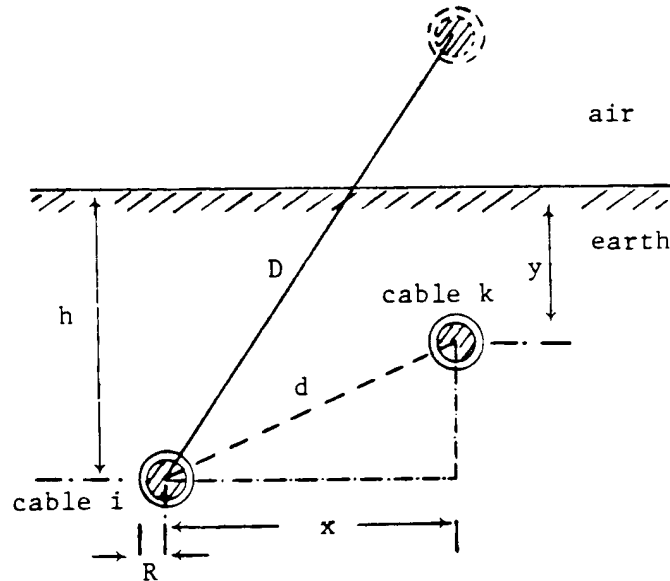
Fig. 5.9 - Geometric configuration of two cables

The self earth-return impedance is obtained from Eq. (5.22) by choosing the x,y- coordinate on the surface of the outermost insulation, e.g., x = R and y = H,

$$Z'_{earth} = \text{(same as Eq. (5.22), with y = h, x = R)} \qquad (5.23)$$

with R = outside radius of outermost insulation. The permeability μ of earth and air are assumed to be identical in these equations. Furthermore, they are written in a slightly different form than in Pollaczek's original paper, but they are in fact identical.

While the K_0 terms in Eq. (5.22) are easy to evaluate, the integral terms in both (5.22) and (5.23) cannot be calculated that easily. Wedepohl [150] gives an infinite series, which has been compared by Srivallipuranandan [168] with a direct numerical integration method based on Romberg extrapolation. Both results agreed to within 0.1%. Since the function under the integral is highly oscillatory, direct numerical integration is not easy, and the series expansion is therefore the preferred approach.

The support routine CABLE CONSTANTS does not use the exact Pollaczek formula. Ametani recognized that the integral terms in Eq. (5.22) and (5.23) become identical with Carson's earth return impedance if the numerator exp $\{-(h+y)\sqrt{\alpha^2+m^2}\}$ is replaced by exp $\{-(h+y)|\alpha|\}$. Accepting this approximation, which is valid for $|\alpha| >> |m|$, he can then use Carson's infinite series or asymptotic expansion discussed in Section 4.1.1.1. Fig.

5.10 and 5.11 show the errors in Ametani's results from support routine CABLE CONSTANTS, as well as the errors of Wedepohl's approximate formulas [150] for self impedance,

$$Z'_{earth} = \frac{\rho m^2}{2\pi} \{-\ln\frac{\gamma mR}{2} + 0.5 - \frac{4}{3} mh\} \tag{5.24}$$

and for mutual impedance

$$Z'_{mutual} = \frac{\rho m^2}{2\pi} \{-\ln\frac{\gamma md}{2} + 0.5 - \frac{2}{3} m\mathcal{L}\} \tag{5.25}$$

with γ = Euler's constant, and

       $\mathcal{L}$ = sum of the depths of burial of the two conductors.

Wedepohl's approximations are amazingly accurate up to 100 kHz (error < 1%), and then become less accurate as the frequency increases (25% error at 1 mHz) where the condition |mR| < 0.25 or |md| < 0.25 is no longer fulfilled.
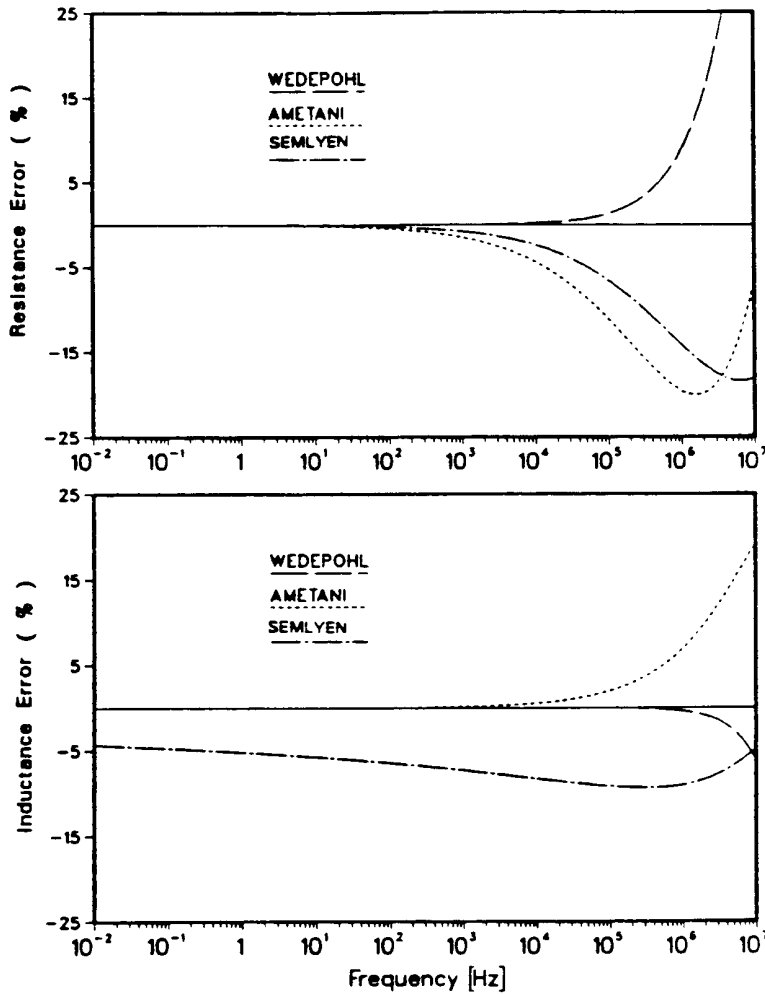
Fig. 5.10 - Relative errors in self earth-return impedance formulas for buried conductors (R = 48.4 mm, ρ = 100 Ωm) [168]. Reprinted by permission of N. Srivallipuranandan

5-14
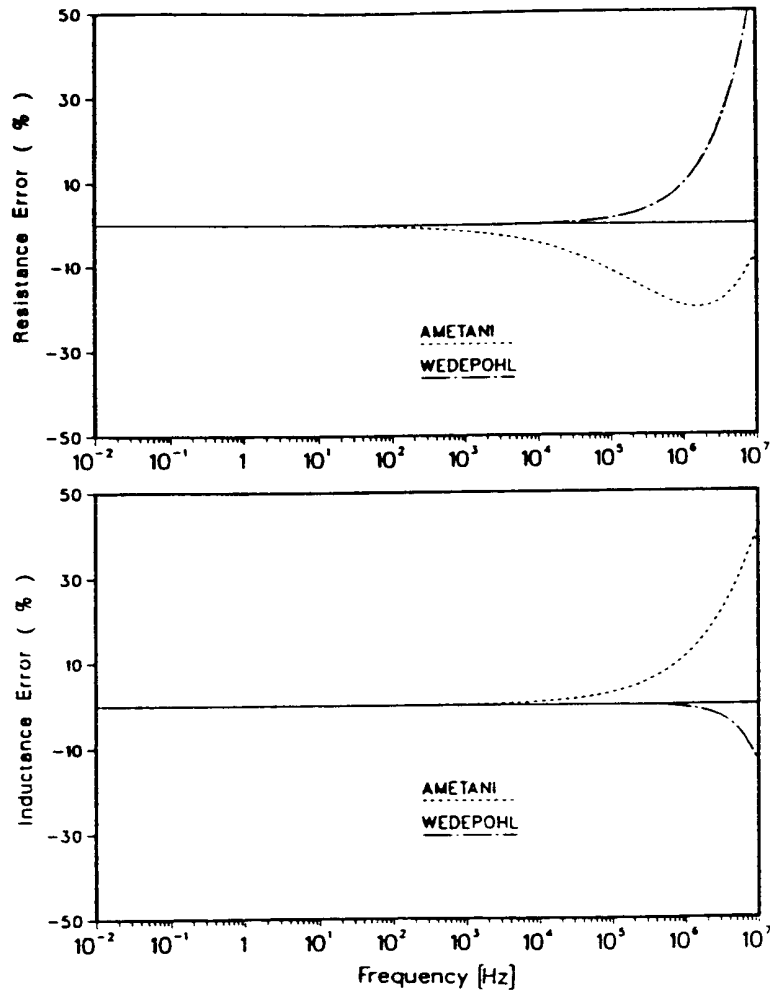
Fig. 5.11 - Relative error in mutual earth-return impedance formulas for
buried conductors (d = 0.3 m, h = 0.75 m, y = 0.75 m) [168].
Reprinted by permission of N. Srivallipuranandan

Semlyen has recently developed a very simple formula based on complex depth (OVERLINE) p = 1/m
[156], analogous to Eq. (4.3) for the case of overhead lines. For the self earth-return impedance, the formula is

$$Z'_{earth} = \frac{j\omega\mu}{2\pi} \ln(R + \frac{1}{mR}) \tag{5.26}$$

while a similar formula for the mutual impedance has not yet been found. The error of Eq. (5.26) is plotted in Fig.
5.10. Considering the extreme simplicity of this formula as compared to Pollaczek's formula, it is amazing to see
how reasonable the results from this approximate formula are.

5.3.2 Buried Conductors in Infinite Earth

In some cases, it may be reasonable to assume that the earth is infinite in all directions around the cable.
This assumption can be made when the depth of penetration in the earth

5-15

$$d_{earth} = \frac{\sqrt{2}}{|m|} = 503 \sqrt{\frac{\rho_{earth(\Omega m)}}{f(Hz)}} \quad (m) \tag{5.27}$$

becomes much smaller than the depth of the burial. For submarine cables, where ρ is typically 0.2 Ωm, this is probably more or less true over the entire frequency range of interest, whereas for underground cables it would only be true above a few MHz or so. Bianchi and Luoni [151] have used this infinite earth assumption to find the sea return impedance of submarine cables.

The self earth-return impedance for infinite earth is easily obtained from the tubular conductor formula (5.7a), by letting the outside radius r go to infinity. Then with q = R,

$$Z'_{earth} = \frac{\rho m}{2\pi R} \frac{K_0(mr)}{K_1(mR)} \tag{5.28}$$

The mutual earth-return impedance was derived in [168] as

$$Z'_{mutual} = \frac{\rho \, K_0(md)}{2\pi R_i R_k K_1(mR_i) K_1(mR_k)} \tag{5.29}$$

5.3.3 Overhead Conductors

If the cable is installed in air, or laid on the surface of the ground, then the earth-return impedances are the same as those discussed for overhead lines in Section 4. The support routine CABLE CONSTANTS uses Carson's formula in that case. For a cable laid on the surface of the ground, the height is equal to R. Ametani has tried a special formula of Sunde for conductors on the surface of the ground, but the answers were found to be very oscillatory around the seemingly correct answer. Sunde's formula was therefore not implemented.

5.3.4 Mutual Impedance Between Overhead Conductor and Buried Conductor

There is inductive coupling between the loop of an overhead conductor with earth return and the loop of a buried conductor with earth return. The mutual impedance between these two loops is needed, for example, for studying the coupling effects in pipelines from overhead lines, as discussed in Section 5.6. This case was treated by Pollaczek as well, with

$$Z'_{mutual} = \int_{-\infty}^{\infty} \frac{\exp\{-h|\alpha| - y\sqrt{\alpha^2 + m^2}\}}{|\alpha| + \sqrt{\alpha^2 + m^2}} \exp(j\alpha x) \, d\alpha \tag{5.30}$$

As in the case of buried conductors, Ametani uses an approximation for this integral by replacing $y\sqrt{\alpha^2 + m^2}$ with $y|\alpha|$. With this approximation, the formula becomes identical with Carson's equations, with the height of the buried conductor having a negative value. In connection with a pipeline study [158], it was verified that Carson's formula and Pollaczek's formula give identical results at 60 Hz. At higher frequencies, the differences would probably be similar to those shown in Fig. 5.11.

5.4 Pipe-Type Cable

Compared to the geometry of the single-core cable of Fig. 5.4, the geometry of the pipe-type cable of Fig. 5.3 is more complicated. It is therefore more complicated to obtain the impedances of a pipe-type cable, mainly for two reasons,

(a)   The single-core cables inside the pipe are not concentric with respect to the pipe.

(b)   The steel pipe is magnetic, and subject to current-dependent saturation effects.

The analysis is somewhat simplified by the fact that the depth of penetration into the pipe is less than the pipe thickness at power frequency and above. At 60 Hz, it is 1.5 mm from Eq. (5.27), with typical values of $\rho = 0.2 \bullet 10^{-6}$ Ωm and $\mu_r = 400$, whereas a typical pipe thickness for a 230 kV cable is 6.4 mm. For transient studies with frequencies above power frequency, the pipe thickness can therefore be assumed to be infinite, or equivalently, the earth-return can be ignored. Table 5.2 shows the current returning in the earth for a single-phase-to-ground

Table 5.2 - Earth-return current in a 230 kV pipe-type cable for single-phase fault ($\mu_r = 400$)

f (Hz)	current in earth (percent of core current)
0.6	94.50
6	31.00
60	0.85
600	0.00

fault in a 230 kV pipe-type cable, with the pipe being in contact with the earth. To arrive at these values, it was assumed that the core of the faulted phase was in the center of the pipe, and that the two unfaulted phases can be ignored. With these assumptions, the impedance formulas of Section 5.1 can be used. If the two unfaulted phases were included, the earth-return current would probably be even less because some current would return through the shield tapes and skid wires of the unfaulted phases. The relative permeability μ_r influences the values of Table 5.2; with $\mu_r = 50$, 6% of the current would return through the earth at 60 Hz, or 0.02% with $\mu_r = 1600$.

5.4.1 Infinite Pipe Thickness (No Earth Return)

If the depth of penetration is less than the pipe thickness, then no voltage will be induced on the outside of the pipe ($Z'_{pipe-mutual} = 0$ from Eq. (5.7c)), and consequently, the loop current pipe/earth return will be practically zero. In that case, the pipe is the only return path. The configuration is then essentially the same as that of three single-core cables in Fig. 5.8, except that the pipe replaces the earth as the return path.

If we assume that each phase consists of three conductors (e.g., core, shield tapes represented as sheath, skid wires represented as armor), then the loop impedance matrix is the same as in Eq. (5.18). Coupling will only exist among the three outermost loops of each armor (skid wires) with return through the pipe. What is needed then

is a formula for the self impedances Z'_{33a}, Z'_{33b}, Z'_{33c} of the loops formed by each armor (skid wires) and the pipe, and a formula for the mutual impedances Z'_{ab}, Z'_{bc}, Z'_{ca} between two such loops.

The support routine CABLE CONSTANTS finds these impedances with formulas first derived by Tegopoulos and Kriezis [159], and later used by Brown and Rocamora [160]. In these formulas it is assumed that the current is concentrated in an infinitesimally small filament at the center of each single-core cable. This model can be applied to conductors of finite radius if proximity effects are negligible, either because of symmetrical positioning within the pipe, or because the conductor radius is small compared to the distance to other conductors or the pipe wall. In pipe-type cables, neither condition is met since the conductors are relatively large and lie on the bottom of the pipe. The pipe-type cable impedances from CABLE CONSTANTS are therefore not completely accurate, but no better analytical models are available at this time. Brown and Rocamora, who proposed the formulas originally, recommend methods based on the subdivision into partial conductors discussed in Section 5.7, for more accurate impedance calculation [161]. Hopefully, a support routine based on the subdivision method will become available some day.

The self impedance Z'_{33a}, etc. of the loop between the armor (skid wires) and the pipe consists again of three terms, as in Eq. (5.4). The first term $Z'_{amor\text{-}out}$ is the same as in Eq. (5.7b), with the assumption that proximity effects can be ignored. The second term for the insulation becomes more complicated than Eq. (5.6), because of the eccentric geometry,

$$ Z'_{insulation} = j\omega \frac{\mu_0}{2\pi} \ln \left\{ \frac{q}{R_i} \left[1 - \left(\frac{d_i}{q} \right)^2 \right] \right\} \tag{5.31} $$

with q, R_i and d_i defined in Fig. 5.12. The third term for the internal impedance of the pipe, with return on the inside, replaces Z'_{earth} in Eq. (5.4):
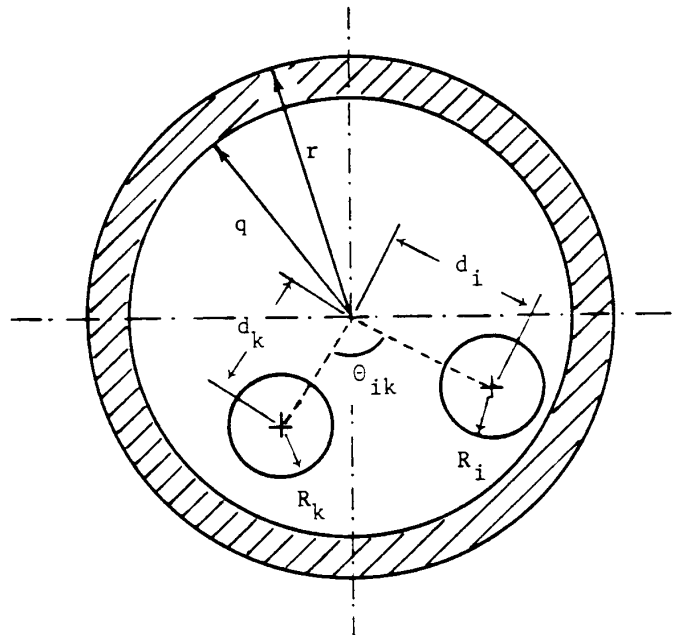
Fig. 5.12 - Geometry of pipe-type cable (q,r = inside and outside radius of pipe; R_i, R_k = outside radius of single-core cables i, k; d_i, d_k = offset from center)

$$Z'_{pipe\text{-}in} = j\omega \frac{\mu}{2\pi} \left\{ \frac{K_0(mq)}{mqK_1(mq)} + 2\sum_{n=1}^{\infty} \left(\frac{d_i}{q}\right)^{2n} \frac{K_n(mq)}{n\mu_r K_n(mq) - mqK'_n(mq)} \right\} \tag{5.32}$$

with m from Eq. (5.7e), and $\mu = \mu_0\mu_r$ = permeability of the pipe,

K_i = modified Bessel function of the second kind of order i

K'_i = derivative of K_i.

For the concentric case with $d_i = 0$, Eq. (5.32) becomes identical with Eq. (5.28).

The mutual impedance Z'_{ab}, etc. between two outermost loops formed by armor (skid wires) and pipe is

$$Z'_{mutual} = j\omega \frac{\mu_0}{2\pi} \{ \ln \frac{q}{\sqrt{d_i^2 + d_k^2 - 2d_i d_k \cos\Theta_{ik}}} + \mu_r \frac{K_0(mq)}{mqK_1(mq)}$$

$$+ \sum_{n=1}^{\infty} (\frac{d_i d_k}{q^2})^n \cos(n\Theta_{ik})(2\mu r \frac{K_n(mq)}{n\mu_r K_n(mq) - mqK'_n(mq)} - \frac{1}{n}) \} \tag{5.33}$$

Except for replacing Z'_{earth} with $Z'_{pipe\text{-}in}$, and for using Z'_{mutual} from Eq. (5.33) instead of (5.22), all calculations remain the same as in Section 5.2, including the transformation from loop to phase quantities. If the cables inside the pipe do not have an armor (skid wires) or a sheath (shield tapes), then some of the matrices will be reduced to 2 x 2, or 1 x 1, as discussed in Section 5.2. In practice, the shield tapes and skid wires can probably be represented as one single sheath.

The magnetic properties of the steel pipe are easily taken into account by using the proper values for the relative permeability μ_r in Eq. (5.32) and (5.33). Unfortunately, μ_r depends on the current because of saturation effects, as shown in Fig. 5.13 [192]. To model saturation effects accurately is not simple, because even at one frequency, say at 60 Hz, the permeability would not remain constant over one cycle. A two-slope saturation curve was tried in [161], with the conclusion that reasonably accurate answers can be obtained with a constant value of μ_r. The sensitivity of the results with respect to μ_r can then be checked by re-running the case with one or more different values of μ_r.
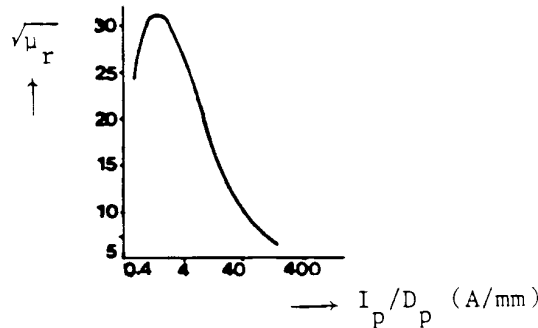
Fig. 5.13 - Relative permeability as a function of pipe current (I_p = pipe current, D_p = pipe diameter) [192]. © 1964 IEEE

Since the shield tapes and skid wires are in contact with the pipe wall, the values of the capacitances between the shield tapes/ skid wires of the three phases and between them and the pipe are immaterial. They are shorted out. Eq. (5.21) can therefore be used directly for the shunt admittance matrix. The support routine CABLE CONSTANTS does not assume this contact with the pipe in the beginning, however, and is therefore more general. For this general case, a potential coefficient matrix is found first,

$$[P'_{phase}] = \begin{bmatrix} [P'_a] & & \\ & [P'_b] & \\ & & [P'_c] \end{bmatrix} + \begin{bmatrix} [P'_{aa}] & [P'_{ab}] & [P'_{ac}] \\ [P'_{ba}] & [P'_{bb}] & [P'_{bc}] \\ [P'_{ca}] & [P'_{cb}] & [P'_{cc}] \end{bmatrix} \tag{5.34}$$

where $[P'_a]$, $[P'_b]$, $[P'_c]$ are the 3 x 3 matrices of each single-core cable found by inversion of Eq. (5.17) with G' = 0,

$$[P'_a] = \begin{bmatrix} C'_1 & -C'_1 & 0 \\ -C'_1 & C'_1+C'_2 & -C'_2 \\ 0 & -C'_2 & C'_2+C'_3 \end{bmatrix}^{-1} \tag{5.35a}$$

or [163]

$$[P_a'] = \begin{bmatrix} P'_1+P'_2+P'_3 & P'_2+P'_3 & P'_3 \\ P'_2+P'_3 & P'_2+P'_3 & P'_3 \\ P'_3 & P'_3 & P'_3 \end{bmatrix} \tag{5.35b}$$

with $P_i' = 1/C_i'$. \hfill (5.35c)

The dielectric between the armors (skid wires) and the pipe is represented by the second term in Eq. (5.34). Each of the submatrices $[P_{ii}']$ and $[P_{ik}']$ in the second term is a 3 x 3 matrix with 9 equal elements,

$$P_{ii}' = \frac{1}{2\pi\varepsilon_0\varepsilon_r} \ln\left\{ \frac{q}{R_i}\left[1 - \left(\frac{d_i}{q}\right)^2 \right] \right\} \tag{5.36a}$$

$$P_{ik}' = \frac{1}{2\pi\varepsilon_0\varepsilon_r} \ln \frac{q}{\sqrt{d_i^2 + d_k^2 - 2d_i d_k \cos\Theta_{ik}}} \tag{5.36b}$$

with the essential terms in Eq. (5.36) being the same expressions appearing in Eq. (5.31) and (5.33). The admittance matrix is then found by inverting $[P'_{phase}]$,

$$[Y'_{phase}] = j\omega [P'_{phase}]^{-1} \tag{5.37}$$

5.4.2 Finite Pipe Thickness with Earth Return

At lower frequencies, there is mutual coupling between the inner and outer surface of the pipe. The induced voltage on the outer surface will then produce a circulating current through the pipe and earth return. This extra loop must be added to the loop impedance matrix of Eq. (5.18),

$$
[Z'_{\text{loop}}] =
\begin{bmatrix}
\begin{array}{ccc|c}
\text{as in Eq. (5.18),} & & & 0 \\
\text{with elements defined} & & & 0 \\
\text{in Section 5.4.1} & & & -Z'_m \\
& & & 0 \\
& & & 0 \\
& & & -Z'_m \\
& & & 0 \\
& & & 0 \\
& & & -Z'_m \\
\hline
0 \ \ 0 \ \ -Z'_m \ \ 0 \ \ 0 \ \ -Z'_m \ \ 0 \ \ 0 \ \ -Z'_m & & & Z'_s
\end{array}
\end{bmatrix}
\tag{5.38a}
$$

with

$$Z'_m = Z'_{\text{pipe-mutual}} \text{ from Eq. (5.7c),} \tag{5.38b}$$

$$Z'_s = Z'_{\text{pipe-out}} + Z'_{\text{insulation}} + Z'_{\text{earth}}. \tag{5.38c}$$

The first two terms in Eq. (5.38c) are found from Eq. (5.7b) and (5.6) ($Z'_{\text{insulation}} = 0$ if pipe in contact with earth), and Z'_{earth} is the earth-return impedance discussed in Section 5.3. Transforming Eq. (5.38a) to phase quantities produces

$$
[Z'_{\text{phase}}] =
\begin{bmatrix}
\begin{array}{ccc|c|cccc|c}
\text{same matrix as} & & & 0 & Z' & Z' & \ldots Z' & Z'_e \\
\text{for infinite} & & & 0 & Z' & Z' & \ldots Z' & Z'_e \\
\text{pipe thickness} & & & . & \ldots\ldots\ldots\ldots & & & . \\
& & & . & \ldots\ldots\ldots\ldots & & & . \\
& & & & Z' & Z' & \ldots Z' & Z'_e \\
\hline
0 \ \ 0 \ \ldots & & & 0 & Z'_e & Z'_e & \ldots Z'_e & Z'_s
\end{array}
\end{bmatrix}
\tag{5.39a}
$$

with Z'_s from Eq. (5.38c)

$$Z'_e = Z'_s - Z'_m \tag{5.39b}$$

$$Z' = Z'_s - 2Z'_m$$

The last row and column in Eq. (5.39a) represent the pipe quantities, while the first 9 rows and columns refer to core, sheath (shield tapes), armor (skid wires) of phases a, b, and c.

If the pipe is in contact with the earth, then the shunt admittance matrix is the same as in Section 5.4.1. If it is insulated, then the potential coefficient matrix of Eq. (5.34) must be expanded with one extra row and column for the pipe, and the same element

$$P^{/} = \frac{1}{2\pi\varepsilon_0\varepsilon_r} \ln \frac{r_{pipe-insulation}}{r_{pipe-outside}} \tag{5.40}$$

must be added to this expanded matrix,

$$
[P'_{phase}] =
\left[
\begin{array}{cccc|c}
\text{same as in} & & & & 0 \\
\text{Eq. (5.34)} & & & & 0 \\
& & & & . \\
& & & & . \\
0 \ 0 \ ... & & & & 0
\end{array}
\right]
+
\left[
\begin{array}{cccc}
P' & P' & & ....P' \\
P' & P' & & ....P' \\
& .... & & \\
P' & P' & & ....P'
\end{array}
\right]
\tag{5.41}
$$

The admittance matrix is then again found by inversion with Eq. (5.37).

5.5 Building of Conductors and Elimination of Grounded Conductors

Conductors are sometimes connected together ("bundled"). For example, the concentric neutral conductors in the cable of Fig. 5.2 are in contact with each other, and therefore electrically connected. In a pipe-type cable, the shield tapes and skid wires are in contact with the pipe. In a submarine cable, the sheath is often bonded to the armor at certain intervals, to avoid voltage differences between the sheath and armor.

In such cases, the connected conductors 1,...m can be replaced by (or bundled into) one equivalent conductor, by introducing the bundling conditions

$$I_1 + I_2 + ...I_m = I_{equiv}; \ V_1 = V_2 = ... V_m = V_{equiv} \tag{5.42}$$

into the equations for the series impedance and shunt admittance matrices. The bundling procedure for reducing the equations from m individual to one equivalent conductor is the same as Method 1 of Section 4.1.2.2 for overhead lines, and is therefore not explained again. It is exact if the conductors are continuously connected with zero connection resistance (as the neutral conductors in Fig. 5.2), and accurate enough if the connections are made at discrete points with negligible resistance (as in bonding of the sheath to the armor), as long as the distance between the connection points is short compared to the wavelength of the highest frequency in the transient simulation.

As in the case of overhead lines with ground wires, some conductors in a cable may be grounded. For example, the steel pipe of a pipe-type cable can usually be assumed grounded, because its asphalt mastic coating is not an electric insulation. Also, neutral conductors may be connected to ground at certain intervals, or at both ends. If a conductor i is grounded, then the condition is simply

$$V_i = 0 \tag{5.43}$$

and conductor i can then be eliminated from the system of equations in the same way as described in Section 4.1.2.1. Again, the elimination is only exact if the conductor is grounded continuously with zero grounding resistance, and accurate enough if the distance between discrete grounding points is short compared to the wavelength of the highest frequency.

An example of bundled as well as grounded conductors would be a single-core submarine cable which has its sheath bonded to the armor. Since the asphalt coating of the armor is not an electric insulation, the armor is in effect

in contact with the sea water, and both sheath and armor are therefore grounded conductors. By eliminating both of them, the submarine cable can be represented by single-phase equations for the core conductor, with the current return combined in sea water, armor and sheath. For an overhead line, the equivalent situation would be a single-phase line with two ground wires.

The case of segmented ground wires in overhead lines discussed in Section 4.1.2.5(b) can exist in cables as well. For example, if the sheath is grounded at one end, but open and ungrounded at the other end, then the sheath could be eliminated in the same way as segmented ground wires, provided the cable length is short compared to the wavelength of the highest frequency. The support routine CABLE CONSTANTS does not have an option for such eliminations. The user must represent the sheath as an explicit conductor, instead, with one end connected to ground. This offers the advantage that the induced voltage at the other end can automatically be obtained, if so desired.

5.6 Buried Pipelines

Pipelines buried close to power lines can be subjected to hazardous induction effects, especially during single-line-to-ground faults. To study these effects, one can include the pipeline as an additional conductor into the transmission line representation (Fig. 5.14(a)). For steady-state analysis, one can also use the single-phase representation of Fig. 5.14(b), with an impressed voltage

steady-state analysis, one can also use the single-phase representation of Fig. 5.14(b), with an impressed voltage

(a) polyphase representation   (b) single-phase representation
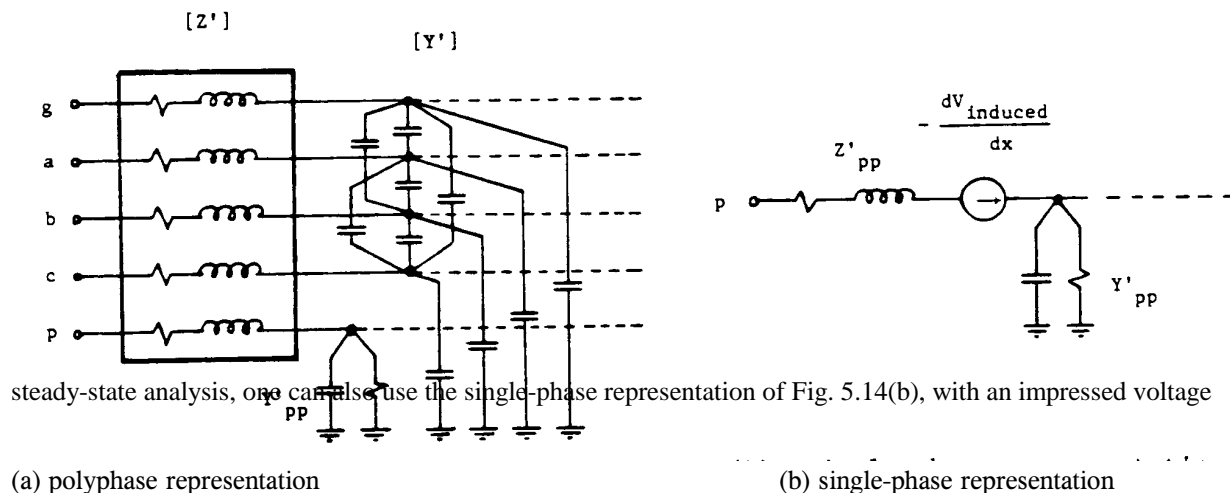
Fig. 5.14 - Pipeline representation (g = ground wire, a, b, c = phase conductors, p = pipeline)

$$-\frac{dV_{induced}}{dx} = Z'_{pa}I_a + Z'_{pb}I_b + Z'_{pc}I_c + Z'_{pg}I_g \tag{5.44}$$

There is no capacitive coupling between the power line and the pipeline if it is buried in the ground.

As explained later, nominal π-circuits can only be used for very short lengths of pipeline (typically ≤ 0.3 km at 60 Hz). The single-phase representation is therefore preferable for steady-state analysis, because the distributed parameters of Fig. 5.14(b) are more easily converted into an exact equivalent π-circuit than the polyphase parameters of Fig. 5.14(a). This results in the active equivalent π-circuit of Fig. 5.15, with Y_{series} and Y_{shunt} being the usual

parameters obtained from Eq. (1.14), while $I_{induced}$ is an active current [158],

$$I_{induced} = \frac{-dV_{induced}/dx}{Z'_{pp}} \tag{5.45}$$
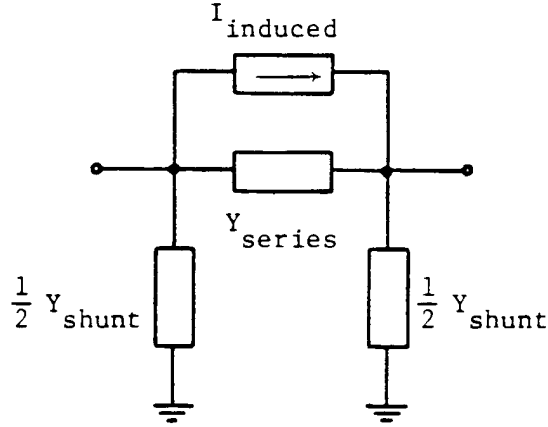
Fig. 5.15 - Active equivalent π-circuit

The correctness of the active π-circuit can easily be shown. Starting from the differential equations

$$-\frac{dV}{dx} = Z'_{pp} + Z'_{pp} I_{induced}$$

$$-\frac{dI}{dx} = Y'_{pp} V$$

the introduction of a modified current

$$I_{modified} = I + I_{induced}$$

transforms the differential equations into the normal form of the line equations, with the assumption that $I_{induced}$ does not change along the line ($dI_{modified}/dx = dI/dx$),

$$-\frac{dV}{dx} = Z'_{pp} I_{modified}$$

$$-\frac{dI_{modified}}{dx} = Y'_{pp} V$$

The solution for a line between nodes k and m is given in Eq. (1.13), except that the current is now $I_{modified}$, or rewritten,

$$\begin{bmatrix} I_{km} + I_{induced} \\ I_{mk} - I_{induced} \end{bmatrix} = \begin{bmatrix} Y_{series} + (1/2)Y_{shunt} & -Y_{series} \\ -Y_{series} & Y_{series} + (1/2)Y_{shunt} \end{bmatrix} \begin{bmatrix} V_k \\ V_m \end{bmatrix}$$

This is exactly the same equations which comes out of the equivalent circuit of Fig. 5.15.

With this single-phase approach, the currents in the power line are assumed to be known, e.g., from the usual type of short-circuit study. It is also assumed that they are constant over the length of the exposure to the pipeline, and that the pipeline runs parallel to the power line (mutual impedances constant). If either assumption is not true, then the power line-pipeline system must be split up into shorter sections as is customarily done in interference studies. The effect of the pipe on the power line zero sequence impedance is usually ignored, but could be taken into account.

In both representations of Fig. 5.14, the mutual impedances between the pipe and the overhead conductors, as well as the self impedance of the pipe with earth return, are needed. The mutual impedances are obtained with the formulas discussed in Section 5.3.4. At 60 Hz, Carson's formula will give practically identical results as the more complicated formula of Pollaczek.

The self impedance Z'_{pp} of the pipeline consists of the same three terms shown for the armor in Eq. (5.4). The first two terms are calculated with Eq. (5.7b) and (5.6), while R'_{earth} is found from the equations discussed in Section 5.3.

For the shunt admittance $Y'_{pp} = G' + j\omega C'$, the capacitive part is calculated in the usual way with Eq. (5.13). In contrast to the underground cable, the shunt conductance G' of the pipeline can no longer be ignored. The insulation around pipelines is electrically poor, either originally or because of puncturing during the laying operation. The loss angle δ in Eq. (5.14) is so large on pipelines insulated with glass-fiber/bitumen that G' becomes much larger than $\omega C'$ at power frequency, and if one part of the shunt admittance is ignored it should be $\omega C'$ rather than G'. On PVC-insulated pipelines, G' may still be smaller than $\omega C'$, though.

If the shunt resistance of the insulation is relatively small, then the grounding resistance of the pipe should be connected in series with it[2] [170], or

$$G' = \frac{1}{R'_{insulation} + R'_{grounding}} \tag{5.46}$$

where $R'_{insulation}$ = resistance of pipe insulation,

$R'_{grounding}$ = grounding resistance.

A useful formula for the grounding resistance is [170]

$$R'_{grounding} = \frac{\rho_{earth}}{4\pi}\left[2\ln\frac{2\mathscr{L}}{D} + \ln\frac{\sqrt{(2h)^2 + \left(\frac{\mathscr{L}}{2}\right)^2} + \frac{\mathscr{L}}{2}}{\sqrt{(2h)^2 + \left(\frac{\mathscr{L}}{2}\right)^2} - \frac{\mathscr{L}}{2}}\right] \tag{5.47}$$

with ρ_{earth} = earth resistivity (e.g., in Ωm),

h = depth of burial of pipe

$\mathscr{L}$ = length of pipe

---

[2]If the sheath, armor, or pipe of an underground cable or the ground wire of an overhead line is grounded, then it has been standard practice to ignore the grounding resistance (V = 0). An alternative would be to use a finite shunt admittance $Y' = 1/R'_{grounding}$, as recently suggested [186].

D = outside diameter of pipe.

Grounding grids must generally be analyzed as three-dimensional problems, even if they consist of only one pipe. The grounding resistance from Eq. (5.47) is therefore no longer an evenly distributed parameter, but depends on the length. Fortunately, the dependence of G' on length is very small for typical values of $G'_{insulation}$ [158]. In the region of measured values for G' between 0.1 S/km for newly-layed pipelines and 0.3 S/km for older pipelines with glass fiber/bitumen insulation [170], the dependence of G' on length is practically negligible, as shown in Fig. 5.16. Treating G' as an evenly distributed parameter is therefore a reasonable approximation.
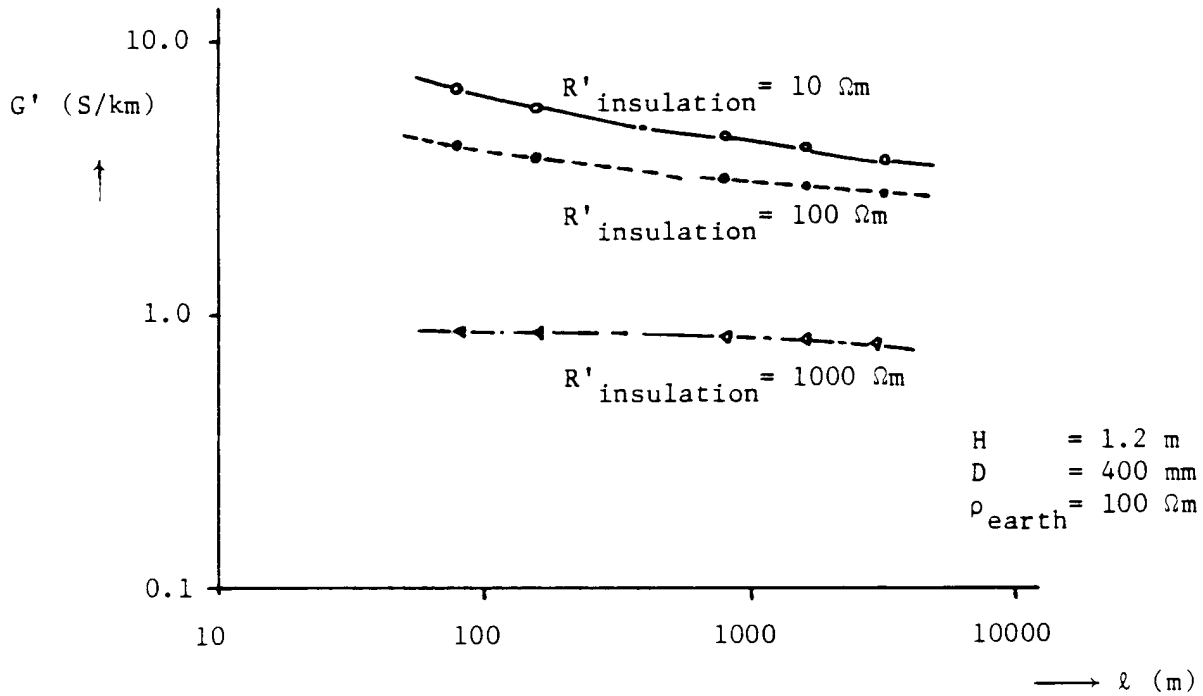
Fig. 5.16 - Shunt conductance of buried pipe

Because of G' >> ωC', the wavelength of buried pipelines is significantly shorter than that of underground cables, as shown in Table 5.3 [170]. Therefore, a nominal π-circuit of a circuit which includes a buried pipeline should not be longer than approximately 0.8 km for

Table 5.3 - Wavelength of pipeline at 50 Hz [170]

G' (S/km)	wavelength (km)
0.1	41.3
1.0	13.1
10.0	4.13

steady-state analysis, or approximately 0.08 km for switching surge studies [158].

Fig. 5.17 shows a comparison between measured and calculated voltages and currents in a pipeline, induced by currents in a neighboring power line, with the pipeline representation as discussed here [158].
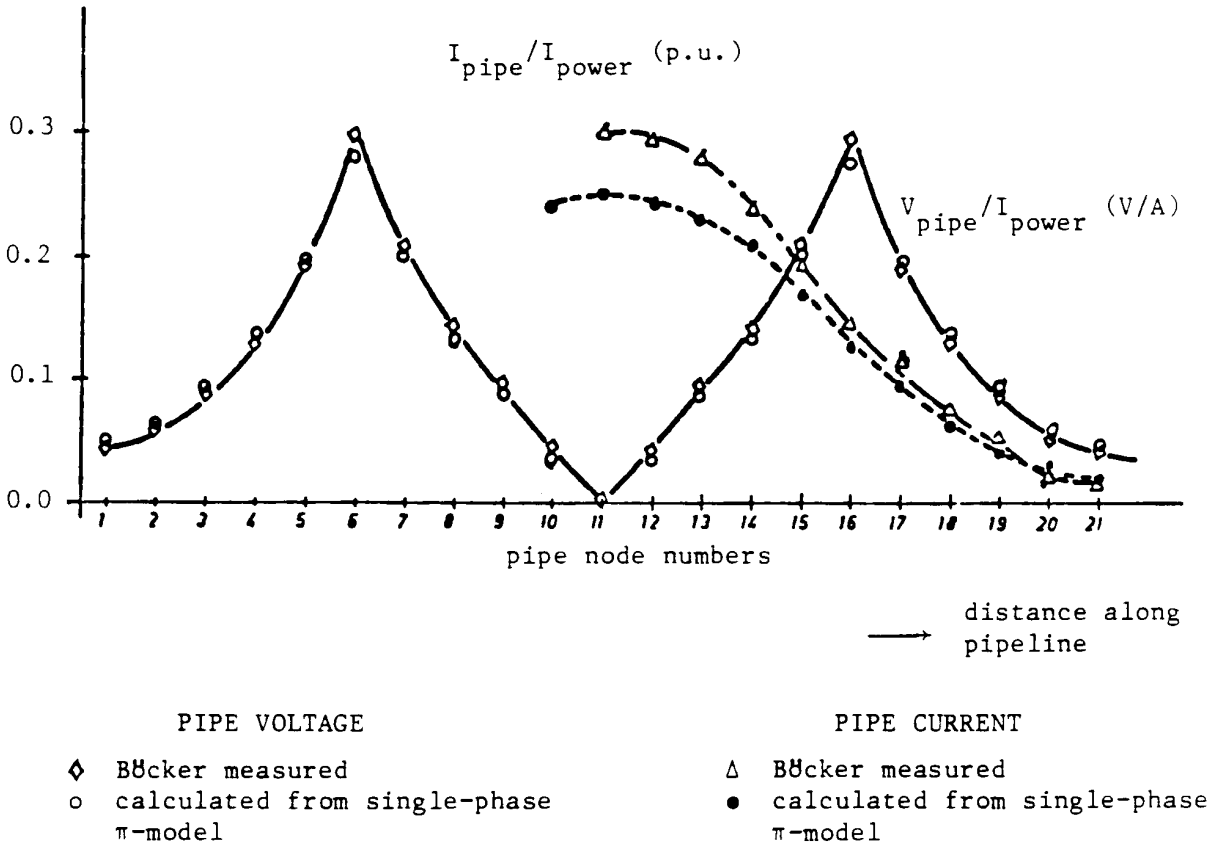
Fig. 5.17 - Induced voltages and currents in a buried pipeline

5.7 Partial Conductor and Finite Element Methods

The support routine CABLE CONSTANTS uses analytical formulas which are essentially only applicable to configurations with axial symmetry. The formulas for the nonconcentric configuration in pipe-type cables (Section 5.5) are only approximate, and the authors of these formulas themselves suggest improvements along the lines discussed here.

To find the impedances and capacitances for conductor systems with arbitrary shapes (e.g., for the cable of Fig. 5.1), numerical methods can be used in place of analytical formulas, which are either based on subdivisions into partial conductors or on finite element methods. There is no support routine yet in the EMTP which uses these numerical methods. The principle of these methods is therefore only outlined very briefly.

5-27

5.7.1 Subdivision into Partial Conductors

With this method, each conductor is subdivided into small "partial" conductors ("subconductors" in [162], "segments" in [164]), as shown in Fig. 5.18. Various shapes can be used for the partial conductors, with rectangles being the preferred shape for strip lines in
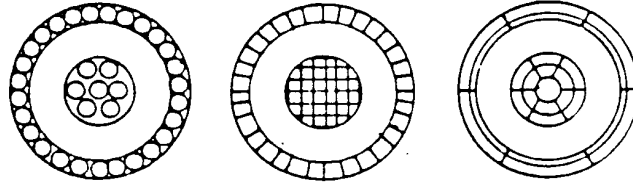
Fig. 5.18 - Subdivision of the main conductors into partial conductors

integrated circuits (Fig. 5.19).
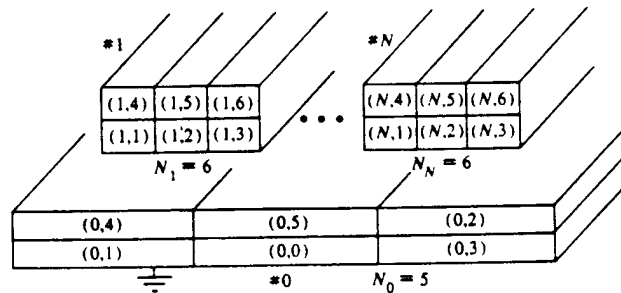
Fig. 5.19 - Subdivision of strip lines into partial conductors of rectangular shape [164]. Copyright 1979 by International Business Machines Corporation; reprinted by permission

In deriving the equations for the system of partial conductors, uniform current density is assumed within each partial conductor. Then the voltage drops along a system of n partial conductors at one frequency are described by the phasor equations

$$
-\begin{bmatrix} dV_1/dx \\ dV_2/dx \\ \cdot \\ \cdot \\ dV_n/dx \end{bmatrix} = \left(\begin{bmatrix} R_1 & & & \\ & R_2 & & \\ & & \cdot & \\ & & & \cdot \\ & & & & R_n \end{bmatrix} + j\omega \begin{bmatrix} L_{11} & L_{12} & \cdot & \cdot & L_{1n} \\ L_{21} & L_{22} & \cdot & \cdot & L_{2n} \\ \cdot & \cdot & \cdot & \cdot & \cdot \\ L_{n1} & L_{n2} & \cdot & \cdot & L_{nn} \end{bmatrix} \right) \begin{bmatrix} I_1 \\ I_2 \\ \cdot \\ \cdot \\ I_n \end{bmatrix}
\tag{5.48}
$$

The diagonal resistance matrix contains the dc resistances, and the full inductance matrix contains the self and mutual inductances of the partial conductors. The formulas for the matrix elements depend on the shape of the partial conductor, but they are well known.

To obtain the frequency-dependent impedance of a cable system, the matrices [R] and [L] are first computed. At each frequency, the complex matrix $[Z] = [R] + j\omega[L]$ is formed, and reduced to the number of actual conductors with Bundling Method 1 of Section 5.5. For example, if partial conductors 1,...50 belong to the core conductor, and partial

conductors 51,...120 to the sheath, then this bundling procedure will reduce the 120 x 120-matrix to a 2 x 2-matrix, which produces the frequency-dependent impedances

$$\begin{bmatrix} Z_{cc}(\omega) & Z_{cs}(\omega) \\ Z_{cs}(\omega) & Z_{ss}(\omega) \end{bmatrix}.$$

This numerical method works well as long as the conductors are subdivided into sufficiently small partial conductors. The size of these partial conductors must be of the same order of magnitude as the depth of penetration.

5.7.2 Finite Element Methods

Finite element methods are more powerful than partial conductor methods in one sense, inasmuch as it is not necessary to assume uniform current density within each element. However, it is very difficult to handle open-boundary conditions with finite element methods, that is configurations where the magnetic field diminishes gradually as one moves away from the conductors, with no clearly defined boundary of known magnetic vector potential reasonably close to the conductors. In situations where a boundary is clearly defined, e.g., in pipe-type cables at high frequency where the depth of penetration becomes much less than the wall thickness, finite element methods can be quite useful.

With finite element methods, the region inside and outside of the conductors is subdivided into small elements, usually of triangular shape. Fig. 5.20(a) shows the example of a stranded conductor inside a pipe of radius R_b as the return path (clearly defined boundary with zero magnetic field $A = 0$ outside the pipe and zero derivative along the two edges of the "wedge"). Because of axial symmetry, it is sufficient to analyze the "wedge" shown in Fig. 5.20(a). This wedge region is then subdivided into triangular elements as shown in Fig. 5.20(b), with longer triangles as one moves away from the conductor.

The magnetic vector potential A is assumed to vary linearly along the edges and inside of each triangle,

$$A = ax + by + c, \tag{5.49}$$

when a first-order method is used (higher-order methods exist as well). The unknowns are essentially the values of A in the node points. If they were shown in the z-direction of a three-dimensional picture, then the triangles would appear in a shape similar to a geodesic dome, with the roof height being the value of A. The equations for finding A are linear algebraic
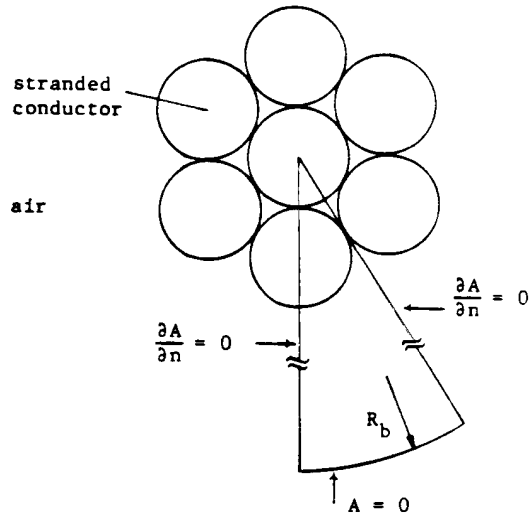
(a) Stranded conductor inside pipe of radius R_b
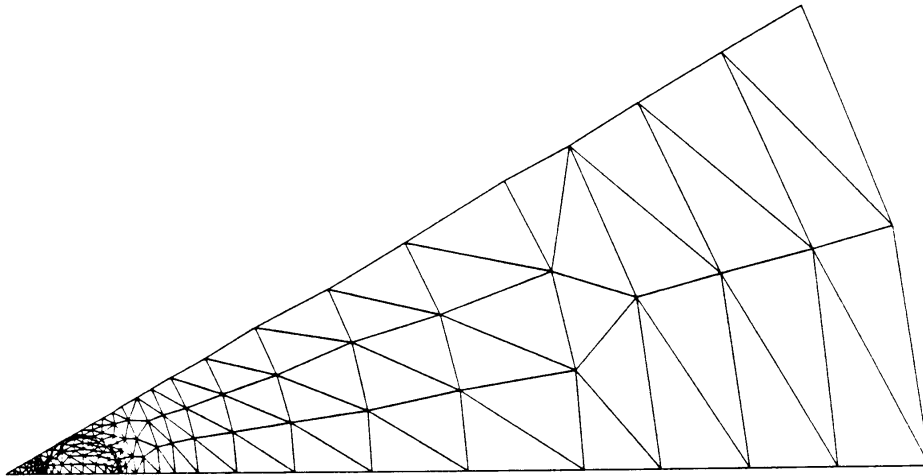
(b) Subdivision of region into triangular elements

Fig. 5.20 - Analysis of stranded conductor with finite element method [171]. Reprinted by permission of Yin Yanan

equations with a sparse matrix, but the number of node points or the number of equations is usually quite high (146 equations for the example of Fig. 5.20). Once the magnetic vector potential is known in the entire region, the impedances can be derived from it.

For readers interested in finite element methods for cable impedance calculations, the papers by Konrad, Weiss and Csendes [165, 166, 167] are a good introduction.

5.8 Modal Parameters

Once the series impedance and shunt admittance matrices per unit length $[Z'_{phase}]$, $[Y'_{phase}]$ are known, the derivation of modal parameters is exactly the same as described in Section 4.1.5 for overhead lines. They could be used, for example, to develop exact equivalent π-circuits for steady-state solutions as explained in Section 4.2.1.3.

For transient simulations, it is more difficult to use modal parameters, as compared to overhead lines, because the transformation matrix $[T_i]$ can no longer be assumed to be constant as for a single-circuit overhead line. Fig. 5.21 shows the variation of the elements in the third column of $[T_i]$ for a typical three-phase arrangement of 230 kV single-core cables with core conductor and sheath in each [155]. Especially around the power frequency of 50 or 60 Hz, the variations are quite pronounced.
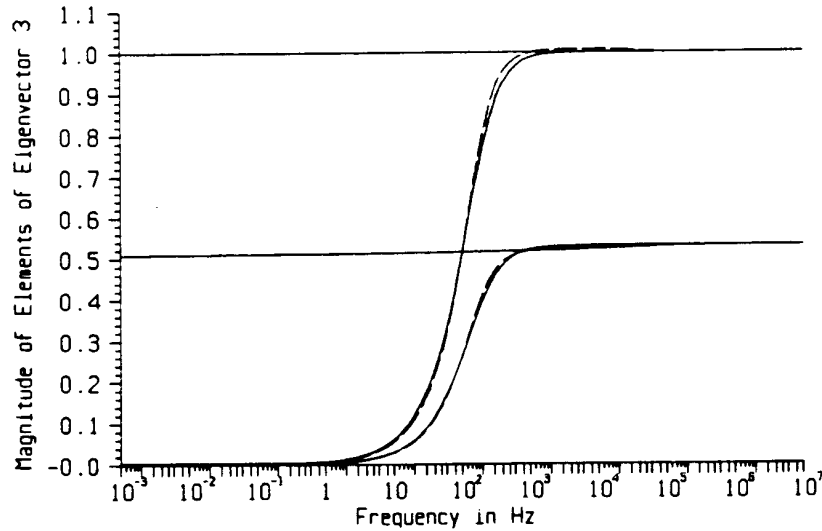
Fig. 5.21 - Magnitude of the elements of column 3 of $[T_i]$

Above a few kHz, the loop between core conductor and sheath becomes decoupled from the outer loop between sheath and earth return, because the depth of penetration on the inside of the sheath for loop 1 becomes much smaller than the sheath thickness. In that case, $Z_{tube-mutual} \sim 0$. This makes the transformation matrix constant above a few kHz, as evident from Fig. 5.21. For a single-phase single-core cable with sheath and armor, the three modes are identical with the 3 loops described in Eq. (5.1) at high frequency where $Z'_{12} \sim 0$ and $Z'_{23} \sim 0$. The transformation matrix between loop and phase quantities of Eq. (5.9),

$$[T_i]^{-1} = \begin{bmatrix} 1 & 0 & 0 \\ 1 & 1 & 0 \\ 1 & 1 & 1 \end{bmatrix} \quad and \quad [T_i] = \begin{bmatrix} 1 & 0 & 0 \\ -1 & 1 & 0 \\ 0 & -1 & 1 \end{bmatrix} \tag{5.50}$$

5.9 Cable Models in the EMTP
Co-author: L. Marti

As of now (Summer 1986), there are no specific cable models in the BPA EMTP. The only way to simulate cables is to fit cable data into the models available for overhead lines. It has long been recognized, of course, that this is only possible in a limited number of cases. A method specifically developed for cables, as discussed in Section 5.9.2.3, will hopefully be implemented in late 1986 or early 1987. It has already been tested extensively in the UBC

EMTP.

5.9.1 Ac Steady-State Solutions

In principle, there is no difficulty in representing cables as nominal or equivalent π-circuits in the same way as overhead lines (Section 4.2.1). If nominal π-circuits are used, it should be realized that the wavelength of underground cables is shorter than on overhead lines. If a nominal π-circuit should not be longer than 100 km at 60 Hz for overhead lines, the limit is more typically 30 km for underground cables. If a pipeline is modelled, the limit can be as low as 1 km, as discussed in Section 5.6.

Underground cables are often very short compared to the length of connected overhead lines. In such cases, the (complicated) series impedances have very little effect on the results because the system sees the cable essentially as a shunt capacitance. The cable can then be modelled as a simple lumped capacitance.

5.9.2 Transient Solutions

The accurate representation of cables with frequency-dependent impedances and frequency-dependent transformation matrices is discussed in Section 5.9.2.3. Situations where simpler models should be accurate enough are discussed first.

5.9.2.1 Short Cables

If a rectangular wave pulse travels on an overhead line and hits a relatively short underground cable, then the cable termination is essentially seen as a lumped capacitance. The voltage then builds up exponentially with a time constant of $T = Z_{overhead} \cdot C_{cable}$, shown in Fig. 5.22(a). If the cable is modelled somewhat more accurately as a lossless distributed-parameter line, then the voltage build-up has the staircase shape of Fig. 5.22(b), with the average of the sending and receiving end curve being more or less the same as the continuous curve in Fig. 5.22(a). As long as the travel time [] of the cable is short compared to the time constant T, reasonably accurate results can be obtained if the cable is represented as a lumped capacitance.

(a)   Cable represented as lumped   (b)   Cable represented as

5-32
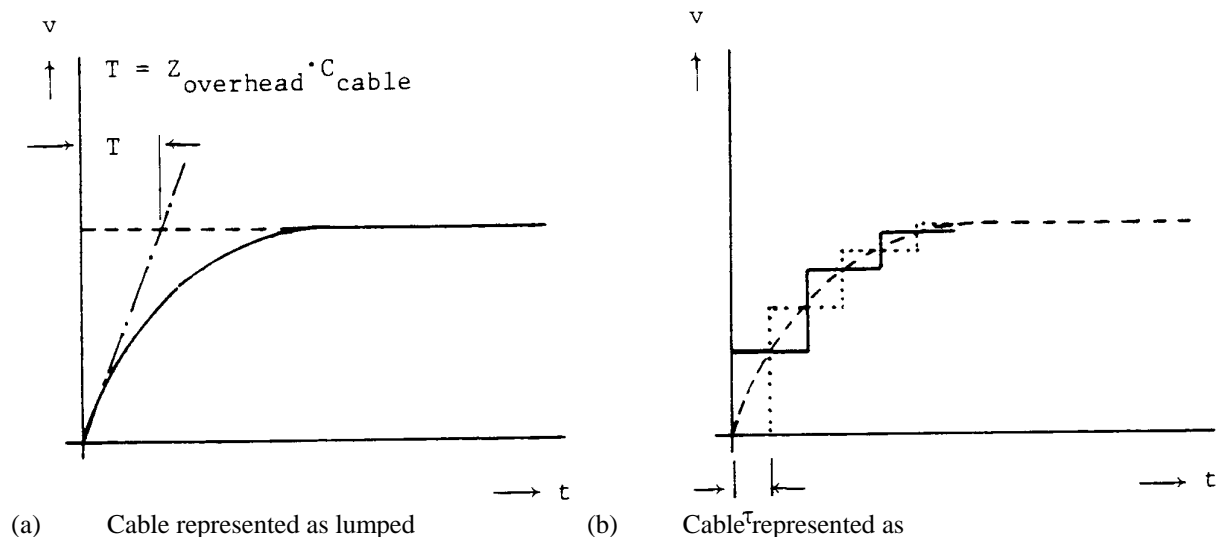
capacitance   lossless transmission line
                                               ------ sending end of cable
                                               ...... receiving end of cable

Fig. 5.22 - Voltage build-up in a cable connected to an overhead line

Nominal π-circuit representations have often been suggested as approximate cable models. They obviously represent the capacitance effect correctly, but the pronounced frequency-dependence in the series impedance is ignored. Nominal π-circuits give reasonable answers probably only in those cases in which the simpler lumped capacitance representation is already accurate enough.

5.9.2.2 Single-Phase Cables

There are situations where single-phase representations are possible. An example is a single-phase submarine cable in which the sheath and armor are bonded together, with the armor being in contact with the sea water. In such a case, the sheath and armor can be eliminated from Eq. (5.10), which results in the reduced single-phase equation

$$ -\frac{dV_c}{dx} = Z'_{core} I_c $$

with Z'_{core} being the impedance of the core conductor with combined current return through sheath, armor and sea water. Coupling to the cables of the other two phases can be ignored because the three cables are layed relatively far apart, to reduce the risk of anchors damaging more than one phase in the same mishap.

When the equations have been reduced to single-phase equations, then it is straightforward to use the frequency-dependent overhead line model described in Section 4.2.2.6.

Sometimes it is not necessary to take the frequency-dependence in the series impedances into account. For example, single phase SF_6-busses have been modelled quite successfully for fast transients with two decoupled lossless single-phase lines, one for the inside coaxial loop and a second one for the outside loop between the enclosure and the earth-return. The coupling between the two loops through the enclosure is negligible at high frequencies because the depth of penetration is much less than the enclosure wall thickness. The only coupling occurs through reflections at the terminations. Agreement between simulation results from such simple models and field tests has been excellent [169].

5.9.2.3 Polyphase Cables [155]

The simple overhead line models with constant parameters discussed in Section 4.2.2 are of limited use for underground cables for two reasons:

(a)   The transformation matrix $[T_i]$ is frequency-dependent up to a few kHz, though a constant $[T_i]$ would be acceptable for transients which contain only high frequencies (e.g., lightning surge studies).

(b)   The modal parameters (e.g., wave velocity and attenuation) are more frequency-dependent than on overhead lines, as shown in Fig. 5.23 for three single-core cables with core and sheath [150].
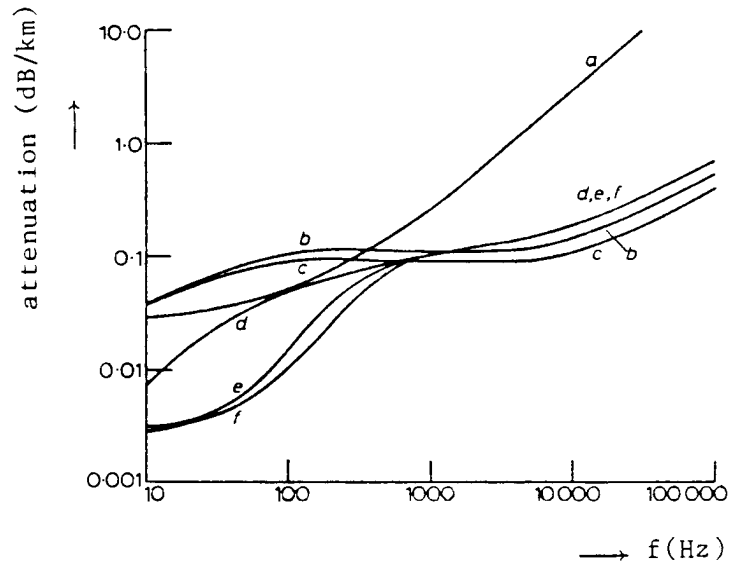
(a) Attenuation
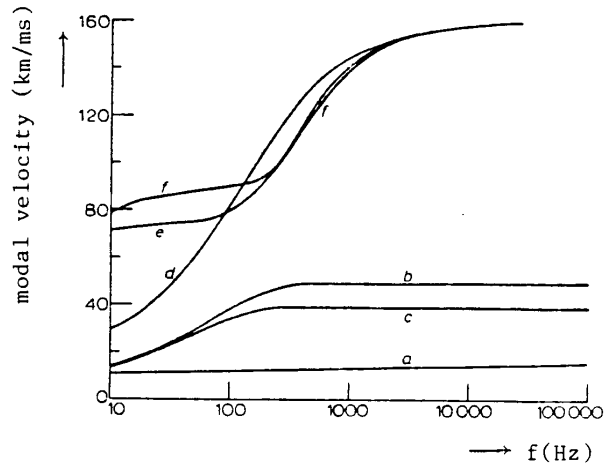
(b) Velocity

Fig. 5.23 - Modal parameters as a function of frequency [150]. Reprinted by permission of IEE and the authors

To derive an accurate model for an n-conductor cable system between nodes k and m, we can start from the phasor equation (4.121) for the overhead line, if we replace that scalar equation, which was written for one phase or mode, by a matrix equation for the n conductors,

$$[Y_c][V_k] - [I_{km}] = [A]\{[Y_c][V_m] + [I_{mk}]\} \tag{5.51}$$

with $[Y_c] = [Z_c]^{-1}$ = characteristic admittance matrix in phase quantities,

$[A] = e^{-[\gamma][l]}$ = propagation factor matrix.

Eq. (5.51) is transformed to modal quantities, with

$$[I] = [T_i][I_{mode}] \tag{5.52a}$$

and

$$[V] = [T_i']^{-1}[V_{mode}] \tag{5.52b}$$

which yields

$$[I_{km-mode}] = [Y_{c-mode}][V_{k-mode}] - [A_{mode}]\{[Y_{c-mode}][V_{m-mode}] + [I_{mk-mode}]\}$$

$$\tag{5.53}$$

with both $[Y_{c-mode}]$ and $[A_{mode}]$ being diagonal matrices,

$$[Y_{c-mode}] = [T_i]^{-1}[Y_c][T_i']^{-1} \tag{5.54a}$$

$$[A_{mode}] = [T_i]^{-1}[A][T_i] \tag{5.54b}$$

The diagonal element of $[A_{mode}]$ is obtained from the i-th eigenvalue γ_i of the product $\lceil Y'_{phase} \rceil \lceil Z'_{phase} \rceil$,

$$A_{mode-i} = e^{-l\lambda_i} \tag{5.54c}$$

and $[T_i]$ is the matrix of eigenvectors of the same product $[Y'_{phase}][Z'_{phase}]$. Eq. (5.53) consists of n decoupled (scalar) equations, with one equation for each mode.

Transforming these scalar equations into the time domain is the same procedure as described in Section 4.2.2.6 for the overhead line. For mode i, the second term in Eq. (5.53) is found with the same convolution integral as in Eq. (4.124),

$$hist_{propagation} = -\int_{\tau_{min}}^{\tau_{max}} i_{m-total}(t-u)a(u)\,du \quad for \ each \ mode \tag{5.55}$$

with the current $i_{m-total}$ being the sum of the line current i_{mk} and of a current which would flow through the characteristic impedance of mode i if the voltage v_m of mode i were connected across it. Only known history terms appear in Eq. (5.55), and $hist_{propagation}$ can therefore be found by n recursive convolutions for the n modes, in the same say as in Section 4.2.2.6. The modal propagation factors are very similar in shape to those of an overhead line, as shown for $A_{mode-3}(\omega)$ in Fig. 5.24.
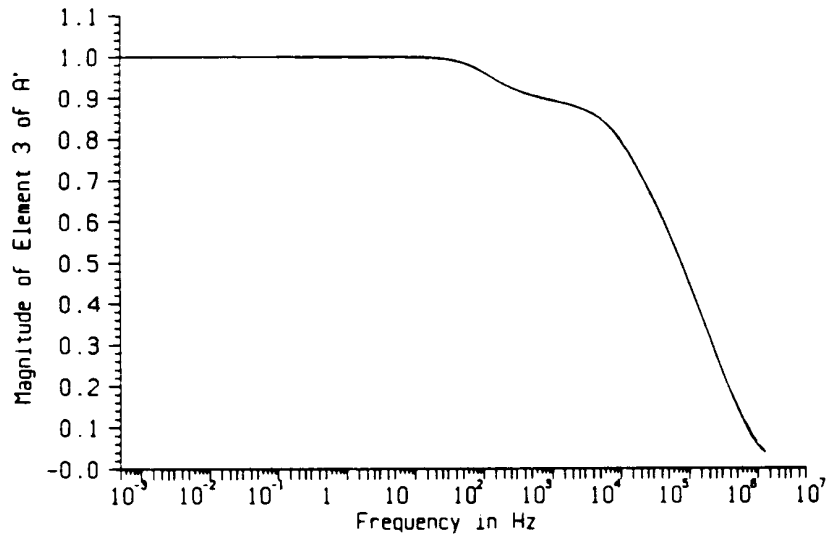
Fig. 5.24 - Magnitude of propagation factor for mode 3 of a 6-conductor system (three single-core cables with core and sheath in each)

With

propagation of the conditions from m to k being taken care of through Eq. (5.55), the only unresolved issue in the modal domain equations is the representation of the term Y_cV_k in Eq. (5.53). Again, the frequency dependence of Y_c is similar to that of an overhead line, as shown in Fig. 5.25, and can be represented with the same type of Foster-I R-C network shown in Fig. 4.42(a), and reproduced here as Fig. 5.26. By applying the trapezoidal rule of integration to the capacitances, or by using recursive convolution as discussed in Appendix V, the R-C
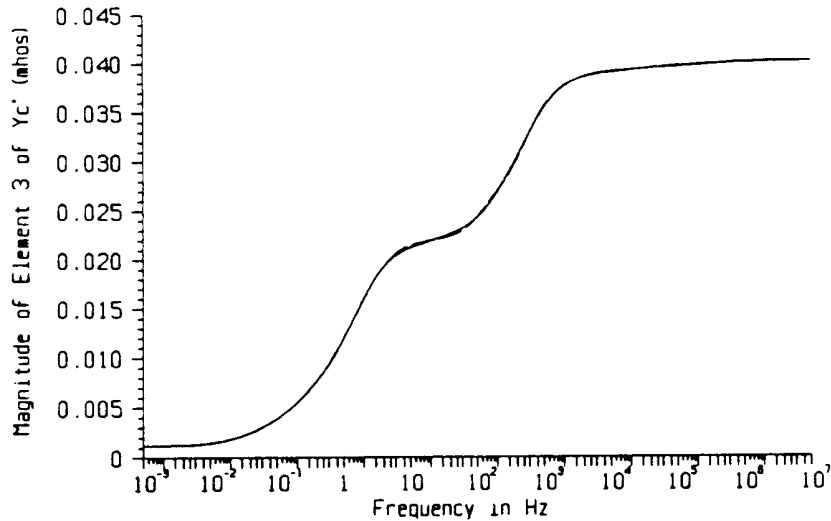
Fig. 5.25 - Magnitude of characteristic admittance for mode 3 (same 6-conductor system as in Fig. 5.24)

5-36
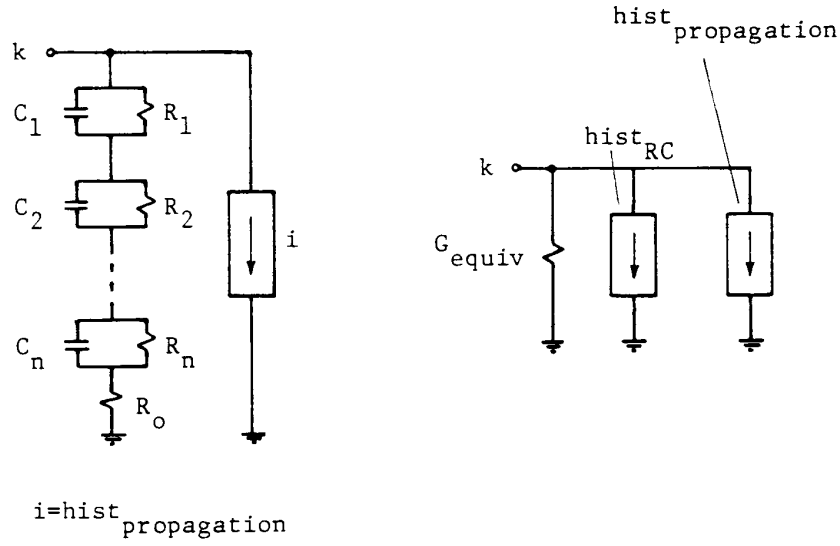
(a)   R-C network   (b)   Equivalent resistance after applying implicit integration to C

Fig. 5.26 - Representation of one mode seen from side k

network is converted into an equivalent conductance G_{equiv} in parallel with a known current source $hist_{RC} + hist_{propagation}$. After the network solution at each time step, the current flowing through the characteristic impedance represented by the R-C network must be calculated for both ends of the cable from $G_{equiv}v + hist_{RC}$, because this term is needed after the elapse of travel time to form the expression $i_{m\text{-}total}$ needed in Eq. (5.55).

From Fig. 5.26(b), it can be seen that each mode is now represented by the scalar, algebraic equation

$$i_{km}(t) = G_{equiv}v_k(t) + (hist_{RC} + hist_{propagation}) \tag{5.56}$$

with an analogous equation for $i_{mk}(t)$ at the other end. If the transformation matrix were constant and real, then Eq. (5.56) could very easily be transformed back to phase quantities,

$$[i_{km\text{-}phase}(t)] = [T_i][G_{equiv}][T_i]^t[v_{k\text{-}phase}] + [T_i][hist]$$

as explained in Eq. (4.109) for the overhead line. As shown in Fig. 5.21, the transformation matrix $[T_i]$ of cables is very much frequency-dependent, and the transformation back to phase quantities now requires convolutions based on Eq. (5.52),

$$[i_{phase}(t)] = \int_{-\infty}^{t} [t_i(t-u)] \, [i_{mode}(u)] \, du \tag{5.57a}$$

$$[v_{mode}(t)] = \int_{-\infty}^{t} [t_i(t-u)]^t \, [v_{phase}(u)] \, du \tag{5.57b}$$

where $[t_i]$ is a matrix obtained from the inverse Fourier transform of the frequency-dependent matrix $[T_i]$. Similar to the curve fitting used for the modal characteristic impedances, each element of $[T_i]$ is again approximated by rational functions of the form

$$T_{\mu\nu}(\omega) = k_0 + \sum_{i=1}^{m} \frac{k_i}{j\omega + p_i} \tag{5.58}$$

with k_0, k_i and p_i being real constants which, when transformed into the time domain, becomes

$$t_{\mu\nu}(t) = k_0 \sigma(t) + \sum_{i=1}^{m} k_i \exp(-p_i t)\, u(t) \tag{5.59}$$

With the simple sum of exponentials in Eq. (5.59), recursive convolution can be applied again (Appendix V). Then, the convolution integrals in Eq. (5.57) can be split up into a term containing the yet unknown voltages and currents at time t, and the known history terms which can be updated recursively,

$$[i_{phase}(t)] = [t_0]\,[i_{mode}(t)] + [hist_{current}] \tag{5.60a}$$

$$[v_{mode}(t)] = [t_0]^t\,[v_{phase}(t)] + [hist_{voltage}] \tag{5.60b}$$

with $[t_0]$ being a real, constant n x n-matrix. With Eq. (5.60), the transformation of the modal equations (5.56) to phase quantities is now fairly simple,

$$[i_{km-phase}(t)] = [G_{phase}]\,[v_{k-phase}(t)] + [hist_{phase}] \tag{5.61a}$$

with

$$[G_{phase}] = [t_0]\,[G_{phase}]\,[t_0]^t \tag{5.61b}$$

and the history term

$$[hist_{phase}] = [hist_{current}] + [t_0]\{[G_{equiv}][hist_{voltage}]$$
$$+ [hist_{RC}] + [hist_{propagation}]\} \tag{5.61c}$$

Since the form of Eq. (5.61a) is identical to that of Eq. (4.109) for the overhead line with constant $[T_i]$, adding the model to the EMTP is the same as described there. The extra effort lies essentially in the evaluation of the two extra history vectors $[hist_{current}]$ and $[hist_{voltage}]$. After the network solution at each time step, Eq. (5.60) is used to obtain the modal quantities from the phase quantities.

The principle of the frequency-dependent cable model is fairly simple, but its correct implementation depends on many intricacies, which are described in [155]. In particular, it is important to normalize the eigenvectors in such a way that the elements of $[T_i]$ as well as the modal surge admittances $Y_{c\text{-mode-}i}$ both become minimum phase shift functions. This is achieved by making one element of each eigenvector a real and constant number through the entire frequency range. Furthermore, standard eigenvalue/eigenvector subroutines do not produce smooth curves of $[T_i]$ and $[Y_{c\text{-mode}}]$ as a function of frequency, because the order in which the eigenvalues are calculated often changes as one moves from one frequency point to the next. This problem was solved by using an extension of the Jacobi method for complex symmetric matrices. Symmetry is obtained by reformulating the eigenproblem

$$[Y'_{phase}] \, [Z'_{phase}] \, [x] \ = \ \lambda[x]$$

in the form

$$[H] \, [r] \ = \ \lambda[r] \tag{5.62a}$$

where

$$[H] \ = \ [L]^t \, [Z'_{phase}] \, [L] \tag{5.62b}$$

and

$$[x] \ = \ [L] \, [r] \tag{5.62c}$$

with [L] being the lower triangular matrix obtained from the Choleski decomposition of $[Y'_{phase}]$ [157]. The Choleski decomposition is a modification of the Gauss elimination method, as explained in Appendix III. One can also replace [L] in Eq. (5.62) with the square root of $[Y'_{phase}]$ obtained from

$$[Y'_{phase}]^{1/2} \ = \ [X] \, [\Lambda^{1/2}] \, [X]^{-1} \tag{5.63}$$

where $[\Lambda^{1/2}]$ is the diagonal matrix of the square roots of the eigenvalues, and [X[is the eigenvector matrix of $[Y'_{phase}]$. Both approaches are very efficient if G' is ignored, or if tanδ is constant for all dielectrics in the cable system, because [L] or $[Y'_{phase}]^{1/2}$ must then only be computed once for all frequencies.

For parallel single core cables layed in the ground (not in air), [Y'] is diagonal if loop equations are used. In that case it is more efficient to find the eigenvalues and eigenvectors for $[Y'_{loop}][Z'_{loop}]$, where both [L] and $[Y'_{loop}]^{1/2}$ become the same diagonal matrix with $\sqrt{Y'_{loop-i}}$ as its elements. The conversion back to phase quantities is trivial with Eq. (5.50).

The reason why the Jacobi procedure produces smooth eigenvectors is that the Jacobi algorithm requires an initial guess for the solution of the eigenvectors. This initial guess is readily available from the solution of the eigenproblem of the preceding frequency step; consequently, the order of the eigenvectors from one calculation to the next is not lost.

Figure 5.27(a) shows the magnitude of the elements of row 3 of the eigenvector matrix $[T_i]$ for the same 6-conductor system as in Fig. 5.24, when standard eigenvalue/eigenvector routines are used. Fig. 5.27(b), on the other hand, shows the same elements of $[T_i]$ calculated with the modified Jacobi algorithm.

As an application for this cable model, consider the case of three 230 kV single-core cables (with core and sheath), buried side by side in horizontal configuration, with a length of 10 km. A unit-step voltage is applied to the core of phase A, and the cores of phases B and C as well as all three sheaths are left ungrounded at both ends. The unit-step function was approximated as a periodic rectangular pulse of 10 ms duration and a period of 20 ms with a Fourier series containing 500 harmonics,

$$v(t) = a_0 + \sum_{i=1}^{500} \{a_i\cos(\omega_i t) + b_i\sin(\omega_i t)\}$$

The wave front of this approximation is shown in Fig. 5.28. Choosing a Fourier series
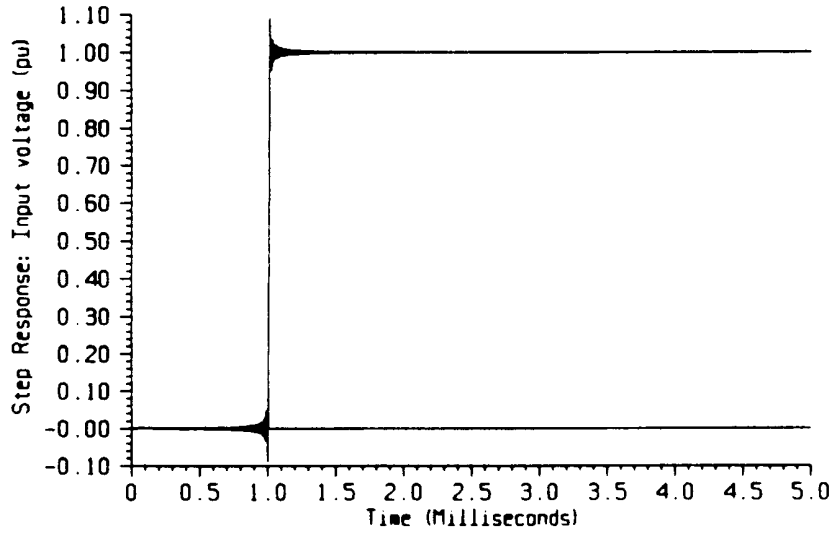
Fig. 5.28 - Fourier series approximation of unit-step

approximation for the voltage source offered the advantage that exact answers could be found as well, by using ac steady-state solutions with exact equivalent π-circuits (Section 4.2.1.3) at each of the 500 frequencies, and by superimposing them. Fig. 5.29 and 5.30 show the EMTP simulation results in the region of the third pulse, superimposed on the exact answers. The two
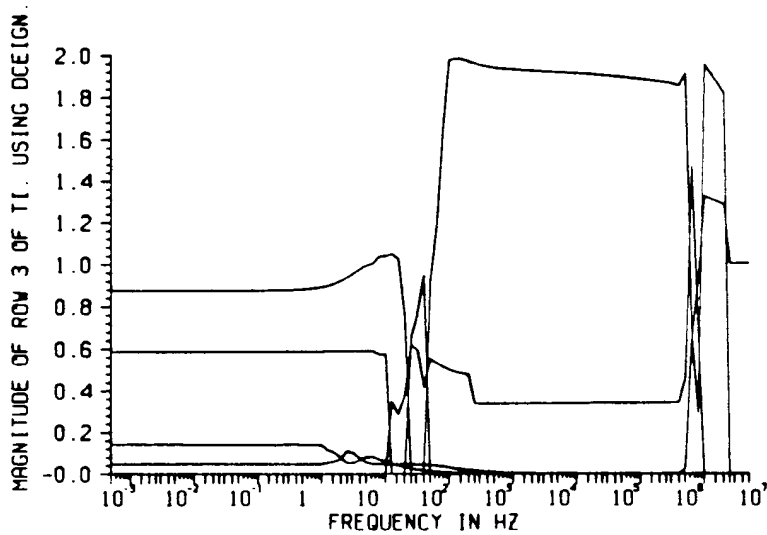
(a) Standard eigenvalue/eigenvector subroutines

5-40
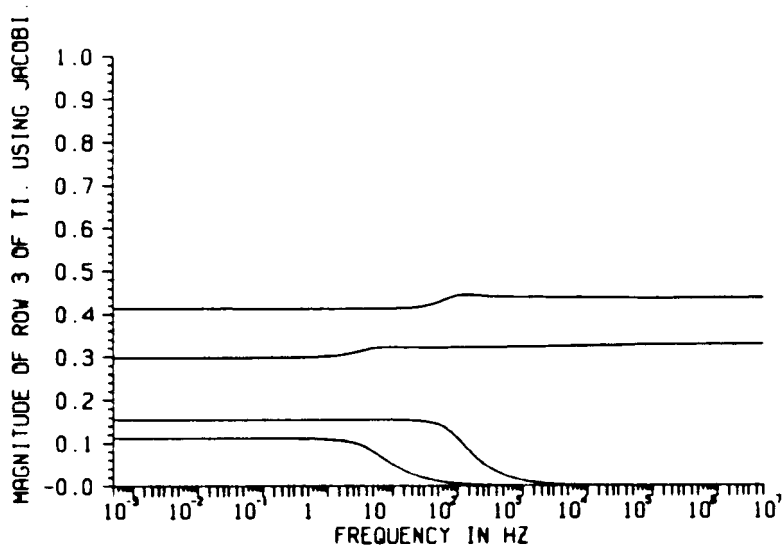
(b) Modified Jacobi algorithm

Fig. 5.27 -
Magnitude of the elements of row 3 of $[T_i]$ (same 6-conductor system as in Fig. 5.24)

curves are indistinguishable in this third pulse region where the phenomena have already become more or less periodic. This shows that the EMTP cable model is capable of producing highly accurate answers. The insert on the right-hand side of Fig. 5.29 shows the response to the first pulse, where the EMTP simulation results differ slightly from the exact answers, not because of inaccuracies in the model but because the EMTP starts from zero initial conditions while the exact answer assumes periodic behavior even for t < 0.
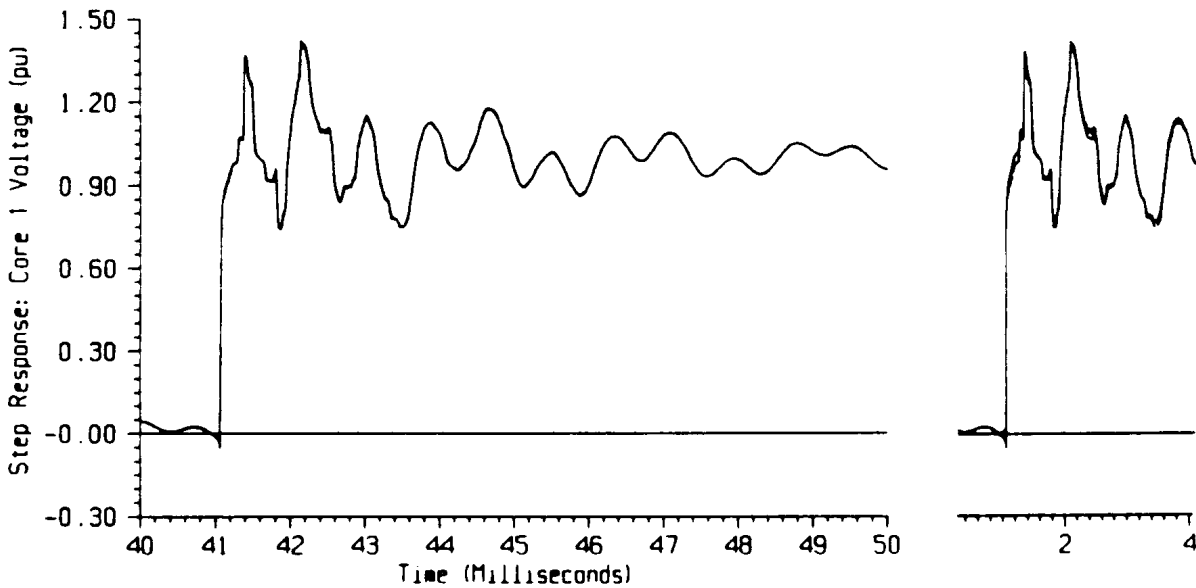
Fig. 5.29 - Step response, receiving end voltage of core (phase A)

5-41
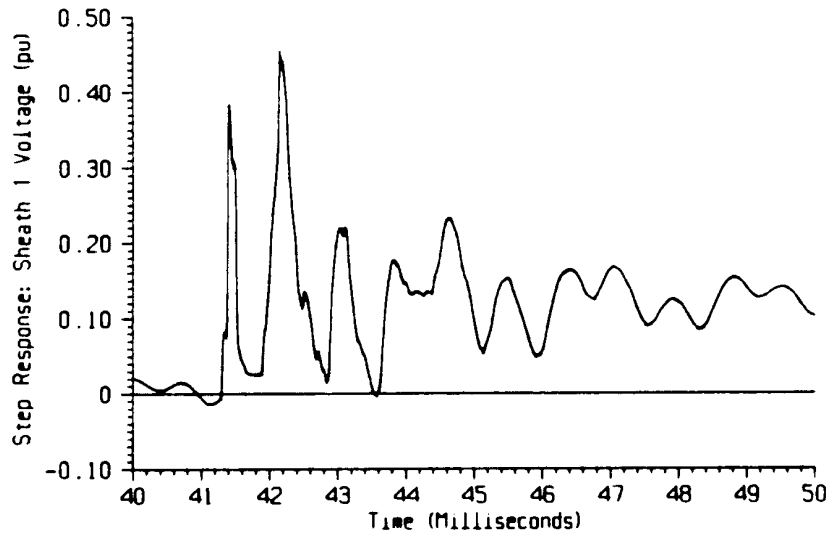
Fig. 5.30 - Step response, receiving end voltage of sheath (phase A)

6. TRANSFORMERS

The first representation of transformers in the EMTP was in the form of branch resistance and inductance matrices [R] and [L]. The support routine XFORMER was written to produce these matrices from the test data of single-phase two- and three-winding transformers. Stray capacitances are ignored in these representations, and they are therefore only valid up to a few kHz.

A star circuit representation for N-winding transformers (called "saturable transformer component" in the BPA EMTP) was added later, which uses matrices [R] and $[L]^{-1}$ with the alternate equation

$$[L]^{-1}[v] = [L]^{-1}[R][i] + [di/dt] \qquad (6.1)$$

in the transient solution. This formulation also became useful when support routines BCTRAN and TRELEG were developed for inductance and inverse inductance matrix representations of three-phase units. An attempt was made to extend the star circuit to three-phase units as well, through the addition of a zero-sequence air-return path reluctance. This model has seldom been used, however, because the zero-sequence reluctance value is difficult to obtain.

Saturation effects have been modelled by adding extra nonlinear inductance and resistance branches to the inductance or inverse inductance matrix representations, or in the case of the star circuit, with the built-in nonlinear magnetizing inductance and iron-core resistance. A nonlinear inductance with hysteresis effects (called "pseudo-nonlinear hysteretic reactor" in the BPA EMTP) has been developed as well. An accurate representation of hysteresis and eddy current effects, of skin effect in the coils, and of stray capacitance effects is still difficult at this time, and some progress in modelling these effects can be expected in the years to come.

Surprisingly, the simplest transformer representation in the form of an "ideal" transformer was the last model to be added to the EMTP in 1982, as part of a revision to allow for voltage sources between nodes.

6.1 Transformers as Part of Thevenin Equivalent Circuits

If a disturbance occurs on the high side of a step-up transformer, then the network behind that transformer, plus the transformer itself, is usually representation as a voltage source behind R-L branches. Since the transformer inductances tend to filter out the high frequencies, such a low-frequency R-L circuit appears to be reasonable.

To explain the derivation of such Thevenin equivalent circuits, the practical example of Fig. 6.1 shall be used [80], where the feeding network consists of three generators and two three-winding transformers. The transformer short-circuit reactances are $X_{HL} = 0.117$ p.u., $X_{HT} = 0.115$ p.u., $X_{LT} = 0.241$ p.u., and the generator reactance is $X''_d = 0.1385$ p.u., all based on 100

three-winding
transformers
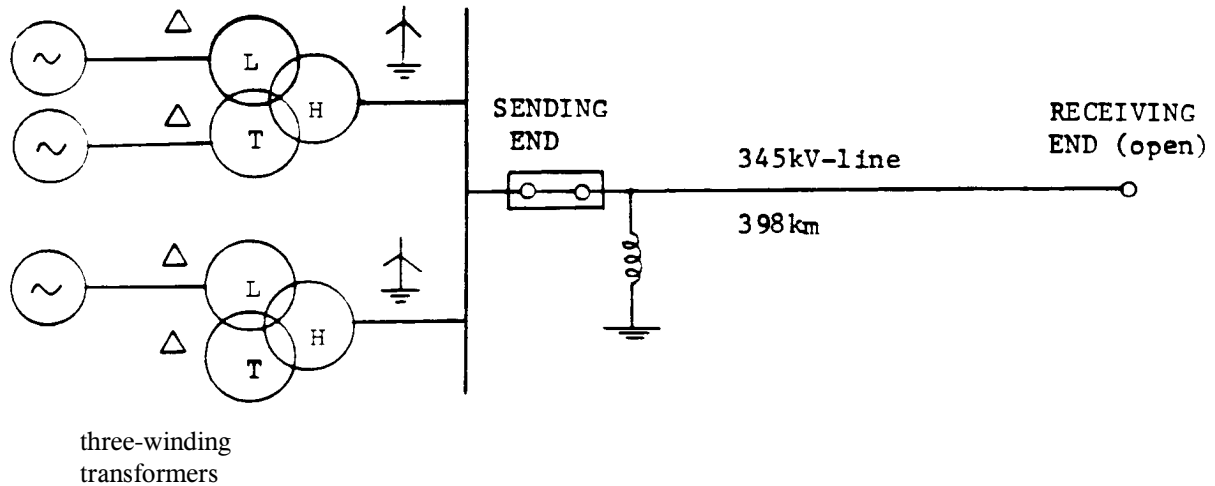
The 4th generator was disconnected
for acceptance testing.

Fig. 6.1 - Network configuration for various field tests at CEMIG, Brazil [80]

MVA at 60 Hz. With the well-known equivalent star circuit for three-winding transformers (see Section 6.3.2), the power plant in Fig. 6.1 can be represented with the positive and zero sequence networks of Fig. 6.2. For simplicity, resistances are ignored, but they could easily be included. It is further assumed here that the zero sequence reactance values of the transformer are the same as the positive sequence values, which is only correct for three-phase banks built from single phase units, but not quite correct for three-phase units (if the zero sequence values were known,

(a)   Positive sequence (negative
      sequence identical, except that
      voltage sources are shorted)

(b)   Zero sequence
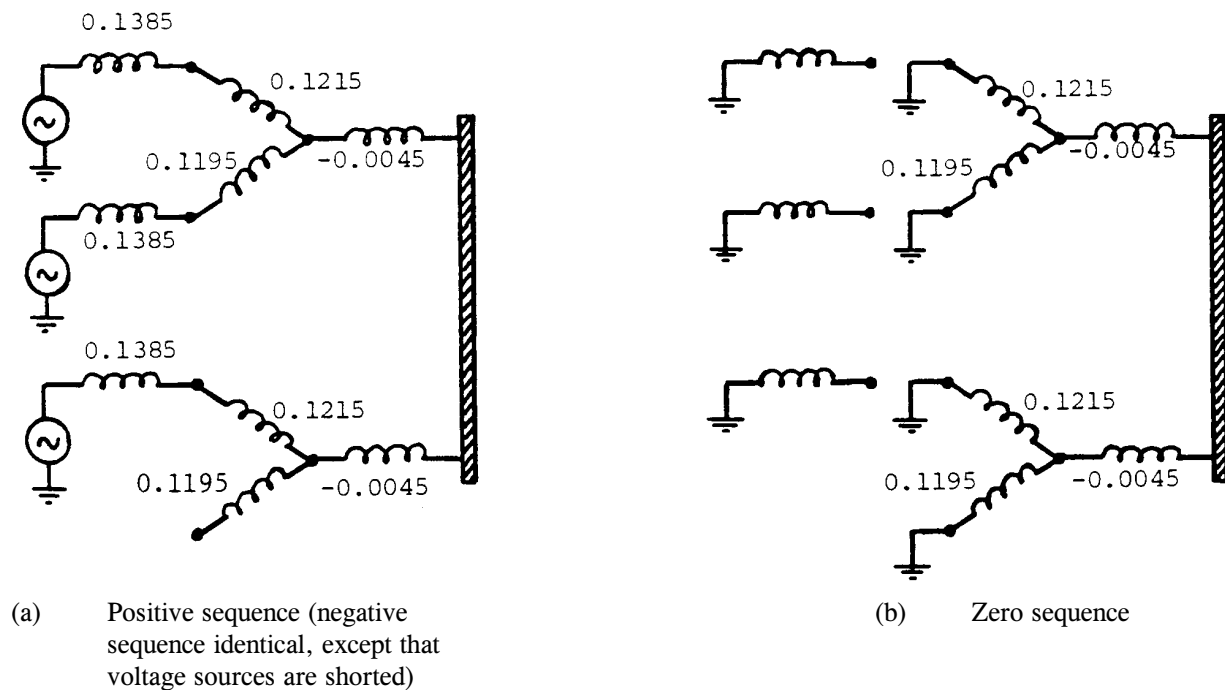
Fig. 6.2 - Equivalent circuits for the power plant (reactance values in p.u. based on 100 MVA at 60 Hz)

then those values could of course be used in Fig. 6.2(b)). Furthermore, the generator is modelled as a symmetrical voltage source E" behind X''_d. Note that the delta-connected windings act as short-circuits for zero sequence currents in Fig. 6.2(b), while the generators are disconnected to force $I_{zero} = 0$. The zero sequence parameters of the generators are therefore irrelevant in this example.

The networks of Fig. 6.2 can now be reduced to the three Thevenin equivalent circuits of Fig. 6.3, which in turn can be converted to one three-phase Thevenin equivalent circuit as shown in Fig. 6.4. This three-phase circuit is used in the EMTP for the representation of the power plant, with the data usually converted from p.u. to actual values seen from the 345 kV side ($X_{pox} = X_{neg} = 99.90\ \Omega$, $X_{zero} = 33.17\ \Omega$, or $X_s = 77.65\ \Omega$, $X_m = -22.25\ \Omega$ at 60 Hz). The symmetrical voltage sources E_a, E_b, E_c behind the coupled inductances in Fig. 6.4 are the open-circuit voltages of the power plant on the 345 kV side. In the transient simulation, the matrix [X] is obviously replaced by the inductance matrix [L].
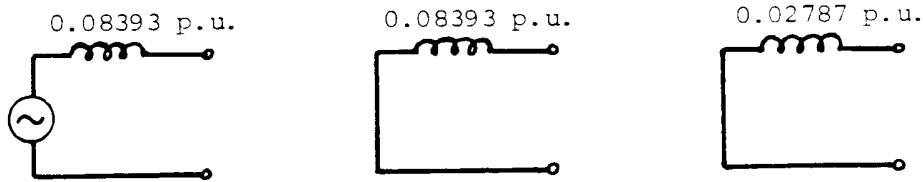
Fig. 6.3 - Thevenin equivalent circuits in sequence quantities
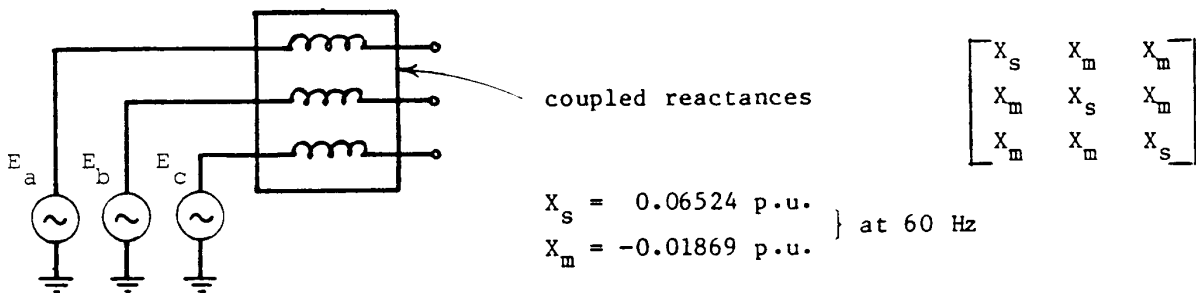
Fig. 6.4 - Three-phase Thevenin equivalent circuit in phase quantities

6.2 Inductance Matrix Representation of Single-Phase Two- and Three-Winding Transformers

Transformers can only be represented as coupled [R]-[L]-branches if the exciting current is not ignored. The derivations are fairly simple, and shall be explained with specific examples.

6.2.1 Two-Winding Transformers

Assume a short-circuit reactance of 10%, short-circuit losses of 0.5%, and an exciting current of 1%, based on the ratings V_{rating}, S_{rating} of the transformer. The excitation losses are ignored, but could be taken into account as explained in Section 6.6. If the given quantities are Z_{pu}, load losses P_{loss}, and power rating S_{rating}, then the resistance and reactance part of the short-circuit impedance are

$$R_{pu} = P_{loss} / S_{rating} \tag{6.2a}$$

$$X_{pu} = \sqrt{Z_{pu}^2 - R_{pu}^2} \tag{6.2b}$$

Since the load losses do not give any information about their distribution between windings 1 and 2, it is best to assume

$$R_{1pu} = R_{2pu} = \frac{1}{2} R_{pu} \tag{6.2c}$$

If the winding resistances are known, and not calculated from P_{loss}, then R_{1pu} and R_{2pu} may of course be different, and $R_{pu} = R_{1pu} + R_{2pu}$ is then used in Eq. (6.2b). With the T-circuit representation found in most textbooks, the p.u. impedances are then as shown in Fig. 6.5. The short-circuit impedance $0.005 + j0.10$ p.u. is divided into two equal parts, and the magnetizing reactance $j99.95$ p.u., which is purely imaginary when excitation losses are ignored, is chosen to give an input impedance of 100 p.u. from one side, with the other side open, to make the exciting current 0.01 p.u. (the resistance 0.0025 p.u. is so small compared to 100 p.u. that it can be ignored in finding the value $j99.95$). The equations with the branch impedance matrix in p.u. are then
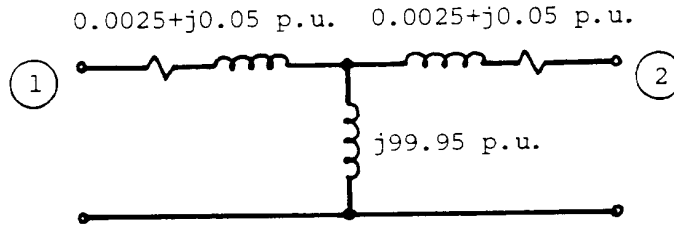
Fig. 6.5 - T-circuit representation of transformer

$$\begin{bmatrix} V_{1pu} \\ V_{2pu} \end{bmatrix} = \left[\begin{bmatrix} 0.0025 & 0 \\ 0 & 0.0025 \end{bmatrix} + j \begin{bmatrix} 100 & 99.95 \\ 99.95 & 100 \end{bmatrix} \right] \begin{bmatrix} I_{1pu} \\ I_{2pu} \end{bmatrix} \tag{6.3a}$$

for steady-state solutions, or

$$\begin{bmatrix} V_1 \\ V_2 \end{bmatrix} = [R] \begin{bmatrix} i_1 \\ i_2 \end{bmatrix} + [L] \begin{bmatrix} di_1 / dt \\ di_2 / dt \end{bmatrix} \tag{6.3b}$$

for transient solutions, with [R] being the same matrix as in Eq. (6.3a), and [L] = 1 / ω [X]. Most EMTP studies are done with actual values rather than with p.u. values. In that case, the matrix in Eq. (6.3) must be converted to actual values, with

$$[Z] = \frac{1}{S_{rating}} \left[\begin{bmatrix} 0.0025 \, V_1^2 & 0 \\ 0 & 0.0025 \, V_2^2 \end{bmatrix} + j \begin{bmatrix} 100 \, V_1^2 & 99.95 \, V_1 V_2 \\ 99.95 \, V_1 V_2 & 100 \, V_2^2 \end{bmatrix} \right] \Omega \tag{6.4}$$

where S_{rating} = apparent power rating of transformer,

   V_1, V_2 = voltage ratings of transformer.

Eq. (6.4) gives the [R] and [X]-matrices of coupled branches in Ω, as required by the EMTP, with the correct turns ratio V_1/V_2. If all quantities are to be referred to one side, say side 1, then simply set $V_2 = V_1$ in Eq. (6.4).

   It is important to realize that the branch impedance matrix [Z] in Eq. (6.4) does not imply that the two coupled branches be connected as shown in the T-circuit of Fig. 6.5. If it were indeed limited to that connection, one could not represent a three-phase bank in wye/delta connection, because both sides would always be connected from node to ground or to some other common node. Instead, [Z] simply represents two coupled coils (Fig. 6.6). The connections are only defined through node name assignments. For example, if three single-phase transformers are connected as a three-phase bank with a grounded wye connection on side 1 and a delta connection on side 2, then the first transformer could have its two coupled branches from node HA to ground and from LA to LB, the second transformer from HB to ground and LB to LC, and the third transformer from HC to ground and LC to LA. This connection will also create the correct phase shift automatically (side 2 lagging behind side 1 by 30° for balanced positive sequence operation in this particular case).
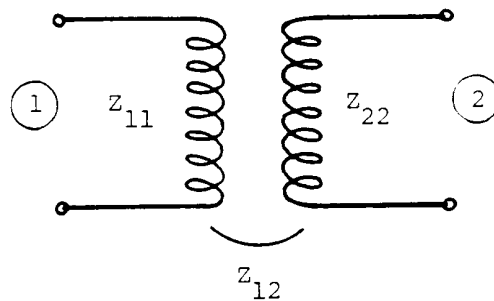
Fig. 6.6 - Two coupled coils

6.2.2 Ill-Conditioning of Inductance Matrix

   The four elements in the [X]-matrix of Eq. (6.3) contain basically the information for the exciting current (magnetizing reactance $X_m = 100$ p.u.), with the short-circuit reactance being represented indirectly through the small differences between X_{11} and X_{12}, and between X_{22} and X_{21}. If all four values were rounded to one digit behind the decimal point ($X_{11} = X_{22} = X_{12} \approx 100$ p.u.), then the short circuit reactance would be completely lost $X^{short} = 0$). In most studies, it is the short-circuit reactance rather than the magnetizing reactance, however, which influences the results. It is therefore important that [X] be calculated and put into the data file with <u>very high accuracy</u>

(typically with at least 5 or 6 digits), to make certain that the short-circuit reactance

$$X^{short} = X_{11} - \frac{X_{12}^2}{X_{22}} \quad seen\ from\ side\ 1 \tag{6.5}$$

is still reasonably accurate. It is highly recommended to calculate X^{short} from Eq. (6.5), to check how much it differs from the original test data. For a transformer with 10% short-circuit reactance and 0.4% exciting current, the values of Z_{11}, Z_{12}, Z_{22} would have to be accurate to within $\pm 0.001\%$ to achieve an accuracy of $\pm 10\%$ for X^{short}! This accuracy problem is one of the reasons why Z_{11}, Z_{12}, Z_{22} cannot be measured directly in tests if this data is to contain the short-circuit test information besides the excitation test information. Mathematically, [X] is almost singular and therefore ill-conditioned, the more so the smaller the exciting current is. Experience has shown that the inversion of [X] inside the EMTP does not cause any problems, as long as very high accuracy is used in the input data. Problems may appear on low-precision computers, however. The author therefore prefers inverse inductance matrix representations, as discussed in Section 6.3.

6.2.3 Three-Winding Transformers

The impedance matrix of single-phase three-winding transformers can be obtained in a similar way with the well-known star circuit used in Fig. 6.2. In that circuit, the magnetizing reactance is usually connected to the star point, but since its unsaturated value is much larger than the short-circuit reactances, it could be connected to either the primary, secondary or tertiary side as well. Assuming that the exciting current for the example of Fig. 6.2 is 1% measured from the primary side, with excitation losses ignored, the magnetizing reactance in the star point would then be 100.0045 p.u. Then

$$[X] = \begin{bmatrix} 100 & 100.0045 & 100.0045 \\ 100.0045 & 100.1260 & 100.0045 \\ 100.0045 & 100.0045 & 100.1240 \end{bmatrix} p.u. \tag{6.6}$$

The particular connection would again be established through the node names at both ends of the branches. For example, the three branches could be connected from node HA to ground, LA to LB, and TA to TB. To convert Eq. (6.6) to actual values, divide all elements by the power rating S_{rating}, and multiply the first row and column with voltage rating V_1, the second row and column with V_2, and the third row and column with V_3.

The [R]- and [X]-matrices can either be derived by hand, or they can be obtained from the support routines XFORMER, BCTRAN, or TRELEG in the BPA version of the EMTP. The latter two support routines were developed for three-phase units, but can be used for single-phase units as well.

6.3 Inverse Inductance Matrix Representation of Single-Phase Two- and Three-Winding Transformers

If the exciting current is ignored, then the only way to represent transformers is with matrices [R] and $[L]^{-1}$, which are handled by the EMTP as described in Section 3.4.2. The author prefers this representation over all others, because the matrices [R] and $[L]^{-1}$ are not ill-conditioned, and because any value of exciting current, including zero,

can be used. The built-in star circuit in the BPA version of the EMTP uses this representation internally as well.

For three-phase transformers, the conversion of the test data to [R]- and [L]$^{-1}$-matrices is best done with the support routine BCTRAN. For single-phase units and for three-phase transformers where $Z_{zero} \approx Z_{pos}$, the conversion is fairly simple, and can easily be done by hand, as explained next.

6.3.1 Two-Winding Transformers

First separate the short-circuit impedance into its resistance and reactance part with Eq. (6.2). The [R]- and $[\omega L]^{-1}$-matrices in p.u. can then be written down by inspection from the equivalent circuit of Fig. 6.5 (after the magnetizing inductance has been removed),

$$[R_{pu}] = \begin{bmatrix} R_{1pu} & 0 \\ 0 & R_{2pu} \end{bmatrix} \quad and \quad [\omega L_{pu}]^{-1} = \begin{bmatrix} \dfrac{1}{X_{pu}} & -\dfrac{1}{X_{pu}} \\ -\dfrac{1}{X_{pu}} & \dfrac{1}{X_{pu}} \end{bmatrix} \tag{6.7}$$

The inverse branch reactance matrix $[\omega L_{pu}]^{-1}$ is the well-known node admittance matrix of a series branch with p.u. reactance X_{pu}. For the example of Fig. 6.5, with exciting current ignored, the p.u. matrices would be

$$[R_{pu}] = \begin{bmatrix} 0.0025 & 0 \\ 0 & 0.0025 \end{bmatrix}, \quad [\omega L_{pu}]^{-1} = \begin{bmatrix} 10 & -10 \\ -10 & 10 \end{bmatrix} \tag{6.8}$$

The matrices in Eq. (6.7) are converted to actual values with

$$[R] = \frac{1}{S_{rating}} \begin{bmatrix} R_{1pu}V_1^2 & 0 \\ 0 & R_{2pu}V_2^2 \end{bmatrix} \quad in \ \Omega \tag{6.9a}$$

$$[\omega L]^{-1} = \frac{S_{rating}}{X_{pu}} \begin{bmatrix} \dfrac{1}{V_1^2} & -\dfrac{1}{V_1 V_2} \\ -\dfrac{1}{V_1 V_2} & \dfrac{1}{V_2^2} \end{bmatrix} \quad in \ S \tag{6.9b}$$

with S_{rating} = apparent power rating

V_1, V_2 = voltage ratings.

Eq. (6.9) contains the correct turns ratio V_1/V_2. If all quantities are to be referred to one side, say side 1, then simply set $V_2 = V_1$ in Eq. (6.9). To obtain [L]$^{-1}$, the matrix in Eq. (6.9) is simply multiplied with ω.

As already mentioned in Section 3.1.2, the two coupled branches described by Eq. (6.9) can also be represented as six uncoupled branches. Ignoring the resistances for the sake of this argument, and setting

$$Y = \frac{S_{rating}}{jX_{pu}V_1^2}$$

$$t = \frac{V_1}{V_2}$$

produces the steady-state branch equations (3.3) and the alternate representations with uncoupled branches of Fig. 3.3.

6.3.2 Three-Winding Transformers

Separating R and X is more complicated now. Therefore, R shall be ignored in the following explanations. Resistances can be included, however, if the support routines BCTRAN or TRELEG are used (see Section 6.10.2 and 6.10.3). The starting point is the well-known star circuit of Fig. 6.7. Its reactances are found from the p.u. short-circuit reactances X_{HLpu}, X_{HTpu},
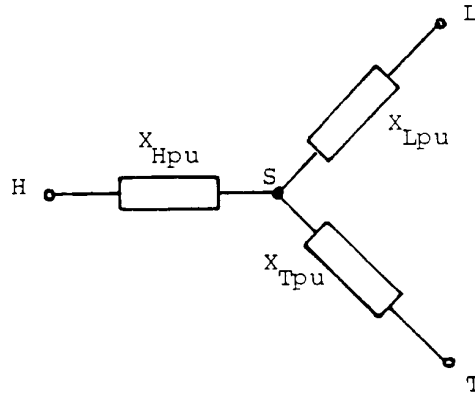
Fig. 6.7 - Star circuit for three-winding transformer with p.u. values based on voltage ratings, or with actual values referred to one side

X_{LTpu}, based on the voltage ratings and one common power base S_{base}. Since the power transfer ratings S_{HL} between H-L, S_{HT} between H-T, and S_{LT} between L-T are usually not identical, a power base conversion is usually needed. If we choose $S_{base} = 1.0$ (in same units as power ratings S_{HL}, S_{HT}, S_{LT}), then

$$X_{Hpu} = \frac{1}{2}\left(\frac{X_{HLpu}}{X_{HL}} + \frac{X_{HTpu}}{S_{HT}} - \frac{X_{LTpu}}{S_{LT}}\right)$$

$$X_{Lpu} = \frac{1}{2}\left(\frac{X_{LTpu}}{S_{LT}} + \frac{X_{HLpu}}{S_{HL}} - \frac{X_{HTpu}}{S_{HT}}\right) \tag{6.10}$$

$$X_{Tpu} = \frac{1}{2}\left(\frac{X_{HTpu}}{S_{HT}} + \frac{X_{LTpu}}{S_{LT}} - \frac{X_{HLpu}}{S_{HL}}\right)$$

For the example used in Section 6.1, with $X_{HL} = 0.117$ p.u., $X_{HT} = 0.115$ p.u., $X_{LT} = 0.241$ p.u. based on 100 MVA, these star-circuit reactances based on 1 MVA would be

$$X_{Hpu} = -0.000045 , \quad X_{Lpu} = 0.001215 , \quad X_{Tpu} = 0.001195$$

Next, the well-known star-delta transformation is used to convert the star-circuit of Fig. 6.7 into the delta circuit of Fig. 6.8,
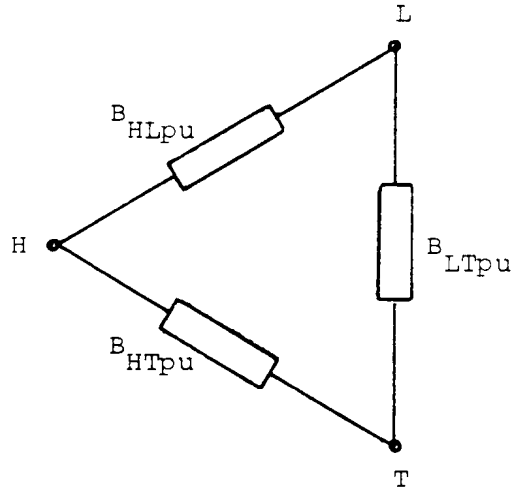
Fig. 6.9 - Delta circuit

which gives us the susceptances[1]

$$B_{HLpu} = \frac{X_{Tpu}}{X^2}$$

$$B_{HTpu} = \frac{X_{Lpu}}{X^2} \tag{6.11a}$$

$$B_{LTpu} = \frac{X_{Hpu}}{X^2}$$

$$with \quad X^2 = X_{Hpu} X_{Lpu} + X_{Lpu} X_{Tpu} + X_{Hpu} X_{Tpu} \tag{6.11b}$$

For the numerical example,

$$B_{HLpu} = 889.484 , \quad B_{HTpu} = 904.371 , \quad B_{LTpu} = -33.495$$

Note that the susceptances in Eq. (6.11a) are not the reciprocals of the short-circuit reactances X used in Eq. (6.10). The p.u. matrix $[\omega L_{pu}]^{-1}$ based on $S_{base} = 1.0$ is easily obtained from Fig. 6.8 with the rules for nodal admittance matrices as

---

[1]"Susceptance" B is used here for the reciprocal of reactance X. This is not strictly correct, because susceptance is the imaginary part of an admittance (which implies B = -1/X).

$$[\omega L_{pu}]^{-1} = \begin{bmatrix} B_{HLpu} + B_{HTpu} & -B_{HLpu} & -B_{HTpu} \\ -B_{HLpu} & B_{HLpu} + B_{LTpu} & -B_{LTpu} \\ -B_{HTpu} & -B_{LTpu} & B_{HTpu} + B_{LTpu} \end{bmatrix} \qquad (6.12)$$

or for the numerical example,

$$[\omega L_{pu}]^{-1} = \begin{bmatrix} 1793.855 & -889.484 & -904.371 \\ -889.484 & 855.989 & 33.495 \\ -904.371 & 33.495 & 870.876 \end{bmatrix} \quad based \ on \ 1 \ MVA$$

The matrix $[\omega L_{pu}]^{-1}$ in actual values is found as

$$[\omega L]^{-1} = \begin{bmatrix} 1st \ row \ and \ column \ of \ (6.12) \ multiplied \ with \ 1/V_H \\ 2nd \ row \ and \ column \ of \ (6.12) \ multiplied \ with \ 1/V_L \\ 3rd \ row \ and \ column \ of \ (6.12) \ multiplied \ with \ 1/V_T \end{bmatrix} \quad in \ S \qquad (6.13)$$

This matrix will contain the correct turns ratios. If all quantities are to be referred to one side, say side H, then simply set $V_L = V_T = V_H$ in Eq. (6.13). Since the p.u. values are based on 1 MVA, the voltages in Eq. (6.13) must be in kV.

6.4 Matrix Representation of Single-Phase N-Coil Transformers

The newer support routines BCTRAN and TRELEG are not limited to the particular case of two or three coils, but work for any number of coils. If each winding is represented as only one coil[2], then transformers with more than three coils will seldom be encountered, but if each winding is represented as an assembly of coils, then transformer models for more than three coils are definitely needed. Breaking one winding up into an assembly of coils may well be required for yet to be developed high-frequency models with stray capacitances.

To explain the concept, only single-phase N-coil transformers are considered in this section. The extension to three-phase units is described in Section 6.5. For such an N-coil transformer, the steady-state equations with a branch impedance matrix [Z] are

---

[2]A coil is "an assemblage of successive convolutions of a conductor," whereas a winding is "an assembly of coils." [76] Since a winding may either be represented as one or as more coils, the more general term "coil" is used here.

$$
\begin{bmatrix} V_1 \\ V_2 \\ . \\ . \\ . \\ V_N \end{bmatrix} = \begin{bmatrix} Z_{11} & Z_{12} & \ldots & Z_1N \\ Z_{21} & Z_{22} & \ldots & Z_2N \\ & & & \\ . & . & . & . & . \\ & & & \\ Z_{N1} & Z_{N2} & \ldots & Z_{NN} \end{bmatrix} \begin{bmatrix} I_1 \\ I_2 \\ . \\ . \\ . \\ I_N \end{bmatrix}
\tag{6.14}
$$

The matrix in Eq. (6.14) is symmetric. Its elements could theoretically be measured in excitation tests: If coil k is energized, and all other coils are open-circuited, then the measured values for I_k and $V_1,\ldots V_N$ produce column k of the [Z] matrix,

$$
Z_{ik} = V_i / I_k
\tag{6.15}
$$

Unfortunately, the short-circuit impedances, which describe the more important transfer characteristics of the transformer, get lost in such excitation measurements, as mentioned in Section 6.2. It is therefore much better to use the branch admittance matrix formulation

$$
[I] = [Y][V]
\tag{6.16}
$$

which is the inverse relationship of Eq. (6.14). Even though [Z] becomes infinite for zero exciting current, or ill-conditioned for very small exciting currents, [Y] does exist, and is in fact the well-known representation of transformers used in power flow studies. Furthermore, all elements of [Y] can be obtained directly from the standard short-circuit test data, without having to use any equivalent circuits. This is especially important for $N > 3$, because the star-circuit "saturable transformer component" in the BPA EMTP) is incorrect for more than three coils.

For an intermediate step in obtaining [Y], the transfer characteristics between coils are needed. Let these transfer characteristics be expressed as voltage drops between coil i and the last coil N,

$$
\begin{bmatrix} V_1 - V_N \\ V_2 - V_N \\ . \\ . \\ . \\ V_{N-1} - V_N \end{bmatrix} = \begin{bmatrix} Z_{11}^{reduced} & Z_{12}^{reduced} & \ldots & Z_{1,N-1}^{reduced} \\ Z_{21}^{reduced} & Z_{22}^{reduced} & \ldots & Z_{2,N-1}^{reduced} \\ & & & \\ . & . & . & . & . \\ & & & \\ Z_{N-1,1}^{reduced} & Z_{N-1,2}^{reduced} & \ldots & Z_{N-1,N-1}^{reduced} \end{bmatrix} \begin{bmatrix} I_1 \\ I_2 \\ . \\ . \\ . \\ I_{N-1} \end{bmatrix}
\tag{6.17}
$$

with [$Z^{reduced}$] again being symmetric. Since the exciting current has negligible influence on these transfer characteristics, it is best to ignore the exciting current altogether. Then the sum of the p.u. currents[3] (based on one common base power S_{base}, and on the transformer voltage ratings of the N coils) must be zero, or

---

[3]From here on it is best to work with p.u. quantities, or with quantities referred to one side, to avoid carrying the turns ratios through all the derivations.

$$\sum_{k=1}^{N} I_{k\,pu} = 0 \tag{6.18}$$

The p.u. values of the matrix elements in Eq. (6.17) can then be found directly from the short-circuit test data, as first shown by Shipley [108]. For a short-circuit test between i and N, only $I_{i\,pu}$ in Eq. (6.17) is nonzero, and $V_{N\,pu} = 0$. Then the i-th row becomes

$$V_{i\,pu} = Z_{ii\,pu}^{reduced} I_{i\,pu} \tag{6.19}$$

The impedance in this equation is the short-circuit impedance between coils i and N by definition,

$$Z_{ii\,pu}^{reduced} = Z_{iN\,pu}^{short} \tag{6.20}$$

based on one common base power S_{base}. The off-diagonal element $Z_{ik\,pu}^{reduced}$ is found by relating rows i and k of Eq. (6.17) to the short-circuit test between i and k. For this test, $I_{k\,pu} = -I_{i\,pu}$, and $V_{k\,pu} = 0$, with all other currents being zero. Then rows i and k become

$$V_{i\,pu} - V_{N\,pu} = \left(Z_{ii\,pu}^{reduced} - Z_{ik\,pu}^{reduced} \right) I_{i\,pu} \tag{6.21a}$$

$$-V_{N\,pu} = \left(Z_{ki\,pu}^{reduced} - Z_{kk\,pu}^{reduced} \right) I_{i\,pu} \tag{6.21b}$$

or after subtracting Eq. (6.21b) from (6.21a), with $Z_{ki}^{reduced} = Z_{ik}^{reduced}$,

$$V_{i\,pu} = \left(Z_{ii\,pu}^{reduced} + Z_{kk\,pu}^{reduced} - 2 Z_{ik\,pu}^{reduced} \right) I_{i\,pu} \tag{6.21c}$$

By definition, the expression in parentheses of Eq. (6.21c) must be the short-circuit impedance $Z_{ik\,pu}^{short}$, or

$$Z_{ik\,pu}^{reduced} = \frac{1}{2} \left(Z_{iN\,pu}^{short} + Z_{kN\,pu}^{short} - Z_{ik\,pu}^{short} \right) \tag{6.22}$$

based on one common base power S_{base}. This completes the calculation of the matrix elements of Eq. (6.17) from the short-circuit test data, which is normally supplied by the manufacturer.

Eq. (6.17) cannot be expanded to include all coils, since all matrix elements would become infinite with the exciting current being ignored. To get to the admittance matrix formulation (6.16), Eq. (6.17) is first inverted,

$$[Y_{pu}^{reduced}] = [Z_{pu}^{reduced}]^{-1} \tag{6.23}$$

In this inverse relationship, the voltage $V_{N\ pu}$ of the last coil already exists, and all terms associated with it can be collected into a N-th column for $V_{N\ pu}$. The N-th row is created by taking the negative sum of rows 1,...N-1 based on Eq. (6.18). This results in the full matrix representation

$$
\begin{bmatrix} I_{1\ pu} \\ I_{2\ pu} \\ . \\ . \\ . \\ I_{N\ pu} \end{bmatrix} = \begin{bmatrix} Y_{11\ pu} & Y_{12\ pu} & \cdots & Y_{1N\ pu} \\ Y_{21\ pu} & Y_{22\ pu} & \cdots & Y_{2N\ pu} \\ & & & \\ . & . & . & . & . \\ & & & \\ Y_{N1\ pu} & Y_{N2\ pu} & \cdots & Y_{NN\ pu} \end{bmatrix} \begin{bmatrix} V_{1\ pu} \\ V_{2\ pu} \\ . \\ . \\ . \\ V_{N\ pu} \end{bmatrix}
\tag{6.24a}
$$

with

$$
Y_{ik\ pu} = Y_{ik\ pu}^{reduced} \quad \textit{from Eq. (6.23) for } i, k \leq N-1
\tag{6.24b}
$$

$$
Y_{iN\ pu} = Y_{Ni\ pu} = -\sum_{k=1}^{N-1} Y_{ik\ pu}^{reduced} \quad \textit{for } i \neq N
\tag{4.24c}
$$

$$
Y_{NN\ pu} = -\sum_{i=1}^{N-1} Y_{iN\ pu}
\tag{6.24d}
$$

To convert from p.u. to actual values, all elements in Eq. (6.24) are multiplied by the one common base power S_{base}, and each row and column i is multiplied with $1/V_i$.

For transient studies, the resistance and inductance parts must be separated, in a way similar to that of Section 6.3. This is best accomplished by building $[Z^{reduced}]$ only from the reactance part of the short-circuit test data, which is

$$
X_{ik\ pu}^{short} = \sqrt{\left(Z_{ik\ pu}^{short}\right)^2 - \left(R_{i\ pu} + R_{k\ pu}\right)^2}
\tag{6.25}
$$

with $\quad Z_{ik\ pu}^{short}$ = p.u. short circuit impedance (magnitude),

$R_{i\ pu} + R_{k\ pu}$ = either p.u. load losses in short-circuit test between i and k, or sum of p.u. winding resistances.

The winding resistances then form a diagonal matrix [R], and

$$
[L]^{-1} = j\omega[Y]
\tag{6.26}
$$

with [Y] being purely built from reactance values $j\omega L$. Both [R] and $[L]^{-1}$ are used in Eq. (6.1) to represent the N-coil transformer.

Support routine BCTRAN uses this procedure for obtaining [R] and $[L]^{-1}$ from the transformer test data, with two additional refinements:

a.   If the winding resistances are not given, but the load losses in the short-circuit tests are known, then the resistances can be calculated from Eq. (6.2) for N=2, and from the following three

equations for $N = 3$,

$$R_{1\ pu} + R_{2\ pu} = P_{12\ pu}^{loss}$$

$$R_{2\ pu} + R_{3\ pu} = P_{23\ pu}^{loss} \quad\quad\quad (6.27)$$

$$R_{1\ pu} + R_{3\ pu} = P_{13\ pu}^{loss}$$

Strictly speaking, Eq. (6.2) and (6.27) are not quite correct, because the load losses contain stray losses in addition to the I^2R-losses, but the results should be reasonable. For transformers with 4 or more coils there is no easy way to find resistances from the load losses, and coil resistances must be specified as input data if $N \geq 4$.

b.   Additional branches can be added to represent the exciting current, as described in Section 6.6.

To short derivations for a numerical example, let us first use the two-winding transformer of Fig. 6.5, with exciting current ignored. The resistance and reactance part is already separated in this case, with $R_{pu} = 0.005$ and $X_{pu} = 0.10$. The reduced reactance matrix of Eq. (6.17) is just a scalar in this case, $jX_{pu}^{reduced} = j0.10$, and its inverse is the reciprocal $Y_{pu}^{reduced} = -j10$. Adding a second row and column with Eq. (6.24) produces

$$\frac{1}{j}[\omega L_{pu}]^{-1} = \frac{1}{j}\begin{bmatrix} 10 & -10 \\ -10 & 10 \end{bmatrix}$$

which, together with $R_{1\ pu} = R_{2\ pu} = 0.0025$, is the same result shown in Eq. (6.8).

For the example of the three-winding transformer used after Eq. (6.10), the reduced reactance matrix (without the factor j) is

$$[X_{pu}^{reduced}] = \begin{bmatrix} 0.1150 & 0.1195 \\ 0.1195 & 0.2410 \end{bmatrix} \quad based\ on\ 100\ MVA$$

which, after inversion, becomes

$$[Y_{pu}^{reduced}] = \frac{1}{j}\begin{bmatrix} 17.9386 & -8.8948 \\ -8.8948 & 8.5599 \end{bmatrix} \quad based\ on\ 100\ MVA$$

or after adding the third row and column with Eq. (6.24),

$$[Y_{pu}] = \frac{1}{j}\begin{bmatrix} 17.93856 & -8.89484 & -9.04372 \\ -8.89484 & 8.55989 & 0.33495 \\ -9.04372 & 0.33495 & 8.70877 \end{bmatrix} \quad based\ on\ 100\ MVA$$

which is the same answer as the one given after Eq. (6.12), except for minor round-off errors and for a change in base power from 1 MVA to 100 MVA. The star-circuit equivalent circuit of a three-winding transformer is therefore just a special case of the general method for N coils discussed here.

6.5 Matrix Representation of Three-Phase N-Coil Transformers

The first attempt to extend single-phase to three-phase transformer models was the addition of a zero-sequence reluctance to the equivalent star-circuit ("saturable transformer element" in the BPA EMTP). This was similar to the approach used on transient network analyzers, where magnetic coupling among the three core legs is usually modelled with the addition of extra delta-connected winding to a three-phase bank consisting of single-phase units. To relate the available test data to the data of the added winding is unfortunately difficult, if not impossible. For example, a two-winding three-phase unit is characterized by only two short-circuit impedances (one from the positive sequence test, and the other from the zero sequence test). Adding delta-connected windings to single-phase two-winding transformers would require three short-circuit impedances, however, because this trick converts the model into a three-winding transformer. Adding extra delta-connected windings becomes even more complicated for three-phase three-winding units, not only in fitting the model data to the test data, but also because a four-winding model would be required for which the star-circuit is no longer valid [109]. It was therefore reasonable to develop another approach, as described here.

The extension from single-phase to three-phase units turned out to be much easier than was originally thought. Conceptually, each coil of a single-phase units becomes three coils on core legs I, II, III in a three-phase unit (Fig. 6.9).

| (a) | Three-legged core design | (b) | Five-legged core design | (c) Shell-type design |
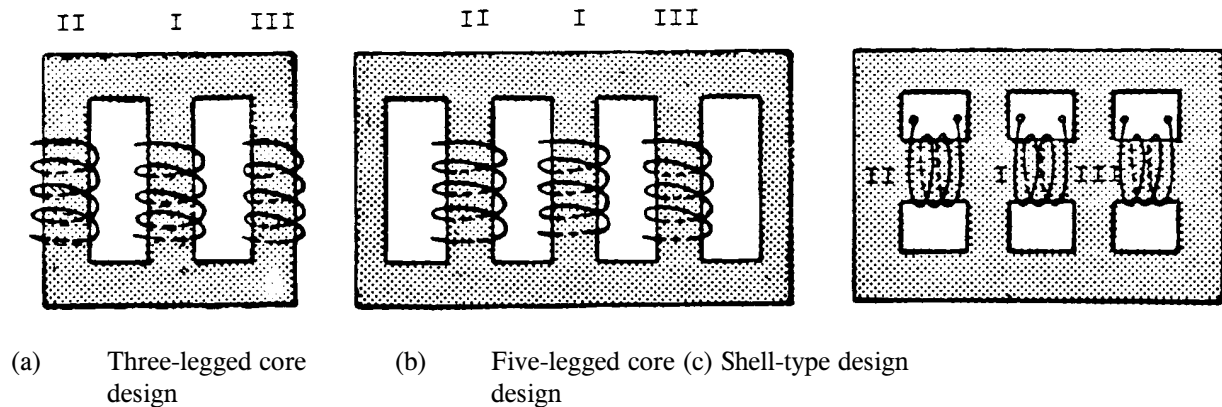
Fig. 6.9 - Three-phase transformers

In terms of equations, this means that each scalar quantity Z or Y must be replaced by a 3 x 3 submatrix of the form

$$\begin{bmatrix} Z_s & Z_m & Z_m \\ Z_m & Z_s & Z_m \\ Z_m & Z_m & Z_s \end{bmatrix} \quad\quad\quad (6.28)$$

where Z_s is the self impedance of the coil on one leg, and Z_m is the mutual impedance to the coils on the other two legs[4]. As in any other three-phase network component (e.g., overhead line), these self and mutual impedances are related to the positive and zero sequence values,

$$Z_s = \frac{1}{3}\left(Z_{zero} + 2Z_{pos}\right)$$

$$Z_m = \frac{1}{3}\left(Z_{zero} - Z_{pos}\right) \quad\quad\quad (6.29)$$

6.5.1 Procedure for Obtaining [R] and [L]$^{-1}$

By simply replacing scalars by 3 x 3 submatrices of the form (6.28), the [R]- and [L]$^{-1}$-matrix representation of a three-phase transformer is found as follows:

1. Set up the resistance matrix [R]. If the winding resistances are known, use them in [R]. If they are to be calculated from load losses, use Eq. (6.2) for N = 2, or Eq. (6.27) for N = 3. For N $\geq$ 4, there is no easy way to calculate the resistances. Use positive sequence test data in these calculations, and assume that the three corresponding coils on legs I, II, III have identical resistances.

2. Find the short-circuit reactances from Eq. (6.25) for positive sequence values. Use the same equation for zero sequence values, provided the zero sequence test between two windings does not involve another winding in delta connection. In the latter case, the data must first be modified according to Section 6.5.2.

3. Build the reduced reactance matrix [$X_{pu}^{reduced}$] from Eq. (6.20) and (6.22), by first calculating the positive and zero sequence values separately from the positive and zero sequence short-circuit reactances, and by replacing each diagonal and off-diagonal element by a 3 x 3 submatrix of the form (6.28). The elements of this matrix are calculated with Eq. (6.29).

   Since the 3 x 3 submatrices contain only 2 distinct values X_s and X_m, it is not necessary to work with 3 x 3 matrices, but only with pairs (X_s, X_m). D. Hedman derived a "balanced-matrix algebra" for the multiplication, inversion, etc., of such "pairs" [110], which is used in the support routines BCTRAN and TRELEG.

---

[4]From Fig. 6.9 it is evident that the mutual impedance between legs I and II is slightly different from the one between legs II and III, etc. Data for this unsymmetry is usually not available, and the unsymmetry is therefore ignored here. To take it into account would require that a three-phase two-winding transformer be modelled as a six-coil transformer (Section 6.4), with 15 measured short-circuit impedances.

4.   Invert $[X_{pu}^{reduced}]$ to obtain $[B_{pu}^{reduced}]$, again using Hedman's "balanced-matrix algebra," and expand $[B_{pu}^{reduced}]$ to the full matrix $[B_{pu}]$ with Eq. (6.24).

5.   Since the reactances were in p.u. based on one common S_{base}, the inverse inductance matrix $[L]^{-1}$ in actual values 1/H is obtained from $[B_{pu}]$ by multiplying each element $B_{ik\ pu}$ with $\omega\ S_{base}\ /\ V_i V_k$, where V_i and V_k are the voltage ratings of coil i and k. For the conversion of p.u. resistances to actual values in Ω, multiply $R_{i\ pu}$ with $V_i^2\ /\ S_{base}$.

6.5.2 Modification of Zero-Sequence Data for Delta Connections

The procedure of Section 6.5.1 cannot be used directly for the zero sequence calculation of transformers with three or more windings if one or more of them are delta-connected. Assume that a three-winding transformer has wye-connected primary and secondary windings, with their neutrals grounded, and a delta-connected tertiary winding. In this case, the zero-sequence short-circuit test between the primary and secondary windings will not only have the secondary winding shorted but the tertiary winding as well, since a closed delta connection provides a short-circuit path for zero-sequence currents. This special situation can be handled by modifying the short-circuit data for an open delta so that the procedure of Section 6.5.1 can again be used. With the well-known equivalent star circuit of Fig. 6.7, the three test values supplied by the manufacturer are ("pu" in the subscript dropped to simplify notation),

$$X_{HL}^{closed\Delta} = X_H + \frac{X_L X_T}{X_L + X_T} \tag{6.30a}$$

$$X_{HT} = X_H + X_T \qquad in\ p.u.\ values \tag{6.30b}$$

$$X_{LT} = X_L + X_T \tag{6.30c}$$

which can be solved for X_H, X_L, X_T:

$$X_H = X_{HT} - \sqrt{X_{LT} X_{HT} - X_{HL}^{closed\Delta} X_{LT}} \tag{6.31a}$$

$$X_L = X_{LT} - X_{HT} + X_H \qquad in\ p.u.\ values \tag{6.31b}$$

$$X_T = X_{HT} - X_H \tag{6.31c}$$

After this modification, the short-circuit reactances $X_H + X_L$, $X_H + X_T$ and $X_L + X_T$ are used as input data, with winding T no longer being shorted in the test between H and L.

The modification scheme becomes more complicated if resistances are included. For instance, Eq. (6.30a) becomes

$$\left| Z_{HL}^{closed\Delta} \right| = \left| R_H + jX_H + \frac{(R_L + jX_L)\ (R_T + jX_T)}{(R_L + R_T)\ + j(X_L + X_T)} \right| \qquad in\ p.u.\ values \tag{6.32}$$

with $\left| Z_{HL}^{closed\ \Delta} \right|$ being the value supplied by the manufacturer, and R_H, R_L, R_T being the winding resistances. This

leads to a system of nonlinear equations, which is solved by Newton's method in the support routine BCTRAN. It works for three-winding transformers with wye/wye/delta- and with wye/delta/delta- connections so far, which should cover most practical cases.

6.6 Exciting Current

The exciting current is very much voltage-dependent above the "knee-point" of the saturation curve $\lambda = f(i)$. Fig. 6.10 shows a typical curve for a modern high-voltage transformer with grain-oriented steel, with the knee-point around 1.1 to 1.2 times rated flux [114]. The value of the incremental inductance $d\lambda/di$ is fairly low in the saturated region, and fairly high in the unsaturated region. The exciting current in the unsaturated region can easily be included in the [L]- or [L]$^{-1}$-representations. Extra nonlinear branches are needed to include saturation effects, and extra resistance branches to include excitation losses.
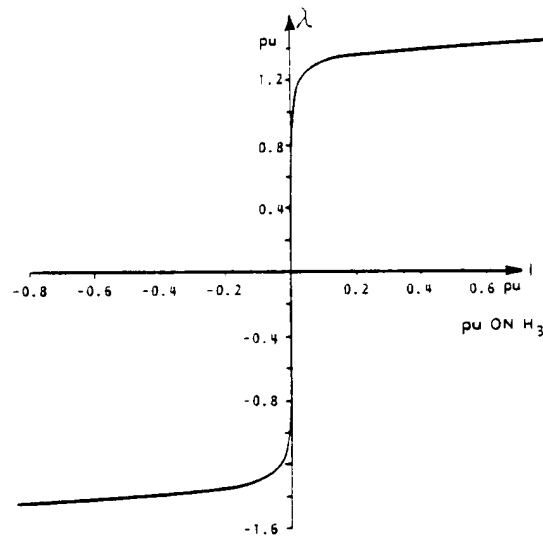
Fig. 6.10 - Typical saturation curve [114]. © 1981 IEEE

6.6.1 Linear (Unsaturated) Exciting Current

For single-phase units and for three-phase units with five-legged core or shell-type design (Fig. 6.9(b) and (c)), the linear exciting current is very small and can often be ignored. If it is ignored, then the [L]$^{-1}$-matrix representation described in Section 6.3 to 6.5 must be used. A (small) exciting current must always be included, however, if [L]-matrices are used, as explained in Section 6.2. For three-phase units with three-legged core design, the exciting current is fairly high in the zero sequence test (e.g., 100%), and should therefore not be neglected.

The exciting current has an imaginary part, which is the "magnetizing current" flowing through the magnetizing inductance L_m. It also has a smaller real part (typically 10% of the imaginary part), which accounts for excitation losses. These losses are often ignored. They can be modelled reasonably well, however, with a shunt conductance G_m in parallel with the magnetizing inductance L_m. The p.u. magnetizing conductance is

$$G_{m\,pu} = \frac{P_{exc}}{S_{rating}}$$

(6.33)

and the reciprocal of the p.u. magnetizing reactance is

$$\frac{1}{X_{m\,pu}} = \sqrt{\left(\frac{I_{exc}}{I_{rating}}\right)^2 - \left(G_{m\,pu}\right)^2}$$

(6.34)

with P_{exc} = excitation loss in excitation test,

          I_{exc} = magnitude of exciting current in excitation test,

          S_{rating} = power rating, and

          I_{rating} = current rating.

To assess the relative magnitudes of G_m and $1/X_m$, let us take the values from the example of Section 6.2 as typical ($X_{short} = 10\%$, $R_{short} = 0.5\%$, $I_{exc} = 1\%$). Furthermore, assume that the excitation loss $V^2 G_m$ at rated voltage is 25% of the load loss $I^2 R_{short}$ at rated current (a typical ratio for power transformers). Then $G_{m\,pu} = 0.00125$ and $I_{exc}/I_{rating} = 0.01$. The reciprocal of the p.u. magnetizing reactance is therefore close to the value of the p.u. exciting current,

$$\frac{1}{X_{m\,pu}} \approx \frac{I_{exc}}{I_{rating}}$$

(6.35)

with the error being less than 1% in the numerical example.

       How to include the linear exciting current in the model depends on whether an $[L]^{-1}$- or $[L]$-matrix representation is used, and whether the transformer is a single-phase or a three-phase unit.

6.6.1.1 Single-Phase Transformers

       In the $[L]$-matrix representation, the magnetizing inductance L_m will already have been included in the model. Usually, the T-circuit of Fig. 6.5, or the star circuit of Fig. 6.7 with L_m connected to star point S, is used in the derivation of $[L]$. Since $L_{m\,pu}$ is much larger than $L_{short\,pu}$, it could be placed across the terminals of the high, low or tertiary side with equal justification. Alternatively, $2L_{m\,pu}$ could be connected to both high and low side, which would convert the T-circuit of the two-winding transformer into a π-circuit, or $3L_{m\,pu}$ could be connected to all 3 sides in the case of a three-winding transformer. The conversion of $L_{m\,pu}$ into actual values is done in the usual way by using the voltage rating for that side to which the inductance is to be connected. For example, connecting the p.u. inductance $3L_{m\,pu}$ to all 3 sides would mean that the actual values of these 3 inductances are

$$L_H = 3L_{m\,pu}\frac{V_H^2}{S_{rating}}$$

$$L_L = 3 L_{m\,pu} \frac{V_L^2}{S_{rating}}$$

$$L_T = 3 L_{m\,pu} \frac{V_T^2}{S_{rating}}$$

In the $[L]^{-1}$-matrix representation, the "internal" nodes of the T- or star circuit are not available, and the magnetizing inductance must therefore be connected across one or all "external" terminals, as discussed above. Connecting it across side i is the same as adding $1/L_m$ to the i-th diagonal element of $[L]^{-1}$. This makes $[L]^{-1}$ nonsingular, and it could therefore be inverted if the user prefers $[R]$- and $[L]$-matrices. This inversion option is available in the support routine BCTRAN, even though this writer prefers to work with $[L]^{-1}$ because $[L]$ is more or less ill-conditioned as discussed in Section 6.2.2.

While L_m does not create extra branches, but "disappears" instead into the $[L]$- or $[L]^{-1}$-matrix, one or more extra resistance branches are needed to model excitation losses with $G_{m\,pu}$ from Eq. (6.33). Again, $G_{m\,pu}$ can either be added to one side, or $1/2\ G_{m\,pu}$ to both sides of a two-winding transformer and $1/3\ G_{m\,pu}$ to all three sides of a three-winding transformer. The conversion to actual values is again straightforward, and $R_m = 1/G_m$ is then used as input data for the extra resistance branch.

6.6.1.2 Three-Phase Transformers

The inclusion of the linear exciting current for three-phase units is basically the same as for single-phase units, except that G_m and $1/X_m$ from Eq. (6.33) and (6.34) are now calculated twice, from the positive as well as from the zero sequence excitation test data. The reciprocals of the two magnetizing inductances,

$$B_{pos} = 1/L_{m-pos}\ , \qquad B_{zero} = 1/L_{m-zero}$$

are converted to a 3 x 3 matrix

$$\begin{bmatrix} B_s & B_m & B_m \\ B_m & B_s & B_m \\ B_m & B_m & B_s \end{bmatrix}$$

where

$$B_s = \frac{1}{3}(B_{zero} + 2B_{pos})$$
$$B_m = \frac{1}{3}(B_{zero} - B_{pos}) \tag{6.36}$$

which is added to the 3 x 3 diagonal block in $[L]^{-1}$ of the high, low, or some other side. Alternatively, 1/N-times the p.u. 3 x 3 matrix could be added to the 3 x 3 diagonal blocks of all sides of an N-winding transformer, after conversion to actual values with the proper voltage ratings. After these additions, $[L]^{-1}$ becomes nonsingular and

can therefore be inverted for users who prefer [L]-matrices. Support routine TRELEG builds an [L]-matrix directly from both the short-circuit and excitation test data, as briefly described in Section 6.10.3.

To include excitation losses, three coupled resistance branches must be added across the terminals of one side. The diagonal and off-diagonal elements of this resistance matrix are

$$R_s = \frac{1}{3}\left(\frac{1}{G_{m-zero}} + \frac{2}{G_{m-pos}} \right)$$

$$R_m = \frac{1}{3}\left(\frac{1}{G_{m-zero}} - \frac{1}{G_{m-pos}} \right) \tag{6.37}$$

The excitation test for the positive sequence is straightforward, and the data is usually readily available. Some precautions are necessary with the zero sequence test data, if it is available, or reasonable assumptions must be made if unavailable.

If the transformer has delta-connected windings, the delta connections should be opened for the zero sequence excitation test. Otherwise, the test really becomes a short-circuit test between the excited winding and the delta-connected winding. On the other hand, if the delta is always closed in operation, any reasonable value can be used for the zero sequence exciting current (e.g., equal to positive sequence exciting current), because its influence is unlikely to show up with the delta-connected winding providing a short-circuit path for zero sequence currents.

If the zero sequence exciting current is not given by the manufacturer, a reasonable value can be found as follows: Imagine that one leg of the transformer (A in Fig. 6.11) is excited, and estimate from physical reasoning how much voltage will be induced in the corresponding coils of the other two legs (B and C in Fig. 6.11). For the three-legged core design of Fig. 6.11, approximately one half of flux λ_A returns through phases B and C, which means that the induced voltages V_B and V_C will be close to 0.5 V_A (with reversed polarity). If k is used for this factor 0.5, then

$$\frac{I_{exc-zero}}{I_{exc-pos}} = \frac{1 + k}{1 - 2k} \tag{6.38}$$
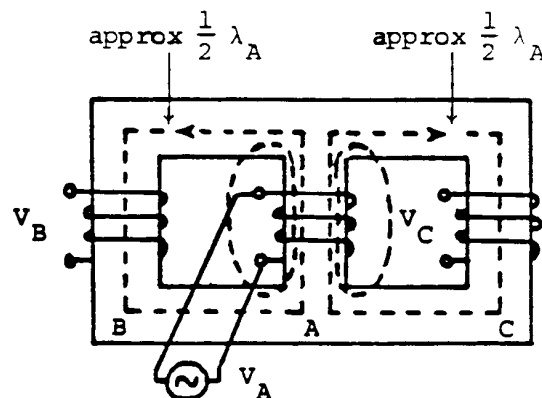
Fig. 6.11 - Fluxes in three-legged core-type design

Eq. (6.38) is derived from

$$V_A = Z_s I_A \tag{6.39a}$$

$$V_B = V_C = Z_m I_A \tag{6.39b}$$

with Z_s, Z_m being the self and mutual magnetizing impedances of the three excited coils. With

$$V_B = V_C = \frac{Z_m}{Z_s} V_A = \frac{Z_{zero} - Z_{pos}}{Z_{zero} + 2Z_{pos}} V_A = -k V_A \tag{6.40}$$

and Z_{pos}, Z_{zero} inversely proportional to $I_{exc-pos}$, $I_{exc-zero}$, Eq. (6.38) follows. Obviously, k cannot be exactly 0.5, because this would lead to an infinite zero sequence exciting current. A reasonable value for $I_{exc-zero}$ in a three-legged core design might be 100%. If $I_{exc-pos}$ were 0.5%, k would become 0.49626, which comes close to the theoretical limit of 0.5. Exciting the winding on one leg with 100 kV would then induce voltages of 49.6 kV (with reversed polarity) in the windings of the other two legs.

For the five-legged core-type design of Fig. 6.9(b), maybe 2/3 of approximately $(1/2)\lambda_A$ would return through legs B and C. In that case, k would be 1/3, or $I_{exc-zero}/I_{exc-pos} = 4$.

The excitation loss in the zero sequence test is higher than in the positive sequence test, because the fluxes λ_A, λ_B, λ_C in the three cores are now equal, and in the case of a three-legged core-type design must therefore return through air and tank, with additional eddy-current losses in the tank. Neither the value of the zero sequence exciting current nor the value of the zero sequence excitation loss are critical if the transformer has delta-connected windings, because excitation tests really become short-circuit tests in such cases.

The modification of $[L]^{-1}$ for magnetizing currents and the addition of resistance branches for excitation losses create a model which reproduces the original test data very well. Table 6.1 compares the test data, which was used to create the model with the support routine BCTRAN, with steady-state EMTP solutions in which this model was used to simulate the test conditions (e.g., voltage sources were connected to one side, and another side was shorted, to simulate a short-circuit test). In this case, the three winding resistances were specified as input data, and an [L]-matrix with 10-digit accuracy was used to minimize the problem of ill-conditioning. The excitation data was specified as being measured from the primary side, but $1/L_m$ and shunt conductance G_m were placed across the tertiary side, for reasons explained in Section 6.6.2. BCTRAN modifies L_m and R_m in this situation, to account for the influence of the short-circuit impedance between the primary and tertiary side. For the zero sequence short-circuit impedance between the primary and secondary side, the modifications of Section 6.5.2 were applied to account for the effect of the delta-connected tertiary winding.

Table 6.1 - Data for three-phase three-winding transformer in Yyd-connection

TYPE OF TEST	TEST DATA	SIMULATION RESULTS

pos. sequence excitation test	exciting current (%)	0.428	0.4281 (in phase A) 0.4280 (in phase B) 0.4230 (in phase C)
	excitation loss (kW)	135.73	135.731
zero sequence excitation test[*]	exciting current (%)	0.428	0.4280 in all phases
	excitation loss (kW)	135.73	135.731
short-circuit test impedances, with three-plane MVA base in paren- thesis	Z_{12}^{pos} (%) (300)	8.74	8.740
	Z_{13}^{pos} (%) (76)	8.68	8.680
	Z_{23}^{pos} (%) (76)	5.31	5.310
	Z_{12}^{zero} (%)[**] (300)	7.343194[***]	7.34318
	Z_{13}^{zero} (%) (300)	26.258183[***]	26.25806
	Z_{23}^{zero} (%) (300)	18.552824[***]	18.55284

[*] With open delta on side 3 (values were unavailable from test; since they are unimportant if delta is closed in operation, as explained in text, the positive sequence values were used for zero sequence as well).
[**] With closed delta on side 3.
[***] These values were calculated from the original test data given as R and X in percent with an accuracy of 2 digits after the decimal point.

6.6.2 Saturation Effects

For the transient analysis of inrush currents, of ferroresonance and of similar phenomena it is clearly necessary to include saturation effects. Only the star circuit representation in the BPA EMTP ("saturable transformer component") accepts the saturation curve directly, while the [L]- and $[L]^{-1}$-representations require extra nonlinear inductance branches for the simulation of saturation effects.

Nonlinear inductances of the form of Fig. 6.10 can often be modelled with sufficient accuracy as two-slope piecewise linear inductances. Fig. 6.12 shows two- and five-slope piecewise linear representations from a practical case [80] for the system shown before in Fig. 6.1. The simulation results (Fig. 6.13) are almost identical, and agree reasonably well with field test results (Fig. 6.14). The slope in the saturated region above the knee is the air-core inductance, which is almost linear and fairly low compared with the slope in the unsaturated region. Typical values for air-core inductances are $2L_{short}$ (L_{short} = short-circuit inductance) for two-winding transformers with separate windings [111], or 4 to 5 times L_{short} for autotransformers. In the unsaturated region, the values can be fairly high on very large transformers (see Fig. 6.10).

While it makes little difference to which terminal the unsaturated inductance is connected,
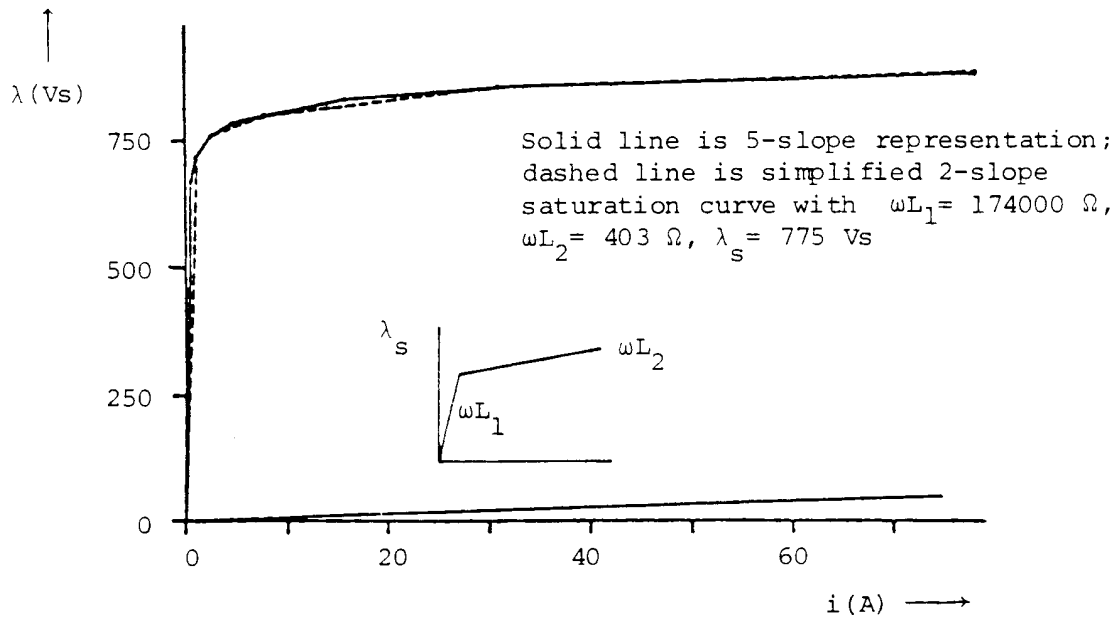
Fig. 6.12 - Two-slope and five-slope piecewise linear inductance
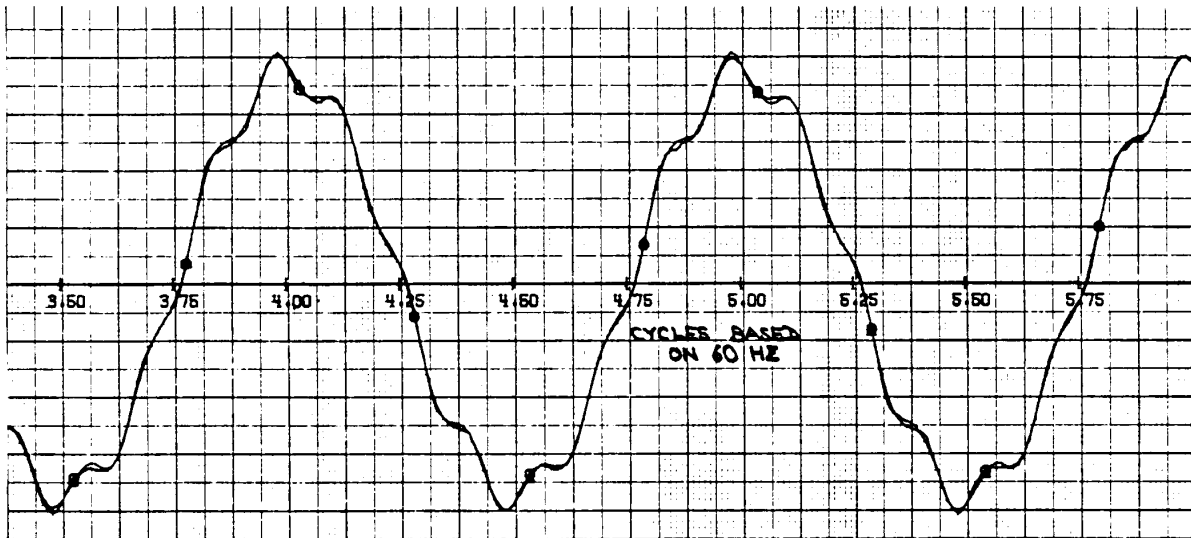
Fig. 6.13 - Superimposed EMTP simulation results with two- and five-slope piecewise linear inductance

6-24
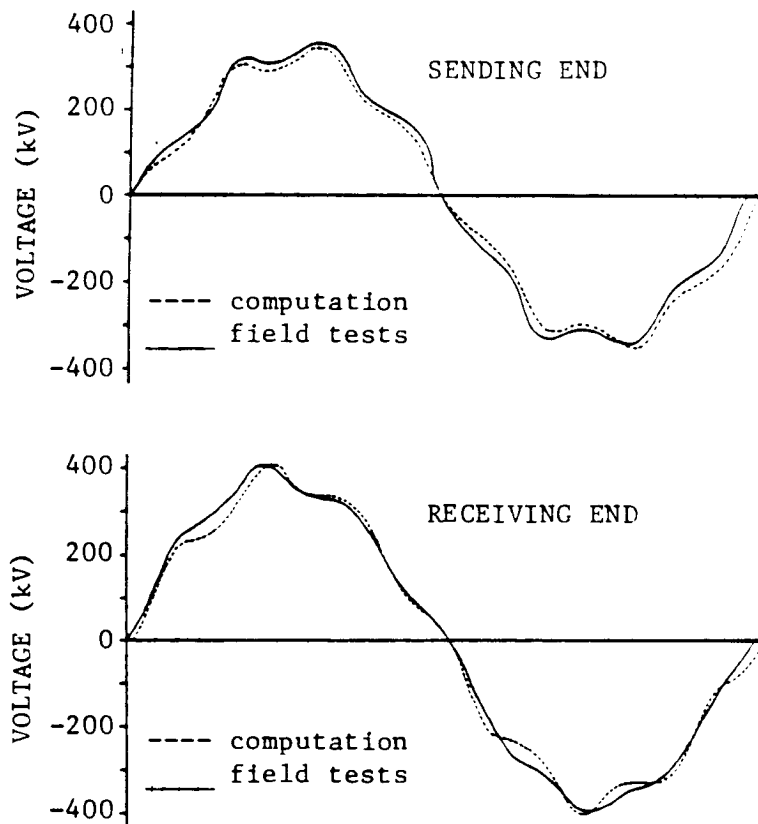
Fig. 6.14 - Comparison between simulation and field test results

it may make a difference for the saturated inductance, because of its low value. Ideally, the nonlinear inductance should be connected to a point in the equivalent circuit where the integrated voltage is equal to the iron-core flux. To identify that point is not easy, however, and requires construction details not normally available to the system analyst. For cylindrical coil construction, it can be assumed that the flux in the winding closest to the core will mostly go through the core, since there should be very little leakage. This winding is usually the tertiary winding in three-winding transformers, and in such cases it is therefore best to connect the nonlinear inductance across the tertiary terminals. Fig. 6.15 shows the star circuit derived by Schlosser [112] for a transformer with three cylindrical windings (T closest to core, H farthest from core, L in between), where the integrated voltage in point A is equal to the flux in the iron-core. The reactances of -0.58 Ω between A and T is normally not known, but it is so small compared to 7.12 Ω between S and T, that the nonlinear inductance can be connected to T instead of A, with little error. Fig. 6.15 also identifies a point B at which the integrated voltage is equal to yoke flux. Zikherman [113] suggests to connect another nonlinear inductance to that point B to represent yoke saturation. Since -4.9 Ω between H and B is small compared to 22 Ω between H and S, this second nonlinear inductance could probably be connected to H without too much error. The knee-point and the slope in the saturated region of this second nonlinear

6-25
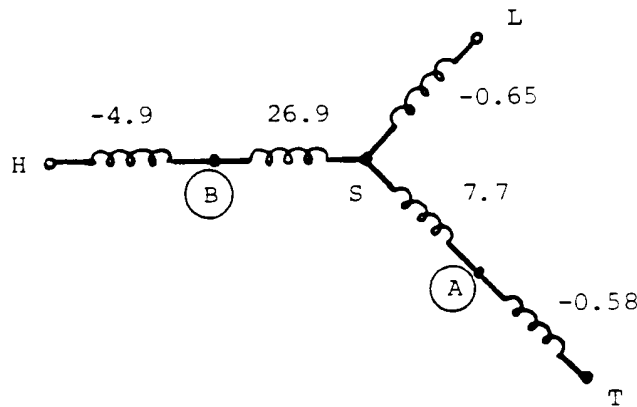
Fig. 6.15 - Reactances (in Ω) of a three-winding transformer (from [112], which provides the data for 5 cylindrical windings; the two windings farthest from the core are ignored here)

inductance are higher than those of the first nonlinear inductance (Fig. 6.16). Since it is already difficult to obtain saturation curves for the core, this secondary effect of yoke saturation is usually ignored. Dick and Watson [114] came to similar conclusions about the proper placement of the nonlinear inductance when they measured saturation curves on a three-winding transformer. Table 6.2 compares the air-core inductance (= slope in saturated region) obtained from laboratory tests with values obtained from the star circuit[5] if the nonlinear inductance is connected to the tertiary T, or to the star point S. The authors also show a more accurate equivalent circuit which would be useful if yoke saturation or unsymmetries in the three core legs are to be included. If L_m is connected to T, then the differences are less than $\pm 5\%$, whereas the differences become very large for the connection to S. Unfortunately, the built-in saturation curve in the BPA star-circuit representation ("saturable transformer component") is always connected to the star point. This model could become more useful if the code were changed so that L_m could be connected to any terminal.

---

[5]This star circuit also had a zero sequence inductance of 1.33 p.u. connected to the high side (see Section 6.6.2.2).
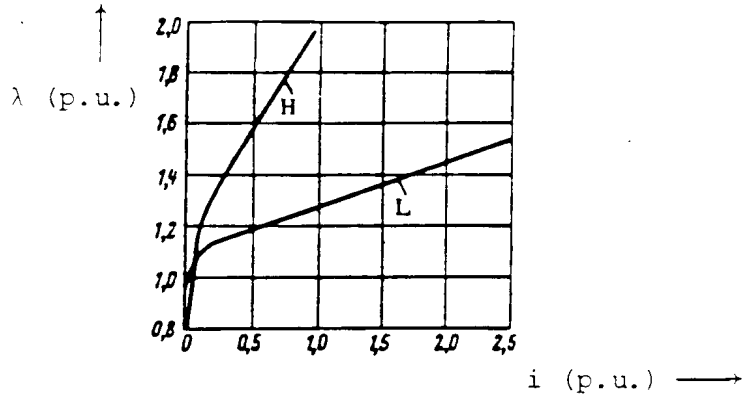
Fig. 6.16 - Nonlinear inductances connected to H (yoke saturation) and L (core saturation) of a two-winding transformer. Reprinted with permission from [113], Copyright 1972, Pergamon Journals Ltd

The proper placement of the nonlinear inductance may or may not be important, depending on the circumstances. For example, if the transformer of Table 6.2 with L_m in S were energized from the high side, then the amplitude of the inrush current would be correct. If it were energized from the tertiary side, however, then the amplitude of the inrush current would be 56% too low for high levels of saturation[6]. If details of the transformer construction are not known, then it is not easy to decide where to place L_m. In the example of Fig. 6.12-6.14, no construction details were known, and L_m was simply placed across the high voltage terminals. In spite of this, simulation results came reasonably close to field test results.

6.6.2.1 Single-Phase Transformers

If the $[L]^{-1}$-model of Section 6.3 or 6.4 is used without the corrections for linear exciting current described in Section 6.6.1, then the nonlinear inductance is simply added across the winding closest to the core. If the [L]-model of Section 6.2 is used, or if $[L]^{-1}$ has already been corrected for the linear exciting current, then a modified nonlinear inductance must be added in which the unsaturated part has been subtracted out (Fig. 6.17). This modified nonlinear inductance has an infinite slope below the knee-point.

Table 6.2 - Comparison between measured and calculated air-core inductances. © 1981 IEEE

		air-core inductance (p.u.)				
excited winding	flux measured at [*)]	test	calculated with L_m in T	error (%)	calculated with L_m in S	error (%)

---

[6]Inrush current approximately proportional to $1/L_{air\text{-}core}$ for flux above knee-point if unsaturated $L_m >> L_{air\text{-}core}$.

H	H	0.198	0.207	+4.5	0.198	0.0
	L	0.124	0.129	+4.0	0.120	-3.2
	T	0.076	0.076	0.0	0.120	+58.0
L	H	0.127	0.129	+1.6	0.120	-5.5
	L	0.131	0.125	-4.8	0.116	-11.0
	T	0.078	0.076	-2.6	0.120	+54.0
T	H	0.076	0.076	0.0	0.120	+58.0
	L	0.076	0.076	0.0	0.120	+58.0
	T	0.076	0.076	0.0	0.173	+128.0

*)Measured by integrating the voltage at that terminal. The measured short-circuit inductances were L_{HL} = 0.0738 p.u., L_{HT} = 0.1305 p.u., L_{LT} = 0.0493 p.u., which produces the star-circuit inductances of L_H = 0.0775 p.u., L_L = -0.0037 p.u., L_T = 0.0530 p.u.

6.6.2.2 Three-Phase Transformers

Usually only the positive sequence saturation curve (or the saturation curve for one core leg) is known. Then it is best to connect the same nonlinear inductance across each one of the three phases (e.g., across the tertiary terminals TA-TB, TB-TC, TC-TA). This implies that the zero sequence values are the same as the positive sequence values, which is probably a reasonable assumption for the five-legged core and shell-type construction.

For the three-legged core design, the zero sequence flux returns outside the windings through an air gap, structural steel and the tank. Fig. 6.18 shows the measured zero sequence magnetization curve for the transformer described in Table 6.2 [114]. Because of the air gap, this curve is not nearly as nonlinear as the core saturation curve of Fig. 6.10. It is therefore reasonable to approximate it as a linear magnetizing inductance. In [114] it is shown that this zero sequence magnetizing inductance should be connected to the high side. With the $[L]^{-1}$-model, this is accomplished by setting B_{pos} = 0 and using B_{zero} = $1/L_{zero}$ in Eq. (6.36), and by adding the 3 x 3 matrix with B_s = B_m = $B_{zero}/3$ to the 3 x 3 diagonal block of the high side[7]. This "buries" the zero sequence magnetizing inductance in $[L]^{-1}$. The positive sequence (core leg) nonlinear inductance (Fig. 6.10 for the example taken from [114]) can then again be added across each one of the phases.

_____

[7]By setting B_{pos} = 0, $[L]^{-1}$ will remain singular. This causes no problems if the inverse inductance is used. Users who prefer [L]-matrices would have to add another 3 x 3 matrix with B_s = $2B_{pos}/3$ and B_m = $-B_{pos}/3$ to one of the sides, with B_{pos} = $1/L_{pos}$, where L_{pos} is the linear (unsaturated) positive sequence magnetizing inductance.
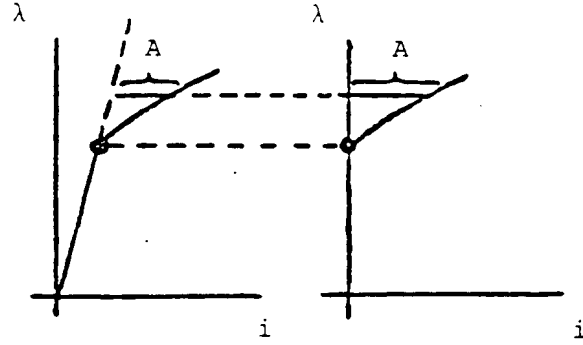
Fig. 6.17 - Subtraction of linear (unsaturated) part in saturation curve (value of A equal in both curves)
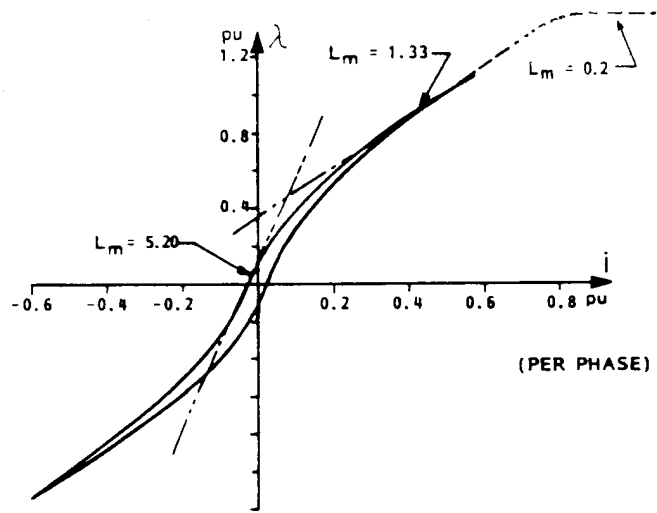
Fig. 6.18 - Zero sequence magnetization curve [114]. © 1981 IEEE

6.6.3 Hysteresis and Eddy Current Losses

The excitation losses obtained from the excitation test are mostly iron-core losses, because the I^2R-losses are comparatively small for the low values of the exciting current. These iron-core losses are sometimes ignored, but they can easily be approximated with the linear shunt conductance of G_m of Eq. (6.33).

A linear shunt conductance G_m cannot represent the iron-core losses completely accurately. These losses consist of two parts,

$$P_{iron-core} = P_{hysteresis} + P_{eddy\ current} \tag{6.41}$$

namely of hysteresis losses $P_{hysteresis}$ and of eddy current losses $P_{eddy\ current}$. In the excitation tests, these two parts cannot be separated, and only the sum $P_{iron-core}$ is obtained. Before discussing more accurate representations, it is useful to have some idea about the ratio between the two parts. Ref. [51], which may be somewhat outdated, gives ratios of

$$P_{hysteresis}/P_{eddy\ current} = 3 \qquad for\ silicon\ steel$$

6-29

$$P_{hysteresis}/P_{eddy\ current} = 2/3 \qquad for\ grain\text{-}oriented\ steel$$

while a more recent reference [125] quotes a typical ratio of 1/3. On modern transformers, hysteresis losses are therefore much less important than they used to be before the introduction of grain-oriented steel.

It is generally agreed that eddy current losses are proportional to λ^2 and to f^2 [51], at least in the low-frequency range, which seems to change to $f^{1.5}$ in the high-frequency range because of skin effect in the laminations. Frequency-dependent eddy current representations were discussed in [115], where R_m is replaced by a number of parallel R-L branches. It is doubtful whether this sophistication is needed, however, because the reduction caused by a proportionality change from f^2 to $f^{1.5}$ at high frequencies is probably offset by other types of loss increases (e.g., by increases in coil resistance due to skin effect, etc.). At any rate, laboratory tests would first have to be done to verify the correctness of the frequency dependence proposed in [115]. In such tests it may be difficult to separate eddy current and hysteresis losses. If we accept a proportionality with λ^2 and f^2, then a constant resistance R_m does model these losses very well, because $P_{eddy\ current} = V_{RMA}^2/R_m$ and $V_{RMS}^2 = \omega^2 \lambda^2_{RMS}$ for sinusoidal excitation.

Hysteresis losses are a nonlinear function of flux and frequency,

$$P_{hysteresis} = k\,(\lambda)^a \cdot (f)^b \tag{6.42}$$

In [51], a is said to be close to 3 for grain-oriented steel, and b = 1. In [116], a = 2.7 and b = 1.5. If a = b = 2 were used, then the sum of hysteresis and eddy current losses could be modelled by the constant resistance R_m or conductance G_m of Eq. (6.33). This is a reasonable first approximation [125], especially if one considers that hysteresis losses are only 25% of the total iron-core losses in transformers with grain-oriented steel. Fig. 6.19(a) shows the nonlinear inductance of a current transformer, which was used by C. Taylor to duplicate field test results in a case where the secondary current was distorted by saturation effects [117]. Fig. 6.19(b) shows λ as a function of the exciting current in the transient simulation, if iron-core losses are modelled with a constant resistance R_m = 80 Ω. It can be seen that R_m not only creates the typical shape of a normal magnetization curve (with lower $d\lambda/di$ coming out of the origin, compared to λ = f(i) in Fig. 6.19(a)), but also creates minor loops with reasonable shapes.
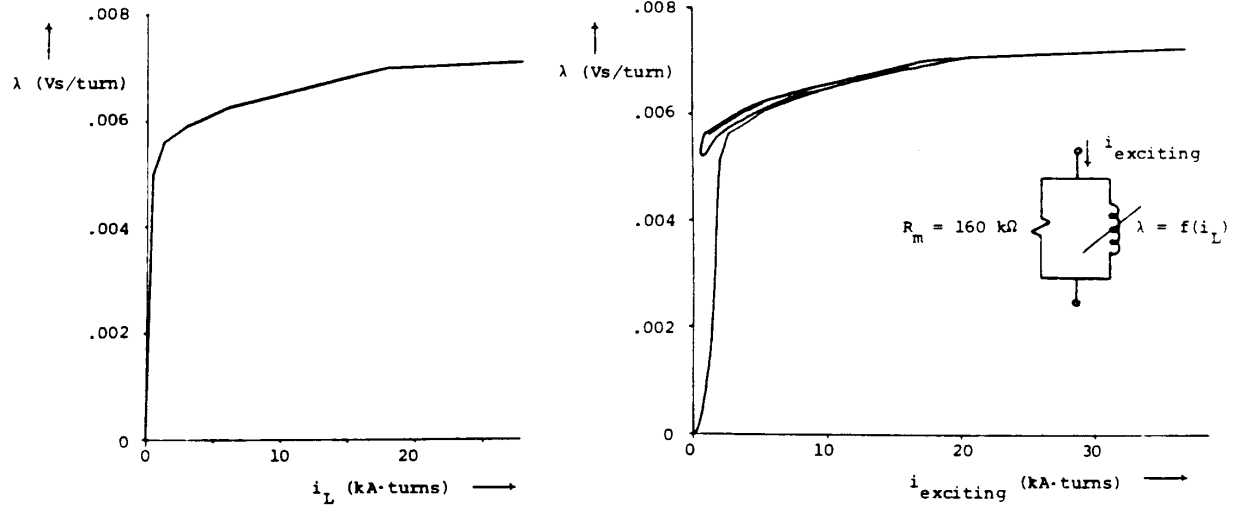
(a)   Nonlinear magnetizing   (b)   Loops created by constant R_m
      of current transformer   for hysteresis and eddy
                                             current losses

Fig. 6.19 - Saturation in current transformer [117]. Reprinted by permission of
C.W. Taylor

If the flux-current loop[8] for sinusoidal excitation is available, then R_m can also be calculated from

$$R_m = \frac{v}{\Delta i} \tag{6.43}$$

as an alternative to Eq. (6.33), with Δi being half of the horizontal width of the loop at $\lambda = 0$ (Fig. 6.20), and $v = \omega\lambda_{max}$. Eq. (6.43) is derived from realizing that at $\lambda = 0$ all the current must flow through the parallel resistance R_m and that the voltage reaches its peak value $\omega\lambda_{max}$ at $\lambda = 0$ because of the 90° phase shift between voltage and flux.

   If more values of Δi are used at various points along the λ-axis, together with the corresponding values for $v = d\lambda/dt$, then a resistance R_m can be constructed which becomes nonlinear. This parallel combination of nonlinear resistance and nonlinear inductance has been proposed by L.O. Chua and K.A. Stromsmoe [118] to model flux-current loops caused by hysteresis and eddy current effects. They give convincing arguments why this representation is reasonable. In particular, they did make comparisons between simulations and laboratory tests, not only for a small audio output transformer with laminated silicon steel, but for a supermalloy core inductor as well. Fig. 6.21 shows the nonlinear inductances and resistances for this audio output transformer [118]. Fig. 6.22 compares the laboratory test results with simulation results [118] (first row laboratory results, second row simulation results). Fig.

---

[8]The author is reluctant to call it "hysteresis loop" because the losses associated with this loop are the sum of hysteresis and eddy current losses, with the latter actually being the larger part in transformers with grain-oriented steel.

6.22(a) is a family of flux-current loops for 60 Hz sinusoidal flux linkage of various amplitudes. Fig. 6.22(b) shows two loops, one with a sinusoidal flux linkage and the second with a sinusoidal current. Fig. 6.22(c) is a family of loops obtained at 60 Hz for various amplitudes of sinusoidal current. Fig. 6.22(d) shows a family of loops for sinusoidal flux linkages at 60, 120, and 180 Hz. In all cases, the agreement between measurements and simulation results is excellent. The minor loops in Fig. 6.22(e) were obtained with a 60 Hz sinusoidal current superimposed on a dc bias current. Again, there appears to be excellent agreement.
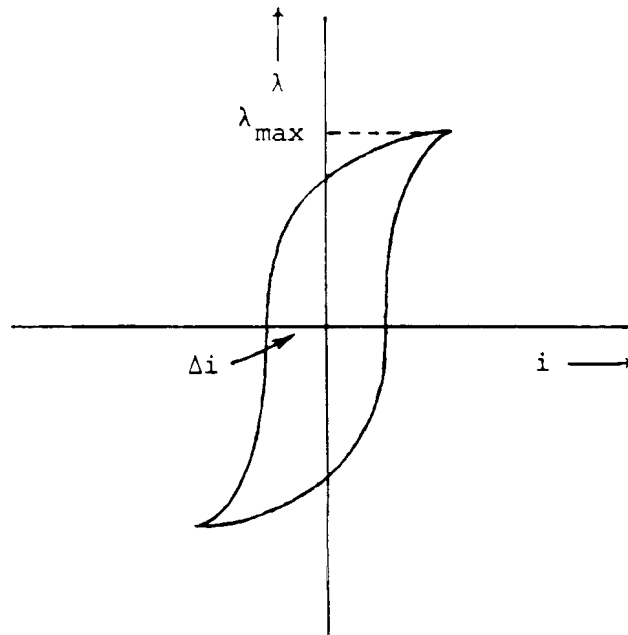
Fig. 6.20 - Flux-current loop

The major drawback of this core-loss representation with a linear or nonlinear resistance is its inability to produce the correct residual flux when the transformer is switched off. This was one of the motivations for the development of more sophisticated hysteresis models, but even these models do not seem to produce the residual flux very accurately. This writer believes that there are no models available at this time which can predict residual fluxes reliably, and that reasonable assumptions should therefore be made. There is no difficulty with the linear or nonlinear R_m-representation in starting a transient simulation with a residual flux if its value is provided as input data, as explained in Section 6.6.4.
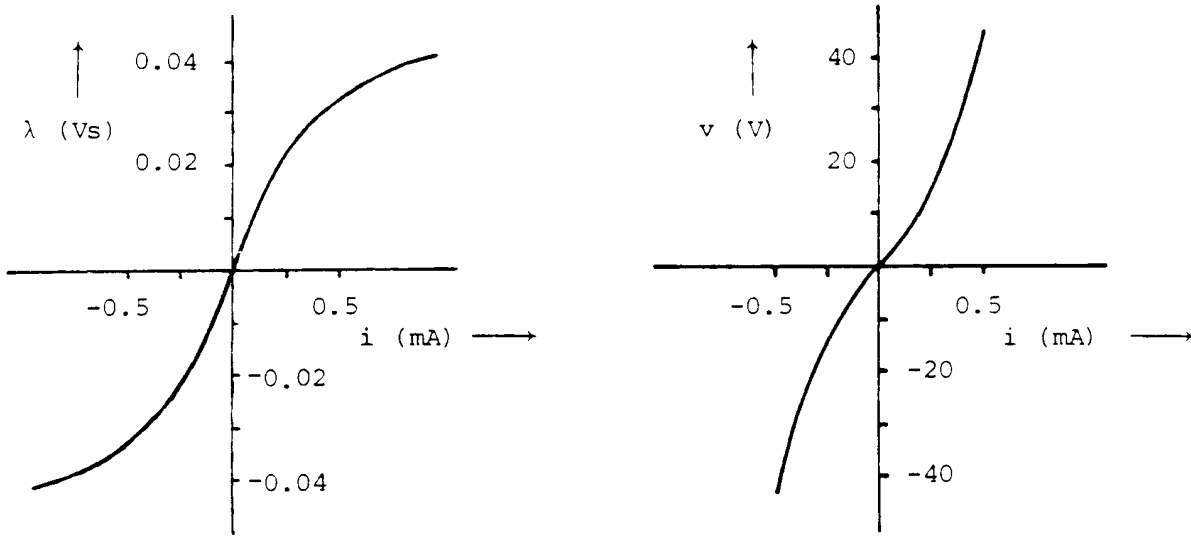
Fig. 6.21 - Model for exciting current with parallel, nonlinear resistances and inductances [118]. © 1970 IEEE

The more sophisticated models mentioned above use pre-defined trajectories or "templates" in the λ, i-plane to decide in which direction the curve will move if the flux either increases or decreases [114, 119]. The technique of [119] has been implemented in the BPA-EMTP ("pseudolinear hysteretic reactor") but a careful comparison with the simpler R_m-representations (either linear or nonlinear) has not yet been done. More research may be needed before reliable hysteresis models become available. Such models may be based on the duality between magnetic and electric circuits, which would then require the dimensions of the iron-core as input data [121], or they may be based on the physics of magnetic materials [120].
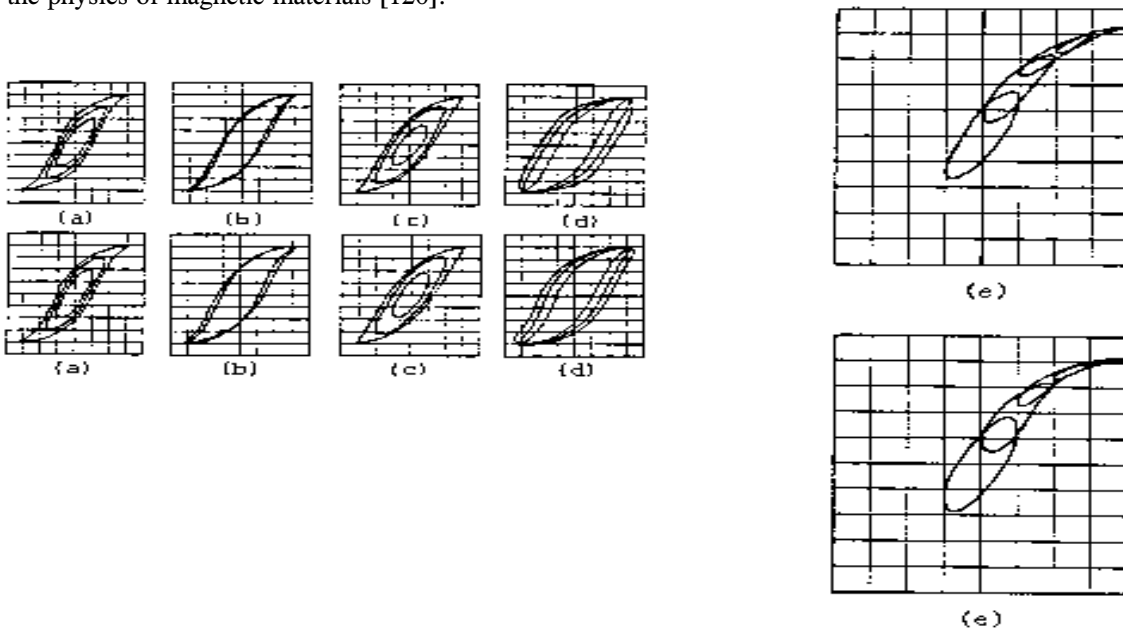
Fig. 6.22 - Comparison between measured and simulated flux-current loops [118]. © 1970 IEEE

6.6.4 Residual Flux

Residual flux is the flux which remains in the iron core after the transformer is switched off[9]. It has a major influence on the magnitude of inrush currents. Starting an EMTP simulation from a known residual flux is relatively easy, with simple as well as with sophisticated hysteresis models. To find the residual flux from a simulation is more complicated, and the results still seem to be unreliable at this time, even with sophisticated hysteresis models. Until this situation improves, it might be best to use a typical value for the residual flux as part of the input data. Unfortunately, not much data is available on residual flux. A recent survey by CIGRE [122] has not added much to it either, except for the quotation of 2 maximum values of 0.75 and 0.90 p.u. This survey does contain a reasonable amount of information about values of air-core inductances and saturation curves, however.

The UBC version of the EMTP starts the simulation from a nonzero residual flux with the following approach, in connection with piecewise linear inductances[10] (see also Section 12.1.3): At t = 0, the starting point A lies at $\lambda_{residual}$ and i = 0, and the simulation moves along a slope of L_1 (unsaturated value), as shown in Fig. 6.23. The slope is changed to L_2 (saturated value) in point B as soon as $\lambda \geq \lambda_{knee}$. At the same time, a value λ_{switch} is calculated which will bring the characteristic back through the origin when the slope is changed back to L_1 as soon as $\lambda \leq \lambda_{switch}$. Thereafter, the normal λ/i-curve will be followed. More details, in particular the problem of overshoot (λ slightly larger than λ_{knee} when going into saturation), are discussed in Section 12.1.3.3. For typical saturation curves, such as the one shown in Fig. 6.10, the linear slope is almost infinite; in that case, the first move into saturation practically lies on the given λ/i-curve, rather than somewhat higher as in Fig. 6.23.

---

[9]There seems to be some confusion in terminology between "residual" and "remanent" flux. It appears that remanent flux is the flux value at i = 0 in the hysteresis curve under the assumption of sinusoidal excitation.

[10]In the BPA version, this branch type has been generalized from 2 to n slopes ("pseudolinear inductor"), but it appears that is no longer accepts residual flux as input data.
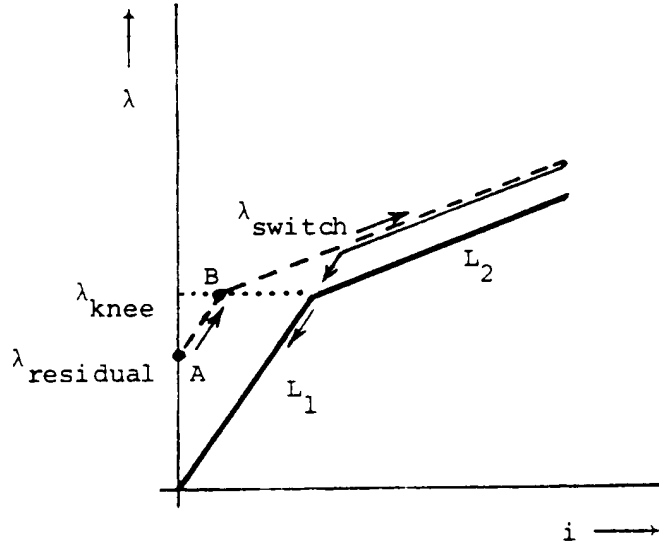
Fig. 6.23 - Starting from residual flux

The simple hysteresis model of a nonlinear L_m in parallel with a resistance R_m cannot be used to predict the residual flux after the transformer is switched off. The energy stored in L_m will simply be dissipated in R_m in this model, with an exponential decay in current and flux to zero values. The flux value at the instant of switching could possibly be close to the residual flux, but this has never been checked. Also, this value would only be meaningful if the transformer is switched off by itself, without lines or other equipment connected to it.

6.7 Autotransformers

If an autotransformer is treated the same way as a regular transformer, that is, if the details of the internal connections are ignored, the models discussed here will probably produce reasonably accurate results, except at very low frequencies. At dc, the voltage ratio between the low and high side of a full-winding transformer will be zero, whereas the voltage ratio of the autotransformer of Fig. 6.24 becomes R_{II}/R_I (dc voltage divider effect).

For a more accurate representation, series winding I and common winding II should be used as building blocks, in place of high side H and low side L. This requires a re-definition of the short-circuit data in terms of windings I and II. Since most autotransformers have a tertiary winding, this winding T shall be included in the re-definition.

First, the voltage ratings are

$$V_I = V_H - V_L$$
$$V_{II} = V_L \tag{6.44}$$
$$V_{III} = V_T$$

The test between H and L provides the required data for the test between I and II directly, since II is shorted

and since the voltage applied to H is actually applied to I (b and c are at the same potential through the short-circuit connection). Only the voltage ratings are different, and the conversion from H to I is simply

$$Z_{I,II} = Z_{HL} \left(\frac{V_H}{V_H - V_L} \right)^2 \qquad \text{in p.u. values} \tag{6.45}$$

No modifications are needed for the test between II and III,

$$Z_{II,III} = Z_{LT} \qquad \text{in p.u. values} \tag{6.46}$$
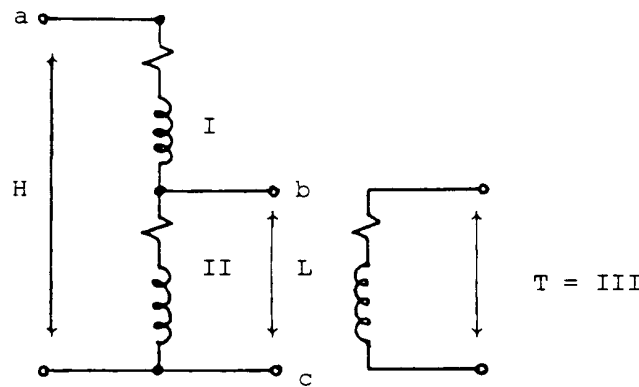
Fig. 6.24 - Autotransformer with tertiary winding

For the test between H and T, the modification can best be explained in terms of the equivalent star-circuit of Fig. 6.7, with the impedances being Z_I, Z_{II}, Z_{III}, based on V_I, V_{II}, V_{III} in this case. With III short-circuited, 1 p.u. current (based on $V_{III} = V_T$) will flow through Z_{III}. This current will also flow through I and II as 1 p.u. based on V_H, or converted to bases V_I, V_{II}, $I_I = (V_H - V_L)/V_H$ and $I_{II} = V_L/V_H$. With these currents, the p.u. voltages become

$$V_I = Z_I \frac{V_H - V_L}{V_H} + Z_{III} \qquad \text{in p.u. values} \tag{6.47}$$

$$V_{II} = Z_{II} \frac{V_L}{V_H} + Z_{III} \qquad \text{in p.u. values} \tag{6.48}$$

Converting V_I and V_{II} to physical units by multiplying Eq. (6.47) with (V_H - V_L) and Eq. (6.48) with V_L, adding them, and converting the sum back to a p.u. value based on V_H produces the measured p.u. value

$$Z_{HT} = Z_I \left(\frac{V_H - V_L}{V_H} \right)^2 + Z_{II} \left(\frac{V_L}{V_H} \right)^2 + Z_{III} \qquad \text{in p.u. values} \tag{6.49}$$

Eqs. (6.45), (6.46) and (6.49) can be solved for Z_I, Z_{II}, Z_{III} since $Z_{I,II} = Z_I + Z_{II}$ and $Z_{II,III} = Z_{II} + Z_{III}$,

$$Z_{I,III} = Z_{HL}\frac{V_H V_L}{(V_H - V_L)^2} + Z_{HT}\frac{V_H}{V_H - V_L} - Z_{LT}\frac{V_L}{V_H - V_L} \quad \text{in p.u. values} \tag{6.50}$$

The autotransformer of Fig. 6.24 can therefore be treated as a transformer with 3 windings I, II, III by simply re-defining the short-circuit impedances with Eqs. (6.45), (6.46) and (6.50). This must be done for the positive sequence tests as well as for the zero sequence tests. If the transformer has a closed delta, then the zero sequence data must be further modified as explained in Section 6.5.2, after the re-definition of the short-circuit data.

6.8 Ideal Transformer

An ideal transformer was not added to the BPA EMTP until 1982. The ideal transformer has no impedances and simply changes voltages and current from side 1 to side 2 (Fig. 6.25) as follows:

$$\frac{v_1}{v_2} = \frac{1}{n} \; ; \qquad \frac{i_1}{i_2} = n \tag{6.51}$$
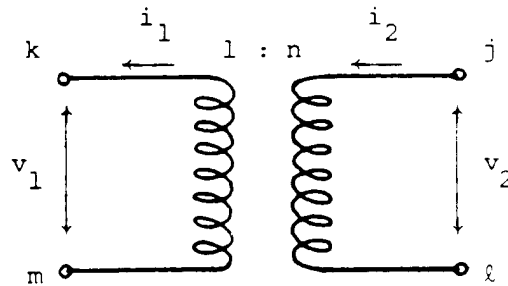
Fig. 6.25 - Ideal transformer

It is handled in the system of nodal equations (1.8a) or (1.20) by treating current i_2 as a variable, and by adding the equation

$$n v_k - n v_m - (v_j - v_\ell) = 0 \tag{6.52}$$

The matrix of the augmented system of equations, with an extra column for variable i_2, and an extra row for Eq. (6.52), then has the form of Fig. 6.26.
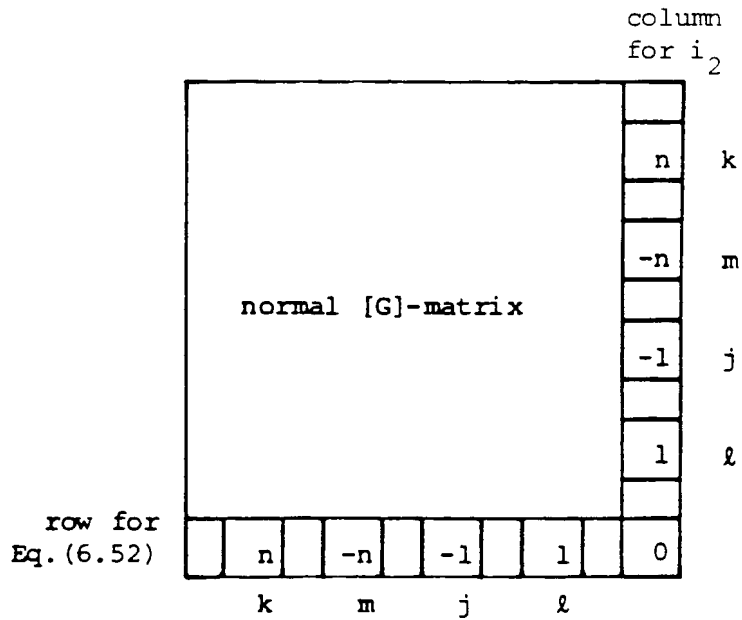
Fig. 6.26 - Augmented [G]-matrix

The ideal transformer can also be simulated with 8 resistance branches and one extra node "extra," as shown in Fig. 6.27, because these branches augment the matrix in the same way as shown in Fig. 6.26. In both approaches it is important that node "extra" (or Eq. (6.52)) is eliminated after nodes k, m, j, ℓ, to assure that the diagonal element becomes nonzero during the elimination process.
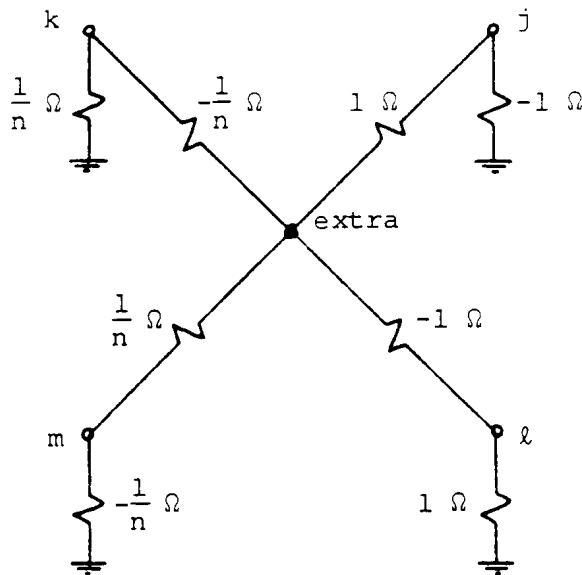
Fig. 6.27 - Resistance modelling of ideal transformer

If the transformer is unloaded ($i_2 = 0$), the elimination process will fail with a zero diagonal element. The UBC version would stop in that case with an appropriate error message, while the BPA version will first print a warning, and then continue after automatic connection of a very large resistance to the node where the zero diagonal

element has been encountered. This problem is related to the treatment of floating subnetworks (see next Section 6.9).

6.9 Floating Delta Connections

Most transmission autotransformers have delta-connected tertiary windings for the suppression of third harmonics. Frequently, nothing is connected to such tertiary windings. In that case, and in similar cases, the delta windings have floating potential with respect to ground (Fig. 6.28): only the voltages across the windings a-b, b-c, c-a are defined, but not the voltages in a, b, or c with respect to ground. Since the EMTP solves for node voltages with respect to ground, the Gauss elimination will fail with a zero diagonal element.
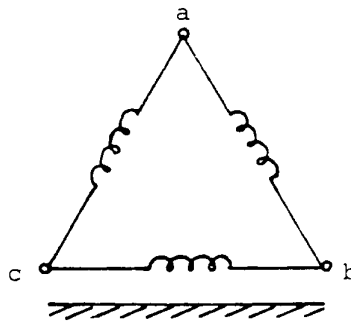
Fig. 6.28 - Floating delta connection

To prevent the solution algorithm from failing, one can either ground one of the nodes (e.g., node a), or connect stray capacitances or large shunt resistances to one or all 3 nodes. Connecting identical branches to each of the 3 nodes has the "cosmetic" advantage that the voltages in a, b, c will be symmetrical, rather than one of them being zero. The BPA version connects a large shunt resistance automatically, with an appropriate warning, whenever a zero or near-zero diagonal element is encountered. For example, if the zero diagonal is encountered at node c, then a large resistance will be connected from c to ground which will make $v_c = 0$.

6.10 Description of Support Routines and Saturable Transformer Component

Except for the "Saturable Transformer Component" in the BPA EMTP, which is an input option specifically for transformers, all other transformer representations discussed here use the general branch input option for π-circuits (with $C = 0$), and possibly additional linear or nonlinear, uncoupled resistance and inductance branches for the representation of the exciting current. There are three support routines XFORMER, TRELEG, and BCTRAN, which convert the transformer data into impedance or admittance matrices, as well as a support routine CONVERT for the conversion of saturation curves $V_{RMS} = f(I_{RMS})$ into $\lambda = f(i)$. These support routines, as well as the built-in saturable transformer component, are briefly described here.

6.10.1 Support Routine XFORMER

This support routine for single-phase transformers is somewhat obsolete, and has been superseded by support routine BCTRAN. For two-winding transformers, it uses essentially the approach of Section 6.3.1 to form an admittance matrix

$$[Y_{pu}] = \begin{bmatrix} \dfrac{1}{Z_{pu}} & -\dfrac{1}{Z_{pu}} \\[2mm] -\dfrac{1}{Z_{pu}} & \dfrac{1}{Z_{pu}} \end{bmatrix}$$

without first separating R and L as in Eq. (6.7). One half of $1 / jX_{m\,pu}$ from Eq. (6.35) is then added to $Y_{11\,pu}$ and $Y_{22\,pu}$, which makes the matrix nonsingular. After its inversion, and conversion from p.u. to actual values, the 2 x 2 branch impedance matrix is obtained. By not separating R and L, this impedance matrix has nonzero off-diagonal resistances, which would produce wrong results at extremely low frequencies when the magnitude of R becomes comparable with the magnitude of ωL (in one particular example, $R \approx \omega L$ at f = 0.002 Hz). At dc, an off-diagonal resistance would imply a nonzero induced voltage in the secondary winding, which should really be zero in a full-winding transformer.

For three-winding transformers, the approach of Section 6.3.2 is used. First, the impedances of the equivalent star circuit are found with Eq. (6.10), which is then converted to the delta circuit with Eq. (6.11) to obtain the 3 x 3 admittance matrix $[Y_{pu}]$ of Eq. (6.12). Again, there is no separation between R and L, and complex impedances Z are used in place of X in all these equations. One third of $1 / jX_{m\,pu}$ from Eq. (6.35) is then added to $Y_{11\,pu}$, $Y_{22\,pu}$ and $Y_{33\,pu}$, followed by matrix inversion and conversion to actual values. Again, nonzero off-diagonal resistances will appear in the branch impedance matrix, as already discussed for the two-winding transformer.

Except for errors at extremely low frequencies, which is caused by not separating R and L, the model produced by XFORMER is useful if the precautions for ill-conditioned matrices discussed in Section 6.2.2 are observed.

6.10.2 Support Routine BCTRAN

This support routine works for any number of windings, and for single-phase as well as for three-phase units. It uses the approach of Section 6.4 and 6.5 to produce the [R] and $[L]^{-1}$-matrices of coupled branches. BCTRAN has an option for inductance matrices [L] as well, in cases where the exciting current is nonzero. Because of the ill-conditioning problem (Section 6.2.2), the author prefers to work with $[L]^{-1}$ instead of [L], however.

Impedance matrices produced by BCTRAN and XFORMER differ mainly in the existence of off-diagonal resistance values in the latter case, which should make the model from BCTRAN more accurate than that from XFORMER at very low frequencies.

6.10.3 Support Routine TRELEG

This support routine was developed by V. Brandwajn at Ontario Hydro, concurrently with the development

of BCTRAN at UBC. It builds the impedance matrix (6.14) of N-winding single-phase or three-phase transformers directly from short-circuit and excitation test data, without going through the reduced impedance matrix described in Section 6.4. The exciting current must always be nonzero, and for very small values of exciting current, the matrices are subject to the ill-conditioning problem described in Section 6.2.2.

Recall that Eq. (6.14) is valid for three-phase transformers as well, if each element is replaced by 3 x 3 submatrix as discussed in Section 6.5. With this in mind, the imaginary parts of the diagonal element pairs (X_{s-ii}, X_{m-ii}) of the excited winding "i" are first calculated from the current of the positive and zero sequence excitation tests. If excitation losses are ignored, then X_{ii} in per unit is simply the reciprocal of the per-unit exciting current. With positive and zero sequence values thus known, the pair of self and mutual reactances is found from Eq. (6.29). For the other windings, it is reasonable to assume that the p.u. reactances are practically the same as for winding "i," since these open-circuit reactances are much larger than the short-circuit impedances. This will produce the imaginary parts of the other diagonal elements[11]. The real part of each diagonal element is the resistance of the particular winding.

With the diagonal element pairs known, the off-diagonal element pairs (Z_{s-ik}, Z_{m-ik}) are calculated from Eq. (6.5), except that real values X are replaced by complex values Z,

$$Z_{ik} = Z_{ki} = \sqrt{(Z_{ii} - Z_{ik}^{short}) Z_{kk}} \qquad (6.53)$$

These impedances are first calculated for positive and zero sequence, and then converted to self and mutual impedances with Eq. (6.29).

As pointed out in Section 6.2.2, the elements of [Z] must be calculated with high accuracy; otherwise, the short-circuit impedances get lost in the open-circuit impedances. The lower the exciting current is, the more equal the p.u. impedances Z_{ii}, Z_{kk} and Z_{ik} become among themselves in Eq. (6.5). Experience has shown that the positive sequence exciting current should not be much smaller than 1% for a single-precision solution on a UNIVAC computer (word length of 36 bits) to avoid numerical problems. On computers with higher precision, the value could obviously be lower. On large, modern transformers, exciting currents of less than 1% are common, but this value can usually be increased for the analysis without influencing the results. Since these ill-conditioning problems do not exist with $[L]^{-1}$, support routine BCTRAN should make TRELEG unnecessary, after careful testing of both routines has been carried out.

6.10.4 Support Routine CONVERT

Often, saturation curves supplied by manufacturers give RMS voltages as a function of RMS currents. The

---

[11]If it is known that the magnetizing impedance should be connected across a particular terminal, then the diagonal elements are modified to account for the differences caused by the short-circuited impedances between the terminals.

support routine CONVERT[12] changes V_{RMS}/I_{RMS}-curves into flux/current-curves $\lambda = f(i)$ with the following simplifying assumptions:

1.   Hysteresis and eddy current losses in the iron-core are ignored,

2.   resistance in the winding is ignored, and

3.   the λ/i-curve is to be generated point by point at such distances that linear interpolation is acceptable in between points.

For the conversion it is necessary to assume that the flux varies sinusoidally at fundamental frequency as a function of time, because it is most likely that the V_{RMS}/I_{RMS}-curve has been measured with a sinusoidal terminal voltage. With assumption (2), $v = d\lambda/dt$. Therefore, the voltage will also be sinusoidal and the conversion of V_{RMS} values to flux values becomes a simple re-scaling:

$$\lambda = \frac{V_{RMS}\sqrt{2}}{\omega} \tag{6.54}$$

The re-scaling of currents is more complicated, except for point i_B at the end of the linear region A-B (Fig. 6.29):

$$i_B = I_{RMS-B}\sqrt{2} \tag{6.55}$$

The following points i_C, i_D,... are found recursively: Assume that i_E is the next value to be found. Assume further that the sinusoidal flux just reaches the value λ_E at its maximum,

$$\lambda = \lambda_E \sin \omega t \tag{6.56}$$
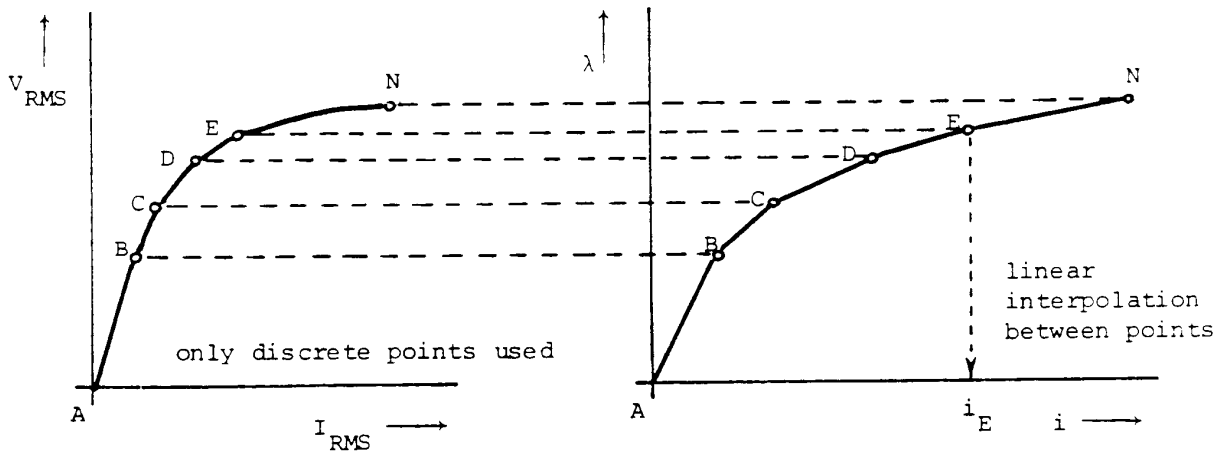
Fig. 6.29 - Recursive conversion of a V_{RMS}/I_{RMS}-curve into a λ/i-curve

Within each segment of the curve already defined by its end points, in this case A-B and B-C and C-D, i is known as a function of λ (namely piecewise linear), and with Eq. (6.56) is then also known as a function of time. Only the

---

[12]CONVERT was developed with the assistance of C.F. Cunha, CEMIG, Belo Horizonte, Brazil.

last segment is undefined inasmuch as i_E is still unknown. Therefore, $i = f(t, i_E)$ in the last segment. If the integral needed for RMS-values,

$$F = \frac{2}{\pi} \int_0^{\frac{\pi}{2}} i^2 \, d(\omega t) \tag{6.57}$$

is evaluated segment by segment, the result will contain i_E as an unknown variable. With the trapezoidal rule of integration (reasonable step size $= 1°$), F has the form

$$F = a + bi_E + ci_E^2 \tag{6.58}$$

with a, b, c known. Since F must be equal to I_{RMS-E}^2 by definition, Eq. (6.58) can be solved for the unknown value i_E. This process is repeated recursively until the last point i_N has been found.

If the λ/i-curve thus generated is used to re-compute a V_{RMS}/I_{RMS}-curve, it will match the original V_{RMS}/I_{RMS}-curve, except for possible round-off errors. As an example, support routine CONVERT would convert the table of per-unit RMS exciting currents as a function of per-unit RMS voltages,

V_{RMS} (p.u.)	I_{RMS} (p.u.)
0	0
0.9	0.0056
1.0	0.0150
1.1	0.0401

with base power $= 50$ MVA and base voltage 635.1 kV, into the following flux/current relationship:

λ (Vs)	i (A)
0	0
2144.22	0.6235
2382.46	2.7238
2620.71	7.2487

This λ/i-curve is then converted back into a V_{RMS}/I_{RMS}-curve as an accuracy check. In this case, the V_{RMS} and I_{RMS} values were identical with the original input data.

Very often, the V_{RMS}/I_{RMS}-curve is only given around the knee-point, and not for high values of saturation. In such cases, it is best to do the conversion first for the given points, and then to extrapolate on the λ/i-curve with the air-core inductance.

6.10.5 Saturable Transformer Component

This built-in model was originally developed for single-phase N-winding transformers. It uses the star-circuit representation of Fig. 6.30. The primary branch with R_1, L_1 is handled as an uncoupled R-L branch between nodes $BUS1_1$, and star point S, whereas each of the other windings 2,…N is treated as a two-winding transformer (first branch from S to $BUS2_1$, second branch from $BUS1_k$ to $BUS2_k$, with $k = 2,…N$). The equations for each of

these two-winding transformers are derived from the cascade connection of an ideal transformer with an R-L-branch (Fig. 6.31). This leads to

$$
\begin{bmatrix} di_{star}/dt \\ di_k/dt \end{bmatrix} = \frac{1}{L_k} \begin{bmatrix} \left(\dfrac{n_k}{n_1}\right)^2 & -\dfrac{n_k}{n_1} \\ -\dfrac{n_k}{n_1} & 1 \end{bmatrix} \begin{bmatrix} v_{star} \\ v_k \end{bmatrix} - \begin{bmatrix} \dfrac{R_k}{L_k} & 0 \\ 0 & \dfrac{R_k}{L_k} \end{bmatrix} \begin{bmatrix} i_{star} \\ i_k \end{bmatrix}
\tag{6.59}
$$
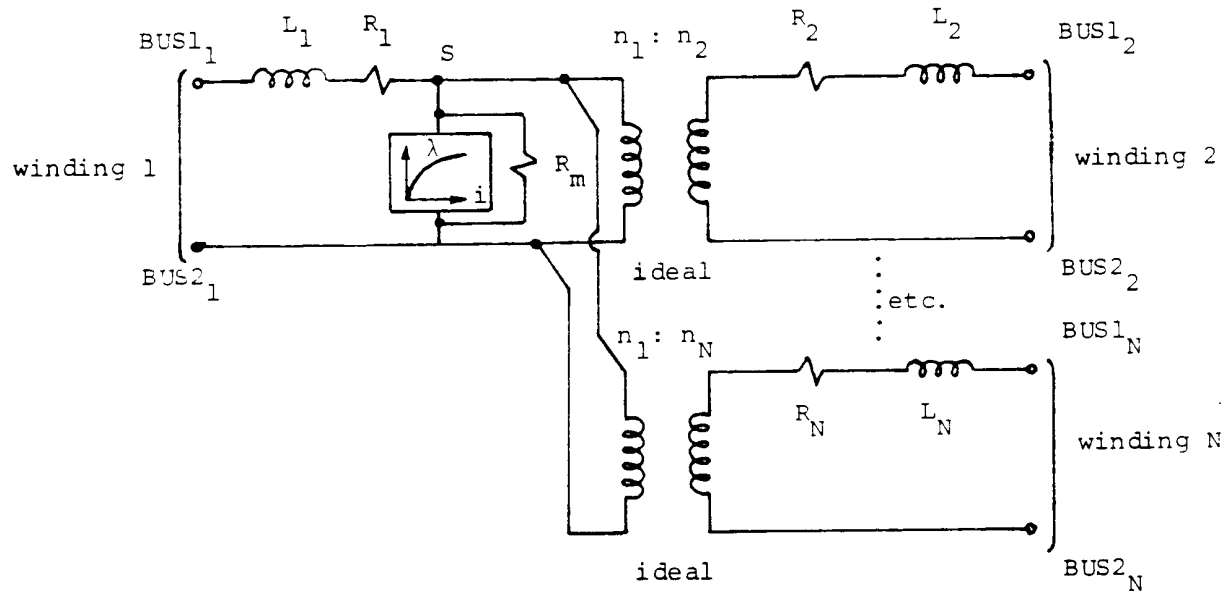
Fig. 6.30 - Star-circuit representation of N-winding transformers

Fig. 6.30 - Star-circuit representation of N-winding transformers
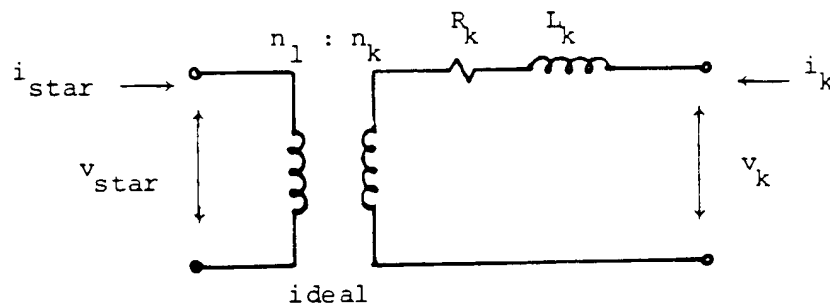
Fig. 6.31 - Cascade connection of ideal transformer and R-L-branch

which is the alternate equation (6.1) with an inverse inductance matrix $[L]^{-1}$. In the particular case of Eq. (6.59), the product $[L]^{-1}[R]$ is symmetric, which is not true in the general case.

The input data consists of the R, L-values of each star branch, and the turns ratios, as well as information for the magnetizing branch. For three-winding transformers, the impedances of the star branches are usually available in utility companies from the data files kept for short-circuit studies. If these values are in p.u., they must

be converted to actual values by using the proper voltage rating V_k for each of the star branches k = 1,...N. If the short-circuit impedances are known, then the star branch impedances can be calculated from Eq. (6.10).

The saturable transformer component has some limitations, which users should be aware of:

1. It cannot be used for more than three windings, because the star circuit is not valid for N > 3. This is more an academic than a practical limitation, because transformers with more than three windings are seldom encountered.

2. The linear or nonlinear magnetizing inductance, with R_m in parallel, is connected to the star point, which is not always the best connecting point, as explained in Section 6.6.

3. Numerical instability has occasionally been observed for the three-winding case. It is not believed to be a programming error. The source of the instability has never been clearly identified, though it is felt that it is caused by the accumulation of round-off errors. V. Brandwajn ran a case in 1985 in which the instability disappeared when the ordering of the windings was changed (e.g., first winding changed to low side from high side).

4. While the saturable transformer component has been extended from single-phase to three-phase units through the addition of a zero-sequence reluctance parameter, its usefulness for three-phase units is limited. Three-phase units are better modelled with inductance or inverse inductance matrices obtained from support routines BCTRAN or TRELEG.

6.11 Frequency-Dependent Transformer Models

At this time, no frequency-dependent effects have yet been included in the transformer model. There are basically three such effects:

a. Frequency-dependent damping in the short-circuit impedances,

b. frequency dependence in the exciting current, and

c. influence of stray capacitances at frequencies above 1 to 10 kHz.

CIGRE Working Groups [8, 18] have collected some information on the frequency-dependent L/R-ratios of short-circuit impedances (Fig. 2.17). As explained in Section 2.2.3, this frequency dependence can easily be modelled with parallel resistances, which matches the experimental curves reasonably well (Fig. 2.19). When dealing with matrices [L] or $[L]^{-1}$, resistance or conductance matrices $[R_p]$ or $[G_p]$ could be added automatically by the program, with the user simply specifying the factor k in

$$[R_p] = k\,[L]\,, \quad or \quad [G_p] = \frac{1}{k}\,[L]^{-1} \tag{6.60}$$

Frequency-dependent effects in the exciting current were modelled with parallel R-L branches in [115], as discussed in Section 6.3.3. Whether the linear frequency dependence in these parallel R-L branches can be separated easily from the nonlinear saturation effects would have to be verified in laboratory experiments.

For transient studies which involve frequencies above a few kHz, capacitances must be added to the R-L-models. As suggested in [123], capacitances should be included

a.   between the winding closest to the core, and the core,

b.   between any two windings, and

c.   across each winding from one end to the other.

    In reality, inductances and capacitances are distributed, but reasonably accurate results, as seen from terminals, can be obtained by lumping one half of the capacitance at each end of winding for effects (a) and (b), and by lumping the total capacitance in parallel with the winding for effect (c), as shown in Fig. 6.32. Each of these capacitances can be calculated from the geometry of the transformer design. Obviously, the internal voltage distribution across a winding, which is of such great concern to the transformer design, cannot be obtained with the simple model of Fig. 6.32. Fig. 6.33 compares measured impedances of a transformer (500 MVA, 765/345/17.25 kV) and calculated impedances with a model where the capacitances were added according to Fig. 6.32. The agreement is quite good. Similar suggestions for the addition of capacitances have been made by others (e.g., [124]).
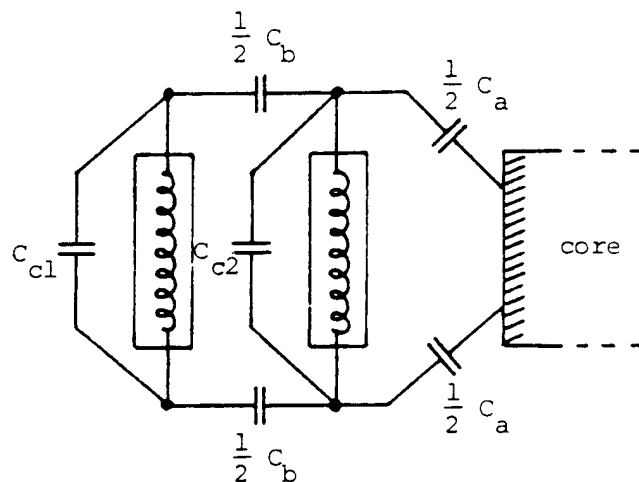
Fig. 6.32 - Addition of capacitances to R-L-model (subscripts a, b, c refer to the three effects mentioned in text)
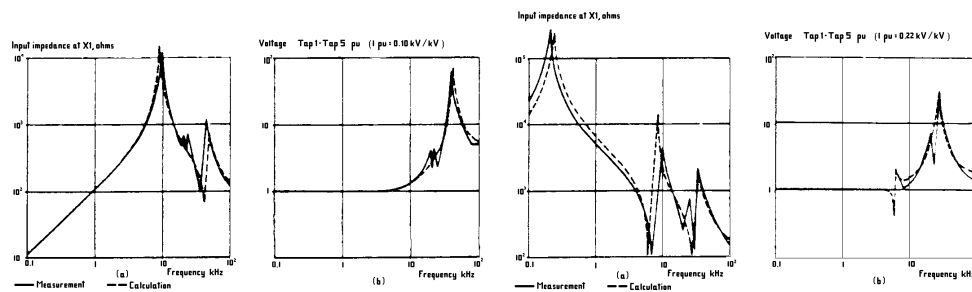
(a)   X1 excited, H1, Y1, Y2   (b)   X1 excited, H1, Y1, Y2
        grounded   open-circuited

Fig. 6.33 - Frequency response of single-phase autotransformer with tertiary winding (marking of terminals according to North American standards: H1 = high voltage terminal, X1 = low voltage terminal, Y1, Y2 = terminals at both ends of tertiary winding) [123]. © 1981 IEEE

7. SIMPLE VOLTAGE AND CURRENT SOURCES

Most of the simple sources are either voltage or current sources defined as a time-dependent function f(t),

$$v(t) = f(t), \quad or \quad i(t) = f(t) \tag{7.1}$$

Frequently used functions f(t) are built into the EMTP. There is also a current-controlled dc voltage source for simplified HVDC simulations, which is more complicated than Eq. (7.1). In addition to the built-in functions, the BPA version of the EMTP allows the user to define functions through user-supplied FORTRAN subroutines, and to declare TACS output variables as voltage or current source functions. The UBC version of the EMTP does not have these two options, but allows the user to read f(t) step by step in increments at Δt. This option has rarely been used, however.

Note that f(t) = 0 for a current source implies that the source is disconnected from the network (i = 0), whereas for a voltage source it implies that the source is short-circuited (v = 0).

7.1 Connection of Sources to Nodes

If a voltage or current source is specified at a node, it is assumed to be connected between that node and local ground, as shown in Fig. 7.1. A voltage source of v(t) = +1.0 V means that the potential at that node is +1.0 V with respect to local ground, whereas a current source of +1.0 A implies that 1.0 A flows from the local ground into that node.
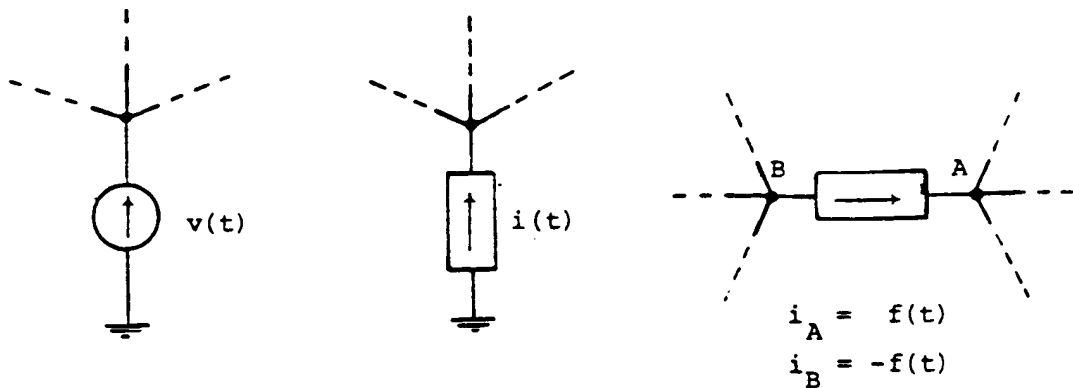
(a) Voltage source between node and local ground

(b) Current source from local ground into node

(c) Current source between two nodes

Fig. 7.1 - Source connections

7.2 Current Sources Between Two Nodes

Current sources between two nodes, e.g., a current leaving node B and entering into node A as shown in Fig. 7.1(c), must be specified as two current sources, namely as

$$i_A(t) = f(t) , \qquad and \quad i_B(t) = -f(t) \tag{7.2}$$

7.3 Voltage Sources Between Two Nodes

Until recently, voltage sources could not be connected between two nodes. With the addition of ideal transformers to the BPA EMTP in 1982 (Section 6.8), voltage sources between two nodes are easy to set up now. In Fig. 6.25, simply ground node $\mathcal{L}$, connect the voltage source from node j to ground, and use a transformer ratio of 1:1. This will introduce a voltage source between nodes k and m. A special input option has been provided for using the ideal transformer for this particular purpose.

The UBC EMTP and older versions of the BPA EMTP do not accept voltage sources between nodes. One could use the equivalent circuit of Fig. 6.27 for the ideal transformer, however, which turns into the circuit of Fig. 7.2. This representation works in the transient solution part of the UBC EMTP, provided the branches of Fig. 7.2 are read in last. In that case, the node "extra" will be forced to the bottom of the equations as shown in Fig. 6.26. The steady-state subroutine in both versions, as well as the transient solution in the BPA version, use optimal re-ordering of nodes, which may not force the row for node "extra" far enough down to assure nonzero diagonal elements during the Gauss elimination. Using Fig. 7.2 may therefore not always work, unless minor modifications are made to the re-ordering subroutine.
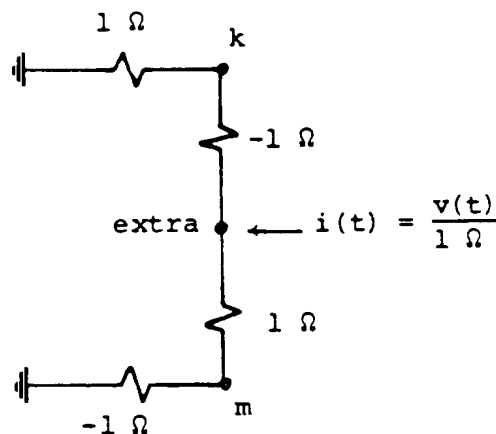
Fig. 7.2 - Equivalent circuit for voltage source v(t) between nodes k and m

In all versions, a voltage source in series with a (nonzero) impedance can always be converted into a current source in parallel with that impedance. The current source between the two nodes is then handled as shown in Eq.

(7.2). The conversion from a Thevenin equivalent circuit (v in series with Z) to a Norton equivalent circuit (i in parallel with Z) is especially simple if the impedance is a pure resistance R, as shown in Fig. 7.3.
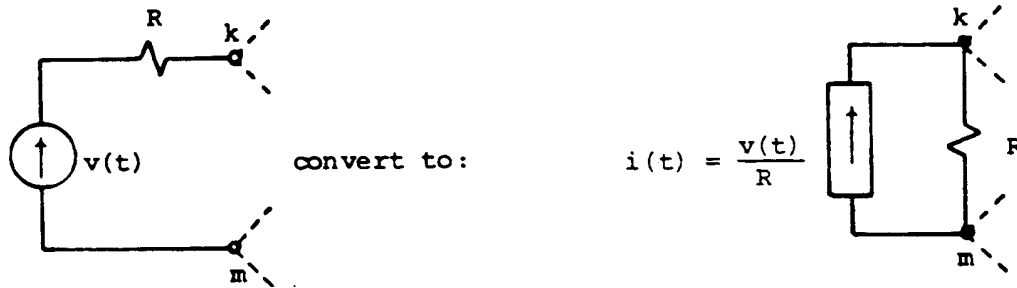
Fig. 7.3 - Conversion of v(t) in series with R into i(t) = v(t)/R in parallel with R

Converting a voltage source in series with an inductance L into a current source with parallel L is slightly more complicated. L is again connected between nodes k and m, in the same way as R in Fig. 7.3. The definition of the current source depends on the initial conditions, however. For example, if

$$v(t) = V_{max} \cos(\omega t + \phi) \tag{7.3}$$

and if the case starts from zero initial conditions, then

$$i(t) = \frac{V_{max}}{\omega L} [\sin(\omega t + \phi) - \sin\phi] \tag{7.4a}$$

If the case starts from linear ac steady-state conditions, with that voltage source being included in the steady-state solution, then

$$i(t) = \frac{V_{max}}{\omega L} \cos(\omega t + \phi - 90°) \tag{7.4b}$$

7.4 More Than One Source on Same Node

If more than one voltage source is connected to the same node, then the EMTP simply adds their functions $f_1(t),...f_n(t)$ to form one voltage source. This implies a series connection of the voltage sources between the node and local ground, as shown in Fig. 7.4(a).

(a)   Series connection of   (b)   Parallel connection of
      sources   current sources
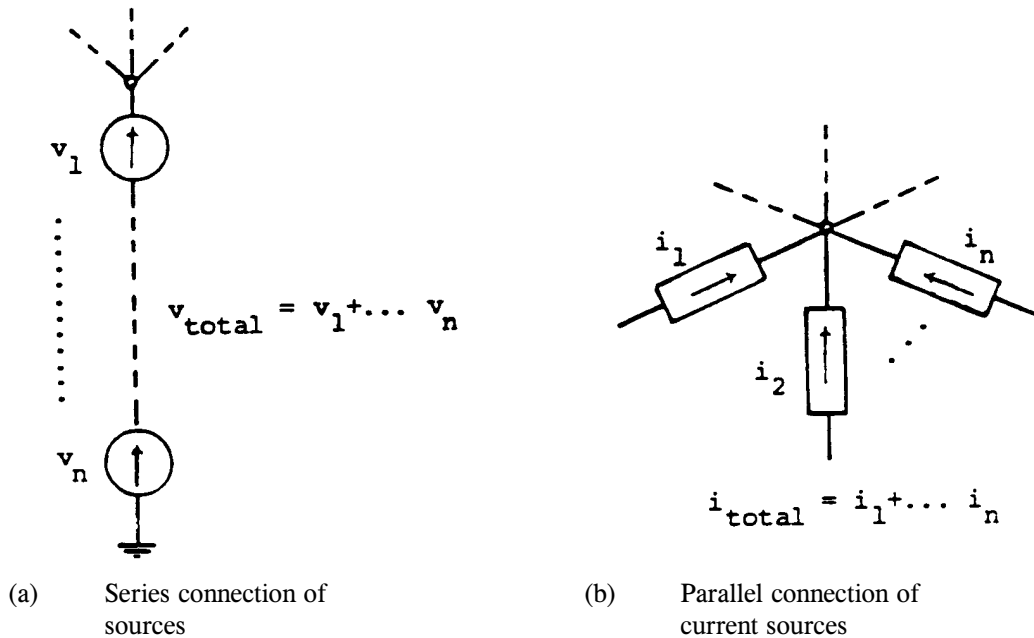
Fig. 7.4 - Multiple voltage or current sources on same node

If more than one current source is connected to the same node, then the EMTP again adds their functions $f_1(t),\ldots f_n(t)$ to form one current source. This implies a parallel connection of the current sources, as shown in Fig. 7.4(b).

Source functions can be set to zero by using parameters t_{START} and T_{STOP}. The EMTP sets $f(t) = 0$ for $t <$ T_{START} and for $t \geq T_{STOP}$. By using more than one source function at the same node with these parameters, more complicated functions can be built up from the simple functions, as explained in the UBC User's Manual and in the BPA Rule Book.

If voltage and current sources are specified at the same node, then only the voltage sources are used by the EMTP, and the current sources are ignored. Current sources would have no influence on the network in such a case, because they would be directly short-circuited through the voltage sources.

7.5 Built-in Simple Source Functions

Commonly encountered source functions are built into the EMTP. They are:

(a) <u>Step function</u> (type 11). In cases which start from zero initial conditions, the step function is approximate in the sense that the EMTP will see a finite rise time from $f(0) = 0$ to $f(\Delta t)$ $= F_{max}$, as shown in Fig. 7.5.
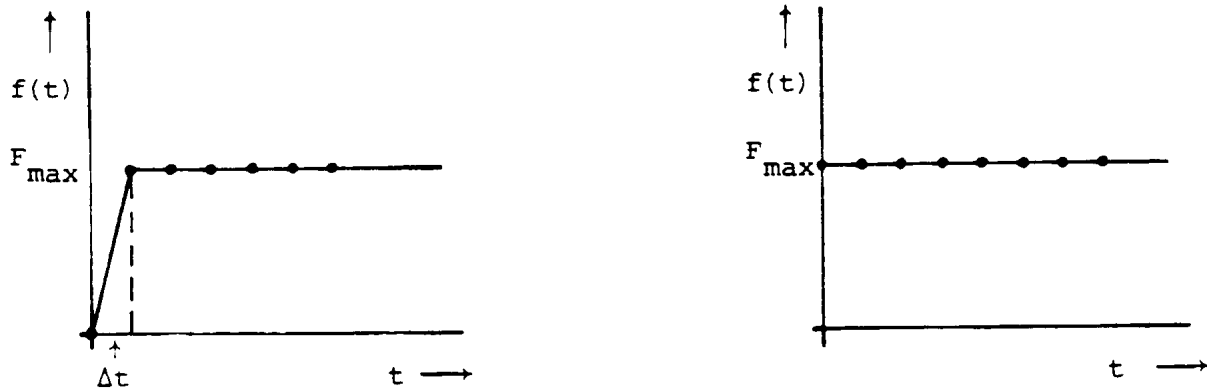
(a) Starting from zero
    initial conditions

(b) Starting from initial
    value F_{max}

Fig. 7.5 - Step function

(b) <u>Ramp function</u> (type 12) with f(t) as shown in Fig. 7.6. The value of the function rises linearly from T_{START} to $T_{START} + T_0$ to a value of F_{max}, and then remains constant until it is zeroed at $t \geq T_{STOP}$.
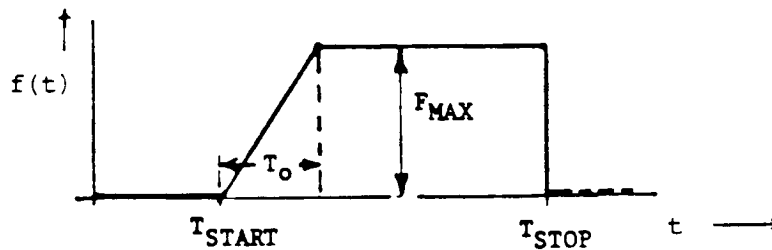
Fig. 7.6 - Ramp function

A modified ramp function (type 13) has the same rise to F_{max} at $T_{START} + T_0$ as in Fig. 7.6, but decays or rises with a linear slope thereafter. By setting $T_{START} = 0$ and $T_0 = 0$, this becomes a step function with a superimposed linear decay or rise.

(c) <u>Sinusoidal function</u> (type 14) with

$$f(t) = F_{max} \cos(\omega t + \phi) \qquad if \ \ T_{START} \leq 0 \tag{7.5a}$$

or

$$f(t) = F_{max} \cos(\omega(t - T_{START}) + \phi) \qquad if \ \ T_{START} > 0 \tag{7.5b}$$

$$with \qquad f(t) = 0 \qquad for \ t < T_{START}$$

This is probably one of the most used source functions. Note that the peak value F_{max} must be specified, rather than the RMS value. To start a case from linear ac steady-state conditions, or to obtain a sequence of steady-

state solutions at a number of frequencies, use $T_{START} < 0$ to indicate to the EMTP that this sinusoidal source should be used for the steady-state solution. The value of T_{START} is immaterial as long as its value is negative, and the complex peak phasor used for that source is then

$$V \text{ or } I = F_{max} \, e^{j\phi} \qquad\qquad (7.6)$$

(d) <u>Impulse function</u> (type 15) of the form

$$f(t) = k \left(e^{-\alpha_1 t} - e^{-\alpha_2 t} \right) \qquad\qquad (7.7)$$

This function has been provided for the representation of lightning or switching impulses, as used in standard impulse tests on transformers and other equipment. A typical lightning impulse voltage is shown in Fig. 7.7 [126], and a typical switching impulse voltage is shown in Fig. 7.8 [126]. There is no simple relationship between the time constants $1/\alpha_1$ and a/α_2 in Eq. (7.7) and the virtual front time T_1 (or time to crest T_{cr}) and the virtual time to half-value T_2. Table 7.1 shows the values for frequently used waveshapes, as well as values for k which produce a maximum value of $f_{max} = 1.0$ in Eq. (7.7). The time at which the maximum occurs is found by setting the derivative $df/dt = 0$ from Eq. (7.7) and solving for t_{max}. Inserting t_{max} into Eq. (7.7) then produces f_{max}. Note that $1/\alpha_1$ and $1/\alpha_2$ in Table 7.1 are in μs, whereas the EMTP input is usually in s.
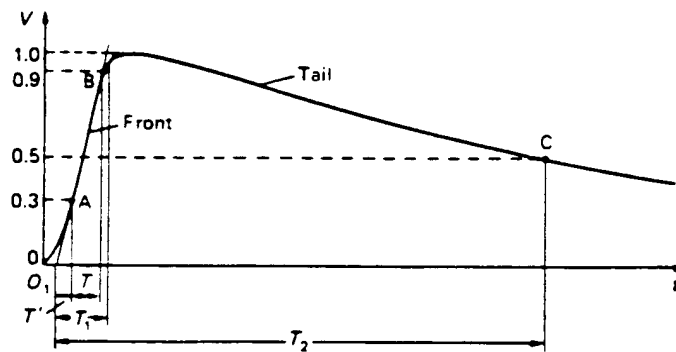
Fig. 7.7 - General shape of lightning impulse voltage (IEC definitions: T_1 = virtual front time, typically 1.2 μs $\pm$ 30%; T_2 = virtual time to half-value, typically 50 μs $\pm$ 20%). Reprinted with permission from [126], © 1984, Pergamon Books Ltd

7-6

In impulse testing, the capacitance of the test object is usually much smaller than the capacitance of the impulse generator. It is then permissible to regard the impulse generator as a voltage source with the function of Eq. (7.7). In cases where the impulse generator is discharged into lines, or into other test objects with impedances which can influence the wave

Table 7.1 - Relationship between T_1, T_2, and α_1, α_2. Reprinted with permission from [126], $^{©}$ 1984, Pergamon Books Ltd

T_1/T_2 (μs)	T_{cr}/T_2 (μs)	$\dfrac{1}{\alpha_1}$ (μs)	$\dfrac{1}{\alpha_2}$ (μs)	k to produce f_{max} = 1.0
1.2/5	-	3.48	0.80	2.014
1.2/50	-	68.2	0.405	1.037
1.2/200	-	284	0.381	1.010
250/2500	-	2877	104	1.175
-	250/2500	3155	62.5	1.104

shape, it may be better to simulate the impulse generator as a capacitance and resistance network, as shown in Fig. 7.9 for a simple single-stage impulse generator. The initial voltage across C_1 would be nonzero, and the switch closing would simulate the gap firing. Fig. 7.10 compares measurements against EMTP simulation results for the waveshape of a multistage impulse generator, where the generator was modelled as a network of capacitances, resistances in inductances [127]. The spark gaps were represented as time-dependent resistances based on Toepler's formula.

(a) Circuit type a   (b) Circuit type b

Fig. 7.9 - Single-stage impulse generators
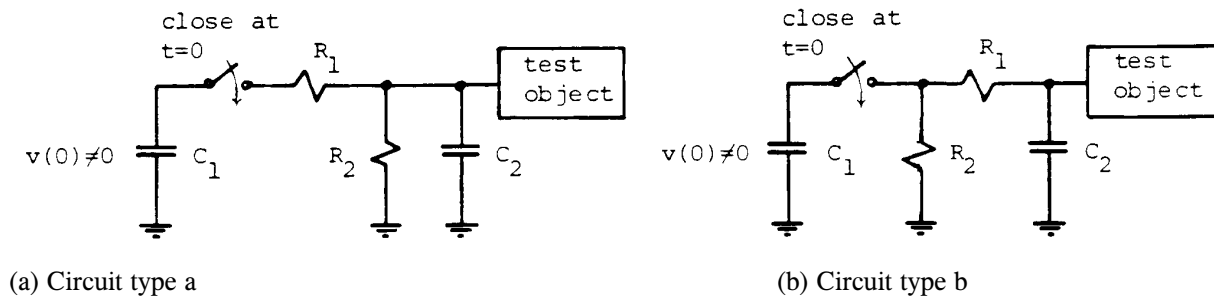
(a)   Measurement   (b)   Simulation results (1 = exact with nonsimultaneous firing of spark gaps, 2 = simultaneous firing, 3 = simultaneous firing with gaps as ideal switches)
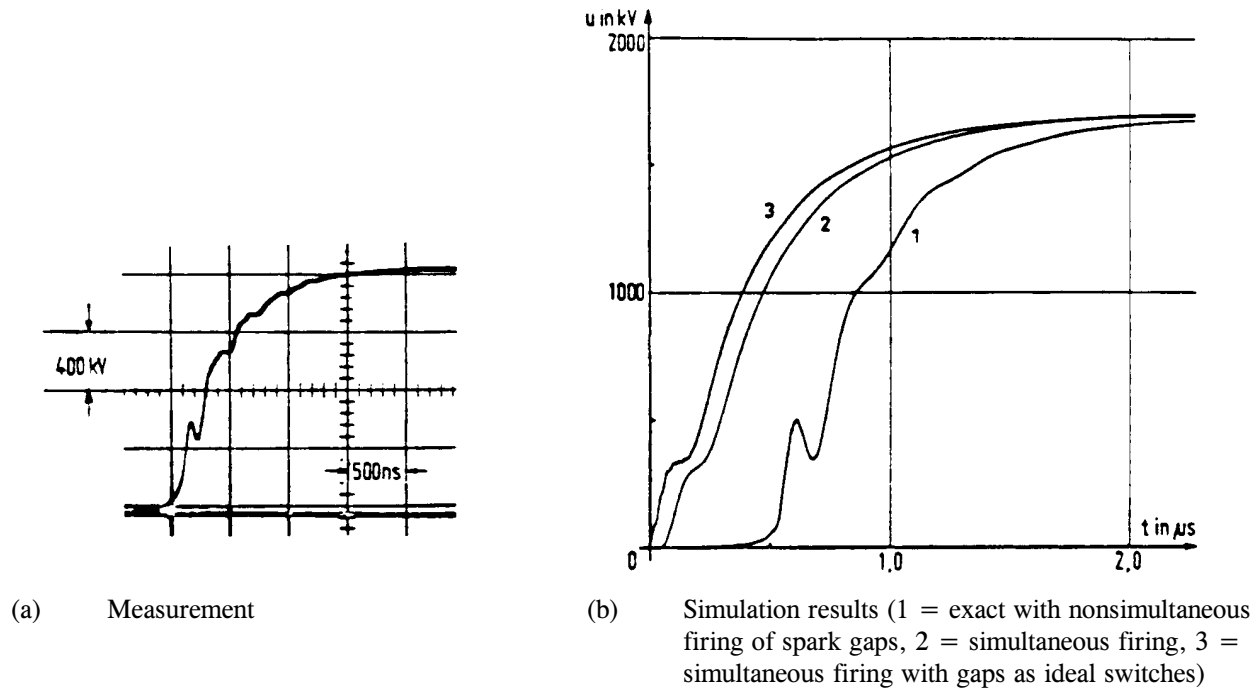
Fig. 7.10 - Waveshape of a multistage impulse generator [127]. © 1971 IEEE

7.6 Current-Controlled dc Voltage Source

This source provides a simplified model of an HVDC converter station [128], and produces simulation results which come reasonably close to field tests [129]. The current-dependent voltage source is connected between two nodes (cathode and anode), as indicated in Fig. 7.11. The current can only flow in one direction (from anode to cathode). This is simulated internally with a switch on the anode side, which opens to prevent the current from going negative and closes again at the proper voltage polarity. Spurious voltage oscillations may occur between the anode and cathode side after the switch opens, unless the damping circuits across the valves are also modelled. Good results were obtained in [128] when an RC branch was added between the anode and cathode (R = 900 Ω and C = 0.15 μs in that case).

The current regulator is assumed to be an amplifier with two inputs (one proportional to current bias I_{BIAS}, and the other proportional to measured current i), and with one output e_α which determines the firing angle. The transfer function of the regulator is

$$G(s) = \frac{K(1 + sT_2)}{(1 + sT_1)(1 + sT_3)} \tag{7.8}$$

with limits placed on the output e_α in accordance with rectifier minimum firing angle, or inverter minimum extinction angle.

The current-controlled dc voltage source is a function of e_α,

$$v_{dc} = k_1 + k_2 e_\alpha \qquad (7.9)$$

as shown in Fig. 7.12. The current regulator output e_α, minus a bias value (10V in Fig. 7.12) is proportional to $\cos\alpha$. The inverter normally operates at minimum extinction angle at the limit $e_{\alpha min}$, and the rectifier normally operates on constant current control between the limits. The user defines steady-state limits for v_{dc}, which are converted to limits on e_α with Eq. (7.9). If the converter operates at the maximum limit $e_{\alpha max}$ (or at the minimum limit $e_{\alpha min}$), either in initial steady state or later during the transient simulation, it will be back off the limit as soon as the derivative de_α/dt becomes negative (or positive) in the differential equation

$$(T_1 + T_3) \frac{de_\alpha}{dt} = K(I_{BIAS} - i) - kT_2 \frac{di}{dt} - T_1 T_3 \frac{d^2 e_\alpha}{dt^2} - e_\alpha \qquad (7.10)$$

The value for $d^2 e_\alpha/dt^2$ is zero in Eq. (7.10) as long as the converter operates at the limit.
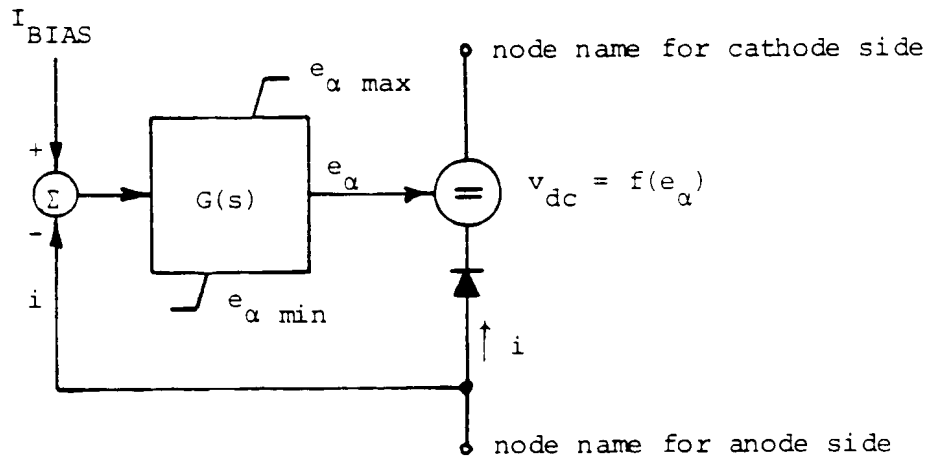
Fig. 7.11 - Current-controlled dc voltage source
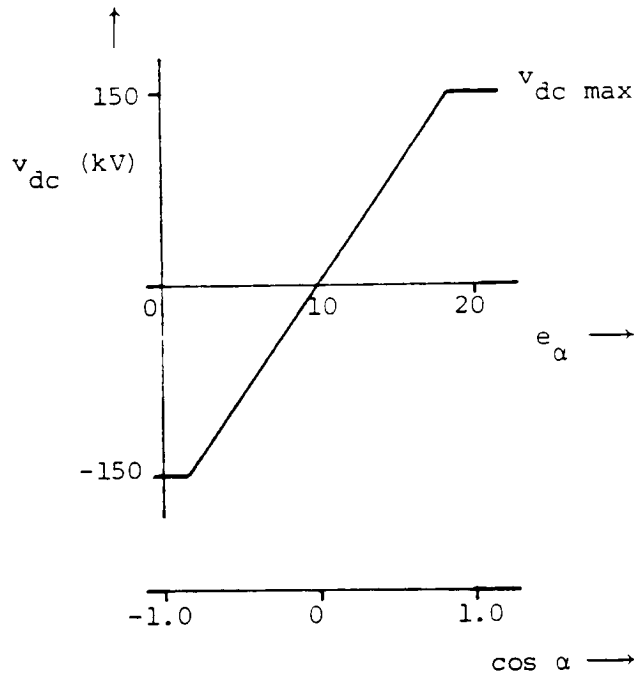
Fig. 7.12 - Relationship between v_{dc} and e_α ($k_1 = -150\,000$, $k_2 = 15\,000$)

7.6.1 Steady-State Solution

Steady-state dc initial conditions are automatically computed by the program with the specified value $v_{dc}(0)$. Since the steady-state subroutine was only written for ac phasor solutions, the dc voltage is actually represented as $v_{dc} = v_{dc}(t) \cos(\omega t)$ with a very low frequency of $f = 0.001$ Hz. Practice has shown that this is sufficiently close to dc, and still makes reactances ωL and susceptances ωC large enough to avoid numerical problems in the ac steady-state solution. When the current-controlled dc voltage source was added to the EMTP, voltage sources between two nodes were not yet permitted. For the steady-state solution, a resistance R_{equiv} is therefore connected in series with the voltage source, which is then converted into a current source in parallel with R_{equiv}. This produces accurate results if the user already knows what the initial current $i_{dc}(0)$ is, because the specified voltage source of the rectifier is automatically increased by $R_{equiv} i_{dc}(0)$, and that of the inverter is decreased by $R_{equiv} i_{dc}(0)$. The program user should check, however, whether the computed current i_{dc} does indeed agree with what the user thought it would be. This nuisance of having to specify $i_{dc}(0)$, without knowing whether it will agree with the computed value, could be removed by using the methods described in Section 6.3, if this HVDC model is used often enough to warrant the program changes. The value of R_{equiv} is the same as the one used in the transient solution (Section 7.5.2).

The normal steady-state operation of an HVDC transmission link, measured somewhere at a common point (e.g., in the middle of the line) is indicated in Fig. 7.13. For the converter operating between the limits on constant current control (which is normally the rectifier), I_{BIAS} is automatically computed to produce the characteristic A-A' of Fig. 7.13,

7-10

$$I_{BIAS} = i(0) + \frac{e_\alpha(0)}{K} , \qquad if \quad e_{\alpha min} < e_\alpha < e_{\alpha max} \tag{7.11}$$

with $i(0)$, $e_\alpha(0)$ being the dc initial conditions. For the converter operating at maximum or minimum voltage (which is normally the inverter), the current setting $I_{SETTING}$ must be given as part of the input, which defines the point where the converter backs off the limit and goes into constant current control. I_{BIAS} is again automatically computed, which in this case is

$$I_{BIAS} = I_{SETTING} + \frac{e_\alpha(0)}{K} \qquad if \quad e_\alpha(0) = e_{\alpha max} \quad or \quad e_{\alpha min} \tag{7.12}$$

$I_{SETTING}$ is typically 15% lower than the current order I_{ORDER} at the steady-state operating point for inverters (or 15% higher for rectifiers).

7.6.2 Transient Solution

In the transient solution, the dynamics of the current controller in the form of Eq. (7.9) and (7.10) must obviously be taken into account. First, rewrite the second-order differential equation (7.10) as two first-order differential equations,

$$e_\alpha + Tx + P\frac{dx}{dt} = K(I_{BIAS} - i) - KT_2\frac{di}{dt} \tag{7.13a}$$

$$x = \frac{de_\alpha}{dt} \tag{7.13b}$$

with the new variable x and with the new parameters

$$T = T_1 + T_3 \tag{7.13c}$$

$$P = T_1 T_3 \tag{7.13d}$$

After applying the trapezoidal rule of integration to Eq. (7.13a) and (7.13b) (replacing x by $[x(t - \Delta t) + x(t)]/2$ and dx/dt by $[x(t) - v(t - \Delta t)]/\Delta t$, etc.), and after eliminating $x(t)$, one linear algebraic equation between $e_\alpha(t)$ and $i(t)$ is obtained. Inserting this into Eq. (7.9) produces an equation of the form

$$v_{dc}(t) = v_0(t) - R_{equiv} i(t) \tag{7.14}$$

which is a simple voltage source $v_0(t)$ in series with an internal resistance R_{equiv}. This Thevenin equivalent circuit is converted into a current source $i_0(t)$ in parallel with R_{equiv} (Fig. 7.14).
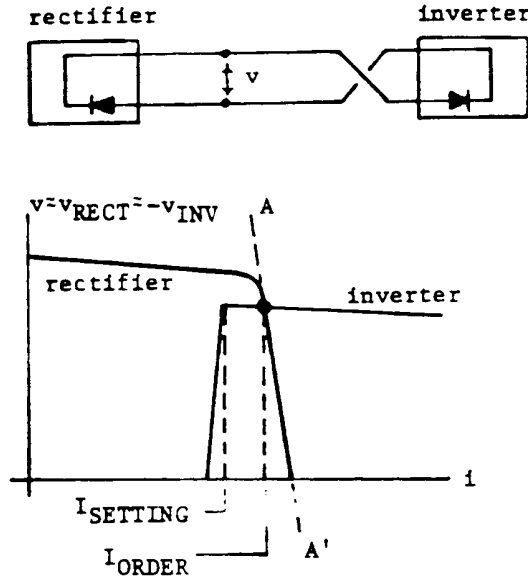
Fig. 7.13 - Normal operation of HVDC transmission link
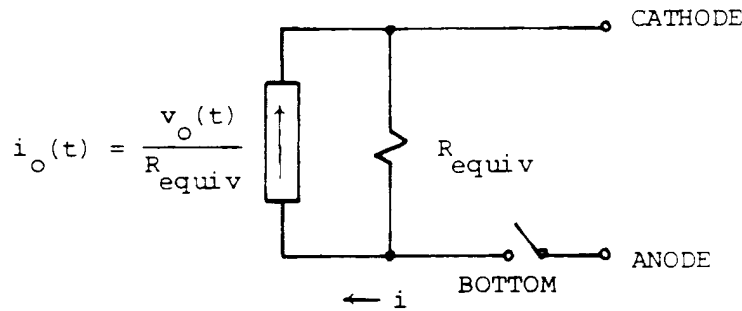
Fig. 7.14 - Norton equivalent circuit

The equivalent resistance R_{equiv} remains constant for a given step size Δt,

$$R_{equiv} = \frac{k_2 K \left(1 + \dfrac{2 T_2}{\Delta t} \right)}{1 + \dfrac{2T}{\Delta t} + \dfrac{4P}{(\Delta t)^2}} \tag{7.15}$$

whereas the current source $i_0(t)$ depends on the values $e_\alpha(t - \Delta t)$ and $x(t - \Delta t)$ of the preceding time step. After the complete network solution at each time step, with the converter representation of Fig. 7.14, the current is calculated with Eq. (7.14), and then used to update the variables e_α and x.

If e_α hits one of the limits $e_{\alpha max}$ or $e_{\alpha min}$, it is kept at the appropriate limit in the following time steps, with x and dx/dt set to zero. B.C. Chiu has recently shown, however, that simply setting x and dx/dt to zero at the limit does not represent the true behavior of the current controller [130]. The treatment of limits should therefore be revised, if this current-controlled dc voltage source remains in use. Backing off the limit occurs when the derivative

de_α/dt calculated from Eq. (7.10) becomes negative in case of $e_\alpha = e_{\alpha max}$, or positive in case of $e_\alpha = e_{\alpha min}$.

The switch opens as soon as $i(t) < 0$, and closes again as soon as $V_{ANODE} > v_{BOTTOM}$, to assure that current can only flow in one direction. This updating of the current source $i_0(t)$ from step to step is not influenced by the switching actions.

8. THREE-PHASE SYNCHRONOUS MACHINE

Co-author: V. Brandwajn

The details with which synchronous machines must be modelled depend very much on the type of transient study. Most readers will be familiar with the simple representation of the synchronous machine as a voltage source E" behind a subtransient reactance X_d". This representation is commonly used in short-circuit studies with steady-state phasor solutions, and is also reasonably accurate for transient studies for the first few cycles of a transient disturbance. Switching surge studies fall into that category. Another well-known representation is E' behind X_d' for simplified stability studies. Both of these representations can be derived from the same detailed model by making certain assumptions, such as neglecting flux linkage changes in the field structure circuits for E" behind X_d", and in addition, assuming that the damper winding currents have died out for E' behind X_d'.

The need for the detailed model described here arose in connection with subsynchronous resonance studies in the mid-1970's. In such studies, the time span is too long to allow the use of simplified models. Furthermore, the torsional dynamics of the shaft with its generator rotor and turbine rotor masses had to be represented as well. Detailed models are now also used for other types of studies (e.g., simulation of out-of-step synchronization). To cover all possible cases, the synchronous machine model represents the details of the electrical part of the generator as well as the mechanical part of the generator and turbine. For studies in which speed variations and torsional vibrations can be ignored, an option is provided for by-passing the mechanical part of the UBC EMTP.[1]

The synchronous machine model was developed for the usual design with three-phase ac armature windings on the stator and a dc field winding with one or more pole pairs on the rotor. For a reversed design (armature windings on the rotor and field winding on the stator), it is probably possible to represent the machine in some equivalent way as a machine with the usual design. Even though the model was developed with turbine-driven generators in mind, it can be used for synchronous motors as well (e.g., pumping mode in a pumped-storage plant).

The model cannot be used for dual-excited machines (one field winding in direct axis and another field winding in quadrature axis) at this time, thought it would be fairly easy to change the program to allow for it. Since such machines have not yet found practical acceptance, it was felt that the extra programming was not justified. Induction machines can also not be modelled with it, though program changes could again be made for that purpose. For these and other types of machines, the universal machine of Section 9 should be used.

While the equations for the detailed machine model have been more or less the same in all attempts to incorporate them into the EMTP, there have been noticeable differences in how their solution is interfaced with the rest of the network. K. Carlsen, E.H. Lenfest and J.J. LaForest were probably the first to add a machine model to the EMTP, but the resulting "MANTRAP" - program [97] was not made available to users outside General Electric Co. M.C. Hall, J. Alms (Southern California Edison Co.) and G. Gross (Pacific Gas & Electric Co.), with the assistance of W.S. Meyer (Bonneville Power Administration), implemented the first model which became available

---

[1]The synchronous machine model is the UBC EMTP is experimental and has not been released.

to the general public. They opted for an iterative solution at each time step, with the rest of the system, as seen from the machine terminals, represented by a three-phase Thevenin equivalent circuit [98]. To keep this "compensation" approach efficient, machines had to be separated by distributed-parameter lines from each other. If that separation did not exist in reality, short artificial "stub lines" had to be introduced which sometimes caused problems. V. Brandwajn suggested another alternative in which the machine is basically represented as an internal voltage source behind some impedance. The voltage source is recomputed for each time step, and the impedance becomes part of the nodal conductance matrix [G] in Eq. (1.8). This approach depends on the prediction of some variables, which are not corrected at one and the same time step in order to keep the algorithm non-iterative. While the prediction can theoretically cause numerical instability, it has been refined to such an extent by now that the method has become quite stable and reliable. Whether an option for repeat solutions as correctors will be added someday remains to be seen. Numerical stability has been more of a problem with machine models partly because the typical time span of a few cycles in switching surge studies has grown to a few seconds in machine transient studies, with the step size Δt being only slightly larger, if at all, in the latter case.

8.1 Basic Equations for Electrical Part

Since there is no uniformity on sign conventions in the literature, the sign conventions used here shall first be summarized:

(a)   The flux linkage λ of a winding, produced by current in the same winding, is considered to have the same sign as the current ($\lambda = Li$, with L being the self inductance of the winding).

(b)   The "generator convention" is used for all windings, that is, each winding k is described by

$$v_k(t) = -R_k i_k(t) - \frac{d\lambda_k(t)}{dt} \tag{8.1}$$

(with the "load convention," the signs would be positive on the right-hand side).

(c)   The newly recommended position of the quadrature axis lagging 90° behind the direct axis in the machine phasor diagram is adopted here [99]. In Park's original work, and in most papers and books, it is leading, and as a consequence the terms in the second row of $[T]^{-1}$ of Eq. (8.7b) have negative signs there.

The machine parameters are influenced by the type of construction. Salient-pole machines are used in hydro plants, with 2 or more (up to 50) pole pairs. The magnetic properties of a salient-pole machine along the axis of symmetry of a field pole (direct axis) and along the axis of symmetry midway between two field poles (quadrature axis) are noticeably different because a large part of the path in the latter case is in air (Fig. 8.1a). Cylindrical-rotor machines have long cylindrical rotors with slots in which distributed field windings are placed (Fig. 8.1b). They are used in thermal plants, and have 1 or 2 pole pairs. For cylindrical-rotor machines the magnetic properties on the two axes differ only slightly (because of the field windings embedded in the slots), and this difference ("saliency") can often be ignored. The word saliency is used as a short expression for the fact that the rotor has

different magnetic properties on the two axes.

(a) Salient-pole machine   (b) Cylindrical-rotor machine
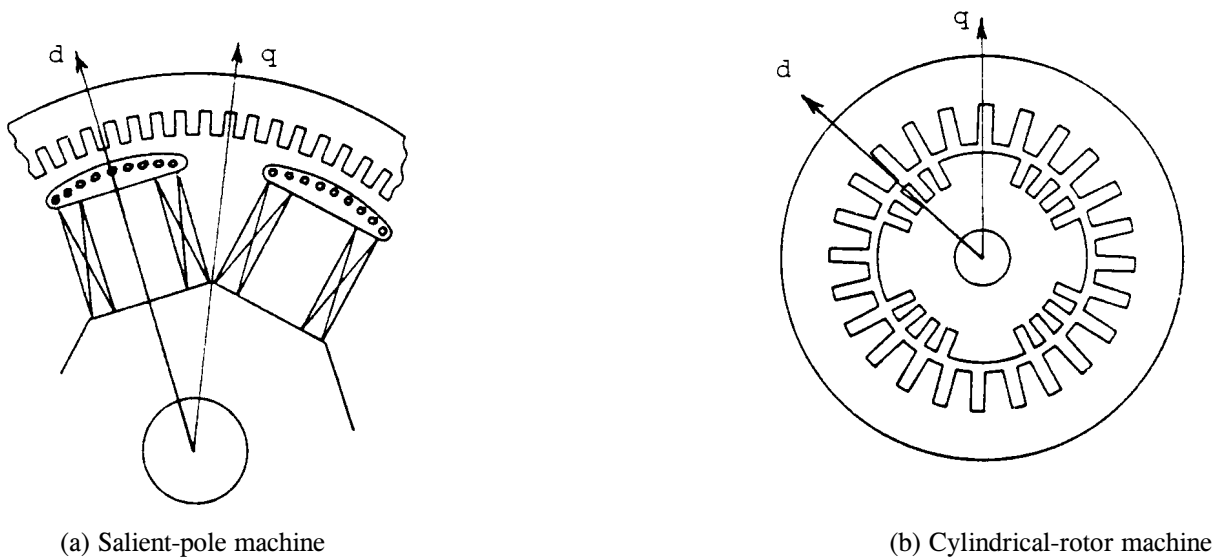
Fig. 8.1 - Cross sections of synchronous machines (d = direct axis, q = quadrature axis)
[101]. Reprinted by permission of I. Kimbark

The machine model in the EMTP always allows for saliency; if saliency is ignored, the same equations will still be used, except that certain parameters will have been set equal at input time ($X_q = X_d$, etc.).

The electrical part of the synchronous machine is modelled as a two-pole machine with 7 coupled windings[2]:

1

2   three armature windings (connected to the power system),

3

f   one field winding which produces flux in the direct axis (connected to the dc source of the excitation system),

g   one hypothetical winding in the quadrature axis to represent slowly changing fluxes in the quadrature axis which are produced by deep-flowing eddy currents (normally negligible in salient-pole machines)

D   one hypothetical winding in the direct axis to represent damper bar effects,

Q   one hypothetical winding in the quadrature axis to represent damper bar effects.

For machines with more than one pole-pair, the electrical equations are the same as for one pole-pair, except that the angular frequency and the torque being used in the equations of the mechanical part must be converted as follows:

---

[2]Another, more modern approach is to measure the frequency response from the terminals, which can then be used to represent the machine with transfer functions between the terminals, without assuming a given number of lumped windings a priori. One can also use curve fitting techniques to match this measured response with that from a series and parallel combination of R-L branches [100]. The end results in the latter case is basically the same model as described here, except that damper bars are sometimes represented by more than one winding, and that the data is obtained from frequency response tests.

$$\omega_{actual} = \frac{\omega_{2-pole-machine}}{p/2}$$ (8.2a)

$$T_{actual} = \frac{p}{2} T_{2-pole-machine}$$ (8.2b)

where p/2 is the number of pole pairs.

The behavior of the 7 windings is described by two systems of equations, namely by the voltage equations

$$[v] = -[R][i] - \frac{d}{dt}[\lambda]$$ (8.3)

with

$[i] = \quad [i_1, i_2, i_3, i_f, i_g, i_D, i_Q],$

$[\lambda] = \quad [\lambda_1, \lambda_2, \lambda_3, \lambda_f, \lambda_g, \lambda_D, \lambda_Q],$

$[v] = \quad [v_1, v_2, v_3, v_f, 0, 0, 0]$ (zero in last 3 components because g-, D-, and Q- windings are short-circuited)

$[R] = \quad$ diagonal matrix of winding resistances $R_a, R_a, R_a, R_f, R_g, R_D, R_Q$ (subscript "a" for armature),

and by the flux-current relationship

$$[\lambda] = [L][i] \quad with \ [L] = \begin{bmatrix} L_{11} & L_{12} & \dots & L_{1Q} \\ L_{21} & L_{22} & \dots & L_{2Q} \\ . & . & . & . & . \\ L_{Q1} & L_{Q2} & \dots & L_{QQ} \end{bmatrix}$$ (8.4)

To make the equations manageable, a number of idealized characteristics are assumed, which are reasonable for system studies. These assumptions for the "ideal synchronous machine" [76, p. 700] are[3]:

(1)   The resistance of each winding is constant.

(2)   The permeance of each portion of the magnetic circuit is constant (corrections for saturation effects will be introduced later, however).

(3)   The armature windings are symmetrical with respect to each other.

(4)   The electric and magnetic circuits of the field structure are symmetrical about the direct or quadrature axis.

(5)   The self inductance of each winding on the field structure (f, g, D, Q) is constant.

(6)   The self and mutual inductances of the armature windings are a constant plus a second-harmonic sinusoidal function of the rotor position β (second-harmonic component zero if saliency ignored), with the amplitude of the second-harmonic component being the same for all self and mutual

---

[3]For a detailed design analysis of synchronous machines, many of these idealizations cannot be made. Since they imply that the field distribution across a pole is a fundamental sinusoid, harmonics produced by the nonsinusoidal field distribution in a real machine could not be studied with the ideal machine implemented in the EMTP.

inductances.

(7)   The mutual inductance between any winding on the field structure and any armature winding is a fundamental sinusoidal function of the rotor position β.

(8)   Effects of hysteresis are negligible.

(9)   Effects of eddy currents are negligible or, in the case of cylindrical-rotor machines, are represented by the g-winding.

Then,

$$
\begin{aligned}
L_{11} &= L_s + L_m\cos2\beta, \qquad similar\ for\ L_{22},\ L_{33} \\
L_{12} &= L_{21} = M_s + L_m\cos(2\beta - 120°) \quad similar\ for\ L_{13},\ L_{23} \\
L_{1f} &= L_{f1} = M_{af}\cos\beta \qquad similar\ for\ L_{2f},\ L_{3f} \\
L_{1D} &= L_{D1} = M_{aD}\cos\beta \qquad similar\ for\ L_{2D},\ L_{3D} \\
L_{1g} &= L_{g1} = M_{ag}\sin\beta \qquad similar\ for\ L_{2g},\ L_{3g} \\
L_{1Q} &= L_{Q1} = M_{aQ}\sin\beta \qquad similar\ for\ L_{2Q},\ L_{3Q} \\
L_{ff}&,\ L_{gg},\ L_{DD},\ L_{QQ},\ M_{fD},\ M_{gQ} \quad constant \quad (not\ functions\ of\ \beta)
\end{aligned}
\tag{8.5}
$$

with β being the angular position of the assumed two-pole rotor relative to the stator ($\beta_{actual} = \beta_{2\text{-pole-machine}}\ /\ p/2$), which is related to the angular frequency,

$$
\omega = \frac{d\beta}{dt}
\tag{8.6}
$$

Some authors (e.g., Kimbark [101]) use a different sign for M_s in Eq. (8.5). With the sign used here, the numerical value will be negative.

The solution of the two systems of equations (8.3) and (8.4) is complicated by the fact that the inductances in Eq. (8.4) are functions of time through their dependence on β in Eq. (8.5). While it is possible to solve them directly in phase quantities[4], most authors prefer to transform them from phase quantities to d, q, 0- quantities because the inductances become constants in the latter reference frame. This transformation projects the rotating fluxes onto the field axis, from where they appear as stationary during steady-state operation. The transformation was first proposed by Blondel, and further developed by Doherty, Nickle and Park; in North America, it is now often called Park's transformation. The transformation is identical for fluxes, voltages, and currents, and converts phase quantities 1, 2, 3 into d, q, 0- quantities, with quantities on the field structure remaining unchanged,

$$
[\lambda_{dq0}] = [T]^{-1}[\lambda] \quad identical\ for\ [v],\ [i]
\tag{8.7a}
$$

with

---

[4]If space harmonics in the magnetic field distribution had to be taken into account, then L_{11} and L_{12} in Eq. (8.5) would have added 4th, 6th, and higher harmonics terms, and L_{1f} etc. would have added 3rd, 5th,…harmonics terms. In that case, solutions in phase quantities would probably be the best choice.

$$[\lambda_{dq0}] \;=\; [\lambda_d,\; \lambda_q,\; \lambda_0,\; \lambda_f,\; \lambda_g,\; \lambda_D,\; \lambda_Q]\;, \quad \textit{and}$$

Remain unchanged

$$[T]^{-1} = \begin{bmatrix}
\dfrac{\sqrt{2}}{\sqrt{3}}\cos\beta & \dfrac{\sqrt{2}}{\sqrt{3}}\cos(\beta - 120°) & \dfrac{\sqrt{2}}{\sqrt{3}}\cos(\beta + 120°) & 0 & 0 & 0 & 0 \\[2mm]
\dfrac{\sqrt{2}}{\sqrt{3}}\sin\beta & \dfrac{\sqrt{2}}{\sqrt{3}}\sin(\beta - 120°) & \dfrac{\sqrt{2}}{\sqrt{3}}\sin(\beta + 120°) & 0 & 0 & 0 & 0 \\[2mm]
\dfrac{1}{\sqrt{3}} & \dfrac{1}{\sqrt{3}} & \dfrac{1}{\sqrt{3}} & 0 & 0 & 0 & 0 \\[1mm]
0 & 0 & 0 & 1 & 0 & 0 & 0 \\
0 & 0 & 0 & 0 & 1 & 0 & 0 \\
0 & 0 & 0 & 0 & 0 & 1 & 0 \\
0 & 0 & 0 & 0 & 0 & 0 & 1
\end{bmatrix} \qquad (8.7b)$$

Eq. (8.7) is an orthogonal transformation; it therefore follows that

$$[T] \;=\; [T]^{-1}_{transposed} \qquad (8.8)$$

The matrices [T] and [T]$^{-1}$ are normalized here. This has the advantage that the power is invariant under transformation, and more importantly, that the inductance matrix in d, q, 0- quantities is always symmetric. The lack of symmetry with unnormalized quantities can easily lead to confusion, because it is often removed by rescaling of field structure quantities which in turn imposes unnecessary restrictions on the choice of base values if p.u. quantities are used. Authors who work with unnormalized transformations use a factor 2/3 in the first two rows of Eq. (8.7b), and 1/3 in the third row. In many older publications the position of the quadrature axis is assumed 90° ahead of the direct axis, rather than lagging 90° behind d-axis as here, and the second row of Eq. (8.7b) has therefore negative signs there.

Transforming Eq. (8.3) to d, q, 0- quantities yields

$$[v_{dq0}] \;=\; -[R]\,[i_{dq0}] \;-\; \frac{d}{dt}[\lambda_{dq0}] \;+\; \begin{bmatrix} -\omega\lambda_q \\ +\omega\lambda_d \\ 0 \\ 0 \\ 0 \\ 0 \\ 0 \end{bmatrix} \qquad (8.9)$$

which is almost identical in form to Eq. (8.3), except for the "speed voltage terms" $-\omega\lambda_q$ and $\omega\lambda_d$ (voltage induced

in armature because of rotating field poles). They come out of Eq. (8.3) by keeping in mind that [T] is a function of time,

$$[T]^{-1} \frac{d}{dt} \{[T] [\lambda_{dq0}]\} = \frac{d}{dt} [\lambda_{dq0}] + [T]^{-1} \left\{ \frac{d}{dt} [T] \right\} [\lambda_{dq0}]$$

Transforming Eq. (8.4) yields flux-current relationships which can be partitioned into two systems of equations for the direct and quadrature axis, and one equation for zero sequence,

$$\begin{bmatrix} \lambda_d \\ \lambda_f \\ \lambda_D \end{bmatrix} = \begin{bmatrix} L_d & M_{df} & M_{dD} \\ M_{df} & L_{ff} & M_{fD} \\ M_{dD} & M_{fD} & L_{DD} \end{bmatrix} \begin{bmatrix} i_d \\ i_f \\ i_D \end{bmatrix} \qquad (8.10a)$$

$$where \quad M_{df} = \frac{\sqrt{3}}{\sqrt{2}} M_{af}, \qquad M_{dD} = \frac{\sqrt{3}}{\sqrt{2}} M_{aD}$$

$$\begin{bmatrix} \lambda_q \\ \lambda_g \\ \lambda_Q \end{bmatrix} = \begin{bmatrix} L_q & M_{qg} & M_{qQ} \\ M_{qg} & L_{gg} & M_{gQ} \\ M_{qQ} & M_{gQ} & L_{QQ} \end{bmatrix} \begin{bmatrix} i_q \\ i_g \\ i_Q \end{bmatrix} \qquad (8.10b)$$

$$where \quad M_{qg} = \frac{\sqrt{3}}{\sqrt{2}} M_{ag}, \qquad M_{qQ} = \frac{\sqrt{3}}{\sqrt{2}} M_{aQ}$$

$$and \qquad \lambda_0 = L_0 i_0 \qquad (8.10c)$$

Most elements of these inductance matrices with constant coefficients have already been defined in Eq. (8.5), except for

direct axis synchronous inductance $L_d = L_s - M_s + 3/2 \, L_m$,
quadr. axis synchronous inductance $L_q = L_s - M_s - 3/2 \, L_m$,   (8.11)
zero sequence inductance $L_0 = L_s + 2M_s$.

8.2 Determination of Electrical Parameters[5]

A set of resistances and of self and mutual inductances is needed in the two systems of equations (8.9) and (8.10), which are not directly available from calculations or measurements. According to IEEE or IEC standards [102, 103] the known quantities are

armature resistance R_a,

armature leakage reactance X_ℓ,

zero sequence reactance X_o,

transient reactances X_d', X_q',

subtransient reactances X_d'', X_q'',

transient short-circuit time constants T_d', T_q',

subtransient short-circuit time constants T_d'', T_q''.

All reactances and time constants must be unsaturated values, because saturation is considered separately, as explained in Section 8.6. This is the reason why short-circuit time constants are preferred as test data over open-circuit time constants, because the measurement of the latter is influenced by saturation effects [104]. Fortunately, one set of time constants can be converted precisely into the other set [104], as explained in Appendix VI in Eq. (VI. 14c) and (VI. 21),

$$T_{d0}' + T_{d0}'' = \frac{X_d}{X_d'} T_d' + \left(1 - \frac{X_d}{X_d'} + \frac{X_d}{X_d''} \right) T_d''$$

$$T_{d0}' T_{d0}'' = T_d' T_d'' \frac{X_d}{X_d''} \tag{8.12}$$

for the direct axis, and identically for the quadrature axis by replacing subscript "d" with "q."

The number of known parameters is less than the number of resistance and inductance values in Eq. (8.9) and (8.10), and some assumptions must therefore be made before the data can be converted. Since the procedure for data conversion is the same for the direct and quadrature axis parameters, only the direct axis will be discussed from here on.

Winding D is a hypothetical winding which represents the effects of the damper bar squirrel cage. We can therefore assume any number of turns for it, without loss of generality. In particular, we can choose the number of turns in such a way that

$$M_{dD} = M_{df} \tag{8.13a}$$

in Eq. (8.10a), and similarly

$$M_{qQ} = M_{qg} \tag{8.13b}$$

in Eq. (8.10b). Many authors represent the flux-current relationships with an equivalent star circuit, which requires

all three mutual inductances in Eq. (8.10a) to be equal. This is achieved by modifying (rescaling) the field structure quantities as follows:

$$\lambda_{fm} = \frac{\sqrt{3}}{\sqrt{2}} k \cdot \lambda_f, \quad and \quad i_{fm} = \frac{1}{\frac{\sqrt{3}}{\sqrt{2}} k} \cdot i_f \qquad (8.14a)$$

$$with \qquad k = \frac{M_{af}}{M_{fD}} \qquad (8.14b)$$

(identical for λ_D and i_D). Then Eq. (8.10a) becomes

$$\begin{bmatrix} \lambda_d \\ \lambda_{fm} \\ \lambda_{Dm} \end{bmatrix} = \begin{bmatrix} L_d & M_m & M_m \\ M_m & L_{ffm} & M_m \\ M_m & M_m & L_{DDm} \end{bmatrix} \begin{bmatrix} i_d \\ i_{fm} \\ i_{Dm} \end{bmatrix} \qquad (8.15a)$$

with

$$M_m = \frac{3}{2} k M_{af}, \qquad L_{ffm} = \frac{3}{2} k^2 L_{ff}, \qquad L_{DDm} = \frac{3}{2} k^2 L_{DD} \qquad (8.15b)$$

and

$$R_{fm} = \frac{3}{2} k^2 R_f, \qquad R_{Dm} = \frac{3}{2} k^2 R_D \qquad (8.16)$$

Fig. 8.2 shows the equivalent star-circuit for the direct axis, with the speed voltage term and resistances added to make it correct for Eq. (8.9) as well. Modifying the field structure quantities is the same as changing the number of turns in the field structure windings. It does not influence the data conversion, but it is simpler to carry out if the modified form of Eq. (8.15a) is used. The correct turns ratio is then introduced later from the relationship between rated no-load excitation current and rated terminal voltage.

The best data conversion procedure seems to be that of Canay [104]. It uses the four equations which define the open- and short-circuit time constants, as derived in Appendix VI.2, to find R_{fm}, R_{Dm}, L_{ffm} and L_{DDm} ("m" dropped in Appendix VI to simplify the notation). Usually, only one pair of time constants (either T_{d0}', T_{d0}'' or T_d', T_d'') plus X_d', X_d'' are known; in that case, the other pair must first be found from Eq. (8.12). Solving the four equations for the four field structure quantities presupposes that the mutual inductance M_m in Eq. (8.15a) is already known. Its value has traditionally been found from leakage flux calculations. While turns ratios have been
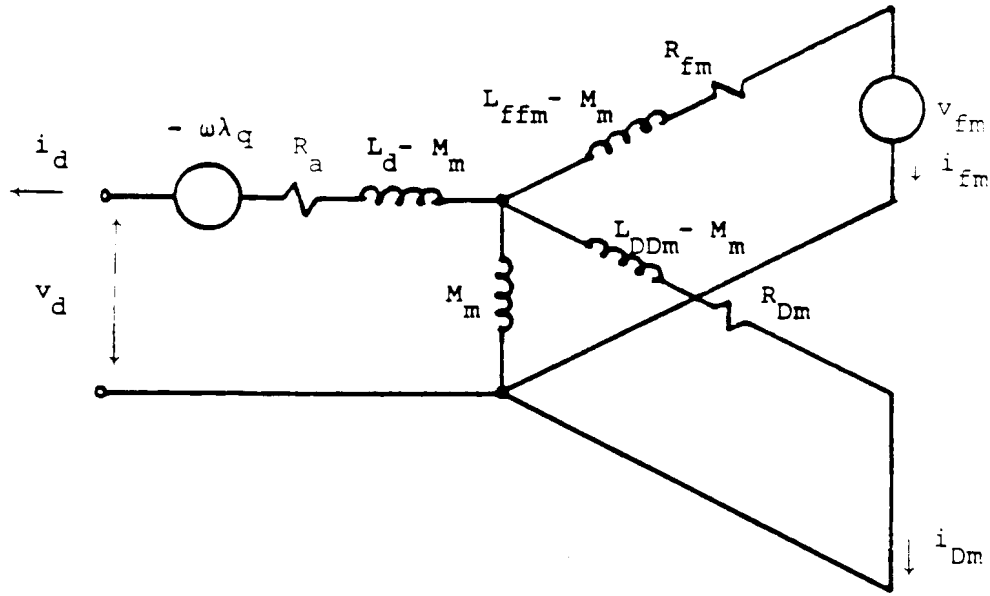
Fig. 8.2 - Equivalent circuit for direct axis with modified field structure quantities

unimportant so far, they must be considered in the definition of leakage flux, since it is the actual flux ϕ, rather than the flux linkage $\lambda = N\phi$ (N = number of turns) which is involved. In defining the leakage flux we must either use actual flux quantities, or flux linkages with turns ratios of 1:1. The leakage flux linkage produced by i_d is then

$$\lambda_{\ell} = L_d i_d - L_{df} i_d, \qquad provided \quad N_d : N_f = 1:1 \tag{8.17}$$

Let us assume that all field structure quantities are referred to the armature side, which implies $N_a : N_f = 1:1$ in the original equations (8.4) with phase quantities, with the mutual inductance being M_{af} (cos $\beta = 1.0$ if magnetic axis of phase 1 armature winding lined up with direct axis). After transforming to d, q, 0- quantities, the mutual inductance in Eq. (8.10a) between d and f changes to $\sqrt{3}/\sqrt{2}\, M_{af}$, which implies that the ratio is now $N_d : N_f = \sqrt{3}/\sqrt{2}$: 1. To convert back to a ratio of 1:1, the second row and column in Eq. (8.10a) must be multiplied with $\sqrt{3}/\sqrt{2}$, which changes the mutual inductance to $3/2\, M_{af}$. Then the leakage flux linkage produced by i_d with a 1:1 ratio becomes

$$\lambda_{\ell} = L_d i_d - \frac{3}{2} M_{af} i_d$$

or for the leakage inductance,

$$L_{\ell} = L_d - \frac{3}{2} M_{af} \tag{8.18}$$

Unfortunately, this equation is still not enough for finding M_m in the modified matrix of Eq. (8.15a) because of the unknown factor k in Eq. (8.14b). To find k, an additional test quantity must be measured which has not yet been

prescribed in the IEEE or IEC standards. It has therefore been common practice to assume k = 1, which implies $M_{fD} = M_{af}$. With this assumption, the results for armature quantities will be correct, but the amplitude of the fast oscillations in the field current will be incorrect, as pointed out by Canay [104] and others. Fig. 8.3 shows the measured field current after a three-phase short-circuit [104], compared with EMTP simulation results with k = 1, and with the correct value of k. Note that the "d-branch" in the star circuit of Fig. 8.2 is the leakage inductance only if all quantities are referred to the armature
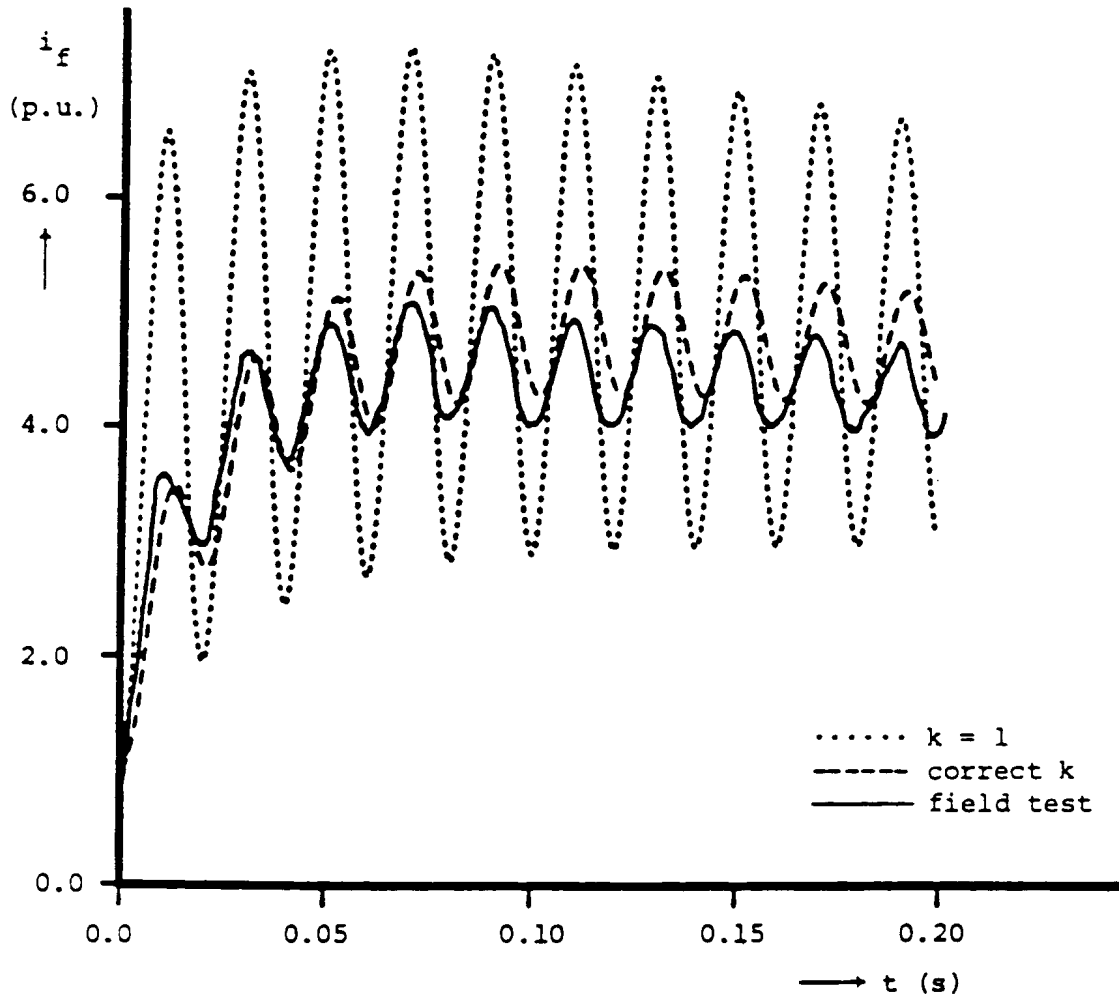
Fig. 8.3 - Field current after three-phase short-circuit [104]. Reprinted by permission of IEE and the author

side and if k = 1. If the factor k is known, then the "d-branch" with field structure quantities referred to the armature becomes Canay's "characteristic inductance"

$$L_c = L_d - \frac{3}{2} k M_{af} \tag{8.19}$$

The data conversion of the modified quantities on the direct axis can now be done as follows: If k is unknown, assume k = 1, find M_m from Eq. (8.18),

$$M_m = L_d - L_q \tag{8.20a}$$

and realize that the fast oscillations in the field current will have a wrong amplitude, but the armature quantities will be correct. If the characteristic inductance is known (which can be calculated from k), find M_m from Eq. (8.19),

$$M_m = L_d - L_c \tag{8.20b}$$

and the fast oscillations in the field current will be correct. Then use the conversion procedure of Appendix VI.4 to obtain the field structure quantities R_{fm}, R_{Dm}, L_{ffm}, L_{DDm} ("m" dropped in Appendix VI), which will be rescaled according to Eq. (8.14). It is not necessary to undo the rescaling if one is only interested in quantities on the armature side, because scaling of field structure quantities does not influence the armature quantities. If the conversion was done with p.u. quantities, which will usually be the case, then multiply all resistances and inductances with V_{rated}^2/S_{rated} to obtain physical values (V_{rated} = rated line-to-line RMS armature voltage, S_{rated} = rated apparent power) for wye-connected machines, followed by another multiplication with a factor 3 for delta-connected machines.

The data conversion for the quadrature axis quantities is the same as that for the direct axis, except that one does not have to worry about correct amplitudes in the oscillations of the current i_g. This current cannot be measured, because the g-winding is a hypothetical winding which represents eddy or damper bar currents. It is therefore best to use k = 1 and

$$M_{m(quadrature\ axis)} = L_q - L_q \tag{8.20c}$$

on the quadrature axis.

Rather than undo the rescaling of Eq. (8.14) by using t = 1 / ($\sqrt{3}/\sqrt{2}$ k) with the procedure described after Eq. (8.22), it makes more sense to choose a factor t which introduces the correct turns ratio between physical values of the armature and field structure quantities. To find this factor, we must look at the open-circuit terminal voltage produced by the no-load excitation current $i_{f\text{-no load}}$. For open circuit, $i_d = i_q = i_D = 0$, and, in steady-state operation, $d\lambda_q/dt = 0$, which leads to

$$v_q = \omega M_m i_{fm}$$

Since we know that the modified current must be t-times the actual current,

$$i_{fm} = t \cdot i_f$$

and since v_q is equal to $\sqrt{3} \bullet V_{1\text{-RMS}}$ (assuming symmetrical voltages in the three phases), we can find t from

$$t = \frac{\sqrt{3}\ V_{phase}}{\omega M_m i_{f\text{-no load}}} \tag{8.21}$$

with V_{phase} = rated RMS line-to-ground voltage for wye connection, and line-to-line voltage for delta connection, $i_{f\text{-no load}}$ = rated no-load excitation current which produces rated voltage at the terminal.

Sometimes the no-load excitation current is not known. Then any system of units can be used for the field structure. One possibility is to set t = 1 (field structure quantities referred to the armature side). Another possibility is to say that a field voltage $|v_f| = 1.0$ should produce the rated terminal voltage. Then

$$i_{f\text{-no load}} = \frac{|v_f|}{R_f} = \frac{1.0}{t^2 R_{fm}}$$

which, when inserted into Eq. (8.21) gives

$$t = \frac{\omega M_m}{\sqrt{3} V_{phase} R_{fm}} \tag{8.22}$$

Once t is known, the inductances are converted by multiplying the second and third row and column of the inductance matrix in Eq. (8.15a) with t, and by multiplying R_{fm} and R_{Dm} with t^2. The quadrature axis inductances and resistances are also multiplied with t or t^2, respectively.

Sometimes, generators are modelled with less than 4 windings on the field structure (D-winding on the direct axis missing, and/or g- or Q-winding on the quadrature axis missing). In such cases, the EMTP still uses the full 7-winding model and simply "disconnects" the unwanted winding by setting its off-diagonal elements in the inductance matrix to zero, and its diagonal element to an arbitrary value of $\omega L = 1 \ \Omega$. Its resistance is arbitrarily set to zero. The inductances and resistances of the other windings on the same axis are calculated from Eq. (VI.4) and (VI.5) (Appendix VI), e.g., for a missing g-winding,

$$M_{qg} = 0, \quad M_{gQ} = 0, \quad R_g = 0, \quad \omega L_{gg} = 1$$

and

$$L_{QQ} = \frac{M^2}{L_q - L_q''}, \quad R_Q = \frac{L_{QQ}}{T_{q0}''}, \quad where \ M = L_q - L_g$$

8.3 Basic Equations for Mechanical Part

There are many transient cases where the speed variation of the generator is so small that the mechanical part can be ignored. Simulating short-circuit currents for a few cycles falls into that category. In that case, ω in Eq. (8.6) and in the other equations is constant, and the angular position β of the rotor needed in Eq. (8.7) and (8.9) is simply

$$\beta(t) = \beta(0) + \omega t \tag{8.23}$$

with β and ω being angle and speed on the electrical side.

For other types of studies it may be necessary to take the speed variations into account. The simplest model

for the mechanical part is the single mass representation as used in stability studies,

$$J \frac{d^2\beta}{dt^2} + D \frac{d\beta}{dt} = T_{turbine} - T_{gen} \qquad (8.24a)$$

and

$$\frac{d\beta}{dt} = \omega \qquad (8.24b)$$

with J =   moment of inertia of rotating turbine-generator mass,

        β =   rotor position,

        ω =   speed

        D =   damping coefficient for viscous and windage friction (linear dependence on speed is a crude approximation),

        $T_{turbine}$ =   torque input to turbine,

        T_{gen} =   electromagnetic torque of generator.

Eq. (8.24) is valid for quantities referred to the electrical or the mechanical side with the conversion from one to the other being[6]

$$J_{e\ell} = \frac{J_{mech}}{(p/2)^2}$$

$$\beta_{e\ell} = \frac{p}{2} \beta_{mech} \qquad (8.25)$$

$$D_{e\ell} = \frac{D_{mech}}{(p/2)^2}$$

$$T_{e\ell} = \frac{T_{mech}}{p/2}$$

With voltages given in V, and power in W, the unit for the torque T becomes N $\bullet$ m, for the damping coefficient D it becomes N$\bullet$m / rad/s and for the moment of inertia J it becomes kgm^2 (kg as mass).

Instead of the moment of inertia, the kinetic energy at synchronous speed is often given, which is identical for the mechanical and electrical side,

$$E = \frac{1}{2} J_{mech} \omega_{mech}^2 = \frac{1}{2} J_{e\ell} \omega_{e\ell}^2 \qquad (8.26)$$

The inertia constant h (in seconds) is the kinetic energy E (e.g., in kWs) divided by the generator rating S_{rating} (e.g.,

---

[6]Subscript "mech" is used for the mechanical side, and subscript "eℓ" for the electrical side.

in kVA),

$$h = \frac{E}{S_{rating}} \tag{8.27}$$

The relationship between the inertia constant h and the acceleration time T_a of the turbine-generator is

$$h = \frac{T_a P_{rating}}{2 S_{rating}} \tag{8.28}$$

with $P_{rating} =$ rated power of turbine-generator (e.g., in MW),

            $S_{rating} =$ rated apparent power of generator (e.g., in MVA).

       A single mass representation is usually adequate for hydro units, where turbine and generator are close together on a stiff shaft. It is not good enough, however, for thermal units, if subsynchronous resonance or similar problems involving torsional vibrations are being studied. In such cases, a number of lumped masses must be represented. Usually 6 to 20 lumped masses provide an adequate model[7]. The model in the EMTP allows any number of lumped masses $n \geq 1$, and automatically includes the special case of $n = 1$ in Eq. (8.24). Each major element (generator, high pressure turbine, etc.) is considered to be a rigid mass connected to adjacent elements by massless springs. Fig. 8.4 shows a typical 7-mass model.

       The shaft/rotor system is assumed to be linear, which is reasonable for the small amplitudes of typical torsional vibrations. The n spring-connected rotating masses are then described by the rotational form of Newton's second law,
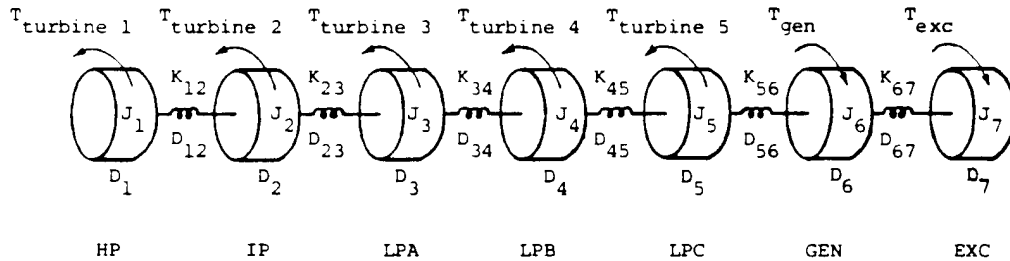
Fig. 8.4 - Mechanical part of a steam turbine generator with 7 masses (HP = high pressure turbine, IP = intermediate pressure turbine, LPA, LPB, LPC = low pressure turbine stages A, B, C, GEN = generator, EXC = exciter)

$$[J]\frac{d^2}{dt^2}[\theta] + [D]\frac{d}{dt}[\theta] + [K][\theta] = [T_{turbine}] - [T_{gen/exc}] \tag{8.29a}$$

and

---

[7]There are studies where the lumped mass representation is no longer adequate, and where continuum models must be used.

$$\left[\frac{d\theta}{dt}\right] = [\omega] \tag{8.29b}$$

where

[J]　　=　　diagonal matrix of moments of inertia ($J_1,\ldots J_7$ in Fig. 8.4),

[θ]　　=　　vector of angular positions ($\theta_1,\ldots\theta_7$ in Fig. 8.4, with $\theta_6 = \beta$),

[ω]　　=　　vector of speeds,

[D]　　=　　tridiagonal matrix of damping coefficients,

[K]　　=　　tridiagonal matrix of stiffness coefficients,

[$T_{turbine}$]　=　　vector of torques applied to the turbine stages ($T_{turbine6} = 0$ and $T_{turbine7} = 0$ in Fig. 8.4),

[$T_{gen/exc}$] =　　vector of electromagnetic torques of generator and exciter (components 1 to 5 = 0 in Fig. 8.4).

The moments of inertia and the stiffness coefficients are normally available from design data. The spring action of the shaft section between masses i - 1 and i creates a torque which is proportional to the angle twist θ_{i-1}-θ_i. The proportionality factor is the stiffness coefficient or spring constant $K_{i-1,i}$. This spring action torque acts in opposite directions on masses i - 1 and i,

$$T_{spring,i-1} = -T_{spring,i} = K_{i-1,i}\left(\theta_{i-1}-\theta_i\right) \tag{8.30}$$

If these torques are included in Eq. (8.29), they create the term [K][θ]. From Eq. (8.30) it can be seen that [K] has the following form

$$[K] = \begin{bmatrix} K_{12} & -K_{12} & & & \\ -K_{12} & K_{12}+K_{23} & -K_{23} & & \\ & -K_{23} & K_{23}+K_{34} & -K_{34} & \\ . & . & . & . & . \\ & & & -K_{n-1,n} & K_{n-1,n} \end{bmatrix}$$

Two damping effects are included with the damping coefficients, namely the self-damping D_i of mass i (mostly friction between the turbine blades and steam), and the damping $D_{i-1,i}$ created in the shaft when the shaft between masses i - 1 and i is twisted with the speed ω_i - ω_{i-1}. The damping torque acting on mass i is therefore

$$T_{damping,i} = D_i\frac{d\theta_i}{dt} + D_{i-1,i}\left(\frac{d\theta_i}{dt} - \frac{d\theta_{i-1}}{dt}\right) + D_{i,i+1}\left(\frac{d\theta_i}{dt} - \frac{d\theta_{i+1}}{dt}\right) \tag{8.31}$$

From Eq. (8.31) it can be seen that [D] has the same structure as [K], except that the diagonal element is now $D_{i-1,i} + D_i + D_{i,i+1}$,

$$[D] = \begin{bmatrix} D_1 + D_{12} & -D_{12} & & & \\ -D_{12} & D_{12} + D_2 + D_{23} & -D_{23} & & \\ . & . & . & . & . \\ & & & -D_{n-1,n} & D_{n-1,n} + D_n \end{bmatrix}$$

It is very difficult to obtain realistic values for these damping coefficients. Fortunately, they have very little influence on the peak torque values during transient disturbances. However, for estimating the low cycle fatigue one must consider the damping terms, which, unfortunately until now, have often been derived from unsuitable models [107]. The damping of torsional oscillations is measured by observing the rate of decay when the shaft system is excited at one of its natural frequencies (modes). It is difficult to convert these modal damping coefficients into the diagonal and off-diagonal elements of [D].

For the vector of turbine torques it is best to assume that the turbine power $P_{turbine} = \omega \bullet T_{turbine}$ remains constant. This implies that the torque decreases with an increase in speed, which is more reasonable than constant torque because if the turbine were to reach the same speed as the steam (or water) jet the torque on the blades would obviously drop to zero. It is possible to include the effects of the speed governor through TACS modelling, but usually the time span of transient simulations is so short that the governor effects will normally not show up.

The vector of electromagnetic torques and the rotor position of the generator provide the link between the equations of the mechanical and electrical part, with

$$\theta_{mech-gen} \cdot \frac{p}{2} = \beta_{el} \tag{8.32a}$$

$$T_{mech-gen} = \frac{p}{2} (\lambda_d i_q - \lambda_q i_d) \tag{8.32b}$$

$$T_{mech-exc} = \frac{-v_f i_f + i_f^2 R_{exc}}{\omega_{mech}} \tag{8.32c}$$

where it is assumed that (Eq. 8.29) is written for the mechanical side. If it is written for the electrical side, then the conversion of Eq. (8.25) must be used. The term $i_f^2 R_{exc}$ in Eq. (8.32c) represents the losses incurred in the exciter machine; the negative sign for v_f comes from the source convention of Eq. (8.1). If there is no exciter machine, as in the case of rectifier excitation systems, then mass no. 7 in Fig. 8.4 would obviously be deleted, and Eq. (8.32c) would not be needed. $T_{mech-exc}$ is not in the BPA EMTP.

8.4 Steady-State Representation and Initial Conditions

Transient studies with detailed turbine-generator models practically always start from power frequency

steady-state conditions. The EMTP goes therefore automatically into an ac steady-state solution whenever the data file contains turbine-generator models.

In some versions of the BPA EMTP, the machine is represented as a symmetrical voltage source at its terminals. This approach is only correct if the generator feeds into a balanced network. In that case, the generator currents are purely positive sequence. In an unbalanced network, there are negative and zero sequence currents, which would see the generator as a short-circuit. This is incorrect, because generators do have nonzero negative and zero sequence impedances Z_{neg} and Z_{zero}. In the M39 version of the BPA EMTP, the user can specify unsymmetrical voltage sources at the terminals. This is still not good enough, however, unless the user adjusts the negative and zero sequence components of the terminal voltage iteratively until $V_{neg} = -Z_{neg}I_{neg}$ and $V_{zero} = -Z_{zero}I_{zero}$, with I_{neg}, I_{zero} being the currents from the steady-state network solution. The UBC EMTP does include negative and zero sequence impedances correctly, as explained next.

The negative sequence impedance can be calculated as part of the data conversion. Its imaginary part is very close to

$$X_{neg} \approx \frac{X_{d''} + X_{q''}}{2} \tag{8.33}$$

and this value can be used without too much error if the negative sequence impedance is needed for preliminary calculations. The real part R_{neg} is larger than the armature resistance R_a because of double-frequency circulating currents in the field structure circuits; its value is difficult to guess, and is therefore best taken from the data conversion. For calculations internal to the UBC EMTP, the correct values from the data conversion are always used. The zero sequence impedance $Z_{zero} = R_a + kX_{zero}$ is part of the input data, but its value becomes immaterial if the generator step-up transformer is delta-connected on the generator side and if the disturbance occurs on the line side.

The positive sequence representation can be a voltage source behind any impedance, as long as it produces the desired values for the terminal voltage V_{pos} and the current I_{pos}. Knowing only V_{pos} may require a preliminary steady-state solution with a voltage source V_{pos} at the terminal, to find I_{pos}. Then the value needed for the voltage source behind the impedance is

$$V_{source} = V_{pos} + ZI_{pos}$$

Any value can be chosen for Z, but $Z = Z_{neg}$ simplifies programming for the following reason: The EMTP solves the network in phase quantities, and assumes that all phase impedance matrices are symmetric. Only $Z = Z_{neg}$ will produce a symmetric phase impedance matrix, however. Changing the program to handle unsymmetric matrices just for generators would have required a substantial amount of re-programming.

The generator positive sequence representation is then a voltage source behind Z_{neg} while the negative and zero sequence representations are passive impedances Z_{neg} and Z_{zero}, respectively (or zero voltage sources or short-circuits behind Z_{neg} and Z_{zero}). Converted to phase quantities, these 3 single-phase sequence representations become

a three-phase symmetrical voltage source (E_1'', E_2'', E_3'') behind a 3 x 3 impedance matrix, as shown in Fig. 8.5(a), with

$$[Z] = \begin{bmatrix} Z_s & Z_m & Z_m \\ Z_m & Z_s & Z_m \\ Z_m & Z_m & Z_s \end{bmatrix} \tag{8.34}$$

where $Z_s = \dfrac{1}{3}(Z_{zero} + 2 Z_{neg})$, $Z_m = \dfrac{1}{3}(Z_{zero} - Z_{neg})$

To be able to handle any type of connection, including delta and impedance-grounded or ungrounded wye connections, the voltage sources behind [Z] are converted into current sources in parallel with [Z], as indicated in Fig. 8.5(b), with
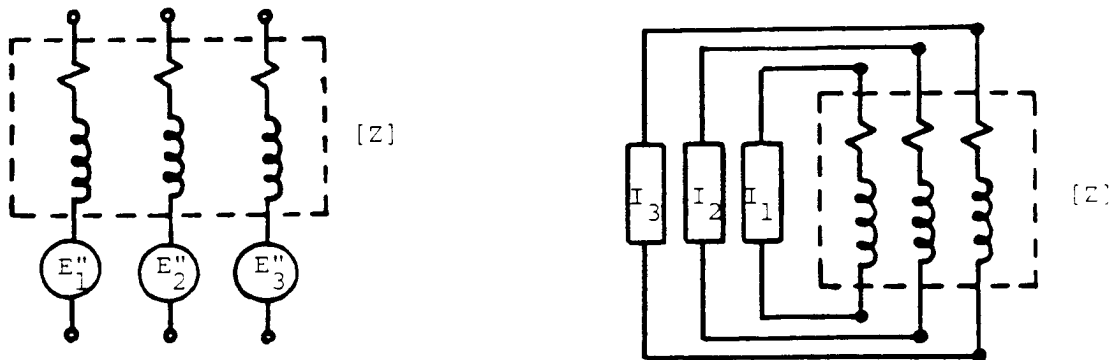
(a) Thevenin equivalent circuit   (b) Norton equivalent circuit

Fig. 8.5 - Turbine-generator representation for steady-state solution

$$\begin{bmatrix} I_1 \\ I_2 \\ I_3 \end{bmatrix} = [Z]^{-1} \begin{bmatrix} E_1'' \\ E_2'' \\ E_3'' \end{bmatrix} \tag{8.35}$$

This is done because the EMTP could not handle voltage sources between nodes until recently and even after such voltage sources are allowed now, this Norton equivalent circuit is at least as efficient. For armature winding 1, the internal voltage source is

$$E_1'' = V_{pos} + Z_{neg}I_{pos} \tag{8.36}$$

with V_{pos}, I_{pos} being the unnormalized positive sequence values. Unnormalized values are a more convenient input form for the user, because with the unnormalized transformation of Eq. (8.38) the positive sequence values are identical with the phase values V_1 and I_1 for armature winding 1 for balanced network conditions. For armature windings 2 and 3, the internal voltages are

$$E_2'' = a^2 E_1'' \quad and \quad E_3'' = a E_1'' \tag{8.37}$$

$a = e^{j120°}$).

In the UBC EMTP, either V_{pos} and I_{pos} can be specified as input data, in which case E_1'' is calculated from Eq. (8.36), or E_1'' can be specified directly. Specifying E_1'' is not as unusual as it may seem, because short-circuit programs use essentially the same generator representation (E'' behind X_d''). If users want to specify active and reactive power at the terminals, or active power and voltage magnitude, then the load flow option described in Section 12.2 can be invoked, which will automatically produce the required V_{pos} and I_{pos}.

The UBC EMTP connects the generator model of Fig. 8.5(b) to the network for the steady-state solution, which will produce the terminal voltages and currents at fundamental frequency. For unbalanced network conditions, this solution method is not quite correct because it ignores all harmonics in the armature windings and in the network. Experience has shown, however, that such an approximate initialization is accurate enough for practical purposes. Fig. 8.6 shows simulation results for a generator feeding into a highly unbalanced load resistance ($R_A = 1.0 \, \Omega$, $R_B = 1.0 \, \Omega$, $R_C = 0.05 \, \Omega$), with an initialization procedure which ignores the harmonics on the armature side, and considers only the second harmonics on the field structure side, as discussed in Section 8.4.2. The final steady state is practically present from the start. The mechanical part is totally ignored in the steady-state solution, because it is assumed that the generator runs at synchronous speed. Again, for unbalanced conditions this is not quite correct
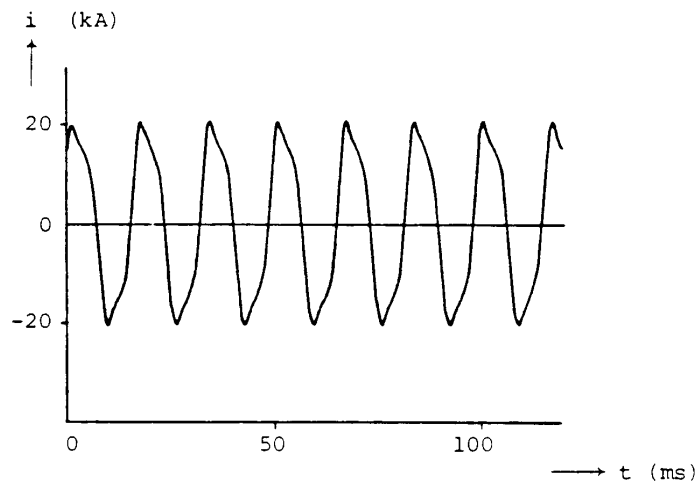
Fig. 8.6 - Steady-state behavior of generator with highly unbalanced load

because, in that case, the constant electromagnetic torque has oscillations superimposed on it which produce torsional

vibrations whose effects are ignored.

After the steady-state solution at fundamental frequency has been obtained, the terminal voltages and currents are converted to unnormalized symmetrical components to initialize the machine variables:

$$
\begin{bmatrix} V_{zero} \\ V_{pos} \\ V_{neg} \end{bmatrix} = \frac{1}{3} \begin{bmatrix} 1 & 1 & 1 \\ 1 & a & a^2 \\ 1 & a^2 & a \end{bmatrix} \begin{bmatrix} V_1 \\ V_2 \\ V_3 \end{bmatrix}, \quad \textit{identical for currents} \tag{8.38}
$$

$(a = e^{j120°})$. The inverse transformation is

$$
\begin{bmatrix} V_1 \\ V_2 \\ V_3 \end{bmatrix} = \begin{bmatrix} 1 & 1 & 1 \\ 1 & a^2 & a \\ 1 & a & a^2 \end{bmatrix} \begin{bmatrix} V_{zero} \\ V_{pos} \\ V_{neg} \end{bmatrix}, \quad \textit{identical for currents} \tag{8.39}
$$

8.4.1 Initialization with Positive Sequence Values

If the positive sequence voltage is obtained as a peak (not RMS) phasor value $|V_{pos}|e^{j\gamma pos}$, then from Eq. (8.39),

$$
v_1(t) = |V_{pos}| \cos(\omega t + \gamma_{pos})
$$

$$
v_2(t) = |V_{pos}| \cos(\omega t + \gamma_{pos} - 120°) \tag{8.40}
$$

$$
v_3(t) = |V_{pos}| \cos(\omega t + \gamma_{pos} + 120°)
$$

Inserting these voltages into the transformation of Eq. (8.7) produces

$$
v_{d-pos}(t) = \frac{\sqrt{3}}{\sqrt{2}} |V_{pos}| \sin(\gamma_{pos} - \delta)
$$

$$
v_{q-pos}(t) = \frac{\sqrt{3}}{\sqrt{2}} |V_{pos}| \cos(\gamma_{pos} - \delta) \tag{8.41}
$$

where δ is the angle between the position of the quadrature axis and the real axis for phasor representations (Fig. 8.7). This angle is related to the rotor position β_{el} on the electrical side by

$$
\beta_{el} = \omega t + \delta + \frac{\pi}{2} \tag{8.42}
$$

The positive sequence values v_d and v_q in Eq. (8.41) are dc quantities and hence do not change as a function of time; the argument (t) can therefore be dropped. From Eq. (8.41) it is evident that v_d and v_q can be combined into a complex expression

$$v_{q-pos} + jv_{d-pos} = \frac{\sqrt{3}}{\sqrt{2}} V_{pos} e^{-j\delta} \tag{8.43}$$

with V_{pos} being the complex quantity $|V_{pos}|e^{j\gamma pos}$. While V_{pos} is a phasor of frequency ω in the network solution reference frame, $V_{pos} e^{-j\delta}$ in Eq. (8.43) becomes a dc quantity in the d, q-axes reference frame. Similarly,

$$i_{q-pos} + ji_{d-pos} = \frac{\sqrt{3}}{\sqrt{2}} I_{pos} e^{-j\delta} \tag{8.44}$$

with I_{pos} being the complex current $|I_{pos}|e^{j\alpha pos}$ with respect to the real axis. With V_{pos} and I_{pos}
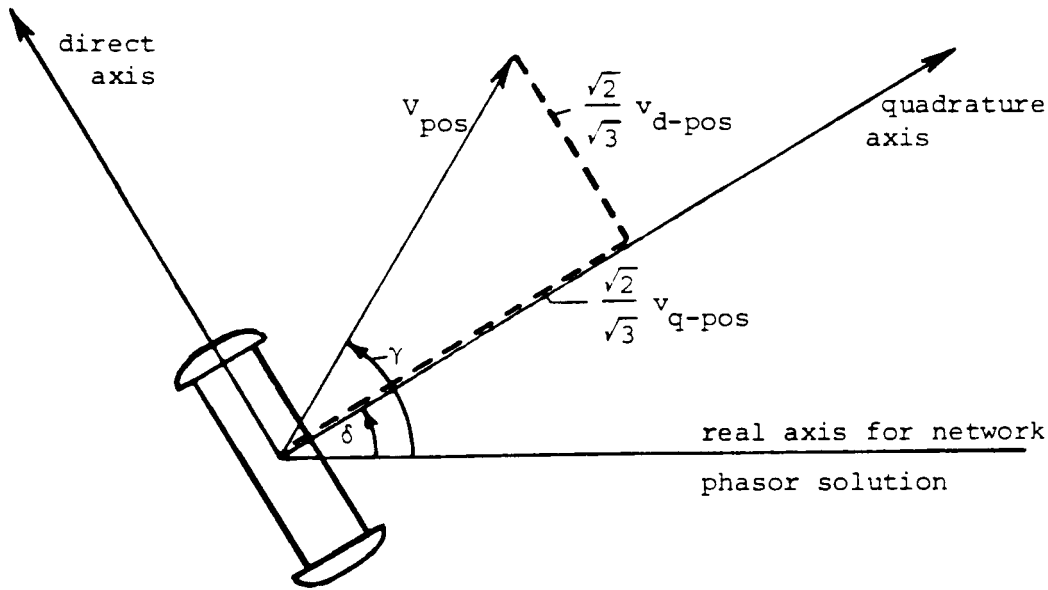
Fig. 8.7 - Definition of δ

known, we still need the angle δ to find the d, q-values. To calculate δ, use Eq. (8.9) and Eq. (8.10), with $i_D = i_g = i_Q = 0$, as well as $d\lambda_d/dt = 0$ and $d\lambda_q/dt = 0$ (no currents in damper windings and all d, q-quantities constant in symmetrical operation with positive sequence values only),

$$v_{d-pos} = -R_a i_{d-pos} - \omega L_q i_{q-pos} \tag{8.45a}$$

$$v_{q-pos} = -R_a i_{q-pos} + \omega L_d i_{d-pos} + \omega M_{df} i_{f-pos} \tag{8.45b}$$

Eq. (8.45a) and (8.45b) can be rewritten as a complex equation relative to the quadrature axis

$$v_{q\text{-}pos} + jv_{d\text{-}pos} = -(R_a + j\omega L_q)(i_{q\text{-}pos} + ji_{d\text{-}pos}) + E_{q\text{-}pos} \tag{8.45c}$$

where $E_{q\text{-}pos}$ is a quantity whose position on the quadrature axis is important, but whose magnitude

$$E_{q\text{-}pos} = (\omega L_d - \omega L_q)i_{d\text{-}pos} + \omega M_{df} i_{f\text{-}pos}$$

is immaterial here. By inserting Eq. (8.43) and Eq. (8.44) into Eq. (8.45c), and by multiplying with $(\sqrt{2}/\sqrt{3})e^{j\delta}$, all dc quantities become phasors in the network solution reference frame again. The angle δ is then obtained from the phasor equation

$$\frac{\sqrt{2}}{\sqrt{3}} \Delta v_{q\text{-}pos} e^{j\delta} = V_{pos} + (R_a + j\omega L_q) I_{pos} \tag{8.46}$$
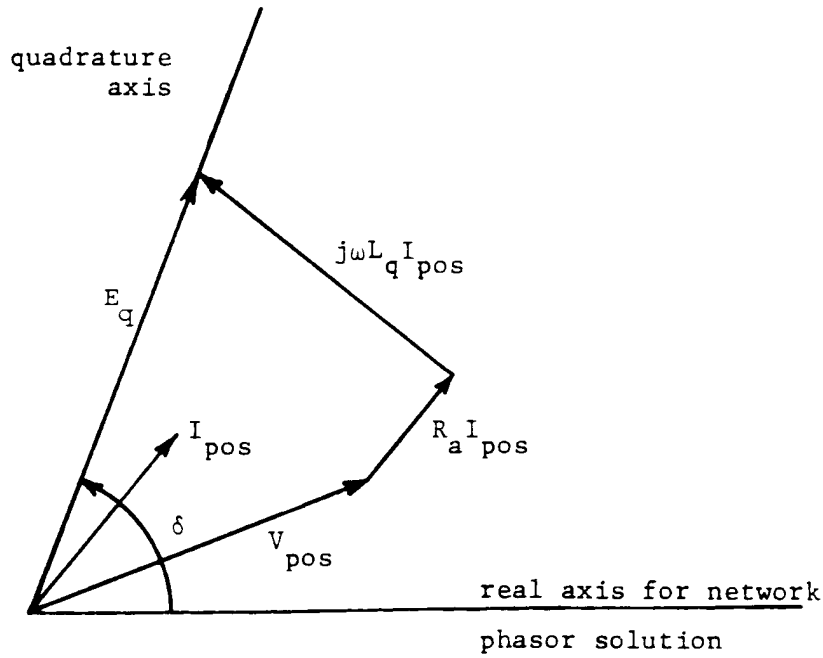
Fig. 8.8 - Calculation of angle δ

With δ known, the initial values $v_{d\text{-}pos}(0)$, $v_{q\text{-}pos}(0)$, $i_{d\text{-}pos}(0)$, $i_{q\text{-}pos}(0)$ are found from Eq. (8.43) and (8.44). As mentioned before, the remaining currents i_D, i_g, i_Q are zero from the positive sequence effects, except for i_f, whose initial value is calculated from Eq. (8.45b),

$$i_{f\text{-}pos}(0) = \frac{v_{q\text{-}pos}(0) + R_a i_{q\text{-}pos}(0) - \omega L_d i_{d\text{-}pos}(0)}{\omega M_{df}} \tag{8.47}$$

$i_{f\text{-}pos}(0)$ is used to initialize v_f

$$v_{f\text{-}pos}(0) = -R_f i_{f\text{-}pos}(0) \tag{8.48}$$

The initial value of the torque produced by the positive sequence quantities is needed in the mechanical part. It is calculated from the fluxes $\lambda_{d\text{-}pos}(0) = L_d i_{d\text{-}pos}(0) + M_{df} i_{f\text{-}pos}(0)$ and $\lambda_{q\text{-}pos}(0) = L_q i_{q\text{-}pos}(0)$ as

$$T_{gen-pos}(0) = \lambda_{d-pos}(0)\, i_{q-pos} - \lambda_{q-pos}(0)\, i_{d-pos}(0) \tag{8.49}$$

The initial positive sequence torque can also be calculated from energy balance considerations (ωT = power delivered to the network + losses in the armature windings),

$$\omega T_{gen-pos}(0) = \frac{3}{2} Re\{I_{pos} V_{pos}^*\} + \frac{3}{2} |I_{pos}|^2 R_a \tag{8.50}$$

(division by 2 because the phasors are peak values).

8.4.2 Initialization with Negative Sequence Values[8]

If the network is balanced in steady state, then there are no negative sequence values. This part of the initialization can therefore be skipped if the negative sequence (peak) phasor current

$$I_{neg} = |I_{neg}|\, e^{j\alpha_{neg}} \tag{8.51}$$

obtained from the steady-state solution is negligibly small.

Negative sequence currents in the armature windings create a magnetic field which rotates backwards at a relative speed of 2ω with respect to the field structure. Second harmonic currents are therefore induced in all windings on the field structure, which the EMTP takes into account in the initialization. These second harmonic currents induce third harmonics in the armature windings, which in turn produce fourth harmonics in the field structure windings, etc. Fortunately, these higher harmonics decrease rapidly in magnitude. They are therefore ignored. Calculating the field structure harmonics or order higher than 2 could be done fairly easily, but the calculation of the armature harmonics of order 3 and higher would involve solutions of the complete network at these higher frequencies. While the network solutions for harmonics may be added to the EMTP someday, this addition does not appear to be justified for this particular purpose.

First, the negative sequence current must be defined on the direct and quadrature axis. By starting with the negative sequence currents in the three armature windings,

$$i_1(t) = |I_{neg}|\, \cos(\omega t + \alpha_{neg})$$
$$i_2(t) = |I_{neg}|\, \cos(\omega t + \alpha_{neg} + 120°) \tag{8.52}$$
$$i_3(t) = |I_{neg}|\, \cos(\omega t + \alpha_{neg} - 120°)$$

---

[8]The negative sequence currents in the BPA EMTP can be incorrect (see beginning of Section 8.4).

these d, q-axes values are obtained through the transformation (8.7),

$$i_{d-neg}(t) = -\frac{\sqrt{3}}{\sqrt{2}} |I_{neg}| \sin(\alpha_{neg} + \delta + 2\omega t)$$

$$i_{q-neg}(t) = \frac{\sqrt{3}}{\sqrt{2}} |I_{neg}| \cos(\alpha_{neg} + \delta + 2\omega t) \tag{8.53}$$

While the positive sequence d, q-axes currents are dc quantities, the negative sequence d, q-axes currents are second harmonics. This is important to keep in mind when we represent them with a phasor of frequency 2ω,

$$I_{dq-neg} = \frac{\sqrt{3}}{\sqrt{2}} I_{neg} e^{j\delta} \tag{8.54}$$

with the understanding that

$$i_{d-neg}(t) = -Im\{I_{dq-neg} e^{j2\omega t}\}$$

$$i_{q-neg}(t) = Re\{I_{dq-neg} e^{j2\omega t}\} \tag{8.55}$$

For the initialization of i_d and i_q, the negative sequence values at $t = 0$ from Eq. (8.55) must be added to the respective positive sequence values from Eq. (8.44) to obtain the total initial values $i_d(0)$ and $i_q(0)$. The negative sequence d, q-axes voltages are not needed in the initialization, but they could be obtained analogously to the currents.

The second harmonic currents in the field structure windings are found by using the d, q-axes phasor current of frequency 2ω as the forcing function. The procedure is outlined for the direct axis; it is analogous for the quadrature axis. From Eq. (8.1),

$$v_{f-neg} = -R_f i_{f-neg} - \frac{d}{dt}(M_{df} i_{d-neg} + L_{ff} i_{f-neg} + M_{fD} i_{D-neg})$$

$$v_{D-neg} = -R_D i_{D-neg} - \frac{d}{dt}(M_{dD} i_{d-neg} + M_{fD} i_{f-neg} + L_{DD} i_{D-neg}) \tag{8.56}$$

The voltages on the left-hand side are zero because the damper winding is always shorted, and the dc voltage source supplying the field winding is seen as a short-circuit by second harmonic currents. With zero voltages, and knowing that all currents are second harmonics, Eq. (8.56) can be rewritten as two phasor equations

$$\begin{bmatrix} R_f + j2\omega L_{ff} & j2\omega M_{fD} \\ j2\omega M_{fD} & R_D + j2\omega L_{DD} \end{bmatrix} \begin{bmatrix} I_{f\text{-}neg} \\ I_{D\text{-}neg} \end{bmatrix} = - \begin{bmatrix} j2\omega M_{df} \\ j2\omega M_{dD} \end{bmatrix} I_{dq\text{-}neg} \tag{8.57}$$

which are solved for the two phasors $I_{f\text{-}neg}$, $I_{D\text{-}neg}$. Their initial values are found on the basis of Eq. (8.55) as

$$i_{f\text{-}neg}(0) = - Im\{I_{f\text{-}neg}\}$$

$$i_{D\text{-}neg}(0) = - Im\{I_{D\text{-}neg}\} \tag{8.58}$$

The value $i_{f\text{-}neg}(0)$ is then added to $i_{f\text{-}pos}(0)$ from Eq. (8.47) for the total initial field current, whereas $i_{D\text{-}neg}(0)$ is already the value of the total damper current.

The phasor currents $I_{g\text{-}neg}$ and $I_{Q\text{-}neg}$ for the quadrature axis are obtained analogous to Eq. (8.58), by replacing subscripts f and D with g and Q. Their initial values on the basis of Eq. (8.55) are then

$$i_{g\text{-}neg}(0) = Re\{I_{g\text{-}neg}\}$$

$$I_{Q\text{-}neg}(0) = Re\{I_{Q\text{-}neg}\} \tag{8.59}$$

which are the total initial values since the respective positive sequence values are zero.

The negative sequence phenomena produce torques which influence the initialization of the mechanical part. Recall that the electromagnetic torque on the electrical side is $\lambda_d i_q - \lambda_q i_d$. With both fluxes and currents consisting of positive and negative sequence parts, the total torque can be expressed as the sum of three terms,

$$T_{gen} = T_{gen\text{-}pos} + T_{gen\text{-}neg} + T_{gen\text{-}pos/neg} \tag{8.60}$$

The positive sequence torque was already defined in Eq. (8.49), and the negative sequence torque is

$$T_{gen\text{-}neg} = \lambda_{d\text{-}neg} i_{q\text{-}neg} - \lambda_{q\text{-}neg} i_{d\text{-}neg} \tag{8.61}$$

The third term

$$T_{gen\text{-}pos/neg} = \lambda_{d\text{-}pos} i_{q\text{-}neg} + \lambda_{d\text{-}neg} i_{q\text{-}pos} - \lambda_{q\text{-}pos} i_{d\text{-}neg} - \lambda_{q\text{-}neg} i_{d\text{-}pos} \tag{8.62}$$

is an oscillating torque produced by the interaction between positive and negative sequence quantities, with an average value of zero. That it is purely oscillatory can easily be seen since all positive sequence values in Eq. (8.62) are constant, and all negative sequence values oscillate at a frequency of 2ω. This and other oscillating terms are ignored in the initialization of the mechanical part, where torsional vibrations are not taken into account.

The negative sequence torque of Eq. (8.61) consists of a constant part, which must be included in the initialization of the mechanical part, and of an oscillating part with frequency 4ω which is ignored. To find the constant part, the fluxes are first calculated as phasors,

$$\Lambda_{d-neg} = L_d I_{dq-neg} + M_{df} I_{f-neg} + M_{dD} I_{D-neg} \tag{8.63a}$$

$$\Lambda_{q-neg} = L_q I_{dq-neg} + M_{qg} I_{g-neg} + M_{qQ} I_{Q-neg} \tag{8.63b}$$

With the definition of Eq. (8.55) for the instantaneous values of currents and fluxes, and after some manipulations of the equations, it can be shown that the constant part is

$$T_{gen-neg-constant} = Re\{\Lambda_{average}\} Im\{I_{dq-neg}\} - Im\{\Lambda_{average}\} Re\{I_{dq-neg}\}$$

$$\tag{8.64a}$$

with

$$\Lambda_{average} = \frac{1}{2}(\Lambda_{d-neg} + \Lambda_{q-neg}) \tag{8.64b}$$

The oscillatory part is not needed, but could be calculated from

$$T_{gen-neg-oscillatory} = Im\left\{\frac{\Lambda_{q-neg} - \Lambda_{d-neg}}{2} I_{dq-neg} e^{j4\omega t}\right\} \tag{8.65}$$

Identical values for the constant part are obtained from energy balance considerations (ωT = power delivered to network + losses in all windings),

$$\begin{aligned}
\omega T_{gen-neg-constant} = \frac{1}{2}\{&-3|I_{neg}|^2(R_{neg} - R_a) + |I_{f-neg}|^2 R_f + |I_{g-neg}|^2 R_g \\
&+ |I_{D-neg}|^2 R_D + |I_{Q-neg}|^2 R_Q\}
\end{aligned} \tag{8.66}$$

Because 3rd and higher order harmonics are ignored in the armature windings, and 4th and higher order harmonics are ignored in the windings on the field structure, the initial torque values are not exact. They are good approximations, however, as can be seen from Table 8.1. This table compares the values obtained from the initialization equations with the values obtained from a transient simulation (Fig. 8.9), for the severely unbalanced case described in Fig. 8.6. The constant torque from the initialization procedure is almost identical with the average torque of the transient simulation (difference 1.6%). Fig. 8.9 further shows that the initial torque from Eq. (8.73) can be quite different from the average torque. Table 8.1 also compares the values for the 2nd and 4th harmonics (not needed in the initialization, though). The values for the 2nd harmonic agree quite well, but not the values for the smaller 4th harmonic. This is to be expected, because the 4th harmonic torque is influenced by 3rd harmonic currents in the armature windings, which are ignored in this initialization procedure. The average value in Fig. 8.9 lies not exactly halfway between the maximum and minimum values because the 4th harmonic is phase-shifted with respect to the second harmonic.
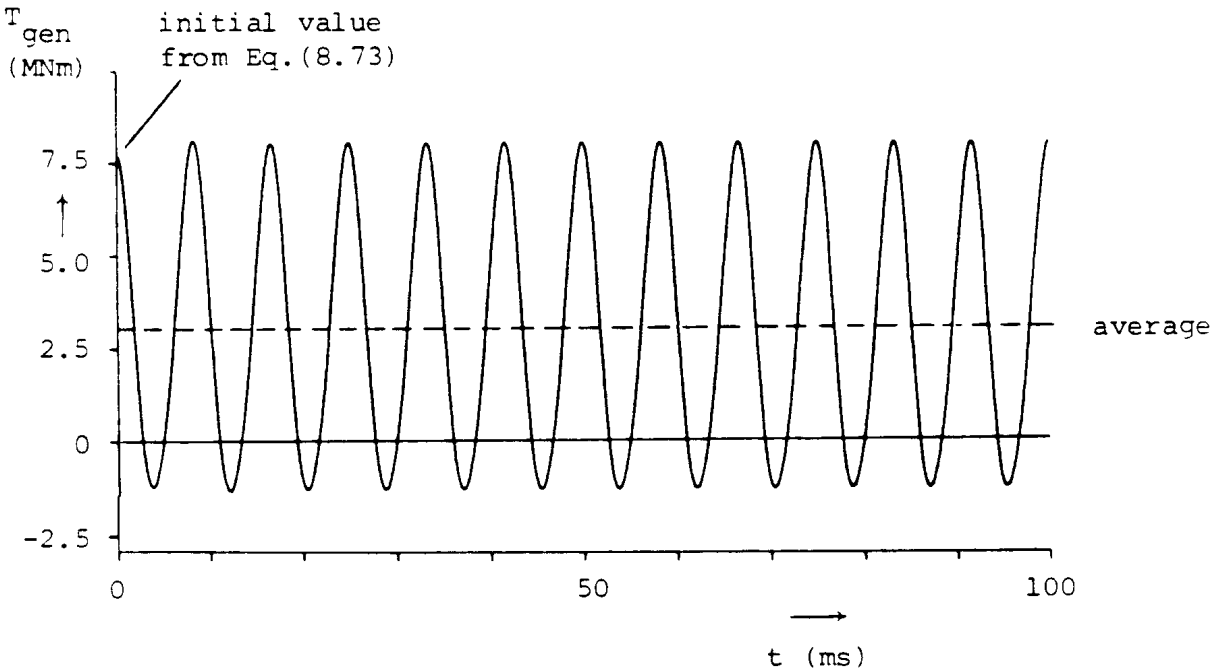
Fig. 8.9 - Torque obtained with transient simulation for case described in Fig. 8.6

Table 8.1 - Electromagnetic torque for test case of Fig. 8.6 ($\Delta t = 46.2963$ μs)

Torque Component	From Equations (MNm)	From Fourier Analysis Between 80 ms and 100 ms (MNm)	Relative Error (%)
average	pos = 2.953 from (8.49) or (8.50) neg = 0.017 from (8.64) or (8.66) ——————— sum = 2.970	3.019	1.62
2nd harmonic	4.673	4.634	0.84
4th harmonic	0.262	0.517	49.32

8.4.3 Initialization with Zero Sequence Values[9]

The initial zero sequence values are easy to obtain, either from the d, q, 0-transformation of Eq. (8.7), or from the symmetrical component transformation of Eq. (8.38). Physically, both are the same quantities, except that

---

[9]The zero sequence currents in the BPA EMTP can be incorrect (see beginning of Section 8.4).

the d, q, 0-transformation is normalized and the symmetrical component transformation chosen in Eq. (8.38) is not. Since the d, q, 0-quantities are normalized,

$$i_0(0) \; = \; \frac{1}{\sqrt{3}} \, (i_a(0) \; + \; i_b(0) \; + \; i_c(0)) \tag{8.67a}$$

or

$$i_0(0) \; = \; \sqrt{3} \, Re \, \{I_{zero}\} \tag{8.67b}$$

The zero sequence quantities do not produce any torque, and therefore do not influence the initialization of the mechanical part.

8.4.4 Initialization of the Mechanical Part[10]

The links between the electrical and the mechanical part are the angle $\beta_{el}(0)$ from Eq. (8.42), which is converted to the mechanical side with Eq. (8.25), and the electromagnetic torques T_{gen} and T_{exc} from Eq. (8.32). For the generator torque, the constant part is

$$T_{gen-constant} \; = \; T_{gen-pos}(0) \; + \; T_{gen-neg-constant} \tag{8.68}$$

on the electrical side, which is converted with Eq. (8.25) to the mechanical side. Since torsional vibrations coming from the oscillating torques of Eq. (8.62) and Eq. (8.65) in unbalanced cases are ignored in the steady-state initializations, the oscillating term is left off in Eq. (8.68). For the exciter torque, the oscillating terms are ignored as well. Then,

$$\omega T_{exc-constant} \; = \; -v_{f-pos}(0) \, i_{f-pos}(0) \; + \; \frac{1}{2} \, |I_{f-neg}|^2 \, R_{exc} \tag{8.69}$$

with I_{f-neg} from Eq. (8.57).

Without torsional vibrations, the speeds of all turbine-generator masses are one and the same, and the acceleration of each mass is zero. Then Eq. (8.29) simplifies to

$$[K] \, [\theta] \; = \; [T_{turbine}] \; - \; [T_{gen/exc}] \; - \; \omega [D_{self}] \tag{8.70}$$

with ω being the synchronous angular speed and $[D_{self}]$ being the diagonal matrix of self-damping terms D_i. The sum of the turbine torques must, of course, equal the sum of the electromagnetic and speed self-damping torques, so that there is zero accelerating torque initially,

$$\sum T_{turbine-i} \; = \; T_{gen-constant} \; + \; T_{exc-constant} \; + \; \omega \sum_i D_i \tag{8.71}$$

---

[10]The initial angles in the BPA EMTP can be incorrect in unbalanced cases, because the negative sequence torques are not included in Eq. (8.68) and (8.69). If Table 8.1 is typical, these torques are very small, however.

Eq. (8.71) is used to find the sum of the turbine torques first, and then to apportion the total to the individual stages from the percentage numbers to be supplied in the input (e.g., 30% of torque in high pressure stage, 26% in intermediate pressure stage, etc.). The right-hand side of Eq. (8.70) is then known, as well as the angle of the generator mass from Eq. (8.32a). [K] is singular. Assume the generator to be mass no. k (with θ_k known); then the remaining initial angles may be found in 2 ways:

(1) Multiply the diagonal element K_{kk} with an arbitrary large number (e.g., 10^{30}), and reset the k-th right-hand side value to this number times θ_k. This will, in effect, change the k-th equation to variable θ_k = specified value of θ_k. Then solve the system of linear equations (8.70), preferably with a subroutine for tri-diagonal matrices (required in the time-step loop anyhow).

(2) Starting to the left of generator mass k, find the angles of the lower-numbered masses recursively from

$$\theta_{i-1} = \theta_i + \frac{\sum_{1}^{i-1} RHS}{K_{i-1,i}}, \quad i = k,\ldots 1 \tag{8.72a}$$

(RHS = right-hand side terms of Eq. (8.70)), and starting to the right of generator mass k, find the angles of the higher-numbered masses recursively from

$$\theta_{i+1} = \theta_i + \frac{\sum_{i+1}^{n} RHS}{K_{i,i+1}}, \quad i = k,\ldots n \tag{8.72b}$$

These recursive equations are derived by summing up rows 1,...i, or by summing up rows i,...n in Eq. (8.70); in either case, most terms on the left-hand side cancel out because of the special structure of [K], as shown after Eq. (8.30).

While the oscillating terms of T_{gen} and T_{exc} are ignored in finding the initial angles of the mechanical part, they must be included in initializing the electromagnetic torques for solving the differential equations in the time-step loop. This is best done using

$$T_{gen-total}(0) = \lambda_d(0) i_q(0) - \lambda_q(0) i_d(0) \tag{8.73}$$

where the currents are

$$i_d(0) = i_{d-pos}(0) + i_{d-neg}(0)$$

$$i_q(0) = i_{q-pos}(0) + i_{q-neg}(0)$$

and the initial fluxes are calculated from Eq. (8.10). Similarly,

$$\omega T_{exc-total}(0) = -v_{f-pos}(0) i_f(0) + R_{exc} \{i_f(0)\}^2 \tag{8.74}$$

where

$$i_f(0) \;=\; i_{f\text{-}pos}(0) \;+\; i_{f\text{-}neg}(0)$$

8.5 Transient Solution

The numerical methods for the transient solution part are based on [13]. The basic idea is to reduce the machine equations to a three-phase Thevenin equivalent circuit, similar to that of Fig. 8.5 for the steady-state initialization. The equivalent circuit for the transient solution differs from Fig. 8.5 mainly in two aspects:

(a)   The impedance matrix [Z] of Fig. 8.5 becomes a resistance matrix [R], after integrating the machine equations (8.9) with the trapezoidal rule of integration, and after reducing the seven equations for all windings to three equations for the armature windings.

(b)   The sinusoidal voltage sources E″ of Fig. 8.5 become instantaneous voltage sources which must be updated from step to step.

The updating procedure for the voltage sources requires the prediction of certain variables from the known solution at t - Δt to the yet unknown solution at t. Different prediction methods have been tried over the years, and their behavior with respect to numerical stability has gradually improved. Some earlier versions of the TYPE-59 synchronous machine model produced too much numerical noise [131], but beginning with version M36, the prediction methods are quite stable and the simulation results are fairly reliable now [132]. Further progress with respect to numerical stability can only be achieved if the overall EMTP algorithm is changed from a direct to an iterative solution in each time step.

8.5.1 Brief Outline of Solution Method

Assume that the solution at t - Δt is already known, and that the solution at t has to be found next. Then the method works roughly as follows:

(1)   Predict the generator rotor angle β(t) (first predicted variable).

(2)   Apply the trapezoidal rule of integration to the R-L branches of Fig. 8.2, in the direct axis as well as in the quadrature axis. Conceptually, this converts each R-L branch into an equivalent resistance in parallel with a known current source, as indicated in Fig. 8.10(a) and (b). The zero sequence consists of only one branch (Fig. 8.10(c)).

(a) d-axis

(b) q-axis

(c) zero sequence
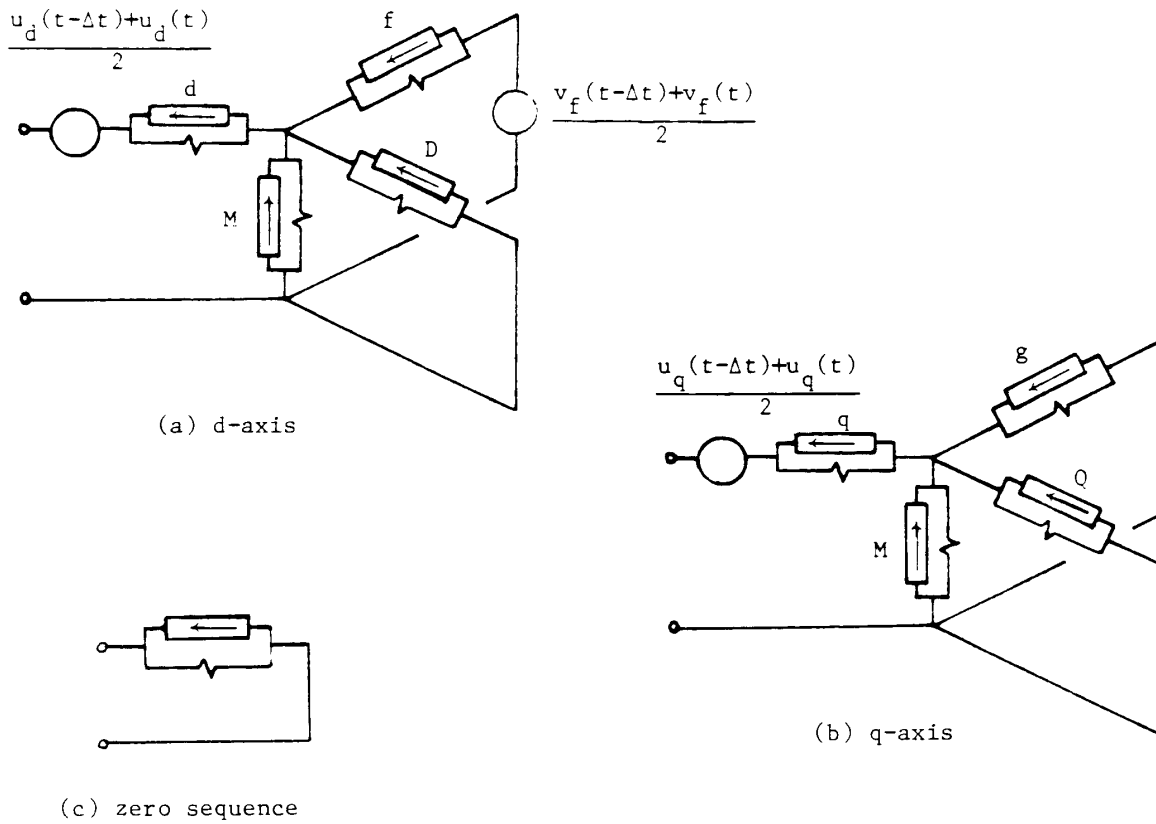
Fig. 8.10 - Resistive networks resulting from trapezoidal rule of integration (u = speed voltages defined in Eq. (8.75))

(3) Reduce the e- and q-axis resistive networks of Fig. 8.10 to one equivalent resistance in series with one equivalent voltage source as shown in Fig. 8.11. For this reduction, assume that $v_f(t) = v_f(t - \Delta t)$, which is exact if the excitation system is not modelled, or use some other prediction (e.g. linear extrapolation).

(a) Direct axis

(b) Quadrature axis

(c) Zero sequence
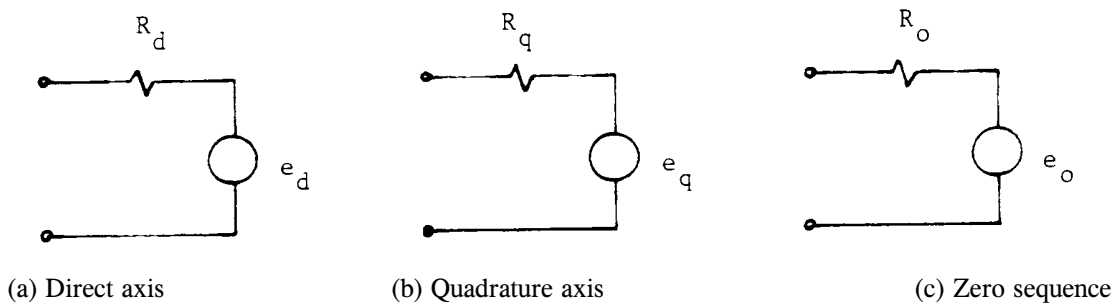
Fig. 8.11 - Resistive networks

Unfortunately, the speed voltages

$$u_d = -\omega \lambda_q$$

8-32

$$u_q = \omega \lambda_d \tag{8.75}$$

at time t are also unknown, but since fluxes can never change abruptly, their values can be predicted reasonably well. With predicted values for $u_d(t)$, $u_q(t)$ and $v_f(t)$ (2nd, 3rd and 4th predicted variable), the reduction is straightforward. Conceptually, branches M, f, D for the d-axis in Fig. 8.10(a) are paralleled, and then connected in series with the c-branch (analogous for the q-axis).

(4)   Convert the 3 resistive Thevenin equivalent circuits for d, q, 0-quantities to phase quantities. If this were done directly, then the resulting 3 x 3 resistance matrix would be time-dependent as well as unsymmetric. To obtain a constant, symmetric matrix, the equivalent resistances of the d- and q-axis are averaged, as indicated in Fig. 8.12, and the "saliency terms" R_d-R_q / 2 • $i_d(t)$ and R_q-R_d / 2 • $i_q(t)$ are combined with the voltage sources e_d and e_q into one voltage source.

(a) direct axis

(b) quadrature axis

(c) zero sequence
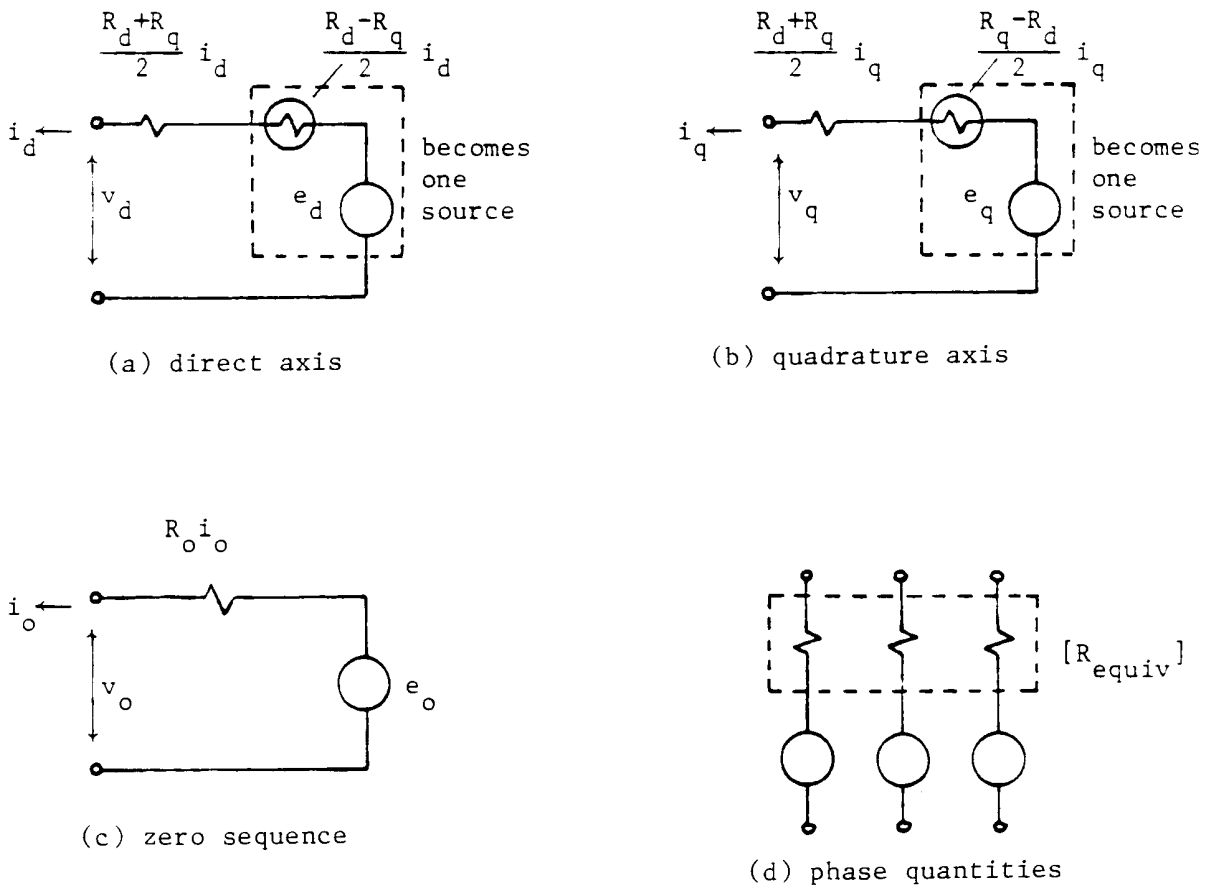
(d) phase quantities

Fig. 8.12 - Modified resistive networks

This can only be done at the expense of having to use a predicted value for $i_d(t)$ and $i_q(t)$ (5th and 6th predicted variable). After conversion to phase quantities, the d, q, 0-networks become one three-phase network, with three source voltages behind a symmetric, constant resistance matrix

[R_equiv].

(5)   Solve the complete network, with the machine representation of Fig. 8.12(d). In the EMTP, current sources in parallel with [R_equiv] are used in place of voltage sources in series with [R_equiv].

(6)   From the complete network solution in phase quantities, extract the generator voltages and convert them to d, q, 0-quantities. Calculate the armature currents in d, q, 0-quantities and the field structure currents, and use them to find the electromagnetic torques of the generator and exciter from Eq. (8.32) at time t. Then solve the equations of the mechanical part.

(7)   Compare the predicted values of β, u_d, u_q, i_d, i_q with the corrected values from the solution of step (6), and repeat steps (6) and (7) if the difference is larger than the acceptable tolerance. When returning to step (6), it is assumed that the terminal voltages in phase quantities remain the same.

(8)   Return to step (1) to find the solution at the next time step.

Some of the implementation details, which have been omitted from this brief outline, are discussed next. Variations of the iteration and prediction methods are described in Section 8.5.4.

8.5.2 Transient Solution of the Electrical Part

Consider the equations for the direct axis first, which are obtained from rows 1, 4, 6 of Eq. (8.9) and from Eq. (8.10a) as

$$
\begin{bmatrix} v_d \\ v_f \\ 0 \end{bmatrix} = -\begin{bmatrix} R_a \\ R_f \\ R_d \end{bmatrix}\begin{bmatrix} i_d \\ i_f \\ i_D \end{bmatrix} - \begin{bmatrix} L_d & M_{df} & M_{dD} \\ M_{df} & L_{ff} & M_{fD} \\ M_{dD} & M_{fD} & L_{DD} \end{bmatrix}\begin{bmatrix} di_d/dt \\ di_f/dt \\ di_D/dt \end{bmatrix} + \begin{bmatrix} u_d \\ 0 \\ 0 \end{bmatrix}
\tag{8.76a}
$$

with u_d being the speed voltage from Eq. (8.75), or in short-hand notation,

$$
[v] = -[R][i] - [L]\left[\frac{di}{dt}\right] + [u]
\tag{8.76b}
$$

Because of numerical noise problems in pre-M32 versions of the BPA EMTP, this equation is integrated with the "damped trapezoidal rule" of Section 2.2.2[11], with a damping resistance matrix $[R_p]$ in parallel with $[L]$,

$$
[R_p] = \frac{1 + \alpha}{1 - \alpha} \cdot \frac{2}{\Delta t} [L]
\tag{8.77}
$$

where α is the reciprocal of the damping factor defined in Eq. (2.21). For $\alpha = 1$ there is no damping, while $\alpha = 0$ is the critically damped case. In the present version of the BPA EMTP, a default value of $(1 + \alpha)/(1 - \alpha) = 100$ is used.

---

[11]The (unreleased) UBC version with synchronous machines uses the normal trapezoidal rule. By setting α = 1 in the input, the BPA EMTP would use the normal trapezoidal rule as well.

Applying the damped trapezoidal rule of Eq. (2.20) for v = L di/dt to Eq. (8.76), with v replaced by [u] - [v] - [R][i], results in

$$[v(t)] = [u(t)] + [hist(t - \Delta t)] - \left\{ [R] + \frac{1 + \alpha}{\Delta t} [L] \right\} [i(t)] \qquad (8.78a)$$

with the known history term

$$[hist(t - \Delta t)] = \left\{ - \alpha [R] + \frac{1 + \alpha}{\Delta t} [L] \right\} [i(t - \Delta t)] - \alpha [v(t - \Delta t)] + \alpha [u(t - \Delta t)] \qquad (8.78b)$$

Eq. (8.78a) described a voltage source [u(t)] + [hist(t - Δt)] behind a resistance matrix

$$[R_{comp}] = [R] + \frac{1 + \alpha}{\Delta t} [L] \qquad (8.79)$$

Subscript "comp" is used because such equivalent resistive networks are called "resistive companion models" in network theory [133].

For interfacing the synchronous machine equations with the network equations, the field structure quantities are eliminated from Eq. (8.78). Dropping subscript "comp" and using subscripts d, f, D again, the field structure currents can be expressed from the last two rows of Eq. (8.78a) with [R$_{comp}$] from Eq. (8.79) as

$$\begin{bmatrix} i_f(t) \\ i_D(t) \end{bmatrix} = \begin{bmatrix} R_{ff} & R_{fD} \\ R_{fD} & R_{DD} \end{bmatrix}^{-1} \left[\begin{bmatrix} hist_f(t - \Delta t) \\ hist_D(t - \Delta t) \end{bmatrix} - \begin{bmatrix} v_f(t) \\ 0 \end{bmatrix} - \begin{bmatrix} R_{df} \\ R_{dD} \end{bmatrix} i_d(t) \right] \qquad (8.80)$$

which, when inserted into the first row of Eq. (8.78a), produces a single equation for the d-axis,

$$v_d(t) = e_d - R_d i_d(t) \qquad (8.81)$$

with the reduced companion resistance

$$R_d = R_{dd} - [R_{df} \quad R_{dD}] \begin{bmatrix} R_{ff} & R_{fD} \\ R_{fD} & R_{DD} \end{bmatrix}^{-1} \begin{bmatrix} R_{df} \\ R_{dD} \end{bmatrix} \qquad (8.82a)$$

the voltage source

$$e_d = u_d(t) + hist_d^{red}(t - \Delta t) \qquad (8.82b)$$

and the reduced history term

$$hist_d^{red} = hist_d - [R_{df} \quad R_{dD}] \begin{bmatrix} R_{ff} & R_{fD} \\ R_{fD} & R_{DD} \end{bmatrix}^{-1} \begin{bmatrix} hist_f - v_f(t) \\ hist_D \end{bmatrix} \qquad (8.82c)$$

By predicting the speed voltage $u_d(t) = -\omega(t)\lambda_q(t)$, and by assuming that $v_f(t) = v_f(t - \Delta t)$, the simple resistive network of Fig. 8.11(a) is obtained, with a voltage source e_d behind the companion resistance R_d. If $R << 2L/\Delta t$ in all R-L branches of Fig. 8.10(a), then

$$R_d \approx \frac{2 L_d^{//}}{\Delta t} \tag{8.83a}$$

Therefore, Eq. (8.81) essentially represents the trapezoidal rule solution of a voltage source behind the subtransient reactance $X_d"$. In publications based on [13]. R_d is called a_{11}.

If the dynamic behavior of the excitation system is to be simulated as well, then using $v_f(t) = v_f(t - \Delta t)$ implies a one time-step delay in the effect of the excitation system on the machine. Such a delay is usually acceptable, because Δt is typically much smaller than the effective time constant between the input and output of the excitation systems. Alternatively, some type of prediction could be used for $v_f(t)$.

The derivations for the q-axis are obviously analogous to those just described for the d-axis, and lead to the single equation for the q-axis,

$$v_q(t) = e_q - R_q i_q(t) \tag{8.84}$$

with the voltage source

$$e_q = u_q(t) + hist_q^{red}(t - \Delta t) \tag{8.85}$$

Here, only the speed voltage $u_q(t) = \omega(t)\lambda_d(t)$ must be predicted because the voltage v (t) is zero. The q-axis resistive network is shown in Fig. 8.11(b). Again, if $R << 2L/\Delta t$ in all R-L branches of Fig. 8.10(b), then

$$R_q \approx \frac{2 L_q^{//}}{\Delta t} \tag{8.83b}$$

Therefore, Eq. (8.84) essentially represents the trapezoidal rule solution of a voltage source behind the subtransient reactance $X_q"$. In publications based on [13], R_q is called a_{22}.

The equations for the zero sequence quantities (row 3 in Eq. (8.9) and Eq. (8.10c)) are also integrated with the damped trapezoidal rule, which leads to

$$v_0(t) = hist_0(t - \Delta t) - R_0 i_0(t) \tag{8.86a}$$

with the companion resistance

$$R_0 = R_a + \frac{1 + \alpha}{\Delta t} L_0 \tag{8.86b}$$

and the known history term

$$hist_0(t - \Delta t) = \left(\frac{1 + \alpha}{\Delta t} L_0 - \alpha R_a \right) i_0(t - \Delta t) - \alpha v_0(t - \Delta t) \tag{8.86c}$$

The zero sequence resistive network of Eq. (8.86a) with $e_0 = hist_0(t - \Delta t)$ is shown in Fig. 8.11(c). In publications based on [13]. R_0 is called a_{33}.

The reduced generator equations (8.81), (8.84) and (8.86a) can be solved in one of two ways:

(1)   Find a three-phase Thevenin equivalent circuit (resistive companion model) for the network seen from the generator terminals, and solve it together with the generator equations.

(2)   Add the reduced generator equations to the network equations, and solve them simultaneously.

The first approach was used in [98]. It has the advantage that iterations can easily be implemented for the correction of predicted values. However, generator must be separated by distributed-parameter lines with travel time for reasons of numerical efficiency, so that an independent three-phase Thevenin equivalent circuit can be generated for each generator (otherwise, M generators would have to be interfaced with one 3 x M-phase Thevenin equivalent circuit). If there are no such lines in reality, artificial stub-lines with $\tau = \Delta t$ must be used to separate the generators. This can result in incorrect answers. For this reason, the first approach has been abandoned in the EMTP.

With the second approach, there is no restriction on the number of generators connected to the network, or even to the same bus. However, it does require the prediction of certain variables, which makes this approach more sensitive to the accumulation of prediction errors. It is the only method retained in the present BPA EMTP, and only this method is discussed here. To solve the generator equations with the network equations, the generator resistive networks of Fig. 8.12 in d, q, 0-quantities must be converted to phase quantities, which produces a time-dependent and unsymmetric 3 x 3 resistance matrix. To accommodate such matrices would have required a complete restructuring of the basic (non-iterative) solution algorithm of the EMTP. Instead, an average resistance

$$R_{av} = (R_d + R_q)/2 \tag{8.87}$$

is used on both axes. This requires "saliency terms" $i_d(R_d - R_q)/2$ on the d-axis and $i_q(R_q - R_d)/2$ on the q-axis, which are added to the known voltage sources e_d, e_q by using predicted values for i_d, i_q (Fig. 8.12). For generators with $X_d" = X_q"$, these saliency terms are practically negligible. For the IEEE benchmark model [74] with different values of $X_d" = 0.135$ p.u. and $X_q" = 0.200$ p.u., the companion resistances are $R_d = 3.5844$ p.u. and $R_q = 5.3103$ p.u. for $\Delta t = 200$ μs. These values are practically identical with $2L_d"/\Delta t = 3.5810$ p.u. and $2L_q"/\Delta t = 5.3052$ p.u., as mentioned in Eq. (8.83). The voltage drop across the saliency terms $(R_d - R_q)/2$ would be 20% of the voltage drop across $(R_d + R_q)/2$ with $\Delta t = 200$ μs.

With the average resistance of Eq. (8.87), the modified equations in d, q, 0-quantities become

$$\begin{bmatrix} v_d(t) \\ v_q(t) \\ v_0(t) \end{bmatrix} = \begin{bmatrix} e_{d\text{-mod}} \\ e_{q\text{-mod}} \\ e_0 \end{bmatrix} - \begin{bmatrix} R_{av} & & \\ & R_{av} & \\ & & R_0 \end{bmatrix} \begin{bmatrix} i_d(t) \\ i_q(t) \\ i_0(t) \end{bmatrix} \tag{8.88a}$$

where

$$e_{d\text{-mod}} = e_d - \frac{R_d - R_q}{2} i_d(t) \tag{8.88b}$$

$$e_{q\text{-mod}} = e_q + \frac{R_d - R_q}{2} i_q(t) \tag{8.88c}$$

Predicted values i_d, i_q are used in the last two equations, and the voltage sources behind resistances are then converted into current sources in parallel with the resistances,

$$i_{d\text{-source}} = \frac{1}{R_{av}} e_{d\text{-mod}} \tag{8.89a}$$

$$i_{q\text{-source}} = \frac{1}{R_{av}} e_{q\text{-mod}} \tag{8.89b}$$

$$e_{0\text{-source}} = \frac{1}{R_0} e_0 \tag{8.89c}$$

Finally, the d, q, 0-quantities are converted to phase quantities with a predicted angle $\beta(t)$, which produces a resistive companion model with current sources

$$
\begin{bmatrix} i_{1\text{-source}} \\ i_{2\text{-source}} \\ i_{3\text{-source}} \end{bmatrix} = \frac{\sqrt{2}}{\sqrt{3}} \begin{bmatrix} \cos\beta & \sin\beta & \frac{1}{\sqrt{2}} \\ \cos(\beta-120°) & \sin(\beta-120°) & \frac{1}{\sqrt{2}} \\ \cos(\beta+120°) & \sin(\beta+120°) & \frac{1}{\sqrt{2}} \end{bmatrix} \begin{bmatrix} i_{d\text{-source}} \\ i_{q\text{-source}} \\ i_{0\text{-source}} \end{bmatrix} \tag{8.90}
$$

and parallel with

$$
[R_{equiv}] = \begin{bmatrix} R_s & R_m & R_m \\ R_m & R_s & R_m \\ R_m & R_m & R_s \end{bmatrix} \tag{8.91a}
$$

where

$$R_s = (R_0 + 2R_{av})/3 , \qquad R_m = (R_0 - R_{av})/3 \tag{8.91b}$$

Since this model is identical with the resistive companion model of Eq. (3.8) for coupled inductances, generators are interfaced with the network equations as if they were coupled inductances. The matrix $[R_{equiv}]^{-1}$ enters the nodal conductance matrix [G] of Eq. (1.8) once and for all outside the time step loop, while the parallel current sources are updated from step to step.

After the complete network solution has been obtained at time t, the generator phase voltages are converted

to d, q, 0-quantities,

$$
\begin{bmatrix} v_d \\ v_q \\ v_0 \end{bmatrix} = \frac{\sqrt{2}}{\sqrt{3}} \begin{bmatrix} \cos\beta & \cos(\beta-120°) & \cos(\beta+120°) \\ \sin\beta & \sin(\beta-120°) & \sin(\beta+120°) \\ 1\sqrt{2} & 1\sqrt{2} & 1\sqrt{2} \end{bmatrix} \begin{bmatrix} v_1 \\ v_2 \\ v_3 \end{bmatrix} \tag{8.92}
$$

and the armature currents are found from

$$
i_d = (e_{d\text{-mod}} - v_d)/R_{av}
$$
$$
i_q = (e_{q\text{-mod}} - v_q)/R_{av} \tag{8.93}
$$
$$
i_0 = (e_0 - v_0)/R_0
$$

The field structure currents are recovered from Eq. (8.80) for the d-axis, and from an analogous equation for the q-axis. Finally, the fluxes λ_d, λ_q are calculated from Eq. (8.10a) and (8.10b), and the electromagnetic torques from Eq. (8.32), which are then used to solve the mechanical equations as described next.

8.5.3 Transient Solution of the Mechanical Part

The mechanical part is described by Eq. (8.29), which can be rewritten as

$$
[J]\begin{bmatrix} \dfrac{d\omega}{dt} \end{bmatrix} + [D][\omega] + [K][\theta] = [T_{net}] \tag{8.94a}
$$

with the speeds of the system of masses

$$
[\omega] = \begin{bmatrix} \dfrac{d\theta}{dt} \end{bmatrix} \tag{8.94b}
$$

and the net torque

$$
[T_{net}] = [T_{turbine}] - [T_{gen/exc}] \tag{8.94c}
$$

The torque $[T_{gen/exc}]$ provides the only direct link with the electrical part, with another indirect link through $\theta_{gen} = \beta$ which had to be predicted to solve the electrical part.

Applying the trapezoidal rule (or central difference quotients) to Eq. (8.94a) and (8.94b) yields

$$
[J]\frac{[\omega(t)] - [\omega(t-\Delta t)]}{\Delta t} + [D]\frac{[\omega(t)] + [\omega(t-\Delta t)]}{2} + [K]\frac{[\theta(t)] + [\theta(t-\Delta t)]}{2}
$$

$$= \frac{[T_{net}(t)] + [T_{net}(t-\Delta t)]}{2} \tag{8.95}$$

and

$$\frac{[\omega(t)] + [\omega(t-\Delta t)]}{2} = \frac{[\theta(t)] - [\theta(t-\Delta t)]}{\Delta t} \tag{8.96}$$

Replacing $[\theta(t)]$ in Eq. (8.95) with the expression from Eq. (8.96) produces

$$\left\{\frac{2}{\Delta t}[J] + [D] + \frac{\Delta t}{2}[K]\right\}[\omega(t)] = [T_{net}(t)] + [hist(t-\Delta t)] \tag{8.97a}$$

with the known history term

$$[hist(t-\Delta t)] = \left\{\frac{2}{\Delta t}[J] - [D] - \frac{\Delta t}{2}[K]\right\}[\omega(t-\Delta t)] - 2[K][\theta(t-\Delta t)]$$
$$+ [T_{net}(t-\Delta t)] \tag{8.97b}$$

Normally, it is assumed that the turbine power is constant. In that case, the torque on each mass i is calculated by using predicted speeds ω_i,

$$T_{turbine,i} = \frac{P_{turbine,i}}{\omega_i} \tag{8.98}$$

If constant turbine torque is assumed, then Eq. (8.98) is skipped. With the turbine torques from Eq. (8.98), and with the electromagnetic torques at time t already calculated in the electrical part, Eq. (8.97a) can be solved directly for the speeds $[\omega(t)]$. The matrices

$$[A] = \frac{2}{\Delta t}[J] + [D] + \frac{\Delta t}{2}[K] \quad and \quad [B] = \frac{2}{\Delta t}[J] - [D] - \frac{\Delta t}{2}[K]$$

are tridiagonal, and remain constant from step to step. They are triangularized once and for all before entering the time step loop, with a Gauss elimination subroutine specifically written for tridiagonal matrices, which saves storage as well as computer time. Inside the time step loop, the information in the triangularized matrix is used to apply the elimination to the right-hand sides, followed by backsubstitution ("repeat solution," as explained in Section III.1).

It is worth noting that the form of Eq. (8.94) is the same as the system of branch equations for coupled R-L-C branches. In that analogy, the matrix [J] is equivalent to a matrix [L] of uncoupled inductances, the matrix [D]

to a matrix [R] of coupled resistances, and the matrix [K] to an inverse capacitance matrix $[C]^{-1}$ of coupled capacitances. $[T_{net}]$ would be equivalent to the derivatives [dv/dt] of the applied branch voltages.

8.5.4 Prediction and Correction Schemes

The synchronous machine code in the EMTP has undergone many changes, especially with respect to the prediction and correction schemes. The presently used schemes, as well as variations of it, are summarized here.

8.5.4.1 Prediction of ω and β

The speeds of all masses are predicted with linear extrapolation,

$$[\omega(t)] = 2[\omega(t - \Delta t)] - [\omega(t - 2\Delta t)] \tag{8.99}$$

Since the speeds change slowly, in comparison with the electrical quantities, this prediction should be accurate enough. Predicted speeds are needed in two places, namely for the prediction of speed voltages (see Section 8.5.4.3), and for the calculation of turbine torques from Eq. (8.98). The accuracy of the predicted generator rotor speed ω_{gen} is more important because there is no speed voltage correction in the present iteration scheme. The accuracy of the turbine rotor speeds prediction is less important, because the torque calculations Eq. (8.98) are corrected in the iteration scheme of Section 8.5.1, if constant turbine power is assumed (default option in UBC EMTP, only option in BPA EMTP). If constant turbine torque is assumed, then the turbine speed predictions are not needed at all.

Fig. 8.13 shows the speed and the electromagnetic torque of a generator by itself (no turbine connected to it), which runs unloaded at synchronous speed and is then switched into a resistance load at t = 0 [134] (data in Table 8.2). The generator slows down very quickly in this case. The curves were obtained with the UBC EMTP without iterations (no return from step 7 to 6 in Section 8.5.1), and verified with a 4th-order Runge-Kutta-Merson method (agreement to within 4 digits). Both the UBC and BPA EMTP had bugs in the speed calculation, which were not noticed before in cases of small speed changes. They were corrected after J. Mechenbier proved their existence by using principles of energy conservation as suggested by H. Boenig and S. Ranade [134].

The angle β of the generator rotor must be predicted so that the d, q, 0-networks of Fig. 8.12 can be converted to phase quantities for the complete network solution in step 5 of Section 8.5.1. There is no correction for this conversion in the present iteration scheme. The angle β is also needed for converting the voltage solution back from phase to d, q, 0-quantities in step 6 of Section 8.5.1; here, corrected values are obtained from the solution of the mechanical part if steps (6) and (7) are iterated.
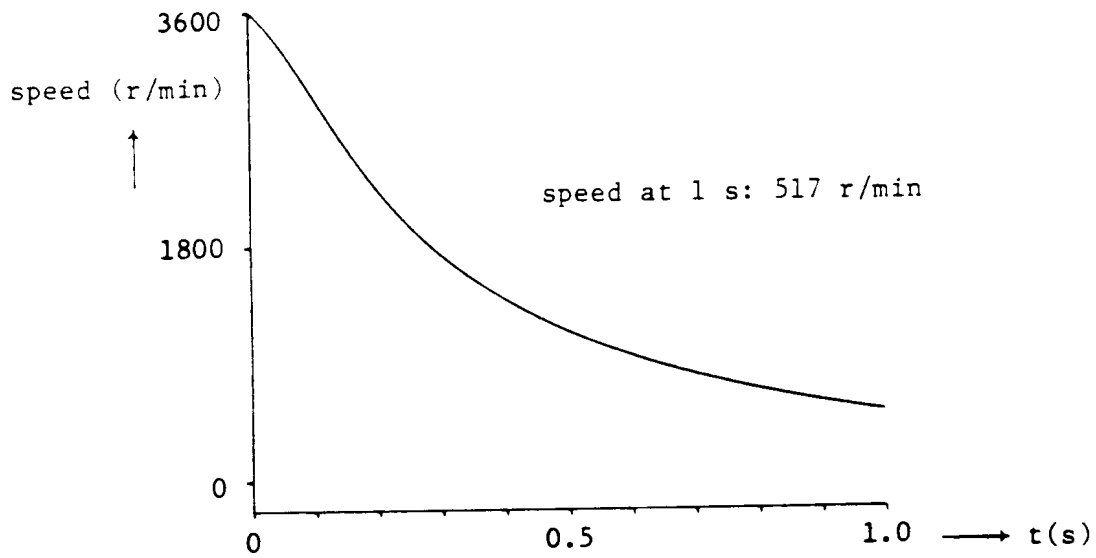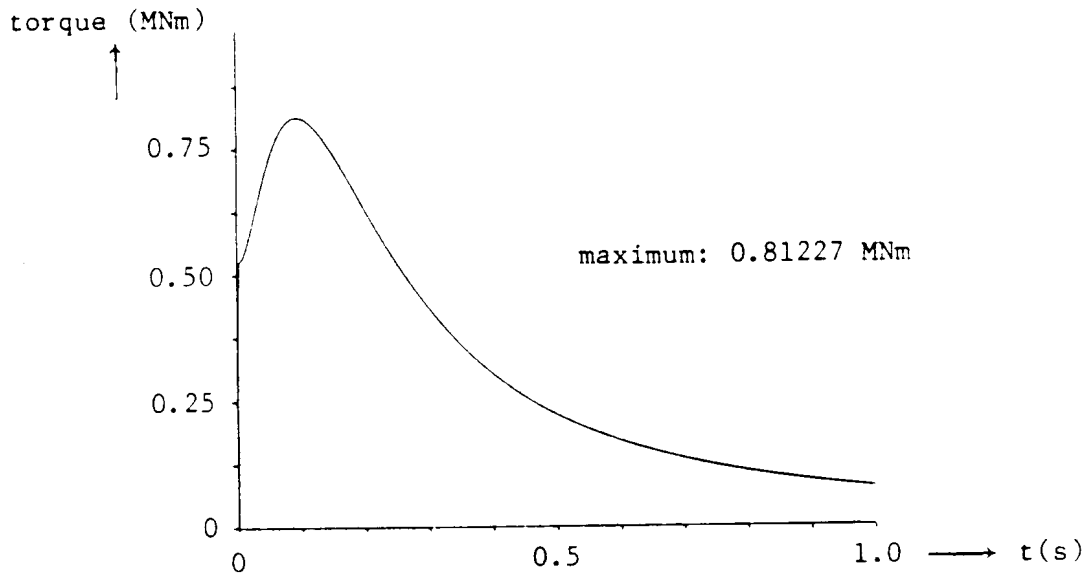
Fig. 8.13 - Speed and electromagnetic torque of an unloaded generator when switched into a resistance load. (a) Speed, (b) Electromagnetic torque.

In the UBC EMTP, the predicted value for β is calculated from the predicted speed ω_{gen} with the trapezoidal rule of integration (8.96),

$$\beta(t) = \beta(t - \Delta t) + \frac{\Delta t}{2} \{\omega_{gen}(t - \Delta t) + \omega_{gen}(t)\} \qquad (8.100)$$

M36 and later versions of the BPA EMTP use a predictor formula suggested by Kulicke [135], which is based on the assumption that β is a fourth-order polynomial of t,

$$\beta = a_0 + a_1 t + a_2 t^2 + a_3 t^3 + a_4 t^4 \tag{8.101}$$

By using three known values of β at t - Δt, t - 2Δt, t - 3Δt, and two known values of the speed

$$\omega = \frac{d\beta}{dt} = a_1 + 2a_2 t + 3a_3 t^2 + 4a_4 t^3 \tag{8.102}$$

at t - Δt, t - 2Δt, the coefficients $a_0,\ldots a_4$ can be found from the solution of 5 linear equations. This is a Hermite interpolation formula and leads to the predictor formula [7; p. 184, P6 in Table 5.1]

$$\beta(t) = -9\{\beta(t-\Delta t) - \beta(t-2\Delta t)\} + \beta(t-3\Delta t) + 6\Delta t\{\omega_{gen}(t-\Delta t) + \omega_{gen}(t-2\Delta t)\} \tag{8.103}$$

Table 8.2 - Generator test case no. 1 [134]

Ratings:	160 MVA (three-phase), 15 kV (line-to-line), wye-connected.
Reactances:	X_d = 1.7 p.u., X_d' = 0.245 p.u., X_d'' = 0.185 p.u.
	X_q = 1.64 p.u., X_q'' = 0.185 p.u. (no g-winding)
	X_l = 0.15 p.u., X_O = 0.14 p.u.
Time constants:	T_{do}' = 5.9 s, T_{do}'' = 0.03046 s
	T_{qp}'' = 0.075 s
Resistances:	R_a = 0.001096 p.u.
	R_{load} = 10^8 Ω in steady state (no effect; added because some versions cannot handle isolated generator)
	R_{load} = 1 Ω after switching at t = 0
Moment of inertia:	J = 999.947 (N-m)s^2. One pole pair.
Terminal voltage:	V_1 = 12.247 $e^{j216°}$ kV (peak) in steady state in phase 1 (symmetrical in 3 phases).
Step size	Δt = 200 μs. f = 60 Hz

With coefficients $a_0,\ldots a_4$ known, a predictor formula for ω_{gen} = dβ/dt for use in the speed voltages could be written down with Eq. (8.102) as well,

$$\Delta t\,\omega(t) = 14\,\Delta t\,\omega(t-\Delta t) + 17\,\Delta t\,\omega(t-2\Delta t) - 27\,\beta(t-\Delta t) + 24\beta(t-2\Delta t)$$

$$+ 3\beta(t-3\Delta t) \tag{8.104}$$

The BPA EMTP uses the predicted speed from Eq. (8.99), though. It is not clear whether the 4th order predictor of Eq. (8.103) is really superior to the predictor of Eq. (8.99).

### 8.5.4.2. Averaging of d- and q-Axis Companion Resistances

Instead of an average resistance (R_d + R_q_/2 in Fig. 8.12, the M39 version of the BPA EMTP uses R_d on both d- and q-axes. To compensate for this, a term (R_q-R_d) $\bullet$ i_q is added to the voltage source on the q-axis, and no compensating term is needed on the d-axes. Whether this method is better than the averaging procedure of Fig. 8.12 is unclear. Both procedures are special cases of a class of averaging methods discussed in [136].

8.5.4.3. Prediction of i_d, i_q

The armature currents i_d, i_q must be predicted so that the saliency terms $i_d(R_d$-$R_q)/2$ and $i_q(R_q$-$R_d)/2$ can be combined with the known voltage sources e_d, e_q (Fig. 8.12). No correction is made for this in the present iteration scheme. Note that the saliency terms are practically zero if $X_q" = X_d"$. In the UBC version and in BPA versions until M32, the predicted currents i_d, i_q are also used to find predicted speed voltages, as described in the next section. In the UBC EMTP, linear extrapolation is used,

$$i(t) = 2i(t - \Delta t) - i(t - 2\Delta t) \qquad (8.105)$$

where "i" is either i_d or i_q. The BPA version uses a linear three-point predictor formula which smoothes numerical oscillations. With the current known at t - Δt, t - 2Δt and t - 3Δt as
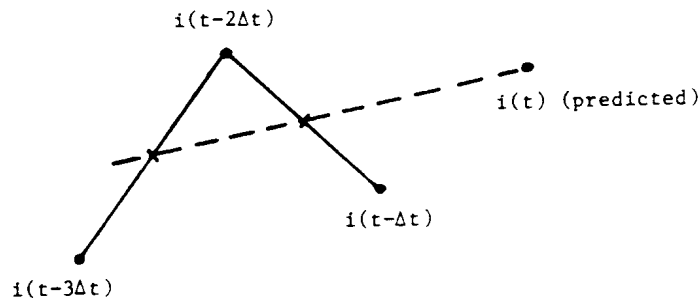
Fig. 8.14 - Linear prediction with smoothing

indicated in Fig. 8.14, averaged values are first found at the two midpoints by linear interpolation

$$i(t - 2\frac{1}{2}\Delta t) = \frac{i(t - 3\Delta t) + i(t - 2\Delta t)}{2}$$

$$i(t - 1\frac{1}{2}\Delta t) = \frac{i(t - 2\Delta t) + i(t - \Delta t)}{2}$$

Then a straight line is drawn through the two midpoints, with a slope of

$$slope = \frac{i(t - \Delta t) - i(t - 3\Delta t)}{2\,\Delta t}$$

to predict the current i(t),

$$i(t) = \frac{5}{4}i(t - \Delta t) + \frac{1}{2}i(t - 2\Delta t) - \frac{3}{4}i(t - 3\Delta t) \qquad (8.106)$$

This linear prediction with smoothing is conceptually similar to fitting a straight line through three points in the least squares sense. Such a straight line least square fitting would have the same slope, but a value at t - 2Δt of {i(t - 3Δt) + i(t - 2Δt) + i(t - Δt)}/3 instead of {i(t - 3Δt) + 2i(t - 2Δt) + i(t - Δt)}/4 in Fig. 8.14, which would yield a predictor

$$i(t) = \frac{4}{3}i(t - \Delta t) + \frac{1}{3}i(t - 2\Delta t) - \frac{2}{3}i(t - 3\Delta t) \qquad (8.107)$$

Which predictor performs best is difficult to say. All predictor formulas discussed in this section depend solely on past points, and not on the form of the differential equations for i_d, i_q. Eq. (8.76), and an analog equation for the q-axis, were tried at one time as Euler predictor formulas, but they performed worse than the predictors discussed here. It might be worth exploring other predictor formulas, because the accuracy of the solution depends primarily on the prediction of i_d, i_q, especially if the speed voltages are calculated from i_d, i_q as well, as discussed in the next section. One could use Eq. (8.103), for example, by replacing β with i and ω with di/dt calculated from Eq. (8.76).

Fig. 8.15 shows the current in phase 1 after a three-phase short-circuit of a generator with unrealistically low armature resistance R_a = 0.0001 p.u. The data for this case is summarized in Table 8.3. Since speed changes were ignored, the only predicted values are i_d, i_q, as well as speed voltages in the BPA EMTP.
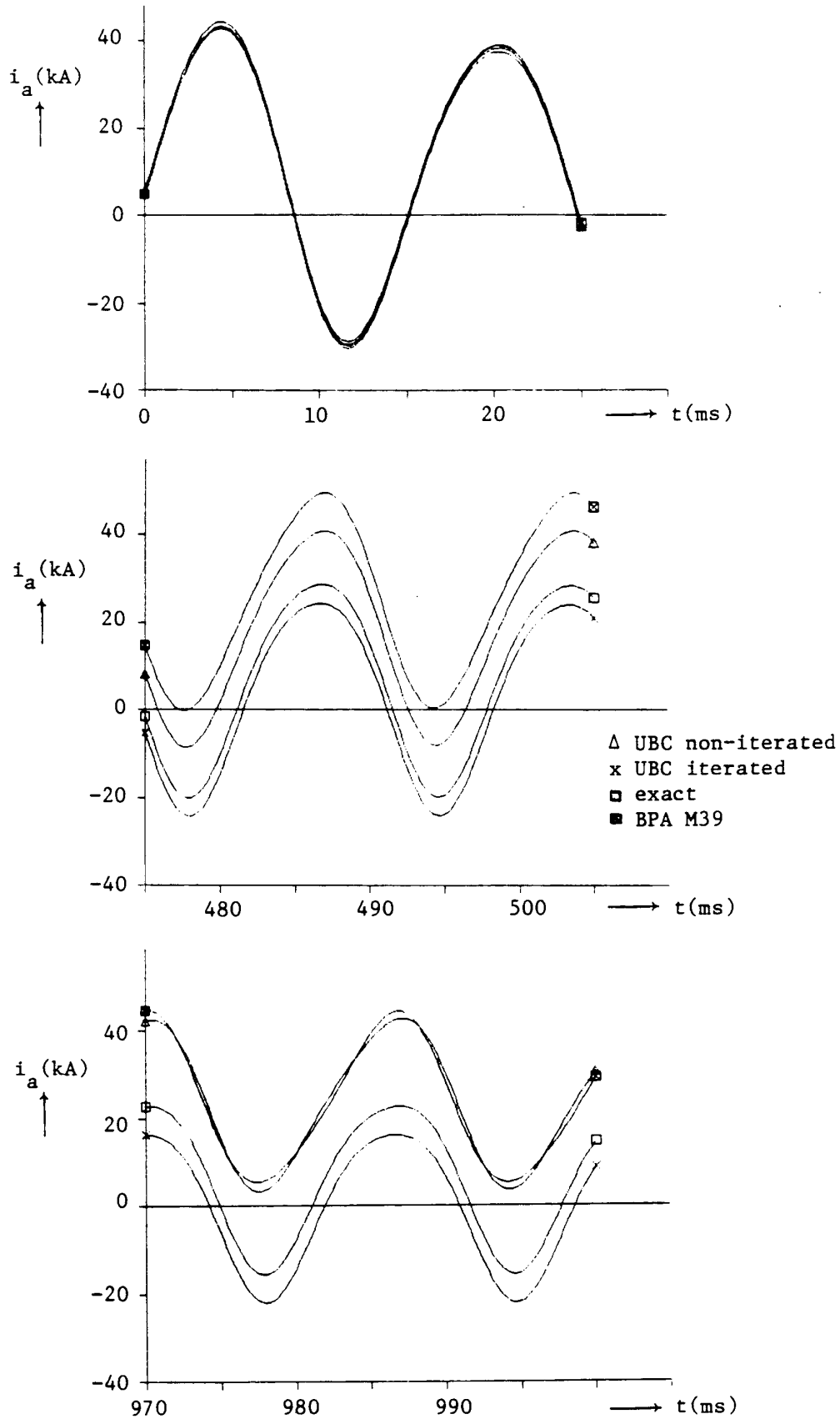
Fig. 8.15 - Current in phase 1 after a three-phase short-circuit. $R_a = 0.0001$ p.u.

Table 8.3 - Generator test case no. 2

Ratings:	400 MVA (three-phase), 18 kV (line-to-line), wye-connected
Reactances:	X_d = 0.92 p.u., X_d' = 0.18 p.u., X_d'' = 0.161 p.u.
	X_q = 0.748 p.u., X_q'' = 0.161 p.u. (no g-winding)
	X_ℓ = X_O = 0.082 p.u.
Time constants:	T_{do}' = 6.6 s, T_{do}'' = 0.05 s
	T_{qO}'' = 0.05 s
Resistances:	R_a = 10^{-4} p.u. (unrealistically low value)
	R_a = 10^{-3} p.u. (more realistic value)
	R_{load} = 1 Ω
Moment of inertia:	J = ∞ (constant speed)
Terminal voltage:	V_1 = 4.926 $e^{j \cdot 7.391°}$ kV (peak) in steady state in phase 1 (symmetrical in 3 phases).
Step size	Δt = 200 μs. f = 60 Hz
Disturbance:	Three-phase short-circuit at terminals at t = 0

In such a case with low damping, the errors caused by the prediction do accumulate noticeably if the simulation runs over 5000 steps to t_{max} = 1 s. The errors are decreased if the complete network solution is iterated (not yet available as an option in the production codes of the EMTP). For comparison purposes, the exact solution is shown as well, which was found for i_d, i_q, with the eigenvalue/eigenvector method discussed in Appendix I.1, and then transformed to phase quantities with β from Eq. (8.23). Fig. 8.16 shows the results if the armature resistance is changed to a more realistic value of R_a = 0.001 p.u. As can be seen, the answers are now closer to the exact solution.

8.5.4.4. Prediction of Speed Voltages

Starting with M32 of the BPA EMTP, the speed voltages u_d, u_q of Eq. (8.75) are predicted in the same way as i_d, i_q with Eq. (8.106). In some of these versions, the prediction was done in a synchronously rotating reference frame, and then converted directly to phase quantities without going through d, q-axes parameters. This has been abandoned in Feb. 1986, and the speed voltages are now again predicted in d, q-quantities because the latter turned out to be superior when applied to test case no. 1 of Table 8.2.
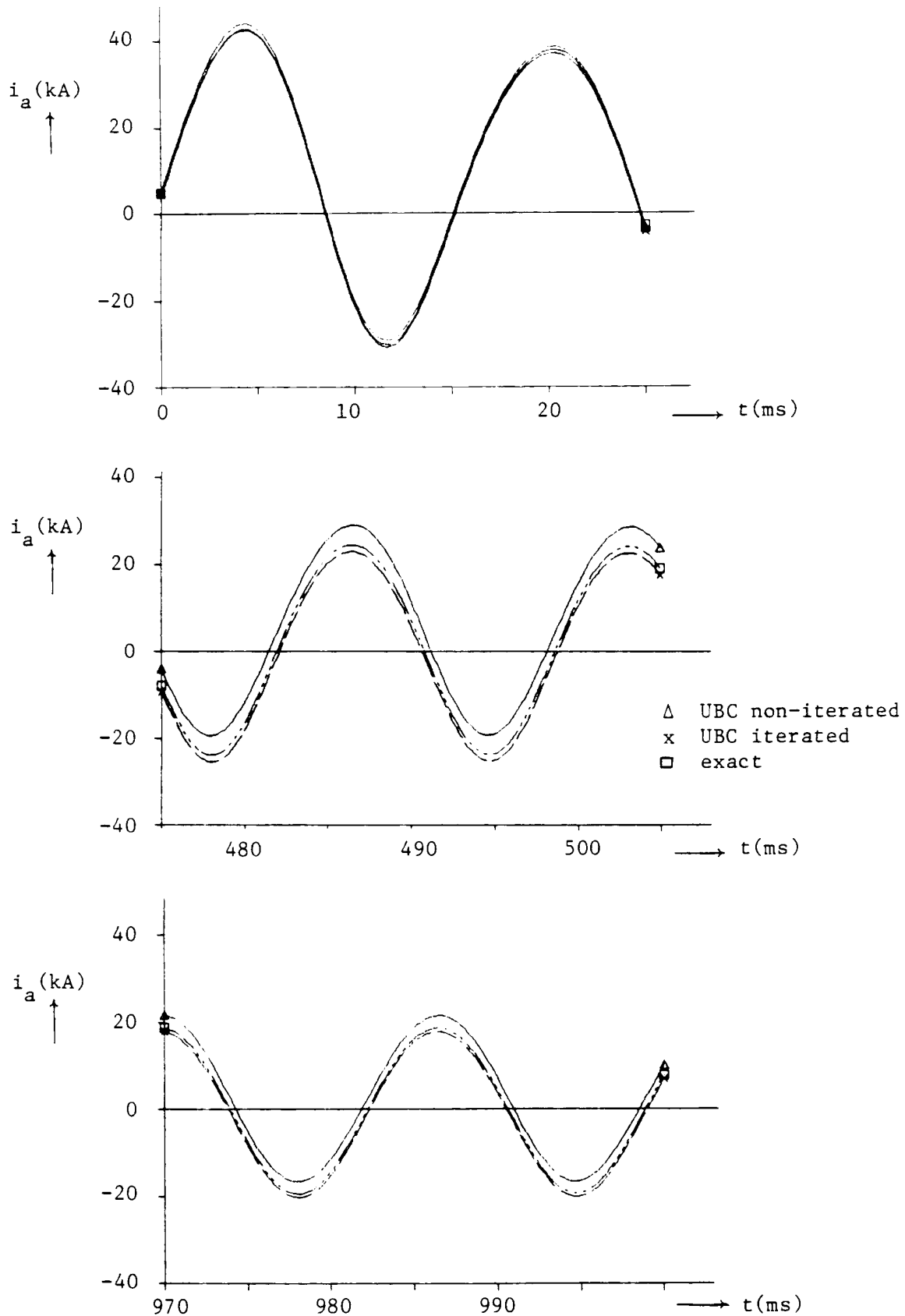
Fig. 8.16 - Current in phase 1 after a three-phase short-circuit. $R_a = 0.001$ p.u.

In pre-M32 versions of the BPA EMTP, and in the (unreleased) UBC version with synchronous machines, the speed voltages $u_d = -\omega\lambda_q$ and $u_q = \omega\lambda_d$ are not predicted explicitly. Instead, the predicted currents $i_d(t)$, $i_q(t)$ and the predicted speed $\omega_{gen}(t)$ are used to calculate the speed voltages from Eq. (8.10a) and (8.10b). The field structure currents appearing in these equations are expressed as a function of i_d with Eq. (8.80), which leads to the expression

$$\lambda_d(t) = L_d^{reduced} i_d(t) + \lambda_{d-0} \tag{8.108}$$

with the known reduced inductance

$$L_d^{reduced} = L_d - [L_{df} \ L_{dD}] \begin{bmatrix} R_{ff} & R_{fD} \\ R_{fD} & R_{DD} \end{bmatrix}^{-1} \begin{bmatrix} R_{df} \\ R_{dD} \end{bmatrix} \tag{8.109}$$

and the known flux λ_{d-0} for zero current ($i_d = 0$),

$$\lambda_{d-0} = [L_{df} \ L_{dD}] \begin{bmatrix} R_{ff} & R_{fD} \\ R_{fD} & R_{DD} \end{bmatrix}^{-1} \begin{bmatrix} hist_f - v_f(t) \\ hist_D \end{bmatrix} \tag{8.110}$$

The reduced inductance $L_d^{reduced}$ is practically identical with L_d'' if $R << 2L/\Delta t$. For the IEEE benchmark model [74] with $\Delta t = 200\ \mu s$, $\omega L_d = 0.135129$ p.u. compared to $\omega L_d'' = 0.135$ p.u. In publications based on [13], $\omega L_d^{reduced}$ is called $-a_{21}$ and $\omega L_q^{reduced}$ is called a_{12}.

8.5.4.5. Iteration Schemes

Up to now, the complete network solution is direct, without iterations. The iteration scheme of Section 8.5.1 does not repeat the network solution, and predicted values are therefore never completely corrected. There is only one exception, namely the three-phase short-circuit at the generator terminals with zero fault resistance. In that case the terminal voltages are always zero, and going back to step 6 in the iteration scheme of Section 8.5.1 should be a complete correction of all predicted values.

It is doubtful whether the predictors can be improved much more. Further improvements can probably only be made if the network solution is included in the iterations as well. This could be a worthwhile option, not only for machines, but for other nonlinear or time-varying elements as well.

8.6 Saturation

Saturation effects in synchronous machines can have an influence on load flow, on steady-state and transient stability, and on electromagnetic transients. While transformer saturation usually causes more problems than machine saturation (e.g., in the creation of so-called "temporary overvoltages"), there are situations where saturation in machines must be taken into account, too.

To model machine saturation rigorously is very difficult. It would require magnetic field calculations, e.g.

by finite element methods [181], which is already time-consuming for one particular operating condition, and practically impossible for conditions which change from step to step. Also, the detailed data for field calculations would not be available to most EMTP users. An approximate treatment of saturation effects is, therefore, commonly accepted. The modelling of saturation effects is discussed in four parts,

> (a) basic assumptions,
>
> (b) saturation effects in steady-state operation, and
>
> (c) saturation effects under transient conditions, and
>
> (d) implementation in the EMTP

8.6.1 Basic Assumptions

The data which is normally available is the "open-circuit saturation curve" (Fig. 8.17), which shows the terminal voltage as a function of the field current for open-circuited armature windings (no-load condition). In the transient simulation, a flux-current relationship is required, rather than $V = f(i_f)$. This is easily obtained from Eq. (8.9), which becomes

$$v_q = \omega \lambda_d \tag{8.111a}$$
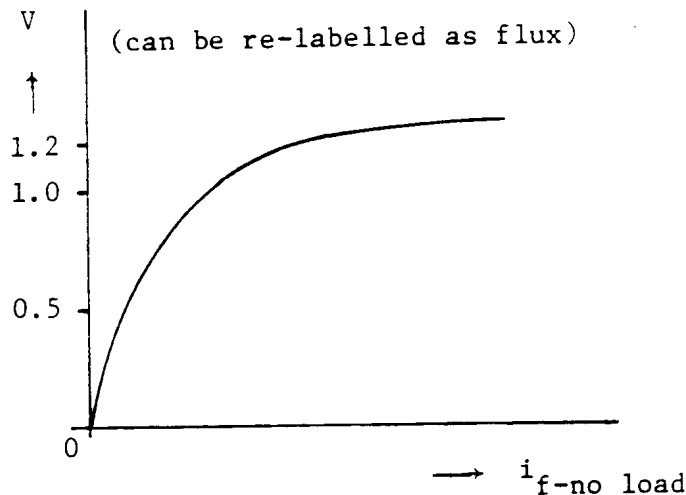
Fig. 8.17 - Open-circuit saturation curve

for balanced, open-circuit steady-state conditions, where both λ_q and the transformer voltages $d\lambda_d/dt$, $d\lambda_q/dt$ are zero. Since v_q is equal to $\sqrt{3}V_{1\text{-RMS}}$, this equation can be rewritten as

$$\sqrt{3}\, V_{1-RMS} = \omega \lambda_d \tag{8.111b}$$

where $V_{1\text{-RMS}}$ is the RMS terminal voltage of armature winding 1 (line-to-ground RMS voltage for wye-connected machines). It is therefore very simple to re-label the vertical axis in Fig. 8.17 from voltage to flux values with Eq. (8.111).

The saturation effects in synchronous machines do not produce harmonics during balanced steady-state

8-50

operation, because the open-circuit saturation curve describes a dc relationship between the dc flux of the rotating magnets (poles) and the dc field current required to produce it. The magnitude of the dc flux determines the magnitude of the induced voltages in the armature, while the shape of the flux distribution across the pole face determines the waveshape of the voltage. If the distribution is sinusoidal, as assumed in the ideal machine implemented in the EMTP, then the voltage will be sinusoidal as well. In reality, the distribution is distorted with "space harmonics," and it is this effect which produces the harmonics in synchronous machines.

There are many different ways of representing saturation effects [182], and it is not completely clear at this time which one comes closest to field test results. More research on this topic is needed. At this time, the representation of saturation effects in the EMTP is based upon the following simplifying assumptions:

1. The flux linkage of each winding in the d- or q-axis can be represented as the sum of a leakage flux (which passes only through that winding) and of a mutual flux (which passes through all other windings on that axis as well), as illustrated in Fig. 8.18,

$$\lambda = \lambda_{\ell} + \lambda_m \tag{8.112}$$

where

λ_{ℓ} = leakage flux unaffected by saturation,

λ_m = mutual flux subjected to saturation effects.

In reality, the leakage fluxes are subjected to saturation effects as well because they pass partly through iron [180], but to a much lesser degree than the mutual flux. Saturation effects are therefore ignored in the leakage fluxes. The data is not available anyhow if only one saturation curve (open-circuit saturation curve) is given. In terms of equivalent circuits, this assumption means that only some of the inductances are nonlinear (shunt branch in star point in Fig. 8.2), while the others remain constant.

2. The degree of saturation is a function of the total air-gap flux linkage λ_{m-u},

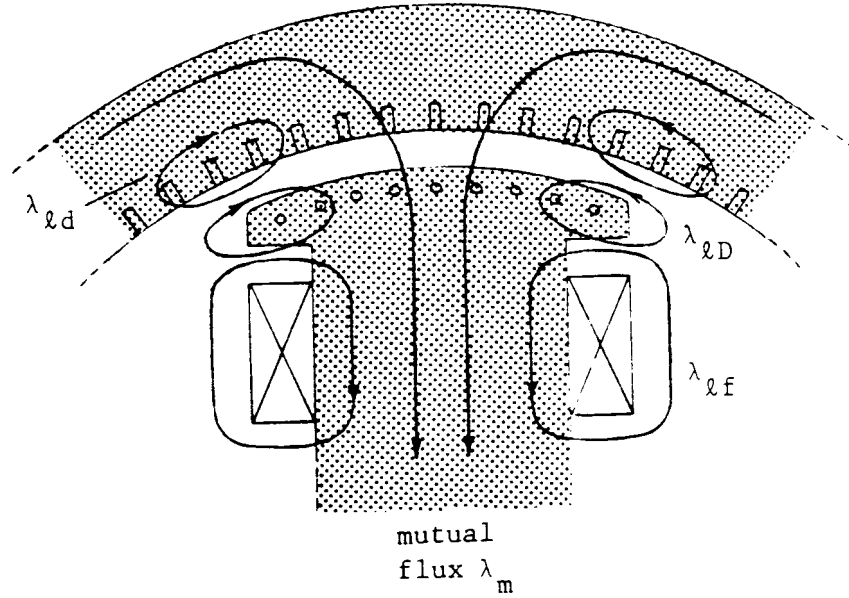$$\lambda_m = f(\lambda_{m-u}) \tag{8.113a}$$

with

$$\lambda_{m-u} = \sqrt{\lambda_{md-u}^2 + \lambda_{mq-u}^2} \tag{8.113b}$$

and

$$\lambda_{md-u} = M_{du}(i_d + i_f + i_D) ; \qquad \lambda_{mq-u} = M_{qu}(i_q + i_g + i_Q) \tag{8.113c}$$

Fig. 8.18 - Leakage fluxes and mutual flux

where subscript "m" indicates mutual, and "u" indicates unsaturated values. In Eq. (8.113c) it is important to use the proper mutual inductances for the representation of the mutual flux. This leads back to the data conversion problem discussed in Section 8.2. If Canay's characteristic reactance X_c is not known, then assume $k = 1$ in Eq. (8.14b), and use

$$M_{du} = L_d - L_\ell \; ; \qquad M_{qu} = L_q - L_\ell$$

from Eq. (8.20a) and (8.20c). In this case, the equivalent star circuit of Fig. 8.2 shows the correct separation into the mutual inductance $M_m = M_{du}$ or M_{qu} for the mutual flux (subject to saturation) and into the leakage inductances for the leakage fluxes (linear d-, f-, and D-branches). If Canay's characteristic reactance is used, then Fig. 8.2 can no longer be used, as explained in Section 8.6.5.

3. Only one flux, namely the total air-gap flux, is subjected to saturation. The saturated mutual fluxes λ_{md}, λ_{mq} on both axes are found from their unsaturated values by reducing them with the same ratio (similar triangles in Fig. 8.19),
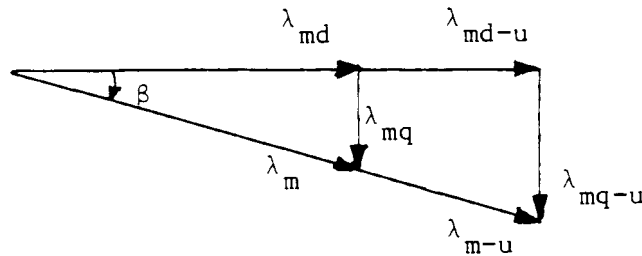
Fig. 8.19 - Unsaturated and saturated mutual fluxes

$$\lambda_{md} = \lambda_{md-u} \cdot \frac{\lambda_m}{\lambda_{m-u}} \; ; \qquad \lambda_{mq} = \lambda_{mq-u} \cdot \frac{\lambda_m}{\lambda_{m-u}} \tag{8.114}$$

8-52

This assumption is based on the observation that there is only one mutual flux, which lines up with the pole axis if λ_{mq} is very small, and which will shift to one side of the pole as λ_{mq} increases (Fig. 8.20).

(a)   flux from i_f alone ($\lambda_{mq} = 0$)   (b)   flux from i_f and stator currents $\lambda_{mq} \neq 0$
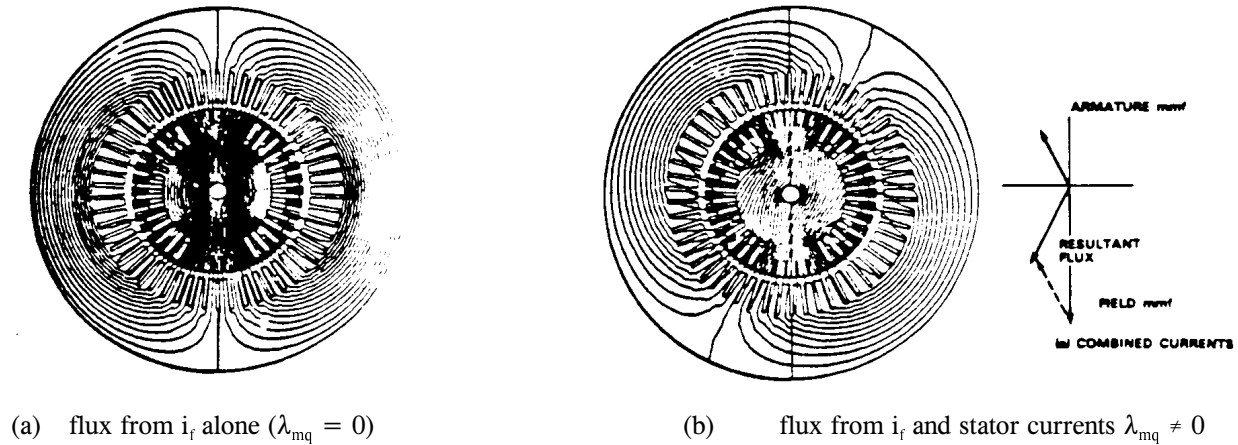
Fig. 8.20 - Flux in turbogenerator [181]. $^{©}$ 1981 IEEE

4.   Saturation does not destroy the sinusoidal distribution of the magnetic field over the face of the pole, and all inductances therefore maintain their sinusoidal dependence on rotor position according to Eq. (8.5).

5.   Hysteresis is ignored, while eddy currents are approximately modelled by the g-winding, and maybe to some extent with the D- and Q-windings. More windings could be added, in principal, to represent eddy currents more accurately.

8.6.2 Saturation in Steady-State Operation

        At this time, the saturation effects are only modelled correctly in the ac steady-state initialization if the terminal voltages and currents are balanced. More research is needed before saturation can be represented properly in unbalanced cases.

        As explained in Section 8.4, the initialization of the machine variables follows after the phasor steady-state solution of the complete network. The initialization for balanced (positive sequence) conditions is described in detail in Section 8.4.1, and only the modifications required to include saturation effects will be discussed here.

        The nonlinear characteristic of Fig. 8.17 makes it impossible to use the initialization procedure of Section 8.4.1 in a straightforward way. To get around this problem, it is customary to use an "equivalent linear machine" in steady-state analysis which gives correct answers at the particular operating point and approximate answers in the neighborhood. This equivalent linear machine is represented by a straight line through the operating point and the origin (dotted line in Fig. 8.21). Whenever the operating point moves, a new straight line through the new operating point must be used.

        The concept of the equivalent linear machine is used in the EMTP as follows.

1.   Obtain the ac steady-state solution of the complete network. From the terminal voltages and currents of the

machine (positive sequence values), find the internal machine variables with the method of Section 8.4.1. Assume that the machine operates in the unsaturated region at this time.
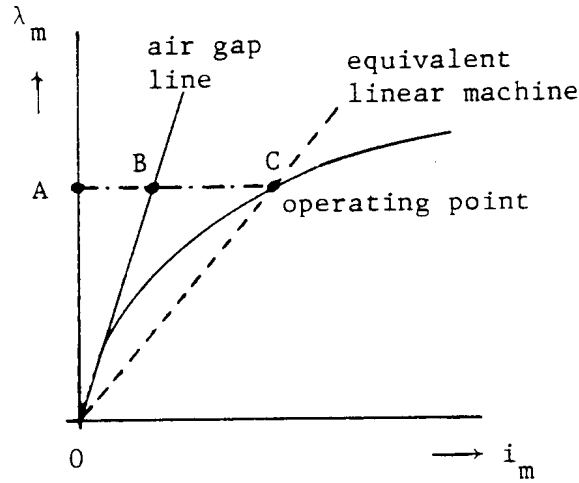
Fig. 8.21 - Linearization for steady-state analysis

2. Determine the total magnetizing current

$$i_m = \sqrt{(i_d + i_f + i_D)^2 + \left(\frac{M_{qu}}{M_{du}}\right)^2 (i_q + i_g + i_Q)^2} \tag{8.115a}$$

with i_D, i_g, i_Q being zero for balanced conditions. Eq. (8.115) assumes turns ratios of $N_d:N_f:N_D = 1:1:1$ (same for quadrature axis). If any other turns ratios are used, the first term would be

$$M_{du} i_{md} = M_{du} i_d + M_{df-u} i_f + M_{dD-u} i_D \tag{8.115b}$$

and the second term

$$M_{qu} i_{mq} = M_{qu} i_q + M_{qg-u} i_g + M_{qQ-u} i_Q \tag{8.115c}$$

with

$$M_{du} i_m = \sqrt{(M_{du} i_{md})^2 + (M_{qu} i_{mq})^2} \tag{8.115d}$$

Find the operating point on the nonlinear characteristic of Fig. 8.21. If this point lies in the linear region, then the initialization is complete. Otherwise:

3. Calculate the ratio K from Fig. 8.21,

$$K = \frac{AB}{AC} \tag{8.116a}$$

and multiply the unsaturated mutual inductances with that ratio to obtained the saturated values of the equivalent linear machine,

$$M_d = K \cdot M_{du} \; ; \qquad M_q = K \cdot M_{qu} \tag{8.116b}$$

Use these values to repeat the initialization procedure of Section 8.4.1. Then re-calculate the magnetizing current from Eq. (8.115). If it agrees with the previously calculated value within a prescribed tolerance, then the initialization is finished. If not, repeat step 3. Convergence is usually achieved with 1 to 2 iterations of step 3.

In the BPA EMTP steady-state solution, machines are now represented as voltage sources at the terminals, and the terminal currents are obtained from that solution. With terminal voltages and currents thus known, their positive sequence components can be calculated and then used to correct the internal variables for saturation effects. Since this correction does not change the terminal voltages and currents, the complete network solution does not have to be repeated in step 3.

This will also be true in future versions of the EMTP, where the machine will be represented as symmetrical voltage sources behind an impedance matrix. Again, the terminal voltages and currents and their positive sequence components will be known from the steady-state solution.

In unbalanced cases, the present representation will produce negative sequence values, while the future representation will produce correct values. How to use these negative sequence values in the saturation corrections has not yet been worked out. Since they produce second harmonics in the direct and quadrature axes fluxes, it may well be best to ignore saturation effects in the negative sequence initialization procedure of Section 8.4.2 altogether.

The equivalent linear machine produces correct initial conditions for the different model used in the transient simulation, as can easily be verified if a steady-state solution is followed by a transient simulation without any disturbance.

8.6.3 Saturation under Transient Conditions

The equivalent linear machine described in Section 8.6.2 cannot be used in the transient solution, because the proper linearization for small disturbances (as they occur from step to step) is not the straight line 0-C in Fig. 8.21 ("linear inductance"), but the tangent to the nonlinear curve in point C ("incremental inductance").

The saturation effect enters the transient solution discussed in Section 8.5 in two places, namely through the speed voltages and through the transformer voltages. Consider the direct axis equations (8.76) first, which can be rewritten as

$$[v] = -[R][i] - \frac{d}{dt}\begin{bmatrix} \lambda_{\ell d} \\ \lambda_{\ell f} \\ \lambda_{\ell D} \end{bmatrix} - \frac{d}{dt}\begin{bmatrix} \lambda_{md} \\ \lambda_{md} \\ \lambda_{md} \end{bmatrix} + \begin{bmatrix} -\omega\lambda_{\ell q} \\ 0 \\ 0 \end{bmatrix} + \begin{bmatrix} -\omega\lambda_{mq} \\ 0 \\ 0 \end{bmatrix} \tag{8.117}$$

for the d, f, D-quantities if each flux linkage is separated into its leakage flux and the common mutual flux,

$$\lambda_d = \lambda_{\ell d} + \lambda_{md}$$
$$\lambda_f = \lambda_{\ell f} + \lambda_{md} \tag{8.118}$$
$$\lambda_D = \lambda_{\ell D} + \lambda_{md}$$

assuming turns ratios of $N_d:N_f:N_D = 1:1:1$ (analogous for quadrature axis). Only the terms with λ_{md} and λ_{mq} in Eq. (8.117) are influenced by saturation, and only those terms are therefore discussed.

Consider first the speed voltage term $-\omega\lambda_{mq}$ in Eq. (8.117), which is properly corrected for saturation by simply using the correct saturated value λ_{mq}. The saturation correction has already been described in Eq. (8.114), and is conceptually the same as the one used in Eq. (8.116) for the steady-state solution. Since the transient solution works with predicted values of speed voltages $\omega\lambda_d$ and $\omega\lambda_q$, as explained in Section 8.5.4.4, they are used directly in Eq. (8.117) (not split up into two terms).

Next consider the transformer voltages $-[d\lambda_{md}/dt]$ in Eq. (8.117), where incremental changes ("incremental inductances") are important. By using the tangent of the nonlinear characteristic in the last solution point, one can linearize the flux-current relationship to

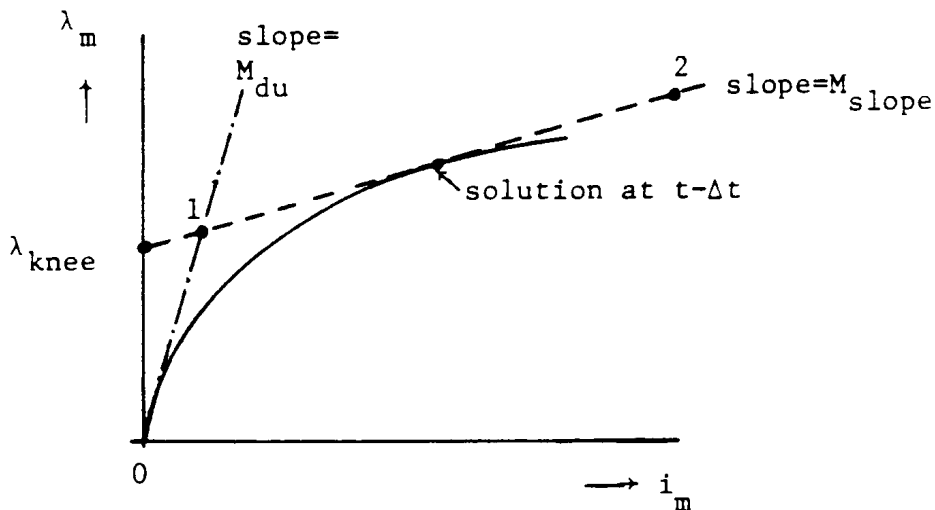$$\lambda_m = \lambda_{knee} + M_{slope}\, i_m \tag{8.119}$$

Fig. 8.22 - Linearization around last solution point

with M_{slope} being an incremental inductance (Fig. 8.22). This equation can be used over the next time step, because

the fluxes change only very slowly with typical step sizes of 50 to 500 μs. In the EMTP implementation, the problem is even simpler because the saturation curve is represented as a two-slope piecewise linear curve. In that case, the linearization of Eq. (8.119) changes only at the instant where the machine goes into saturation, and at the instant when it comes out again. With Eq. (8.113) and (8.115), the unsaturated total flux is

$$\lambda_{m-u} = M_{du} i_m \tag{8.120}$$

which, inserted into Eq. (8.119), produces

$$\lambda_m = \lambda_{knee} + b \lambda_{m-u} \tag{8.121a}$$

with the ratio between incremental inductance M_{slope} and linear (unsaturated) inductance M_{du},

$$b = \frac{M_{slope}}{M_{du}} \tag{8.121b}$$

After saturation has been defined for the total flux, it must be separated into d- and q-components again. With assumption (3) from Section 8.6.1, and with Fig. 8.19,

$$\lambda_{md} = \lambda_{knee-d} + b \lambda_{md-u}$$
$$\lambda_{mq} = \lambda_{knee-q} + b \lambda_{mq-u} \tag{8.122a}$$

where

$$\lambda_{knee-d} = \lambda_{knee} \cos\beta ; \quad \lambda_{knee-q} = \lambda_{knee} \sin\beta ; \quad \beta = \tan^{-1}(\lambda_{mq-u}/\lambda_{md-u})$$

$$\tag{8.122b}$$

If Eq. (8.117), and the analogous equation for the quadrature axis, are solved with the trapezoidal rule of integration, then the transformer voltage term affected by saturation,

$$[v_{md}] = -d[\lambda_{md}]/dt$$

is transformed with Eq. (8.122) into

$$[v_{md}(t)] = -\frac{2b}{\Delta t} \{[\lambda_{md-u}(t)] - [\lambda_{md-u}(t - \Delta t)]\}$$

$$-\frac{2}{\Delta t}\{[\lambda_{knee-d}(t)] - [\lambda_{knee-d}(t - \Delta t)]\} - [v_{md}(t - \Delta t)] \tag{8.123}$$

This equation shows how the transformer voltages must be corrected for saturation effects:

      (a)   multiply all mutual inductances by the factor b, and

(b)   add correction terms to account for the variation of the knee fluxes $[\lambda_{knee\text{-}d}]$, and $[\lambda_{knee\text{-}q}]$

8.6.4 Implementation in the EMTP

Saturation effects were modelled for the first time in the M27 version of the BPA EMTP, based on the concept of two independent saturation effects, one in the direct axis and the other in the quadrature axis. This was replaced with a newer model in the M32 version, which was essentially the model discussed here. It was not quite correct, however, because the correction terms in Eq. (8.123) related to the knee fluxes were not included. The model described here was implemented for the first time in the DCG/EPRI version to be released in 1986.

The open-circuit saturation curve is approximated as a two-slope piecewise linear characteristic (0-1 and 1-2 in Fig. 8.22). The number of linear segments could easily be increased, but a two-slope representation is usually adequate.

8.6.4.1 Steady-State Initialization

The initialization procedure is only correct for balanced networks at this time. The extension to unbalanced cases is planned for the future. Until this is done, some transients caused by incorrect initialization can be expected in unbalanced cases. Hopefully, they will settle down within the first few cycles.

The initialization follows the procedure of Section 8.6.2. For the reactances X_d, X_q, which consist of a constant leakage part and a saturable mutual part,

$$X_d = X_{\ell} + \omega M_d ; \qquad X_q = X_{\ell} + \omega M_q \tag{8.124}$$

unsaturated values M_{du}, M_{qu} are first used to obtain the internal machine variables with the method of Section 8.4.1. If the resulting magnetizing current lies in the saturated region, then the mutual reactances M_d, M_q in Eq. (8.124) must be corrected with Eq. (8.116). The calculation of the internal machine variables is then repeated with saturated reactances one or more times, until the changes in the magnetizing current become negligibly small.

With the two-slope piecewise linear representation implemented in the EMTP, the ratio K needed in Eq. (8.116) is

$$K = \frac{M_{slope}\, i_m + \lambda_{knee}}{M_{du}\, i_m} \tag{8.125}$$

with the meaning of the parameters shown in Fig. 8.22, and with i_m calculated from Eq. (8.115).

8.6.4.2 Transient Solution

Saturation effects in the time step loop are modelled according to Section 8.6.3. The coefficient b of Eq. (8.121b) is set to 1.0 in the unsaturated region, and to M_{slope}/M_{du} in the saturated region. Whenever the solution moves from one region into the other, it is reset accordingly.

This coefficient b affects the values in the equivalent resistance matrix $[R_{equiv}]$ of Eq. (8.91a) and in the history term matrix of Eq. (8.82c). To include this coefficient, the inductance matrix of Eq. (8.76) is split up into

$$[L] = b \begin{bmatrix} L_{md-u} & L_{md-u} & L_{md-u} \\ L_{md-u} & L_{md-u} & L_{md-u} \\ L_{md-u} & L_{md-u} & L_{md-u} \end{bmatrix} + \begin{bmatrix} L_{\mathfrak{L}d} & & \\ & L_{\mathfrak{L}f} & \\ & & L_{\mathfrak{L}D} \end{bmatrix} \tag{8.126}$$

(analogous for quadrature axis). Whenever b changes, [L] is recalculated and then used to recalculate [R$_{equiv}$] and the history term matrix of Eq. (8.82c). With the two-slope representation implemented in the EMTP, there are only two values of b, and the matrices could therefore be precalculated outside the time step loop for the two values of b = 1 and b = M$_{slope}$/M$_{du}$. The major effort lies in the re-triangularization of the network conductance matrix [G] of Eq. (8.18), however, which contains [R$_{equiv}$]$^{-1}$ and therefore changes whenever the machine moves into the saturated region, or out of it.

An additional modification is required in the calculation of the history terms with Eq. (8.78b). As shown in Eq. (8.123), the knee fluxes λ_{knee}(t) and λ_{knee}(t - Δt) must now be included. Since the trapezoidal rule of integration is not very good for the calculation of derivatives, the knee fluxes are included with the backward Euler method. First, the knee fluxes λ_{knee-d}(t) and λ_{knee-q}(t) are predicted, using the three-point predictor of Eq. (8.106). Then the trapezoidal rule expression

$$\frac{2}{\Delta t} \{ [\lambda_{knee-d}(t)] - [\lambda_{knee-d}(t - \Delta t)] \}$$

is replaced with the backward Euler expression

$$\frac{1}{\Delta t} \{ [\lambda_{knee-d}^{predicted}(t)] - [\lambda_{knee-d}(t - \Delta t)] \} \tag{8.127}$$

and the voltage term [v$_{md}$(t - Δt)] is replaced by a voltage term which excludes the knee flux.

8.6.5 Saturation Effects with Canay's Characteristic Reactance

If saturation is ignored, then it does not matter whether Canay's characteristic reactance is used or not, because it only affects the data conversion part. With saturation included, however, the nonlinear inductance can only be identified as the shunt branch M$_m$ in Fig. 8.2 if k = 1 in Eq. (8.14b). If Canay's characteristic reactance is known, then k ≠ 1. This factor k must then be removed again from the rotor quantities in Eq. (8.15a), by multiplying the second and third row and column with its reciprocal value,

$$\begin{bmatrix} \lambda_d \\ \dfrac{\sqrt{3}}{\sqrt{2}} \lambda_f \\ \dfrac{\sqrt{3}}{\sqrt{2}} \lambda_D \end{bmatrix} = \begin{bmatrix} L_d & cM_m & cM_m \\ cM_m & c^2 L_{ffm} & c^2 M_m \\ cM_m & c^2 M_m & c^2 L_{DDm} \end{bmatrix} \begin{bmatrix} i_d \\ \dfrac{\sqrt{2}}{\sqrt{3}} i_f \\ \dfrac{\sqrt{2}}{\sqrt{3}} i_D \end{bmatrix} \tag{8.128}$$

where

$$c = \frac{1}{k} \qquad (8.129)$$

and where M_m, L_{ffm} and L_{DDm} are the modified parameters straight out of the data conversion routine of Appendix VI.4. As explained in the text between Eq. (8.17) and (8.18), the factor $\sqrt{3}/\sqrt{2}$ in Eq. (8.128) is needed to produce turns ratios of $N_d:N_f:N_D = 1:1:1$. Only with turns ratios of 1:1 can the fluxes be separated into their main and leakage parts. The circuit of Fig. 8.23, which is equivalent to Eq. (8.128), has the correct separation into the mutual inductance $cM_m = 3/2\ M_{af}$ subjected to saturation (for the mutual flux), and into the linear leakage
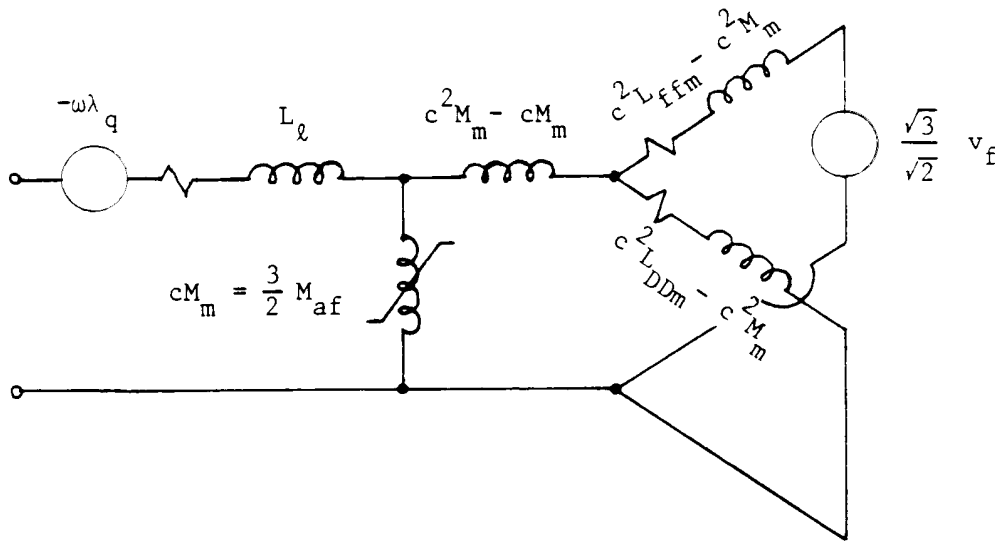
Fig. 8.23 - Equivalent circuit for direct axis with identity of leakage and main fluxes restored from Fig. 8.2

inductances in the three branches d, f, D. For the quadrature axis, Fig. 8.2 can still be used, with M_m being the nonlinear inductance, because Canay's characteristic reactance cannot be measured on that axis (current split between g- and Q-windings unmeasurable because both windings are hypothetical windings).

Most EMTP users will not know Canay's characteristic reactance because it is not supplied with the standard test data. Therefore, it has not yet been included in the saturation model in the EMTP, e.g. in the form of Fig. 8.23, because of lower priority compared to other issues. When it is implemented, one would have to decide whether the inductance $c^2M_m - cM_m$, which is mutual to both f- and D- windings, should be constant or saturable as well.

9. UNIVERSAL MACHINE

Co-author: H.K. Lauw

The universal machine was added to the EMTP by H.K. Lauw and W.S. Meyer [137,140], to be able to study various types of electric machines with the same model. It can be used to represent 12 major types of electric machines:

(1)   synchronous machine, three-phase armature;

(2)   synchronous machine, two-phase armature;

(3)   induction machine, three-phase armature;

(4)   induction machine, three-phase armature and three-phase rotor;

(5)   induction machine, two-phase armature;

(6)   single-phase ac machine (synchronous or induction), one-phase excitation;

(7)   same as (6), except two-phase excitation;

(8)   dc machine, separately excited;

(9)   dc machine, series compound (long shunt) field;

(10)   dc machine, series field;

(11)   dc machine, parallel compound (short shunt) field;

(12)   dc machine, parallel field.

The user can choose between two interfacing methods for the solution of the machine equations with the rest of the network. One is based on compensation, where the rest of the network seen from the machine terminals is represented by a Thevenin equivalent circuit, and the other is a voltage source behind an equivalent impedance representation, similar to that of Section 8.5, which requires prediction of certain variables.

The mechanical part of the universal machine is modelled quite differently from that of the synchronous machine of Section 9. Instead of a built-in model of the mass-shaft system, the user must model the mechanical part as an equivalent electric network with lumped R, L, C, which is then solved as if it were part of the complete electric network. The electromagnetic torque of the universal machine appears as a current source in this equivalent network.

9.1 Basic Equations for Electrical Part

Any electric machine has essentially two types of windings, one being stationary on the stator, the other rotating on the rotor. Which type is stationary and which is rotating is irrelevant in the equations, because it is only the relative motion between the two types which counts. The two types are:

(a)   Armature windings (windings on "power side" in BPA Rule Book). In induction and (normally) in synchronous machines, the armature windings are on the stator. In dc machines, they are on the rotor, where the commutator provides the rectification from ac to dc.

(b)   Windings on the field structure ("excitation side" in BPA Rule Book). In synchronous machines the field

structure windings are normally on the rotor, while in dc machines they are on the rotor, either in the form of a short-circuited squirrel-cage rotor, or in the form of a wound rotor with slip-ring connections to the outside. The proper term is "rotor winding" in this case, and the term "field structure winding" is only used here to keep the notation uniform for all types of machines.

These two types of windings are essentially the same as those of the synchronous machine described in Section 8.1. It is therefore not surprising that the system of equations (8.9) and (8.10) describe the behavior of the universal machine along the direct and quadrature axes as well. The universal machine is allowed to have up to 3 armature windings, which are converted to hypothetical windings d, q, 0a ("a" for armature) in the same way as in Section 8.1. The special case of single-phase windings is discussed in Section 9.3. The field structure is allowed to have any number of windings D1, D2,...Dm on the direct axis, and any number of windings Q1, Q2,...Qn on the quadrature axis, which can be connected to external circuits defined by the user. In contrast to Section 8, the field structure may also have a single zero sequence winding 0f ("f" for field structure), to allow the conversion of three-phase windings on the field structure (as in wound-rotor induction machines) into hypothetical D, Q, 0-windings.

With these minor differences to the synchronous machine of Section 8 in mind, the voltage equations for the armature windings in d, q-quantities become

$$\begin{bmatrix} v_d \\ v_q \end{bmatrix} = - \begin{bmatrix} R_a & 0 \\ 0 & R_a \end{bmatrix} \begin{bmatrix} i_d \\ i_q \end{bmatrix} - \frac{d}{dt} \begin{bmatrix} \lambda_d \\ \lambda_q \end{bmatrix} + \begin{bmatrix} -\omega\lambda_q \\ +\omega\lambda_d \end{bmatrix} \qquad (9.1a)$$

with ω being the angular speed of the rotor referred to the electrical side, and in zero sequence,

$$v_{0a} = -R_a i_{0a} - d\lambda_{0a}/dt \qquad (9.1b)$$

The voltage equations for the field structure windings are

$$\begin{bmatrix} v_{D1} \\ v_{D2} \\ . \\ . \\ . \\ v_{Dm} \end{bmatrix} = - \begin{bmatrix} R_{D1} & & \\ & R_{D2} & \\ & & . \\ & & . \\ & & . \\ & & R_{Dm} \end{bmatrix} \begin{bmatrix} i_{D1} \\ i_{D2} \\ . \\ . \\ . \\ i_{Dm} \end{bmatrix} - \frac{d}{dt} \begin{bmatrix} \lambda_{D1} \\ \lambda_{D2} \\ . \\ . \\ . \\ \lambda_{Dm} \end{bmatrix} \qquad (9.2a)$$

$$\begin{bmatrix} v_{Q1} \\ v_{Q2} \\ . \\ . \\ . \\ v_{Qm} \end{bmatrix} = - \begin{bmatrix} R_{Q1} & & \\ & R_{Q2} & \\ & & . \\ & & . \\ & & . \\ & & R_{Qm} \end{bmatrix} \begin{bmatrix} i_{Q1} \\ i_{Q2} \\ . \\ . \\ . \\ i_{Qm} \end{bmatrix} - \frac{d}{dt} \begin{bmatrix} \lambda_{Q1} \\ \lambda_{Q2} \\ . \\ . \\ . \\ \lambda_{Qm} \end{bmatrix} \qquad (9.2b)$$

and

$$v_{0f} = -R_{0f} i_{0f} - \frac{D \lambda_{0f}}{dt}$$ (9.2c)

The flux-current relationships on the two axes provide the coupling between the armature and field structure sides,

$$
\begin{bmatrix} \lambda_d \\ \lambda_{D1} \\ \lambda_{D2} \\ . \\ . \\ . \\ \lambda_{Dm} \end{bmatrix} =
\begin{bmatrix}
L_d & M_{dD1} & M_{dD2} & \cdots & M_{dDm} \\
M_{dD1} & L_{D1} & M_{D1D2} & \cdots & M_{D1Dm} \\
M_{dD2} & M_{D1D2} & L_{D2} & \cdots & M_{D2Dm} \\
. & . & . & . & . \\
M_{dDm} & M_{D1Dm} & M_{D2Dm} & \cdots & L_{Dm}
\end{bmatrix}
\begin{bmatrix} i_d \\ i_{D1} \\ i_{D2} \\ . \\ . \\ . \\ i_{Dm} \end{bmatrix}
$$ (9.3a)

$$
\begin{bmatrix} \lambda_q \\ \lambda_{Q1} \\ \lambda_{Q2} \\ . \\ . \\ . \\ \lambda_{Qn} \end{bmatrix} =
\begin{bmatrix}
L_q & M_{qQ1} & M_{qQ2} & \cdots & M_{qQn} \\
M_{qQ1} & L_{Q1} & M_{Q1Q2} & \cdots & M_{Q1Qn} \\
M_{qQ2} & M_{Q1Q2} & L_{Q2} & \cdots & M_{Q2Qn} \\
. & . & . & . & . \\
M_{qQn} & M_{Q1Qn} & M_{Q2Qn} & \cdots & L_{Qn}
\end{bmatrix}
\begin{bmatrix} i_q \\ i_{Q1} \\ i_{Q2} \\ . \\ . \\ . \\ i_{Qn} \end{bmatrix}
$$ (9.3b)

with both inductance matrices being symmetric. The zero sequence fluxes on the armature and field structure side are not coupled at all,

$$\lambda_{0a} = L_{0a} i_{0a}$$ (9.3c)

$$\lambda_{0f} = L_{0f} i_{0f}$$ (9.3d)

The universal machine has been implemented under the assumption that the self and mutual inductances in Eq. (9.3a) and (9.3b) can be represented by a star circuit if the field structure quantities are referred to the armature side, as shown in Fig. 9.1. This assumption
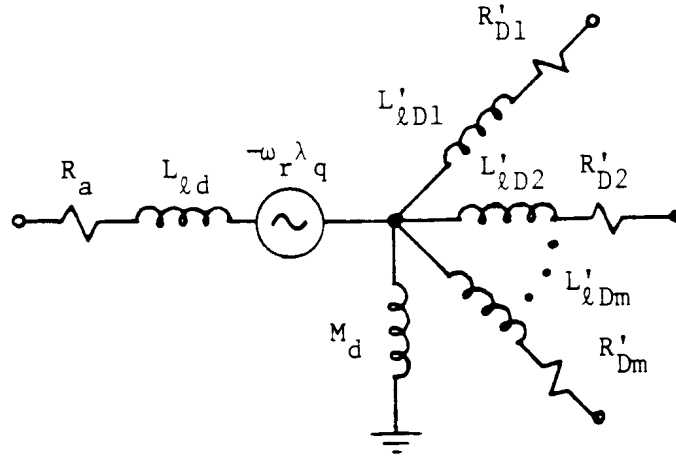
Fig. 9.1 - Star circuit representation of coupled windings in direct axis (analogous in quadrature axis)

implies that there is only one mutual (or main) flux which links all windings on one axis (λ_m in Fig. 8.18), and that the leakage flux of any one winding is only linked with that winding itself. Strictly speaking, this is not always true. For example, part of the leakage flux of the field winding (λ_{lf} in Fig. 8.18) could go through the damper winding as well, but not through the armature winding, which leads to the modified star circuit of Fig. 8.23 (synchronous machines) or Fig. 9.2 (induction machines). The data for such models with unequal mutual inductances is seldom available, however (e.g., Fig. 8.23 requires Canay's characteristic reactance, which is not available from standard test data). The star circuit is therefore a reasonable assumption in practice. At any rate, the code could easily be changed to work with the self and mutual inductances of Eq. (9.3) instead of the star circuit of Fig. 9.1.

With the star circuit representation of Fig. 9.1, the flux-current equations (9.3a) can be simplified to

$$\lambda_d = L_{\ell d}\, i_d + \lambda_{md}$$

$$\lambda'_{D1} = L'_{\ell D1}\, i'_{D1} + \lambda_{md} \tag{9.4a}$$

$$\lambda'_{Dm} = L'_{\ell Dm}\, i'_{Dm} + \lambda_{md}$$

with

$$\lambda_{md} = M_d\,(i_d + i'_{D1} \dots + i'_{Dm}) \tag{9.4b}$$

where the prime indicates that field structure quantities have been referred to the armature side with the proper turns ratios between d and D1, d and D2,...d and D_m. All referred mutual inductances are equal to M_d in this representation, and the referred self inductances of Eq. (9.3a) are related to the leakage inductances of the star

branches by

$$L_d = L_{\ell d} + M_d$$

$$L'_{D1} = L'_{\ell D1} + M_d \qquad\qquad (9.5)$$

.

.

$$L'_{Dm} = L'_{\ell Dm} + M_d$$

The voltage equations (9.1) and (9.2) are valid for referred quantities as well, if R_{D2}, i_{D2},... are replaced by R_{D2}', i_{D2}',... The quadrature axis equations are obtained by replacing subscripts d, D in the direct axis equations with q, Q.

In the BPA EMTP Rule Book, the turns ratios are called "reduction factors," and the process of referring quantities to the armature side is called "reduction" (referring quantities from one side to another is discussed in Appendix IV.3).

9.2 Determination of Electrical Parameters

By limiting the universal machine representation to the star circuit of Fig. 9.1, the input parameters are simply the resistances and leakage inductances of the star branches and the mutual inductance, e.g., for the direct axis,

$$R_a , \qquad L_{\ell d}$$

$$R'_{D1} , \qquad L'_{\ell D1}$$

.

.

.

$$R'_{Dm} , \qquad L'_{\ell Dm}$$
$$M_d ,$$

(analogous for the quadrature axis), and for the zero sequence on the armature and field structure side,

$$L_{0a} ,$$

$$R'_{0f} , \qquad L'_{0f}$$

If the armature leakage inductance L_ℓ is known instead of the mutual inductance, then find M from Eq. (9.5),

$$M_d = L_d - L_{\ell d} , \qquad M_q = L_q - L_{\ell q}$$

If neither L_{ϑ} nor M is known, then use a reasonable estimate. The BPA EMTP Rule Book recommends

$$L_{\vartheta d} = 0.1 L_d \ , \qquad L_{\vartheta q} = 0.1 L_q \tag{9.6}$$

which seems to be reasonable for round rotor synchronous machines, while for salient pole machines the factor is closer to 0.2 than to 0.1. Compared to the large value of the magnetizing inductance of transformers, the value of the mutual (or magnetizing) inductance M_d, M_q from Eq. (9.6) (90% of self inductance) is relatively low because of the air gap in the flux path.

Compared to the $(m + 1)(m + 2) / 2$ inductance values in Eq. (9.3a), the star circuit has only $m + 2$ inductance values. For the most common machine representation with 2 field structure windings, Eq. (9.3a) requires 6 values, compared to 4 values for the star circuit. This means that the star circuit is not as general as Eq. (9.3a), but this is often a blessing in disguise because available test or design data is usually not sufficient anyhow to determine all self and mutual inductances (see requirement of obtaining an extra inductance value X_c in Section 8.2).

As already discussed for the synchronous machine in Section 8.2, the resistances and self and mutual inductances (or the star branch inductances here) are usually not available from calculations or measurements. If the universal machine is used to model a synchronous machine, then the data conversion discussed in Section 8.2 can be used (input identical to synchronous machine model in version M32 and later).

For three-phase induction machines, the data may be given in phase quantities. If so, Eq. (8.11) must be used to convert them to d, q, 0-quantities,

$$L_d = L_q = L_s - M_s$$
$$L_o = L_s + 2M_s$$

with $\quad L_s$ = self inductance of one armature winding,

$\quad M_s =$ mutual inductance between two armature windings (BPA Rule Book uses opposite sign for M_s). L_m in Eq. (8.11) is zero for an induction machine, where the saliency term defined in Eq. (8.5) does not exist. The same conversion is used if the rotor windings are three-phase. The mutual inductance between stator and rotor follows from Eq. (8.10).

$$M_{d-Di} = \frac{\sqrt{3}}{\sqrt{2}} M_{a-Di}$$

(same for q-axis), with $M_{a-Di}\cos \beta$ being the mutual inductance between armature winding 1 and rotor winding Di $(i = 1,...m)$, as defined in Eq. (8.5). Note that the factor $\sqrt{3}/\sqrt{2}$ changes the turns ratio; if the turns ratio between phase 1 and the rotor winding is 1:1, it changes to $\sqrt{3}:\sqrt{2}$ in d, q, 0-quantities (see also Section 8.2). This extra factor must be taken into account when rotor quantities are referred to the stator side.

For modelling three-phase induction machines, a modified universal machine with its own data conversion routine has recently been developed by Ontario Hydro [138]. It uses the standard NEMA specification data to find the resistances and self and mutual inductances of the equivalent circuit. It is beyond the scope of this treatise to describe the conversion routine in detail. Essentially, the field structure (which is the rotor in the induction machine)

has two windings to represent the rotor bars as well as the eddy currents in the deep rotor bars of large machines, or the double-squirrel cage rotor in smaller machines. Since there is no saliency, d- and q-axis parameters are identical. The assumption of equal mutual inductances (or the star circuit) is dropped, and the equivalent circuit of Fig. 9.2 is used instead. Not surprisingly, this equivalent circuit is identical with that of the synchronous machine in Fig. 8.23, because a synchronous
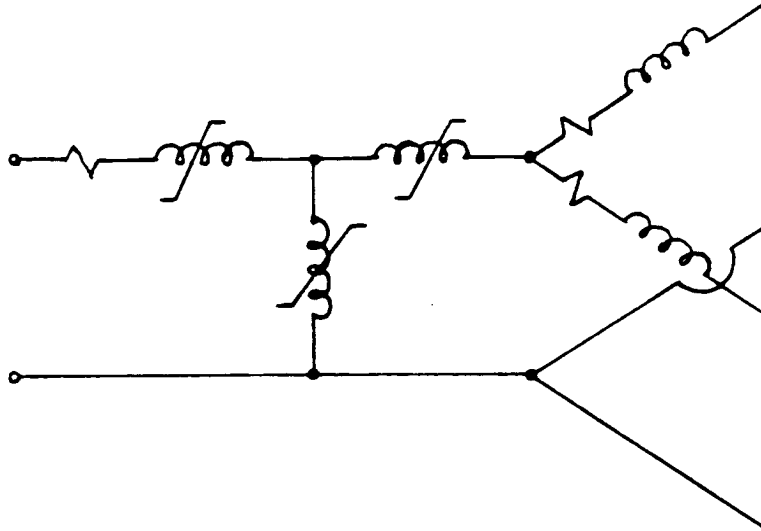
Fig. 9.2 - Equivalent circuit of induction machine with deep rotor bars

machine becomes an induction machine if the field winding is shorted. In contrast to the standard universal machine, saturation is included in the leakage inductance branch of the armature as well, and another nonlinear inductance is added between the star point and the star branches of the field structure windings. Fig. 9.3 shows comparisons between measurements and simulation results with this modified universal machine model [138, 139], for a case of a cold start-up of an induction-motor-driven heat transfer pump (1100 hp, 6600 V). Excellent agreement with the field test results is evident for the whole start-up period, which proves the validity of the modified universal machine model over the whole range of operation.
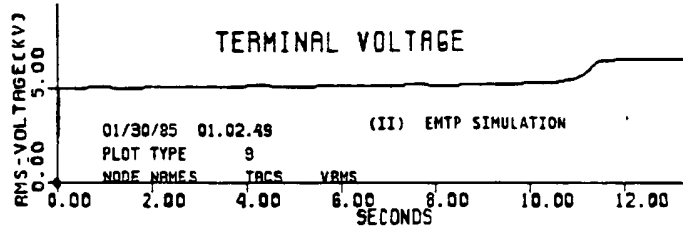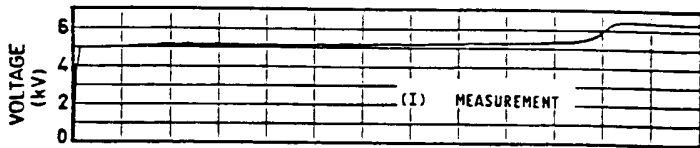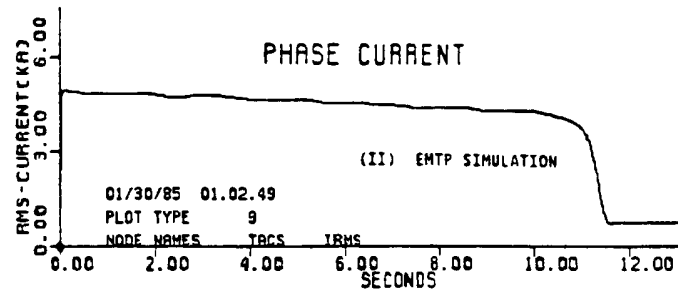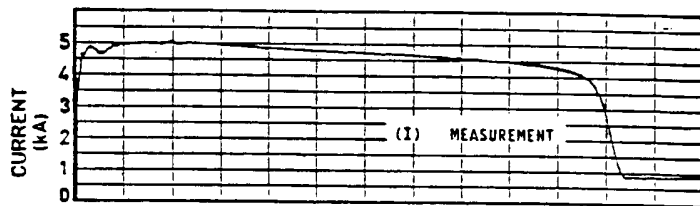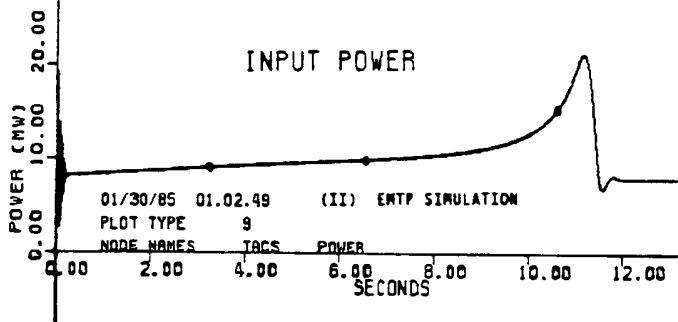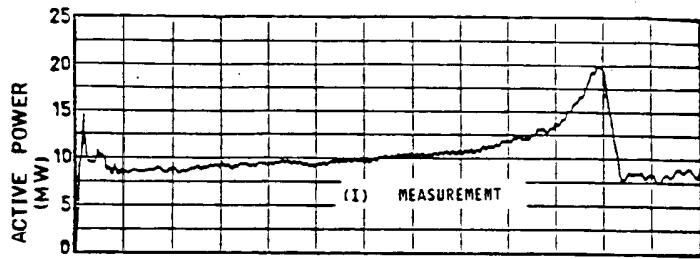
Fig. 9.3 - Comparison between field test and simulation results for starting up an induction motor with a heat transfer pump [138, 139]. Reprinted by permission of G.J. Rogers and D. Shirmohammadi

9-8

9.3 Transformation to Phase Quantities

Eq. (9.1) to (9.3) completely describe the universal machine in d, q, 0-quantities, irrespective of which type of machine it is. To solve these machine equations together with the rest of the network, they must be transformed to phase quantities. It is in this transformation where the various types of machines must be treated differently. Fortunately it is possible to work with the same transformation matrix for all types, by simply using different matrix coefficients.

For the case of a three-phase synchronous machine, the transformation has already been shown in Eq. (8.7). If this equation is rewritten for the armature quantities only, then[1]

$$
\begin{bmatrix} \lambda_d \\ \lambda_q \\ \lambda_{0a} \end{bmatrix} = [T]^{-1} \begin{bmatrix} \lambda_1 \\ \lambda_2 \\ \lambda_3 \end{bmatrix} \quad \textit{identical for } [v], \ [i]
\tag{9.7a}
$$

with

$$
[T]^{-1} = \frac{\sqrt{2}}{\sqrt{3}} \begin{bmatrix} \cos\beta & \cos(\beta-120°) & \cos(\beta+120°) \\ \sin\beta & \sin(\beta-120°) & \sin(\beta+120°) \\ \dfrac{1}{\sqrt{2}} & \dfrac{1}{\sqrt{2}} & \dfrac{1}{\sqrt{2}} \end{bmatrix}
\tag{9.7b}
$$

being an orthogonal matrix, which means that

$$
[T] = [T]^{-1}_{transposed}
\tag{9.7c}
$$

The rotor position β is related to the angular speed ω of the rotor by

$$
\omega = d\beta / dt
\tag{9.7d}
$$

The transformation matrix $[T]^{-1}$ can be rewritten as a product of two matrices [137],

$$
[T]^{-1} = [P(\beta)]^{-1} [S]^{-1}
\tag{9.8a}
$$

with

---

[1] In [137] and [139], $[T]^{-1}$ is called [T]; similarly, [P] and [S] are called $[P]^{-1}$ and $[S]^{-1}$ there.

$$[P(\beta)]^{-1} = \begin{bmatrix} \cos\beta & -\sin\beta & 0 \\ \sin\beta & \cos\beta & 0 \\ 0 & 0 & 1 \end{bmatrix} \tag{9.8b}$$

$$[S]^{-1} = \begin{bmatrix} \dfrac{\sqrt{2}}{\sqrt{3}} & -\dfrac{1}{\sqrt{6}} & -\dfrac{1}{\sqrt{6}} \\ 0 & -\dfrac{1}{\sqrt{2}} & \dfrac{1}{\sqrt{2}} \\ \dfrac{1}{\sqrt{3}} & \dfrac{1}{\sqrt{3}} & \dfrac{1}{\sqrt{3}} \end{bmatrix} \tag{9.8c}$$

each being orthogonal again,

$$[P] = [P]^{-1}_{transposed} \ , \qquad [S] = [S]^{-1}_{transposed} \tag{9.8d}$$

The first transformation with the $[S]^{-1}$-matrix replaces the three-phase coils (displaced by $120°$ in space) by the three equivalent coils d and q (perpendicular to each other) and 0 (independent by itself). This is the same transformation matrix used for α, β, 0-components in Eq. (4.48), except for a sign reversal of the β-quantities. The second transformation with $[P]^{-1}$ makes the d, q-axes rotate with the same speed as the field poles, so that they become stationary when seen from the field structure. The field structure quantities are not transformed at all.

This approach with two transformations can be applied to any type of machine. For a three-phase induction machine with a three-phase wound rotor, both the armature and field structure quantities are transformed with $[S]^{-1}$ to get equivalent windings on the d- and q-axes, while the transformation with $[P]^{-1}$ is only applied to the armature side. For direct current machines, there is not transformation at all for both the armature and field structure side.

For two-phase armature windings displaced by $90°$ in space, the windings are already on the d, q-axes. Therefore

$$[S_2]^{-1} = \begin{bmatrix} 1 & 0 \\ 0 & -1 \end{bmatrix} \tag{9.9a}$$

and

$$[P_2]^{-1} = \begin{bmatrix} \cos\beta & -\sin\beta \\ \sin\beta & \cos\beta \end{bmatrix} \tag{9.9b}$$

with the zero sequence winding missing.

For single-phase armature windings, there is only flux along one axis, or

$$[S_1]^{-1} = 1 \tag{9.10a}$$

and

$$[P_1]^{-1} = \cos\beta \tag{9.10b}$$

with both the quadrature axis and zero sequence winding missing.

The EMTP uses only one transformation matrix $[S]^{-1}$ and $[P]^{-1}$ for all cases, and makes the distinction by resetting the coefficients c_1, c_2, c_3 in these matrices,

$$[S]^{-1} = \begin{bmatrix} c_1 + c_2 + c_3\sqrt{2/3} & -c_3/\sqrt{6} & -c_3/\sqrt{6} \\ 0 & -c_2 - c_3/\sqrt{2} & c_3/\sqrt{2} \\ c_3/\sqrt{3} & c_3/\sqrt{3} & c_3/\sqrt{3} \end{bmatrix} \tag{9.11}$$

with

$c_3 =$ 1 for three-phase ac windings, and $c_3 = 0$ otherwise,

$c_2 =$ 1 for two-phase ac windings, and $c_2 = 0$ otherwise,

$c_1 =$ 1 for single-phase ac windings and dc machines, and $c_1 = 0$ otherwise.

Since $[S]^{-1}$ in Eq. (9.11) degenerates into 2 x 2 and 1 x 1 matrices for two-phase and single-phase windings, its inverse cannot be found by inversion. Using Eq. (9.8d) instead of inversion works in all cases, however. The matrix in Eq. (9.11) is slightly different from that in [137], because it is assumed here that only phases 1, 2 exist for two-phase machines, and only phase 1 exists for single-phase machines. In [137], phase 1 is dropped for two-phase machines, and phases 1 and 2 are dropped for single-phase machines.

For ac armature windings, $[P]^{-1}$ of Eq. (9.8b) is used, realizing that the zero sequence does not exist in the two-phase case, and that the zero sequence as well as the q-winding do not exist in the single-phase case. For dc armature windings, there is not second transformation with $[P]^{-1}$.

9.4 Mechanical Part

In contrast to the synchronous machine model, the universal machine does not have a built-in model for the mechanical part. Instead, the user must convert the mechanical part into an equivalent electric network with lumped R, L, C, which is then treated by the EMTP as if it were part of the overall electric network. The electromagnetic torque of the universal machine appears as a current source injection into the equivalent electric network.

Table 9.1 describes the equivalence between mechanical and electrical quantities. For each mass on the shaft system, a node is created in the equivalent electric network, with a

Table 9.1 - Equivalence between mechanical and electrical quantities

Mechanical			Electrical		
T	(torque acting on mass)	[Nm]	i	(current into node)	[A]
ω	(angular speed)	[rad/s]	v	(node voltage)	[V]
θ	(angular position of mass)	[rad]	q	(capacitor charge)	[C]
J	(moment of inertia)	[kgm^2]	C	(capacitance to ground)	[F]
K	(stiffness coefficient or spring constant)	[Nm/rad]	1/L	(reciprocal or inductance)	[1/H]
D	(damping coefficient)	[Nms/rad]	1/R	(conductance)	[S]

(1 Nm = 0.73756 lb-ft; 1 kgm^2 = 23.73 lb-ft^2)

capacitor to ground with value J for the moment of inertia. If there is damping proportional to speed on this mass, a resistor with conductance D is put in parallel with the capacitor (D_i in Eq. (8.31)). If there is a mechanical torque acting on that mass (turbine torque on generators, mechanical load on motors), a current source is connected to that node (positive for turbine torque, negative for load torque). If there are two or more masses, inductors are used to connect adjacent shunt capacitors, with their inductance values being equal to 1/K (reciprocal of stiffness coefficient of the shaft coupling between two masses). If there is damping associated with this shaft coupling, then the inductor is paralleled with a resistor whose conductance value is D ($D_{i,k}$ in Eq. (8.31)). The electromagnetic torque is automatically added to the proper node as a current source by the EMTP.

Fig. 9.4 summarizes the equivalence between the mechanical and electric components. Representing the mechanical system by an equivalent electric network can provide more
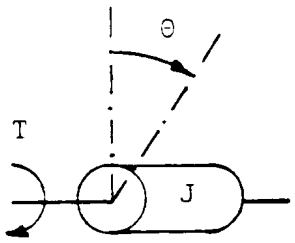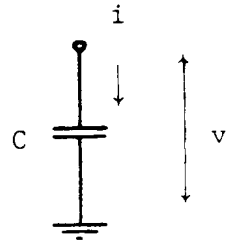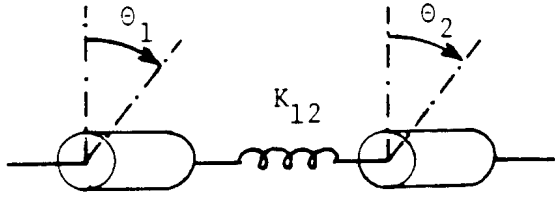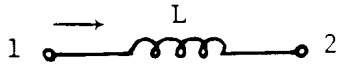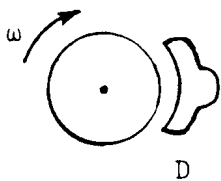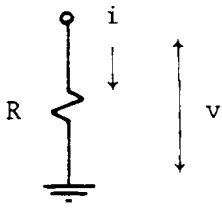
MECHANICAL	ELECTRICAL
Θ T J $T = J \dfrac{d^2\Theta}{dt^2} = J \dfrac{d\omega}{dt}$	i C v $i = C \dfrac{dv}{dt}$
Θ_1 Θ_2 K_{12} $T_{12} = K_{12}\,(\Theta_1 - \Theta_2)$ $= K_{12}\displaystyle\int(\omega_1 - \omega_2)\,dt$	L $1 \quad\longrightarrow\quad 2$ $i_{12} = \dfrac{1}{L}\displaystyle\int(v_1 - v_2)\,dt$
ω D $T = D\cdot\omega$	i R v $i = \dfrac{1}{R}\,v$

Fig. 9.4 - Equivalence between mechanical and electric components

flexibility than the built-in model of the synchronous machine of Section 8. With this approach it should be easy to incorporate gear boxes, distributed-parameter modelling of rotors, etc. The EMTP further provides for up to three

universal machines sharing the same mechanical system.

9.5 Steady-State Representation and Initial Conditions

The steady-state representation of the ac-type universal machine is based on the assumption that the network to which it is connected is balanced and linear. Only positive sequence quantities are used in the initialization, and negative and zero sequence quantities are ignored if there are unbalances. The initialization procedure could obviously be extended to handle unbalanced conditions as well, along the lines discussed in Section 8, but this extension has been given low priority so far.

9.5.1 Three-Phase Synchronous Machine

For three-phase synchronous machine representations, any positive sequence voltage source behind any positive sequence impedance can be used, as long as it produces the desired terminal voltages and currents when solved with the rest of the network. For simplicity, a three-phase symmetrical voltage source directly at the terminals is used for the steady-state solution. If the current (or active and reactive power output) from that solution is not what the user wants, then the power flow iteration option of the EMTP can be used, which will iteratively adjust the magnitude and angle of the three-phase voltage source until the desired active and reactive power output (or some other prescribed criteria) have been achieved. Once the terminal voltages and currents are known, the rest of the electrical machine variables are initialized in the same way as described in Section 8.4.1.

If the excitation system is represented by an electric network (rather than constant v_f), then the EMTP performs a second ac steady-state solution for the excitation systems of all universal machines, with the field currents i_f being treated as current sources $I_f\cos(\omega_f t)$, with ω_f being an angular frequency which is so low that i_f is dc for practical purposes. This trick is used because the EMTP cannot find an exact dc steady-state solution at this time (the network topology for dc solutions is different from that of ac steady-state solution; inductances would have to be treated as closed switches, capacitances as open switches, etc.).

From the initialization of the electrical variables, the electromagnetic torque $T_{mech\text{-}gen}$ on the mechanical side is known from Eq. (8.32b) as well. These torques are used as current sources $i(t) = T_{mech\text{-}gen}\cos(\omega_{mech} t)$ in the equivalent networks which represent the mechanical systems of all universal machines, with ω_{mech} again being an angular frequency so low that $i(t)$ is practically dc. The EMTP then performs a third ac steady-state solution for the initialization of the mechanical system quantities. Note that this three-step initialization procedure is direct, and does not require either predictions or iterations.

9.5.2 Two-Phase Synchronous Machine

Armature currents in two-phase machines with equal amplitudes and displacements of $90°$ produce a rotating magnetic field in the same way as symmetrical three-phase armature currents displaced by $120°$. As long as this condition is met (which is the balanced or positive sequence condition for two-phase machines), the initialization is identical with the three-phase case after proper conversion to d, q, 0-quantities. If the phase quantities are

$$i_1(t) = |I| \cos(\omega_s t + \alpha)$$
$$i_2(t) = |I| \cos(\omega_s t + \alpha - 90°) \tag{9.12}$$

with ω_s being the (synchronous) frequency of the supply network, then the d, q, 0-quantities are obtained with $[S_2]^{-1}$ and $[P_2]^{-1}$ from Eq. (9.9) with $\omega = \omega_s$ as

$$i_d = |I| \sin(\alpha - \delta)$$
$$i_q = |I| \cos(\alpha - \delta) \tag{9.13}$$

where δ is the angle between the position of the quadrature axis and the real axis of the ac phasor representation. Eq. (9.13) is indeed identical with Eq. (8.41) for the balanced three-phase machine, except for a factor of $\sqrt{3}/\sqrt{2}$ there.

9.5.3 Single-Phase Synchronous Machine

Converting a single-phase armature current

$$i_1(t) = |I| \cos(\omega_s t + \alpha) \tag{9.14}$$

into d, q, 0-quantities results in

$$i_d(t) = \frac{1}{2} |I| \sin(\alpha - \delta) - \frac{1}{2} |I| \sin(2\omega_s t + \alpha + \delta)$$
$$i_q = 0 \qquad i_0 = 0 \tag{9.15}$$

with the first term being the dc quantity analogous to the positive sequence effect in three-phase machines, and the second double-frequency term analogous to the negative sequence effect in Eq. (8.53) in three-phase machines. This is a mathematical expression of the fact that an oscillating magnetic field in a single-phase armature winding can be represented as the sum of a constant magnetic field rotating forward at synchronous speed (angular speed = 0 relative to field winding) and a constant magnetic field rotating backwards at synchronous speed (angular speed = 2ω relative to field winding).

Since only the first term in Eq. (9.15) is used in the initialization now, the initial conditions are not totally correct, and it may take many time steps before steady state is reached. The steady-state torque includes a pulsating term very similar to Fig. 8.9 for the case of an unbalanced three-phase synchronous machine. As an alternative to universal machine modelling, the three-phase synchronous machine model of Section 8 could be used for single-phase machines, by keeping two armature windings open-circuited. Unfortunately, the initialization with negative sequence quantities described in Section 8.4.2 is not yet fully correct in the BPA EMTP either, as explained in the beginning of Section 8.4, though it has been implemented in an unreleased version of the UBC EMTP.

9.5.4 DC Machines

The initialization of dc machine quantities is straightforward, and follows the same procedure outlined in

Section 9.5.1. In d, q, 0-quantities, balanced three-phase ac quantities appear as dc quantities. Therefore, there is essentially no difference between the equations of a balanced three-phase synchronous generator and a dc machine.

9.5.5 Three-Phase Induction Machine

In balanced steady-state operation, the angular speed ω of the rotor (referred to the electrical side with Eq. (8.25)) differs from the angular frequency ω_s of the supply network by the p.u. slip s,

$$s = \frac{\omega_s - \omega}{\omega_s} \tag{9.16}$$

The network sees the induction machine as a positive sequence impedance whose value depends on this slip s. The negative and zero sequence impedances are of no interest if the initialization is limited to balanced cases.

Fig. 9.5 shows the well-known equivalent circuit for the balanced steady-state behavior of a three-phase induction machine, which can be found in many textbooks. Its impedance can
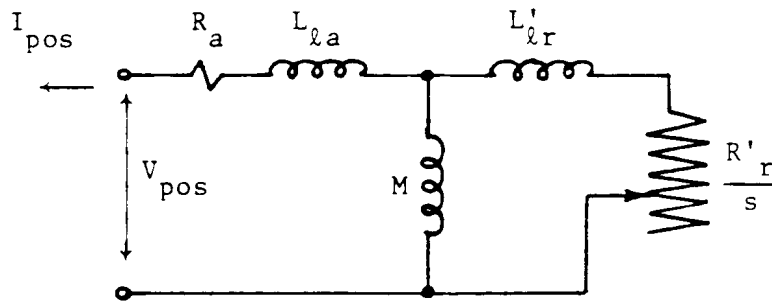
Fig. 9.5 - Conventional equivalent circuit for steady-state behavior of induction machines (subscript a for armature side, subscript r for rotor side)

easily be calculated, and with the relationship between leakage, self and mutual inductances

$$L_{aa} = L_{\ell a} + M$$

$$L_{rr}^{/} = L_{\ell r}^{/} + M \tag{9.17a}$$

becomes

$$Z_{pos} = R_a + j\omega_s L_{aa} - \frac{(j\omega_s M)^2}{\dfrac{R_r^{/}}{s} + j\omega_s L_{rr}^{/}} \tag{9.17b}$$

This single-phase impedance is used in phases 1, 2, 3 for the steady-state solution, provided there is only one winding on the field structure (rotor).

For the general case of m windings on the field structure, the calculation is slightly more complicated. First,

let us assume that the armature currents are

$$i_1(t) = |I| \cos(\omega_s t + \alpha)$$

$$i_2(t) = |I| \cos(\omega_s t + \alpha - 120°)$$

$$i_3(t) = |I| \cos(\omega_s t + \alpha - 240°)$$

in balanced operation. Transformed to d, q, 0-quantities, the currents become

$$i_d(t) = \frac{\sqrt{3}}{\sqrt{2}} |I| \sin(s\omega_s t + \alpha - \delta)$$

$$i_q(t) = \frac{\sqrt{3}}{\sqrt{2}} |I| \cos(s\omega_s t + \alpha - \delta) \qquad (9.18a)$$

$$i_o(t) = 0$$

which can be represented as a phasor of slip frequency $s\omega_s$, projected onto the q, d-axes,

$$I_{qd} = \frac{\sqrt{3}}{\sqrt{2}} I_{phase} \, e^{-j\delta} \qquad (9.18b)$$

with $I_{phase} = |I| e^{j\alpha}$ being the (peak) phasor current in the ac network solution reference frame, and with the understanding that

$$i_q(t) = R_e\{I_{qd} \, e^{js\omega_s t}\}$$

$$i_d(t) = Im\{I_{qd} \, e^{js\omega_s t}\} \qquad (9.18c)$$

All d, q-quantities vary with the slip frequency $s\omega_s$, and can therefore be represented as phasors in the same way as the armature currents.

To obtain the impedance, the rotor currents must first be expressed as a function of armature currents. Since all rotor voltages are zero, Eq. (9.2a) can be rewritten as

$$0 = - [R_r] [i_r] - \frac{d}{dt} [\lambda_r] \qquad (9.19)$$

with

$$[\lambda_r] = [L_{ra}] i_a + [L_{rr}][i_r] \qquad (9.20)$$

from Eq. (9.3a) (subscript "r" for rotor or field structure quantities, and "a" for armature quantities). Since there is no saliency in three-phase induction machines, Eq. (9.19) and (9.20) are identical for the d- and q-axes, except

that i_a is i_d in one case, and i_q in the other case. The submatrices $[L_{ra}]$ and $[L_{rr}]$ are obtained from the matrix of Eq. (9.3a) by deleting the first row; $[L_{ra}]$ is the first column and $[L_{rr}]$ the m x m-matrix of what is left. If the rotor windings are not shorted, but connected to an R-L network, then $[R_r]$ and $[L_{rr}]$ must be modified to include the resistances and inductances of this connected network (for connected networks with voltage or current sources see Section 9.5.8). Since $[i_r]$ and i_a can both be represented as phasors with Eq. (9.18), the flux in Eq. (9.20) is also a phasor which, after differentiation, becomes

$$\frac{d}{dt}[\Lambda_r] = js\omega_s[L_{ra}]I_{qd} + js\omega_s[L_{rr}][I_r] \tag{9.21}$$

Inserting this into Eq. (9.19) produces the equation which expresses the rotor currents as a function of the armature current phasor,

$$[I_r] = -\{[R_r] + js\omega_s[L_{rr}]\}^{-1}js\omega_s[L_{ra}]I_{qd} \tag{9.22}$$

To obtain the direct axis rotor currents as complex phasor quantities, use $\text{Im}\{I_{q,d}\}$ on the right-hand side of Eq. (9.22), while the use of $\text{Re}\{I_{qd}\}$ will produce the quadrature axis rotor currents.

The next step in the derivation of the impedance is the rewriting of the armature equations (9.1a) in terms of phasor quantities. Since

$$\frac{d}{dt}\Lambda_{qd} = js\omega_s\Lambda_{qd}$$

Eq. (9.1a) becomes

$$V_{qd} = -R_aI_{qd} - js\omega_s\Lambda_{qd} - j\omega\Lambda_{qd}$$

or with $s\omega_s = \omega_s - \omega$ from Eq. (9.16),

$$V_{qd} = -R_aI_{qd} - j\omega_s\Lambda_{qd} \tag{9.23}$$

With the flux from the first row of Eq. (9.3a)

$$\Lambda_{qd} = L_{aa}I_{qd} + [L_{ar}][I_r] \tag{9.24}$$

where $[L_{ar}] = [L_{ra}]^t$, and with Eq. (9.22), Eq. (9.23) finally becomes

$$V_{qd} = -\{(R_a + j\omega_sL_{aa}) - j\omega_s[L_{ar}]\{[R_r] + js\omega_s[L_{rr}]\}^{-1}js\omega_s[L_{ra}]\}I_{qd}$$

Therefore, the positive sequence impedance is

$$Z_{pos} = R_a + j\omega_sL_{aa} - j\omega_s[L_{ar}]\{[R_r] + js\omega_s[L_{rr}]\}^{-1}js\omega_s[L_{ra}] \tag{9.25}$$

If there is only one winding on the rotor, then it can easily be shown that the impedance of Eq. (9.17b) is identical

with that of Eq. (9.25), by using the definitions of Eq. (9.17a).

To summarize: The three-phase induction machine is represented as three single-phase impedances Z_{pos} from Eq. (9.25) in the three phases 1, 2, 3. After the ac network solution of the complete network, the armature currents are initialized with Eq. (9.18b), and the rotor currents with Eq. (9.22). The calculation with Eq. (9.22) is done twice, with the imaginary part of I_{qd} to obtain the direct axis quantities, and with the real part of I_{qd} to obtain the quadrature axis quantities.

As mentioned before, the initialization works only properly for balanced cases at this time. If initialization for unbalanced cases is to be added some day, then the procedures of Section 8.4.2 and 8.4.3 for the synchronous machines should be directly applicable, because negative and zero sequence currents see the field winding as short-circuits. Therefore, there is no difference between synchronous and induction machines in the negative and zero sequence initialization.

9.5.6 Two-Phase Induction Machine

As already discussed in Section 9.5.2 for the two-phase synchronous machine, the equations for balanced operation of a two-phase machine are identical on the d, q-axes with those of the three-phase machine. The only difference is the missing factor $\sqrt{3}/\sqrt{2}$ in the conversion from phase quantities to d, q-quantities.

9.5.7 Single-Phase Induction Machine

The problem is essentially the same as discussed in Section 9.5.3 for the synchronous machine. Only positive sequence values are used now, and the second term in

$$i_d(t) = \frac{1}{2}\,|I|\,\sin(s\omega_s\,t + \alpha - \delta)\ -\ \frac{1}{2}\,|I|\,\sin((\omega_s + \omega)t + \alpha + \delta) \tag{9.26}$$

is presently ignored.

9.5.8 Doubly-Fed Induction Machine

If the rotor (field structure) windings are connected to an external network with ac voltage and/or current sources, then the EMTP will automatically assume that their frequency is equal to the specified slip frequency $s\omega$, and ignored the frequency values given for these sources.

Feeding the rotor windings from sources requires two modifications to the procedure of Section 9.5.5. In these modifications, it is assumed that the external network is represented by a Thevenin equivalent circuit, with voltage sources $[V_{Thev}]$ behind an impedance matrix $[Z_{Thev}]$ defined at slip frequency.

First, the rotor impedance matrix $[R_r] + js\omega_s[L_{rr}]$ must be modified to include the external impedances,

$$[Z_{rr}^{mod}] = [R_r] + js\omega_s[L_{rr}] + [Z_{Thev}] \tag{9.27}$$

This modification must be done twice, for the direct axis quantities and for the quadrature axis quantities. Since

$[Z_{Thev}]$ is in general different for the two axes, $[Z_{rr}{}^{mod}]$ is no longer the same on both axes.

Secondly, the left-hand side of Eq. (9.19) is no longer zero, but $[V_{Thev}]$. This will change Eq. (9.22) into

$$[I_r] = -[Z_{rr}^{mod}]^{-1}\{[V_{Thev}] + js\omega_s [L_{ra}]I_{qd}\} \qquad (9.28)$$

Again, this calculation must be done twice. For the direct axis, use $\text{Im}\{I_{qd}\}$ and the direct axis values $[Z_{rr}{}^{mod}]$ and $[V_{Thev}]$, for the quadrature axis $\text{Re}\{I_{qd}\}$ and quadrature axis values $[Z_{rr}{}^{mod}]$ and $[V_{Thev}]$.

With these two modifications, the steady-state model of the induction machine is no longer a passive impedance Z_{pos}, but becomes a three-phase voltage source $[E_{source}]$ behind three single-phase impedance branches

$$Z_{pos}^{mod} = R_a + j\omega_s L_{aa} - j\omega_s [L_{ar}] [Z_{rr}^{mod}]^{-1} js\omega_s [L_{ra}] \qquad (9.29)$$

The voltage source is found by calculating the direct axis contribution,

$$E_d = j\omega_s [L_{ar}] [Z_{rr-d}^{mod}]^{-1} [V_{Thev-d}] \qquad (9.30a)$$

and the quadrature axis contribution,

$$E_q = j\omega_s [L_{ar}] [Z_{rr-q}^{mod}]^{-1} [V_{Thev-q}] \qquad (9.30b)$$

and then transforming to phase quantities,

$$
\begin{aligned}
E_{source-1} &= \frac{\sqrt{2}}{\sqrt{3}} e^{j\delta} (E_q + jE_d) \\
\text{with} \quad E_{source-2} &= E_{source-1} \cdot e^{-j120°} \\
\text{and} \quad E_{source-3} &= E_{source-1} \cdot e^{+j120°}
\end{aligned}
\qquad (9.30c)
$$

Once the ac steady-state solution of the complete network has been obtained, the d, q, 0-armature currents are initialized with Eq. (9.18b), while the rotor currents are initialized with Eq. (9.28).

9.6 Transient Solution with Compensation Method

For the transient solution with the compensation method, the machine differential equations (9.1) and (9.2) are first converted to difference equations with the trapezoidal rule of integration. Then Eq. (9.1) becomes

$$
\begin{bmatrix} v_d(t) \\ v_q(t) \\ v_{0a}(t) \end{bmatrix} = - \begin{bmatrix} R_a & 0 & 0 \\ 0 & R_a & 0 \\ 0 & 0 & R_a \end{bmatrix} \begin{bmatrix} i_d(t) \\ i_q(t) \\ i_{0a}(t) \end{bmatrix} - \frac{2}{\Delta t} \begin{bmatrix} \lambda_d(t) \\ \lambda_q(t) \\ \lambda_{0a}(t) \end{bmatrix} + \begin{bmatrix} -\omega(t)\lambda_q(t) \\ +\omega(t)\lambda_d(t) \\ 0 \end{bmatrix} + \begin{bmatrix} hist_d \\ hist_q \\ hist_{0a} \end{bmatrix}
\tag{9.31a}
$$

with the history terms known from the preceding time step,

$$
\begin{bmatrix} hist_d \\ hist_q \\ hist_{0a} \end{bmatrix} = - \begin{bmatrix} v_d(t-\Delta t) \\ v_q(t-\Delta t) \\ v_{0a}(t-\Delta t) \end{bmatrix} - \begin{bmatrix} R_a & 0 & 0 \\ 0 & R_a & 0 \\ 0 & 0 & R_a \end{bmatrix} \begin{bmatrix} i_d(t-\Delta t) \\ i_q(t-\Delta t) \\ i_{0a}(t-\Delta t) \end{bmatrix} + \frac{2}{\Delta t} \begin{bmatrix} \lambda_d(t-\Delta t) \\ \lambda_q(t-\Delta t) \\ \lambda_{0a}(t-\Delta t) \end{bmatrix} +
$$

$$
\begin{bmatrix} -\omega(t-\Delta t)\lambda_q(t-\Delta t) \\ +\omega(t-\Delta t)\lambda_d(t-\Delta t) \\ 0 \end{bmatrix}
\tag{9.31b}
$$

The field structure equations (9.2) on the direct axis become

$$
\begin{bmatrix} v_{D1}(t) \\ \cdot \\ \cdot \\ \cdot \\ v_{Dm}(t) \end{bmatrix} = - \begin{bmatrix} R_{D1} & & & \\ & \cdot & & \\ & & \cdot & \\ & & & \cdot \\ & & & R_{Dm} \end{bmatrix} \begin{bmatrix} i_{D1}(t) \\ \cdot \\ \cdot \\ \cdot \\ i_{Dm}(t) \end{bmatrix} - \frac{2}{\Delta t} \begin{bmatrix} \lambda_{D1}(t) \\ \cdot \\ \cdot \\ \cdot \\ \lambda_{Dm}(t) \end{bmatrix} + \begin{bmatrix} hist_{D1} \\ \cdot \\ \cdot \\ \cdot \\ hist_{Dm} \end{bmatrix}
\tag{9.32a}
$$

with the known history terms

$$
\begin{bmatrix} hist_{D1} \\ \cdot \\ \cdot \\ \cdot \\ hist_{Dm} \end{bmatrix} = - \begin{bmatrix} v_{D1}(t-\Delta t) \\ \cdot \\ \cdot \\ \cdot \\ v_{Dm}(t-\Delta t) \end{bmatrix} - \begin{bmatrix} R_{D1} & & & \\ & \cdot & & \\ & & \cdot & \\ & & & \cdot \\ & & & R_{Dm} \end{bmatrix} \begin{bmatrix} i_{D1}(t-\Delta t) \\ \cdot \\ \cdot \\ \cdot \\ i_{Dm}(t-\Delta t) \end{bmatrix} + \frac{2}{\Delta t} \begin{bmatrix} \lambda_{D1}(t-\Delta t) \\ \cdot \\ \cdot \\ \cdot \\ \lambda_{Dm}(t-\Delta t) \end{bmatrix}
\tag{9.32b}
$$

On the quadrature axis, they are identical in form to Eq. (9.32), except that subscripts D1,…Dm must be replaced by Q1,…Qn. Finally for Eq. (9.2c),

$$
v_{of}(t) = - R_{of} i_{of}(t) - \frac{2}{\Delta t} \lambda_{of} + hist_{of}
\tag{9.33a}
$$

with

$$hist_{of} = -v_{of}(t-\Delta t) - R_{of} i_{of}(t-\Delta t) - R_{of} i_o f(t-\Delta t) + \frac{2}{\Delta t} \lambda_{of}(t-\Delta t) \tag{9.33b}$$

As explained in Section 12.1.2, the network connected to the armature side of the machine can be represented by the instantaneous Thevenin equivalent circuit equation

$$\begin{bmatrix} v_1(t) \\ v_2(t) \\ v_3(t) \end{bmatrix} = \begin{bmatrix} v_{1-0} \\ v_{2-0} \\ v_{3-0} \end{bmatrix} + \begin{bmatrix} R_{equiv} \end{bmatrix} \begin{bmatrix} i_1(t) \\ i_2(t) \\ i_3(t) \end{bmatrix} \tag{9.34}$$

with a sign reversal for the current compared to Section 12.1.2, to change from a load to source convention. Similarly, if external networks are connected to the field structure windings, they will also be represented by Thevenin equivalent circuits with equations of the form

$$\begin{bmatrix} v_{D1}(t) \\ \cdot \\ \cdot \\ \cdot \\ v_{Dm}(t) \end{bmatrix} = \begin{bmatrix} v_{D1-0} \\ \cdot \\ \cdot \\ \cdot \\ v_{Dm-0} \end{bmatrix} + \begin{bmatrix} R_{D-equiv} \end{bmatrix} \begin{bmatrix} i_{D1}(t) \\ \cdot \\ \cdot \\ \cdot \\ i_{Dm}(t) \end{bmatrix} \tag{9.35a}$$

$$\begin{bmatrix} v_{Q1}(t) \\ \cdot \\ \cdot \\ \cdot \\ v_{Qn}(t) \end{bmatrix} = \begin{bmatrix} v_{Q1-0} \\ \cdot \\ \cdot \\ \cdot \\ v_{Qn-0} \end{bmatrix} + \begin{bmatrix} R_{Q-equiv} \end{bmatrix} \begin{bmatrix} i_{Q1}(t) \\ \cdot \\ \cdot \\ \cdot \\ i_{Qn}(t) \end{bmatrix} \tag{9.35b}$$

and

$$v_{of}(t) = v_{of-o} + R_{of-equiv} i_{of}(t) \tag{9.35c}$$

The external network connected to the first three field structure windings is represented by a three-phase Thevenin equivalent circuit (Section 12.1.2.3), whereas the external networks connected to the rest of the field structure windings are represented by single-phase Thevenin equivalent circuits (Section 12.1.2.1). This limitation results from the fact that the BPA EMTP could handle M-phase Thevenin equivalent circuits only for M ≤ 3 at the time the Universal Machine was first implemented. In practice, this limitation should not cause any problems because the field structure windings are usually connected to separate external networks. An exception is the three-phase wound rotor of induction machines, which is the reason why a three-phase equivalent circuit was chosen for the first three rotor windings.

The solution of the machine equations is then roughly as follows:

(1)   Solve the complete network without the universal machines. Extract from this solution the Thevenin equivalent open-circuit voltages of Eq. (9.34) and (9.35), as well as the open-circuit voltages of the network which represents and mechanical system.

(2)   Predict the rotor speed $\omega(t)$ with linear extrapolation.

(3)   Transform Eq. (9.34) from phase to d, q, 0-quantities with Eq. (9.7) if the armature windings are ac windings,

$$
\begin{bmatrix} v_d \\ v_q \\ v_{oa} \end{bmatrix} = \begin{bmatrix} v_{d-o} \\ v_{q-o} \\ v_{oa-o} \end{bmatrix} + \begin{bmatrix} R_{phase-equiv} \end{bmatrix} \begin{bmatrix} i_d \\ i_q \\ i_{oa} \end{bmatrix}
\tag{9.36a}
$$

where

$$
\begin{bmatrix} v_{d-o} \\ v_{q-o} \\ v_{oa-o} \end{bmatrix} = [T]^{-1} \begin{bmatrix} v_{1-o} \\ v_{2-o} \\ v_{3-o} \end{bmatrix} \quad and \quad [R_{phase-equiv}] = [T]^{-1} [R_{equiv}] [T]
\tag{9.36b}
$$

For dc armature windings, the Thevenin equivalent circuit is already in the form of Eq. (9.36a) without transformation.

(4)   Substitute Eq. (9.36a) into Eq. (9.31a), and substitute Eq. (9.35) into Eq. (9.32). This eliminates the voltages as variables. Then solve the resulting linear equations for the m + n + 4 currents by Gauss elimination, after the fluxes are first replaced by linear functions of currents with Eq. (9.3). Using the star circuit of Fig. 9.1 instead of the more general inductance matrix of Eq. (9.3) simplifies this solution process somewhat.

(5)   Calculate the electromagnetic torque on the electrical side,

$$
T_{el}(t) = i_q(t) \lambda_d(t) - i_d(t) \lambda_q(t)
\tag{9.37}
$$

and convert it to $T_{mech}(t)$ on the mechanical side with Eq. (8.25) if the mechanical system is not modelled as a one pole-pair machine. Use $T_{mech}(t)$ as a current source in the Thevenin equivalent circuit which represents the mechanical system and solve it to obtain the speed (as an equivalent voltage). Up to 3 universal machines can share the same mechanical system, because the EMTP uses an M-phase compensation method for $M \leq 3$ (see Section 12.1.2.3).

(6)   If the speed calculated in (5) differs too much from the predicted speed, then return to step (3). Otherwise:

(7)   Update the history terms of Eq. (9.31b), (9.32b) for d- and q-axes, and (9.33b) for the next time step.

(8)   Transform the armature currents from d, q, 0-quantities to phase quantities with Eq. (9.7) (only if the windings are ac windings).

(9)   Find the final solution of the complete network by super-imposing the effects of the armature currents, of

the field-structure currents (if they have externally connected networks) and of the current representing the electromagnetic torque in the network for the mechanical system, with Eq. (12.8) of Section 12.

(10)   Proceed to the next time step.

Since the variables of the mechanical system usually change much slower than the electrical variables, because of the relatively large moment of inertia of practical machines, the prediction of the speed is fairly good. As a consequence, the number of iterations typically lies between 1 and 3.

Interfacing the solution of the machine equations with the solution of the electric network through compensation offers the advantage that the iterations are confined to the machine equations only. Furthermore, if a small tolerance is used for checking the accuracy of the speed, the solution is practically free of any interfacing error.

The only limitation of the compensation method is the fact that the universal machines must be separated from each other, and from other compensation-based nonlinear elements, through distributed-parameter lines with travel time. Stub lines can be used to introduce such separations artificially, but such stub lines create their own problems. Because of this limitation, a second solution option has been developed, as described in the next section.

9.7 Transient Solution with Armature Flux Prediction

In the transient solution of the synchronous machine of Section 8, essentially voltage sources behind resistances R_a and average subtransient inductances $(L_d'' + L_q'')/2$ are used, with the trapezoidal rule applied to the inductance part. The voltage sources contain predicted currents and the predicted speed.

The prediction-based interface option for the universal machine also uses voltage sources with elements of prediction in them, but just behind resistances R_a, with no inductance part (Fig. 9.6). If we think of R_a as belonging to the electric network and not to the machine, then Eq.
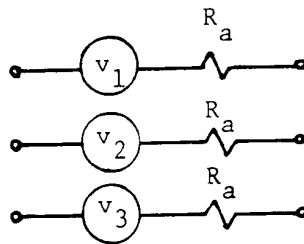
Fig. 9.6 - Thevenin equivalent circuit for universal machine

(9.1) becomes a simple relationship between armature voltages and fluxes,

$$
\begin{bmatrix} v_d \\ v_q \\ v_{oa} \end{bmatrix} = -\frac{d}{dt}\begin{bmatrix} \lambda_d \\ \lambda_q \\ \lambda_{oa} \end{bmatrix} + \begin{bmatrix} -\omega\lambda_q \\ +\omega\lambda_d \\ 0 \end{bmatrix}
\tag{9.38}
$$

The fluxes always change smoothly, in contrast to the voltages which can suddenly jump in case of short-circuits. Therefore, the fluxes are chosen as variables suitable for prediction. Furthermore, the fluxes λ_d, λ_q of induction machines vary sinusoidally with slip frequency during steady-state operation, whereas the fluxes seen from a synchronously rotating reference frame (rotating at the supply frequency ω_s) would remain constant. Because of this, the fluxes seen from a synchronously rotating reference frame are predicted, rather than λ_d, λ_q. This requires a transformation of Eq. (9.38) from the d, q-axes to the synchronously rotating reference frame [140]. Alternatively, one can forget about the original transformation from phase quantities to the d, q-axes altogether, and transform the phase quantities directly to the ds, qs-axes of the synchronously rotating reference frame. That means that $d\beta/dt = \omega$ must be replaced by ω_s, which leads to

$$
\begin{bmatrix} v_{ds} \\ v_{qs} \\ v_{oa} \end{bmatrix} = -\frac{d}{dt}\begin{bmatrix} \lambda_{ds} \\ \lambda_{qs} \\ \lambda_{oa} \end{bmatrix} + \begin{bmatrix} -\omega_s\lambda_{qs} \\ +\omega_s\lambda_{ds} \\ 0 \end{bmatrix}
\tag{9.39}
$$

The only difference with Eq. (9.38) is the replacement of rotor speed ω by the ac supply frequency ω_s. This simple change works only for the voltage equations; for the flux-current relationships the synchronously rotating reference frame cannot be used because that would make the inductances time-dependent rather than constant.

The fluxes λ_{ds}, λ_{qs}, λ_{oa} on the synchronously rotating axes are now predicted linearly,

$$
\begin{bmatrix} -\lambda_{ds-pred} \\ \lambda_{qs-pred} \\ \lambda_{oa-pred} \end{bmatrix} = 2\begin{bmatrix} \lambda_{ds}(t-\Delta t) \\ \lambda_{qs}(t-\Delta t) \\ \lambda_{oa}(t-\Delta t) \end{bmatrix} - \begin{bmatrix} \lambda_{ds}(t-2\Delta t) \\ \lambda_{qs}(t-2\Delta t) \\ \lambda_{oa}(t-2\Delta t) \end{bmatrix}
\tag{9.40}
$$

and the backward Euler method (see Appendix I.9) is then applied to Eq. (9.39),

$$
\begin{bmatrix} v_{ds}(t) \\ v_{qs}(t) \\ v_{oa}(t) \end{bmatrix} = -\frac{1}{\Delta t}\begin{bmatrix} \lambda_{ds-pred} - \lambda_{ds}(t-\Delta t) \\ \lambda_{qs-pred} - \lambda_{qs}(t-\Delta t) \\ \lambda_{oa-pred} - \lambda_{oa}(t-\Delta t) \end{bmatrix} + \begin{bmatrix} -\omega_s\lambda_{qs-pred} \\ +\omega_s\lambda_{ds-pred} \\ 0 \end{bmatrix}
\tag{9.41}
$$

With all quantities on the right-hand side known (either from the preceding time step or from prediction), the terminal voltages are now known, too, and can be transformed back to phase quantities with

$$
\begin{bmatrix} v_1(t) \\ v_2(t) \\ v_3(t) \end{bmatrix} = \begin{bmatrix} \cos(\omega_s t) & \sin(\omega_s t) & 0 \\ -\sin(\omega_s t) & \cos(\omega_s t) & 0 \\ 0 & 0 & 1 \end{bmatrix}\begin{bmatrix} v_{ds}(t) \\ v_{qs}(t) \\ v_{oa}(t) \end{bmatrix}
\tag{9.42}
$$

The representation of the universal machine as three voltage sources $v_1(t)$, $v_2(t)$, $v_3(t)$ behind resistances R_a

in the complete electric network is only used on the armature side, whereas compensation-based interfaces are still maintained for the field structure windings and for the mechanical system. With this in mind, the solution process works roughly as follows:

(1)   With the universal machine represented as voltage sources behind R_a (implemented as current sources in parallel with R_a in the EMTP), solve the complete electric network. Extract from this solution the Thevenin equivalent open-circuit voltages of Eq. (9.35) if there are any external networks connected to the field structure windings (see Section 9.6 for details about three-phase compensation on the first three windings, and single-phase compensation on the rest). Extract as well the open-circuit voltages of the network which represents the mechanical system.

(2)   Execute steps (2) to (9) of the compensation-based procedure described in the preceding Section 9.6, except that the armature currents i_1, i_2, i_3 (and i_d, i_q, i_{oa} after transformation with $[T^{-1}]$) are now known from step (1) and used directly in place of the Thevenin equations (9.36) for the armature part. The calculations for the other parts remain unchanged.

(3)   Rotate the armature fluxes λ_d, λ_q, λ_{oa} from the d, q-axes to the synchronously rotating ds, qs-axes

$$\begin{bmatrix} \lambda_{ds} \\ \lambda_{qs} \\ \lambda_{oa} \end{bmatrix} = \begin{bmatrix} \cos(\omega_s t - \beta) & -\sin(\omega_s t - \beta) & 0 \\ \sin(\omega_s t - \beta) & \cos(\omega_s t - \beta) & 0 \\ 0 & 0 & 1 \end{bmatrix} \begin{bmatrix} \lambda_d \\ \lambda_q \\ \lambda_{oa} \end{bmatrix} \tag{9.43}$$

and use them to predict the voltage sources for the next time step with Eq. (9.40) to (9.42). Note that no predictions for the speed and angle are needed here.

(4)   Proceed to (1) to find the solution at the next time step.

Experience has shown [140] that this interfacing option is as accurate as the compensation-based interface of Section 9.6. It also requires less computation time. Its numerical stability can be partly attributed to the backward Euler method in Eq. (9.41). As shown in Appendix I.9, the backward Euler method is identical to the trapezoidal rule of integration with critical damping, and is therefore absolutely numerically stable. However, Eq. (9.41) involves predictions as well, and the comparison is therefore not completely correct.

9.8 Saturation

Saturation effects are only represented for the main flux (M_d in Fig. 9.1), except for the special induction machine model of Ontario Hydro, which includes saturation effects in the leakage fluxes as well.

The saturation curve of the universal machine is approximated as two piecewise linear segments for the d-axis, the q-axis, or for both (Fig. 9.7). By using the star circuit of Fig. 9.1,
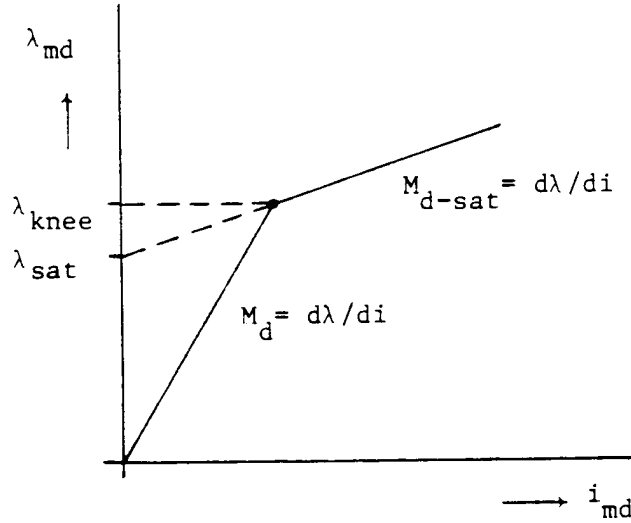
Fig. 9.7 - Piecewise linear inductance

the piecewise linear representation can easily be implemented. Whenever the flux lies above the knee-point value λ_{knee}, the relationship of Eq. (9.4b) in the form of

$$\lambda_{md} = M_d\, i_{md} \tag{9.44a}$$

is simply replaced by

$$\lambda_{md} = \lambda_{sat} + M_{d-sat}\, i_{md} \tag{9.44b}$$

on the direct axis, and analogous on the quadrature axis.

Residual flux can be represented as well. In that case, the characteristic of Fig. 9.8 is used. If the absolute value of the flux is less than $\lambda_{\text{residual}}$, then the M_d-branch is open-circuited,

$$i_{md} = 0 \qquad if \;\; |\lambda_{md}| \;<\; \lambda_{residual} \tag{9.45a}$$

$$\lambda_{md} = \lambda_{residual} + M_d\, i_{md} \qquad if \;\; \lambda_{residual} \;\leq\; |\lambda_{md}| \;\leq\; \lambda_{knee} \tag{9.45b}$$

and

$$\lambda_{md} = \lambda_{sat} + M_{d-sat}\, i_{md} \qquad if \;\; |\lambda_{md}| \;>\; \lambda_{knee} \tag{9.45c}$$
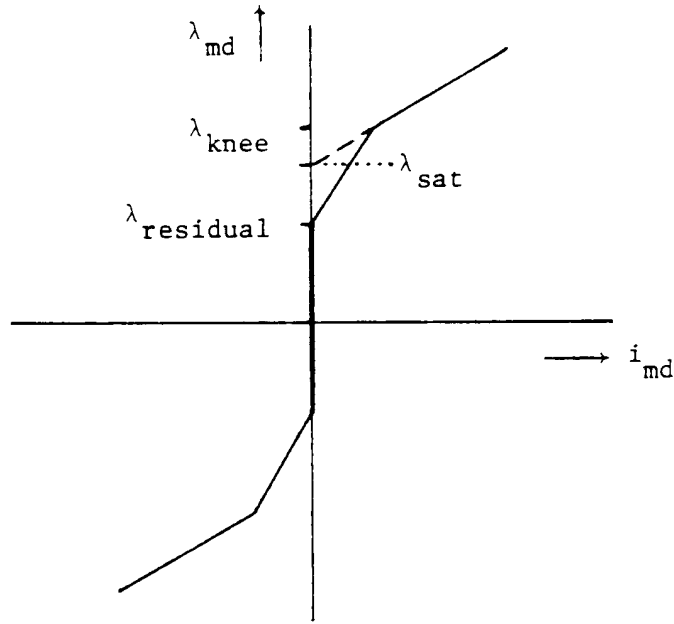
Fig. 9.8 - Residual flux

T   h   e
decoupled approach of d- and q-axis saturation works reasonably well for salient-pole synchronous machines and for dc machines with a definite field coil in one axis. However, when both the armature and field structures are round with no pronounced saliency, as in most induction machines and in round-rotor synchronous machines, then this decoupled approach leads to unacceptable results. Therefore, a "total saturation" option is available, which uses a solution method very similar to that discussed in Section 8.6.

10. SWITCHES

Any switching operation in a power system can potentially produce transients. For the simulation of such transients, it is necessary to model the various switching devices, such as

> circuit breakers,
>
> load breakers,
>
> dc circuit breakers,
>
> disconnectors,
>
> protective gaps,
>
> thyristors, etc.

So far, all these switching devices are represented as ideal switches in the EMTP, with zero current ($R = \infty$) in the open position and zero voltage ($R = 0$) in the closed position. If the switch between nodes k and m is open, then both nodes are represented in the system of nodal equations, whereas for the closed switch, both k and m become one node (Fig. 10.1). It is

(a) open   (b) closed
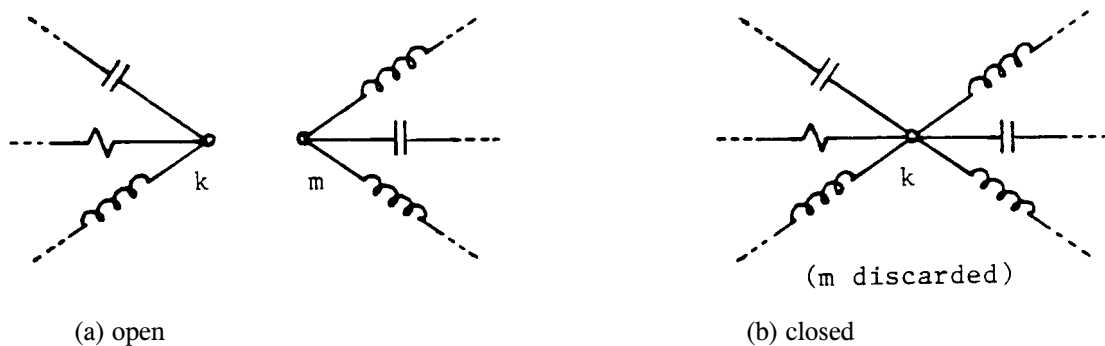
Fig. 10.1 - Representation of switches in the EMTP

possible, of course, to add other branches to the ideal switch, to more closely resemble the physical behavior, e.g., to add a capacitance from k to m for the representation of the stray capacitance or the R-C grading network of an actual circuit breaker. The characteristics of the arc in the circuit breaker are not yet modelled, but work is in progress to include them in future versions.

Switches are not needed for the connection of voltage and current sources if they are connected to the network at all times. The source parameters T_{START} and T_{STOP} can be used in place of switches to have current sources temporarily connected for $T_{START} \leq t \leq T_{STOP}$, as explained in Section 7. For voltage sources, this definition would mean that the voltage is zero for $t < T_{START}$ and for $t > T_{STOP}$, which implies a short-circuit rather than a disconnection. Therefore, switches are needed to disconnect voltage sources.

Switches are also used to create piecewise linear elements, as discussed in Section 12.

10.1 Basic Switch Types

There are five basic switch types in the EMTP, which are all modelled as ideal switches. They differ only in the criteria being used to determine when they should open or close.

10.1.1 Time-Controlled Switch

This type is intended for modelling circuit breakers, disconnectors, and similar switching devices, as well as short-circuits. The switch is originally open, and closes at T_{CLOSE}. It opens again after T_{OPEN} (if $< t_{max}$), either as soon as the absolute value of the switch current falls below a user-defined current margin, or as soon as the current goes through zero (detected by a sign change), as indicated in Fig. 10.2 For the simulation of circuit breakers, the latter criterion for opening should normally be used. The time between closing and opening can be delayed by a user-defined time delay.

(a) current going through zero   (b) current less than margin
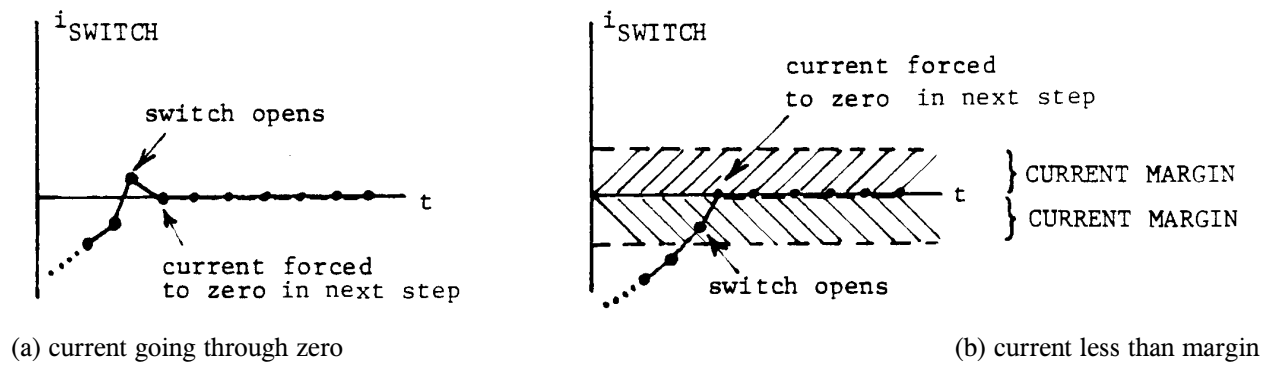
Fig. 10.2 - Opening of time-controlled switch

The closing takes place at the time step nearest to T_{CLOSE} in the UBC version (Fig. 10.3(a)), and at the time step where $t \geq T_{CLOSE}$ for the first time in the BPA version (Fig. 10.3(b)).
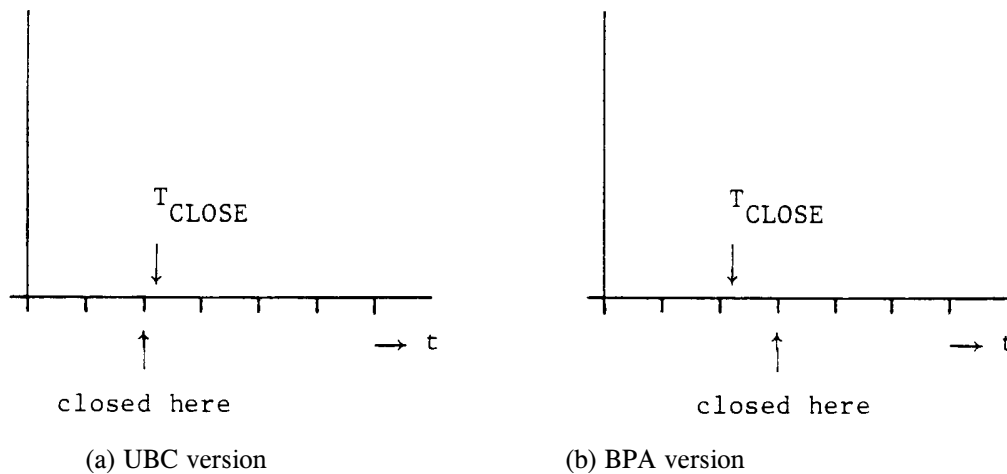

(a) UBC version   (b) BPA version

Fig. 10.3 - Closing of time-controlled switch

10-2

$T_{CLOSE} < 0$ signals to the EMTP that the switch should be closed from the very beginning. If the simulation starts from automatically calculated ac steady-state conditions, then the switch will be recognized as closed in the steady-state phasor solution.

The BPA EMTP has an additional time-controlled switch type (TACS-controlled switch type 13), in which the closing and opening action is controlled by a user-specified TACS variable from the TACS part of the EMTP. With that feature it is easy to build more complicated opening and closing criteria in TACS.

10.1.2 Gap Switch

This switch is used to simulate protective gaps, gaps in surge arresters, flashovers across insulators, etc. It is always open in the ac steady-state solution. In the transient simulation, it is normally open, and closes as soon as the absolute value of the voltage across the switch exceeds a user-defined breakdown or flashover voltage. For this checking procedure, the voltage values are averaged over the last two time steps, to filter out numerical oscillations. Opening occurs at the first current zero, provided a user-defined delay time has already elapsed. This close-open cycle repeats itself whenever the voltage exceeds the breakdown or flashover voltage again, as indicated in Fig. 10.4
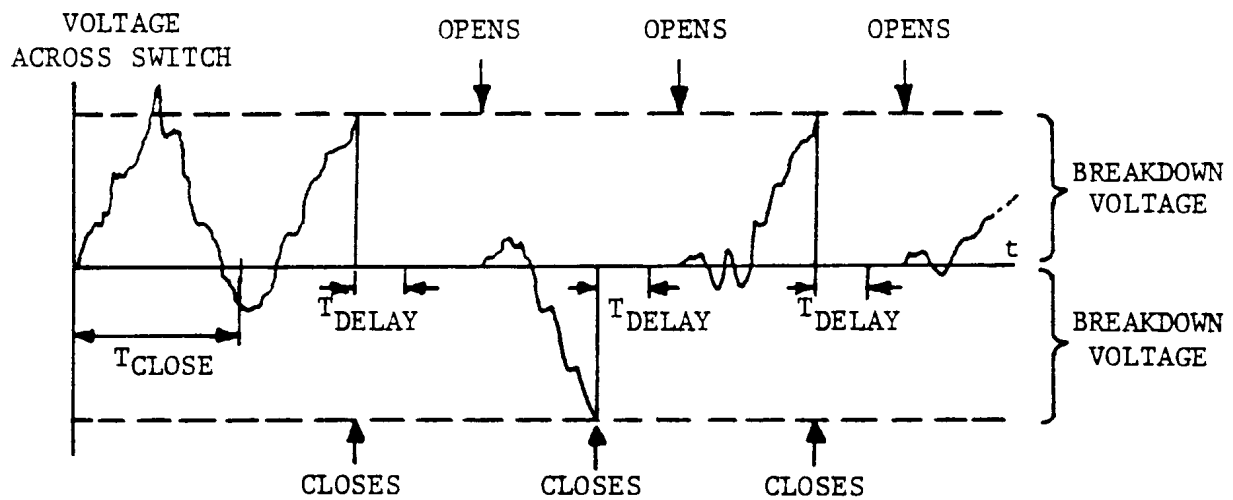
Fig. 10.4 - Repetition of close-open operation for gap switch

It is well known that the breakdown voltage of a gap or the flashover voltage of an insulator is not a simple constant, but depends on the steepness of the incoming wave. This dependence is usually shown in the form of a voltage-time characteristic (Fig. 10.5), which can be measured in the laboratory for standard impulse waveshapes. Unfortunately, the waveshapes of power system transients are usually very irregular, and voltage-time characteristics can seldom be used, therefore. Analytical methods based on the integration of a function

$$F = \int_{t_1}^{t_2} (v(t) - v_0)^k \, dt \tag{10.1}$$

10-3
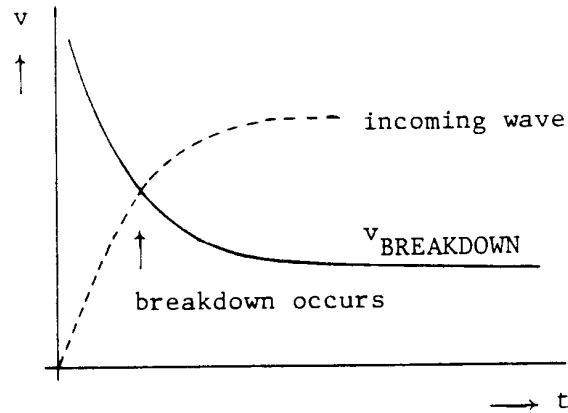
Fig. 10.5 - Voltage-time characteristic of a gap

could easily be implemented. In Eq. (10.1), v_o and k are constants, and breakdown occurs at instant t_2 where the integral value F becomes equal to a user-defined value [8]. For k = 1, this is the "equal-area criterion" of D. Kind [172]. Neither the voltage-time characteristic nor Eq. (10.1) has been implemented so far.

The BPA EMTP has an additional gap switch type (TACS-controlled switch type 12), in which the breakdown or flashover is controlled by a firing signal received from the TACS part of the EMTP (Section 13). With that feature, voltage-time characteristics or criteria in the form of Eq. (10.1) can be simulated in TACS by skilled users.

10.1.3 Diode Switch

This switch is used to simulate diodes where current can flow in only one direction, from anode m to cathode k (Fig. 10.6). The diode switch closes whenever $v_m \geq v_k$ (voltage values averaged over two successive time steps to filter out numerical oscillations), and opens after the elapse of a user-defined time delay as soon as the current i_{mk} becomes negative, or as soon as its magnitude becomes less than a user-defined margin.
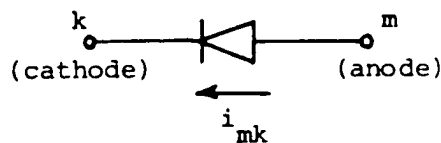
Fig. 10.6 - Diode switch

In the ac steady-state solution, the diode switch can be specified as either open or closed.

10.1.4 Thyristor Switch (TACS Controlled)

This switch is the building block for HVDC converter stations. It behaves similarly to the diode switch, except that the closing action under the condition of $v_m \geq v_k$ only takes place if a firing signal has been received from the TACS part of the EMTP (Section 13).

10.1.5 Measuring Switch

A measuring switch is always closed, in the transient simulation as well as in the ac steady-state solution. It is used to obtain current, or power and energy, in places where these quantities are not otherwise available.

The need for the measuring switch arose because the EMTP does not calculate currents for certain types of branches in the updating procedure inside the time step loop. These branches are essentially the polyphase coupled branches with lumped or distributed parameters. The updating procedures could be changed fairly easily to obtain the currents, as an alternative to the measuring switch.

10.2 Statistical Distribution of Switching Overvoltages

Since circuit breakers can never close into a transmission line exactly simultaneously from both ends, there is always a short period during which the line is only closed, or reclosed, from one end, with the other end still open. Travelling waves are then reflected at the open end with the well-known doubling effect, and transient overvoltages of 1 p.u. at the receiving end are therefore to be expected. In reality, the overvoltages can be higher for the following reasons:

(a)   the line is three-phase with three different mode propagation velocities,

(b)   the network on the source side of the circuit breaker may be fairly complicated, and can therefore create rather complicated reflections,

(c)   the line capacitance may still be charged up from a preceding opening operation ("trapped charge" in reclosing operations),

(d)   the magnitude of the overvoltage depends on the instant of closing (point on waveshape),

(e)   the three poles do not close simultaneously (pole spread).

In the design of transmission line insulation, it would make little sense to base the design on the highest possible switching surge overvoltage, because that particular event has a low probability of ever occurring, and because the line insulation could not be designed economically for that single high value. Furthermore, it is impossible or very difficult to know which combination of parameters would produce the highest possible overvoltage. Instead, 100 or more switching operations are usually simulated, with different closing times and possibly with variation of other parameters, to obtain a statistical distribution of switching surge overvoltages. This is usually shown in the form of a cumulative frequency distribution (Fig. 10.7).
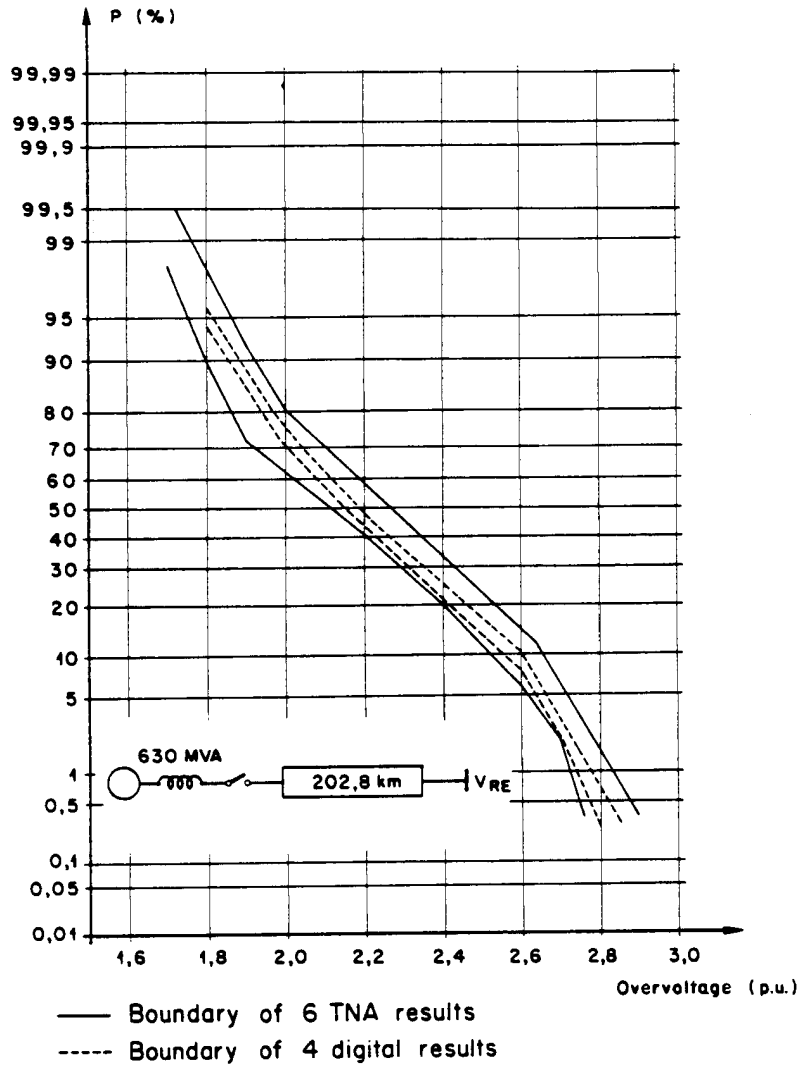
Fig. 10.7 - Cumulative frequency distribution of receiving end overvoltages from 100 digital computer and TNA simulations [18]. Reprinted by permission of CIGRE

For the left-most curve in Fig. 10.7, an overvoltage of 1.6 p.u. or higher would have to be expected in 5% of the switching operations. Insulation design for withstanding a certain overvoltage often refers to a 2% probability. The withstand voltage of insulators does not only depend on the peak value, but on the waveshape as well. For irregular waveshapes, as they occur in switching surges, it is very difficult to take the waveshape into account, and it is therefore usually ignored.

The BPA EMTP has special switch types for running a large number of cases in which the opening or closing times are automatically varied. The output includes statistical overvoltage distributions, e.g., in the form of Fig. 10.7. There are two types, one in which the closing times are varied statistically, and the other in which they are varied systematically. How well these variations represent the true behavior of the circuit breaker is difficult to say. Before the contacts have completely closed, a discharge may occur across the gap and create "electrical" closing slightly ahead of mechanical closing ("prestrike"). There is very little data available on prestrike values, however.

10.2.1 Statistics Switch

The closing time T_{CLOSE} of each statistics switch is randomly varied according to either a Gaussian (normal) distribution, or a uniform distribution, as shown in Fig. 10.8. After each variation, for all such switches, the case is rerun to obtain the peak overvoltages. The mean closing time T and the standard deviation σ are specified by the user. In addition to closing time variations of each individual switch, a random delay can be added, which is the same for all statistics switches, and which always follows a uniform distribution.
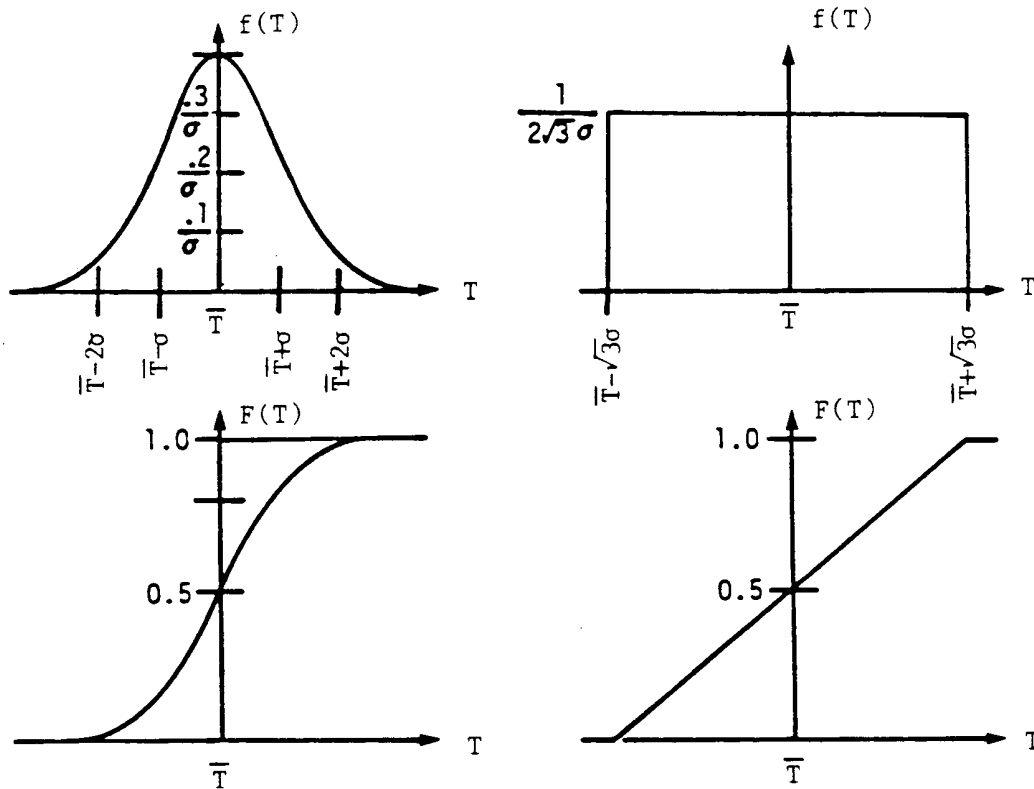
Fig. 10.8 - Probability distribution for the closing time T_{CLOSE} of the statistics switch. f(T) = density function, F(T) = cumulative distribution function

There is also an option for dependent "slave" switches, in which the closing time depends on that of a "master" switch,

$$T_{CLOSE-slave} = T_{CLOSE-master} + T_{random} \qquad (10.2)$$

with

$T_{CLOSE-master}$ =   statistically determined closing time of a "master" statistics switch,

T_{random} =   random time delay defined by a mean time and standard deviation.

This slave switch may in turn serve as a master switch for another slave switch. Slave switches are usually used to model circuit breakers with closing resistors. The first contact to close would be the master switch, with the next one or more contacts to close being slave switches.

Statistics switches can also be used for random openings, instead of closings, but this option is less

important. In realistic simulations, the current interruption only occurs at the first current zero after T_{OPEN}, and there are only a few combinations of phase sequences in which the three poles of a three-phase circuit can interrupt. It may be just as easy to simulate these combinations directly, rather than statistically.

10.2.2 Systematic Switch

Each systematic switch has its closing time systematically varied, from T_{min} to T_{max} in equal increments of ΔT. If this is done for the three poles of a three-phase circuit breaker, it can result in a very large number of cases which have to be run automatically, as indicated in Fig. 10.9.
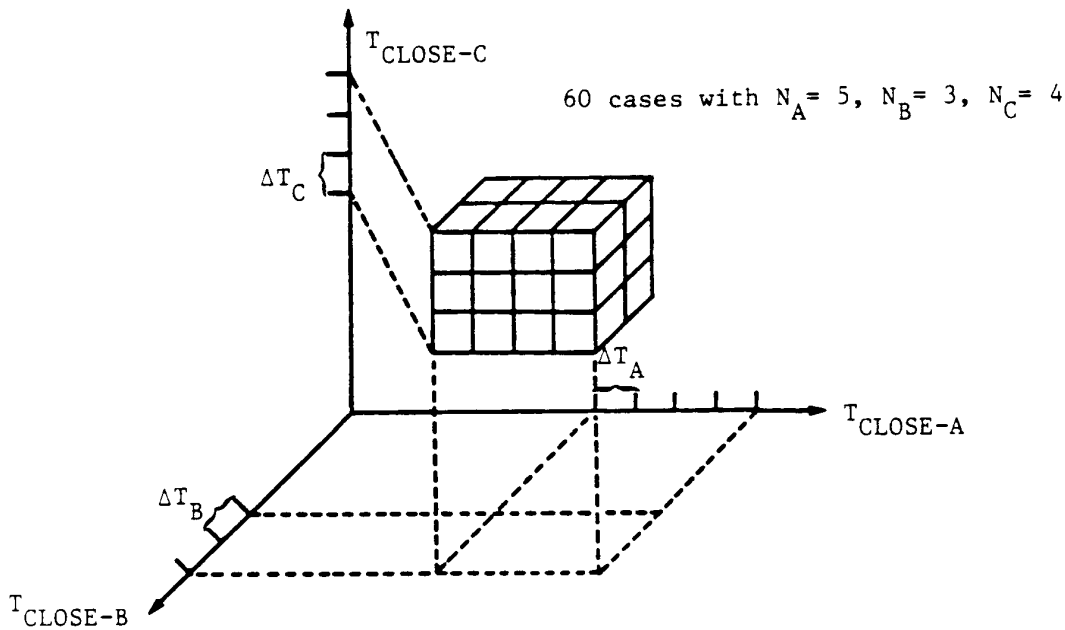
Fig. 10.9 - Three-dimensional space for three closing times $T_{CLOSE-A}$, $T_{CLOSE-B}$, $T_{CLOSE-C}$

Again, there is an option for dependent "slave" switches, in which the closing time is

$$T_{CLOSE-slave} = T_{CLOSE-master} + T_{OFFSET} \tag{10.3}$$

where T_{OFFSET} is now a constant, rather than a random variable as in Eq. (10.2). As in the case of statistics switches, slave switches are used to model the second (or third,…) contact to close in circuit breakers with closing resistors. Slave switches do not increase the dimension of the vector space shown in Fig. 10.9 for three master switches.

10.3 Solution Methods for Networks with Switches

There is more than one way of handling changing switch positions in the transient solution part of the EMTP. For the ac steady-state solution part, the problem is simpler, because the equations are only solved once. In that case, it is best to use 2 nodes for open switches, and 1 node for closed switches, as shown in Fig. 10.1.

In some programs, the switch is represented as a resistance R, with a very large value if the switch is open and a very small value if the switch is closed. As explained in Section 2.1, very large values of R do not cause numerical problems in solution methods based on nodal equations, but very small values can cause numerical problems. This approach was therefore not chosen for the EMTP. The calculation of the switch current is trivial in this approach, with

$$i_{km} = (v_k - v_m)/R \tag{10.4}$$

The compensation method described in Section 12.1.2 provides another approach for handling switches. To represent M-switches, an M-phase Thevenin equivalent circuit would be precomputed with an equation of the form

$$[v_k] - [v_m] = [v_{k-0}] - [v_{m-o}] - [R_{Thev}][i_{km}] \tag{10.5}$$

The switch currents, which are needed for the superposition calculation (Eq. (12.8) in Section 12.1.2), are simply $[i_{km}] = 0$ if all switches are open or

$$[i_{km}] = [R_{Thev}]^{-1}\{[v_{k-0}] - [v_{m-0}]\} \tag{10.6}$$

if all switches are closed. If only some switches are closed, then $[R_{Thev}]$ in Eq. (10.6) is a submatrix obtained from the full matrix after throwing out the rows and columns for the open switches. The switch currents are automatically obtained in this approach, and there should not be any numerical problems. The compensation-based method is not used in the EMTP now, though it may be chosen in future versions for the inclusion of arc characteristics. It was used in a predecessor version of the EMTP developed by the author in Munich. The treatment of switches in the UBC EMTP, as discussed next in Section 10.3.1, is essentially the same as the compensation-based method, even though the programming details are different.

A third approach is to change the network connections whenever a switch position changes. As indicated in Fig. 10.1, there are two nodes whenever the switch is open, and only a single node whenever the switch is closed. This approach has been implemented in the EMTP, in two different ways.

10.3.1 Network Reduction to Switch Nodes

In the UBC EMTP, and in an older version of the BPA EMTP, nodes which have switches connected are eliminated last, as indicated in Fig. 10.10. Before entering the time step

(a)   initial reduction   (b)   completion of triangularization whenever switches change position
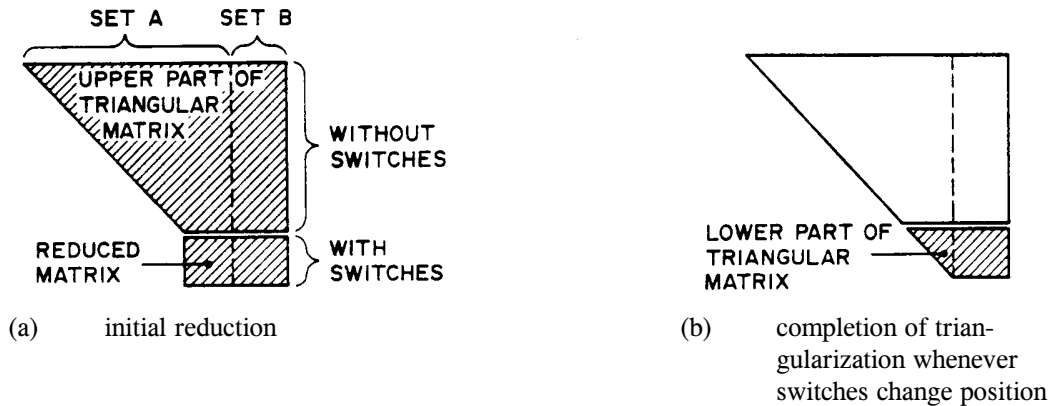
Fig. 10.10 - Matrix reduction for nodes with switches

loop, normal Gauss elimination is used on those nodes with unknown voltages (subset A) which do not have switches connected to them. For the rest of the nodes of subset A with switches, the Gauss elimination is stopped at the vertical line which separates the non-switch nodes from the switch nodes. This creates the reduced matrix illustrated in Fig. 10.10(a). All switches are assumed to be open in this calculation.

Whenever a switch position changes in the time step loop, this reduced matrix is first modified to reflect the actual switch positions. If the switch between nodes k and m is closed, then the two respective rows and columns are added to form one new row and column using the higher node number between k and m, and the other row and column for the lower node number is discarded. If the switch is open, no changes are made in the reduced matrix. After these modifications, the triangularization is completed for the entire matrix of subset A, as indicated in Fig. 10.10(b). In repeat solutions, the addition of rows for closed switches must be applied to the right-hand sides as well. In the backsubstitution, the voltage of the discarded lower node number is set equal to the voltage of the retained higher node number.

Using this reduced matrix scheme has the advantage that the triangularization does not have to be done again for the entire matrix whenever switch positions change. Instead, re-triangularization is confined to the lower part. This scheme works well if the network contains only a few switches. If there are many switches, as in HVDC converter station simulations, then this method becomes less and less efficient, and straightforward re-triangularization may then be the best approach, as described in Section 10.3.2. When the method was first programmed, only two rows and columns could be added. This has led to the restriction that a node with unknown voltage can only have one switch connected to it in this scheme, because two closed switches connected to one node would require the addition of three rows and columns (to collapse three nodes into one). This restriction no longer applies to newer BPA versions which use the method of Section 10.3.2.

The current calculation for closed switches in the time step loop uses the row of either node k or m in the reduced matrix (where the switch was assumed to be open) after the right-hand sides have been modified by the downward operations with the upper part of the triangular matrix. In effect, this sums up the currents through the branches connected to k or m, which must be equal to the switch current. In the ac steady-state solution, the switch

currents are no calculated at all, but simply set to zero at t = 0. This is obviously incorrect, but the values will be correct at Δt, $2\Delta t$,...t_{max}.

10.3.2 Complete Re-Triangularization

In newer versions of the BPA EMTP, the reduction scheme discussed in the preceding section is no longer used. Instead, the matrix is built and triangularized completely again whenever switch positions change, or when the slope of piecewise linear elements changes. The current is calculated from the original row or either node k or m, with all switches open, with the proper right-hand side.

With this newer scheme, any number of switches can be connected to any node, as long as the current in each switch is uniquely defined. A delta-configuration of closed switches, or two closed switches in parallel, would therefore not be allowed. Also, a switch cannot connect two voltage sources together, which is unrealistic anyhow because it would create an infinite current. The switch currents are now calculated in the ac steady-state solution as well, and switch currents are therefore correct at all times, including at t = 0.

10.3.3 Switch-Closing

When the EMTP prints a message that a switch is closed after T seconds, T will always be an integer multiple of Δt, because the EMTP cannot handle variable step sizes so far. The actual closing time T will therefore differ somewhat from the user-specified time T_{CLOSE}, as explained in Fig. 10.3.

The network will already have been solved, with the switch still open, when the decision is made to close the switch at time T. As shown in Fig. 10.11, all voltages and currents at t = T are therefore the "preclosing" values. After the network solution at t = T, the matrix is rebuilt and re-triangularized for the closed switch position, and in the transition from T to T + Δt, it is assumed that all variables change linearly with finite slope, rather than abruptly.
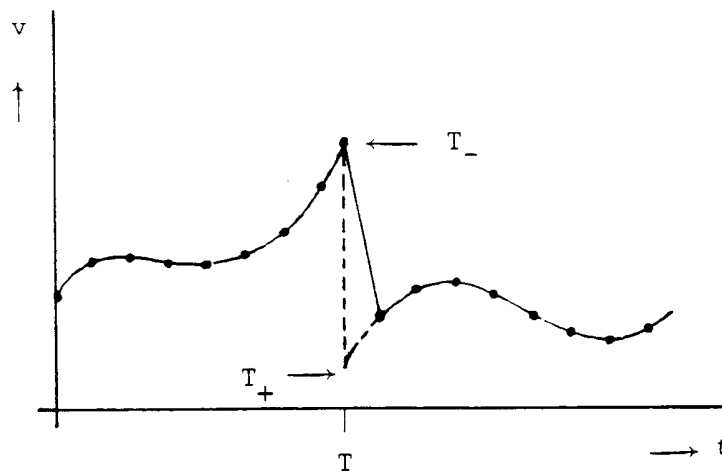

Fig. 10.11 - Switch closing or opening at time T

In many cases, the linear transition with a finite slope indicated in Fig. 10.11 is a reasonable assumption. For example, if the voltage v were the voltage across a capacitor, then v could not change abruptly anyhow. On the other

hand, if it were the voltage across an inductance it could indeed jump, as indicated by the dotted line in Fig. 10.11. Such voltage jumps are very common in HVDC converter stations. The exact method for handling such jumps would be the addition of a second "post-change" solution at T_+ after the "pre-change" solution at T_-, without advancing in time. As explained in Appendix II, methods are now known to re-initialize at T_+, but they have not yet been implemented in the EMTP.

10.3.4 Switch Opening

The treatment of switch opening in the solution is similar to that of switch closing. Again, the network will already have been solved, with the switch still closed, when the decision is made to open the switch at time T. To explain the transition from T to T + Δt, Fig. 10.11 can again be used: all voltage and currents at t = T will be the "pre-change" values, and after these values have been obtained, the matrix will be rebuilt and re-triangularized for the "post-change" configuration. All variables are then assumed to vary linearly rather than abruptly in the transition from T to T + Δt.

As already explained in Section 2.2.2,, not re-initializing the variables at T_- with a second "post-change" solution creates numerical oscillations in the voltages across inductances. They can be prevented with the re-initialization method of Appendix II, which has not yet been implemented in the EMTP, or with the damping resistances discussed in Section 2.2.2. For many years it was thought that the numerical oscillations occur only because the current is never exactly zero when the switch opens, with a residual energy $L(\Delta i)^2/2$ left in the inductance. It is now known that they also occur if Δi = 0. Decreasing Δt will not cure the oscillations either.

There are cases where the numerical oscillation, in place of the correct sudden jump, can serve as an indicator of improper modelling. An example is transient recovery voltage studies, where a sudden jump in voltage would indicate that the proper stray capacitances are missing from the model. Fig. 10.12 shows a simple example: both switches I and II in the network of Fig. 10.12(a) are closed at t = 0 to charge the capacitor. Switch II opens when the capacitor is charged up and when the current is more or less zero. Fig. 10.12(b) shows the numerical oscillations in the voltage v_2 on the feeding network side. By adding a stray capacitance to the left side of the switch, as illustrated in Fig. 10.12(c), the transient recovery voltage on the feeding side would no longer have the unrealistic jump, as shown in Fig. 10.12(d).

10.4 Arc Phenomena in Circuit Breakers

When the contacts of a circuit breaker open, they draw an electric arc which maintains the current flow until interruption takes place at current zero. In high voltage circuit breakers, the arc resistance is negligibly small if normal load currents or high short-circuit currents are
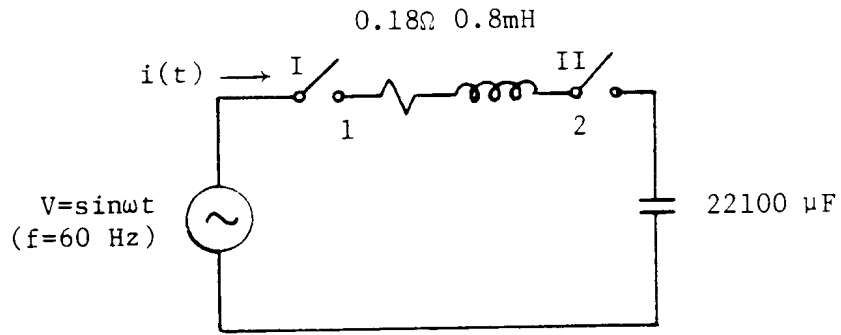
(a) network
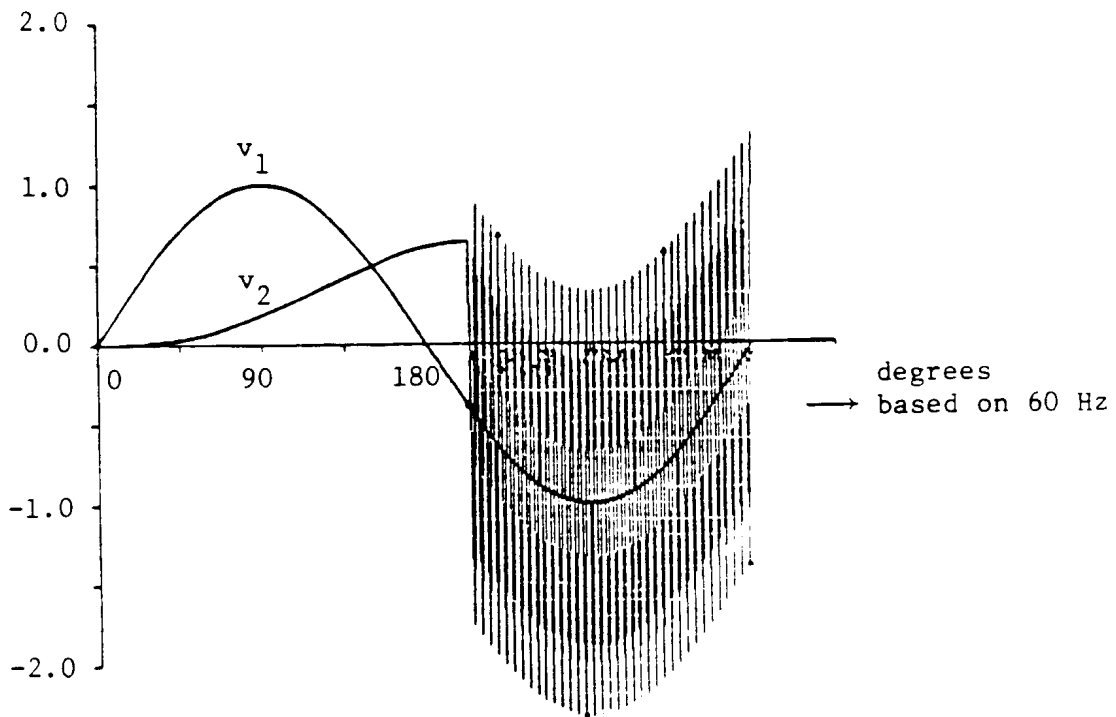
(b) voltage across inductance
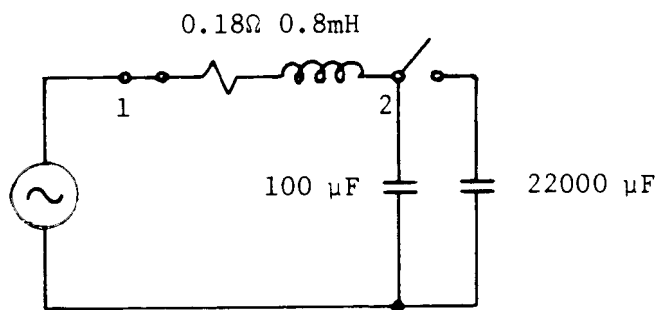
(c) modified network

10-13
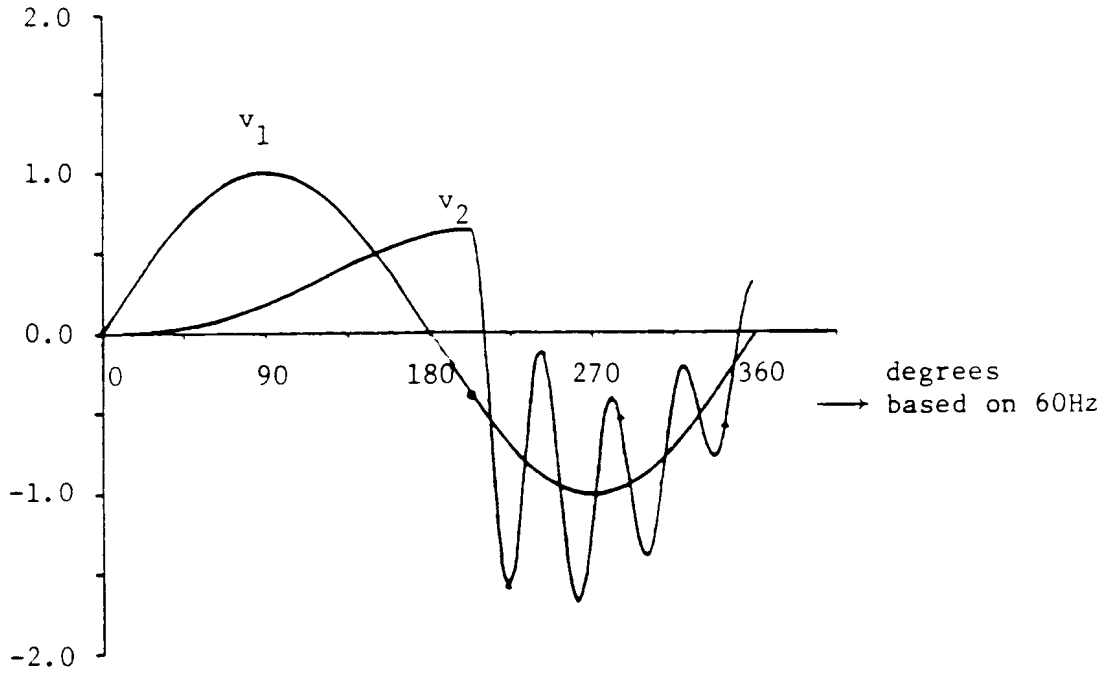
(d) voltage across inductance

Fig. 10.12 - Capacitor charging and discharging

interrupted. In the interruption of small inductive currents (e.g., in switching off an unloaded transformer), the arc resistance is higher because of the falling arc characteristic, and may be important in deciding whether current interruption is successful or not. Immediately after current interruption, a transient recovery voltage builds up across the contacts, which can lead to reignition if it exceeds the dielectric strength which re-appears as the gap between the contacts is being de-ionized.

There is no circuit breaker arc model in the EMTP now, but work is in progress to add one. Static arc models are not good enough, and differential equations describing the arc must be used instead. Most experts working on current interruption problems use a modification of an equation first proposed by Mayr, of the form

$$\frac{dg}{dt} = \frac{1}{\tau(g)}\left(\frac{i^2}{P(g)} - g \right) \tag{10.7}$$

where

g = arc conductance,

i = arc current,

$\tau(t)$ = conductance-dependent time constant,

$P(g)$ = conductance-dependent heat dissipation.

The parameters $\tau(t)$ and $P(g)$ are dependent on the characteristics of the particular circuit breaker. A detailed investigation into the usefulness of various arc equations is presently being done by CIGRE Working Group 13.01

("Practical Application of Arc Physics in Circuit Breakers").

If high-frequency oscillations develop in the arc current prior to interruption, as they sometimes do in switching off small inductive currents or in other current-chopping situations, then reignition may occur within 1/4 cycle after current interruption (the term "restrike" is used to describe resumption of current conduction if it occurs 1/4 cycle or longer after current interruption, which most likely occurs in the interruption of capacitive currents). For deciding whether reignition occurs, the arc equation of Eq. (10.7) cannot be used. Instead, the transient recovery voltage is compared again the dielectric strength, which increases as a voltage is compared against the dielectric strength, which increases as a function of time, and if it exceeds it, then reignition occurs. For the breakdown itself, Toepler's equation can be used, which is of the form [173]

$$g = \frac{1}{ks} \int_0^t i(u)\, du \qquad\qquad (10.8)$$

where

  k = constant,

  s = gap spacing

  i = current in gap (starting from an extremely small value).

  v = voltage across gap.

11. SURGE ARRESTERS AND PROTECTIVE GAPS

To protect generators, transformers, cables, SF_6-basses, and other devices against levels of overvoltages which could permanently destroy their non-self-restoring insulation, surge arresters are installed as close as possible to the protected device. Short connections are important to avoid the doubling effect of travelling waves on open-ended lines, even if they are short busses. Surge arresters have normally not been used for the protection of transmission lines, because one can easily recover from insulator flashovers with fast opening and reclosing of circuit breakers (self-restoring insulation). Some utilities are studying the possibility of using surge arresters on transmission lines, too, to limit switching surge overvoltages.

Protective gaps are seldom used nowadays, except in the protection of series-capacitor stations.

11.1 Protective Gaps

Protective gaps are crude protection devices. They consist of air gaps between electrodes of various shapes. Examples are horns or rings on insulators and bushings, or rod gaps on or near transformers. They do protect against overvoltages by collapsing the voltage to practically zero after sparkover, but they essentially produce a short-circuit which must then be interrupted by circuit breakers. Also, their voltage-time characteristic (Fig. 10.5) rises steeply for fast fronts, which makes the protection against fast-rising impulses questionable.

Protective spark gaps are still used to protect series capacitors. There, the sparkover does not increase the transmission line current, but actually reduces it because the line impedance increases when the series capacitor is by-passed. Since the spark gap is unable to interrupt the current, a by-pass circuit breaker must be closed to extinguish the arc in the spark gap (Fig. 11.1). This by-pass breaker must be opened again if the series capacitor is to be re-inserted. In the future, protective spark gaps may be replaced by metal-oxide surge arresters.
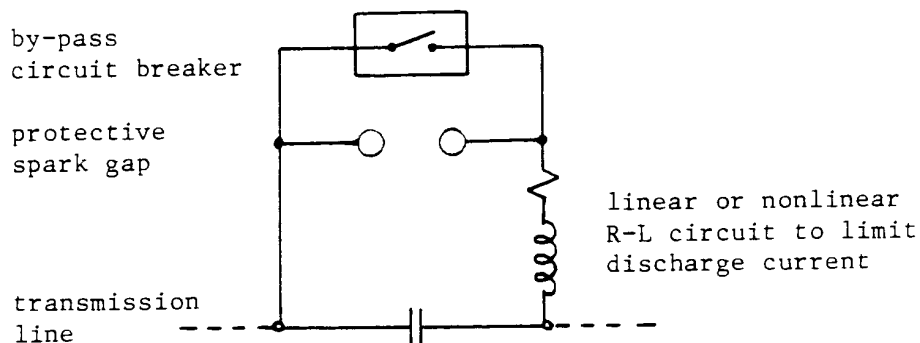

Fig. 11.1 - Series capacitor protection scheme

Protective gaps are simulated in the EMTP with the gap switch discussed in Section 10.1.2.

11.2 Surge Arresters

There are two basic types of surge arresters, namely silicon-carbide surge arresters, and metal-oxide surge arresters. Until about 10 years ago, only silicon-carbide arresters were used, but the metal-oxide arrester is quickly replacing the older type to the extent that some manufacturers produce only metal-oxide arresters now.

11.2.1 Silicon-Carbide Surge Arrester

Silicon-carbide arresters consist of a silicon-carbide resistor with a nonlinear v-i characteristic, in series with a spark gap (Fig. 11.2). The spark gap connects the arrester to the system when the overvoltage exceeds the sparkover voltage, and the resistor limits the follow current and enables the arrester to "reseal" (interrupt the current in the gap). To facilitate resealing, so-called "active spark gaps" have been designed in which an arc voltage builds up after some time. A resistor block in series with the gap is not very high (typically 4 cm), and to produce the desired sparkover voltage and nonlinear resistance for a particular voltage level, many such blocks are stacked together in a series connection. To achieve reasonably uniform

i in kA	v in kV
0	0
0,5	440
1	510
1,5	540
2,5	580
3	590
10	660

$v_{sparkover} = 610$ kV
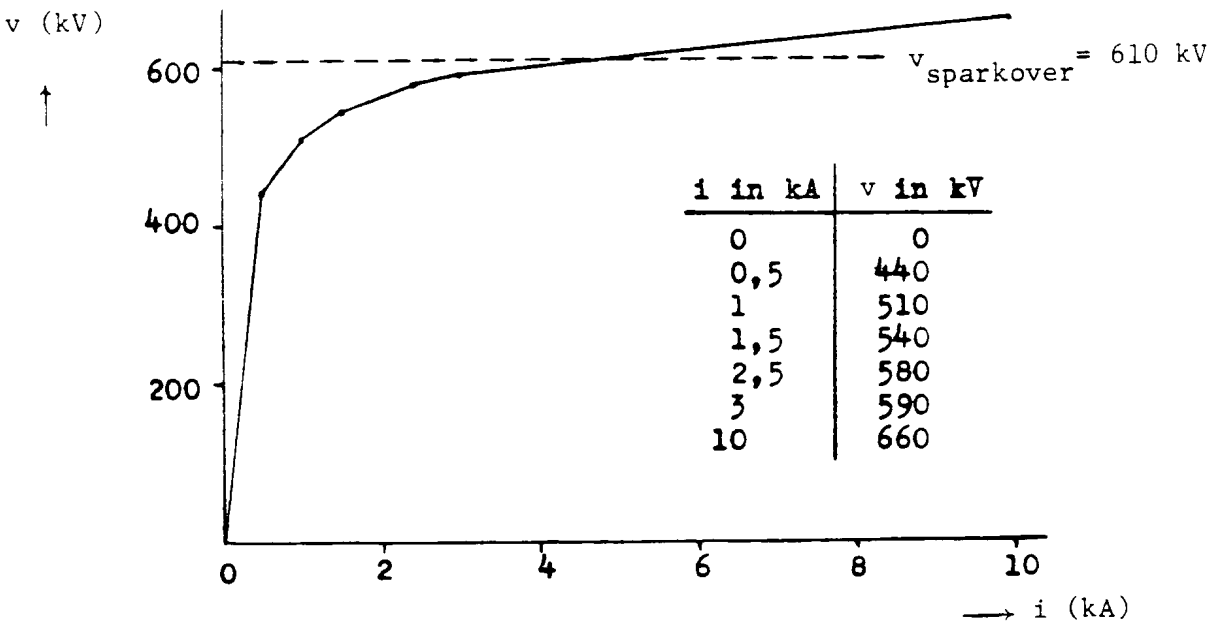
Fig. 11.2 - Nonlinear characteristic of a 220 kV silicon-carbide surge arrester

voltage distribution along the stack, parallel R-C grading networks are used, which are normally ignored in simulations.

Silicon-carbide arresters are modelled in the EMTP as a nonlinear resistance in series with a gap which has a constant sparkover voltage. In reality the sparkover voltage depends on the steepness of the incoming wave, as shown in Fig. 11.3 [174]. Since surges in a system have very irregular shapes, rather than the linear rise used in

11-2

the measurements of Fig. 11.3, the steepness dependence of the sparkover voltage is not easy to implement, as already discussed in Section 10.1.2. The nonlinear resistance in series with the gap is either solved with the compensation method (Section 12.1.2), or with the piecewise linear representation (Section 12.1.3).

In silicon-carbide surge arresters with current-limiting gaps, a voltage builds up across the gap after 200 to 400 μs, which is best modelled as an inserted ramp-type voltage source [175], as shown in Fig. 11.4. This ramp voltage source is not part of the EMTP arrester model now, but it can easily be added as an extra voltage source, after one trial run to determine when sparkover occurs. This gap voltage is only important in switching surge studies. In lightning surge studies, it can be ignored because of the time delay of 200 to 400 μs. Useful IEEE guidelines for modelling silicon-carbide arresters are found in [175].

a = medium voltage
b = high voltage, lightning surge protection
c = high voltage, lightning and switching surge protection
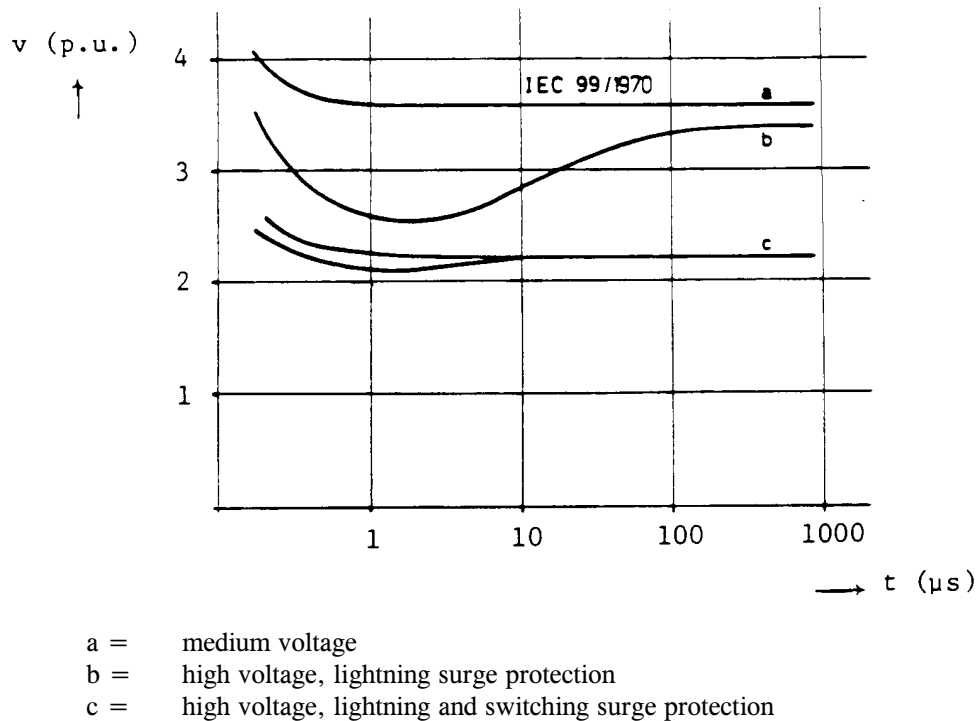
Fig. 11.3 - Arrester sparkover voltage-time characteristic for wavefronts with linear rise [174]. Reprinted by permission of Plenum Publishing Corp. and Brown Boveri Oerlikon

It is doubtful whether very sophisticated models with dynamic characteristics, such as the "type-94 modern-style SiC surge arrester" based on [176] in the BPA EMTP, are useful, because it would be almost impossible to obtain the required data. Brauner [177] has developed a model with dynamic characteristics with special reference to GIS insulation coordination, which appears to require less data than the type-94 arrester.
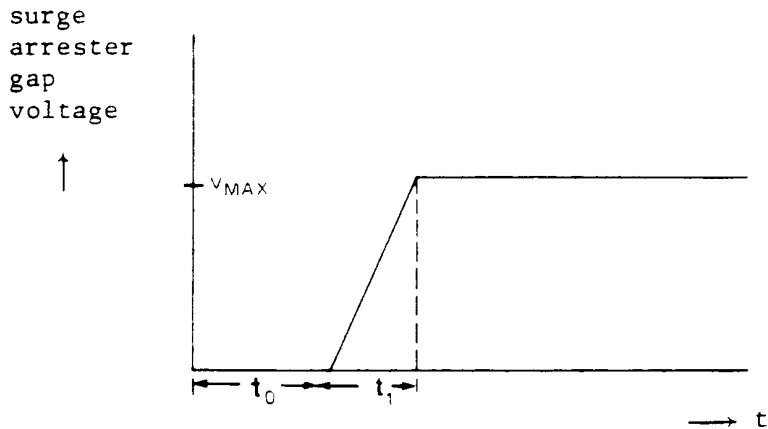
Fig. 11.4 - Arrester gap characteristic

11.2.2 Metal-Oxide Surge Arrester

Metal-oxide or zinc-oxide surge arresters are highly nonlinear resistors, with an almost infinite slope in the normal-voltage region, and an almost horizontal slope in the overvoltage protection region, as shown in Fig. 11.5. They were originally gapless, but some manufacturers
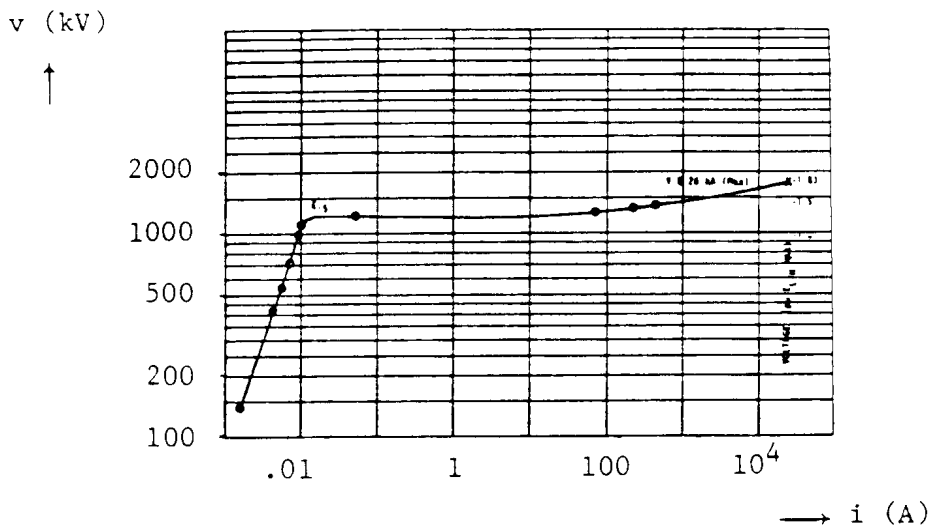
Fig. 11.5 - Voltage-current characteristic of a 1200 kV gapless metal-oxide surge arrester [183]. © 1982 IEEE

have re-introduced gaps into the design. Its nonlinear resistance is represented by a power function of the form

$$i = p\left(\frac{v}{v_{ref}}\right)^{q} \tag{11.1}$$

where p, v_{ref} and q are constants (typical values for q = 20 to 30). Since it is difficult to describe the entire region with one power function, the voltage region has been divided into segments in the BPA EMTP, with each segment defined by its own power function. In the UBC EMTP, only one function is allowed so far. For voltages

11-4

substantially below v_{ref}, the current is extremely small (e.g., $i = p \bullet 0.5^{30} = p \bullet 10^{-9}$ for $v/v_{ref} = 0.5$), and a linear representation is therefore used in this low voltage region. In the meaningful overvoltage protection region, two segments with power functions (11.1) are usually sufficient.

The static characteristic of Eq. (11.1) can be extended to include dynamic characteristics similar to hysteresis effects, through the addition of a series inductance L, whose value can be estimated once the arrester current is approximately known from a trial run [10]. A metal-oxide surge arrester model for fast front current surges with time to crest in the range of 0.5 to 10 μs was proposed and compared against laboratory tests by Durbak [178]. The basic idea is to divide the single nonlinear resistance into m parallel nonlinear resistances, which are separated by low pass filters, as illustrated in Fig. 11.6 for two parallel nonlinearities, which is usually sufficient in practice. The R_1-L_1 circuit is the low pass filter which separates the two nonlinear resistances defined by $i_o(v_o)$ and $i_1(v_1)$. The inductance L_o represents the small but finite inductance associated with the magnetic fields in the immediate vicinity of the surge arrester, while R_o is used only to damp numerical oscillations (see Section 2.2.2). C is the stray capacitance of the surge arrester. The model of Fig. 11.6 can easily be created from existing EMTP elements. If three such models were connected to phases a, b, c, then the six nonlinear resistances would have to be solved with the compensation method with a six-phase Thevenin equivalent circuit.
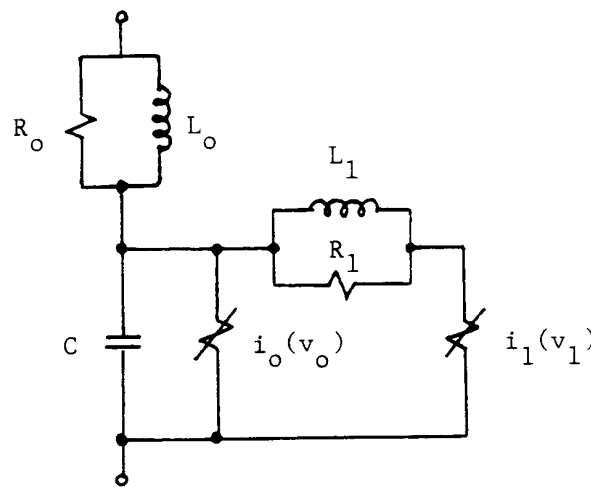
Fig. 11.6 - Two-section surge arrester model for fast front surges [178]

A somewhat different model (Fig. 11.7) has been proposed by Knecht [179]. It consists of a nonlinear resistance R(v), a more or less constant capacitance C, and a linear, but frequency-dependent impedance $Z(\omega)$.

No IEEE guidelines have yet been published for the modelling of metal-oxide surge arresters. The energy absorbed in them is an important design factor, and should therefore be computed in whatever type of model is used. Since energy absorption may change as the system is expanded, it is important to check whether ratings which were appropriate initially may possibly be exceeded in future years. Energy absorption capability is probably more of a limitation for switching surges than for lightning surges. The sharp change from the almost vertical to the almost horizontal slope, which limits overvoltages almost ideally at the arrester location, could produce oscillations with overshoot at locations some distance from the arrester, especially in substations with long bus runs. This may be

another factor worth watching for.

Metal-oxide surge arresters are generally solved with the compensation method in the EMTP, with iterations using Newton's method as explained in Section 12.1.2. The piecewise linear representation is less useful because the highly nonlinear characteristic of Eq. (11.1) is not easily described by piecewise linear segments.
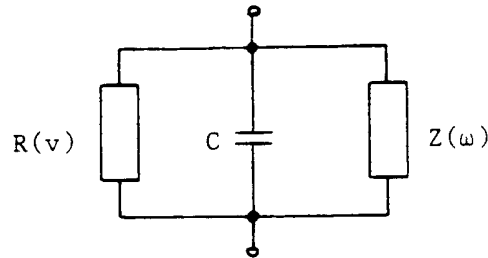
Fig. 11.7 - Alternative surge arrester model

If the surge arrester is equipped with a shunt spark gap, as illustrated in Fig. 11.8, then it is still represented as a nonlinear resistance in the solution process except that the function for
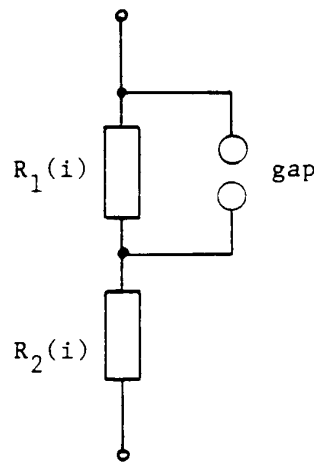
Fig. 11.8 - Metal oxide surge
arrester with shunt spark gap

that resistance will change abruptly from $R_1(i) + R_2(t)$ before sparkover to $R_2(i)$ after sparkover. If the surge arrester is equipped with a series spark gap, then a very high resistance is added to $R_1(i) + R_2(i)$ to represent the series gap before sparkover.

12. SOLUTION METHODS IN THE EMTP

The basic theory behind the solution methods for the transient simulation and for the ac steady-state phasor solution has already been explained in Section 1. Extensions of the basic theory for more complicated network elements have mostly been discussed in the sections dealing with these elements. What remains to be explained here are the various options for handling nonlinearities, the load flow option, and methods for initializing variables with more than one frequency component.

12.1 Inclusion of Nonlinear Elements

The most common types of nonlinear elements are nonlinear inductances for the representation of transformer and shunt reactor saturation, and nonlinear resistances for the representation of surge arresters. Nonlinear effects in synchronous and universal machines are handled in the machine equations directly, and are therefore not described here.

Usually, the network contains only a few nonlinear elements. It is therefore sensible to modify the well-proven linear methods more or less to accommodate nonlinear elements, rather than to use less efficient nonlinear solution methods for the entire network. This has been the philosophy which has been followed in the EMTP. Three modification schemes have been used over the years, namely

(1)   current-source representations with time lag Δt (no longer used),

(2)   compensation methods, and

(3)   piecewise linear representations.

12.1.1 Current-Source Representation with Time Lag Δt

Assume that the network contains a nonlinear inductance with a given flux/current characteristic $\lambda(i)$, and that the network is just being solved at instant t. All quantities are therefore known at t - Δt, including flux $\lambda(t - \Delta t)$, which is found by integrating the voltage across the nonlinear inductance up to t - Δt. Provided Δt is sufficiently small, one could use $\lambda(t - \Delta t)$ to find a current i(t - Δt) from the nonlinear characteristic, and inject this as a current source between the two nodes to which the nonlinearity is connected for the solution at instant t. In principle, any number of nonlinearities could be handled this way.

Fig. 12.1 shows a current-limiting device where this simple method was used for the two

12-1
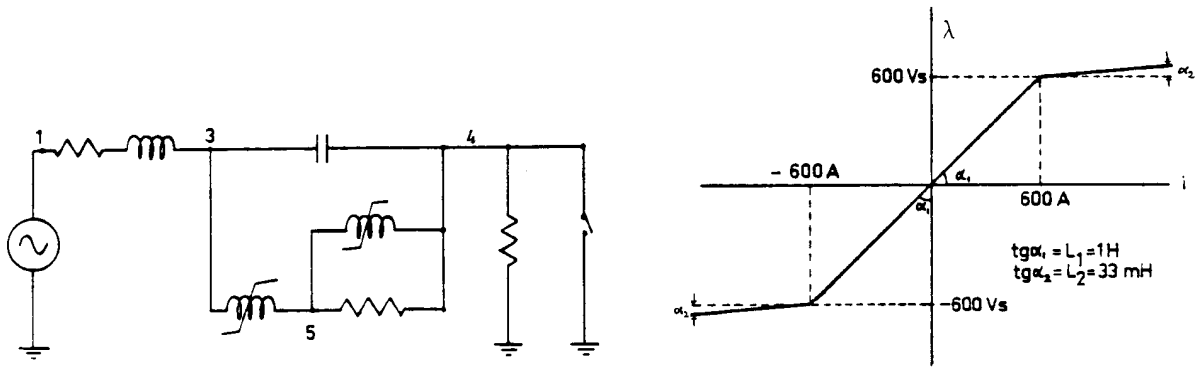
(a)   circuit diagram (branch 1-3 = feeding network, branches between 3 and 4 = current limiting device, shunt R in 4 = load, switch in 4 = short circuit)

(b)   characteristics of saturable reactors (both identical)

Fig. 12.1 - Current-limiting device

nonlinear inductances. The simulation results are plotted in Fig. 12.2. The numerical oscillations around t = 1.4 cycles seem to be caused by the time lag Δt, since they disappear with more sophisticated techniques in Fig. 12.11.

Since this method is very easy to implement, it may be useful in special cases, provided that the step size Δt is sufficiently small. It is not a built-in option in any of the available EMTP versions, however.
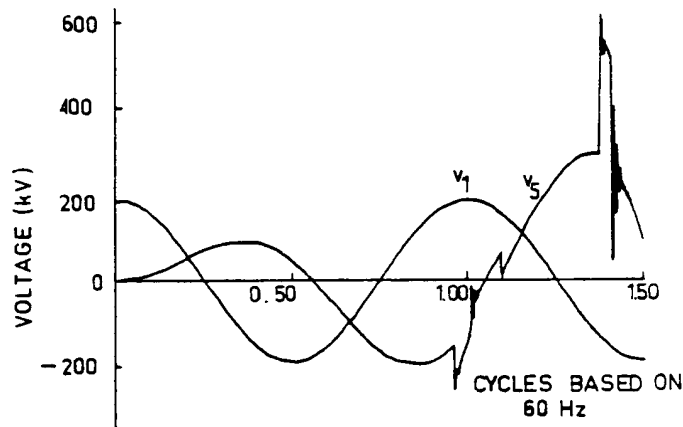
Fig. 12.2 - Simulation results with current source representation

12.1.2 Compensation Method

In earlier versions of the EMTP, the compensation method worked only for a single nonlinearity in the network, or in case of more nonlinearities, if they were all separated from each other through distributed-parameter lines. It appears that the type-93 nonlinear inductance in the BPA EMTP still has this restriction imposed on it, but for most other types, more nonlinearities without travel time separation are allowed now.

The extension of the compensation method to more than one nonlinearity was first implemented for metal

oxide surge arresters, and later used for other nonlinear elements as well.

In compensation-based methods, the nonlinear elements are essentially simulated as current injections, which are super-imposed on the linear network after a solution without the nonlinear elements has first been found. There are rare situations where a network solution without the nonlinearity is impossible, as in the case of Fig. 12.3. With the nonlinear branch removed, the current injected into node 1 from the current source would not have any path to return to neutral. The EMTP would stop with the error message "diagonal element of node-2 very small" (matrix singularity). A remedy would be to represent the nonlinearity as a parallel combination of a (normal) linear branch and of a (modified) nonlinear branch. A related problem occurs if the nonlinear branch is disconnected from the network, as in Fig. 12.4. When the
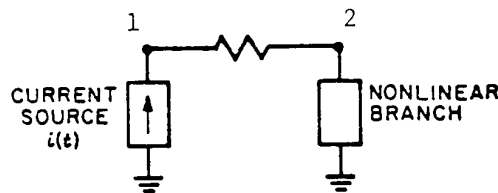
Fig. 12.3 - Unsolvable network if nonlinear branch removed
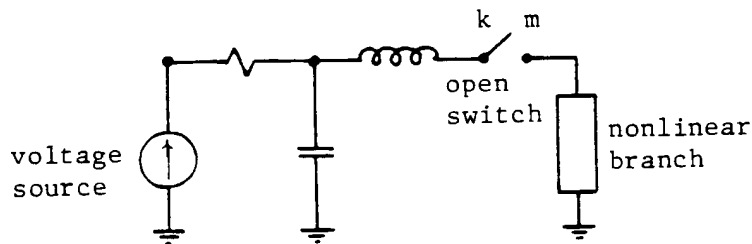
Fig. 12.4 - Disconnected nonlinear branch

EMTP tries to calculate the Thevenin equivalent resistance for the nonlinear branch by injecting current into node m, a zero diagonal element will be encountered in the nodal conductance matrix, and the EMTP will stop with the error message "diagonal element in node-m too small." The remedy in this case is the same: represent the nonlinear branch as a linear branch in parallel with a (modified) nonlinear branch. The BPA manual also suggests the insertion of high-resistance paths where needed, but warns that the resistance values cannot be arbitrarily large.

12.1.2.1 One Nonlinear Element

Let us assume that the network contains only one nonlinear element between nodes k and m, as indicated in Fig. 12.5. The compensation theorem states that this nonlinear branch can be
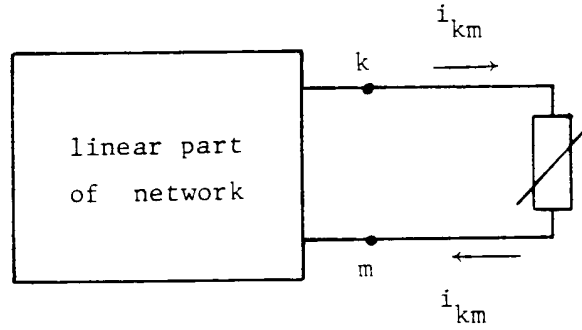
Fig. 12.5 - One nonlinear element connected to linear
network

excluded from the network, and be simulated as a current source i instead, which leaves node k and enters node m if the nonlinear element is treated as a load and not as a source. The current i_{km} must fulfill two equations, namely the network equations of the linear part (instantaneous Thevenin equivalent circuit between nodes k and m),

$$v_{km} = v_{km-0} - R_{Thev} i_{km} \qquad (12.1)$$

(subscript "0" indicates solution without the nonlinear branch, $v_{km} = v_k - v_m$), and the relationship of the nonlinear branch itself,

$$v_{km} = f(i_{km}, di_{km}/dt, t, ...) \qquad (12.2)$$

The value of the Thevenin resistance R_{Thev} in Eq. (12.1) is pre-computed once before entering the time step loop, and re-computed whenever switches open and close.

The network equations (1.8b) can be rewritten as

$$[G_{AA}][V_A] = [k_A] \qquad (12.3)$$

with $[k_A]$ being the known right-hand side from Eq. (1.8b). To find the Thevenin resistance, a current of 1 A must be injected into node k, and drawn out from node m. Therefore, replace $[k_A]$ with a vector whose components are all zero, except for +1.0 in row k and -1.0 in row m. Then perform one repeat solution with this right-hand side vector, which will produce a vector $[r_{Thev}]$. This vector is the difference of the k-th and m-th columns of the inverse matrix $[G_{AA}]^{-1}$. Then

$$R_{Thev} = r_{Thev-k} - r_{Thev-m} \qquad (12.4)$$

If one of the voltages, say in node m, is known (voltage source, or grounded node), then -1.0 does not appear in $[k_A]$ because node m belongs to set B of the nodes rather than to set A. In that case,

$$R_{Thev} = r_{Thev-k} \qquad (12.5)$$

If the voltages in both nodes k and m are known, then

$$R_{Thev} = 0 \tag{12.6}$$

If the solution fails because of matrix singularity, it is likely that one of the situations illustrated in Fig. 12.3 and 12.4 has been encountered, and remedies discussed there should then be used.

The solution with compensation proceeds as follows in each time step:

(1)   Compute the node voltages $[v_{A-0}]$ without the nonlinear branch, with a repeat solution of Eq. (12.3). From this vector, and from the other known voltages $[v_B]$, extract the open-circuit voltage $v_{km-0} = v_{k-0} - v_{m-0}$.

(2)   Solve the two scalar equations (12.1) and (12.2) simultaneously for i_{km}. If Eq. (12.2) is given analytically, then the Newton-Raphson method is usually used (example: zinc-oxide arrester models). If Eq. (12.2) is defined point-by-point as a piecewise linear curve, then the intersection of the two curves must be found through a search procedure, as indicated in Fig. 12.6 for a nonlinear resistance.
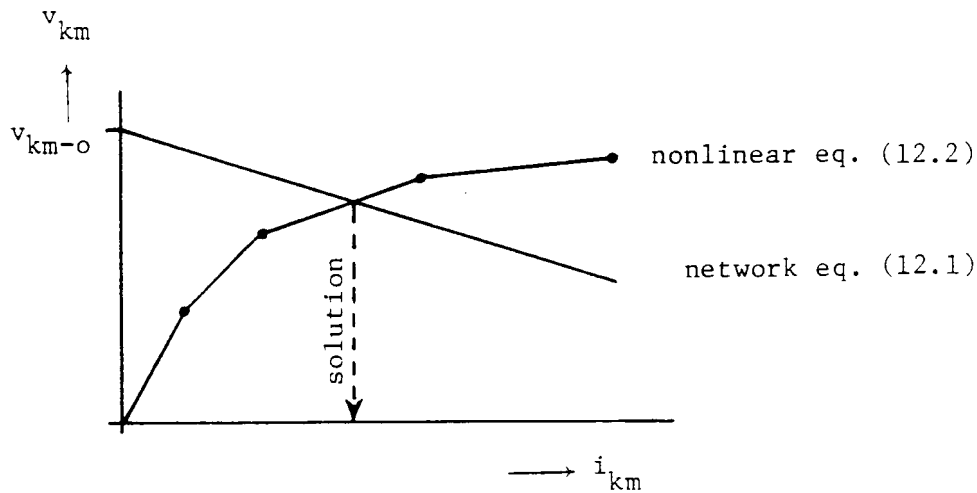
Fig. 12.6 - Simultaneous solution of two equations

(3)   Find the final solution by superimposing the response to the current i_{km},

$$[v_A] = [v_{A-0}] - [r_{Thev}] i_{km} \tag{12.7}$$

Superposition is permissible as long as the rest of the network is linear.

Step (1) is the normal solution procedure for linear networks. Step (2) takes little extra time because it involves only two scalar equations. Step (3) requires N additional multiplications and additions if N = number of voltages in set A. Therefore, the extra work of steps (2) and (3) is rather small compared to repeated refactorizations of $[G_{AA}]$, which would be required for general, nonlinear networks.

12.1.2.2 Two or More Nonlinear Elements Separated by Travel Time

Lines with distributed parameters decouple the network equations for the two ends. This is not astonishing because the phenomena at one end are not immediately seen at the other end, but travel time τ later. Nonlinear elements decoupled by distributed-parameter lines can therefore be solved independent of each other, because each

has its own "area" Thevenin equivalent equation (12.1) decoupled from the others. The $[r_{Thev}]$-vector of a particular nonlinearity will only have nonzero entries for the nodes of its own area. Therefore, all $[r_{Thev}]$-vectors can be merged into a single vector, at the expense of another vector which contains the area number for each component [50]. This is schematically indicated in Fig. 12.7.
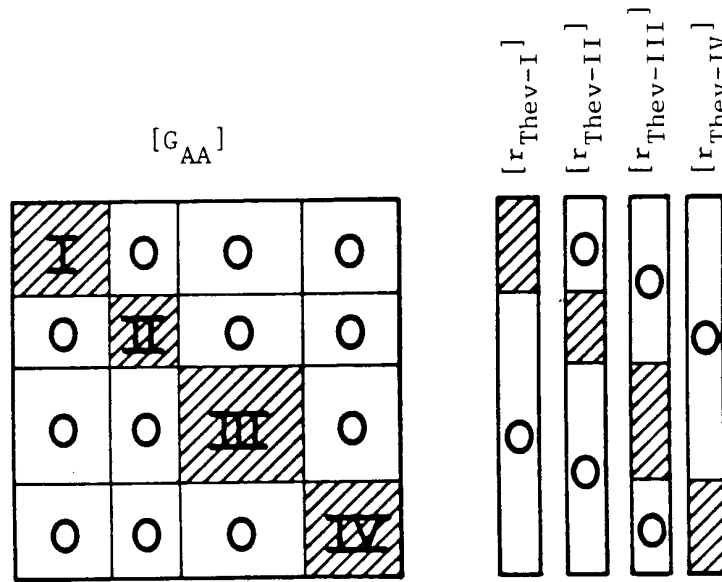
Fig. 12.7 - Disconnected subnetworks I, II, III, IV

12.1.2.3 Two or More Connected Nonlinear Elements

The compensation method can also be used to simulate the effect of M nonlinear branches with current sources. Then, M vectors $[r_{Thev-1}],...[r_{Thev-M}]$ must be pre-computed (and re-computed whenever switches change position). The first vector is found by inserting $+1.0$ and -1.0 into the appropriate locations for the first nonlinear element, and then performing a repeat solution. This procedure is repeated for the 2nd,...M-th nonlinear element. The Thevenin equivalent resistance becomes an M x M- matrix $[R_{Thev}]$ in this case. The first column of this matrix is created by calculating the differences $r_{Thev-ki} - r_{Thev-mi}$ for all M nonlinear elements $i = 1,...M$ from $[r_{Thev-1}]$, the second column by doing the same from $[r_{Thev-2}]$, etc.

In the solution process, step (1) in Section 12.1.2.1 remains identical, but step (2) now requires the solution of M nonlinear equations

$$[v_{km}] = [v_{km-0}] - [R_{Thev}][i_{km}]$$ (12.8a)

Step (3) uses M vectors $[r_{Thev-1}],...[r_{Thev-M}]$ in place of one vector,

$$[v_A] = [v_{A-0}] - \left[[r_{Thev-1}],...[r_{Thev-M}]\right][i_{km}]$$ (12.8b)

with $[i_{km}]$ being a vector with M components. If there are N voltages in set A, then N x M multiplications and additions are required in Eq. (12.8). As M becomes large, this effort may become larger than simply re-solving

12-6

$$[G_{AA}]\,[v_A] \;=\; [k_A \;+\; (i_{km} \; \textit{added in appropriate places})\,] \tag{12.9}$$

with one repeat solution, because the N x M-matrix in Eq. (12.8) is full, whereas sparsity methods are used in performing a repeat solution with the triangularized matrix of Eq. (12.9). In the BPA EMTP, repeat solutions of Eq. (12.9) are used if M > 1, whereas Eq. (12.8) is used in the UBC EMTP.

The M-phase compensation method can be combined with the advantages of element separation through travel time discussed in Section 12.1.2.2. For example, three surge arresters in phases A1, B1, C1 at the sending end of a line and three surge arresters in phases A2, B2, C2 at the receiving end are best solved as two disconnected groups, each with M = 3, rather than as one group with M = 6, though the latter approach would work as well if the program allows for M > 3. The merging procedure discussed in Section 12.1.2.2 is essentially the same, except that each vector is replaced by M vectors.

12.1.2.4 Nonlinear Inductance

The simultaneous solution of the network equation with the nonlinear equation, as illustrated in Fig. 12.6, is straightforward if the nonlinear branch is a nonlinear resistance defined by $v_{km} = f(i_{km})$, or if it is a time-varying resistance with $v_{km} = R(t) \bullet i_{km}$. For nonlinear inductances, this solution process is not so direct because the nonlinear characteristic is now in the form

$$\lambda \;=\; f(i) \tag{12.10}$$

with the flux λ being the integral over the voltage $v = v_k - v_m$,

$$\lambda(t) \;=\; \lambda(t - \Delta t) \;+\; \int_{t - \Delta t}^{t} v(u)\,du \tag{12.11}$$

In the EMTP, this problem is solved by using the trapezoidal rule of integration on Eq. (12.11), which converts the flux $\lambda(t)$ into a linear function of $v(t)$,

$$\lambda(t) \;=\; \frac{\Delta t}{2}\, v(t) \;+\; hist(t - \Delta t) \tag{12.12a}$$

with the known history term

$$hist(t - \Delta t) \;=\; \lambda(t - \Delta t) \;+\; \frac{\Delta t}{2}\, v(t - \Delta t) \tag{12.12b}$$

Inserting Eq. (12.12a) into Eq. (12.10) produces a resistance relationship, by first shifting the origin by + hist (t - Δt), and then rescaling the λ-axis into a v-axis with a multiplication factor of 2/Δt. This v(i)-characteristic is solved with the network equation in the same way as for any other nonlinear resistance.

As an alternative, the network equation $v = v_o - R_{Thev}i$ could also be converted into a flux-current relationship, by using $v = 2(\lambda\text{-hist})/\Delta t$ from Eq. (12.12).

12.1.2.5 Newton-Raphson Method

If an M-phase Thevenin equivalent circuit must be used, in cases where the M nonlinear elements are not separated by travel time, then a system of nonlinear equations must be solved. The Newton-Raphson iteration method is the best approach for systems of nonlinear equations. It includes the scalar case (one nonlinear equation) as well.

To illustrate the method, assume that the nonlinear elements are nonlinear resistances. Then Eq. (12.8a), rewritten here for convenience as

$$[v_{km}] - [v_{km-0}] + [R_{Thev}][i_{km}] = 0 \qquad\qquad (12.13a)$$

must be solved, whereby $[i_{km}]$ can be replaced by a diagonal matrix $[f(v_{km})]$, whose elements are the i-v-characteristics of the M nonlinear resistances (e.g., as defined in Eq. (11.1)),

$$[i_{km}] = [f(v_{km})] \qquad\qquad (12.13b)$$

Experience has shown that convergence is faster if Eq. (12.13) is solved for voltages rather than for currents. Applying the Newton-Raphson method to Eq. (12.13) produces

$$[R_{Thev}]\left[\frac{df_{km}}{dv_{km}}\right] + [U]\,[\Delta v_{km}] = [v_{km-0}] - [v_{km}] - [R_{Thev}][f(v_{km})] \qquad\qquad (12.14)$$

where the matrix on the left-hand side ("Jacobian matrix") and the right-hand side are evaluated with approximate answers from the last iteration step h-1. The improved solution is found by solving the system of linear equations for $[\Delta v_{km}]$, with

$$[v_{km}^{(h)}] = [v_{km}^{(h-1)}] + [\Delta v_{km}] \qquad\qquad (12.15)$$

In Eq. (12.14), $[df_{km}/dv_{km}]$ is a diagonal matrix of the derivatives of the i-v-characteristics, which destroys the symmetry of the Jacobian matrix. To maintain symmetry, the following modification can be used: multiply the Jacobian matrix with the inverse matrix $[df_{km}/dv_{km}]^{-1}$, and solve the equations for the variables $[\Delta x]$,

$$\left\{[R_{Thev}] + \left[\frac{df_{km}}{dv_{km}}\right]^{-1}\right\}[\Delta x] = [v_{km-0}] - [v_{km}] - [R_{Thev}][f(v_{km})] \qquad\qquad (12.16a)$$

The Jacobian matrix is now symmetric, and the diagonal elements of $[df_{km}/dv_{km}]^{-1}$ are simply the reciprocals of df_{km}/dv_{km}. After $[\Delta x]$ has been found, the voltage corrections are

$$\Delta v_{km} = \frac{\Delta x_{km}}{df_{km}/dv_{km}} \qquad\qquad (12.16b)$$

This modification is used in the UBC EMTP.

In the BPA EMTP, symmetry is achieved by working with the inverse matrix $[R_{Thev}]^{-1}$. Multiplying Eq. (12.13a) with this inverse matrix and applying the Newton-Raphson method to it produces

12-8

$$\left\{ [R_{Thev}]^{-1} + \left[\frac{df_{km}}{dv_{km}} \right] \right\} [\Delta v_{km}] = [R_{Thev}]^{-1} \left\{ [v_{km-0}] - [v_{km}] \right\} - [f(v_{km})] \qquad (12.17)$$

If the inverse matrix exists, then this procedure is as straightforward as Eq. (12.16). $[R_{Thev}]$ can be singular, however, if nonlinear elements are directly connected to voltage sources. In the scalar case, R_{Thev} would become zero, as shown in Eq. (12.6), whereas the respective row and column in $[R_{Thev}]$ becomes zero in the M-phase case. This has to be treated in a special way in Eq. (12.17), whereas no special cases arise with Eq. (12.16).

To start the iterations with either Eq. (12.16) or (12.17), an initial guess for the voltages is needed. Since currents in nonlinear elements tend to change less from step to step than voltages, it is best to use the old currents $[i_{km}(t - \Delta t)]$ from the preceding time step and the new open-circuit voltages $[v_{km-0}(t)]$ to obtain an initial voltage guess from Eq. (12.13a). This voltage guess is used for $[v_{km}]$ in Eq. (12.16a) or (12.17), as well as for $[df_{km}/dv_{km}]$ and $[f(v_{km})]$. This procedure seems to require the least number of iterations, and has therefore been implemented in the UBC EMTP.

12.1.2.6 Numerical Problems

As long as the EMTP works with a fixed step size Δt, numerical problems can arise with nonlinear elements. If Δt is too large, artificial negative damping or hysteresis can occur, as illustrated in Fig. 12.8 (solution proceeds from 1 to 2 to 3 in consecutive steps). This can cause
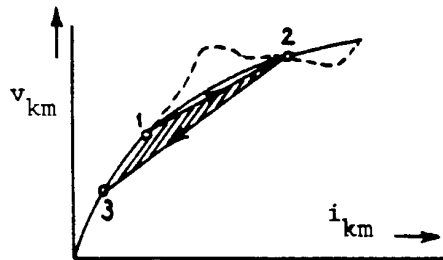
Fig. 12.8 - Artificial negative damping

numerical instability. Since the dotted nonlinear characteristic would give identical answers, it is obvious that the shape of the characteristic between sampled points does not enter into the solution, that is, the nonlinear characteristic is only used in a "spotty" way. Piecewise linear resistances and inductances, as discussed in the next section, appear to be more stable numerically (or possibly absolutely stable), but they may cause "overshooting" problems.

Another problem is related to automatic ac steady-state initialization. Since nonlinear elements are approximated as linear elements in the ac phasor solution, a sudden jump can occur at $t = 0$ between the linear and nonlinear representations. For nonlinear inductances, the problem can be minimized through proper voltage source rotations, as discussed in Section 12.1.3.3. The problem will be resolved when the superposition of harmonics (Section 12.4) becomes available to the users.

12.1.3 Piecewise Linear Representation

12.1.3.1 Piecewise Linear Inductance

As discussed in Section 6.6.2, the saturation characteristics of modern transformers can often be represented accurately enough as a piecewise linear inductance with two slopes (Fig. 12.9). Such a piecewise linear inductance can be simulated with two linear inductances L_1 and
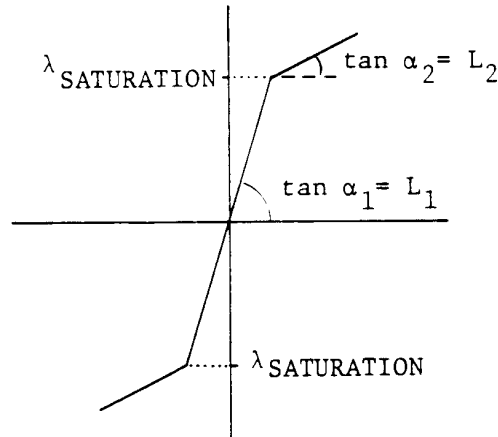
Fig. 12.9 - Piecewise linear inductance with two slopes

L_p in parallel (Fig. 12.10), provided that the flux in L_p is always computed by integrating the voltage $v_k - v_m$ independent of the switch position. The switch is close whenever $|\lambda| \geq \lambda_{SATURATION}$, and opened again as soon as $|\lambda| < \lambda_{SATURATION}$. Fig. 12.11 shows the simulation results for the current-limiting device of Fig. 12.1 if two-slope piecewise linear inductances are
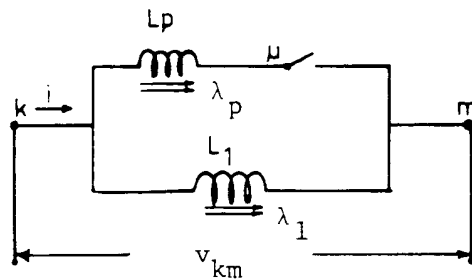
Fig. 12.10 - "Switched inductance' implementation of two-slope piecewise linear inductance
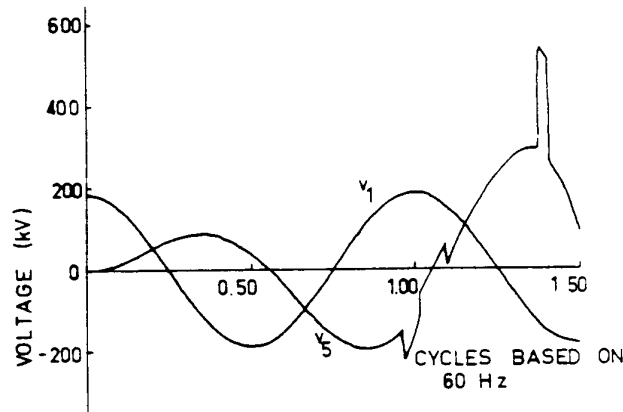
Fig. 12.11 - Simulation results for case of Fig. 12.1 with
two-slope piecewise linear inductances

used. The numerical oscillations around 1.4 cycles present in Fig. 12.2 have now disappeared.

Using a switch to make the changeover from an inductance value of L_1 to L_2 in [G] of Eq. (1.8) is simply a programming trick, which has been used in the UBC EMTP and in older versions of the BPA EMTP, and has sometimes been called "switched inductance" (or "switched resistance"). In newer versions of the BPA EMTP, [G] is changed directly and re-triangularized whenever the solution moves from one straight-line segment of a piecewise linear inductance to another segment ("pseudolinear inductance or resistance in BPA EMTP Rule Book). In this direct matrix change approach, the recursive updating of the history term of Eq. (2.8) would be wrong whenever the slope changes. It is therefore better to use the non-recursive formula (2.7), where the branch current must first be determined from Eq. (2.6) with the inductance value of the old slope, while Eq. (2.7) requires the inductance value of the new slope at instants of changeover.

The two-slope piecewise linear inductance in the UBC EMTP has an option for starting the simulation from a user-specified residual flux $\lambda_{residual}$, which overrides any internally calculated flux. With this option, the piecewise linear characteristic 1-2 with slope L_1 is used to point 2 where the slope is switched to L_2 (Fig. 12.12). The flux λ_2 at the switching point is precalculated in such a way that the simulation will move directly into the normal two-slope characteristic thereafter. This procedure works well if the saturation is driven high enough to reach at least point 3. If not, some special tricks are used, which are described in more detail in the UBC User's Manual (parameter IFLUX on time card).

In addition to the normal piecewise linear inductance, the BPA EMTP also has one with hysteresis behavior ("type-96 pseudo-nonlinear hysteretic reactor"), as illustrated in Fig. 12.13. Moving along any linear segment is still described by the same differential equation $v = L \, di/dt$ used for any other linear inductance. Therefore, the representation in the transient solution part of the EMTP is the simple equivalent resistance $2L/\Delta t$ in parallel with a current source known from the history in the preceding time step (Fig. 2.8). The equivalent resistance must be changed, however, whenever the simulation moves from one segment into another. The fact that

12-11
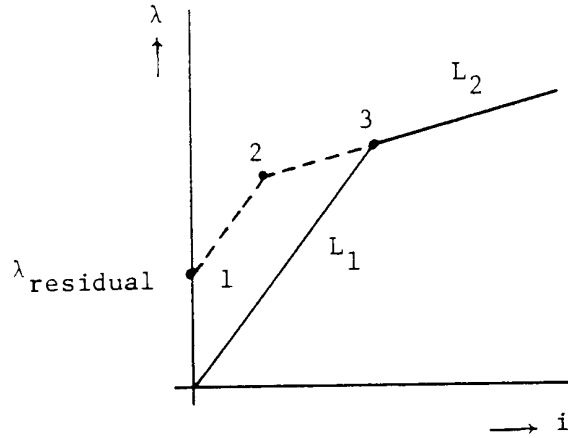
Fig. 12.12 - Representation of residual flux in UBC EMTP
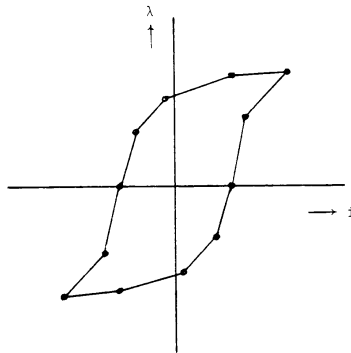
Fig. 12.13 - Piecewise linear inductance with hysteresis

the linear segment does (in general) not pass through the origin is automatically taken care of by the history terms. Starting from a residual flux is permitted. This representation with hysteresis can be tricky to use, and the reader is therefore referred to [119] for more details.

12.1.3.2 Piecewise Linear Resistance

Either the "switching" approach or the direct matrix change approach for nonlinear inductances works equally well for nonlinear resistances. History terms are of course not needed in this case. Each linear segment with a slope of $R = dv/di$ is represented in the EMTP as a voltage source v_{KNEE} in series with a resistance R, or a current source v_{KNEE}/R in parallel with a resistance R (Fig. 12.14).

| (a) | piecewise linear segment | (b) | voltage source representation | (c) | current source representation |
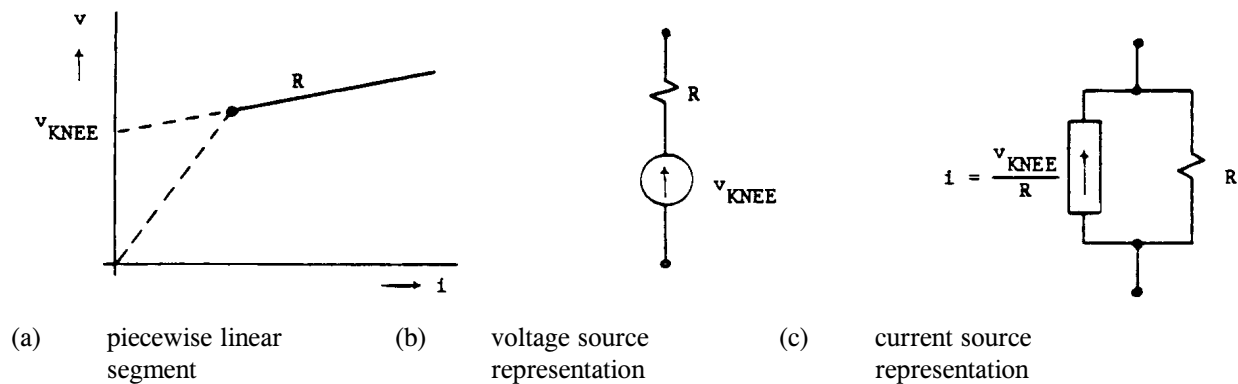
Fig. 12.14 - Piecewise linear resistance

12.1.3.3 Numerical Problems

With the direct matrix change approach, there is no reason to limit the shape of the nonlinear characteristic to only two slopes. Newer versions of the BPA EMTP therefore permit essentially any number of piecewise linear segments ("type-98 pseudo-linear reactor" and "type-99 pseudo-linear resistance" in the BPA EMTP Rule Book). While multi-slope piecewise linear elements are more useful than two-slope elements, they can also create special problems which do not exist with two-slope elements, especially for the nonlinear resistance: if the piecewise linear resistance is used to model a silicon-carbide surge arrester with a spark gap, then the EMTP does not automatically know which segment it should jump to after sparkover (Fig. 12.15). The user must therefore specify the segment number as part of the input data (e.g., segment 2-3 in Fig. 12.15). This may require a trial run, unless the network seen from the surge
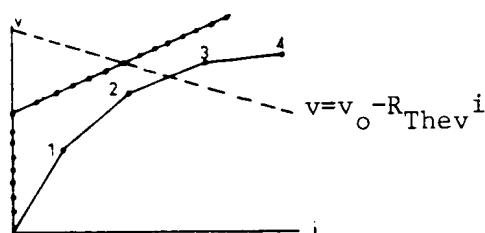
Fig. 12.15 - Jump after sparkover (--- generally unknown network characteristic at instant of sparkover)

arrester location is relatively simple[1]. For the 2-slope resistance in the UBC EMTP shown in Fig. 12.15, this problem does not arise.

All piecewise linear representations cause "overshoots," because the need for changing to the next segment

---

[1]If only single-phase lossless lines were connected to the surge arrester, then the slope of the network equation would simply be $R_{Thev} = \Sigma \, 1/Z_{surge}$.

12-13

is only recognized after the last point (c in Fig. 12.16) has gone outside its proper range. The simulation will therefore follow the dotted line into the next segment, rather
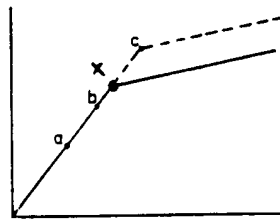
Fig. 12.16 - Overshoot in piecewise linear representation

than the specified solid line at point x. Caution is therefore needed in the choice of Δt to keep the overshoot small. The overshoot is usually less severe on piecewise linear inductances because the flux, being the integral over the voltage, cannot change very quickly. The proper cure for the overshoot problem would be an interpolation method which moves the solution backwards by a fraction of Δt to point x in Fig. 12.16, and then restarts the solution again at that point with Δt. The points along the time axis would then no longer be spaced at equal distances. This method is used in the transients program NETOMAC [15].

Both the piecewise linear representation and the compensation method suffer from the fact that nonlinear inductances are approximated as linear inductances in the ac phasor solution, at least until the superposition of harmonics discussed in Section 12.4.2 has become available to most users. The problem should not occur with nonlinear resistances which represent surge arresters. The voltages across these nonlinear resistances should be low enough in the steady-state solution to either draw negligibly small currents (metal oxide arresters), or be below sparkover voltage (silicon-carbide arresters). Transformers and shunt reactors do saturate in normal steady-state operation, however, and a jump from the linear to the nonlinear characteristic will therefore occur at t = 0 (Fig. 12.17). Whether the jump occurs in λ or i, or in both depends
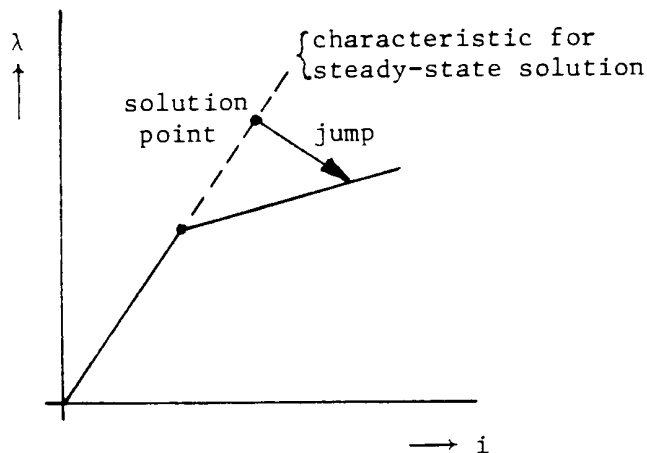
Fig. 12.17 - Jump between steady-state and transient solution

to some extent on the type of representation. This problem can be minimized by rotating the voltage sources in such a way that one of the three flux phasor Λ_A, Λ_B, Λ_C has zero angle (Fig. 12.18). For balanced network conditions, one flux would be at zero value at t = 0, and the other
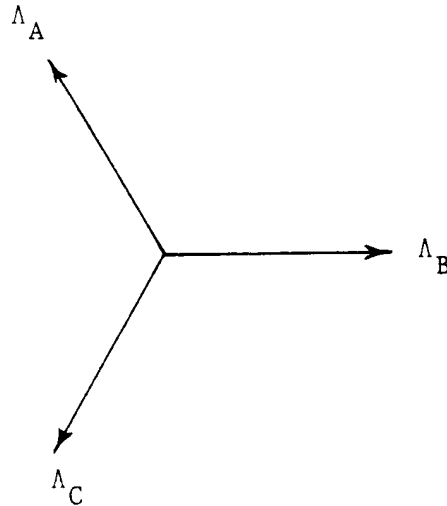
Fig. 12.18 - Flux phasors ($\lambda(0) = \text{Re}\{\Lambda\}$)

two fluxes would be 86.6% of their peak value. Hopefully, this would be below the knee point of the saturation curve. Note that fluxes and voltages are 90° out of phase when doing this rotation (checking that one of the currents is close to zero at t = 0 will verify the correctness of the rotation).

12.2 Load Flow Option

A load flow (power flow) option was added to the EMTP in 1983 by F. Rasmussen (Elkraft, Denmark). It adjusts the magnitudes and angles of sinusoidal sources iteratively in a sequence of steady-state solution, until specified active and reactive power, or specified active power and voltage magnitude, or some other specified criteria, are achieved. This will create the initial conditions for the subsequent transient simulation.

Without the load flow option, the steady-state conditions are obtained by solving the system of linear nodal equations (1.21) only once. These equations are

$$[Y_{AA}][V_A] = [I_A] - [Y_{AB}][V_B] \qquad (12.18)$$

with user-specified magnitudes and angles for the voltage sources $[V_B]$ and for the current sources $[I_A]$. The resulting power flows may or may not be what the user wants. There are many cases, however, where the details of the initial power flows in the network do not influence the results of the transient simulation. For example, the switching surge overvoltages on the line in the network of Fig. 12.19 are not influenced by the power flow pattern within the feeding
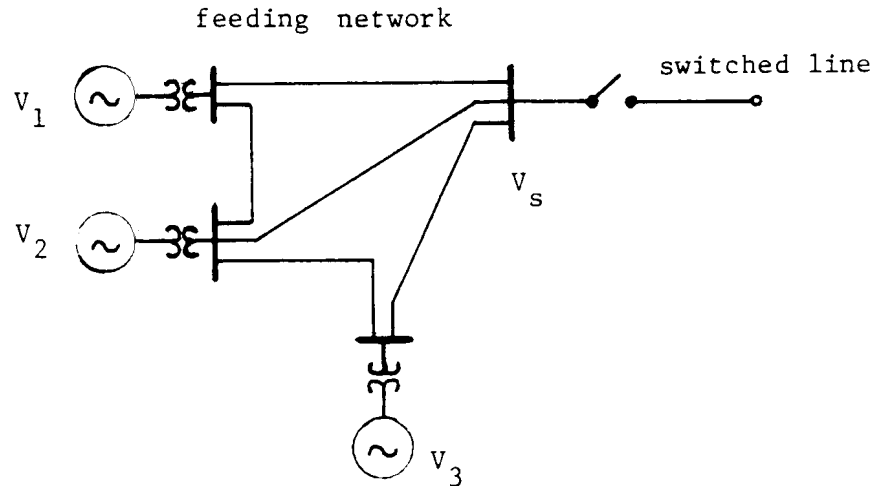
Fig. 12.19 - Network configuration for switching surge study

network, as long as the feeding network does not contain nonlinear elements. The only important parameters are the (frequency-dependent) impedance of the feeding network (which does not depend on power flows anyhow), and the pre-closing voltage V_S. This is true because a linear network can always be represented by a Thevenin equivalent circuit which requires only these two parameters. The value of the open-circuit voltage V_S is normally specified by the user (e.g., 5% above rated voltage), rather than obtained from a load flow solution. Any combination of source voltages V_1, V_2, V_3 which produces the same V_S would create identical overvoltages. One could therefore simply assume equal source voltages $V_1 = V_2 = V_3$, make one trial steady-state solution to get V_S^{trial}, and then multiply the voltages with the factor V_S/V_S^{trial} for the final simulation. A load flow solution is not needed in this case.

The best methods for load flow solutions are based on the Newton-Raphson method. When Rasmussen added a load flow option in 1983, he was aware of that, but he could not afford the tremendous programming effort involved in its implementation. Instead, he developed a simpler method, which would serve his needs and at the same time require as little program changes as possible. This led to the method discussed next, which is somewhat similar to the Gauss-Seidel methods used in the early days of load flow program development. An improved approach, which also requires a minimum of program changes, is discussed in Section 12.2.2. It is clear, however, that one would eventually have to use Newton-Raphson methods, and re-program the steady-state solution routine completely, if further improvements are needed.

12.2.1 Rasmussen's Load Flow Method

Nodes at which the user specifies active power P and reactive power Q (or some other combination of P, Q, voltage magnitude, and voltage angle) are treated as voltage sources in the direct solution of the system of linear equations (12.18). For a network with 100 nodes, in which P, Q is specified at 9 nodes, and where one node is the slack node ($|V|$, θ specified), the solution of the 90 equations (12.18) amounts essentially to a reduction of the network to 10 voltage source nodes. After this solution, Rasmussen calculates the current at P, Q-nodes from the equations of set B which have been left out in Eq. (12.18),

$$I_k = \sum_{m=1}^{n} Y_{km} V_m \qquad \text{for all nodes k of set B, except for slack node} \qquad (12.19)$$

and then the power from

$$P_k - jQ_k = L_k V_k^* \qquad (12.20)$$

The calculated values of P_k, Q_k are then compared with the values specified by the user. Based on these differences, corrections are made to the angle θ_k and magnitude $|V_k|$ of each voltage V_k,

$$\Delta\theta_k = \frac{P_k - P_{k-specified}}{\frac{1}{2}(|P_k| + |P_{k-specified}|)} \cdot 2.5 \; F \qquad (12.21)$$

and

$$\Delta|V_k| = \frac{Q_k - Q_{k-specified}}{\frac{1}{2}(|Q_k| + |Q_{k-specified}|)} \cdot 2000 \; F \qquad (12.22)$$

F is a deceleration factor which decreases from 1.0 to 0.25 in 500 iterations, with the formula

$$F = \left(\frac{1000 - h}{1000}\right)^2 \qquad (12.23)$$

(h = iteration step). Once the voltages have been corrected, another direct solution of Eq. (12.18) is obtained. This cycle of calculations is repeated until $\Delta\theta_k$ and $\Delta|V_k|$ become sufficiently small.

The method of Rasmussen is comparable to the Gauss-Seidel load flow solution method applied to the reduced system

$$[Y_{BB}^{reduced}] = [V_B] = [I_B] \qquad (12.24a)$$

where

$$[Y_{BB}^{reduced}] = [Y_{BB}] - [Y_{BA}][Y_{AA}]^{-1}[Y_{AB}] \qquad (12.24b)$$

and where $[I_A]$ was assumed to be zero to simplify the explanations. For the 100-node example, the performance of Rasmussen's method would therefore have to be compared against the Gauss-Seidel method for a 10-node system (with one slack node), and not for a 100-node system. Since the Gauss-Seidel method converges faster for smaller systems, the reduction implied in the Rasmussen method is an advantage over straightforward Gauss-Seidel methods.

12-17

If the standard Gauss-Seidel load flow method were applied to the reduced system, the corrected voltages would be found from

$$Y_{kk}^{reduced} V_k^{(h)} = \frac{P_{k\text{-}specified} - jQ_{k\text{-}specified}}{V_k^{*(h-1)}} - \sum_{nodes\ of\ set\ B\ except\ K} Y_{km}^{reduced} V_m^{(h-1)}$$

for each node k of subset B (except for the slack node). A slightly modified method uses equations in the form in which they are normally written for Newton's methods,

$$(-Q_k - B_{kk}^{reduced} |V_k|^2) \Delta\theta_k = P_k - P_{k\text{-}specified} \tag{12.25}$$

$$(P_k + G_{kk}^{reduced} |V_k|^2) \frac{\Delta |V_k|}{|V_k|} = Q_k - Q_{k\text{-}specified} \tag{12.26}$$

The coefficients on the left-hand side are often called H_{kk} and L_{kk} in the load flow solution literature. By comparing Eq. (12.25) and (12.26) with Eq. (12.21) and (12.22), one can see that Rasmussen basically assumed fixed values for H_{kk} and L_{kk}, independent of the type of network and the system of units used (p.u., VA, kVA, or MVA). The influence of the chosen system of units seems to be more or less eliminated by using relative values $\Delta P/P$ and $\Delta Q/Q$ in Eq. (12.21) and (12.22). The method of Rasmussen may be sensitive to the type of network being studied. Convergence may be slow, as for any Gauss-Seidel related method, even if the reduced system is small.

12.2.2 Current Source Iteration Method[2]

From stability studies it is known that much better convergence can be obtained by representing the P, Q-nodes as current sources in the reduced network of Eq. (12.24). The current sources are obtained from the voltage solution of the preceding iteration step,

$$I_k^{(h)} = \frac{P_{k\text{-}specified} - jQ_{k\text{-}specified}}{V_k^{*(h-1)}} \tag{12.27}$$

for all nodes k of set B except for slack node

With $[I_B]$ thus known, Eq. (12.24) is solved directly for an improved voltage solution $[V_B]$ (except for the slack node). For the 100-node example, 99 equations would have to be solved, compared to 90 equations in Rasmussen's method. However, convergence is potentially much faster. For the single-phase 5-node test system of Fig. 12.20, it took 9 iterations to converge to an accuracy of $|\Delta P| / |P|$, $|\Delta Q| / |Q| \leq 10^{-5}$ for all nodes. Rasmussen's method was not run for this case, but it would probably require many more iterations.
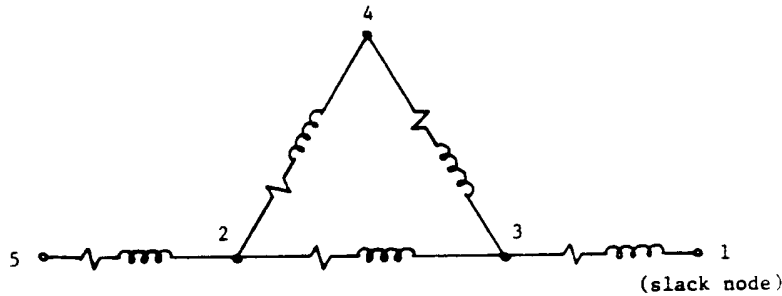
Fig. 12.20 - Single-phase 5-node test system (node 1 = slack node, nodes 2, 3, 4, 5 = P, Q-nodes)

The test case supplied by BPA for the load flow option is shown in Fig. 12.21. It consists of a three-phase generator (terminals A1, B1, C1) with series resistances, which feeds through a delta/wye-connected transformer and through coupled inductances into a three-phase voltage source (slack nodes). P, Q is specified at the three generator terminals A1, B1, C1. The entire system is balanced, and is therefore equivalent to a 2-node single-phase (positive sequence) network with only one P, Q-node and one slack node. Rasmussen's method takes 133 iterations to converge to accuracy defined in the BPA test case data. When the current source iteration method was first tried on it (with high hopes), it failed unexpectedly. The reason turned out to be the floating delta connection of the transformer, which makes the admittance matrix on the generator side singular (or extremely ill-conditioned). The sum of the three currents $I_{A1} + I_{B1} + I_{C1}$ becomes slightly nonzero (because of round-off errors) in the iteration process, and this extremely small zero sequence current will be injected into an infinite zero sequence impedance on the delta side, which produces a large zero sequence voltage. This causes the method to diverge.
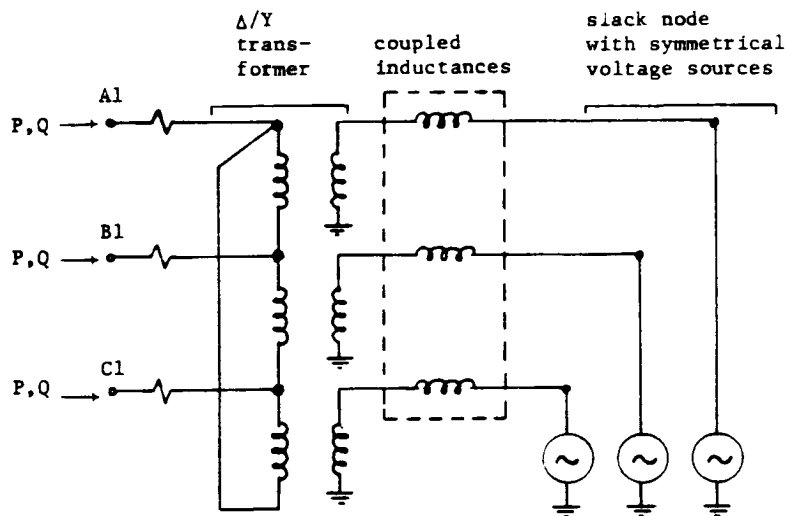
Fig. 12.21 - BPA test case for load flow option

To resolve this problem, one can connect shunt impedances to nodes A1, B1, C1 to make the matrix nonsingular. Since node 1 is a synchronous machine, and since such a machine should properly be represented as current sources in parallel with the negative sequence impedances to handle unbalanced cases (Section 8.4), a natural

choice would be

$$Z_{shunt} = j \frac{X_d^{//} + X_q^{//}}{2} \qquad (12.28)$$

With this shunt impedance, and with a modification of Eq. (12.27) to account for the current in this impedance,

$$I_k^{(h)} = \frac{R_{k\text{-}specified} - j\, Q_{k\text{-}specified}}{V_k^{*(h-1)}} + \frac{V^{(h-1)}}{Z_{shunt}} \qquad (12.29)$$

the current source iterations converge in 45 iterations, which is faster than Rasmussen's method, but much slower than expected from the experience with the 5-node test system of Fig. 12.20.

It is known from stability studies that shunt impedances speed up convergence if they are determined in such a way that they would produce the specified power at the rated voltage, or

$$Z_{shunt} = - \frac{|V_{rated}|^2}{P_{specified} - j\, Q_{specified}} \qquad (12.30)$$

where P, Q is negative for loads and positive for generation. With this shunt impedance, the current source iteration method does indeed converge quickly in 5 iterations. Fig. 12.22 shows
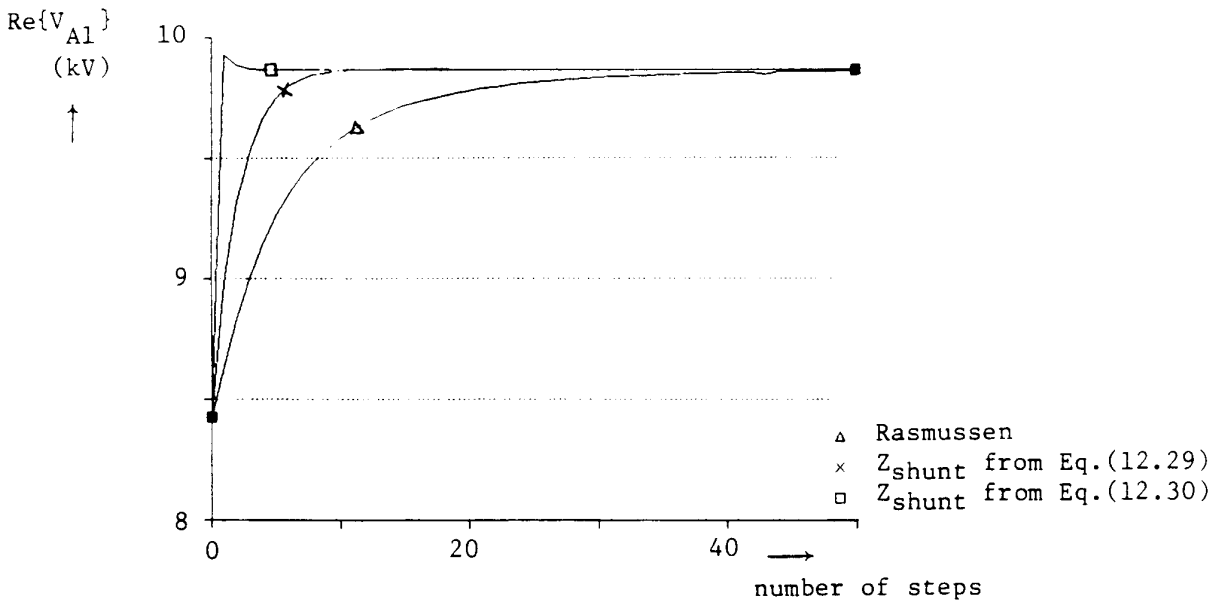
(a) Real part of V_{A1}
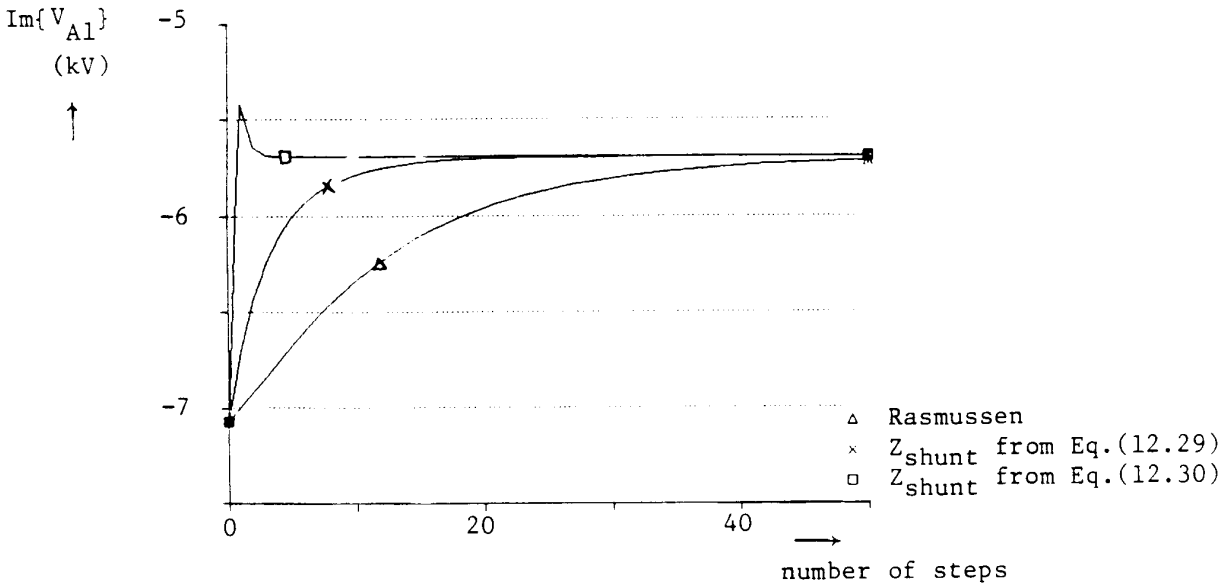
(b) Imaginary part of V_{A1}

Fig. 12.22 - Voltages as a function of iteration step for test case of Fig. 12.21

the real and imaginary part of voltage V_{A1} for Rasmussen's method, and for the current source iteration method with Z_{shunt} from Eq. (12.29) and from Eq. (12.30). From a convergence standpoint, Z_{shunt} from Eq. (12.30) is obviously best, but if one wants to represent the synchronous machine properly in unbalanced cases, Z_{shunt} from Eq. (12.29) should be used.

A. Yan started implementing this method in Ontario Hydro in 1985/86. A few issues remain to be resolved. One is the treatment of P, |V|-nodes where active power and voltage magnitude are specified. If one is willing to pre-calculate the internal impedance of the network as seen from each P, |V|-node, then one can construct an approximate Thevenin equivalent circuit after the solution at each iteration step. With V_{known} and I_{known} being the known values at a P, |V|-node, and with Z_{Thev} having been pre-calculated once and for all, the open-circuit voltage V_{Thev} of the Thevenin equivalent circuit (Fig. 12.23) is simply

$$V_{Thev} = V_{known} - Z_{Thev} I_{known} \qquad (12.31)$$

| (a) Circuit | (b) Relationship between $\lvert V \rvert$ and Q |
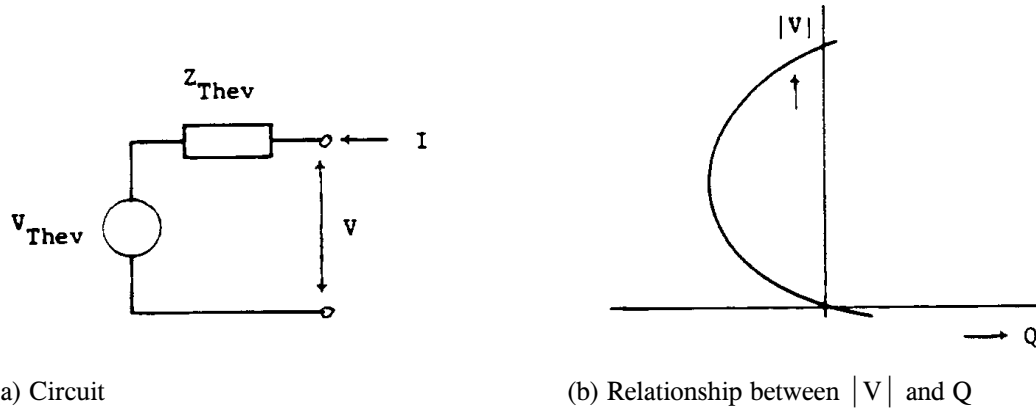
Fig. 12.23 - Thevenin equivalent circuit

If we assume that this Thevenin equivalent circuit is now correctly defined by V_{Thev} and Z_{Thev}, and that V and I are allowed to change, then we obtain a relationship between Q and $\lvert V \rvert$,

$$Q = B \left(\lvert V_{Thev} \rvert \, \lvert V \rvert \, \cos\alpha \; - \; \lvert V \rvert^2 \right) \; + \; G \lvert V_{Thev} \rvert \, \lvert V \rvert \, \sin\alpha \qquad (12.32)$$

where α is the angle between V_{Thev} and V, and $G + jB = 1/Z_{Thev}$. Since the angle α is more related to active power flows than reactive power flows, it is reasonable to assume that α does not change if the Q - $\lvert V \rvert$-relationship is altered. With α, G, B and $\lvert V_{Thev} \rvert$ known, and with the specified node voltage magnitude being used for $\lvert V \rvert$, Eq. (12.32) can be solved for Q. This value of Q is then used in calculating the current for the next iteration step from Eq. (12.29). For the 5-node test system of Fig. 12.20, this method converged in 16 iterations when nodes 4 and 5 were treated as P, $\lvert V \rvert$-nodes, with nodes 2 and 3 remaining P, Q-nodes.

The treatment of P, Q-nodes and P, $\lvert V \rvert$-nodes in three-phase unbalanced cases is still under development. To obtain realistic answers, the user cannot specify power or voltage magnitude values more or less arbitrarily at each one of the three phases. Instead, one must know how the load or generator reacts to unbalanced conditions. As explained in Section 8.4, synchronous machines must be modelled as symmetrical voltage sources behind (or symmetrical current sources in parallel with) a 3 x 3 impedance matrix calculated from $Z_{pos} = Z_{neg}$ and Z_{zero}. To obtain results which are physically possible, the same representation would have to be used in the load flow iterations. Similar models valid for unbalanced conditions would have to be developed for the universal machine, and for other devices which appear in the EMTP as loads or generators.

12.3 Steady-State Solutions without Harmonics

The linear ac steady-state phasor solution at one frequency has already been described in Section 1, and the models of the various elements which must be used in that solution have been discussed in the respective sections. The routine for the steady-state solution was added by J.W. Walker, originally to obtain ac steady-state initial conditions automatically. Later, it became a useful tool on its own, e.g., for studying complicated coupling effects between circuits on the same right-of-way (example in Fig. 4.25). The EMTP therefore has an option to terminate

the run after the steady-state solution, and to tabulate the phasor values in as much detail as the user may wish.

12.3.1 Thevenin Equivalent Circuits

If a large network is to be solved repeatedly, with only a few parameters varied each time, then it may be best to generate an M-phase Thevenin equivalent circuit for the large network first, as illustrated in Fig. 12.24. The parameters of the Thevenin equivalent circuit can easily be obtained with the EMTP from M + 1 steady-state solutions of the large network as follows:
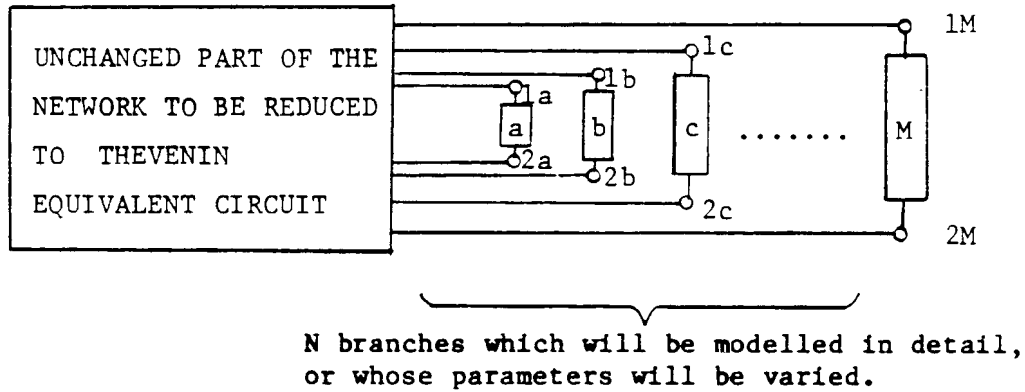
Fig. 12.24 - Parameter variation in branches 1, … M

(1)   Remove the branches 1,…M (which may be coupled among themselves) from the large network. Obtain a steady-state solution, and record the open-circuit branch voltages across the node pairs 1a-2a, 1b-2b,… at the locations where the M branches were removed. If the branches are all connected from node to ground, then these branch voltages are simply node voltages. This first steady-state solution produces the open-circuit voltage vector of the M-phase Thevenin equivalent circuit,

$$[V_{Thev}] = \begin{bmatrix} V_{1a-2a} \\ V_{1b-2b} \\ . \\ . \\ V_{1M-2M} \end{bmatrix} \tag{12.33}$$

(2)   Find the impedance matrix

$$[Z_{Thev}] = \begin{bmatrix} Z_{aa} & Z_{ab} & \dots & Z_{aM} \\ Z_{ba} & Z_{bb} & \dots & Z_{bM} \\ Z_{Ma} & Z_{Mb} & \dots & Z_{MM} \end{bmatrix} \tag{12.34}$$

of the Thevenin equivalent circuit column by column with M steady-state solutions. First, short-circuit all voltage sources in the large network (easiest way to do this is to set their amplitudes to zero; simply removing

12-23

them from the data file would create open circuits), and cancel all current sources (set amplitudes to zero or remove them from data file). To obtain column k of $[Z_{Thev}]$, connect one current source of 1.0 A (RMS) to node 1k, and a second current source of -1.0 A (RMS) to node 2k, and ask for a steady-state solution. Then the elements of the k-th column of $[Z_{Thev}]$ are simply the RMS-branch voltages,

$$
\begin{bmatrix} Z_{ak} \\ Z_{bk} \\ . \\ . \\ Z_{Mk} \end{bmatrix} = \begin{bmatrix} V_{1a-2a} \\ V_{1b-2b} \\ . \\ . \\ V_{1M-2M} \end{bmatrix}
\tag{12.35}
$$

With $[V_{Thev}]$ and $[Z_{Thev}]$ known, the large (unchanged) part of the network is described by the M-phase Thevenin equivalent circuit of Fig. 12.25, with its branch equation

$$[V] = [V_{Thev}] - [Z_{Thev}][I] \tag{12.36}$$
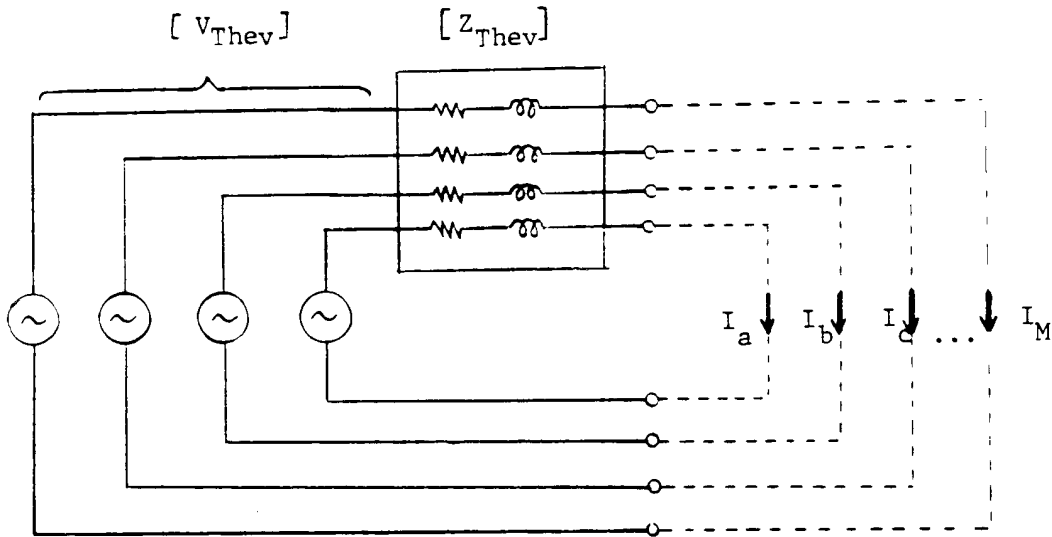
Fig. 12.25 - M-branch Thevenin equivalent circuit

where [V] and [I] are branch voltages and currents. If these branches are passive, with a branch impedance matrix $[Z_{branch}]$ whose values are to be varied repeatedly, then

$$[V] = [Z_{branch}][I] \tag{12.37}$$

which can be solved with Eq. (12.36) for the currents,

$$[I] = \{[Z_{Thev}] + [Z_{branch}]\}^{-1}[V_{Thev}] \tag{12.38}$$

EMTP users may want to write their own program to solve Eq. (12.38), rather than use the EMTP for it.

Such a Thevenin equivalent circuit was used by BPA to study resonance problems on a shunt-compensated transmission line which is switched off at both ends, but which is still capacitively coupled to parallel circuits on the same right-of-way. Because of complicated transposition schemes, the complete network is fairly large, whereas the Thevenin equivalent circuit of the network seen from the three shunt reactor connection points A, B, C has only a 3 x 3 $[Z_{Thev}]$-matrix. Fig. 12.26 shows the results of this study, in which the inductance of the shunt reactors was varied in small steps from 5.85 to 6.00 H.
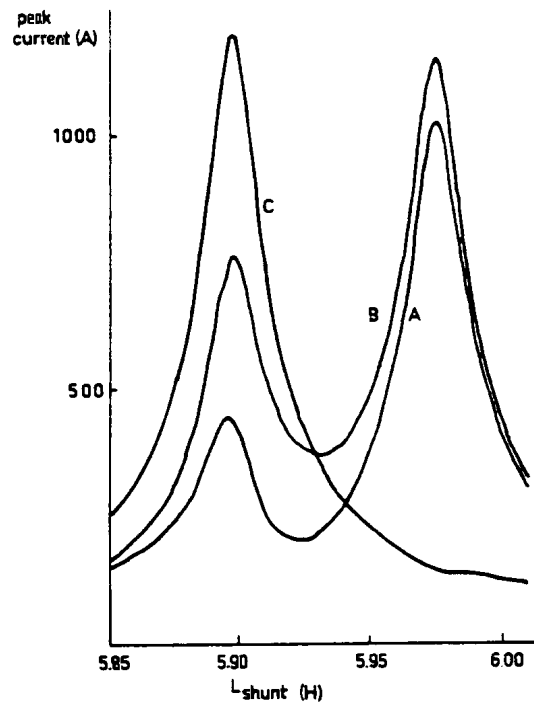
Fig. 12.26 - Resonance in shunt reactors

Thevenin equivalent circuits are in principle only valid at the frequency at which they are calculated. In the preceding example it would be known, however, that an open-ended line is seen by the shunt reactor as a capacitance up to some frequency way above 60 Hz, and that the coupling to energized lines is capacitive as well. The Thevenin impedance is therefore $Z_{Thev} = 1/(j\omega C)$, or in the matrix case

$$[C]^{-1} = j\omega [Z_{Thev}]$$

The capacitance matrix representation would then be useful for transient studies (up to a certain frequency) as well.

12.3.2 Frequency Scan

The first addition to the steady-state solution routine was a loop to vary the frequency automatically from f_{min} to f_{max}, either in linear steps of Δf or on a logarithmic scale. At each frequency, the solution is obtained in the same way as before. This option has become known as "frequency scan." Instead of getting voltages and currents as a function of time, their magnitudes and angles are obtained as a function of frequency. This option is very useful

for finding the frequency-dependent impedance of a network seen from a particular location. To obtain the impedance, all voltage sources are short-circuited and all current sources are removed. A current source of 1 A is then added across the two nodes between which the impedance is to be obtained. The branch voltage will be equal to the impedance. Fig. 12.27 shows an example, where the impedance between two phases was computed with the frequency-scan option of the EMTP, as well as indirectly measured with a phase-to-phase fault (time response Fourier transformed to frequency response), as part of a study to investigate potential subsynchronous resonance problems.
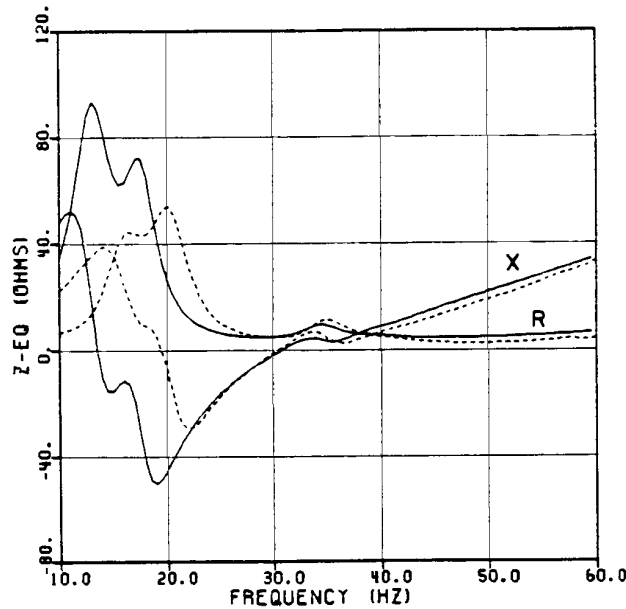
Fig. 12.27 - Comparison between impedance calculated with frequency scan and measured impedance [184]. © 1984 IEEE

12.3.3 Different Frequencies in Disconnected Parts

The BPA EMTP is capable of finding the steady-state solution in networks with sources having different frequencies, provided that the network is disconnected into subnetworks, with each subnetwork only containing sources with the same frequency. The need for this capability arose primarily in connection with universal machine initialization (Section 9.5). For example, the armature windings of a synchronous machine and the connected power system must be solved for ac conditions, whereas the field circuit requires a dc solution.

The same capability can be used to handle trapped charge on an isolated line, and HVDC links. In the latter case, the converters are either represented as impedances or current sources on the ac side, and as voltage sources on the dc side. This ignores the current harmonics on the ac side and the voltage harmonics on the dc side, but it does produce reasonable initial conditions for the transient simulation. Fig. 12.28 shows simulation results for a dc transmission line with six-pulse converters, which were connected through converter transformers to ac networks
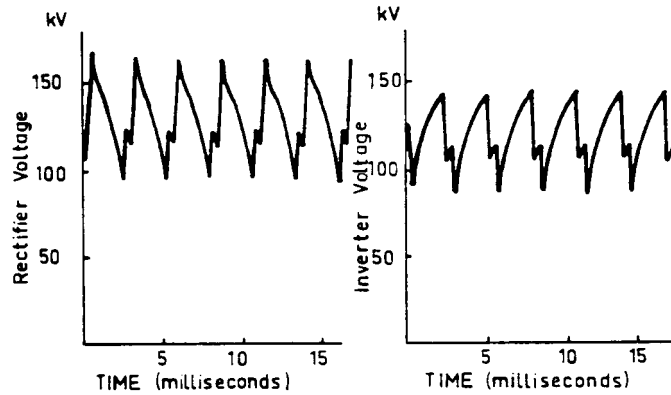
Fig. 12.28 - Rectifier and inverter voltage, with simulation
starting from approximate initial conditions

represented as three-phase Thevenin equivalent circuits. At least in this case, the final steady state was reached almost immediately.

The theory behind this single solution with multiple frequencies is very simple. Assume that there are two subnetworks 1 and 2 with frequencies f_1 and f_2. Since they must be disconnected, Eq. (1.20) has the form

$$\begin{bmatrix} [Y_1] & 0 \\ 0 & [Y_2] \end{bmatrix} \begin{bmatrix} [V_1] \\ [V_2] \end{bmatrix} = \begin{bmatrix} [I_1] \\ [I_2] \end{bmatrix} \tag{12.39}$$

and all that is required is that frequency f_1 be used in forming $[Y_1]$ and f_2 in forming $[Y_2]$.

For dc solutions, an inductance branch becomes a short-circuit and the two nodes therefore collapse into one node. To solve dc conditions exactly would therefore require program modifications, which have been regarded as a low-priority item until now. Instead, dc sources are represented as ac sources of the form $V\cos\omega t$ or $I\cos\omega t$, with ω being very low (typically $f = 10^{-3}$ Hz). Inductances are then very low impedances, rather than short circuits.

12.4 Steady-State Solution with Harmonics

Steady-state harmonics in high-voltage transmission systems are primarily produced by transformer (and possibly shunt reactor) saturation, by HVDC converter stations, and by large rectifier loads (e.g., aluminum reduction plants). In rectifiers and inverters, the magnitude of harmonics is reasonably well known, and these harmonics can therefore be represented as given current or voltage sources in harmonic load flow programs specifically designed for harmonics studies. In contrast, harmonics generated by transformer saturation depend critically on the peak magnitude and waveform of the voltage at the transformer terminals, which in turn are influenced by the harmonic currents and the frequency-dependent network impedances.

Transient simulations with the EMTP will contain harmonics effects either from transformer saturation of from converters. If the simulation is carried out long enough to let the transients settle down to steady-state conditions, then the waveforms will contain the harmonics with reasonable accuracy up to a certain order, depending

on the step size Δt. A Fourier analysis program is available as a support routine in the EMTP to analyze such waveforms. This approach is discussed first. There are cases, however, where it would be desirable to have the harmonics already included in the steady-state initial conditions, because steady-state harmonics do sometimes have an effect on the transients. This is discussed next in Section 12.4.2.

12.4.1 Harmonics from Linear ac Steady-State Solution followed by Transient Simulation

A simple method for obtaining saturation-generated harmonics is to perform a transient simulation with the EMTP which starts from approximate linear ac steady-state conditions. For the initial ac steady-state solution, the magnetizing inductances of transformers are represented by their unsaturated values. In the transient simulation, the only disturbances will then be the deviations between the linear and nonlinear magnetizing inductance representations. The transients caused by these deviations will often settle down to the distorted steady state within a few cycles.

This simple method works only well if the final distorted steady state is reached quickly in a few cycles. Such is the case in the example cited in Section 6.6.2 (Fig. 6.13 and 6.14), where steady state was reached within approximately 3 cycles. For lightly damped systems, it may take a long time before the final steady state is reached. Fig. 12.29 shows the voltages at
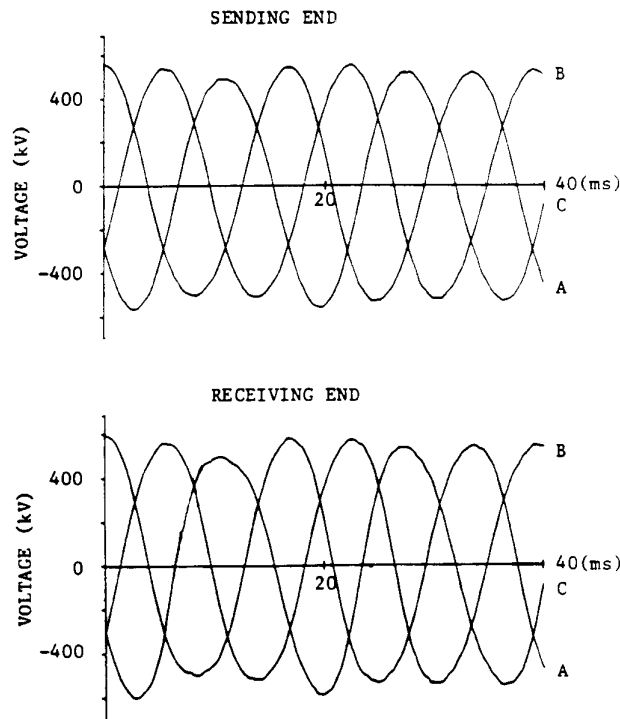
Fig. 12.29 - Voltages with harmonic distortion on a 500 kV line (simulation starts from approximate linear steady state)

both ends of a 500 kV-line with shunt reactors which go into saturation at 0.92 p.u. of rated flux at the sending end and at 1.05 p.u. of rated flux at the receiving end. Because of low damping, the steady state is reached only after a long time. It is such cases where the steady-state solution method described in the next section is useful.

12.4.2 Harmonics from Steady-State Solutions

The method described in this section [185] has been implemented in Ontario Hydro's EMTP by A. Yan in 1985, as part of joint work undertaken by the EMTP Development Coordination Group (DCG) and EPRI. It should become available to users of the DCG/EPRI version of the EMTP in 1986 or 1987.

To obtain the harmonics directly from phasor equations, the nonlinear inductances must be replaced by current sources, which contain the fundamental frequency component as well as the harmonic frequency components (Fig. 12.30). The network itself is then linear, and the voltages at any frequency are therefore easily found by solving the system of linear equations (12.18). The nonlinear effects are represented as current sources in the vector $[I_A]$. The complete solution is found with two iterative loops. First "power flow" iterations are used to obtain an approximate solution at fundamental frequency, while the second "distortion" iterations take the higher harmonics into account and correct the fundamental frequency solution as well.
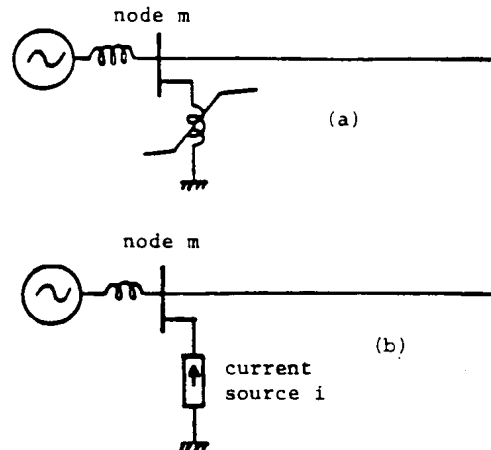
Fig. 12.30 - Replacing nonlinear inductances by current sources. (a) Network with nonlinear inductance, (b) network with current source

12.4.2.1 "Power Flow" Iterations

In the "power flow" iterations, an approximate linear ac steady-state solution is found which represents the V_{RMS}/I_{RMS}-curves of the nonlinear inductances correctly, but does not include harmonic distortion. For the nonlinear inductance, say at node m in Fig. 12.30, the original data may already be in the form of a V_{RMS}/I_{RMS}-curve, as shown in Fig. 12.31. If not, it is straightforward to convert the λ/i-curve into a V_{RMS}/I_{RMS}-curve, with the support routine CONVERT (Section 6.10.4). To start the iteration process, a guess for the RMS voltage V_m is used to find the RMS current I_m (Fig. 12.31). This current, with the proper phase shift of $90°$ with respect to V_m, is inserted into the current vector $[I_A]$ in Eq. (12.18), and a new set of voltages $[V_A]$ is then found by solving the system of linear equations. This solution process is repeated, until the prescribed error criterion for the current I_m is satisfied. Note that the admittance matrix $[Y]$ in Eq. (12.18) remains constant for all iteration steps; therefore, $[Y]$ is only triangularized once outside the iteration loop. Inside the iteration loop, the downward operations and

backsubstitutions are only performed on the right-hand side, by using the information contained in the triangularized matrix ("repeat solutions").
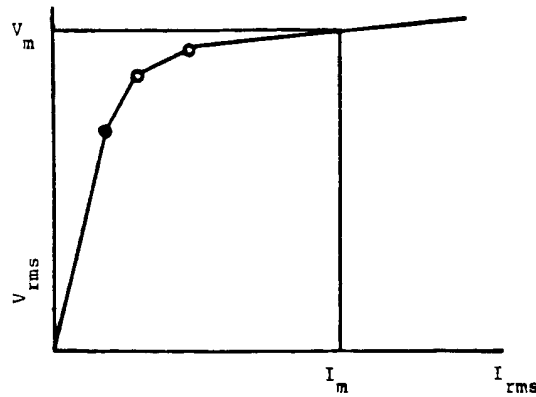
Fig. 12.31 - V_{RMS}/I_{RMS} characteristic of a nonlinear inductance

In these "power flow" iterations at fundamental frequency, the V_{RMS}/I_{RMS}-curve is used as an approximation to the curve relating the fundamental frequency current I_1 to the fundamental frequency voltage V_1. If V_{RMS} were equal to V_1, then I_{RMS} would contain harmonics,[3] which are ignored. The approximation does provide a good starting point, however, for the following "distortion" iterations, in which harmonics are included.

If the network contains nodes of the load flow option type, e.g., active power P and reactive power Q specified rather than current I, then the adjustments to achieve constant power can easily be incorporated into this iterative loop by using Eq. (12.29), or a similar equation, at the beginning of each iteration step.

12.4.2.2 "Distortion" Iterations

The "power flow" iterations produce a steady-state solution at fundamental frequency only, without harmonic distortion. To obtain the harmonics, the RMS voltages found from the "power flow" iterations are used in an initial estimate for the flux. Since $v = d\lambda/dt$, and assuming that the peak voltage phasor is $|V|e^{j\phi}$, or

$$v(t) = |V| \cos(\omega_1 t + \phi) \tag{12.40}$$

as a function of time (ω_1 = angular fundamental frequency), it follows that the flux is

$$\lambda(t) = \frac{|V|}{\omega_1} \sin(\omega_1 t + \phi) \tag{12.41}$$

With $\lambda(t)$ known, one full cycle of the distorted current i(t) is generated point-by-point with the λ/i-curve (Fig. 12.32). If hysteresis is ignored, then it is sufficient to produce one quarter of a cycle of i(t), since each half-cycle wave is symmetric, and since the second half is the negative of the first half of each cycle.

---

[3]Subscripts 1, 2,... are used in this section to indicate the order of the harmonic (1 = fundamental).

The distorted current i(t) in each nonlinear inductance is then analyzed with the support routine Fourier Analysis, which produces the harmonic content expressed by

$$i(t) = \sum_{n=1}^{k} |I_n| \sin(\omega_n t + \phi_n)$$ (12.42)

with

$$\omega_n = n\omega_1$$ (12.43)

being the angular frequency of the n-th harmonic. Experience has shown that it is usually sufficient to consider the fundamental and the odd harmonics of order 3 to 15, and to ignore the higher and even harmonics. At each harmonic considered (including the fundamental), the harmonic component from Eq. (12.42) is entered into $[I_A]$ with its proper magnitude and angle for all nonlinear inductances, and the voltages at that harmonic frequency are then found by solving the system of linear equations (12.18). Known harmonic current sources from converters and other harmonic producing equipment are added into the vector $[I_A]$.
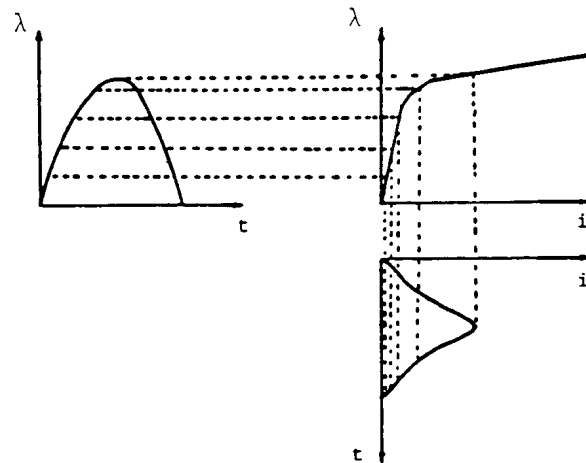
Fig. 12.32 - Generating i(t) from λ(t)

Taking the fundamental and the odd harmonics 3, 5, 7, 9, 11, 13 and 15 into consideration requires 8 solutions of that system of equations, with [Y] obviously being different for each of the harmonic frequencies. For lumped inductances L and capacitances C, it is clear that values $\omega_n L$ and $\omega_n C$ must be used as reactances and susceptances in building [Y]. Lines can be modelled as cascade connections of nominal π-circuits, as long as the number of π-circuits per line is high enough to represent the line properly at the highest harmonic frequency. It is safer, however, to define the line data as distributed parameters, and to generate the exact equivalent π-circuit at each frequency, as explained in Sections 4.2.1.2 and 4.2.1.3.

Once the voltages have been found for the fundamental and for the harmonics, an improved flux function λ(t) can be calculated for each nonlinear inductance from the peak voltage phasors $|V_1|e^{j\phi 1}$, $|V_3|e^{j\phi 3}$, etc.,

$$\lambda(t) = \sum_{n=1}^{k} \frac{|V_n|}{\omega_n} \sin(\omega_n t + \phi_n) \tag{12.44}$$

With $\lambda(t)$ known, i(t) is again generated point-by-point as shown in Fig. 12.32, and then analyzed with the support routine Fourier Analysis to obtain an improved set of harmonics expressed as Eq. (12.42). These are then again used to find an improved set of harmonic voltages. This iterative process is repeated until the changes in the harmonic currents are sufficiently small. Experience has shown that 3 iterations are usually enough to obtain the harmonic currents with an accuracy of $\pm 5\%$.

12.4.3 Discrepancies between Harmonics in Steady-State and Transient Solution

The method described in the preceding section turns the EMTP into a harmonics load flow program. If it is used that way, without a transient simulation following the steady-state solution, then the problems discussed in this section do not apply.

If the method is used as an improved initialization procedure for a subsequent transient simulation, then discrepancies can appear between the results from the steady-state and transient solutions. These discrepancies were not expected at first. They are cased by the unavoidable discretization error of the trapezoidal rule, which is used for lumped inductances and capacitances in the EMTP. In the steady-state solution for the n-th harmonic, correct reactance values $\omega_n L$ would normally be used, while the transient simulation would see a somewhat larger reactance $k\omega_n L$, with

$$k = \frac{\tan\left(\omega_n \frac{\Delta t}{2}\right)}{\omega_n \frac{\Delta t}{2}} \tag{12.45}$$

as explained in Section 2.2.1. The susceptance is also too large by the same factor k (Section 2.3.1). While a small Δt can keep the correction factor k of Eq. (12.45) reasonably close to 1.0 (e.g., $\Delta t = 50 \ \mu s$ leads to a correction factor of $k_7 = 1.0015$ at the 7th harmonic, or to an error of 0.15%), it can never be avoided completely. Even small errors can shift the resonance frequencies of the network. Fig. 12.33 compares the impedance at the location of the nonlinear inductance in the problem of Fig. 6.13, as it would be seen by a steady-state phasor solution and by a transient solution with the correction factor of Eq. (12.45). To emphasize the difference in Fig. 12.33, the line was modelled as a cascade connection of three-phase nominal π-circuits,
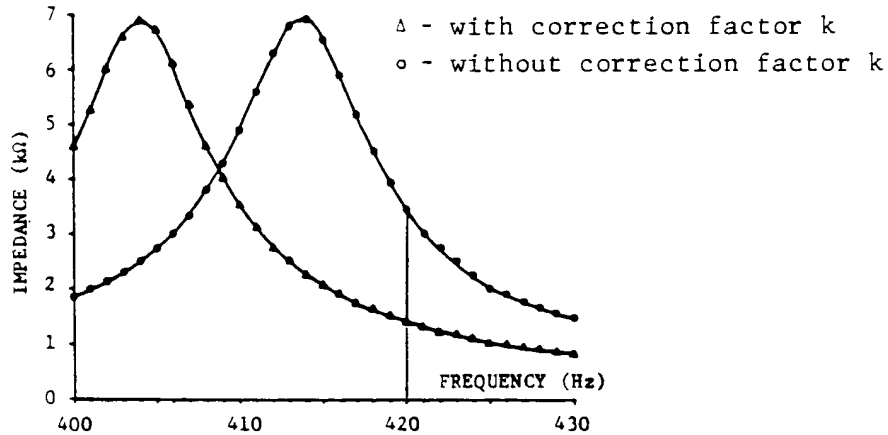
Fig. 12.33 - Frequency response with and without correction factor k (Δt = 200 μs)

rather than with distributed parameters. Since the EMTP uses other, more accurate, method for solving the equations of distributed-parameter lines, the differences would be much less with distributed-parameter representations.

In the transient simulation, the discretization correction factor of Eq. (12.45) is unavoidable, and the answers will therefore be slightly incorrect. In such situations, it may be best to introduce the same correction factor into the initialization with the steady-state solution method of Section 12.4.2, to avoid discrepancies between initial conditions and transient simulations. With this modification, the discrepancies between the initialization procedure of Section 12.4.2 and subsequent transient simulations of an otherwise undisturbed network become practically negligible.

Fig. 12.34 shows the transient simulation results for the same case used for Fig. 6.13, except that the initialization procedure of Section 12.4.2 was now used. It can be seen that the initial conditions must have contained more or less correct harmonics because no disturbance is noticeable after t = 0. Fig. 12.35 shows similar results
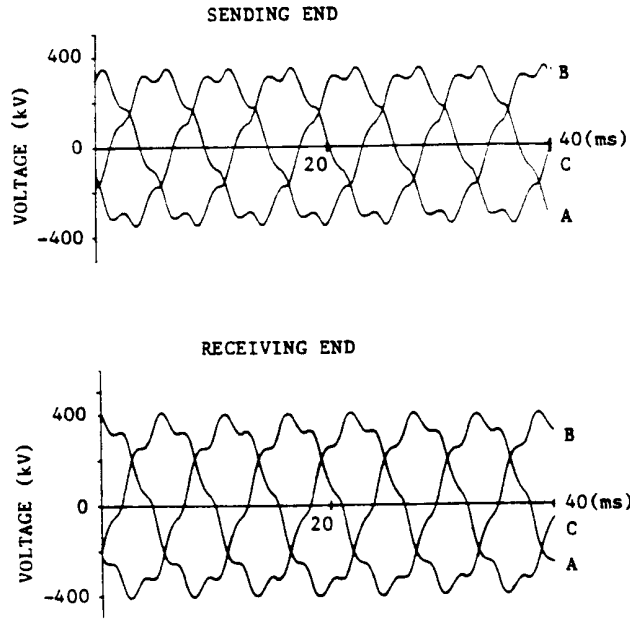
Fig. 12.34 - Same case as in Fig. 6.13, except simulation starts from steady state with harmonics

for the case used in Fig. 12.29, with the initialization procedure of Section 12.4.2. The improvement from the inclusion of harmonics in the initialization is quite evident in the second example.
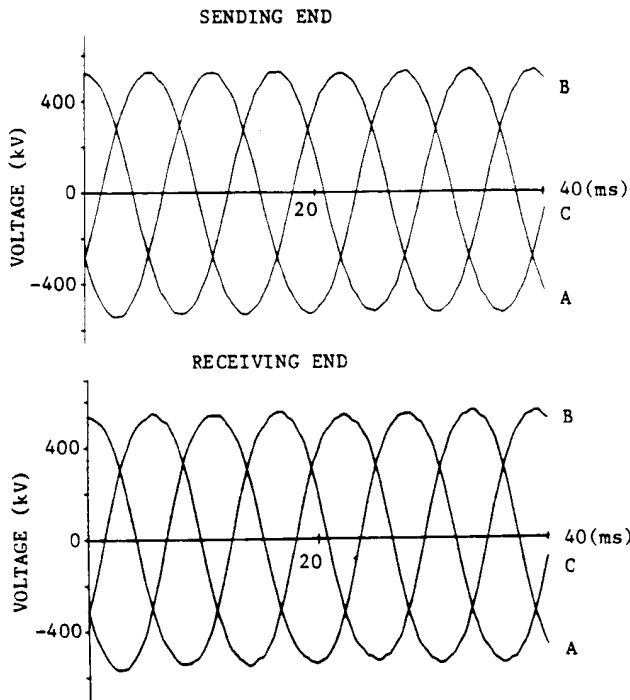
Fig. 12.35 - Same case as in Fig. 12.29, except simulation starts from steady state with harmonics

12.4.4 Ferroresonance

An attempt was made to apply the method of Section 12.4.2 to ferroresonance cases, but with little success. In ferroresonance phenomena, more than one steady-state solution is possible. It depends very much on the initial conditions and on the type of disturbance which one of these possible steady states will be reached. The method of Section 12.4.2 is therefore not useful for ferroresonance studies. The EMTP can be used for the simulation of ferroresonance phenomena, however, though it will not give any insight into all possible steady-state conditions. In that sense, EMTP simulations are somewhat similar to transient stability simulations, which also do not give global answers about the overall stability of the system.

13. TRANSIENT ANALYSIS OF CONTROL SYSTEMS (TACS)

Co-Author: S. Bhattacharya

The program part TACS (acronym for Transient Analysis of Control Systems) was developed 10 years ago by L. Dubé. In 1983/84, Ma Ren-ming did a thorough study of the code, and made major revisions in it, particularly with respect to the order in which the blocks of the control system are solved [187]. More improvements will be made in the future by L. Dubé and others. Because changes are expected anyhow, and because L. Dubé was not available for co-authoring this section, the general philosophy of the solution method in TACS and possible alternatives are emphasized more than details of implementation.

TACS was originally written for the simulation of HVDC converter controls, but it soon became evident that it had much wider applications. It has been used for the simulation of

    (a)   HVDC converter controls,

    (b)   excitation systems of synchronous machines,

    (c)   current limiting gaps in surge arresters,

    (d)   arcs in circuit breakers,

and for other devices or phenomena which cannot be modelled directly with the existing network components in the EMTP.

Control systems are generally represented by block diagrams which show the interconnections among various control system elements, such as transfer function blocks, limiters, etc. Fig. 13.1 is a typical example. A block diagram representation is also used in TACS because it makes the data specification by the user simple. All signals are assigned names which are defined by 6 alphanumeric characters (blank is included as one of the characters). By using the proper names for the input and output signals of blocks, any arbitrary connection of blocks can be achieved. Amazingly, there is no uniform standard for describing the function of each block in an unambiguous way, except in the case of linear transfer functions [189]. Users of the EMTP should be aware of this.

The control systems, devices and phenomena modelled in TACS and the electric network are solved separately at this time. Output quantities from the network solution can be used as input quantities in TACS over the same time step, while output quantities from TACS can become input quantities to the network solution only over the next time step. TACS accepts as input network voltage and current sources, node voltages, switch currents, status of switches, and certain internal variables (e.g., rotor angles of synchronous machines). The network solution accepts output signals from TACS as voltage or current sources (if the sources are declared as TACS controlled sources), and as commands to open or close switches (if the switch is a thyristor or a TACS controlled switch).
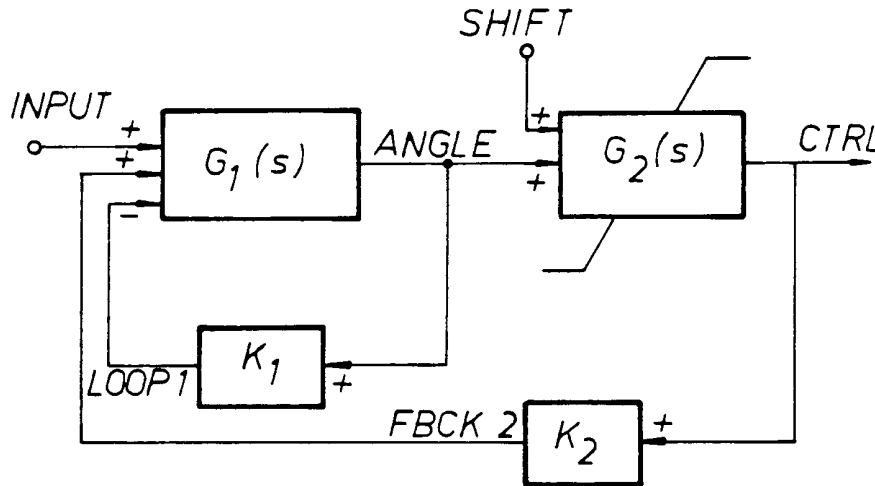
Fig. 13.1 - Typical block diagram representation of a control system

The present interface between the network solution and TACS, and possible alternatives to it, are explained first. The models available in TACS are described next, followed by a discussion of the initialization procedures.

13.1 Interface between TACS and the Electric Network

To solve the models represented in TACS simultaneously with the network is more complicated than for models of power system components such as generators or transformers. Such components can essentially be represented as equivalent resistance matrices with parallel current sources, which fit directly into the nodal network equations (1.8). The equations of control systems are quite different in that respect. Their matrices are unsymmetric, and they cannot be represented as equivalent networks.

Because of these difficulties, L. Dubé decided to solve the electric network (briefly called NETWORK from here on) and the TACS models (briefly called TACS from here on) separately. This imposes limitations which the users should be aware of. As illustrated in Fig. 13.2, the NETWORK solution is first advanced from $(t - \Delta t)$ to t as if TACS would not exist directly. There is an indirect link from TACS to NETWORK with a time delay of Δt, inasmuch as NETWORK can contain voltage and current sources defined between $(t - \Delta t)$ and t which were computed as output signals in TACS in the preceding step between $(t - 2\Delta t)$ to $(t - \Delta t)$. NETWORK also receives commands for opening and closing switches at time t, which are determined in TACS in the solution from $(t - 2\Delta t)$ to $(t - \Delta t)$. In the latter case, the error in the network solution due to the time delay of Δt is usually negligible. First, Δt for this type of simulation is generally small, say 50 μs. Secondly, the delay in closing a thyristor switch is compensated by the converter control, which alternately advances and retards the firing of thyristor switches to keep the current constant in steady-state operation. With continuous voltage and current source functions coming from TACS, the time delay can become more critical, however, and the user must be aware of its consequences. Cases have been documented where this time delay of Δt can cause numerical instability, e.g., in modeling the arc of circuit breakers with TACS [188].
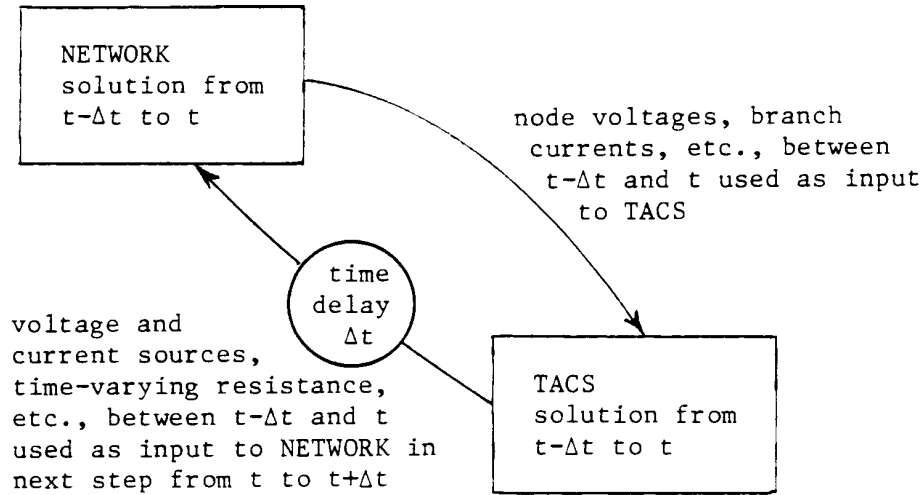
Fig. 13.2 - Interface between NETWORK and TACS solution

Once NETWORK has been solved, the network voltages and currents specified as input to TACS are known between (t - Δt) and t, and are then used to bring the solution of TACS from (t - Δt) to t. No time delay occurs in this part of the interface, except that TACS itself has built-in delays which may not always be transparent to the user.

If the EMTP is re-written some day to eliminate the time delay from TACS to NETWORK, two approaches (and possibly others) could be used:

(a)   Predict the output from TACS at time t, and use the predicted values to solve the NETWORK and then TACS from (t - Δt) to t. Use the output from TACS as corrected values, and repeat the solution of the two parts again from (t - Δt) to t. If the differences between the predicted and corrected values are still larger than a specified tolerance, then do another iteration step with a repeat solution, until the values have converged to their final values. This approach is conceptually easy to implement, but its usefulness depends on the convergence behavior. Two or three iteration steps, on average, would probably be acceptable. This method would make it possible to add other corrections in NETWORK and TACS where only predictions are used now (e.g. correction of predicted armature currents in synchronous machines).

(a) before reduction   (b) after reduction

13-3
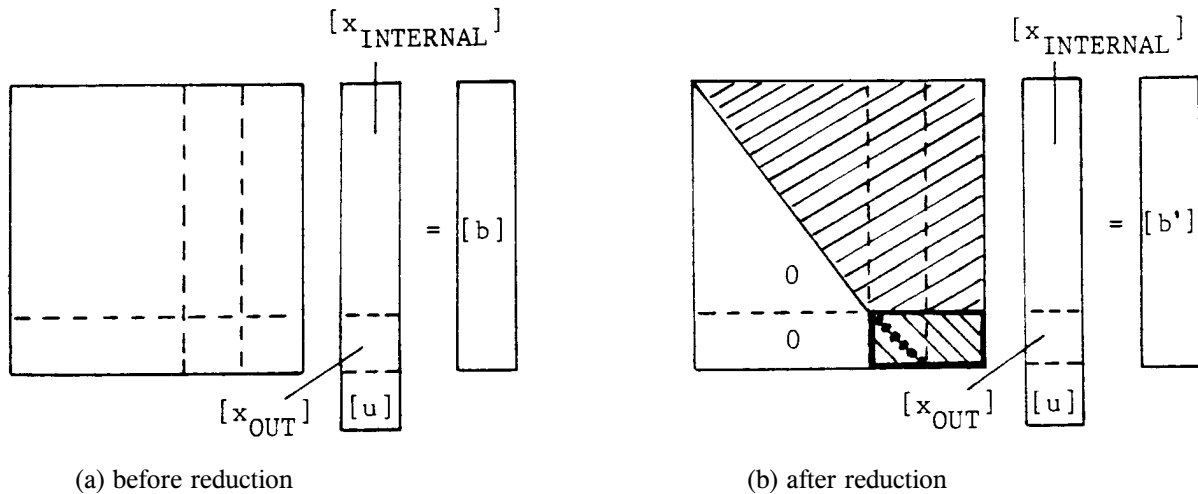
Fig. 13.3 - Form of difference equations for a control system. $[x_{INTERNAL}]$ = internal variables, $[x_{OUT}]$ = output signals, and $[u]$ = input signals

b)   Do not solve the equations in TACS completely, but reduced them to an input-output relationship at time t, by eliminating variables which are internal to TACS. This approach has been used successfully in a stability program for the representation of excitation systems [72]. Assume that the trapezoidal rule of integration (or any other implicit integration method) is applied to the differential equations of the control system. Assume further that the variables are ordered in such a way that the internal variables $[x_{INTERNAL}]$ come first, then the output signals $[x_{OUT}]$ which become input to NETWORK (v_f in an excitation system) and finally the input signals [u] which come from the output of NETWORK ($v_{TERMINAL}$ in an excitation system). Then the equations would have the form of Fig. 13.3(a). By eliminating the internal variables $[x_{INTERNAL}]$ with Gauss elimination, the reduced system of equations in the bottom rectangle of Fig. 13.3(b) is obtained, which has the form

$$[A_{OUT}] [x_{OUT}] + [A_{IN}] [u] = [b']$$ (13.1)

or in the case of an excitation system,

$$a_{OUT} v_f + a_{IN} v_{TERMINAL} = b'$$

In the latter case, this equation would have to be incorporated into the synchronous machine model of Section 8. Limiters can be handled as well with this approach, as explained in [72].

Method (b) could be implemented in a number of different ways. For control systems which can be represented by one transfer function, the implementation would be very simple, because TACS already produces an equation of the form of Eq. (13.1), as explained later in Eq. (13.7). For more complicated systems, the existing code of TACS could be used to solve the equations of system twice, e.g., in the case of the excitation system, for 2 predicted values of $v_{TERMINAL}$. The two solutions $v_{f1}(t)$ and $v_{f2}(t)$ would create 2 points in the $v_{TERMINAL}$ - v_F - plane, and a straight line through them would produce Eq. (13.1) indirectly.

13.2 Transfer Function Block with Summer

The transfer function block (Fig. 13.4) is used to describe a relationship between input U(s) and output X(s) in the Laplace domain,

$$X(s) = G(s) U(s)$$ (13.2a)

where the transfer function is a rational function of order n,

$$G(s) = K \frac{N_0 + N_1 s \dots + N_m s^m}{D_0 + D_1 s \dots + D_n s^n} \qquad with \quad m \le n$$ (13.2b)

The Laplace operator is replaced by jω to obtain the steady-state frequency response at any angular frequency ω, including dc. For transient solutions, s is replaced by the differential operator d/dt, which converts Eq. (13.2) into a linear n-th order differential equation

$$D_0 x \ + \ D_1 \frac{dx}{dt} \ldots + \ D_n \frac{d_n x}{dt^n} \ = \ K \left(N_0 u \ + \ N_1 \frac{du}{dt} \ldots + \ N_m \frac{d^m u}{dt^m} \right) \tag{13.3}$$

$$U(s) \quad \longrightarrow \quad K \ \frac{N_0 + N_1 s \ \cdots \ + N_m s^m}{D_0 + D_1 s \ \cdots \ + D_n s^n} \quad \longrightarrow X(s)$$
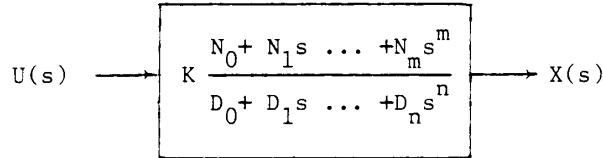
Fig. 13.4 - Transfer function block

In TACS, the n-th order differential equation is re-written as a system of n first-order differential equations by introducing internal variables for the derivatives of u and x

$$x_1 \ = \ \frac{dx}{dt}, \quad x_2 \ = \ \frac{dx_1}{dt}, \quad \ldots \quad \ldots \ x_n \ = \ \frac{dx_{n-1}}{dt}$$

$$u_1 \ = \ \frac{du}{dt}, \quad u_2 \ = \ \frac{du_1}{dt}, \quad \ldots \quad \ldots \ u_m \ = \ \frac{du_{m-1}}{dt} \tag{13.4}$$

With these internal variables, Eq. (13.3) becomes an algebraic equation

$$D_0 x \ + \ D_1 x_1 \ \ldots \ + \ D_n x_n \ = \ K (N_0 u \ + \ N_1 u_1 \ \ldots \ + \ N_m u_m) \tag{13.5}$$

To eliminate these internal variables again, the differential equations (13.4) are first converted into difference equations with the trapezoidal rule of integration,

$$x_i(t) \ = \ \frac{2}{\Delta t} x_{i-1}(t) \ - \ \{ x_i(t-\Delta t) \ + \ \frac{2}{\Delta t} x_{i-1}(t-\Delta t) \} \quad for \ \ i \ = \ 1, \ldots \ n \tag{13.6a}$$

$$u_j(t) \ = \ \frac{2}{\Delta t} u_{j-1}(t) \ - \ \{ u_j(t-\Delta t) \ + \ \frac{2}{\Delta t} u_{j-1}(t-\Delta t) \} \quad for \ j \ = \ 1, \ldots \ m \tag{13.6b}$$

where $x_0 = x$ and $u_0 = u$.

Expressing x_n as a function of x_{n-1} in Eq. (13.5) with Eq. (13.6), and then again expressing x_{n-1} as a function of x_{n-2} etc., until only x is left, and using the same procedure for u, produces a single output-input relationship of the form [189]

$$cx(t) = K\,du(t) + hist(t - \Delta t) \tag{13.7}$$

This is the equation which is used in the transient solution of the control system. After the solution at each time step, n history terms must be updated to obtain the single term "hist" for the solution over the next time step. If recursive formulas are used, then

$$hist_1(t) = Kd_1u(t) - c_1x(t) - hist_1(t-\Delta t) + hist_2(t-\Delta t)$$
$$\dots = \dots$$
$$\dots = \dots$$
$$hist_i(t) = Kd_iu(t) - c_ix(t) - hist_i(t-\Delta t) + hist_{i+1}(t-\Delta t)$$
$$\dots = \dots$$
$$\dots = \dots$$

$$hist_n(t) = Kd_nu(t) - c_nx(t)$$
$$with$$
$$hist = hist_1 \tag{13.8}$$

The coefficients c_i, d_i are calculated once at the beginning from the coefficients N_i, D_i of the transfer function, with the recursive formula

$$c_i = c_{i-1} + (-2)^i \{ \tbinom{i}{i} (\tfrac{2}{\Delta t})^i D_i + \tbinom{i+1}{i} (\tfrac{2}{\Delta t})^{i+1} D_{i+1} \dots + \tbinom{n}{i} (\tfrac{2}{\Delta t})^n D_n \} \tag{13.9}$$

where $\binom{i}{j}$ is the binomial coefficient, and where the starting value is

$$c_0 = \sum_{i=0}^{n} \left(\frac{2}{\Delta t} \right)^i D_i , \qquad with \quad c = c_0 \tag{13.10}$$

The formulas for d_i are identical, if D is replaced by N, and if the upper limit is m rather than n.

Instead of a single input signal u, TACS accepts the sum of up to five input signals $u_i, \dots u_5$, as illustrated in Fig. 13.5 (subscripts 1,2,… are no longer used to indicate internal variables of a block from here on). To model a summer by itself, a zero-order transfer function block is used with $K = N_0 = D_0 = 1$. This zero-order transfer function is contained in Eq. (13.7) as a special case, with $K = c = d = 1$ and hist = 0.
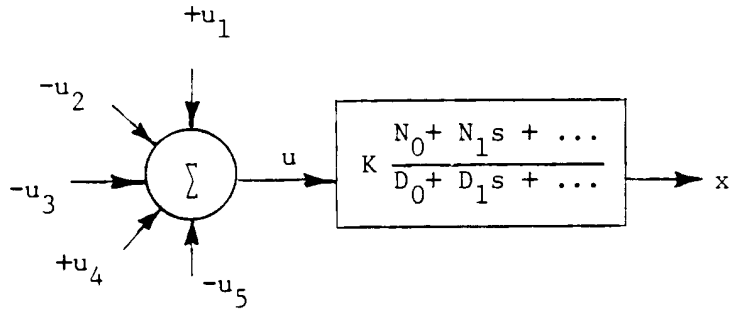
Fig. 13.5 - Transfer function with summer ($u = u_1 - u_2 - u_3 + u_4 - u_5$)

If the control system consists solely of interconnected transfer function blocks and summers, then the entire system is described by using an equation of the form (13.7) for each one of the blocks. For the example of Fig. 13.6, there would be four equations

$$
\begin{bmatrix}
c_a & -K_a d_a & -K_a d_a & 0 & K_a d_a & 0 \\
-K_b d_b & 0 & 0 & c_b & 0 & -K_b d_b \\
-K_c d_c & c_c & 0 & 0 & 0 & 0 \\
0 & 0 & -K_d d_d & c_d & 0 & 0
\end{bmatrix}
\begin{bmatrix}
x_1 \\ x_2 \\ x_3 \\ x_4 \\ u_1 \\ u_2
\end{bmatrix}
=
\begin{bmatrix}
hist_a \\ hist_b \\ hist_c \\ hist_d
\end{bmatrix}
$$

which is the same form as in Fig. 13.2(a), with

$$[x_{INTERNAL}] = [x_1 \ x_2 \ x_3]$$

$$[x_{OUT}] = [x_4]$$

$$[u] = [u_1 \ u_2]$$
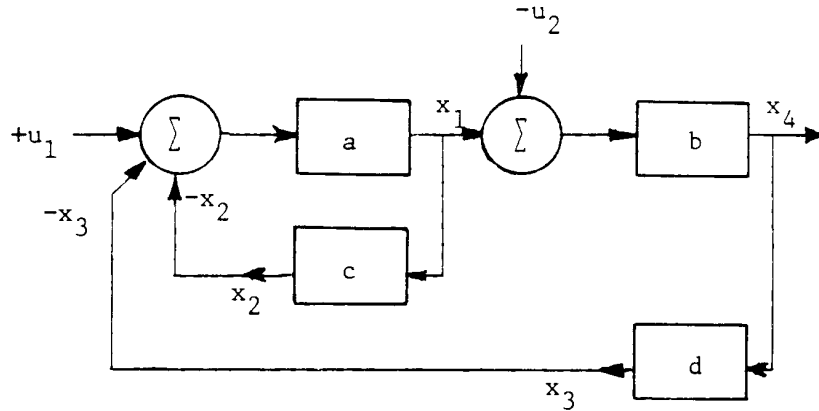
Fig. 13.6 - Control system with linear transfer functions

In TACS, this system of equations

$$[A_{xx}] [X] + [A_{xu}] [u] = [hist] \qquad (13.11)$$

is solved by first performing a triangular factorization on $\{[A_{xx}]. [A_{xu}]\}$ before entering the time step loop. In each time step, the unknown variables [x] are then found by

(a)   assembling the right-hand side [hist],

(b)   performing a downward operation on it,

(c)   doing a backsubstitution to obtain [x], and

(d)   updating the history terms of each block.

The solution procedure is very similar to the one indicated in Fig. 13.3(b), except that the elimination does not stop on the vertical line which separates the columns of $[x_{INTERNAL}]$ and $[x_{OUT}]$, but continues to the diagonal (indicated by dots in Fig. 13.3(b)). Since the matrix is unsymmetric here, both the upper and lower triangular matrix coming out of the triangularization must be stored, in contrast to the matrix in NETWORK where only the upper triangular matrix is stored. Since the matrix is sparse, optimal ordering techniques are used to minimize the number of fill-in elements. Only the nonzero elements are stored with a compact storage scheme similar to the one discussed in Appendix III. Whether pivoting is needed is unclear to the authors.

13.3 Limiters

There are two types of limiters, the windup limiter with clipped output ("static limiter" in the EMTP Rule Book) and the non-windup limiter with clamped output ("dynamic limiter" in the EMTP Rule Book). The windup limiter can be visualized as a measuring instrument in which the needle (position = output signal) can only be seen within a limited window, but the needle is allowed to move freely (wind up) outside the window (Fig. 13.7(a)). In the non-windup limiter, the needle is restrained from moving outside the window (Fig. 13.7(b)). In both cases, the movement of the needle is described by differential equations. The equation describing the limiting function has the

same form in both cases, but the criteria for backing off are different.

(a) Windup limiter   (b) Non-windup limiter
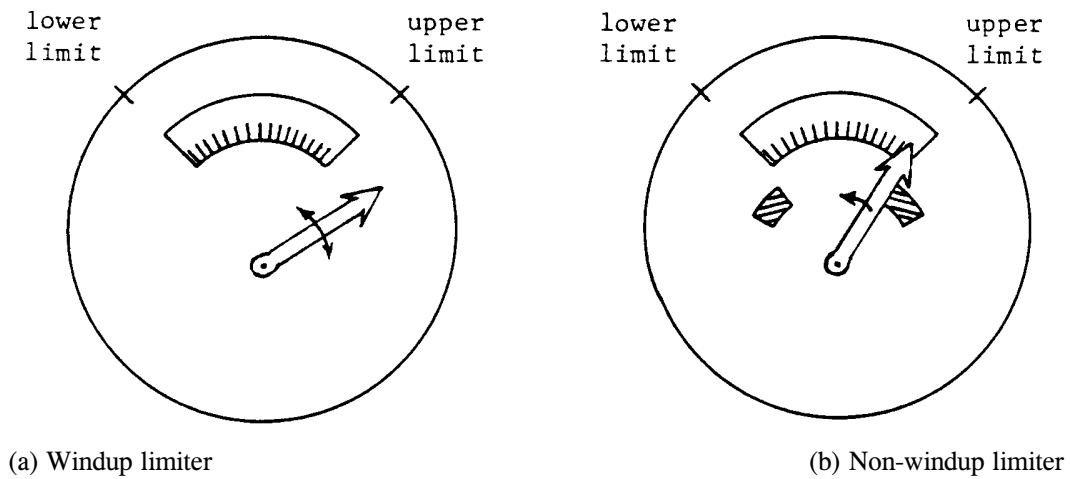
Fig. 13.7 - Limits in a measuring instrument

13.3.1 Windup Limiter

The output x of the windup limiter of Fig. 13.8 is

$$x = \begin{cases} Ku, & \text{if } x_{min} < Ku < x_{max} \\ x_{min}, & \text{if } Ku \leq x_{min} \\ x_{max}, & \text{if } Ku \geq x_{max} \end{cases} \qquad (13.12)$$

Either one of the three equations is still a linear algebraic equation of the form of Eq. (13.7), with $c = d = 1$, hist $= 0$ inside the limits, and $c = 1$, $d = 0$, hist $= (x_{max}$ or $x_{min})$ at the limit. The proper way of handling this limiter is to change the linear equations (13.11) at instants when x hits the limit and when it moves off the limit again. This requires occasional re-triangularizations, which are no different in principle from those required in NETWORK whenever switch positions change or when the solution in piecewise linear elements moves from one segment to another.

(a) Block diagram representation   (b) Limiting action
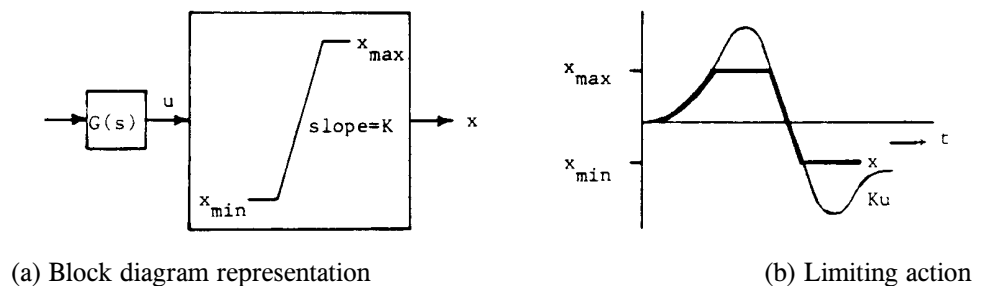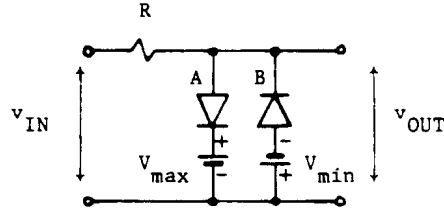
(c) Clipping circuit implementation for
K=1 (diode A conducts when $v_{IN} > v_{max}$,
diode B conducts when $v_{IN} < v_{min}$

Fig. 13.8 - Windup limiter

If there are only a few limiters, one could also use the compensation method described in Section 12.1.2. Assume that the control system contains only two limiters which limit x_i and x_k. In that case, one could precalculate column i and column k of the inverse matrix of $[A_{xx}]$ with two repeat solutions before entering the time step loop. In each time step, the variables would first be calculated as if no limits exist. Call this solution $[x_{without}]$. If both $x_{i-without}$ and $x_{k-without}$ are outside their limits, then the necessary corrections $\Delta hist_i$ and $\Delta hist_k$ in the right-hand side of Eq. (13.11) to produce limited values are found by solving the two equations

$$\begin{bmatrix} x_{i-limit} \\ x_{k-limit} \end{bmatrix} = \begin{bmatrix} x_{i-without} \\ x_{k-without} \end{bmatrix} + \begin{bmatrix} b_{ii} & b_{ik} \\ b_{ki} & b_{kk} \end{bmatrix} \begin{bmatrix} \Delta hist_i \\ \Delta hist_k \end{bmatrix} \tag{13.13a}$$

If only $x_{i-without}$ is outside its limits, then

$$x_{i-limit} = x_{i-without} + b_{ii} \Delta hist_i$$
$$\Delta hist_k = 0 \tag{13.13b}$$

The final solution is found by superposition,

$$[x] = [x_{without}] + \begin{bmatrix} b_{1i} & b_{1k} \\ b_{2i} & b_{2k} \\ . & . \\ . & . \\ . & . \end{bmatrix} \begin{bmatrix} \Delta hist_i \\ \Delta hist_k \end{bmatrix} \tag{13.13c}$$

The coefficients b in Eq. (13.3) are the elements of column i and k of $[Z_{ss}]^{-1}$.

At the time when TACS was first written, both the re-triangularization procedure and the compensation method were regarded as too costly, and the simpler method discussed in Section 13.4 was introduced instead. It suffered initially from unnecessary time delays, which have now been mostly removed with the recent code changes of Ma Ren-ming in version M36. Whether re-triangularization or compensation will be used in future versions to remove the remaining time delays remains to be seen.

In comparing Fig. 13.8(a) with the piecewise linear representation of network elements discussed in Section

12.1.3, one notices that the slope in the saturated region is always zero (hard limit) rather than finite (soft limit). In rewriting TACS, it may be worth considering whether soft limits would be a useful enhancement. In Fig. 13.8(c) the limits become soft if the internal resistances of the diodes and dc voltage sources are taken into account, or if resistors are specifically added for that purpose. The equation for soft limits, with the notation from Fig. 13.9, would be

$$X = \begin{cases} Ku & if \ x_{min} < Ku < x_{max} \\ x_{min} + K_{min}(u-u_{min}) & if \ Ku \leq x_{min} \\ x_{max} + K_{max}(u-u_{max}) & if \ Ku \geq x_{max} \end{cases} \tag{13.14}$$

These equations have again the form of Eq. (13.7), and soft limits can therefore be implemented in the same way as hard limits. As a matter of fact, the hard limit would become a special case of the soft limit of Eq. (13.14) by simply setting K_{max} or K_{min} to zero.
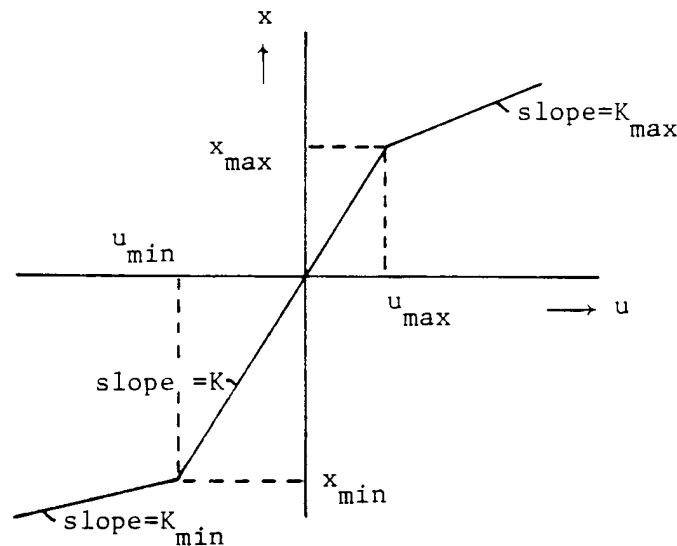
Fig. 13.9 - Soft limits

13.3.2 Non-Windup Limiter

In the windup limiter, the output of a transfer function block is just clipped, without affecting the dynamic behavior of the transfer function block on the input side itself. In a non-windup limiter, this is no longer true. Here, the dynamic behavior of the transfer function block is changed by the limiting action.

Before describing the limiting action with equations, it is important to understand that non-windup limiters should only be used with first-order transfer functions. For second and higher-order transfer functions, it is no longer clear which variables should be limited. Take a second-order transfer function $G(s) = 1/2$ as an example. It can easily be shown [190] that backing off the limit will occur in three different ways in this case, depending on whether the internal variables dx/dt or d^2x/dt^2, or both, are forced to remain at zero after the limit is hit. This ambiguity can only be removed if the user defines the problem as two cascaded first-order transfer function blocks,

with the proper limits on each of them. Even for the first-order transfer function, the meaning of the limiting function is confused if it has any zeros ($N_1 \neq 0$) [191]. It is because of these ambiguities why the limiter in the current-controlled dc voltage source described in Section 7.6.2 may be incorrect.

To make the definition of non-windup limiters unique, they should only be allowed on first-order transfer functions with no zeros of the form

$$G(s) = \frac{K}{1 + sT} \tag{13.15}$$

The equations are

$$
\begin{aligned}
x + T\frac{dx}{dt} &= Ku && \text{if } x_{min} < x < x_{max} \\
x = x_{min} && \text{if } x \leq x_{min} && \text{and } (Ku - x) < 0 \\
x = x_{max} && \text{if } x \geq x_{max} && \text{and } (Ku - x) > 0
\end{aligned}
\tag{13.16}
$$
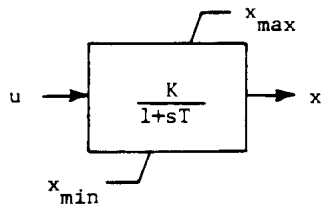
(a) Block diagram representation
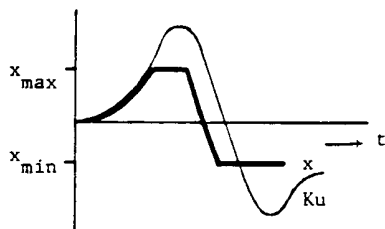
(b) Limiting action
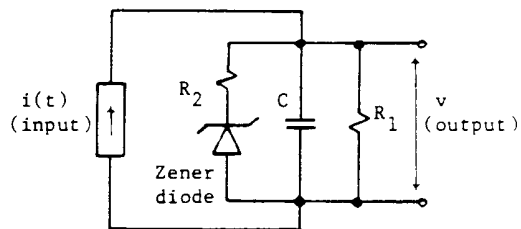
(c) Circuit implementation

Fig. 13.10 - Non-windup limiter

For operation within the limits, the differential equation is converted to the algebraic equation (13.7). That equation, and the equations valid at the limit, are all linear algebraic equations, as in Eq. (13.12) for the windup limiter. The non-windup limiter can therefore be handled in exactly the same way as the windup limiter, either with re-triangularization or with the compensation method. While the windup limiter has the coefficients $c = d = 1$, and

hist = 0 inside the limits, the non-windup limiter has

$$d = K$$

$$c = \left(1 + \frac{2T}{\Delta t}\right)$$

$$hist = Ku(t - \Delta t) - \left(1 - \frac{2T}{\Delta t}\right) x(t - \Delta t)$$

For deciding when to back off, the derivative T dx/dt = Ku - x must be used, rather than Ku.

Changing from a hard to a soft limit would also be possible with the non-windup limiter. In the implementation of Fig. 13.10(c), the limits would become soft if $R_2 \neq 0$, where R_2 can either be the internal resistance of the Zener diode, or a resistor specifically added to create soft limits.

From the limited (unpublished) information available to the authors, it appears that TACS handles the non-windup limiters with a pseudo-compensation method, in which corrections are made to the right-hand sides [hist] in Eq. (13.11) a priori at the beginning of each time step. As explained above Eq. (13.13), a correct implementation of the compensation method requires a complete solution of the control system without limiters, followed by superposition of correction terms for which elements of $[A_{xx}]^{-1}$ are needed. This does not seem to be done in TACS, and the treatment of limiters is therefore somewhat suspicious. Since TACS does reset the variable to its limit value whenever it exceeds its limits, the answers are probably correct, except that the procedure is unable to eliminate the time delays in closed loops discussed in Section 13.4.

The pseudo-compensation method also seems to create subtle differences in the way it backs off the limit. It seems to use the equation

$$\frac{T}{\Delta t} \{2x(t) - x_{limit}\} = K u(t) - x(t)$$

in the first step after backing off, which would be the backward Euler formula if the factor 2 were missing, while Eq. (13.7) would back off with

$$\frac{T}{\Delta t} \{x(t) - x_{limit}\} = K \frac{u(t) + u(t-\Delta t)}{2} - \frac{x(t) + x_{limit}}{2}$$

13.4 Limiter Implementation with Possible Time Delay

With the code changes of Ma Ren-ming in 1983/84, the variables are now ordered in such a way that most of the time delays which were caused by limiters no longer exist in version M36 and later versions. For example, the open loop control system of Fig. 13.11 was originally solved in the sequence S_1, $G_2(s)$, $G_3(s)$, S_2, S_3 and finally $G_1(s)$, because of a rule that transfer function blocks feeding into special or supplemental device blocks S should be solved first. This has been changed, and the blocks are now solved in their functional order S_1, $G_1(s)$, $G_2(s)$, S_2,

$G_3(s)$, S_3. With this order, it is simple to observe the limits on the output x_1, without having to re-triangularize the matrix or without having to use the compensation method, because x_1 is limited first before any other variables are computed. In the system of equations (13.11), this means that the equation for $G_1(s)$ must be the last one, with enforcement of the limits on x_1 being done in the backsubstitution. Ma Ren-ming observes correctly [187] that there is no difference between n-th order and zero order transfer functions, or between windup and non-windup limiters in this simple ordering scheme.

A more complicated example for the new ordering rule is shown in Fig. 13.12, with 10 transfer function blocks of which three have limits. The first four blocks G_1, G_2, G_3, and G_4 form one set of equations which are disconnected from the others. This first set of equations is solved simultaneously, with rows in Eq. (13.7) ordered G_1, G_4, G_3, and G_2. With this order, the output of G_2 is the first variable to be found in the backsubstitution. By keeping it within its limits at that point, the properly limited value will be used in the rest of the backsubstitution in finding the outputs of G_3, G_4, and G_1. Using the known output of G_2, the output of G_5 is found from one single equation, and knowing the output of G_5, the output of G_0 is found from another single equation and then kept within its limits. Finally, the equations for G_7, G_8, G_9, and G_{10} for another independent set of equations, and if ordered in that sequence, the limits on the output of G_{10} can again be easily observed because it is the first variable found in the backsubstitution. So in spite of feedback loops and limiters, the control system of Fig. 13.12 is now solved simultaneously without the time delays observed in pre-M36 versions. Note that this ordering scheme developed for easy implementation of limiters may not completely minimize the fill-ins in the triangularization, but this is a small price to pay for the proper implementation of limiters.
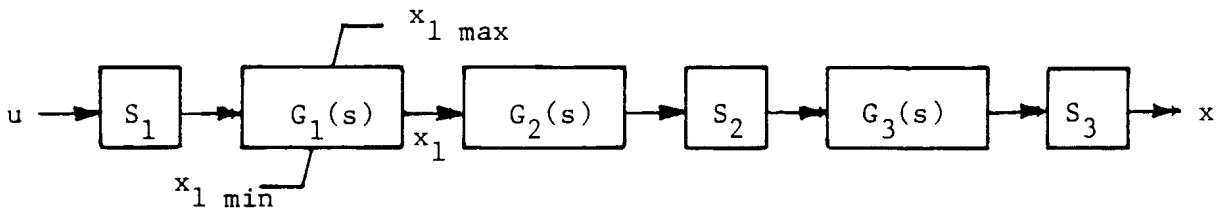
Fig. 13.11 - Simple open loop control system

Time delays cannot be avoided completely with the new ordering scheme. Fig. 13.13 shows an example where two limiters are within the same loop. In this case, TACS inserts a time delay of Δt (if not explicitly done so by the user) and the solution is then no longer simultaneous. Note that with re-triangularization or with the compensation method, the solution of that system would again become simultaneous.
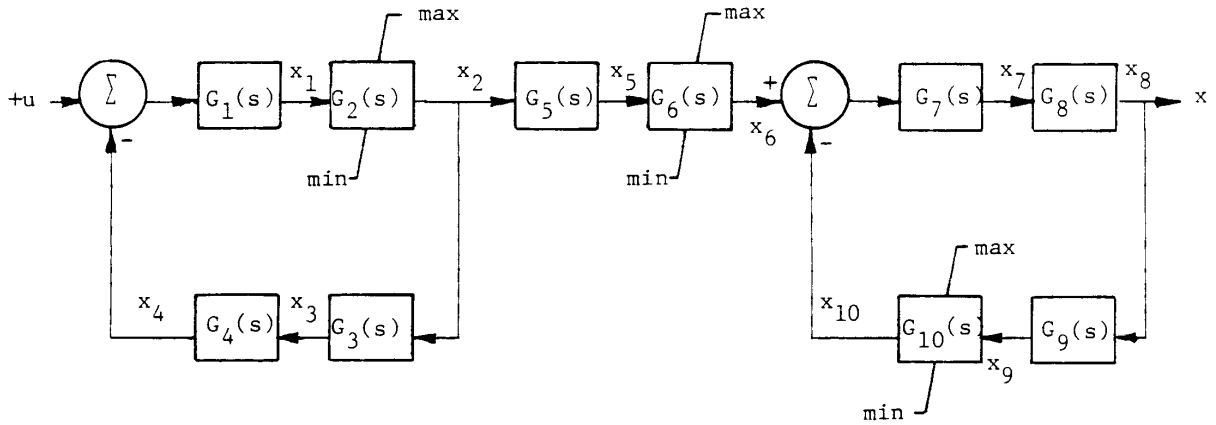
Fig. 13.12 - Control system with feedback loops
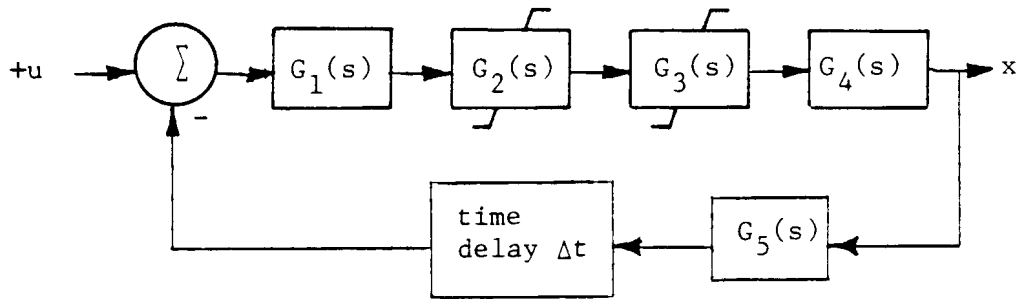
Fig. 13.13 - Two limiters within same loop

13.5 Signal Sources

TACS has signal sources built into it, similar to the voltage and current sources in NETWORK. They serve as input signals to transfer function blocks and other blocks. In the system of equations (13.11), they are handled as known values in vector [u].

Resident sources are signal sources with reserved names, which are available by simply referring to their names. Resident sources can also be used as voltage or current sources in NETWORK through the TACS-NETWORK interface. They are

TIMEX = simulation time in seconds (0 in steady state),

ISTEP = number of time step,

DELTAT = step size in seconds,

FREQHZ = network frequency in Hz of first sinusoidal source,

OMEGAR = 2πFREQHZ,

ZERO = 0.0,

MINUS1 = -1.0,

PLUS1 = +1.0,

INFTY $= +\infty$ (very large number which still fits computer system),

PI $= \pi$.

There are also signal sources with data specifications supplied by the user, such as

single rectangular pulse,

sinusoidal function,

repetitive pulse,

repetitive ramp function,

node voltage from NETWORK,

switch current from NETWORK,

special NETWORK variables (e.g., rotor angle of machines),

switch status,

any voltage or current source defined in NETWORK.

13.6 Special Devices

Transfer function blocks, limiters and signal sources are not enough to model realistic control systems. Other building blocks have therefore been added to TACS under the heading of "Special Devices" ("Supplemental variables and devices" in the EMTP Rule Book). They make TACS extremely versatile, but they do not fit neatly into the control system equations (13.7). They are therefore solved sequentially, rather than simultaneously as for the transfer function blocks, with the user controlling the sequence. In Fig. 13.11, the special device S_1 would be solved after G_2 has been solved, and S_2 would be solved after G_3 has been solved. The solution would still be simultaneous in this case. In general, the sequence of calculations is more complicated, with non-simultaneous solutions through time delays. For details, the reader should consult the EMTP Rule Book.

All special devices can either be designated as input devices, as output devices, or as internal devices by the user. To make the solution as much simultaneous as possible, the user should keep the number of internal devices as low as possible, and use input or output devices instead whenever possible. The rules for the designation are as follows:

(a)   Input devices: All inputs must either be TACS signal sources or output from other input devices. They are essentially used to pre-process signals before they enter transfer function blocks (e.g., S_1 in Fig. 13.11).

(b)   Output devices: Their output must not be used as input to any other block, except to other output devices. They are essentially used to post-process control system outputs for its own sake, or before passing them on as voltage or current sources or switching commands to NETWORK (e.g. S_3 in Fig. 13.11).

(c)   Internal devices: They are inside the control system (e.g., S_2 in Fig. 13.11).

The behavior of the special devices is either defined through user-supplied FORTRAN expressions, or with built-in types.

13.6.1 FORTRAN-Defined Special Devices

The FORTRAN expression can be more or less as general as allowed by the FORTRAN-IV language itself (for details see the EMTP Rule Book). Algebraic operators (+-* etc.), relational operators (.EQ. etc.), logical operators (.AND. etc.), FORTRAN intrinsic functions (SIN, EXP, etc.) and special functions defined in the EMTP Rule Book can be used. In the example

$$ANGLE = DEG(AT\ AN(CNTRL - BIAS2)) + 36.2,$$

the output signal is ANGLE, while the input signals are CNTRL and BIAS2. AT AN is the arctangent function, while DEG is a special function for converting radians to degrees.

A FORTRAN expression of the form

$$VARIABLE = VARIABLE + \{Arithmetic\ Expression\}$$

is not allowed, because it gives rise to sorting problem within TACS.

13.6.2 Built-In Special Devices

There are 17 built-in special devices at this time, for which the user supplies the parameters only. They are

(a) accumulator and counter,

(b) controlled integrator,

(c) digitizer,

(d) frequency sensor,

(e) input-IF component,

(f) instantaneous min/max,

(g) level-triggered switch,

(h) min/max tracking,

(i) multi-operation time-sequenced switch,

(j) point-by-point user defined nonlinearity,

(k) pulse transport delay,

(l) relay-operated switch,

(m) RMS value,

(n) sample and track hold,

(o) signal selector,

(p) simple derivative (backward Euler),

(q) transport delay.

Details about their characteristics can be found in the EMTP Rule Book.

13.7 Initial Conditions

The ac steady-state solution for the electric network is found first, before TACS variables are initialized. All variables from NETWORK are therefore available for the automatic initialization in TACS, but not the other way

around. This may cause problems, e.g., if a TACS output defines a sinusoidal voltage source in NETWORK whose initial amplitude and phase angle, supplied by the user, could differ from the values coming out the TACS initialization. An iterative steady-state solution between NETWORK and TACS would resolve such discrepancies, but they are probably so rare that such an iteration scheme cannot be justified. An error message (possibly with termination) would be useful, however.

The automatic initialization of TACS variables is complicated and not foolproof at this time, and improvements are likely to be added in the future. The present initialization procedure is therefore only described in broad terms.

The input and output signals of transfer function blocks are usually dc quantities in steady state. For dc quantities, the output-input relationship of the transfer function (13.2b) becomes

$$x_{dc} = K \frac{N_0}{D_0} u_{dc} \tag{13.17}$$

which is the same form as Eq. (13.7) for the transient solution, with $c = 1$, $d = N_0/D_0$, and hist $= 0$. If the entire control system consists of transfer function blocks only, a system of equations can be formed, similar to Eq. (13.11), and solved for the unknown TACS variables $[x_{dc}]$. This is essentially what TACS does automatically now. The variables $[x_{dc}]$ are not needed directly, but only indirectly for initializing [hist] in Eq. (13.11) before entering the time step loop.

Unfortunately, control systems are more complicated. Any sophisticated control system has integrators G(s) $= K 1/$. Their steady-state output must now be supplied by the user, but these values are not always easy to find. For example, the output of an unbounded integrator with nonzero input is a continuously increasing ramp function. In practice, integrators are always bounded within upper and lower limits. Therefore, the steady-state output of a bounded integrator is either at its minimum or maximum value, which TACS could distinguish from the sign of the input signal. A realistic steady-state equation of a bounded integrator for nonzero input would therefore be

$$x_{dc} = \{ \begin{matrix} x_{\min} & if & u_{dc} < 0 \\ x_{\max} & if & u_{dc} > 0 \end{matrix} \tag{13.18}$$

Evaluation of the steady-state output value of a bounded integrator with zero input or of an unbounded integrator is impossible from the knowledge of its input alone.

Further complications are introduced because TACS signal sources are not restricted to dc quantities in steady state. They could be pulse trains, sinusoidal functions, and other periodic functions. To automate the initialization procedure for all such eventualities is therefore still an unresolved issue. At this time, the user must supply initial conditions in complicated cases and for most special devices.

APPENDIX I - NUMERICAL SOLUTION OF ORDINARY DIFFERENTIAL EQUATIONS

"Computers are influencing network theory by demanding methods of analysis adapted to the solution of computer-sized problems," as stated by F.H. Branin [2], but very little of this influence has shown up yet in textbooks on electric circuits and networks, not even in most of the recently published books. In this appendix, an attempt is made to summarize some of the numerical solution techniques for solving ordinary differential equations, which one might consider in developing a general-purpose program, such as the EMTP. Since power system networks are mostly linear, techniques for linear ordinary differential equations are given special emphasis.

I.1 Closed Form Solution

Let us assume that the differential equations are written in "state-variable form," and that the equations are linear,

$$\left[\frac{dx}{dt}\right] = [A][x] + [g(t)], \tag{I.1}$$

with a constant square matrix [A], and a vector of known forcing functions [g(t)]. There is no unique way of writing equations in state variable form, but it is common practice to choose currents in inductances and voltages across capacitances as state variables. For example, Eq. (I.1) could have the following form for the network of Fig. I.1:
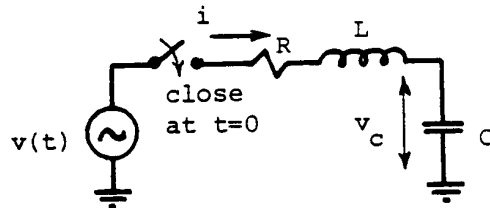
Fig. I.1 - Energization of an R-L-C network

$$\begin{bmatrix} \dfrac{di}{dt} \\ \dfrac{dv_c}{dt} \end{bmatrix} = \begin{bmatrix} -\dfrac{R}{L} & -\dfrac{1}{L} \\ \dfrac{1}{C} & 0 \end{bmatrix} \begin{bmatrix} i \\ v_c \end{bmatrix} + \begin{bmatrix} \dfrac{1}{L}v(t) \\ 0 \end{bmatrix} \tag{I.2}$$

With Laplace transform methods, especially when one output is expressed as a function of one input, the system is often described as one n^{th}-order differential equation, e.g., for the example of Fig. I.1 in the form

Such an nth-order differential equation can of course always be rewritten as a system of n first-order differential equations, by introducing extra variables $x_2 = dx_1/dt$, $x_3 = dx_2/dt$, to $x_n = dx_{n-1}/dt$, for the higher-order derivatives,

with $x_1 = x$. In the example, with $x_1 = i$ and $x_2 = di/dt$,

$$\begin{bmatrix} R & L \\ & \\ 1 & 0 \end{bmatrix} * \begin{bmatrix} \dfrac{dx_1}{dt} \\ \dfrac{dx_2}{dt} \end{bmatrix} = \begin{bmatrix} -\dfrac{1}{C} & 0 \\ & \\ 0 & 1 \end{bmatrix} * \begin{bmatrix} x_1 \\ x_2 \end{bmatrix} + \begin{bmatrix} \dfrac{dv(t)}{dt} \\ \\ 0 \end{bmatrix}$$

which, after pre-multiplication with

$$\begin{bmatrix} R & L \\ 1 & 0 \end{bmatrix}^{-1} = \begin{bmatrix} 0 & 1 \\ \dfrac{1}{L} & -\dfrac{R}{L} \end{bmatrix}$$

produces another state-variable formulation for this example. While [A] of this formulation differs from that in Eq. (I.2), its eigenvalues are the same.

The closed-form solution of Eq. (I.1), which carries us from the state of the system at $t - \Delta t$ to that at t, is

$$[x(t)] = e^{[A]\Delta t} \cdot [x(t-\Delta t)] + \int_{t-\Delta t}^{t} e^{[A](t-u)}[g(u)]du, \tag{I.3}$$

where the matrix $e^{[A]\Delta t}$ is called the "transition matrix." Eq. (I.3) contains the case where [x(t)] is simply desired as a function of t by setting $\Delta t = t$. The computational task lies in finding this transition matrix. Since there is no closed-form solution for the matrix exponential $e^{[A]\Delta t}$, the way out is to transform this matrix to a diagonal matrix, whose elements can easily be evaluated by using the eigenvalues λ_1 of [A] and the matrix of eigenvectors (modal matrix) [M] of [A]. and then to transform back again. An efficient method for finding eigenvalues appears to be the "QR transformation" due to J.G.F. Francis [3], and for finding eigenvectors the "inverse iteration scheme" due to J.H. Wilkinson [4], which has also been described in modified form by J.E. Van Ness [5]. With [Λ] and [M] known, where [Λ] is the diagonal matrix of eigenvalues λ_i, $e^{[A]\Delta t}$ is diagonalized[1],

$$[M]^{-1}e^{[A]\Delta t}[M] = [e^{\Lambda\Delta t}]$$

Once the diagonal elements $e^{\lambda_i \Delta t}$ have been found, this can be converted back to give

$$e^{[A]\Delta t} = [M]\ [e^{\Lambda\Delta t}]\ [M^{-1}] \tag{I.4}$$

where

$\quad$ $[e^{\Lambda\Delta t}]$ = diagonal matrix with elements $e^{\lambda_i \Delta t}$,

$\quad$ [M] $\quad$ = eigenvector (modal) matrix of [A], and

---

[1]If [M] diagonalizes [A], it will also diagonalize $e^{[A]\Delta t}$. The matrix exponential is defined as the series of Eq. (I.13), and then one simply has to show that [M] not only diagonalizes [A], but all positive powers $[A]^n$ as well. Since $[A] = [M][\Lambda][M]^{-1}$ it follows that $[A]^n = ([M][\Lambda][M]^{-1})([M][\Lambda][M]^{-1})...([M][\Lambda][M]^{-1})$ of $[A]^n = [M][\Lambda^n][M]^{-1}$. Therefore, $[M]^{-1}[A]^n[M] = [\Lambda^n]$ is again diagonal.

λ_i = eigenvalues of [A].

With Eq. (I.4), Eq. (I.3) becomes

$$[x(t)] = [M] [e^{\Lambda \Delta t}] [M]^{-1}[x(t-\Delta t)] + \int_{t-\Delta t}^{t} [M] [e^{\Lambda(t-u)}] [M]^{-1} [g(u)] \, du \tag{I.5}$$

The "convolution integral" in Eq. (I.5) can be evaluated in closed form for many types of functions [g(t)].

For the network of Fig. I.1, the eigenvalues can be obtained by setting the determinant of $[A]-\lambda[U]$ to zero ([U] = identity matrix),

$$\begin{vmatrix} -\dfrac{R}{L} - \lambda & -\dfrac{1}{L} \\[2mm] \dfrac{1}{C} & -\lambda \end{vmatrix} = 0$$

or

$$\lambda_{1,\,2} = -\frac{R}{2L} \pm \sqrt{(\frac{R}{2L})^2 - \frac{1}{LC}} \tag{I.6}$$

If $R < 2\sqrt{(L/C)}$, then the system is underdamped[2], and the argument under the square root will be negative, giving a pair of complex eigenvalues

$$\lambda_{1,\,2} = \alpha \pm j\beta; \quad with \quad \alpha = -\frac{R}{2L}, \quad \beta = \sqrt{\frac{1}{LC} - (\frac{R}{2L})^2} \tag{I.7}$$

For a specific case, let us assume that R = 1Ω, L = 1H, C = 1F. then

$$\lambda_{1,\,2} = -\frac{1}{2} \pm j\frac{\sqrt{3}}{2} = e^{\pm j120^\circ}$$

and

$$[M] = \frac{1}{\sqrt{2}} \begin{bmatrix} 1 & 1 \\ e^{-j120^\circ} & e^{j120^\circ} \end{bmatrix}, \quad [M]^{-1} = \frac{\sqrt{2}}{j\sqrt{3}} \begin{bmatrix} e^{j120^\circ} & -1 \\ -e^{-j120^\circ} & 1 \end{bmatrix}$$

If we set $\Delta t = t$ to obtain the state variables simply as a function of time and of initial conditions, then Eq. (I.5) becomes

---

[2]If $R > 2*sqrt(L/C)$, then the system is overdamped, giving two real eigenvalues. The critically damped case of $R = 2 * sqrt(L/C)$ seldom occurs in practice; it leads to two identical eigenvalues. This latter case of "multiple eigenvalues" may require special treatment, which is not discussed here.

$$
\begin{bmatrix} i(t) \\ v_c(t) \end{bmatrix} = \begin{bmatrix} e^{\alpha t}\left(\cos\beta t \ - \ \dfrac{1}{\sqrt{3}}\sin\beta t\right) & -\dfrac{2}{\sqrt{3}}e^{\alpha t}\sin\beta t \\[2ex] \dfrac{2}{\sqrt{3}}e^{\alpha t}\sin\alpha t & e^{\alpha t}\left(\cos\beta t \ +\dfrac{1}{\sqrt{3}}\sin\beta t\right) \end{bmatrix} \cdot \begin{bmatrix} i(0) \\ v_c(0) \end{bmatrix}
$$

$$
+ \ \frac{2}{\sqrt{3}}\int_0^t \begin{bmatrix} e^{\alpha(t-u)}\ [\cos(\beta(t-u)) \ - \ \dfrac{1}{\sqrt{3}}\sin(\beta(t-u))]v(u) \\[2ex] e^{\alpha(t-u)}\sin(\beta(t-u))v(u) \end{bmatrix} du \tag{I.8}
$$

with α and β as defined in Eq. (I.7). If we were to assume that the voltage source is zero and that $v_c(0) = 1.0$ p.u., then we would have the case of discharging the capacitor through R-L, and from Eq. (I.8) we would immediately get (realizing that i(0) = 0),

$$
i(t) \ = \ -\frac{2}{\sqrt{3}} \ e^{\alpha t} \ \sin\beta t
$$

$$
v_c(t) \ = \ e^{\alpha t}\ (\cos\beta t \ + \ \frac{1}{\sqrt{3}}\sin\beta t)
$$

Could such a closed-form solution be used in an EMTP? For networks of moderate size, it probably could. J.E. Van Ness had no difficulties finding eigenvalues and eigenvectors in systems of up to 120 state variables [5]. If the network contains switches which frequently change their position, then its implementation would probably become very tricky.   Combining it with Bergeron's method for distributed-parameter lines, or with more sophisticated convolution methods for lines with frequency-dependent parameters, should in principle be possible. Where the method becomes almost unmanageable, or useless, is in networks with nonlinear elements. Another difficulty would arise with the state-variable formulation, because Eq. (I.1) cannot as easily be assembled by a computer as the node equations used in the EMTP. This difficulty could be overcome, however, since there are ways of using node equations even for state-variable formulations, by distinguishing node types according to the types of branches (R, L, or C) connected to them.

Where do Laplace transform methods fit into this discussion since they provide closed-form solutions as well? To quote F.H. Branin [2], "…traditional methods for hand solution of networks are not necessarily best for use on a computer with networks of much greater size. the Laplace transform techniques fit this category and should at least be supplemented, if not supplanted, by numerical methods better adapted to the computer>" He then goes on to show that essentially all of the information obtainable by Laplace transforms is already contained in the eigenvalues and eigenvectors of [A]. It is surprising that very few, if any, textbooks show this relationship. The Laplace transform of Eq. (I.1) is

$$
s[X(s)] \ - \ [x(0)] \ = \ [A]{\cdot}[X(s)] \ + \ [G(s)] \tag{I.9a}
$$

or rewritten

$$(\ s \ [U] \ - \ [A] \ ) \cdot [X(s)] \ = \ [x(0) \ + \ [G(s)]]$$ (I.9b)

From which the formal solution in the s-domain is obtained as

$$[X(s)] \ = \ (\ s[U] \ - \ [A] \ )^{-1} \cdot (\ [x(0)] \ + \ [G(s)] \ )$$ (I.10)

The computational task in Eq. (I.10) is the determination of the inverse of (s[U]-[A]). The key to doing this efficiently is again through the eigenvalues and eigenvectors of [A]. With that information, the matrix (s[U]-[A]) is diagonalized,

$$[M]^{-1} \cdot (\ s \ [U] \ - \ [A] \ ) \cdot [M] \ = \ s \ [U] \ - \ [\Lambda]$$ (I.11)

and then the inverse becomes

$$(\ s \ [U] \ - \ [A] \ )^{-1} \ = \ [M] \cdot (\ s \ [U] \ - \ \Lambda \ )^{-1} \cdot [M]^{-1}$$ (I.12)

in which the inverse on the right-hand side i now trivial to calculate since (s[U]-[Λ]) is a diagonal matrix (that is, one simply takes the reciprocals of the diagonal elements). To quote again from F.H. Branin [2], "…one of the more interesting features of this method is the fact that it is far better suited for computer-sized problems than the traditional Laplace transform techniques involving ratio of polynomials and the poles and zeros thereof. In particular, the task of computing the coefficients of the polynomials in a network function P(s)/Q(s) is not only time-consuming but also prone to serious numerical inaccuracies, especially when the polynomials are of a high degree. The so-called "topological" formula approach [25] to computing these network functions involves finding all the trees of a network and then computing the sum of the corresponding tree-admittance products. But the number of trees may run into millions for a network with only 20 nodes and 40 branches. And even if this were not enough of an impediment, the computation of the roots of the polynomials P(s) and Q(s) is hazardous because these roots may be extremely sensitive to errors in the coefficients. In the writer's judgment, therefore, the polynomial approach is just not matched to the network analysis tasks which the computer is called upon to handle. The eigenvalue approach is much better suited and gives all of the theoretical information that the Laplace transform methods are designated to provide. For example, the eigenvalues are identical with the poles of the network functions. Moreover, any network function desired may be computed straightforwardly and its sensitivity obtained, either with respect to frequency or with respect to any network parameter. Finally, even the pole sensitivities can be calculated…"

I.2 Taylor Series Approximation of Transition Matrix

The matrix exponential $e^{[A]\Delta t}$ can be approximated by a power series, derived from a Taylor series expansion,

$$e^{[A]\Delta t} = [U] + \Delta t \cdot [A] + \frac{\Delta t^2}{2!} [A]^2 + \frac{\Delta t^3}{3!} [A]^3 + \frac{\Delta t^4}{4!} [A]^4 + \dots \qquad (I.13)$$

This series is, in effect, the definition of the matrix exponential.

Using Eq. (I.13), necessarily with a finite number of terms, appears to offer a way around the computation of eigenvalues. However, "the method runs headlong into another kind of eigenvalue problem which limits its usefulness: namely, that when the matrix [A] has a large eigenvalue (which means a small time constant), the integration step Δt must be kept small in order to permit rapid convergence of Eq. (I.13)" [2]. This refers to the problem encountered in "stiff systems", where there are large differences between the magnitudes of eigenvalues, and where the largest eigenvalues produce "ripples" of little interest to the engineer, who is more interested in the slower changes dictated by the smaller eigenvalues, as indicated in Fig. I.2. The method of using Eq. (I.13) becomes numerically unstable, for a given finite
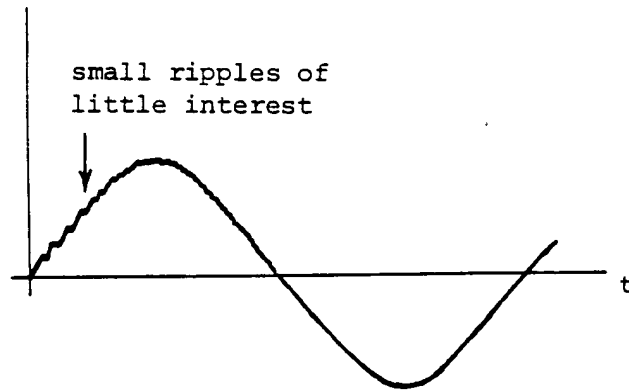
Fig. I.2 - Response of a "stiff system"

number of terms if Δt is not sufficiently small to trace the small, uninteresting ripples. It is, therefore, not a practical method for an EMTP. It exhibits the same proneness to numerical instability as the Runge-Kutta method discussed in Section I.5, which is not too surprising, since this method becomes identical with the fourth-order Runge-Kutta method if 5th and higher-order terms are neglected in Eq. (I.13), at least if the forcing function [g(t)] in Eq. (I.1) is zero ("autonomous system"), as further explained in Section I.5. Since this method is not practical, more details such as the handling of the convolution integral in Eq. (I.3) are not discussed.

I.3 Rational Approximation of Transition Matrix

A rational approximation for the matrix exponential, which is numerically stable and therefore much better than Eq. (I.13), is due to E.J. Davison[3] [6],

---

[3]This was pointed out to the writer by K.N. Stanton when he was at Purdue University (now President of ESCA Corp. in Seattle)

$$e^{[A]\Delta t} \approx (\ [U] - \frac{\Delta t}{2}[A] + \frac{\Delta t^2}{4}[A]^2 - \frac{\Delta t^3}{12}[A]^3\ )^{-1} \cdot$$
$$(\ [U] + \frac{\Delta t}{2}[A] + \frac{\Delta t^2}{4}[A]^2 + \frac{\Delta t^3}{12}[A]^3\ ) \tag{I.14}$$

A lower-order rational approximation, which is also numerically stable for all Δt, neglects the second and high-order terms in Eq. (I.14).

$$e^{[A]\Delta t} \approx (\ [U] - \frac{\Delta t}{2}[A]\ )^{-1} \cdot (\ [U] + \frac{\Delta t}{2}[A]\ ) \tag{I.15}$$

This is identical with the trapezoidal rule of integration discussed in the following section.

Would it be worthwhile to improve the accuracy of the EMTP, which now uses the trapezoidal rule, with the higher-order rational approximation of Eq. (I.14)? This is a difficult question to answer. First of all, the EMTP is not based on state-variable formulations, and it is doubtful whether this method could be applied to individual branch equations as easily as the trapezoidal rule (see Section 1). Furthermore, if sparsity is to be exploited, much of the sparsity in [A] could be destroyed when the higher-order terms are added in Eq. (I.14). By and large, however, the writer would look favorably at this method if the objective is to improve the accuracy of EMTP results, even though it is somewhat unclear how to handle the convolution integral in Eq. (I.3).

I.4 Trapezoidal Rule of Integration

Since this is the method used in the EMTP, the handling of the forcing function [g(t)] in Eq. (I.1), or analogously the handling of the convolution integral in Eq. (I.3), shall be discussed here. Let Eq. (I.1) be rewritten as an integral equation,

$$[x(t)] = [x(t-\Delta t)] + \int_{t-\Delta t}^{t} (\ [A]\ [x(u)] + [g(u)]\ )\ du \tag{I.16}$$

which is still exact. By using linear interpolation on [x] and [g] between t-Δt and t, assuming for the time being that [x] were known at t (which, in reality, is not true, thereby making the method "implicit"), we get

$$[x(t)] = [x(t-\Delta t)] + \frac{\Delta t}{2}[A] \cdot (\ [x(t-\Delta t)] + [x(t)]\ ) + \frac{\Delta t}{2} \cdot (\ [g(t-\Delta t)] + [g(t)]\ ) \tag{I.17}$$

Linear interpolation implies that the areas under the integral of Eq. (I.16) are approximated by trapezoidals (Fig. I.3); therefore the name "trapezoidal rule of integration". The method is identical with using "central difference quotients" in Eq. (I.1),

$$\frac{[x(t)] - [x(t-\Delta t)]}{\Delta t} = [A] \frac{[x(t-\Delta t)] + [x(t)]}{2} + \frac{[g(t-\Delta t)] + [g(t)}{2} \tag{I.18}$$
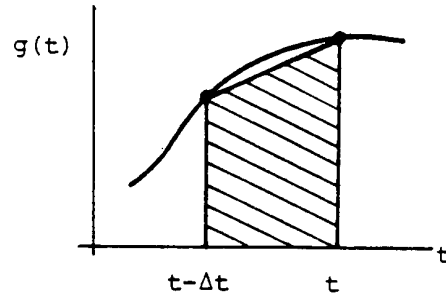
Fig. I.3 - Trapezoidal rule of integration

and could just as well be called the "method of central difference quotients". Eq. (I.17) and (I.18) can be rewritten as

$$([U] - \frac{\Delta t}{2}[A]) \cdot [x(t)] = ([U] + \frac{\Delta t}{2}[A]) \cdot [x(t-\Delta t)] + \frac{\Delta t}{2} (g(t-\Delta t)] + [g(t)]) \tag{I.19}$$

which, after premultiplication with $([U]-\Delta t\bullet[A]/2)^{-1}$, shows that we do indeed get the approximate transition matrix of Eq. (I.15).

Working with the trapezoidal rule of integration requires the solution of a system of linear, algebraic equations in each time step. If Δt is not changed, and as long as no network modifications occur because of switching or nonlinear effects, the matrix $([U]-\Delta t\bullet[A]/2)$ for this system of equations remains constant. It is therefore best and most efficient to triangularize this matrix once at the beginning, and again whenever network changes occur, and to perform the downward operations and backsubstitutions only for the right-hand side inside the time step loop, using the information contained in the triangularized matrix. The solution process is broken up into two parts in this scheme, one being the triangularization of the constant matrix, the other one being the "repeat solution process" for right-hand sides (which is done repeatedly inside the time step loop). this concept of splitting the solution process into one part for the matrix and a second part for the right-hand side is seldom mentioned in textbooks, but it is very useful in many power system analysis problems, not only here, but also in power flow iterations using a triangularized [Y]-matrix, as well as in short-circuit calculations for generating columns of the inverse of [Y] one at a time. For more details, see Appendix III.

It may not be obvious that the trapezoidal rule applied to the state variable equations (I.1) leads to the same answers as the trapezoidal rule first applied to individual branch equations, which are then assembled into node equations, as explained in Section 1. The writer has never proved it, but suspects that the answers are identical. For the example of Fig. I.1, this can easily be shown to be true.

The trapezoidal rule of integration is admittedly of lower order accuracy than many other methods, and it is therefore not much discussed in textbooks. It is numerically stable, however, which is usually much more

important in power system transient analysis than accuracy by itself. Numerical stability more or less means that the solution does not "blow up" if Δt is too large; instead, the higher frequencies will be incorrect in the results (in practice, they are usually filtered out), but the lower frequencies for which the chosen Δt provides an appropriate sampling rate will still be reasonably accurate. Fig. I.4 illustrates this for the case of a three-phase line energization. This line was represented as a cascade connection of 18 three-phase nominal π-circuits. The curve for Δt = 5° (based on f = 60 Hz, i.e., Δt = 231.48 μs)

Fig. I.4 - Switching surge overvoltage at the receiving end in a three-phase open-ended line

cannot follow some of the fast oscillations noticeable in the curve for Δt = 0.5°, but the overall accuracy is not too bad. The error between the exact and approximate value at a particular instant in time is obviously not a good measure by itself for overall accuracy, or for the usefulness of a method for these types of studies. In Fig. I.4, an error as large as 0.6 p.u. (at the location of the arrow, assuming that the curve for Δt = 0.5° gives the exact value) is perfectly acceptable, because the overall shape of the overvoltages is still represented with sufficient accuracy.

A physical interpretation of the trapezoidal rule of integration for inductances is given in Section 2.2.1. This interpretation shows that the equations resulting from the trapezoidal rule are identical with the exact solution of a lossless stub-line, for which the answers are always numerically stable though not necessarily as accurate as desired.

I.5 Runge-Kutta Methods

These methods can be used for any system of ordinary differential equations,

$$[\frac{dx}{dt}] = [\ f\ ([x],\ t)\ ] \qquad\qquad (I.20)$$

There are many variants of the Runge-Kutta method, but the one most widely used appears to be the following fourth-order method: Starting from the known value [x(t-Δt), the slope is calculated at the point 0 (Fig. I.5(a)),

$$\frac{[\Delta x^{(1)}]}{\Delta t} = [\ f(\ [x(t-\Delta t)\ ],\ t-\Delta t\ )\ ] \qquad (I.21a)$$

which is then used to obtain an approximate value $[x^{(1)}]$ at midpoint 1,

$$[x^{(1)}] = [\ x(t-\Delta t)\ ] + \frac{1}{2}\ [\ \Delta x^{(1)}\ ] \qquad (I.21b)$$
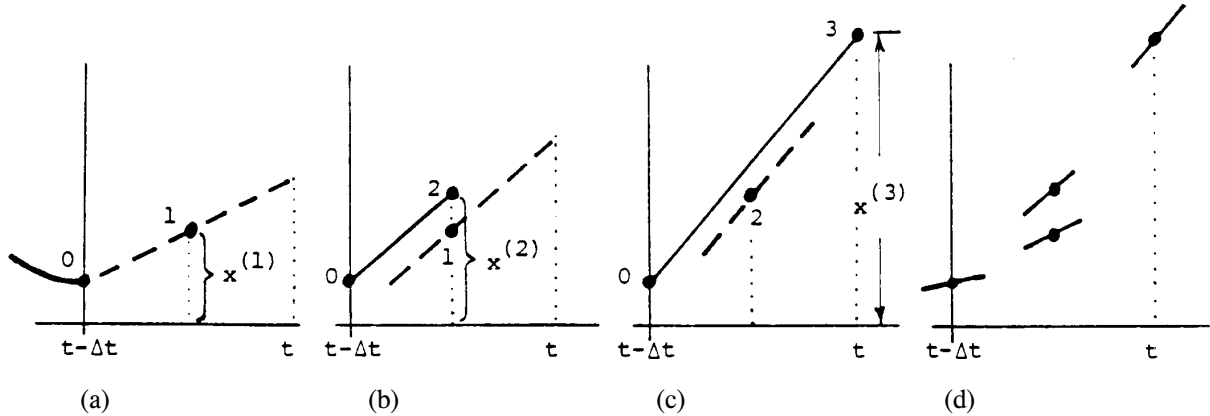
Fig. I.5 - Fourth-order Runge-Kutta method

Now, the slope is recalculated at midpoint 1 (Fig. I.5(b)),

$$\frac{[\ \Delta x^{(2)}\ ]}{\Delta t} = [\ f(\ [x^{(1)}],\ t-\Delta\frac{t}{2}\ ] \qquad (I.21c)$$

and this is used to obtain a second approximate value $[x^{(2)}]$ at midpoint 2,

$$[\ x^{(2)}\ ] = [\ x(t-\Delta t)\ ] + \frac{1}{2}\ [\ \Delta x^{(2)}\ ] \qquad (I.21d)$$

Then the slope is evaluated for a third time, now at midpoint 2 (Fig. I.5(c)),

$$\frac{[\ \Delta x^{(3)}\ ]}{\Delta t} = [\ f\ (\ [x^{(2)}],\ t-\frac{\Delta t}{2}\ )\ ] \qquad (I.21e)$$

which is used to get an approximate solution in point 3 at time t,

$$[\ x^{(3)}\ ] = [\ x(t-\Delta t)\ ] + [\ \Delta x^{(3)}\ ] \qquad (I.21f)$$

Finally, the slope is evaluated for a fourth time in point 3,

$$\frac{[\ \Delta x^{(4)}\ ]}{\Delta t} = [\ f\ (\ [x^{(3)}],\ t\ )\ ]$$

(I.21g)

From these four slopes in 0, 1, 2, 3 (Fig. I.5(d)), the final value at t is obtained by using their weighted averages,

$$[x(t)] = [x(t-\Delta t)] + \frac{\Delta t}{6} \cdot (\ \frac{[\Delta x^{(1)}\ ]}{\Delta t} + 2\ \frac{[\ \Delta x^{(2)}\ ]}{\Delta t} + 2\ \frac{[\ \Delta x^{(3)}\ ]}{\Delta t} + \frac{[\ \Delta x^{(4)}\ ]}{\Delta t}\ )$$

(I.22)

The mathematical derivation of the Runge-Kutta formula is quite involved (see, for example, in [7]). Intuitively, it can be viewed as an exploration of the "direction field"[4] at a number of sample points (0,1,2,3 in Fig. I.5). There are variants as to the locations of the sample points, and hence as to the weights assigned to them. There are also lower-order Runge-Kutta methods which use fewer sample points.

As already mentioned in Section I.2, the fourth-order Runge-Kutta method of Eq. (I.21) and (I.22) is identical with the fourth-order Taylor series expansion of the transition matrix if the differential equations are linear, at least for autonomous systems with $[g(t)] = 0$ in Eq. (I.1). In that case, Eq. (I.1) becomes

$$\frac{[\ \Delta x^{(1)}\ ]}{\Delta t} = [A]\ [x(t-\Delta t)]\ , \qquad [\ x^{(1)}\ ] = (\ [U] + \frac{\Delta t}{2}[A]\ )\ [x\ (t-\Delta t)]$$

With these values, the second slope becomes

$$\frac{[\Delta x^{(2)}]}{\Delta t} = (\ [A] + \frac{\Delta t}{2}\ [A]^2\ ) \cdot [x\ (t-\Delta t)]$$

and

$$[x^{(2)}] = (\ [U] + \frac{\Delta t}{2}[A] + \frac{\Delta t^2}{4}[A]^2\ ) \cdot [x(t-\Delta t)]$$

Then the third slope becomes

$$\frac{[\Delta x^{(3)}]}{\Delta t} = (\ [A] + \frac{\Delta t}{2}\ [A]^2 + \frac{\Delta t^2}{4}\ [A]^3\ ) \cdot [x(t-\Delta t)]$$

and

$$[x^{(3)}] = (\ [U] + \Delta t\ [A] + \frac{\Delta t^2}{2}[A]^2 + \frac{\Delta t^3}{4}[A]^3\ ) \cdot [x(t-\Delta t)]$$

---

[4]If the slopes are calculated at a number of points and graphically displayed as short lines, then one gets a sketch of the "direction field", as indicated in Fig. I.5(d).

from which the fourth slope is calculated as

$$\frac{[\Delta x^{(4)}]}{\Delta t} = (\ [A]\ +\ \Delta t\ [A]^2\ +\ \frac{\Delta t^2}{2}\ [A]^3\ +\ \frac{\Delta t^3}{4}\ [A]^4\ )\ \cdot\ [x(t-\Delta t)]$$

Finally, the new value is obtained with Eq. (I.22) as

$$[x(t)] = (\ [U]\ +\ \Delta t\ [A]\ +\ \frac{\Delta t^2}{2}\ [A]^2\ +\ \frac{\Delta t^3}{6}\ [A]^3\ +\ \frac{\Delta t^4}{24}\ [A]^4\ )\ \cdot\ [x(t-\Delta t)]$$

which is indeed identical with the Taylor series approximation of the transition matrix in Eq. (I.13).

If [A] is zero in Eq. (I.1), that is, if [x] is simply the integral over the known function [g(t)], then the fourth-order Runge-Kutta method is identical with Simpson's rule of integration, in which the curve is approximated as a parabola going through the three known points in t-Δt, t-Δt/2, and t (Fig. I.6).
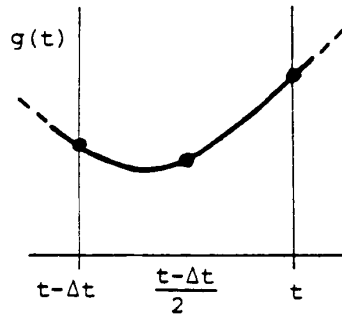
Fig. I.6 - Simpson's rule

The Runge-Kutta method is prone to numerical instability if Δt is not chosen small enough. "It becomes painfully slow in the case of problems having a wide spread of eigenvalues. For the largest eigenvalue (or, equivalently, its reciprocal, the smallest time constant) controls the permissible size of Δt. But the smallest eigenvalues (largest time constants) control the network response and so determine the total length of time over which the integration must be carried out to characterize the response. In the case of a network with a 1000 to 1 ratio of largest to smallest eigenvalue, for instance, it might be necessary to take in the order of 1000 times as many integration steps with the Runge-Kutta method as with some other method which is free of the minimum time-constant barrier" [2}. This problem is indicated in Fig. I.2: Though the ripples may be very small in amplitude, they will cause the slopes to point all over the place, destroying the usefulness of methods based on slopes.

I.6 Predictor-Corrector Methods

These methods can again be used for any system of ordinary differential equations of the type of Eq. (I.20).To explain the basic idea, let us try to apply the trapezoidal rule to Eq. (I.20), which would give us

$$[x^{(h)}] = [x(t-\Delta t)] + \frac{\Delta t}{2} ([f ([x(t-\Delta t)], t-\Delta t)] + [f ([x^{(h-1)}], t)]) \tag{I.23}$$

In the linear case discussed in Section I.4, this equation could be solved directly for [x]. In the general (time-varying or nonlinear) case, this direct solution is no longer possible, and iterative techniques have to be used. This has already been indicated in Eq. (I.23) by using superscript (h) to indicate the iteration step; at the same time, the argument "t" has been dropped to simplify the notation. The iterative technique works as follows:

1. Use a predictor formula, discussed further on, to obtain a "predicted" guess $[x^{(0)}]$ for the solution at time t.

2. In iteration step h (h=1,2,...), insert the approximate solution $[x^{(h-1)}]$ into the right-hand side of Eq. (I.23) to find a "corrected" solution $[x^{(h)}]$.

3. If the difference between $[x^{(h)}]$ and $[x^{(h-1)}]$ is sufficiently small, then the integration from t-Δt to t is completed. Otherwise, return to step 2.

Eq. (I.23) is a second-order <u>corrector</u> formula. To start the iteration process, a <u>predictor</u> formula is needed for the initial guess $[x^{(0)}]$. A suitable predictor formula for Eq. (I.23) can be obtained from the midpoint rule,

$$[x^{(0)}_{(t)}] = [x(t-2\Delta t)] + 2\Delta t [f ([x(t-\Delta t)], t-\Delta t)] \tag{I.24}$$

or from an extrapolation of known values at t-3Δt, t-2Δt, and t-Δt,

$$[x^{(0)}_{(t)}] = [x(t-3\Delta t)] + \frac{3}{2}\Delta t ([f([x(t-\Delta t)], t-\Delta t)] + [f([x(t-2\Delta t)], t-2\Delta t)]) \tag{I.25}$$

The difference in step 3 of the iteration scheme gives an estimate of the error, which can be used

(a) to decide whether the step size Δt should be decreased (error too large) or can be increased (error very small), or

(b) to improve the prediction in the next time step.

It is generally better to shorten the step size Δt than to use the corrector formula repeatedly in step 2 above. In using the error estimate to improve the prediction, it is assumed that the difference between the predicted and corrected values changes slowly over successive time steps. This "past experience" can then be used to improve the prediction with a <u>modifier</u> formula. Such a modifier formula for the predictor of Eq. (I.25) and for the corrector of Eq. (I.23) would be

$$[x^{(0)}_{improved}] = [x^{(0)}] + \frac{9}{10} ([x(t-\Delta t)] - [x^{(0)}_{(t-\Delta t)}]) \tag{I.26}$$

Besides the second-order methods of Eq. (I.23) to Eq. (I.26), there are of course higher-order methods. Fourth-order predictor-corrector methods seem to be used most often. Among these are Milne's method and Hamming's method, with the latter one usually more stable numerically. The theory underlying all predictor-

corrector methods is to pass a polynomial through a number of points at t, t-Δt, t-2Δt, …, and to use this polynomial for integration. The end-point at t is first predicted, and then once or more often corrected. Obviously, the convergence and numerical stability properties of the corrector formula are more important than those of the predictor formula, because the latter is only used to obtain a first guess and determines primarily the number of necessary iteration steps. The predictor and corrector formula should be of the same order in the error terms. There are different classes of predictors: Adams-Bashforth predictors (obtained from integrating Newton' backward interpolation formulas), Milne-type predictors (obtained from an open Newton-Cotes forward-integrating formula), and others. Note that those formulas requiring values at t-2Δt, or further back, are not "self-starting"; Runge-Kutta methods are sometimes used with such formulas to build up enough history points.

It is questionable whether non-self-starting high-order predictor-corrector formulas would be very useful for typical power system transient studies, since waves from distributed-parameter lines hitting lumped elements look almost like discontinuities to the lumped elements, and would therefore require a return to second-order predictor-correctors each time a wave arrives. In linear systems, the second-order corrector of Eq. (I.23) can be solved directly, however, and is then identical with the trapezoidal rule as used in the EMTP.

I.7 Deferred Approach to the Limit (Richardson Extrapolation and Romberg Integration)

The idea behind these methods is fairly simple. Instead of using higher-order methods, the second-order trapezoidal rule (either directly with Eq. (I.17) for linear systems, or iteratively with Eq. (I.23) for more general systems) is used more than once in the interval between t-Δt and t, to improve the accuracy. Assume that the normal step size Δt is used to find $[x^{(1)}]$ at t from $[x(t-\Delta t)]$, as indicated in Fig. I.7. Now repeat the integration with the trapezoidal rule with half
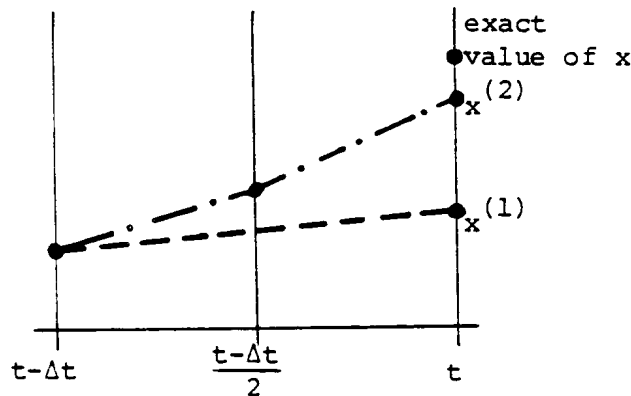
Fig I.7 - Richardson extrapolation

the step size Δt/2, and perform two integration steps to obtain $[x^{(2)}]$. With the two values $[x^{(1)}]$ and $[x^{(2)}]$, an intelligent guess can be made as to where the solution would end up if the step size were decreased more and more. This "extrapolation towards Δt=0" (Richardson's extrapolation) would give us a better answer

I-14

$$[x(t)] = [x^{(2)}] + \frac{1}{3} \left([x^{(2)}] - [x^{(1)}] \right) \tag{I.27}$$

The accuracy can be further improved by repeating the integration between t-Δt and t with 4,8,16,… intervals. The corresponding extrapolation formula for Δt → 0 is known as "Romberg integration."

Whether any of these extrapolation formulas are worth the extra computational effort in an EMTP is very difficult to judge. Some numerical analysts seem to feel that these methods look very promising. They offer an elegant accuracy check as well.

I.8 Numerical Stability and Implicit Integration

The writer believes that the numerical stability of the trapezoidal rule has been one of the key factors in making the EMTP such a success. It is therefore worthwhile to expound on this point somewhat more.

The trapezoidal rule belongs to a class of implicit integration schemes, which have recently gained favor amongst numerical mathematicians for the solution of "stiff systems", that is, for systems where the smallest and largest eigenvalues or time constants are orders of magnitude apart [70]. Most power systems are probably stiff in that sense. While implicit integration schemes of higher order than the trapezoidal rule are frequently proposed, their usefulness for the EMTP remains questionable because they are numerically less stable. A fundamental theorem due to Dahlquist [71] states:

Theorem: Let a multistep method be called A-stable, if, when it is applied to the problem $[dx/dt] = \lambda[x]$, $Re(\lambda) < 0$, it is stable for all $\Delta t > 0$.

Then: (i) No explicit linear multistep method is A-stable.

(ii) No implicit linear multistep method of order greater than two is A-stable.

(iii) The most accurate A-stable linear multistep method of order two is the trapezoidal rule.

To illustrate the problem of numerical stability, let us assume that a fast oscillation somewhere in the network produces "ripples" of very small amplitudes, which do not have any influence on the overall behavior of the network, similar to those shown in Fig. I.2. Such a mode of oscillation could be described by [72]

$$\frac{d^2x}{dt^2} + x = 0, \quad with \ x(0) = 0, \quad dx/dt(0) = 10^{-4} \tag{I.28}$$

with its exact solution being

$$x = 10^{-4} \sin(t) \tag{I.29}$$

The amplitude of 10^{-4} shall be considered as very small by definition. Eq. (I.28) must be rewritten as a system of first-order differential equations in order to apply any of the numerical solution techniques,

$$\begin{bmatrix} dx_1/dt \\ dx_2/dt \end{bmatrix} = \begin{bmatrix} 0 & 1 \\ -1 & 0 \end{bmatrix} \begin{bmatrix} x_1 \\ x_2 \end{bmatrix} \tag{I.30}$$

with $x_1 = x$ and $x_2 = dx/dt$. The exact step-by-step solution with Eq. (I.3) is

$$\begin{bmatrix} x_1(t) \\ x_2(t) \end{bmatrix} = e^{[a]\Delta t} \begin{bmatrix} x_1(t-\Delta t) \\ x_2(t-\Delta t) \end{bmatrix} \tag{I.30a}$$

with

$$[A] = \begin{bmatrix} 0 & 1 \\ -1 & 0 \end{bmatrix} \tag{I.30b}$$

Application of the trapezoidal rule to Eq. (I.30) gives

$$\begin{bmatrix} x_1(t) \\ x_2(t) \end{bmatrix} = \frac{1}{1+\dfrac{\Delta t^2}{4}} \begin{bmatrix} 1-\dfrac{\Delta t^2}{4} & \Delta t \\ -\Delta t & 1-\dfrac{\Delta t^2}{4} \end{bmatrix} \begin{bmatrix} x_1(t-\Delta t) \\ x_2(t-\Delta t) \end{bmatrix} \tag{I.31}$$

It can be shown that

$$x_1^2(t) + x_2^2(t) = x_1^2(t-\Delta t) + x_2^2(t-\Delta t)$$

in Eq. (I.31) for any choice of Δt. Therefore, if the solution is started with the correct initial conditions $x_1^2(0) + x_{22}(0) = 10^{-8}$, the solution for x will always lie between -10^{-4} and $+10^{-4}$, even for step sizes which are much larger than one cycle of oscillation. In other words, the trapezoidal rule "cuts across" oscillations which are very fast but of negligible amplitude, without any danger of numerical instability.

Explicit integration techniques, which include Runge-Kutta methods, are inherently unstable. They require a step size tailored to the highest frequency or smallest time constant (rule of thumb: $\Delta t \leq 0.2\ T_{min}$), even though this mode may produce only negligible ripples, with the overall behavior determined by the larger time constants in stiff systems. Applying the conventional fourth-order Runge-Kutta method to Eq. (I.30) is identical to a fourth-order Taylor series expansion of the transition matrix, as mentioned in Section I.5, and leads to

$$\begin{bmatrix} x_1(t) \\ x_2(t) \end{bmatrix} = \begin{bmatrix} 1-\dfrac{\Delta t^2}{2}+\dfrac{\Delta t^4}{24} & \Delta t-\dfrac{\Delta t^3}{6} \\ -\Delta t+\dfrac{\Delta t^3}{6} & 1-\dfrac{\Delta t^2}{2}+\dfrac{\Delta t^4}{24} \end{bmatrix} \begin{bmatrix} x_1(t-\Delta t) \\ x_2(t-\Delta t) \end{bmatrix} \tag{I.32}$$

Plotting the curves with a reasonably small Δt, e.g., 6 samples/cycle, reveals that the Runge-Kutta method of Eq. (I.32) is more accurate at first than the trapezoidal rule, but tends to lose the amplitude later on (Fig. I.8). This is not serious since the ripple is assumed to be unimportant in the first place. If the step size is increased, however, to $\Delta t > \sqrt{2}/\pi$ cycles,
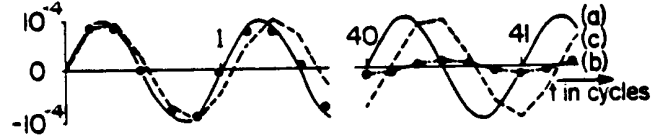
Fig. I.8 - Numerical solution of $d^2x/dt^2 + x = 0$; (a) exact, (b) Runge-Kutta, (c) trapezoidal rule

then the amplitude will eventually grow to infinity. This is illustrated in table I.1 for $\Delta t = 1$ cycle.

Table I.1 - Numerical solution of Eq. (I.28) with $\Delta t = 1$ cycle

t in cycles	1	2	3	4	5	6
exact	0	0	0	0	0	0
trapezoidal rule	$0.58 \cdot 10^{-4}$	$-0.94 \cdot 10^{-4}$	$0.96 \cdot 10^{-4}$	$-0.63 \cdot 10^{-4}$	$0.06 \cdot 10^{-4}$	$0.53 \cdot 10^{-4}$
Runge-Kutta	-0.004	-0.32	-18	-590	-6800	2,600,000

Ref. 72 explains that the trapezoidal rule remains numerically stable even in the limiting case where the time constant T in an equation of the form

$$T \, dx_2/dt = K \, x_1 - x_2 \tag{I.33}$$

becomes zero. For $T = 0$, the trapezoidal rule produces

$$K \, x_1(t) - x_2(t) = - \{ K \, x_1(t-\Delta t) - x_2(t-\Delta t) \} \tag{I.34}$$

which is the correct answer as long as the solution starts from correct initial conditions $K \, x_1(0) - x_2(0) = 0$. Even a slight error in the initial conditions,

$$K \, x_1(0) - x_2(0) = \varepsilon$$

will not cause serious problems. Since Eq. (I.34) just flips the sign of the expression from step to step, the error ε would only produce ripples $\pm \, \varepsilon$ superimposed on the true solution for x_2.

Semlyen and Dabuleanu suggest an implicit third-order integration scheme for the EMTP, in which second-order interpolation (parabola) is used through two known points at $t - 2 \, \Delta t$ and $t - \Delta t$, and through the yet unknown solution point at t [73]. Applying this scheme to Eq. (I.30) produces

$$\begin{bmatrix} x_1(t) \\ x_2(t) \end{bmatrix} = \begin{bmatrix} a & b \\ -b & a \end{bmatrix} \begin{bmatrix} x_1(t-\Delta t) \\ x_2(t-\Delta t) \end{bmatrix} + \begin{bmatrix} c & d \\ -d & c \end{bmatrix} \begin{bmatrix} x_1(t-2\Delta t) \\ x_2(t-2\Delta t) \end{bmatrix} \tag{I.35}$$

with

$$a = (1 - \frac{40}{144}\Delta t^2) / \det$$

$$b = \frac{13}{12} \Delta t / \det$$

$$c = \frac{5}{144} \Delta t^2 / \det$$

$$d = -\frac{\Delta t}{12} / \det$$

$$\det = 1 + \frac{25}{144} \Delta t^2$$

Eq. (I.35) gives indeed higher accuracy than the trapezoidal rule, but only as long as the step size is reasonably small, and as long as the number of steps is not very large. After 40 cycles, with a step size of 6 samples/cycle, Eq. (I.35) would produce peaks which have already grown by a factor of 20,000. This indicates that the choice of the step in Eq. (I.35) is subject to limitations imposed by numerical stability considerations, whereas the trapezoidal rule is not. A step size of 6 samples/cycles is not too large for fast oscillations which have no influence on the overall behavior. The trapezoidal rule simply filters them out. High-order implicit integration schemes are therefore not as useful for the EMTP as one might be thought to believe from recent literature on implicit integration schemes for stiff systems.

I.9 Backward Euler Method

The major drawback of the trapezoidal rule of integration of Section I.4 is the danger of numerical oscillations when it is used as a differentiator, e.g., in

$$v = L \, di / dt \tag{I.36}$$

with current i being the forcing function. A sudden jump in di/dt, which could be caused by current interruption in a circuit breaker, should create a sudden jump in the voltage v. Instead, the trapezoidal rule of integration produces undamped numerical oscillations around the correct answer, as explained in Section 2.2.2. These oscillations can be damped out by adding a parallel resistor R_p across the inductance. Section 2.2.2 shows that critical damping is achieved if $R_p = 2L/\Delta t$. In that case, the "damped" trapezoidal rule of Eq. (2.20) transforms Eq. (I.36) into

$$v(t) = \frac{L}{\Delta t} [i(t) - i(t-\Delta t)] \tag{I.37}$$

which is simply the backward Euler method. Therefore, the "critically damped" trapezoidal rule and the backward Euler method are identical.

In general, the undamped trapezoidal rule is better than the backward Euler method, because the latter method produces too much damping. It is a good method, however, if it is only used for a few steps to get over instants of discontinuities (see Appendix II).

APPENDIX II - RE-INITIALIZATION AT INSTANTS OF DISCONTINUITY

The numerical oscillations which occur in the voltages across inductances at points of discontinuities in di/dt, or in currents through capacitances at points of discontinuities in dv/dt, oscillate around the correct answer. These numerical oscillations can therefore be eliminated from the output if the output is smoothed, e.g., for the voltage across an inductance,

$$v_L(t)_{smoothed} = \frac{1}{2} [v_L(t) + v_L(t-\Delta t)] \qquad (II.1)$$

If this smoothing algorithm is not just applied to the output, but added directly into the trapezoidal rule solution method, then we obtain

$$v_L(t)_{smoothed} = L \frac{i(t) - i(t-\Delta t)}{\Delta t} \qquad (II.2)$$

which is simply the backward Euler method (Appendix I.9). B. Kulicke [15] recognized that such a backward difference quotient can be used to restart the solution process smoothly after a discontinuity, with the correct jumps in v_L across L, or in i_C through C. The backward Euler method does have absolute numerical stability, but it is not as accurate as the trapezoidal rule. It is therefore only used to restart the solution with new initial conditions. B. Kulicke also recognized that it is best to use half the step size with the backward Euler method to make the matrix [G] needed for that backward difference solution identical with the matrix [G] of Eq. (I.8), which is needed for the trapezoidal rule solution after the discontinuity anyhow. In what follows, Kulicke's method of re-initialization is explained in detail for the inductance; the derivations for the capacitance equations are analogous. There are three steps in Kulicke's method, namely

      (a)   interpolation to obtain variables at the point of discontinuity,

      (b)   network solution at $\Delta t/2$ after the discontinuity for the sole purpose of re-initialization,

      (c)   re-initialization of history terms at the point of discontinuity.

These three steps are then followed by the normal trapezoidal rule solution method.

(a)   <u>Interpolation</u>

Assume that current is to be interrupted at current zero in a circuit breaker. The EMTP solution will give us answers at points 1, 2, 3 (Fig. II.1), with current zero crossing being discovered at point 3. Kulicke then uses linear interpolation to locate the zero crossing at point 0, and then calculates the values of all variables and history terms at that point 0, again with linear interpolation. The solution is then restarted at point 0, with the same Δt as before, but the uniform spacing along the time axis will be disturbed at that point, which would have to be recognized in the output. For Kulicke's method to work, e.g., by re-solving the network in point 3 with the switch open, is unclear at this time, and may require more work than linear interpolation. Interpolation would also help to eliminate overshooting of knee-points in piecewise linear elements.
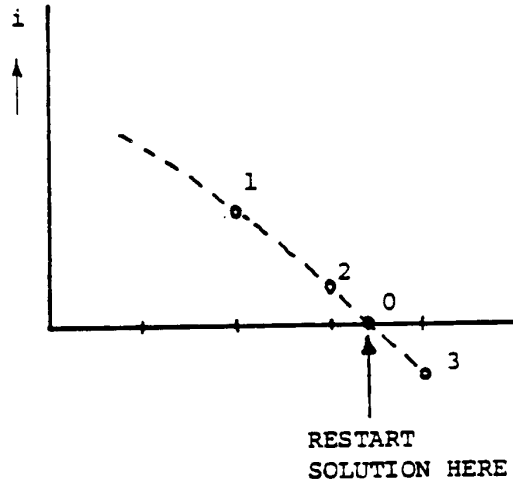
Fig. II.1 - Linear interpolation to locate point of discontinuity

(b) <u>Network solution at $t_o + \Delta t/2$</u>

Let us call the instant of discontinuity t_o, with the argument t_{o-} used for quantities before the jump, and t_{o+} for quantities after the jump (Fig. II.2). Let us also look at the jump in di/dt across an inductance, which is caused by the switch opening. Since no jump can occur in this
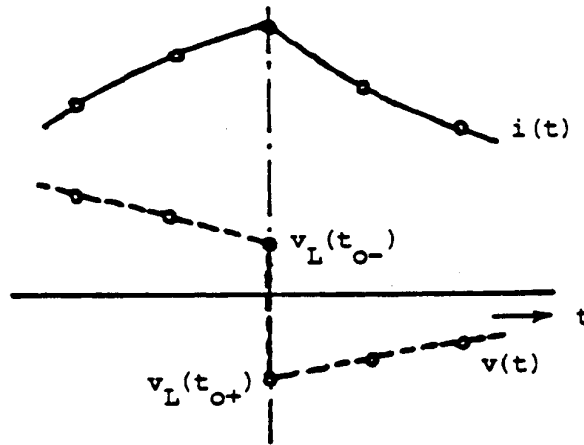
Fig. II.2 - Voltage and current at point of discontinuity

current, we know that

$$i(t_{o+}) = i(t_{o-}) \tag{II.3}$$

If we now use the backward difference quotient of Eq. (II.2) to solve the network at $t_o + \Delta t/2$, then we obtain

$$i(t_o + \frac{\Delta t}{2}) = \frac{\Delta t}{2L} \, v_L(t_o + \frac{\Delta t}{2}) + i(t_{o-}) \tag{II.4}$$

which is the same as Eq. (1.3a), except that the history term is now simply $i(t_{o-})$. For capacitance, the analogous equation would be

$$i_c\left(t_o + \frac{\Delta t}{2}\right) = \frac{2C}{\Delta t}\, v\left(t_o + \frac{\Delta t}{2}\right) - \frac{2C}{\Delta t}\, v(t_{o-}) \tag{II.5}$$

again with a modified history term of $-2C \ast v(t_{o-})/\Delta t$ in this case. The solution at $t_o + \Delta t/2$ is therefore found in the usual way with Eq. (1.8b), after [G] has been modified to account for switch opening or for whatever caused the discontinuity, and after it has been re-triangularized. Notice that this matrix change and re-triangularization process is required anyhow, even if Kulicke's re-initialization method is not used. The only difference for this extra solution is in the right-hand side, since the history term is now $i(t_{o-})$ instead of hist from Eq. (1.3b), with an analogous modification of the capacitance history term.

(c) <u>Re-initialization of history terms at t_{o+}</u>

The extra network solution at $t_o + \Delta t/2$ is made for the sole purpose of re-initializing variables at t_{o+}. For the inductance, assuming a linear change in current between t_{o+} and $t_o + \Delta t/2$, the voltage at t_{o+} simply becomes

$$v_L(t_{o+}) = v_L(t_o + \Delta t/2) \tag{II.6}$$

which would then be used in Eq. (1.3b) to calculate the history term required for the next, normal solution at $t_o + \Delta t$, for which the triangularized matrix has already been obtained in step (b).

Similarly, assuming a linear change of voltage across capacitances, the current at t_{o+} simply become

$$i_C(t_{o+}) = i_C(t_o + \Delta t/2) \tag{II.7}$$

**APPENDIX III - SOLUTION OF LINEAR EQUATIONS, MATRIX
REDUCTION AND INVERSION, SPARSITY**

The fastest direct method for solving a system of linear equations

$$Y_{11}V_1 + Y_{12}V_2 + ... Y_{1N}V_N = I_1$$
$$Y_{21}V_1 + Y_{22}V_2 + ... Y_{2N}V_N = I_2$$
$$............................$$
$$Y_{N1}V_1 + Y_{N2}V_2 + ... Y_{NN}V_N = I_N \qquad \text{(III.1)}$$

for the unknown voltages $V_1, ... V_N$, with given current $I_1, ... I_N$, is Gauss elimination, which in more or less modified forms is also called triangularization, triangular factorization, LU decomposition, Gauss-Banachiewicz, Gauss-Doolittle, Crout, etc.

Gauss-Jordan elimination or diagonalization takes more operations for the solution of linear equations, but for matrix inversion the differences in speed between Gauss and Gauss-Jordan seem to become negligible, since both methods require essentially N^3 operations. The Gauss-Jordan method has therefore been chosen for the inversion of small, but full matrices associated with coupled branches. For solving the complete network with Eq. (1.8b) or Eq. (1.21), Gauss elimination with sparsity techniques is used, as discussed in Section III.4.

A comparison of operation counts between these two basic methods is shown in Table III.1. Choleski's method is a modification of Gauss elimination for positive definite, symmetric matrices, whereby the square root is taken of the diagonal elements to make the lower triangular matrix equal to the transpose of the upper triangular matrix. This requires extra calculations which are difficult to justify. It has been claimed, however, that Choleski's method works better for ill-conditioned matrices, probably because the square root operation brings numbers closer together in orders of magnitude, e.g., 10^6 and 10^{-4} would become 10^3 and 10^{-2}. The writer has never tested this claim, and suspects that it applies only to (obsolete) fixed-point arithmetic.

Table III.1 - Number of operations for direct solution of a system of linear equations

1. Full matrices

Operations count for N equations in N unknowns. Taken from [75]

A. Unsymmetric matrix; storage requirement $= N^2$ for matrix

Number of operations				
Method	Process[a]	Mult.	Add./Sub.	Div.
Gauss elimination (triangularization)	for matrix	$\frac{N^3}{3} - \frac{N}{3}$	$\frac{N^3}{3} - \frac{N^2}{2} + \frac{N}{6}$	N
	1 repeat solution	N^2	$N^2 - N$	O

Gauss elimination using scalar products[b]	for matrix	$\dfrac{N^3}{3} - \dfrac{N^2}{2} + \dfrac{N}{6}$	$\dfrac{N^3}{3} - N^2 + \dfrac{2N}{3}$	N
	1 repeat solution	N^2	$N^2 - N$	O
Gauss-Jordan (diagonalization)	for matrix	$\dfrac{N^3}{2} - \dfrac{N^2}{2}$	$\dfrac{N^3}{2} - N^2 + \dfrac{N}{2}$	N
	1 repeat solution	N^2	$N^2 - N$	O

B. Symmetric matrix; storage requirement = $^{N(N+1)}/_2$ for matrix

Number of operations				
Method	Process[a]	Mult.	Add./Sub.	Div.
Gauss elimination (triangularization)	for matrix	$\dfrac{N^3}{6} + \dfrac{N^2}{2} - \dfrac{2N}{3}$	$\dfrac{N^3}{6} - \dfrac{N}{6}$	N
	1 repeat solution	N^2	$N^2 - N$	O
Choleski (triangular-ization)	for matrix	$\dfrac{N^3}{6} + \dfrac{N^2}{2} - \dfrac{2N}{3}$	$\dfrac{N^3}{6} - \dfrac{N}{6}$	N (+N square roots) O
	1 repeat solution	$N^2 + N$	$N^2 - N$	
Gauss-Jordan (diagonalization)	for matrix	$\dfrac{N^3}{3} - \dfrac{N}{3}$	$\dfrac{N^3}{3} - \dfrac{N^2}{2} + \dfrac{N}{6}$	N
	1 repeat solution	N^2	$N^2 - N$	O

a)   In the process "for matrix" only the elements of the matrix are transformed. In the process "1 repeat solution," the transformation process is extended to the given vector [I] in the system of equations [Y][V] = [I] and then [V] is found. If [I] changes only and [Y] remains unchanged, then only the process "1 repeat solution" is used.

b)   Also called "Gauss-Banachiewicz and in slightly modified form "Gauss-Doolittle" (advantageous only for desk calculators and for digital computers with scalar product as a single operation).

2. Sparse matrices for network solutions

Impressive savings in storage requirements and number of operations possible. See Section III.4.

Because [Y] in Eq. (III.1) has usually strong diagonal elements, "pivoting" is not used in the solution routines of the EMTP and its support programs.

If Eq. (III.1) is solved repeatedly with the same matrix [Y], but with different right-hand sides [I], then it is best to split the elimination process into two parts, one "for the matrix", and the other for "repeat solutions". This situation occurs in the transient simulation over successive time steps as long as the network does not change because of switching operations or nonlinear effects. As shown in Table III.1, the number of operations is much less for repeat solutions than for a complete solution involving the process for the matrix. The savings are even more

pronounced with the sparsity techniques discussed in Section III.4.

III.1 Gauss Elimination

Most readers are probably familiar with this method, which will be explained for the following example:

$$2x_1 + 3x_2 - x_3 \qquad\qquad = 20$$
$$-6x_1 - 5x_2 \qquad + 2x_4 = -45$$
$$2x_1 - 5x_2 + 6x_3 - 6x_4 \qquad = -3 \qquad\qquad\qquad\qquad\text{(III.2)}$$
$$4x_1 + 6x_2 + 2x_3 - 3x_4 \qquad = 58$$

Step 1: Leave the first row unchanged[1], and add such multiples of the first row to rows 2, 3, 4 that zeros are produced in column 1 of these rows:

2	3	-1	0
0	4	-3	2
0	-8	7	-6
0	0	4	-3

20
15
-23
18

unchanged

add 3-times row 1

add (-1)-times row 1

add (-2)-times row 1

this information must be saved if repeat solutions are to be performed later

Step 2: Leave the second row unchanged[2], as well as row 1, and add such multiples of the second row to rows 3, 4 that zeros are produced in column 2 of these rows:

2	3	-1	0
0	4	-3	2
0	0	1	-2
0	0	4	-3

20
15
7
18

unchanged

add 2-times row 2

add 0-times row 2

save information if repeat solutions are to be performed later.

Step 3: Leave the third row unchanged[2], as well as rows 1 and 2, and add such multiples of the third row 4 that zeros are produced in column 3 of that row:

---

[1]In the transient simulation part of the EMTP, this row is divided by the diagonal element before proceeding with the other row modifications.

[2]ibid.

$$\begin{array}{|cccc|} \hline 2 & 3 & -1 & 0 \\ 0 & 4 & -3 & 2 \\ 0 & 0 & 1 & -2 \\ 0 & 0 & 0 & 5 \\ \hline \end{array} \qquad \begin{array}{|c|} \hline 20 \\ 15 \\ 7 \\ -10 \\ \hline \end{array}$$

unchanged

add (-4)-times row 3

save information if repeat solutions are to be performed later.

After these "downward operations" of steps 1 to 3, the matrix has become "triangularized", with an "upper triangular matrix",

$$
\begin{aligned}
2x_1 + 3x_2 - x_3 \qquad\qquad &= 20 \\
4x_2 - 3x_3 + 2x_4 &= 15 \\
x_3 - 2x_4 &= 7 \qquad\qquad\qquad\qquad \text{(III.3)}\\
5x_4 &= -10
\end{aligned}
$$

and the unknowns can now easily be found backwards by "backsubstitution": First, find xo 4, then x_3 from row 3, etc., with the result

$$
\begin{aligned}
x_4 &= -2 \\
x_3 &= 3 \\
x_2 &= 7 \\
x_1 &= 1
\end{aligned}
$$

The determinant is obtained as a byproduct in the downward operations: It is the product of the diagonal elements in the triangular matrix of Eq. (III.3),

$$\det\{[A]\} = 2\bullet4\bullet1\bullet5 = 40$$

In the transient simulation, the system of linear equations is solved repeatedly with no change in the matrix, but with changes in the "right-hand sides". In that case, the downward operations are only repeated for the vector of the right-hand side (process "repeat solution" in Table III.1), using the multiplication factors indicated on the right side in steps 1 to 3, which can conveniently be stored in the columns where the zeros are created. This produces the "lower triangular matrix"

$$\begin{array}{|ccc|} \hline 3 & & \\ -1 & 2 & \\ -2 & 0 & -4 \\ \hline \end{array}$$

As an example, assume that a repeat solution of Eq. (III.2) is sought with right-hand sides of

$$\begin{array}{|c|}\hline 1 \\ -1 \\ 2 \\ 12 \\ \hline \end{array}$$

By repeating step 1 for the right-hand sides, we obtain

$$\begin{array}{|c|}\hline 1 \\ \hline 2 \\ 1 \\ 10 \\ \hline \end{array}$$

and after step 2

$$\begin{array}{|c|}\hline 1 \\ 2 \\ \hline 5 \\ 10 \\ \hline \end{array}$$

and finally after step 3

$$\begin{array}{|c|}\hline 1 \\ 2 \\ 5 \\ \hline -10 \\ \hline \end{array}$$

which, after backsubstitution with the upper triangular matrix of Eq. (III.3), produces the results

$$x_4 = -2$$
$$x_3 = 1$$
$$x_2 = 9/4$$
$$x_1 = -19/8$$

If the matrix is symmetric, then the lower triangular matrix need not be recorded for repeat solutions. The information is already contained in the upper triangular matrix, since the rows of the upper triangular matrix divided by its negative diagonal element are equal to the columns of the lower triangular matrix. Symmetry is exploited in this way by the EMTP in the transient simulation part.

If the inverse of [Y] in Eq. (III.1) were known, then it appears to be more straightforward to make repeat solution with simple matrix multiplications,

$$[V] = [Y]^{-1}[I] \tag{III.4}$$

This notational elegance is deceiving, however, because it ignores the computational burden of obtaining the inverse matrix $[Y]^{-1}$ in the first place. As it turns out, the numerical process for inverting the matrix takes us right back to the elimination techniques for solving linear equations. Essentially, the inverse of a matrix is found by applying the solution process to the N columns of the unit matrix as right-hand sides, which amounts to N repeat solutions, or

N^3 operations. On the other hand, the elimination process "for matrix" in Table III.1 requires only $N^3/3$ operations, with the number of operations in a repeat solution and in the multiplication of Eq. (III.4) both being N^2. Therefore, systems of linear equations should never by solved by using the inverse, because triangularization of the matrix takes only 1/3 of the operations required for matrix inversion. There are only three excused for using the inverse, namely

(a)   in cases where N is so small that computer time is insignificant,

(b)   in cases where the matrix is used so often that the time spent for its one-time inversion is negligible compared with the numerous multiplications with Eq. (III.4), as in the case of updating history terms of couple branches in Eq. (3.9), with N usually being small as well, and

(c)   in cases where the inverse matrix is needed explicitly, as in the computation of the capacitance matrix from the potential coefficient matrix (Eq. (4.23) in Section 4.1.1.2), or in calculating $(\Delta t/2)[L]^{-1}$ of couple branches (Eq. (3.8) in Section 3.2).

III.2 Gauss-Jordan Elimination by Diagonalization

This method is used for the inversion of small, full matrices of coupled branches in the EMTP, and for matrix inversion in the support routine LINE CONSTANTS, in a version which exploits the symmetry of the matrix. The writer chose it over inversion based on Gauss elimination many years ago because it requires basically the same number of operations, namely $N^3/2$ and because it is easier to program in a way which works for matrix inversion as well as for matrix reduction. Gauss-Jordan elimination is very similar to Gauss elimination, except that in step 1 one does not only produce zeros in the column below the diagonal element, but above the diagonal as well. The solution is available immediately after the downward operation; there are no linear equations, with the example of Eq. (III.2).

Step 1: Divide first row by Y_{11}, and add such multiples of the modified first row to all other rows that zeros are produced in column 1 of these rows:

1	3/2	-1/2	0		10
0	4	-3	2		15
0	-8	7	-6		-23
0	0	4	-3		18

Step 2: Divide second row by Y_{22}, and add such multiples of the modified second row to all other rows that zeros are produced in column 2 of these rows:

1	0	5/8	-3/4		35/8
0	1	-3/4	1/2		15/4
0	0	1	-2		7
0	0	4	-3		18

Step 3: Divide third row by Y_{33}, and add such multiples of the modified third row to all other rows that zeros are

produced in column 3 of these rows:

1	0	0	1/2	0
0	1	0	-1	9
0	0	1	-2	7
0	0	0	5	-10

Step 4: Divide fourth row by Y_{44}, and add such multiples of the modified fourth row to all other rows that zeros are produced in column 4 of these rows:

1	0	0	0	1
0	1	0	0	7
0	0	1	0	3
0	0	0	1	-2

This final step gives the solution, since the matrix has now been transformed into a unit matrix.

$$x_1 = 1$$
$$x_2 = 7$$
$$x_3 = 3$$
$$x_4 = -2$$

III.3 Subroutines REDUCT and CXRED for Matrix Inversion, Reduction and Solution of Equations with Symmetric Matrices

By applying the Gauss-Jordan process simultaneously to N right-hand sides in the form of a unit matrix, the inverse matrix will be produced. The unit matrix need not be stored as such, because the nontrivial values generated in each step can conveniently be stored in the columns in which the zeros are created. After the final step, the original matrix will have been changed to its inverse in its own place. Since the matrices requiring inversion are all symmetric in the EMTP, Shipley's version of the Gauss-Jordan process is used [43], which takes advantage of symmetry. In that process, the original matrix is replaced by its <u>negative</u> inverse. The subroutines REDUCT for real matrices and CXRED for complex matrices use this version for matrix inversion as well as for matrix reduction. In the reduction option, the last rows and columns M+1, ... N are eliminated, and operations in certain parts of the matrix are skipped, which in effect changes the process from Gauss-Jordan to Gauss elimination. The subroutine REDUCT has been changed in UBC in 1982 to solve linear equations with symmetric matrices by Gauss elimination as well. The process works as follows, keeping in mind that the matrix is symmetric and that only elements in and below the diagonal are processed, since $a_{ik} = a_{ki}$. In step j, where j is counted backwards[3] from N, N-1, to M+1,

---

[3]Eliminations are done backwards, eliminating X_N first, then X_{N-1}, etc., so that the last rows and columns can be eliminated in the matrix reduction option.

process row j as follows:

$$Y_{jk}^{new} = d \cdot Y_{jk}^{old}, \quad k = 1, \dots N, \text{ except for } j \tag{III.5}$$

with

$$d = -\frac{1}{Y_{jj}^{old}} \quad and \quad Y_{jj}^{new} = d \tag{III.6}$$

$$Y_{ik}^{new} = Y_{ik}^{old} + Y_{ij}^{old} \cdot Y_{jk}^{new}, \quad k = 1, \dots i, \text{ except for } j \tag{III.7}$$

and

$$Y_{ij}^{new} = d \cdot Y_{ij}^{old} \tag{III.8}$$

If M=0, this will produce the negative inverse. If $0 < M < N$, this will produce a reduced matrix of order M.

The case of matrix reduction may warrant further explanations. Let the components in the vectors be partitioned into 2 subsets 1 and 2. With corresponding partitioning of the matrices we get

$$\begin{bmatrix} [Y_{11}] & [Y_{12}] \\ [Y_{21}] & [Y_{22}] \end{bmatrix} \begin{bmatrix} [V_1] \\ [V_2] \end{bmatrix} = \begin{bmatrix} [I_1] \\ [I_2] \end{bmatrix}$$

or

$$[Y_{11}][V_1] + [Y_{12}][V_2] = [I_1] \tag{III.9}$$

$$[Y_{21}][V_1] + [Y_{22}][V_2] = [I_2] \tag{III.10}$$

The objective is to arrive at a reduced system of equations for subset 1. The procedure used in the subroutines is that of Eq. (III.5) to (III.8), but may be easier to understand with the following matrix equations:

Solve Eq. (III.10) for $[V_2]$,

$$[V_2] = -[Y_{22}]^{-1}[Y_{21}][V_1] + [Y_{22}]^{-1}[I_2] \tag{III.11}$$

and insert this into Eq. (III.9), which yields the reduced system of equations

$$[Y_{11}^{reduced}][V_1] = [I_1] + [D_{12}][I_2] \tag{III.12}$$

with the reduced matrix

$$[Y_{11}^{reduced}] = [Y_{11}] - [Y_{12}][Y_{22}]^{-1}[Y_{21}] \tag{III.13}$$

and the distribution factor matrix

$$[D_{12}] = -[Y_{12}][Y_{22}]^{-1} \tag{III.14}$$

The name "distribution factor matrix" for $[D_{12}]$ comes from the fact that, when multiplied with the currents $[I_2]$ at the eliminated nodes, it distributes their effects to the retained nodes 1, as can be seen from the right-hand side of Eq. (III.12). This distribution factor matrix is never needed in the EMTP because reduction is only used in cases

where $[I_2]=0$; the subroutine REDUCT could easily be modified to produce $[D_{12}]$ as well as the reduced matrix, however, by simply omitting three FORTRAN statements. The transpose $[D_{12}]^t$ is the screening factor matrix mentioned in Eq. (4.41) of Section 4.1.2.5

III.4 Gauss Elimination with Sparsity Techniques

Sparsity has been exploited intuitively for a long time. In the days of hand calculations, any body solving the three equations

$$
\begin{array}{rrrrr}
3x_1 + & 2x_2 - & 6x_3 & = & 7 \\
x_1 + & x_2 & & = & 10 \\
x_1 - & & x_3 & = & 2
\end{array}
$$

would have picked the second and third equations first, e.g., to express x_2 and x_3 as a function of x_1, and to insert these expressions into the first equation to find x_1. This is essentially the same ordering scheme which is used in computer programs today.

Sparsity techniques have been used in power system analysis since the early 1960's by W.F. Tinney and his co-workers [141] in the U.S.A., by H. Edelmann [142] in Germany, and by J. Carpentier [143] in France, and by others. There is an extensive list of references on the subject, and improvements are still being made [144]. The following explanations do not cover all the details, but they should be sufficient to understand how sparsity is sued in the EMTP.

III.4.1 Basic Idea

Let us assume that we have to solve the node equations for the network of Fig. III.1, and let us use an "X" to indicate nonzero entries in the nodal admittance matrix of Eq. (III.1). Then the node equations
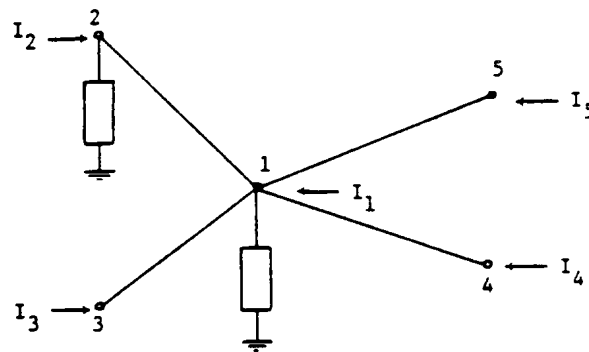
Fig. III.1 - Simple network

have the form

$$
\begin{vmatrix}
X & X & X & X & X \\
X & X & & & \\
X & & X & & \\
X & & & X & \\
X & & & & X
\end{vmatrix}
\begin{bmatrix}
V_1 \\ V_2 \\ V_3 \\ V_4 \\ V_5
\end{bmatrix}
=
\begin{bmatrix}
I_1 \\ I_2 \\ I_3 \\ I_4 \\ I_5
\end{bmatrix}
\tag{III.15}
$$

After triangularization, the equations will have the following form:

$$
\begin{vmatrix}
X & X & X & X & X \\
& X & X & X & X \\
& & X & X & X \\
& & & X & X \\
& & & & X
\end{vmatrix}
\begin{bmatrix}
V_1 \\ V_2 \\ V_3 \\ V_4 \\ V_5
\end{bmatrix}
=
\begin{bmatrix}
I_1' \\ I_2' \\ I_3' \\ I_4' \\ I_5'
\end{bmatrix}
\tag{III.16}
$$

The triangular matrix is now full, in contrast to the original matrix which was sparse. The "fill-in" is, of course, produced by the downward operations in the elimination process. This fill-in depends on the node numbering, or in other words, on the order in which the nodes are eliminated. To show this, let us exchange numbers on nodes 1 and 5 (Fig. III.1), and solve the problem again. It will be the same problem and we will get the same solution because assigning numbers to the nodes is really arbitrary. The node equations now have the form

$$
\begin{vmatrix}
X & & & & X \\
& X & & & X \\
& & X & & X \\
& & & X & X \\
X & X & X & X & X
\end{vmatrix}
\begin{bmatrix}
V_1 \\ V_2 \\ V_3 \\ V_4 \\ V_5
\end{bmatrix}
=
\begin{bmatrix}
I_1 \\ I_2 \\ I_3 \\ I_4 \\ I_5
\end{bmatrix}
\tag{III.17}
$$

which becomes after triangularization:

$$
\begin{vmatrix}
X & & & & X \\
& X & & & X \\
& & X & & X \\
& & & X & X \\
& & & & X
\end{vmatrix}
\begin{bmatrix}
V_1 \\ V_2 \\ V_3 \\ V_4 \\ V_5
\end{bmatrix}
=
\begin{bmatrix}
I_1' \\ I_2' \\ I_3' \\ I_4' \\ I_5'
\end{bmatrix}
\tag{III.18}
$$

III-10
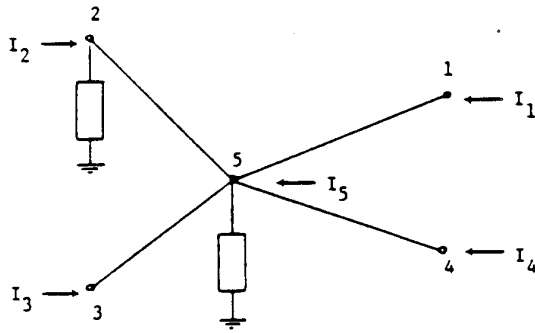
Fig. III.2 - Nodes 1 and 5 re-
numbered

Now there is no fill-in at all (in general, there will be some fill-in). This saving was achieved by just numbering the nodes in a slightly different order, or in other words, sparsity can be preserved by using "good" ordering.

The simplest "good" ordering scheme is as follow: Number nodes with only 1 branch connected first, then number nodes with 2 branches connected, then nodes with 3 branches connected, etc. Better ordering schemes are discussed in [141], with Scheme 2 probably being the best compromise between time spent on finding a near-optimal order and the savings achieved through sparsity. Scheme 2 is used in the steady-state and transient solution part of the BPA EMTP. The UBC EMTP uses re-ordering only in the transient solution part.
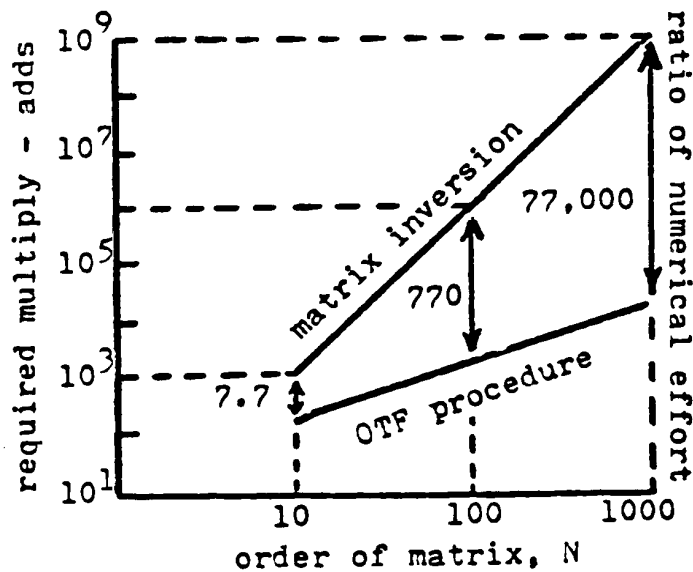
Fig. III.3 - Comparison of the numerical effort between matrix inversion and ordered triangular factorization for typical power networks [145]. © 1973 IEEE

Exploitation of sparsity is extremely important in large power systems because it reduces storage requirements and solution times tremendously. The curves in Fig. III.3, taken from a tutorial paper by Tinney and Meyer [145], clearly show this. The solution time for full matrices is proportional to N^3. For sparse power systems it increases about <u>linearly.</u> Typically, the number of series branches is about 1.6 x (number of nodes) and the

III-11

number of matrix elements in the upper triangular matrix is about 2.5 to 3 times the number of nodes in steady-state equations. The node equations (1.8) for the transient solution are usually sparser because distributed-parameter lines do not contribute any off-diagonal elements.

Fig. III.4 shows the steady-state nodal admittance matrix of a single-phase (positive sequence) network with 127 nodes and 153 branches, before triangularization in the lower triangular part, and after triangularization in the upper triangular part, with optimal ordering base on Scheme 2. The fill-in elements are indicated by the symbol "O", whereas "X" indicates the original elements. Because of fill-in, the number of off-diagonal elements in the upper triangular matrix grows from 153 to 229, but this is still very sparse compared with 8001 elements in a full matrix.
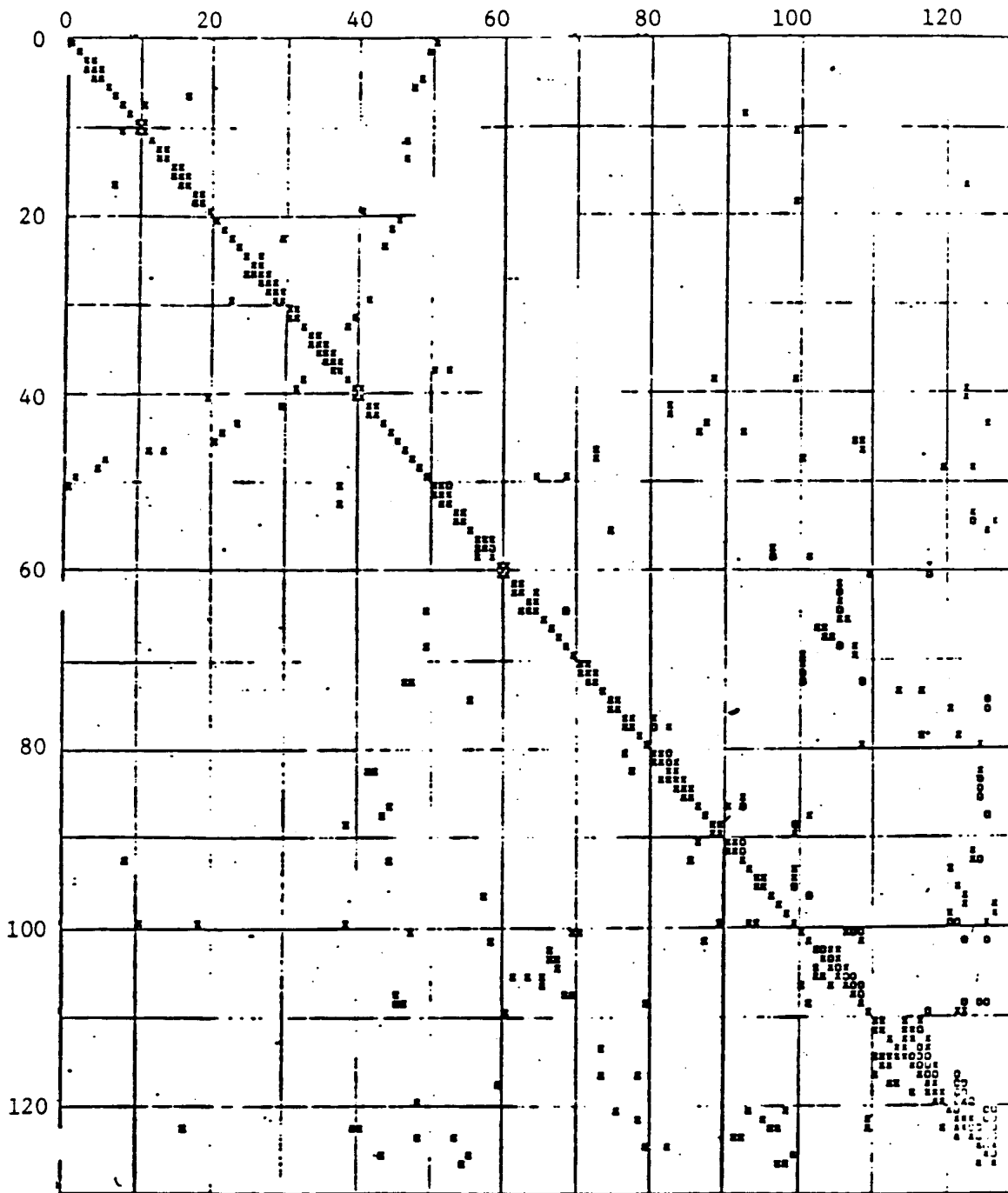
Fig. III.4 - Nonzero pattern of symmetric matrix before triangularization shown below diagonal and after triangularization shown above diagonal, for a network with 127 nodes

III.4.2 Row-by-row Elimination with Static Storage

While there are many variations of the basic Gauss elimination and associated sparse storage schemes, the best choice for power system analysis seems to be row-by-row elimination with static storage. This is the scheme used in the EMTP. Its two basic concepts are:

(a)   The non-zero pattern of the triangularized [Y] - or [G] - matrix need not be known in advance (even though

it could be obtained as a by-product of the re-ordering subroutine), but the nodes must be re-numbered near-optimally for minimum fill-in.

(b)   As each row of the upper triangular matrix is built, it is stored away once and for all and never changed again (static storage). Since the nodal matrices are symmetric in the steady-state as well as in the transient solution part, the lower triangular matrix is not needed.

Concept (b) rules out the "textbook approach" to elimination shown in Section III.1, in which zeros are produced column by column in the lower triangular matrix, because the resulting reduced matrices change with fill-in elements from one elimination step to the next.

Row-by-row elimination on the matrix elements with static storage works basically as follows (Fig. III.5):
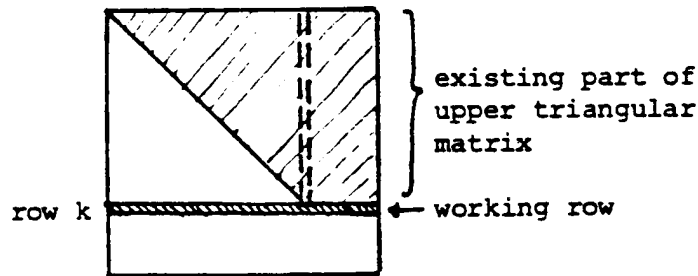
Fig. III.5 - Row-by-row elimination

1.   Set elimination step k = 0.

2.   Increase k by 1.

3.   Stop process if k > N.

4.   Build row k of [Y] from branch tables in a one-dimensional "working row" array (or transfer data into working row if [Y] is already available). Use either a full working row scheme or a packed working row scheme, as discussed in Section III.4.3

5.   In the working row, eliminate $Y_{k,1}$ (if nonzero) by adding the appropriate multiple of row 1 of the already existing part of the upper triangular matrix. Then eliminate $Y_{k,2}$ (if nonzero) in an analogous way, then $Y_{k,3}$ etc., up to $Y_{k,k-1}$. Note that rows of the existing part of the upper triangular matrix are only recalled from storage, but not modified (static storage).

6.   Store the diagonal element in a table of length N (or its reciprocal on computers where division takes more time than multiplication), and add the nonzero elements Ym to the right of it (m > k) in compact form to the existing part of the upper triangular matrix, e.g., with the row pointer/column index scheme of Section III.4.4. Since the matrices in the EMTP are symmetric, only the upper triangular matrix has to be stored.

7.   Return to step 2.

If there is only one solution, as in the steady-state initialization, then the right-hand side [I] is processed together with [Y] as if it were an extra (N+1)-th column.

For the repeat solutions in the transient solution part, the downward operations are made with the rows of the upper triangular matrix, since the elements of row k of the upper triangular matrix, divided by the negative diagonal element, are the multiplication factors usually stored in column k of the lower triangular matrix. If

YREC(K) is reciprocal of the diagonal element, if R(I) is right-hand side, if YU(J) are the off-diagonal elements of row k of the upper triangular matrix, and if MU(J) are the column indices m of these elements, then elimination step k of a repeat solution would be more or less similar to the following Fortran statements:

```
         A = R(K) * YREC(K)
         DO 10  J = (beginning of row), (end of row)
         M = MU(J)
10       R(M) = R(M) - YU(J) * A
```

III.4.3 Working Row

For the working row discussed in step 4 of the preceding section, and indicated in Fig. III.5, a full row can be used with a one-dimensional array of dimension N, in which zero elements are actually represented by zero values. In the eliminations of step 5 and in storing nonzero elements in step 6 of the preceding section, each element must be checked whether it is nonzero. This costs extra computer time, which is the price one has to pay for the simplicity of the full working row scheme, where fill-ins "fall naturally" into their proper location during the elimination process of step 5 (preceding section). A full working row scheme can be used in situations where the extra time of checking for zeros is not very important in the total computer time. This is more or less the case in the transient solution part of the EMTP, where the [G]-matrix is only triangularized occasionally, namely at the beginning of the time step loop and whenever switches change their position. Therefore, the UBC EMTP and older versions of the BPA EMTP use a full working row scheme. No additional storage is needed for that row, because the one-dimensional array needed in the time step loop for the right-hand side is available at the time of triangularization.

For utmost speed, packed working row schemes should be used, especially if the matrix is re-triangularized frequently. This situation arose with the simulation of HVDC systems, where the switches representing the valves open and close after every 20 steps or so. Newer versions of the BPA EMTP therefore use a packed working row scheme, which is essentially the same as the one described in [146] in table IX. In spite of the necessity of additional indexing tables, enough storage space and computer time is saved to justify the additional complications it entails.

III.4.4 Row Pointer/Column Index Storage Scheme

Before discussing the compact storage of the upper triangular matrix, it should be remembered that a separate array is used for the working row, e.g.,

REAL ROW(N) for a full working row and real (not complex)matrix elements,

REAL ROW(M) for a packed working row with $M < N$ according to [146]
INTEGER NEXT(M), KOL(M)

A row pointer/column index scheme in the form discussed next, or in a similar form, seems to offer the best choice in terms of ease of access and economy of space. Note that such a scheme cannot only be used for storing the triangular matrix in compact form, but also for storing the original [Y]-matrix in compact form.

The diagonal elements (or their reciprocals on computers where division takes noticeably longer than

multiplication) are stored in a one-dimensional array of dimension N, say in YDIAG (Fig. III.6). The nonzero off-diagonal elements of the upper triangular matrix are stored row-by-row in another one-dimensional array of dimension larger than N, (typically 3.5*N), say in YU, with the starting address of each row available from a row-pointer table of length N+!, say in KSTART. The address of the last entry in a row is simply the starting address of the following row minus 1, which explains why an (N+1)-th entry is needed in KSTART. Obviously, the column numbers get lost when elements are packed into YU. Therefore, an extra column index table, say MU, is required, as indicated in Fig. III.6. The overhead burden of this extra table,

table of length N for diagonal elements (or their reciprocals)

table of length N + 1 for row pointer

table YU for elements of upper triangular matrix and table MU for associated column indices

	YDIAG		KSTART		YU	MU
1	(real)	1	(integer)	1	(real)	(integer)
.		.		.		
.		.		.		
.		.		.		
N		N				
		N+1		≈ 3.5*N		
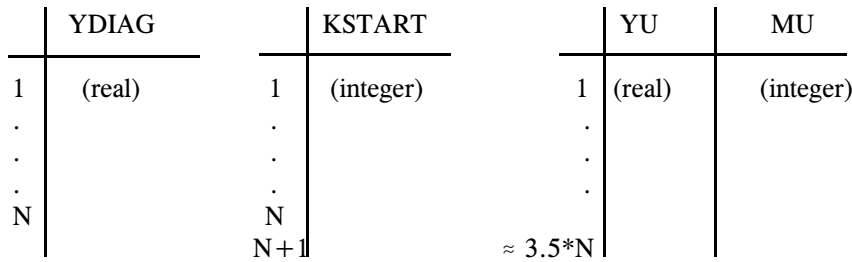
Fig. III.6 - Row pointer/column index storage scheme

of this extra table, which becomes less for complex elements in the steady-state solution because only YU would have to be replaced by two tables but MU would still be a single table, is trivial for large matrices when the total storage requirements are compared with the alternative of storing a full matrix in a two-dimensional array. Experience has shown that the number of words for compact storage is proportional to N (as is the computer time), whereas the number of words required for storing a full matrix is proportional to N^2 (Table III.2). If N = 1000 in Table III.2,

Table III.2 - Storage requirement for upper triangular matrix and for vectors needed for repeat solutions in case of symmetric matrices [147]

	real elements	complex elements
compact storage	9.8 * N	15.2 * N
full storage	$\dfrac{N^2 + N}{2} + 2N$	$N^2 + N + 4N$

then 9,800 words would be needed for a real matrix and 15,200 words for a complex matrix, compared with 502,500 words and 1,005,000 words, respectively, for storing a full matrix. The savings are 98% and 98.5% respectively.

III.4.5 Special Techniques for Symmetric Matrices

The matrices [Y] for the steady-state solution as well as [G] for the transient solution are both symmetric. Symmetry can be exploited in two ways:

(a)   The lower triangular matrix need not be stored for repeat solutions, and

(b)   only elements to the right of the diagonal must be processed in step 5 of Section III.4.2, which cuts the operation count in the elimination process for the matrix approximately in half. No savings can be gained in repeat solutions, however.

Point (a) has been discussed in Section III.4.2; it results from the fact that a column of the lower triangular matrix is equal to the respective row of the upper triangular matrix, divided by the negative diagonal element. This point is exploited in the EMTP.

Point (b) is true because the multiplication factors needed for the elimination of $Y_{k,1}$, $Y_{k,2}$, ... in step 5 of Section III.4.2 are already available in the dotted column of Fig. III.5. This is not exploited in the EMTP, since it is difficult to access this dotted column directly without some additional indexing tables. A simple way out of this problem would be to store elements of the dotted column, as they are created, in a separate table for the rows of the lower triangular matrix, but that would defeat the advantage of point (a) above.

There is some advantage in dividing the rows of the upper triangular matrix by the diagonal element, in the loop where they are stored in step (6) of Section III.4.2. This way, N multiplications are saved in the backsubstitution of the repeat solution, at the expense of one extra multiplication for each off-diagonal element in the triangular matrix. When the EMTP was first written, it was assumed that the matrix will only be triangularized occasionally (before entering the time step loop and whenever switches change their position). Therefore, division by the diagonal elements was chosen to keep the operation count in the repeat solutions inside the time step loop as low as possible. In simulating HVDC systems, the savings in the time step loop may become less than the extra operations needed for multiplying the off-diagonal elements with the reciprocal of the diagonal element.

With division by the diagonal elements, the matrix process is only modified in step (6) of Section III.4.2. In step (2) it must be realized of course that the elements of the upper triangular matrix are no longer Y_{km}, but Y_{km}/Y_{kk}.

The process for repeat solutions with the storage scheme of Section III.4.2 works roughly as follows. Downward operations:

1.   Set elimination step k = 0.

2.   Increase k by 1.

3.   Go to backsubstitution if k > N.

4.   Get compact row k of the triangular matrix from storage, and

(a)   save k-th component of right-hand side, A = R(K),

(b)   multiply k-th component with reciprocal of diagonal element, R(K0 = A * YREC(K)

(c)   modify all components of right-hand side for which entries exist in row k of the triangularized matrix (diagonal element excluded):

DO XX   J = (beginning of row), (end of row)

$$M = MU(J)$$

$$R(M) = R(M) - YU(J)*A$$

5.   Return to step 2.

Backsubstitutions (R will be replaced by solution vector):

1.   Set counter k = N.

2.   Decrease k by 1.

3.   Stop process if k = 1.

4.   Get compact row k of the triangular matrix from storage, and find the solution for k-th component with the following loop (diagonal element excluded):

$$A = R(K)$$

$$DO \; XX \quad J = (beginning \; of \; row), (end \; of \; row)$$

$$M = MU(J)$$

$$XX \;\; A = A - YU(J)*R(J)$$

$$R(K) = A$$

5. Return to step 2.

APPENDIX IV - ACTUAL VALUES VERSUS PER-UNIT QUANTITIES

The use of per-unit quantities has been customary for so many years in the electric power industry, that it is not always recognized that actual values can be used just as easily, and that the per-unit system may have outlived its usefulness. This writer sees no advantages in working with per-unit quantities, and feels much more comfortable with actual values.

The widespread use f per-unit quantities probably started with network analyzers in the 1930's. For power flow and short-circuit studies on network analyzers, per-unit quantities offered two advantages, namely scaling of impedances to values available on the analyzer, and the possibility of representing transformers as simple series impedances as long as their turns ratio was identical to the ratio of the base voltages on the two sides. Somewhat similar arguments for per-unit quantities could be made in the early days of digital computers with fixed-point arithmetic, where the order of magnitude of intermediate and final results had to be about the same. On modern computers with floating-point arithmetic, there is no reason, however, why one shouldn't work directly with actual values.

IV.1 Per-Unit Quantities

A per-unit quantity is the ratio of the actual value of a quantity to the base value of the same quantity [76, p. 482]. It has been customary to use one common base power S_{base} (apparent power) for the entire system (typically 100 MVA), and a different base voltage for each voltage level (e.g., $V_{base} = 115$ kV and $V_{base} = 230$ kV in a 115/230 kV system) as the base values. Then the per-unit quantities in a single-phase network are

$$I_{p.u.} = I_{actual} \cdot \frac{V_{base}}{S_{base}}$$

$$V_{p.u.} = \frac{V_{base}}{V_{base}}$$

$$Y_{p.u.} = Y_{actual} \cdot \frac{V_{base}^2}{S_{base}}$$

$$Z_{p.u.} = Z_{actual} \cdot \frac{S_{base}}{V_{base}^2}$$

(IV.1)

It may be safest to use these single-phase equations for three-phase networks as well. In wy-connected equipment, S_{base} would be the single-phase base power of one winding (e.g., 100/3 MVA) and Vase would be the base voltage across each winding, namely the phase-to-ground base voltage (e.g., 113/√3 kV and 230/√3 kV). In delta-connected equipment, S_{base} would again be the single-phase base power of each winding (e.g., 100/3 MVA), whereas the base voltage V_{base} across each winding would now be the phase-to-phase base voltage (e.g., 115 kV and 23 kV).

The following, well-known formulas with three-phase base values were developed for positive sequence

power flow studies, where the distinction between wye- and delta-connections gets lost in the conversion from three-phase representations to equivalent single-phase representations for balanced operation:

$$I_{p.u.} = I_{actual} \cdot \sqrt{3} \; \frac{V_{base-phase-to-phase}}{S_{base-three-phase}}$$

$$V_{p.u.} = \frac{V_{actual}}{V_{base}} \; (numerator \, and \; denominator \, either \; both \; phase\text{-}to\text{-}phase \, or \; both \, phase\text{-}to\text{-}ground)$$

$$Y_{p.u.} = Y_{actual} \cdot \frac{(V_{base-phase-to-phase})^2}{S_{base-three-phase}} \tag{IV.2}$$

$$Z_{p.u.} = \frac{1}{Y_{p.u.}}$$

Eq. (IV.2) cannot only be used for the conversion of positive sequence parameters, but for negative and zero sequence parameters as well, as shown in the example of Section IV.3.

Per-unit quantities, as ratios of actual to base values, are meaningless if the base values are not listed as part of the data as well. For example, the positive sequence series impedance of an overhead line is fully described by three actual values,

$$R_{pos}^{/} + j\omega L_{pos}^{/} = 0.05 + j0.40 \; \Omega/km, \;\; f = 60 \; Hz$$

or if R'$_{pos}$ and L'$_{pos}$ are independent of frequency, by two values,

$$R'_{pos} = 0.05 \; \Omega/km, \quad L'_{pos} = 1.061 \; mH/km$$

On the other hand, the record for per-unit quantities consists of 5 values,

R'$_{pos}$ + jωL'$_{pos}$ = 9.45$\bullet$10^{-5} + j75.61$\bullet$10^{-5} p.u., f = 60 Hz, S$_{base}$ = 100 MVA (three phase), V$_{base}$ = 230 kV (phase-to-phase).

With R'$_{pos}$ and L'$_{pos}$, the frequency could be dropped from the record, but the time base should then be added,

R'$_{pos}$ = 9.45$\bullet$10^{-5} p.u., L'$_{pos}$ = 20.06$\bullet$10^{-7} p.u., S$_{base}$ = 100 MVA (three-phase), V$_{base}$ = 230 kV (phase-to-phase), t$_{base}$ = 1s.

Adding the time base may seem superfluous, but there are stability programs which use cycles (of 60 Hz) as a time base, in which case L'$_{pos}$ = 12.03$\bullet$10^{-5} p.u., t$_{base}$ = 1/60 s.

IV.2 Conversion from One Base to Another

If per-unit data is to be exchanged among utilities and manufacturers, then it is important to include the base

values, especially if one party customarily uses base values which are different from those used by the other party. For example, a transformer manufacturer lists the short-circuit input impedance in per-unit based on the voltage and power nameplate ratings of the transformers,

$$Z_{p.u.}^{manufacturer} = Z_{actual} \cdot \frac{S_{nameplate}}{(V_{nameplate})^2} \tag{IV.3}$$

In a particular case, these base values might be 660 MVA (three-phase) and 241.5 kV (phase-to-phase). Utility companies generally use different base values (e.g., $S_{base} = 100$ MVA, $V_{base} = 230$ kV). By solving Eq. (IV.3) for Z_{actual} and using Eq. (IV.2) to get back to per-unit quantities, one obtains

$$Z_{p.u.}^{utility} = Z_{p.u.}^{manufacturer} \cdot (\frac{V_{nameplate}}{V_{base}})^2 \cdot \frac{S_{base}}{S_{nameplate}} \tag{IV.4}$$

Obviously, the per-unit quantity of the manufacturer will be quite different from the one used by the utility company.

In general, the formulas for conversion from base "1" to base "2" are

$$
\begin{aligned}
I_{p.u.}^{base\ 2} &= I_{p.u.}^{base\ 1} \cdot \frac{S_{base\ 1}}{S_{base\ 2}} \cdot \frac{V_{base\ 2}}{V_{base\ 1}} \\
V_{p.u.}^{base\ 2} &= V_{p.u.}^{base\ 1} \cdot \frac{V_{base\ 1}}{V_{base\ 2}} \\
Y_{p.u.}^{base\ 2} &= Y_{p.u.}^{base\ 1} \cdot \frac{S_{base\ 1}}{S_{base\ 2}} \cdot (\frac{V_{base\ 2}}{V_{base\ 1}})^2
\end{aligned}
\tag{IV.5}
$$

IV.3 Actual Values Referred to One Side Transformer

The advantage of representing transformers as simple series impedances with per-unit quantities, as long as their turns ratio is identical to the ratio of the base voltages, exists with actual values as well, if the quantities on one side are referred to the other side. In the example of Fig. IV.1, quantities on the low voltage side are referred to the high voltage side with

$$
\begin{aligned}
I_{high} &= I_{low} \cdot \frac{15}{241.5} \\
V_{high} &= V_{low} \cdot \frac{241.5}{15}
\end{aligned}
\tag{IV.6}
$$

$$
\begin{aligned}
Y_{high} &= Y_{low} \cdot (\frac{15}{241.5})^2 \\
Z_{high} &= Z_{low} \cdot (\frac{241.5}{15})^2
\end{aligned}
$$

15 kV / 241.5 kV
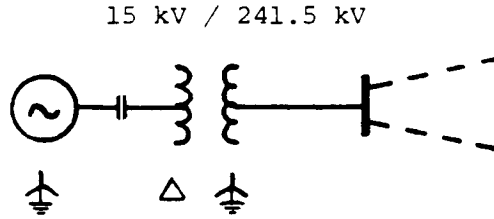
Fig. IV. 1 - Generator with step-up transformer. Generator data: $X_d" = X_q" = 10\%$ based on rating of 13.8 kV and 180 MVA. Transformer data: $X_{pos} = X_{zero} = 8\%$ based on rating of 15/241.5 kV and 250 MVA

(a) positive   (b) negative   (c) zero
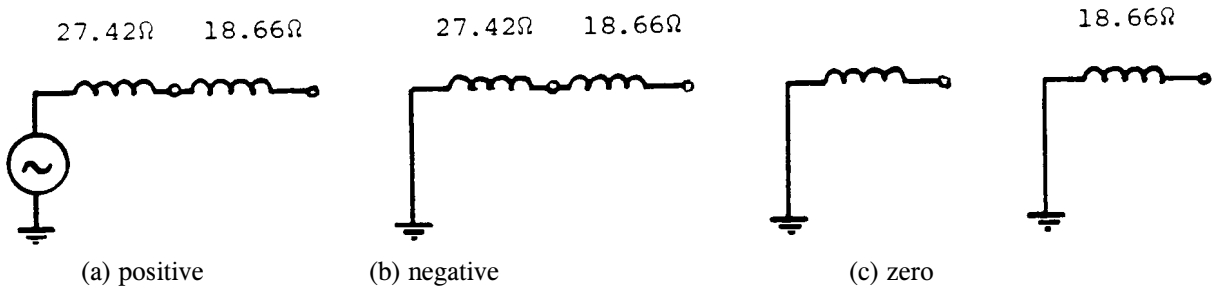
Fig. IV.2 - Positive, negative, and zero sequence networks seen from high side

This conversion to the high side is advantageous if the generator and step-up transformer are to be replaced by a Thevenin equivalent circuit seen from the high side. With the data of Fig. IV.1, the positive, negative and zero sequence networks of Fig. IV.2 are obtained as follows: For the transformer,

$$X_{actual} = 0.08 \ \frac{241.5^2}{250} \ \Omega = 18.66 \ \Omega \quad (seen \ high \ side)$$

and for the generator,

$$X_{actual} = 0.10 \ \frac{13.8^2}{180} \ \Omega = 0.1058 \ \Omega \quad (seen \ high \ side)$$

or

$$X_{actual} = 0.1058 \ (\frac{241.5}{15})^2 \ \Omega = 27.42 \ \Omega \quad (seen \ high \ side)$$

Note that the delta connection provides a short-circuit for the zero sequence currents (Fig. IV.2(c)). With $X_{pos} = X_{neg} = 46.08 \ \Omega$, $X_{zero} = 18.66 \ \Omega$, the final three-phase Thevenin equivalent circuit of Fig. IV.3 is obtained by converting the sequence reactances to self and mutual reactances with Eq. (3.4). The amplitude of the Thevenin

voltages is set equal to the voltage seen on the high side for the particular operating condition, which may be 230 kV phase-to-phase in a particular case.
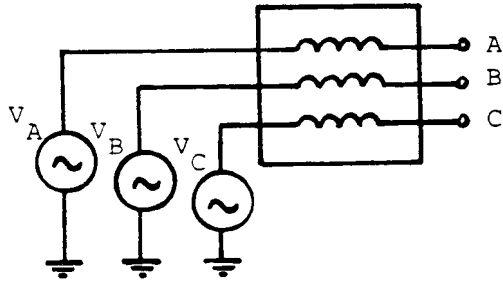
3x3 reactance matrix

$$\begin{bmatrix} X_s & X_m & X_m \\ X_m & X_s & X_m \\ X_m & X_m & X_s \end{bmatrix}$$

Fig. IV.3 - Three-phase Thevenin equivalent circuit. Symmetric voltage sources V_A, V_B, V_C with RMS amplitude of $230/\sqrt{3}$ kV; $x_s = 36.94\ \Omega$, $X_m = -9.14\ \Omega$

One could also use per-unit quantities for the Thevenin equivalent circuits of Fig. IV.2, with the transformer ratings as base values. In that case, $X = 0.08$ p.u. for the transformer, and with Eq. (IV.5),

$$X = 0.10 \cdot (250/180) \cdot (13.8/15)^2 \text{ p.u.} = 0.1176 \text{ p.u.}$$

for the generator. Then, $X_{pos} = X_{neg} = 0.19756$ p.u., $X_{zero} = 0/08$ p.u., which leads to $X_{pos} = X_{neg} = 46.08\ \Omega$, $X_{zero} = 18.66\ \Omega$ with $S_{base} = 250$ MVA (three-phase) and $V_{base} = 241.5$ kV (phase-to-phase).

IV.4 Advantages of Actual Values

This writer prefers actual values over per-unit quantities for the following reasons:

(1)   Confusion may arise with per-unit quantities because the base values are not always clearly stated. This confusion cannot arise with actual values.

(2)   The data record is shorter for actual values, as shown in the last paragraph of Section IV.1, even if S_{base} in the per-unit record is left off, with the understanding that it is always 100 MVA.

(3)   Actual values are fixed characteristics of a piece of equipment, independent of how this equipment is being used. This is not true for per-unit quantities: If a 500 kV shunt reactor is temporarily used on a 345 kV circuit, its per-unit values based on 500 kV would have to be converted to a base of 345 kV.

(4)   Since the ratio of transformer voltage ratings is not always equal to the ratio of base voltages, one has to allow for "off-nominal" turns ratios (unequal 1:1) with per-unit quantities anyhow. If one has to allow for any ratio, then a ratio of 1:1.05 for per-unit quantities is neither easier nor more difficult to handle than a ratio of 15 kV:241.5 kV for actual values. Therefore, one might as well use actual values. Furthermore, the simple series impedance representation of transformers with per-unit ratios of 1:1 (Fig. 3.3(c) with $t = 1.0$) can seldom be used in EMTP studies. For example, a three-phase bank of single-phase transformers in wye-delta connection would require a 2x2 [Y]-matrix model for each transformer, or alternatively, an equivalent circuit representation with uncouple reactances as shown in Fig. 3.3(b). The case of $t = 1.0$ offers no advantage whatsoever in that six-branch circuit.

(5)   If test data is available in per-unit quantities, e.g., for generators or transformers, then conversions are even necessary for per-unit values, since the base values do in general not agree with the nameplate ratings. Therefore, one might as well convert to actual values. Furthermore, the EMTP does this conversion in most cases anyhow, e.g., in the main program in the case of generators, or in supporting routines in the case of transformers.

(6)   All digital computers use floating-point arithmetic nowadays, and therefore accept numbers over a wide range of magnitudes. Therefore, the numbers do not have to be of the same order of magnitude, and a turns ratio of 15 kV:241.5 kV causes no more problems than a turns ratio of 1:1.05.

Sometimes the question is raised whether solutions with per-unit values aren't possibly more accurate than solutions with actual values. Many years ago on computers with fixed-point arithmetic, per-unit values may indeed have produced more accurate than the other. To show this, let us look at the steady-state solution of a single-phase network with nodal equations,

$$[Y_{actual}] \, [V_{actual}] = [I_{actual}] \tag{IV.7}$$

where $[I_{actual}]$ is given, and $[V_{actual}]$ is to be found. In general, the network will have two or more voltage levels, which will be taken into account in $[Y_{actual}]$ with the proper transformer turns ratios. To convert Eq. (IV.7) to per-unit quantities, the base voltages are first defined in the form of a diagonal matrix,

$$[V_{base}] = \begin{bmatrix} V_{base\ 1} & & & & \\ & V_{base\ 2} & & & \\ & & \cdot & & \\ & & & \cdot & \\ & & & & V_{base\ N} \end{bmatrix} \tag{IV.8}$$

with the possibility of each node having its own base voltage. In reality of course, all nodes within one voltage level would have the same base value. With S_{base} being the same for the entire network, the current and voltage vectors in per-unit and actual values are related by

$$[I_{p.u.}] = (1/S_{base})[V_{base}][I_{base}] \tag{IV.9}$$

$$[V_{actual}] = [V_{base}][V_{p.u.}] \tag{IV.10}$$

Premultiplying Eq. (IV.7) with $[V_{base}]/S_{base}$, and replacing $[V_{actual}]$ with Eq. (IV.10) will produce the per-unit equations

$$[Y_{p.u.}][V_{p.u.}] = [I_{p.u.}] \tag{IV.11}$$

with

$$[Y_{p.u.}] = (1/S_{base})[V_{base}][Y_{actual}][V_{base}] \tag{IV.12}$$

Therefore, the conversion from actual to per-unit values consists of the transformation of the coefficient matrix $[Y_{actual}]$ into $[Y_{p.u.}]$ with Eq. (IV.12). This transformation is very simple since $[V_{base}]$ is a diagonal matrix: Aside from dividing all elements by the constant S_{base}, each row i (i = 1, 2, ... N) is multiplied by V_{base-i}, and each row k (k = 1, 2, ...N) is multiplied by V_{base-k}. This is essentially a scaling operation.

This scaling operation has no influence on the solution process if pivoting[1] is not used, but it may influence the accumulation of round-off errors. This influence on round-off errors is difficult to assess. For a system of linear equations, the following can however be said [77, p.39]: If scaling is done in such a way that it changes only the exponent of the floating-point number (e.g., by using $S_{base} = 128$ MVA or 2^7, $V_{base\ 1} = 128$ kV or 2^7 and $V_{base\ 2} = 512$ kV or 2^9 on a computer using base 2 for the exponents), and if the order of eliminations is not changed, then the scaled (per-unit) coefficients will have precisely the same mantissas, and all intermediate and final results will have precisely the same number of significant digits. Therefore, it is reasonable to assume that scaling will neither improve nor degrade the accuracy of the solutions. M.D. Crouch of Bonneville Power Administration has shown that this assumption is correct for power flow solutions with 48 bit precision.

IV.5 Per-Unit Voltage with Actual Impedances

Sometimes, overvoltage studies are made with impedances in actual values, but with voltage source amplitudes scaled to 1.0 p.u. or similar values,

$$V_{p.u.} = V_{actual} / V_{base}$$

This produces overvoltages expressed in per-unit, which is often preferred in insulation co-ordination studies. If there are no nonlinear elements in the network, then this approach is quite straightforward. Actual values can be obtained from the per-unit values by multiplying per-unit voltages <u>and</u> currents with V_{base}, and per-unit power with V^2_{base}.

Some care is required, however, if the network contains nonlinearities. For nonlinear resistances or inductances defined point-by-point with pairs of values v, i or ψ, i <u>both</u> values of each pair must be divided by V_{base} in the input data. If the nonlinearities are defined by their piecewise linear slopes R_1, R_2, ... or L_1, L_2, ..., and by the "knee-point" v_1, v_2, ... or ψ_1, ψ_2, ..., only these knee-point values must be divided by V_{vase} in the input data.

---

[1]Pivoting is generally not used in the EMTP, except in some subroutines for the inversion of small matrices of couple branches.

APPENDIX V - RECURSIVE CONVOLUTION

Consider the convoluted integral

$$s(t) = \int_T^\infty f(t-u)e^{-p(u-T)}du \tag{V.1}$$

to be found at time t, with $s(t-\Delta t)$ already known from the preceding time step. This known value can be expressed as

$$s(t-\Delta t) = e^{p\Delta t}\int_{T+\Delta t}^\infty f(t-u)e^{-p(u-T)}\,du \tag{V.2}$$

by simply substituting a new variable $u_{new} = u + \Delta t$ into Eq. (V.1). At the same time, the integration in Eq. (V.1) can be done in two parts,

$$s(t) = \int_T^{T+\Delta t} f(t-u)e^{-p(u-T)}\,du + \int_{T+\Delta t}^\infty f(t-u)e^{-p(u-T)}\,du$$

which becomes

$$s(t) = \int_T^{T+\Delta t} f(t-u)e^{-p(u-T)}\,du + e^{-p\Delta t}\cdot s(t-\Delta t) \tag{V.3}$$

with Eq. (V.2). Therefore, s(t) is found recursively from $s(t-\Delta t)$ with a simple integration over one single time step Δt. If we assume that f varies linearly between t-T-Δt and t-T, then [94]

$$s(t) = c_1 \bullet s(t-\Delta t) + c_2 \bullet f(t-T) + c_3 \bullet f(t-T-\Delta t) \tag{V.4}$$

with the three constants

$$c_1 = e^{-p\Delta t}$$

$$c_2 = \frac{1}{p} - \frac{1}{\Delta t\, p^2}(1 - e^{-p\Delta t}) \tag{V.5}$$

$$c_3 = -\frac{1}{p}e^{-p\Delta t} + \frac{1}{\Delta t\, p^2}(1 - e^{-p\Delta t})$$

**APPENDIX VI - TRANSIENT AND SUBTRANSIENT PARAMETERS OF
SYNCHRONOUS MACHINES**

The derivations are the same for the direct and quadrature axis. They will therefore only be explained for the direct axis. Furthermore, it is assumed that field structure quantities have been rescaled (in physical or p.u. quantities) in such a way that the mutual inductances among the three windings d, f and D are all equal, as explained in Section 8.2, except that the subscript "m" (fore modified) is dropped from Eq. (8.15a), to simplify the notation. The equations with this simpler notation are then

$$
\begin{bmatrix} \lambda_d \\ \lambda_f \\ \lambda_D \end{bmatrix} = \begin{bmatrix} L_d & M & M \\ M & L_{ff} & M \\ M & M & L_{DD} \end{bmatrix} \begin{bmatrix} i_d \\ i_f \\ i_D \end{bmatrix} \tag{VI.1}
$$

and

$$
- \begin{bmatrix} d\lambda_f/dt \\ d\lambda_D/dt \end{bmatrix} = \begin{bmatrix} R_f & 0 \\ 0 & R_D \end{bmatrix} \begin{bmatrix} i_f \\ i_D \end{bmatrix} + \begin{bmatrix} v_f \\ 0 \end{bmatrix} \tag{VI.2}
$$

In the past, it has often been assumed that the damper windings can be ignored for the transient effects, which are associated with the open-circuit or short-circuit time constants T_{do}' or T_d'. In earlier EMTP versions, this assumption was made for the definition of the transient reactance X'_d with Eq. (VI.4), while for the definition of the time constants the damper winding effects were always included. In later EMTP versions, the definition of the time constants as well as of the transient reactance takes damper winding effects into account.

VI.1 Transient Parameters with Only One Winding on the Field Structure

If there is no damper winding, or if the damper winding were to be ignored, then there is only the field winding f on the field structure[1]. The field current i_f can then be eliminated from the second row of Eq. (VI.1)

$$
i_f = \frac{\lambda_f}{L_{ff}} - \frac{M}{L_{ff}} i_d
$$

which, when inserted into the first row, produces

---

[1] This is true for the direct axis. In the quadrature axis, the analogous assumption is that either the g- or the Q- winding is missing.

$$\lambda_d = (L_d - \frac{M^2}{L_{ff}}) \, i_d + \frac{M}{L_{ff}}\lambda_f \tag{VI.3}$$

The flux λ_f cannot change instantaneously after disturbance, and can therefore be regarded as constant at first. The transient inductance which describes the flux/current relationship in the armature immediately after the disturbance is therefore

$$\lambda_d^{\,/} = L_d - \frac{M^2}{L_{ff}} \tag{VI.4}$$

The open-circuit time constant $T_{do}{}'$, which describes the rate of change of flux λ_f for open-circuit conditions ($i_d = 0$) is obtained from Eq. (VI.2) as

$$T_{do}{}' = L_{ff} / R_f \tag{VI.5}$$

As shown in the next section, the definitions of both L_d' and T_{do}' change in the presence of a damper winding.

VI.2 Subtransient and Transient Time Constants with Two Windings on the Field Structure

The open-circuit time constants are found by solving the equations for the currents i_f, i_D. By substituting the last two rows of Eq. (VI.1),

$$\begin{bmatrix} \lambda_f \\ \lambda_D \end{bmatrix} = \begin{bmatrix} M \\ M \end{bmatrix} i_d + \begin{bmatrix} L_{ff} & M \\ M & L_{DD} \end{bmatrix}\begin{bmatrix} i_f \\ i_D \end{bmatrix} \tag{VI.6}$$

into Eq. (VI.2), and by setting $i_d = 0$ for the open-circuit condition, we get

$$\begin{bmatrix} \dfrac{di_f}{dt} \\ \dfrac{di_D}{dt} \end{bmatrix} = \frac{i}{L_{ff}L_{DD} - M^2} \begin{bmatrix} -L_{DD} & M \\ M & -L_{ff} \end{bmatrix}\left[\begin{bmatrix} R_f & 0 \\ 0 & R_D \end{bmatrix}\begin{bmatrix} i_f \\ i_D \end{bmatrix} + \begin{bmatrix} v_f \\ 0 \end{bmatrix} \right] \tag{VI.7}$$

The field winding voltage v_f is the forcing function in this equation, while the open-circuit time constants must be the negative reciprocals of the eigenvalues of the matrix relating the current derivatives to the currents in Eq. (VI.7)[2]. They are therefore found by solving

$$\left(-R_f \frac{L_{DD}}{L_{ff} \, L_{DD} - M^2} + \frac{1}{T} \right) \left(\frac{-R_D \, L_{ff}}{L_{ff} \, L_{DD} - M^2} + \frac{1}{T} \right) - \frac{R_f \, R_D \, M^2}{(L_{ff} \, L_{DD} - M^2)^2} = 0$$

---

[2] The theory is explained in Appendix I.1, where it is shown that there will be two modes of the oscillations defined by terms multiplied with $e^{\lambda_1 t}$ and $e^{\lambda_2 t}$ (λ = eigenvalues). Since the eigenvalues are real and negative here, their negative reciprocals define the two time constants.

for T. The results are

$$\begin{matrix} T'_{do} \\ T''_{do} \end{matrix} = \frac{1}{2}\left(\frac{L_{ff}}{R_f} + \frac{L_{DD}}{R_D}\right) \pm \frac{1}{2}\sqrt{\left(\frac{L_{ff}}{R_f} - \frac{L_{DD}}{R_D}\right)^2 + 4\frac{M^2}{R_f\,R_D}} \tag{VI.8}$$

with the positive sign of the root for T_{do}', and negative sign for T_{do}''. For some derivations, the sums and differences of these two time constants are more useful because of their simpler form,

$$T'_{do} + T''_{do} = \frac{L_{ff}}{R_f} + \frac{L_{DD}}{R_D} \tag{VI.9a}$$

$$T'_{do}\,T''_{do} = \frac{L_{ff}\,L_{DD} - M^2}{R_f\,R_D} \tag{VI.9b}$$

For the short-circuit time constants, i_d in Eq. (VI.6) is no longer zero. Instead, we express it as a function of i_f, i_D and $\underline{\lambda}_d$ with the first row of Eq. (VI.1),

$$M\,i_d = \frac{M}{L_d}\lambda_d - \frac{M^2}{L_d}i_f - \frac{M^2}{L_d}d_D \tag{VI.10}$$

which, when inserted into (VI.6) and (VI.2), produces

$$\begin{bmatrix} \dfrac{di_f}{dt} \\[2ex] \dfrac{di_D}{dt} \end{bmatrix} = \frac{i}{L_{ffs}\,L_{DDs} - M_s^2}\begin{bmatrix} -L_{DDs} & M_s \\ M_s & -L_{ffs} \end{bmatrix}\left(\begin{bmatrix} R_f & 0 \\ 0 & R_D \end{bmatrix}\begin{bmatrix} i_f \\ i_D \end{bmatrix} + \begin{bmatrix} v_f + \dfrac{M}{L_d}\cdot\dfrac{d\lambda_d}{dt} \\[2ex] \dfrac{M}{L_d}\cdot\dfrac{d\lambda_d}{dt} \end{bmatrix}\right) \tag{VI.11}$$

with subscript "s" added to define the inductances modified for short-circuit conditions,

$$L_{ffs} = L_{ff} - M^2/L_d, \quad L_{DDs} = L_{DD} - M^2/L_d, \quad M_s = M - M^2/L_d \tag{VI.12}$$

Taking v_f and $d\lambda_d/dt$ as the forcing functions, we obtain the short-circuit time constants as the negative reciprocals of the eigenvalues of the matrix in Eq. (VI.11). Since this equation has the same form as Eq. (VI.7), we can immediately give the answer as

$$\begin{matrix} T'_d \\ T''_d \end{matrix} = \frac{1}{2}\left(\frac{L_{ffs}}{R_f} + \frac{L_{DDs}}{R_D}\right) \pm \frac{1}{2}\sqrt{\left(\frac{L_{ffs}}{R_f} - \frac{L_{DDs}}{R_D}\right)^2 + 4\frac{M_s^2}{R_f\,R_D}} \tag{VI.13}$$

with the positive sign of the root for T_d', and the negative sign for T_d''. Again, their sums and differences are easier to work with,

$$T_d' + T_d'' = \frac{L_{ffs}}{R_f} + \frac{L_{DDs}}{R_D} \tag{VI.14a}$$

$$T_d' \, T_d'' = \frac{L_{ffs} \, L_{DDs} - M_s^2}{R_f \, R_d} \tag{VI.14b}$$

There is also a useful relationship between the open- and short-circuit time constants,

$$T_d' \, T_d'' = T_{do}' \, T_{do}'' \, \frac{L_d''}{L_d} \tag{VI.14c}$$

which can easily be derived from Eq. (VI.9b) and (VI.14b) by using the definition for L_d" given later in Eq. (VI.16).

It is not quite correct to treat $d\lambda_d/dt$ in Eq. (VI.11) as a forcing function, unless R_a is ignored. Only for $R_a = 0$ are the fluxes known from the first two rows of Eq. (8.9) as

$$\lambda_d = \lambda_d(0)\cos\omega t, \quad \lambda_q = \lambda_q(0)\sin\omega t$$

with $v_d=0$, $v_q=0$ because of the short circuit. In practice, R_a is not zero, but very small. Then the fluxes are still known with fairly high accuracy if $\lambda_d(0)$ is replaced by $\lambda_d(0)e^{-\alpha t}$, where

$$\alpha = \frac{1}{T_a} = \frac{\omega \, R_a}{2}\left(\frac{1}{X_d''} + \frac{1}{X_q''}\right) \tag{VI.14d}$$

is the reciprocal of the time constant for the decaying dc offset in the short-circuit current [105]. If R_a were unrealistically large, then the time constants could no longer be defined independently for each axis, and the data conversion would be much more complicated than the one described in Section VI.4.

VI.3 Subtransient and Transient Reactances with Two Windings on the Field Structure

The subtransient reactance can easily be defined by knowing that the fluxes λ_f, λ_D cannot change immediately after the disturbance. By treating them as constants, we can express i_f, i_D as a function of i_d with Eq. (VI.6), which after insertion into the first row of Eq. (VI.1), produces

$$\lambda_d = \left(L_d - M^2 \frac{L_{ff}+L_{DD}-2M}{L_{ff} \, L_{DD}-M^2} \right) i_d + \frac{M}{L_{ff}L_{DD}-M^2}[(L_{DD}-M)\lambda_f + (L_{ff}-M)\lambda_D] \tag{VI.15}$$

By definition, the term relating λ_d to i_d must be the subtransient inductance,

$$L_d'' = L_d - M^2 \frac{L_{ff} + L_{DD} - 2M}{L_{ff} \, L_{DD} - M^2} \tag{VI.16}$$

To obtain the definition of the transient reactance is more complicated. For many years people have simply assumed that the damper winding currents have already died out after the subtransient period is over, and have used

Eq. (VI.4). Canay has recently shown, however, that this assumption can lead to noticeable errors [104], and that the data conversion is just as easy without this simplification. For the data given in the first IEEE benchmark model for subsynchronous resonance [74], 80% of the current associated with the transient time constant T_d' flows in the field winding, and another 20% in the damper winding after a short-circuit (values obtained while verifying the theory for this section). Ignoring the damper winding for the definition of X_d' would therefore produce errors in the field structure as well as in the armature currents.

Adkins [105] and others derive the transient reactance with Laplace transform techniques. First, Eq. (VI.2) is solved for the currents, after replacing the fluxes with Eq. (VI.6), which leads to the s-domain expression for their sum,

$$M\left(I_f(s) + I_D(s)\right) = \frac{-sM^2(R_f + sL_{ff} + R_D + sL_{DD} - 2sM)}{(R_f + sL_{ff})\ (R_D + sL_{DD}) - s^2 M^2}\ I_d(s)\ +\ f\left(V_f(s)\right)$$

where $f(V_f)$ is some function of the field voltage which is not of interest here. Inserting this into the first row of Eq. (VI.1) produces

$$\Lambda_d(s) = \left(L_d\ -\ \frac{sM^2(R_f + sL_{ff} + R_D + sL_{DD} - 2sM)}{(R_f + sL_{ff})\ (R_D + sL_{DD}) - s^2 M^2}\right)\ I_d(s)\ +\ f\left(V_f(s)\right)$$

with the expression in parentheses being the operational inductance $L_d(s)$,

$$\Lambda_d(s) = L_d(s)\ I_d(s)\ +\ f(V_f(s)) \tag{VI.17}$$

Through some lengthy manipulations it can be shown that it has the simple form

$$L_d(s) = L_d\ \frac{(1 + sT_d')\ (1 + sT_d'')}{(1 + sT_{do}')\ (1 + sT_{do}'')} \tag{VI.18}$$

The basic definition of L_d' and L_d'' in the IEEE and IEC standards is

$$\frac{1}{L_d(s)} = \frac{1}{L_d}\ +\ (\frac{1}{L_d'} - \frac{1}{L_d})\frac{sT_d'}{1 + sT_d'}\ +\ (\frac{1}{L_d''} - \frac{1}{L_d'})\frac{sT_d''}{1 + sT_d''} \tag{VI.19a}$$

in the s-domain, or

$$\frac{1}{L_d(t)} = \frac{1}{L_d}\ +\ (\frac{1}{L_d'} - \frac{1}{L_d})e^{-t/T_d'}\ +\ (\frac{1}{L_d''} - \frac{1}{L_d'})e^{-t/T_d''} \tag{VI.19b}$$

in the time domain[3]. The transient reactance can therefore be found by expanding $1/L_d(s)$ from Eq. (VI.18) into partial fractions,

$$\frac{1}{L_d(s)} = \frac{1}{L_d} - \frac{1}{L_d} \cdot \frac{(T_d'-T_{do}')\ (T_d'-T_{do}'')}{T_d'\ (T_d'-T_d'')} \cdot \frac{s\ T_d'}{1+s\ T_d'} - \frac{1}{L_d} \cdot \frac{(T_d''-T_{do}')\ (T_d''-T_{do}'')}{T_d''\ (T_d''-T_d')} \cdot \frac{s\ T_d''}{1+s\ T_d''}$$

(VI.20)

and by equating the coefficient of the second term in Eq. (VI.19a), which describes what is read off the oscillogram in the short-circuit test, with the coefficient of the second term in Eq. (VI.20), which describes the mathematical model. Then, with the help of Eq. (VI.14c), we obtain

$$T_d'\ \frac{L_d}{L_d'} + T_d''\ (1 - \frac{L_d}{L_d'} + \frac{L_d}{L_d''}) = T_{do}' + T_{do}''$$

(VI.21)

for the definition of the transient reactance or inductance.

Laplace transform techniques are downgraded in Appendix I for EMTP implementation, but for the type of analytical work just described they are quite useful. The transient reactance can also be derived using the eigenvalue/eigenvector approach of Eq. (I.5). The starting point for that approach is Eq. (VI.11), which has the general form

$$\left[\frac{dx}{dt}\right] = [A]\ [x]\ +[g(t)]$$

of Eq. (I.1), with the solution

$$[x(t)] = [M]\ [e^{\Lambda t}]\ [M]^{-1}\ [x(0)] + \int_0^t [M]\ [e^{\Lambda(t-u)}]\ [M]^{-1}\ [g(u)]\ du$$

(VI.22)

If we treat the variables as deviations from the pre-short-circuit steady-state values, then the initial conditions for these "deviation variables" are zero, and the first term in the above solution with $[x(0)]$ drops out. This is in line with the usual practice of assuming zero initial conditions in Laplace transform techniques. What is of interest then is the expression under the integral. To obtain it, we must first find the eigenvector matrix $[M]$ of

$$[A] = \frac{1}{L_{ffs}L_{DDs} - M_s^2} \begin{bmatrix} -L_{DDs}R_f & M_s R_D \\ M_s R_f & -L_{ffs}R_D \end{bmatrix}$$

(VI.23)

which is

---

[3] These definitions are used to read the inductance and time constant values from the oscillograms of the short-circuit test.

$$[M] = \begin{bmatrix} \dfrac{M_s}{R_f} & \dfrac{L_{ffs}}{R_f} - T_d' \\[3ex] \dfrac{L_{DDs}}{R_D} - T_d'' & \dfrac{M_s}{R_D} \end{bmatrix} \qquad (VI.24a)$$

with its inverse

$$[M]^{-1} = \dfrac{1}{(T_d' - \dfrac{L_{ffs}}{R_f})\ (T_d' - T_d'')} \begin{bmatrix} \dfrac{M_s}{R_D} & T_d' - \dfrac{L_{ffs}}{R_f} \\[3ex] T_d'' - \dfrac{L_{DDs}}{R_D} & \dfrac{M_s}{R_f} \end{bmatrix} \qquad (VI.24b)$$

That $[M][M]^{-1}$ = unit matrix can easily be verified by knowing that $T_d" - L_{DDs}/R_D = L_{ffs}/R_f - T_d'$ from Eq. (VI.14a). The forcing function vector $[g(t)]$ is

$$[g(t)] = \dfrac{M}{L_d T_d' T_d'' R_f R_D} \begin{bmatrix} M_s - L_{DDs} \\ M_s - L_{ffs} \end{bmatrix} \dfrac{d\lambda_d}{dt} \qquad (VI.25)$$

The matrix with exponentials in Eq. (VI.22) contains the two diagonal elements $e^{-(t-u)/Td'}$ and $e^{-(t-u)/Td"}$. Since we are only interested in the part associated with the transient time constant T_d', we ignore the parts containing $T_d"$ and obtain

$$[M]\ [e^{\Lambda(t-u)}]\ [M]^{-1} = \dfrac{1}{T_d' - T_d''} \begin{bmatrix} \dfrac{L_{ffs}}{R_f} - T_d'' & \dfrac{M_s}{R_f} \\[3ex] \dfrac{M_s}{R_D} & \dfrac{L_{DDs}}{R_D} - T_d'' \end{bmatrix} e^{-(t-u)/T_d'} + [a\ 2x2\ matrix]e^{-(t-u)/T_d''} \qquad (VI.26)$$

Then

$$\begin{bmatrix} i_f - transient \\ i_D - transient \end{bmatrix} = \begin{bmatrix} product\ of\ matrix\ and\ vector \\ from\ (VI.26)\ and\ (VI.25) \end{bmatrix} \cdot \int_0^t e^{-(t-u)/T_d'}\ \dfrac{d\lambda_d}{dt}\ du$$

which produces the 80%/20% split in the two field structure currents for the IEEE benchmark case mentioned at the beginning of this section, when numerical values are inserted. Since

$$i_d = \dfrac{1}{L_d}\ \lambda_d - \dfrac{M}{L_d}\ (i_f + i_D)$$

the sum of i_f and i_D, after multiplication with $-M/L_D$, will give us the transient part of i_d associated with $T_{d'}$.

$$i_{d-transient} = -\frac{1}{L_d} \frac{(T_d'-T_{do}') (T_d'-T_{do}'')}{T_d' (T_d'+T_d'')} \int_0^t e^{-(t-u)/T_d'} \frac{d\lambda_d}{dt} du \qquad (VI.27)$$

By comparing the coefficient in front of the integral with the coefficient of the second term in Eq. (VI.20), we can see that the eigenvalue/eigenvector approach does indeed produce the same definition of the transient inductance as the Laplace transform method.

VI.4 Canay's Data Conversion

Assume that M has been found from either Eq. (8.20a) or (8.20b) (subscript "m" dropped here), and that the four time constants T_{do}', T_{do}'', T_d', T_d'' are known. If only one pair of time constants as well as X_d', X_d'' are known, the other pari can be found from Eq. (8.12). We then obtain the two time constants of the "f-branch" and "D-branch" of Fig. 8.2,

$$T_1 = \frac{L_f}{R_f}, \quad T_2 = \frac{L_D}{R_D}, \quad \text{with } L_f = L_{ff} - M, \quad L_D = L_{DD} - M \qquad (VI.28)$$

by solving the two equations

$$T_1 + T_2 = (T_{do}' + T_{do}'') \frac{M-L_d}{M} + (T_d'+T_d'') \frac{L_d}{M} \qquad (VI.29a)$$

$$T_1 T_2 = T_{do}' \, T_{do}'' \, (L_{parallel \, MfD} /M) \qquad (VI.29b)$$

with $L_{parallel \, MfD}$ being the inductance of M, L_f, L_D in parallel, which can be shown with Eq. (VI.16) to be

$$L_{parallel \, MfD} = M - L_d + L_d'' \qquad (VI.29c)$$

Eq. (VI.29a) is obtained by multiplying Eq. (VI.9a) with (1-M/L_d) and then subtracting it from Eq. (VI.14a), while Eq. (VI.29b) is obtained from Eq. (VI.9b) with the definition of L_d'' from Eq. (VI.16). Once T_1 and T_2 are known, the inductance of M, L_f in parallel is found,

$$L_{parallel \, Mf} = \frac{M(T_1 - T_2)}{T_{do}' + T_{do}'' - (1 + \dfrac{M}{L_{parallel \, MfD}})T_2} \qquad (VI.30)$$

This equation is derived from rewriting Eq. (VI.9a) as

$$M \left(\frac{T_1}{L_f} + \frac{T_2}{L_D}\right) = T_{do}' + T_{do}'' - T_1 - T_2$$

and rewriting Eq. (VI.9b) as

$$M \left(\frac{T_2}{L_f} + \frac{T_2}{L_D} \right) = \left(\frac{M}{L_{parallel \ MfD}} - 1 \right) T_2$$

which produces M/L_f after subtracting the second from the first equation. After addition of 1 to M/L_f and division by M the reciprocal of $L_{parallel \ Mf}$ follows. Then

$$L_f = (L_{parallel \ Mf} \bullet M) / (M - L_{parallel \ Mf}) \tag{VI.31a}$$

$$L_D = (L_{parallel \ MfD} \bullet L_{parallel \ Mf}) / (L_{parallel \ Mf} - L_{parallel \ MfD}) \tag{VI.31b}$$

and

$$R_f = L_f/T_1, \quad R_D = L_D/T_2, \quad L_{ff} = L_f + M, \quad L_{DD} = L_D + M \tag{VI.32}$$

Table VI.1 compares the results from the approximate data conversion of [74], from the data conversion which ignores the damper winding in the definition of L_d' by using Eq. (VI.4) instead of (VI.21) [106], and from Canay's data conversion. The approximate data conversion produces an incorrect model with $X_d'=0.156$ instead of 0.169 (transient short-circuit currents 8% too large) and with T_{do}' too large while T_{do}'' is too small. The data conversion with the wrong definition of L_d' produces an incorrect model with $X_d'=0.142$ instead of 0.169 (transient short-circuit currents 19% too large), but with correct time constants T_{do}' and T_{do}''. The iterative method mentioned in [74] is correct and produces the same answers as Canay's conversion, except that no procedure is given there on how to perform the iterations.

To double-check whether Canay's data conversion is indeed correct, a system of seven equations of the form

$$[\ di_{dqo} \ / \ dt \ ] = [A] \ [i_{dqo}] + [B] \ [v_f]$$

was set up which describes the three-phase short-circuit condition. The values of Table VI.1 were first used to find the matrix [A]. Then the eigenvalues of [A] were determined. The reciprocals of four of the eigenvalues differ from the time constants T_d', T_d'', T_q', T_q'' by no more than 0.05% for realistic values of $R_a=0.004$ p.u., the reciprocal of one eigenvalue agrees with T_a of Eq. (VI.14d) to within 0.1%. Unrealistically large values of R_a would produce errors for reasons explained in Section VI.2; for $R_a=0.04$ p.u., the error would still be only 4% for T_q' and 1% or less for the other time constants.

VI.5 Negative Sequence Impedance

Negative sequence currents in the armature produce a magnetic field which rotates in opposite direction to the field rotation, thereby inducing double frequency currents in the field structure windings. The negative sequence impedance can therefore be obtained by setting $s=j2\omega$ in Eq. (VI.18), and adding the armature resistance R_a to it,

$$Z_{d-neg} = R_a + j\omega L_d \ \frac{(1 + j2\omega T_d') \ (1 + j2\omega T_d'')}{(1 + j2\omega T_{do}') \ (1 + j2\omega T_{do}'')} \tag{VI.33}$$

Table VI.1 - Data conversion for direct axis data from [74] (X_d = 1.79 p.u., X_d' = 0.169 p.u., X_d'' = 0.135 p.u., X_ℓ = 0.13 p.u., T_{do}' = 4.3 s, T_{do}'' = 0.032 s, f = 60 Hz).

	Approx.	Wrong L_d' [*)	Canay
Conversion results			
X_{ff} (p.u.)	1.6999	1.7036	1.7218
X_{DD} (p.u.)	1.6657	1.6700	1.6655
R_f (p.u.)	0.00105	0.002086	0.001407
R_D (p.u.)	0.00371	0.002045	0.004070
Implied model parameters			
X_d' (p.u.) from (VI.21)	0.1564	0.1416	0.169
T_{do}' (s) from (VI.8)	5.466	4.3	4.3
T_{do}'' (s) from (VI.8)	0.0252	0.032	0.032
T_d' (s) from (VI.13)	0.4744	0.3388	0.4000
T_d'' (s) from (VI.13)	0.0219	0.0306	0.0259
$T_f = L_{ff}/R_f$ (s)	4.300	2.166	3.246
$T_D = L_{DD}/R_D$ (s)	1.192	2.166	1.085

[*)For conversion of [106] to work, X_ℓ had to be reduced by 1.4%.

and analogous for the quadrature axis. Then

$$Z_{neg} \approx (Z_{d\text{-}neg} + Z_{q\text{-}neg}) / 2 \qquad\qquad (VI.34)$$

with $R_{neg} = Re\{Z_{neg}\}$ and $X_{neg} = Im\{Z_{neg}\}$.

If there is only one winding on the field structure, say only the Q-winding on the q-axis, then

$$Z_{q\text{-}neg} = R_a + j\omega L_q \; \frac{1 + j \; 2\omega T_q''}{1 + j \; 2\omega T_{qo}''} \qquad\qquad (VI.33a)$$

with

$$T_q'' = (L_q'' / L_q) \, T_{qo}'' \qquad\qquad (VI.35b)$$

Eq. (VI.35a) follows from (VI.33) by setting T_q' = 0 and T_{qo}' = 0, and Eq. (VI.35b) from $T_q'' = L_{QQs} / R_Q$, with L_{QQs} defined by Eq. (VI.12) and $T_{qo}'' = L_{QQ} / R_Q$.

APPENDIX VII - INTERNAL IMPEDANCE OF STRANDED CONDUCTORS

For power line carrier problems, reasonably accurate attenuation constants are very important. Replacing a stranded conductor by one tubular conductor of equal cross-section is not good enough for such purposes. Instead, the internal impedance formula from [39] should be used

$$R'_{internal} = \omega L'_{internal} = \frac{2.25 \sqrt{\omega \mu_o \mu_r \varrho}}{r \cdot \pi \cdot (2+n) \cdot \sqrt{2}} \; \Omega/m \tag{VII.1}$$

or with $\rho/(\pi \bullet r^2) = R'$

$$R'_{internal} = \omega L'_{internal} = \frac{4.5 \cdot \sqrt{5} \cdot 10^{-4}}{2+N} \sqrt{\omega \mu_r \, R'} \; \Omega/m \tag{VII.2}$$

where

      R' = dc resistance of one of the outer strands of a stranded conductor (Ω/m)

μ_r	=	relative permeability
μ_o	=	$4 \bullet \pi \bullet 10^{-7}$ (H/m)
ω	=	angular frequency
ρ	=	conductor resistivity (Ωm)
r	=	radius of each outer strand (m)
n	=	number of outer strands

The factor 2.25 was found experimentally from field plotting in an electrolytic tank. The formula give reasonably accurate results at frequencies above 2-5 kHz for the most commonly used stranded conductors with the number of outer strands either being 6, 12, 18 or 24.

Fig. VII.1 compares measured attenuation constants with those calculated with the above formula. In [39] it is shown that the measured attenuation constants come from the aerial mode which has a slightly slower wave velocity than the other aerial mode. That mode was chosen on the same basis here. However, input data were used which differ slightly from those given in [39]:

(1)   Phase conductor 150 mm^2 Aldrey was assumed to have 37 strands (18 on the outside), as defined in DIN 48201, with conductor diameter = 15.8 mm, strand diameter = 2.25 mm, and conductor dc resistance = 0.223 Ω/km (latter from Brown Boveri handbook).

(2)   The relative permeability of the steel earth wire was assumed to be 50 to 100 (a Siemens handbook says that these are typical values, with the actual value depending on the current density).
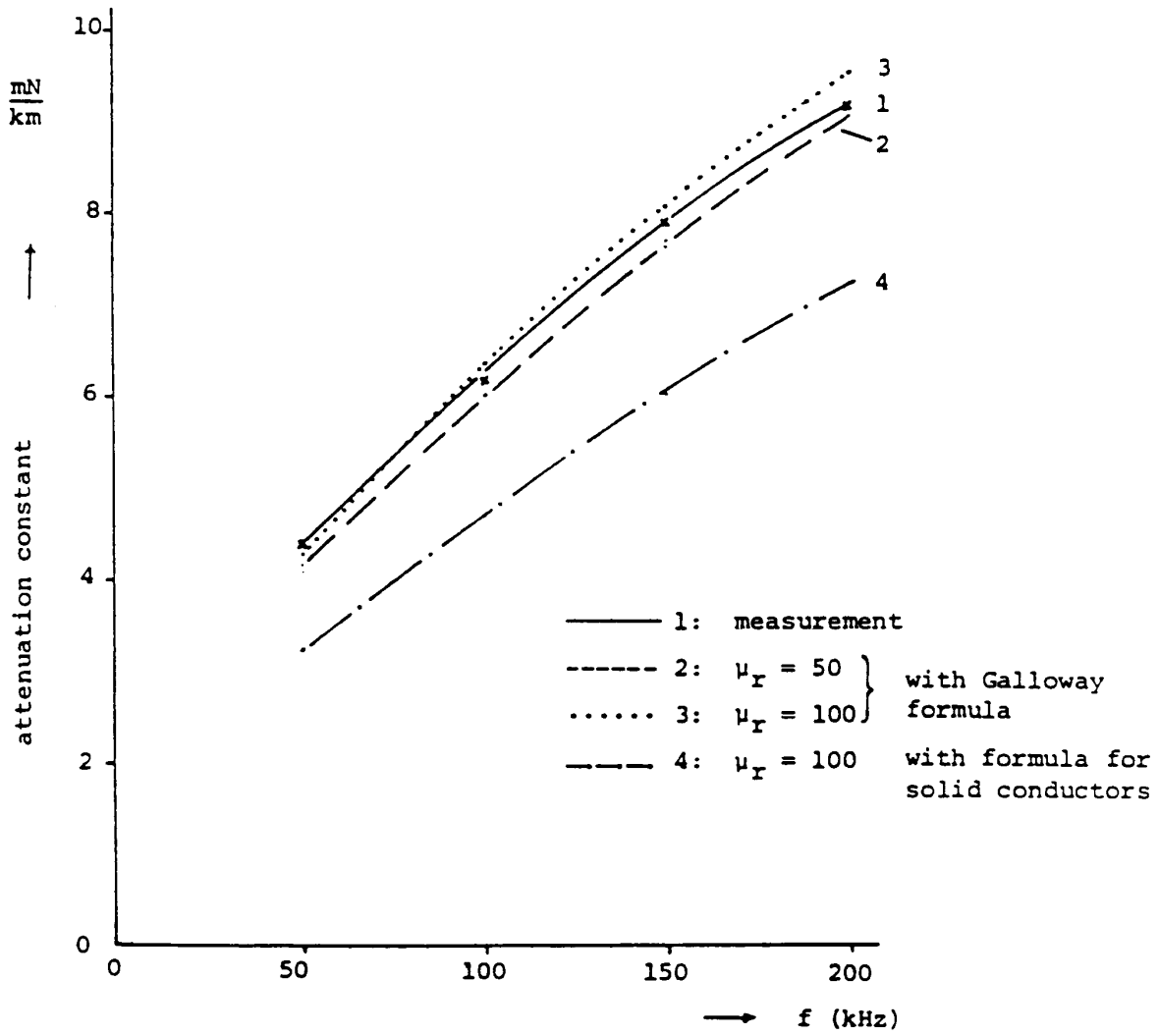
Fig. VII.1 - Comparison between measured and calculated attenuation constants

REFERENCES

[1]   Electromagnetic Transients Program Rule Book. Bonneville Power Administration, Portland, Oregon, April 1982.

[2]   F.H. Branin, "Computer methods of network analysis," Proc. IEEE, vol. 55, pp. 1787-1801, Nov. 1967.

[3]   J.G.F. Francis, "The QR transformation," Computer Journal, vol. 4, pp. 332-345, 1961.

[4]   J.H. Wilkinson, The Algebraic Eigenvalue Problem. Oxford Univ. Press, London, 1965.

[5]   J.E. Van Ness, "The inverse iteration method for finding eigenvectors," IEEE Trans. Automatic Control, vol. AC-14, pp. 63-66, Feb. 1969.

[6]   E.J. Davison, "A high-order Crank-Nicholson technique for solving differential equations," Computer Journal, vol. 10, pp. 195-197, Aug. 1967.

[7]   A. Ralston, A First Course in Numerical Analysis. McGraw-Hill, New York, 1965.

[8]   M. Darveniza et al., "Modelling for lightning performance calculations," IEEE Trans. Power App. Syst., vol. PAS-98, pp. 1900-1908, Nov./Dec. 1979.

[9]   Working Group 36-05, "Harmonics, characteristic parameters, methods of study, estimates of existing values in the network," Electra, no. 77, pp. 35-54, July 1981.

[10]   S. Tominaga, K. Azumi, Y. Shibuya, M. Imataki, Y. Fujiwara and S. Nishida, "Protective performance of metal oxide surge arrester based on the dynamic v-i characteristics," IEEE Trans. Power App. Syst., vol. PAS-98, pp. 1860-1871, Nov./Dec. 1979.

[11]   W.S. Meyer and H.W. Dommel, "Telephone-interference calculation for multiconductor power lines," IEEE Trans. Power App. Syst., vol. PAS-88, pp. 35-41, Jan. 1969.

[12]   A. Wexler (editor), Large Engineering Systems. Pergamon Press, Oxford, 1977. Contribution by P.B. Johns, "Numerical modelling by the TLM method."

[13]   V. Brandwajn, "Synchronous generator models for the analysis of electromagnetic transients," Ph.D. thesis, University of British Columbia, Vancouver, Canada, 1977.

[14]   R.W. Hamming, Numerical Methods for Scientists and Engineers. Second Edition, McGraw-Hill Book Co., New York, 1973, p. 580 (or p. 327 in First Edition, 1962).

[15]   B. Kulicke, "Simulationsprogramm NETOMAC: Differenzenleitwertverfahren bei kontinuierlichen und diskontinuierlichen Systemen (Simulation program NETOMAC: Difference conductance method for continuous and discontinuous systems)," Siemens Forschungs - und Entwicklungsberichte - Siemens Research and Development Reports, vol. 10 (1981), no. 5, pp. 299-302.

[16]   V. Brandwajn, "Damping of numerical noise in the EMTP solution," EMTP Newsletter, vol. 2, no. 3, pp. 10-19, Feb. 1982.

[17]   F. Alvarado, "Eliminating numerical oscillations in trapezoidal integration," EMTP Newsletter, vol. 2, no. 3, pp. 20-32, Feb. 1982.

[18]   CIGRE-Working Group 13.05, "The calculation of switching surges. II. Network representation for energization and re-energization studies on lines fed by an inductive source, Electra, no. 32, pp. 17-42, 1974.

[19]   R. Malewski, V.N. Narancic and Y. Robichaud, "Behavior of the Hydro-Quebec 735-kV system under transient short-circuit conditions and its digital computer simulation," IEEE Trans. Power App. Syst., vol. PAS-94, pp. 425-431, March/April 1975.

[20]   M.I.T. Staff, Magnetic Circuits and Transformers. MIT Press, Cambridge, Mass. (original edition 1943, many reprints thereafter), p. 197.

[21]   P.C. Krause, F. Nozari, T.L. Skvarenina, D.W. Olive, "The theory of neglecting stator transients," IEEE Trans. Power App. Syst., vol. PAS-98, pp. 141-148, Jan./Feb. 1979; discussion by V. Brandwajn and W.A. Mittelstadt.

[22]   R.W. Jensen and L.P. McNamee (editors), Handbook of Circuit Analysis Languages and Techniques. Prentice-Hall, Englewood Cliffs, N.J., 1976.

[23]   G.W.A. Dummer, Modern Electronic Components. Pitman & Sons, London, 1959, p. 131.

[24]   A. Roth, Hochspannungstechnik ("High Voltage Engineering," in German). Springer, Vienna, 1959, p. 605.

[25]   S. Seshu and M.B. Reed, Linear Graphs and Electrical Networks. Addison-Wesley, Reading, Mass., 1961.

[26]   A.G. Phadke (editor), Digital Simulation of Electrical Transient Phenomena. IEEE Tutorial Course, Course Text 81 EHO173-5-PWR, IEEE Service Center, Piscataway, N.J., 1980.

[27]   M.H. Hesse, "Electromagnetic and electrostatic transmission-line parameters by digital computer," IEEE Trans. Power App. Syst., vol. 82, pp. 282-290, 1963.

[28]   J.R. Carson, "Wave propagation in overhead wires with ground return," Bell Syst. Tech. Journal, vol. 5, pp. 539-554, 1926.

[29]   F. Pollaczek, "On the field produced by an infinitely long wire carrying alternating current," Elektrische Nachrichtentechnik (in German), vol. 3, pp. 339-359, 1926, and "On the induction effects of a single phase ac line," Elektrische Nachrichtentechnik (in German), vol. 4, pp. 18-30, 1927 (French translation in Revue General de 1'Electricite, vol. 29, **pp.** 851-867, 1931).

[30]   M. Nakagawa and K. Iwamoto, "Earth-return impedance for the multi-layer case," IEEE Trans. Power App. Syst., vol. PAS-95, pp. 671-676, March/April 1976.

[31]   M.C. Perz and M.R. Raghuveer, "Generalized derivation of fields, and impedance correction factors of lossy transmission lines," IEEE Trans. Power App. Syst., vol. PAS-93, pp. 1827-1841, Nov./Dec. 1974.

[32]   R. Hartenstein, H.J. Koglin and V. Rees, "Equivalent circuit of HVDC lines for symmetric and unsymmetric operation in a frequency region 0 to 100 kHz," ETZ-A (in German), vol. 93, pp. 148-152,

1972.

[33] C. Gary, "Approche Complete de la Propagation multifilaire en haute frequence par utilisation des matrices complexes" ("Complete approach to multiconductor propagation at high frequency with complex matrices," in French), EdF Bulletin de la Direction des Etudes et Recherches, Serie B, no. 3/4, pp. 5-20, 1976.

[34] A. Deri, G. Tevan, A. Semlyen and A. Castanheira, "The complex ground return plane, a simplified model for homogeneous and multi-layer earth return", IEEE Trans. Power App. Syst., vol. PAS-100, pp. 3686-3693, Aug. 1981.

[35] L.M. Wedepohl and A.E. Efthymiadis, "Wave propagation in transmission lines over lossy ground: A new, complete field solution," Proc. IEE, vol. 125, pp. 505-510, June 1978.

[36] A. Semlyen, "Ground return parameters of transmission lines; an asymptotic analysis for very high frequencies," IEEE Trans. Power App. Syst., vol. PAS-100, pp. 1031-1038, March 1981.

[37] IEEE Working Group, "Electromagnetic effects of overhead transmission lines. Practical problems, safeguards, and methods of calculation," IEEE Trans. Power App. Syst., vol. PAS-93, pp. 892-904, May/June 1974.

[38] S. Butterworth, Electrical characteristics of overhead lines, El. Research Assn., Tech. Rpt. Ref. O/T4, 1954.

[39] R.H. Galloway, W.B. Shorrocks and L.M. Wedepohl, "Calculation of electrical parameters for short and long polyphase transmission lines," Proc. IEE, vol. 111, pp. 2051-2059, Dec. 1964.

[40] P. Silvester, "Impedance of nonmagnetic overhead power transmission conductors," IEEE Trans. Power App. Syst., vol. PAS-88, pp. 731-737, May 1969.

[41] A.E. Kennelly, F.A. Laws and P.H. Pierce, "Experimental research on skin effect in conductors," AIEE Trans., pt. II, vol. 34, pp. 1953-2018, 1915.

[42] H.J. West and A.L. Courts, "Current distribution within asymmetrical UHV bundles: A laboratory confirmation of analytical studies," IEEE Trans. Power App. Syst., vol. PAS-95, pp. 1487-1492, July/Aug. 1976.

[43] R.B. Shipley and D.W. Coleman, "A new direct matrix inversion method," AIEE Trans., pt. I (Commun. and Electronics), vol. 78, pp. 568-572, 1959.

[44] E. Clarke, Circuit Analysis of A-C Power Systems, vol. 1. New York: John Wiley & Sons, 1943.

[45] D.E. Hedman, "Propagation on overhead transmission lines. I - Theory of modal analysis. II - Earth-conduction effects and practical results," IEEE Trans. Power App. Syst., vol. PAS-84, pp. 200-211, March 1965, and pp. 489-492, June 1965.

[46] L.M. Wedepohl and R.G. Wasley, "Wave propagation in polyphase transmission systems; resonance effects due to discretely bonded earth wires," Proc. IEE, vol. 112, pp. 2113-2119, Nov. 1965.

[47] General **Electric Co., Transmission** Line Reference Book 345 kV and Above. **New** York: F. Weidner & Son Printers, 1975.

[48]   E.W. Kimbark, Electrical Transmission of Power and Signals. John Wiley & Sons, New York, 1949.

[49]   IEEE Working Group, "Electrostatic effects of overhead transmission lines," IEEE Trans. Power App. Syst., vol. PAS-91, pp. 422-433, March/April 1972.

[50]   H.W. Dommel, "Digital computer solution of electromagnetic transients in single and multiphase networks," IEEE Trans. Power App. Syst., vol. PAS-88, pp. 388-399, April 1969.

[51]   Westinghouse Electric Corp., Electrical Transmission and Distribution Reference Book. Pittsburgh: Westinghouse Electric Corp., 1964.

[52]   E.v. Rziha, Starkstromtechnik-Taschenbuch fuer Elektrotechniker, vol. II. Berlin: Wilhelm Ernst u. Sohn, 1960 (in German).

[53]   Siemens, Formel- und Tabellenbuch fuer Starkstrom- Ingenieure. Essen: Girardet 1965 (in German).

[54]   H. Happoldt and D. Oeding, Elektrische Kraftwerke und Netze ("Electric power plants and networks," in German). Springer, Berlin, 1978.

[55]   G.T. Heydt and R. C. Burchett, discussion to "Six-phase (multi-phase) power transmission systems: Fault analysis" by N.B. Bhatt et al., IEEE Trans. Power App. Syst., vol. PAS-96, pp. 765-766, May/June 1977.

[56]   H. Edelmann, Berechnung elektrischer Verbundnetze ("Analysis of interconnected power systems," in German). Springer, Berlin, 1963.

[57]   H.W. Dommel and W.S. Meyer, "Computation of electromagnetic transients," Proc. IEEE, vol. 62, pp. 983-993, July 1974.

[58]   L.M. Wedepohl, "Application of matrix methods to the solution of travelling-wave phenomena in polyphase systems," Proc. IEE, vol. 110, pp. 2200-2212, Dec. 1963.

[59]   M.C. Perz, "Natural modes of power line carrier on horizontal three-phase lines," IEEE Trans. Power App. Syst., vol. 83, pp. 679-686, discussion pp. 748-754, 1964.

[60]   M.C. Perz, "A method of analysis of power line carrier problems on three-phase lines," IEEE Trans. Power App. Syst., vol. 83, pp. 686-691, discussion pp. 754-756, 1964.

[61]   L.M. Wedepohl, "Electric characteristics of polyphase transmission systems with special reference to boundary-value calculations at powerline carrier frequencies," Proc. IEE, vol. 112, pp. 2103-2112, Nov. 1965.

[62]   O. Nigol, "Analysis of radio noise from high-voltage lines (II) - Propagation theory," IEEE Trans. Power App. Syst., vol. 83, pp. 533-541, discussion pp. 554-558, 1964.

[63]   L.M. Wedepohl and J.N. Saha, "Radio-interference fields in multiconductor overhead transmission lines," Proc. IEE, vol. 116, pp. 1875-1884, Nov. 1969.

[64]   R. Pelissier, "Propagation of electromagnetic waves on a multiphase line," Revue Generale de 1'Electricite, vol. 78, pp. 337-352, 491-506, April and May 1969 (in French).

[65]   J.A. Brandao Faria and J.R. Borges da Silva, "Wave propagation in polyphase transmission lines; a general solution to include cases where ordinary modal theory fails," IEEE Trans. Power Systems, vol. PWRD-1,

pp. 182-189, April 1986.

[66] C.R. Paul, "Solution of the transmission-line equations for lossy conductors and imperfect earth," Proc. IEE, vol. 122, pp. 177-182, Feb. 1975.

[67] B.T. Smith, J. Boyle, B. Garbow, Y. Ikebe, V. Klena and C. Moler, Matrix Eigensystem Routines - EISPACK Guide, Second Edition, Lecture Notes in Comp. Sci., vol. 6, Springer- Verlag, New York, 1976.

[68] K.E. Atkinson, An Introduction to Numerical Analysis. John Wiley & Sons, **New** York, 1978, p. 547.

[69] IEEE Working Group, "Switching Surges: Part IV - Control and reduction on ac transmission lines," IEEE Trans. Power App. & Syst., vol. PAS-101, pp. 2694-2702, Aug. 1982.

[70] R. Willoughby (editor), Stiff Differential Systems. Plenum Press, New York, 1974.

[71] G.G. Dahlquist, "A special stability problem for linear multistep methods," Nordisk Tidskrift for Informations - Behandling, vol. 3, pp. 27-43, 1963.

[72] H.W. Dommel and N. Sato, "Fast transient stability solutions," IEEE Trans. Power App. Syst., vol. PAS-91, pp. 1643-1650, 1972.

[73] A. Semlyen and A. Dabuleanu, "A system approach to accurate switching transient calculations based on state variable component modelling," IEEE Trans. Power App. Syst., vol. PAS-94, pp. 572-578, March/April 1975.

[74] IEEE Task Force, "First benchmark model for computer simulation of subsynchronous resonance," IEEE Trans. Power App. Syst., vol. PAS-96, pp. 1565-1572, Sept./Oct. 1977.

[75] H. Dommel, "Digitale Rechenverfahren fur elektrische Netze" ("digital computer methods for network solutions," in German), Archiv f. Elektrotechnik, vol. 48, pp. 118-132, 1963.

[76] IEEE Standard Dictionary of Electrical and Electronics Terms. Second Edition, published by IEEE. Wiley-Interscience, New York, 1977.

[77] G.E. Forsythe and C.B. Moler, Computer Solution of Linear Algebraic Equations. Prentice-Hall, Englewood Cliffs, N.J., 1967.

[78] P.C. Magnusson, "Travelling waves on multi-conductor open-wire lines - A numerical survey of the effects of frequency dependence of modal composition," IEEE Trans. Power App. Syst., vol. PAS-92, pp. 999-1008, May/June 1973.

[79] V. Brandwajn, "Modifications of User's Instructions for MARTI SETUP," EMTP Newsletter, vol. 3, no. 1, pp. 76-80, Aug. 1982.

[80] H.W. Dommel, A. Yan, R.J. Ortiz de Marcano, A.B. Miliani, "Case studies for electromagnetic transients," Univ. of British Columbia, Vancouver, Canada, May 1983.

[81] L. Bergeron, "Du Coup de Belier en Hydraulique au Coup de Foudre en Electricité." Dunod, Paris 1949 (English translation: Water Hammer in Hydraulics and Wave Surges in Electricity; ASME Committee. Wiley, New York 1961).

[82] CIGRE Working Group 13.05, "The calculation of switching surges. I. A comparison of transient network

analyser results," Electra No. 19, pp. 67-78, Nov. 1971.

[83]   A. Budner, "Introduction of frequency-dependent line parameters into an electromagnetic transients program", IEEE Trans. Power App. Syst., vol. PAS-89, pp. 88-97, Jan. 1970.

[84]   W.S. Meyer and H.W. Dommel, "Numerical modelling of frequency-dependent transmission line parameters in an electromagnetic transients program," IEEE Trans. Power App. Syst., vol. PAS-93, pp. 1401-1409, Sept./Oct. 1974.

[85]   J.K. Snelson, "Propagation of travelling waves on transmission lines - Frequency dependent parameters," IEEE Trans. Power App. Syst., vol. PAS-91, pp. 85-91, Jan./Feb. 1972.

[86]   A. Semlyen and A. Dabuleanu, "Fast and accurate switching transient calculations on transmission lines with ground return using recursive convolutions," IEEE Trans. Power App. Syst., vol. PAS-94, pp. 561-571, March/April 1975.

[87]   A. Ametani, "A highly efficient method for calculating transmission line transients," IEEE Trans. Power App. Syst., vol. PAS-95, pp. 1545-1551, Sept./Oct. 1976.

[88]   J.R. Marti, "Accurate modelling of frequency-dependent transmission lines in electromagnetic transient simulations," IEEE Trans. Power App. Syst., vol. PAS-101, pp. 147-157, Jan. 1982.

[89]   CIGRE Working group 13.05, "The calculation of switching surges - III. Transmission line representation for energization and re-energization studies with complex feeding networks," Electra No. 62, pp. 45-78, Jan. 1979.

[90]   L. Marti, "Voltage and current profiles and low-order approximation of frequency-dependent transmission line parameters," M.A.Sc. Thesis, Univ. of British Columbia, Vancouver, Canada, April 1982.

[91]   F.H. Branin, "Transient analysis of lossless transmission lines", Proc. IEEE, vol. 55, pp. 2012-2013, Nov. 1967

[92]   V. Larsen of EFI in Trondheim, Norway; personal communication.

[93]   R.G. Wasley and S. Selvavinayagamoorthy, "Approximate frequency response values for transmission-line transient analysis," Proc. IEE, vol. 121, pp. 281-286, April 1974.

[94]   J.R. Marti, The problem of frequency dependence in transmission line modelling. Ph.D. thesis, The University of British Columbia, Vancouver, Canada, April 1981.

[95]   L. Marti, "Low-order approximation of transmission line parameters for frequency-dependent models," IEEE Trans. Power App. Syst., vol. PAS-102, pp. 3582-3589, Nov. 1983.

[96]   E. Groschupf, "Simulation transienter Vorgange auf Leitungssystemen der Hochspannungs-Gleichstrom und Drehstrom-Ubertragung" ("Simulation of transient phenomena in systems with HVDC and ac transmission lines," in German). Ph.D. thesis, Technical University, Darmstadt, Germany, 1976.

[97]   K. Carlsen, E.H. Lenfest, and J.J. LaForest, "Mantrap - Machine and Network Transients Program," Proc. IEEE Power Industry Computer Appl. Conf., pp. 144-151, 1975.

[98]   G. Gross, and M.C. Hall, "Synchronous machine and torsional dynamics simulation in the computation of

electromagnetic transients," IEEE Trans. Power App. Syst., vol. PAS-97, pp. 1074-1086, July/Aug. 1978.

[99]   IEEE Working Group Report, "Recommended phasor diagram for synchronous machines," IEEE Trans. Power App. Syst., vol. PAS-88, pp. 1593-1610, Nov. 1969.

[100]   R.P. Schulz, W.D. Jones, and D.N. Ewart, "Dynamic models of turbine generators derived from solid rotor equivalent circuits," IEEE Trans. Power App. Syst., vol. PAS-92, pp. 926-933, May/June 1973.

[101]   E.W. Kimbark, Power System Stability: Synchronous Machines. Dover Publications, New York, 1965 (reprint of 1956 edition by J. Wiley & Sons).

[102]   IEEE, Test Procedures for Synchronous Machines. Standard 115, 1965 (being revised in 1984 to include trial procedure for standstill frequency testing).

[103]   IEC, Recommendations for Rotating Electric Machinery. Publ. 34-4A, 1972.

[104]   I.M. Canay, "Determination of model parameters of synchronous machines," Proc. IEE, **vol.** 130, pt. B, pp. 86-94, March 1983.

[105]   B. Adkins and R.G. Harley, The General Theory of Alternating Current Machines: Application to Practical Problems. Chapman and Hall, London, 1975.

[106]   H.W. Dommel, "Data conversion of synchronous machine parameters," EMTP Newsletter, vol. 1, No. 3, pp. 13-17, April 1980.

[107]   I.M. Canay, H.J. Rohrer, K.E. Schnirel, "Effect of electrical disturbances, grid recovery voltage and generator inertia on maximization of mechanical torques inlarge turbogenerator sets," IEEE State-of-the-Art Symposium - Turbine Generator Shaft Torsionals, Publ. No. 79THOO59-6-PWR, 1979.

[108]   R.B. Shipley, D. Coleman, and C.F. Watts, "Transformer circuits for digital studies," AIEE Trans., Pt. III, vol. 81, pp. 1028-1031, Feb. 1963.

[109]   L.F. Blume et **al,** Transformer Engineering. 2nd Edition. John Wiley & Sons, New York, 1951, p. 117.

[110]   D.E. Hedman, "Theoretical evaluation of multiphase propagation," IEEE Trans. Power App. Syst., vol. PAS-90, pp. 2460-2471, Nov./Dec. 1971.

[111]   D. Povh and W. Schulz, "Analysis of overvoltages caused by transformer magnetizing inrush current," IEEE Trans. Power App. Syst., vol. PAS-97, pp. 1355-1365, July/Aug. 1978.

[112]   K. Schlosser, "An equivalent circuit for N-winding transformers derived from a physical basis," Brown Boveri-Nachrichten, vol. 45, pp. 107-132, March 1963 and "Application of the equivalent circuit of an N-winding transformer," Brown Boveri-Nachrichten, vol. 45, pp. 318-333, June 1963 (in German).

[113]   M. Kh. Zikherman, "Magnetizing characteristics of large power transformers," Elektrichestvo No. 3, pp. 79-82, 1972 (in Russian; English translation in Electric Technology USSR).

[114]   E.P. Dick and W. Watson, "Transformer models for transient studies based on field measurements," IEEE Trans. Power App. Syst., vol. PAS-100, pp. 409-419, Jan. 1981.

[115]   J. Avila-Rosales and F.L. Alvarado, "Nonlinear frequency dependent transformer model for electromagnetic transient studies in power systems," IEEE Trans. Power App. Syst., vol. PAS-101, pp.

4281-4288, Nov. 1982.

[116] **A. Goldstein, Transformer, p.** 330 **(in German). Chapter** in Technik No. **3, edited by Th. Boveri and Th. Wasserrab. Fischer, Frankfurt** (Germany), 1963.

[117] C.W. Taylor, "Simulation of current transformers," Internal Report, Bonneville Power Administration, Feb. 1975.

[118] L.O. Chua and **K.A.** Stromsmoe, "Lumped-circuit models for nonlinear inductors exhibiting hysteresis loops," IEEE Trans. Circuit Theory, vol. CT-17, pp. 564-574, Nov. 1970.

[119] J.G. Frame, N. Mohan and T. Liu, "Hysteresis modeling in an electromagnetic transients program," IEEE Trans. Power App. Syst., vol. PAS-101, pp. 3403-3412, Sept. 1982.

[120] N. Germay, S. Mastero and J. Vroman, "Review of ferroresonance phenomena in high-voltage power systems, and presentation of a voltage transformer model for predetermining them," CIGRE Report No. 33-18, Paris, 1974.

[121] L. Krahenbuhl, B. Kulicke, and A. Webs, "Simulationsmodell eines Mehrwicklungstransformators zur Untersuchung von Sattigungsvorgangen," ("simulation model of an N-winding transformer for the analysis of saturation phenomena", in German), Siemens Forschungs-und Entwicklungs-Berichte (Siemens Research and Development Reports), vol. 12, pp. 232-235, 1983.

[122] E. Colombo and G. Santagostino, "Results of the enquiries on actual network conditions when switching magnetizing and small inductive currents and on transformer and shunt reactor saturation characteristics", Electra No. 94, pp. 35-53, May 1984.

[123] T. Adielson, A. Carlson, H.B. Margolis, and J.A. Halladay, "Resonant overvoltages in EHV transformers - modeling and application", IEEE Trans. Power App. Syst., vol. PAS-100, pp. 3563-3572, July 1981.

[124] R.C. Degeneff, "A method for constructing terminal models for single-phase N-winding transformers", Paper A 78 539-9, presented at IEEE PES **Summer** Meeting, Los Angeles, Calif., July 16-21, 1978.

[125] G.W. Swift, "Power transformer core behavior under transient conditions", IEEE Trans. Power App. Syst., vol. PAS-90, pp. 2206-2210, Sept./Oct. 1971.

[126] E. Kuffel and W.S. Zaengl, High Voltage Engineering. Pergamon Press, Oxford, 1984.

[127] F.W. Heilbronner, "Firing and voltage shape of multistage impulse generators", IEEE Trans. Power App. Syst., vol. PAS-90, pp. 2233-2238, Sept./Oct. 1971.

[128] W.F. Long, "A study on some switching aspects of a double circuit HVDC transmission line", IEEE Trans. Power App. Syst., vol. PAS-92, pp. 734-741, March/April 1973.

[129] D.J. Melvold, P.R. Shockley, W.F. Long, and N.G. Hingorani, "Three terminal operation of the Pacific HVDC Intertie for dc circuit breaker testing", IEEE Trans. Power App. Syst., vol. PAS-95, pp. 1287-1296, July/Aug. 1976.

[130] B.C. Chiu, A converter model for the digital simulation of transients in ac/dc transmission systems.

M.A.Sc. thesis, University of British Columbia, Vancouver, Canada, May 1980.

[131]   V. Brandwajn, "Influence of numerical noise on the stability of Type 59 SM model", EMTP Newsletter, vol. 2, no. 3, pp. 37-43, Feb. 1982.

[132]   V. Brandwajn, "Investigation and improvement of long term stability for the TYPE-59 synchronous machine model", EMTP Newsletter, vol. 4, no. 2, pp. 54-57, Nov. 1983.

[133]   D.A. Calahan, "Numerical considerations for implementation of nonlinear transient circuit analysis program", IEEE Trans. Circuit Theory, vol. CT-18, pp. 66-73, Jan. 1971.

[134]   J. Mechenbier, "Simulation of synchronous machines in cases with large speed changes", EMTP Newsletter, vol. 5, no. 4, pp. 3-7, Oct. 1985.

[135]   B. Kulicke, "Simulation program NETOMAC: modelling of synchronous and induction machines" (in German), Siemens Forschungs-u. Entwicklungs-Berichte, vol. 11, pp. 156-161, 1982.

[136]   R. Ramanujam, "A method of interfacing Olive's model of synchronous machine in an electromagnetic transients program", EMTP Newsletter, vol. 3, no. 1, pp. 46-59, Aug. 1982.

[137]   H.K. Lauw and W.S. Meyer, "Universal machine modelling for the representation of rotating electric machinery in an electromagnetic transients program", IEEE Trans. Power App. Syst., vol. PAS-101, pp. 1342-1351, June 1982.

[138]   G.J. Rogers and D. Shirmohammadi, "Induction machine modelling for electromagnetic transient program", Ontario Hydro Internal Memorandum, 1985.

[139]   D. Shirmohammadi, "Universal machine modelling in Electromagnetic Transient Program (EMTP)", EMTP Newsletter, vol. 5, no. 2, pp. 5-27, April 1985, and Trans. Engineering & Operating Division, Canadian Electrical Association, vol. 24, 1985.

[140]   H.K. Lauw, "Interfacing for universal multi-machine system modelling in an electromagnetic transients program", IEEE Trans. Power App. Syst., vol. PAS-104, pp. 2367-2373, Sept. 1985.

[141]   W.F. Tinney and J.W. Walker, "Direct solutions of sparse network equations by optimally ordered triangular factorization", Proc. IEEE, vol. 55, pp. 1801-1809, Nov. 1967.

[142]   H. Edelmann, "Ordered triangular factorization of matrices", Proc. Power Systems Computation Conference, Stockholm, 1966.

[143]   J. Carpentier, "Ordered eliminations", Proc. Power Systems Computation Conference, London, 1963.

[144]   W.F. Tinney, V. Brandwajn and S.M. Chan, "Sparse vector methods", IEEE Trans. Power App. Syst., vol. PAS-104, pp. 295-301, Febr. 1985.

[145]   W.F. Tinney and W.S. Meyer, "Solution of large sparse systems by ordered triangular factorization", IEEE Trans. Automatic Control, vol. AC-18, pp. 333-346, Aug. 1973.

[146]   W.F. Tinney, "Some examples of sparse matrix methods for power network problems", Proc. 3rd Power Systems Computation Conference, Rome, 1969.

[147]   W.F. Tinney and W.L. Powell, "Comparison of matrix inversion and sparse triangular factorization for

solution of power network problems", Paper presented at a Romania-U.S. Conference on Power Systems, Bucharest, 1974.

[148] B.M. Weedy, Electric Power Systems. Third Edition. John Wiley and Sons, Chichester (England), 1979.

[149] Handbook of Mathematical Functions. Edited by M. Abramowitz and I.A. Stegun, publ. by U.S. Dept. of Commerce, 1964.

[150] L.M. Wedepohl and D.J. Wilcox, "Transient analysis of underground power transmission systems; system-model and wave propagation characteristics", Proc. IEE, vol. 120, pp. 252-259, Feb. 1973.

[151] G. Bianchi and G. Luoni, "Induced currents and losses in single-core submarine cables", IEEE Trans. Power App. syst., vol. PAS-95, pp. 49-58, Jan./Feb. 1976.

[152] S.A. Schelkunoff, "The electromagnetic theory of coaxial transmission lines and cylindrical shields", Bell System Technical Journal, vol. 13, pp. 532-579, 1934.

[153] D.R. Smith and J.V. Barger, "Impedance and circulating current calculations for UD multi-wire concentric neutral circuits", IEEE Trans. Power App. Syst., vol. PAS-91, pp. 992-1006, May/June 1972.

[154] O. Breien and I. Johansen, "Attenuation of travelling waves in single-phase high-voltage cables", Proc. IEE, vol. 118, pp. 787-793, June 1971.

[155] L. Marti, "Simulation of electromagnetic transients in underground cables with frequency-dependent modal transformation matrices", Ph.D. thesis, University of British Columbia, Vancouver, Canada, Nov. 1986.

[156] A. Semlyen, discussion to "Overhead line parameters from handbook formulas and computer programs" by H.W. Dommel, IEEE Trans. Power App. Syst., vol. PAS-104, p. 371, Feb. 1985.

[157] P.W. Hornbeck, Numerical Methods. Quantum Publishers, New York, 1975.

[158] H.W. Dommel and J.H. Sawada, "The calculation of induced voltages and currents on pipelines adjacent to ac power lines", Report to B.C. Hydro and Power Authority for CEA Contract 75-02, 1976 (not released yet).

[159] J.A. Tegopoulous, and E.E. Kriezis, "Eddy current distribution in cylindrical shells of infinite length due to axial current - Part II: shells of finite thickness", IEEE PAS-90, pp. 1287-1294, May 1971.

[160] G.W. Brown and R.G. Rocamora, "Surge propagation in three-phase pipe-type cables. Part I - Unsaturated pipe", IEEE Trans. Power App. Syst., vol. PAS-95, pp. 89-95, Jan./Feb. 1976.

[161] R.G. Rocamora and G.W. Brown, "Surge propagation in three-phase pipe-type cables. Part II - Duplication of field tests including the effects of neutral wires and pipe saturation", IEEE Trans. Power App. Syst., vol. PAS-96, pp. 826-833, May/June 1977.

[162] P. de Arizon and H.W. Dommel, "Computation of cable impedances based on sub-division of conductors", IEEE Trans. Power Delivery, vol. PWRD-2, pp.21-27, Jan. 1987.

[163] A. Ametani, "A general formulation of impedance and admittance of cables", IEEE Trans. Power Syst., vol. PAS-99, pp. 902-910, May/June 1980.

[164]   W.T. Weeks, L.L. Wu, M.F. McAllister, A. Singh, "Resistive and inductive skin effect in rectangular conductors", IBM Journal of Research and Development, **vol.** 23, no. 6, pp. 652-660, Nov. 1979.

[165]   A. Konrad, "The numerical solution of steady-state skin effect problems - an integrodifferential approach", IEEE Trans., Vol. MAG-17, pp. 1148-1152, Jan. 1981.

[166]   A. Konrad, "Integrodifferential finite element formulation of two dimensional steady-state skin effect problems", IEEE Trans., Vol. MAG-18, pp. 284-292, Jan. 1982.

[167]   J. Weiss and Z.J. Csendes, "A one-step finite element method for multiconductor skin effect problems", IEEE Trans., Vol. PAS-101, pp. 3796-3802, Oct. 1982.

[168]   N. Srivallipuranandan, "Series impedance and shunt admittance matrices of an underground cable system", M.A.Sc. Thesis, University of British Columbia, Vancouver, Canada, 1986.

[169]   E.P. Dick, N. Fujimoto, G.L. Ford, and S. Harvey, "Transient ground potential rise in gas-insulated substations - problem identification and mitigation", IEEE Trans. Power App. Syst., vol. PAS 101, pp. 3610-3619, Oct. 1982.

[170]   H. Bocker and D. **Oeding,** "Induced **voltages** in **pipelines close to** high **voltage lines",** **Elektrizitatswirtschaft** (in German), **vol.** 65, pp. 157-170, 1966.

[171]   Yin Yanan "An application of finite element method (FEM) to the calculations of transmission line parameters", Internal Report, Univ. of British Columbia, Vancouver, Canada, April 1986.

[172]   D. Kind, "The equal area criterion for impulse voltage stress of practical electrode configurations in air", ETZ-A (in German), vol. 79, pp. 65-69, 1958.

[173]   F. **Heilbronner, discussion in** [50].

[174]   U. Burger, Surge arresters with spark gaps. Chapter in Surges in High-Voltage Networks, edited by K. Ragaller. Plenum Press, New York, 1980.

[175]   IEEE Working Group, "Modelling of current-limiting surge arresters", IEEE Trans. Power App. Syst., **vol.** PAS-100, pp. 4033-4040, Aug. 1981.

[176]   D.P. Carrol, R.W. Flugum, J.W. Kalb and H.A. Peterson, "A dynamic surge arrester model for use in power system transient studies", IEEE Trans. Power App. Syst., vol. PAS-91, pp. 1057-1067, May/June 1972.

[177]   G. Brauner, "Simulation of the performance of metal-clad substations and open-air substations under lightning surges (in German)", Ph.D. dissertation, Darmstadt, Germany, 1976.

[178]   D.W. Durbak, "Zinc-oxide arrester model for fast surges", EMTP Newsletter, vol. 5, no. 1, pp. 1-9, Jan. 1985.

[179]   B. Knecht, Solid state arresters. Chapter in Surges in High-Voltage Networks, edited by K. Ragaller. Plenum Press, **New** York, 1980.

[180]   J.C. Flores, G.W. Buckley, and G. McPherson, "The effects of saturation on the armature leakage reactance of large synchronous machines", IEEE Trans. Power App. Syst., vol. PAS-103, pp. 593-600,

March 1984.

[181]   M.V.K. Chari, Z.J. Csendes, S.H. Minnich, S.C. Tandon, and J. Berkery, "Load characteristics of synchronous generators by the finite-element method", IEEE Trans. Power App. Syst., vol. PAS-100, pp. 1-13, Jan. 1981.

[182]   R.G. Harley, D.J.N Limebeer, E. Chirricozzi, "Comparative study of saturation methods in synchronous machine models", IEE Proc., vol. 127, pt. B., pp. 1-7, Jan. 1980.

[183]   A. Sweetana, N. Kunkle, N. Hingorani, V. Tahiliani, "Design, development and testing of 1200 kV and 550 kV gapless surge arresters", IEEE Trans. Power App. Syst., vol. PAS-101, pp. 2319-2327, July 1982.

[184]   M.B. Hughes, R.W. Leonard, T.G. Martinich, "Measurement of power system subsynchronous driving point impedance and comparison with computer simulations", IEEE Trans. Power App. Syst., vol. PAS-103, pp. 619-630, 1984.

[185]   H.W. Dommel, A. Yan, Shi Wei, "Harmonics from transformer saturation", IEEE Trans. Power Delivery, vol. PWRD-1, pp. 209-215, April 1986.

[186]   R.E. McCotter, H.A. Smolleck, S.J. Ranade, W.H. Kersting, "An investigation of the fundamental-frequency impedance of a single-phase distribution lateral", IEEE Trans. Power Delivery, vol. PWRD-1, pp. 232-238, Jan. 1986.

[187]   M. Ren-ming, "The challenge of better EMTP TACS variable ordering", EMTP Newsletter, vol. 4, no. 4, pp. 1-6, Aug. 1984.

[188]   J.A. Lima, "Numerical instability due to EMTP-TACS inter-relation", EMTP Newsletter, vol. 5, No. 1, pp. 21-23, Jan. 1985.

[189]   L. Dubé and H.W. Dommel, "Simulation of control systems in an electromagnetic transients program with TACS", Proc. IEEE PICA Conf., pp. 266-271, May 1977.

[190]   N. Dravid, "Comparison of various representations of a limit function in a second order system", handwritten notes, 1972.

[191]   IEEE Task Force, "Conventions for block diagram representations", IEEE Trans. Power Syst., vol. PWRS-1, pp.95-100, Aug. 1986.

[192]   J.H. Neher, "Phase sequence impedance of pipe type cables", IEEE Trans. Power App. Syst., vol. 83, pp. 795-804, August 1964.